NASA CONTRACTOR
REPORT

NASA CR-61322

RANGE AND STRUCTURE OF AMBIENT DENSITY FROM 30 TO 120 KM ALTITUDE

By Raymond A. Minzner, S. Mello and Paul Morgenstern

GCA Corporation
GCA Technology Division
Bedford, Massachusetts

May 1970

Prepared for

NASA-GEORGE C. MARSHALL SPACE FLIGHT CENTER
Marshall Space Flight Center, Alabama 35812

TECHNICAL REPORT STANDARD TITLE PAGE

1. REPORT NO.	2. GOVERNMENT ACCESSION NO.	3. RECIPIENT'S CATALOG NO.
NASA CR-61322		

4. TITLE AND SUBTITLE	5. REPORT DATE
RANGE AND STRUCTURE OF AMBIENT DENSITY FROM 30 TO 120 KM ALTITUDE	May 1970
	6. PERFORMING ORGANIZATION CODE

7. AUTHOR(S)	8. PERFORMING ORGANIZATION REPORT #
Raymond A. Minzner, S. Mello and Paul Morgenstern	

9. PERFORMING ORGANIZATION NAME AND ADDRESS	10. WORK UNIT NO.
GCA Corporation GCA Technology Division Bedford, Massachusetts	11. CONTRACT OR GRANT NO. NAS 8-20098
	13. TYPE OF REPORT & PERIOD COVERED Contractor Report
12. SPONSORING AGENCY NAME AND ADDRESS Aero-Astrodynamics Laboratory George C. Marshall Space Flight Center Marshall Space Flight Center, Alabama 35812	14. SPONSORING AGENCY CODE

15. SUPPLEMENTARY NOTES Contract Technical Monitor: Mr. O. E. Smith, Aerospace Environment Division, Aero-Astrodynamics Laboratory, MSFC.

16. ABSTRACT

Section I of this report deals with two particular investigations involving the validity and applicability of statistical versions of the Gas Law and of the Hydrostatic Equations (as applied to the generation of atmospheric models) with data of various degrees of homogeneity.

Section II consists primarily of a catalogue of two groups of machine-plotted graphs, resulting from a study on the time and space variability of atmospheric density in the height interval 30 to 120 km. The first group consists of 48 graphs comparing various sets of data with the U. S. Standard Atmosphere 1962. The second group consists of 48 graphs comparing the same sets of observed data with the Patrick Reference Atmosphere 1963. The graphs include profiles of mean density and profiles of the standard deviation of density.

17. KEY WORDS	18. DISTRIBUTION STATEMENT
	FOR PUBLIC RELEASE: E. D. Geissler E. D. Geissler Director, Aero-Astrodynamics Laboratory

19. SECURITY CLASSIF. (of this report)	20. SECURITY CLASSIF. (of this page)	21. NO. OF PAGES	22. PRICE
UNCLASSIFIED	UNCLASSIFIED	394	

MSFC - Form 3292 (May 1969)

PREFACE

The two sections of this report previously received very limited distribution as GCA Reports:

(1) GCA-TR-68-15-N (October 1968), "Range and Structure of Ambient Density from 30 to 120 km Altitude," by Minzner and Morgenstern.

(2) GCA-TR-67-16-N (August 1967), "Range and Structure of Ambient Density from 0 to 120 km Altitude," by Minzner and Mello.

The two reports are combined, and distribution is provided in the interest of information exchange. Responsibility for the contents resides with the original authors.

SECTION I

ANALYSIS OF STATISTICAL MODELS

by

R. A. Minzner and P. Morgenstern
GCA Corporation
GCA Technology Division
Bedford, Massachusetts

TABLE OF CONTENTS

RANGE AND STRUCTURE OF AMBIENT DENSITY FROM 30 TO 120 KM ALTITUDE

By R. A. Minzner* and P. Morgenstern**
GCA Corporation, GCA Technology Division
Bedford, Massachusetts

SUMMARY

Altitude profiles of atmospheric temperature, pressure and density obtained from 437 rocket soundings for various portions of the altitude interval 30 to 120 km have been gathered for the purpose of performing various statistical investigations. The soundings have been sorted into homogeneous cells of a three-dimensional array defined by specific diurnal, seasonal and latitudinal categories. Six diurnal categories are defined in terms of solar zenith angles and earth shadow heights rather than in terms of standard or Greenwich time. Eight seasonal categories are defined in terms of astronomical as well as continental climatological considerations. Six latitude bands are defined in 15-degree increments with seasonal inversions to permit combining of southern and northern latitude regions.

The quasi-homogeneous stratification of data has permitted the determination of the independent influence of each of the three mentioned variables on certain atmospheric properties. Two particular investigations involve the validity of statistical versions of the Gas Law and of the Hydrostatic Equations (as applied to the generation of atmospheric models) with data of various degrees of homogeneity. The results of these computations are presented graphically and are discussed theoretically.

INTRODUCTION

A continuing and pressing requirement exists for reliable models of the atmosphere for the purpose of aircraft, missile and booster design, and for the purpose of planning reentry patterns for Apollo and other space missions. To be most useful, these models must describe not only the average state of the entire atmosphere, but should also provide estimates of its time and space variability. The need also exists for extending our knowledge of these statistics to higher regions of the atmosphere than those for which such knowledge is now available.

---

*Now at National Aeronautics and Space Administration, Electronics Research Center, Cambridge, Massachusetts.

**Now at Walden Research Corp., Cambridge, Mass.

The missile and booster design requirements which this study serves, deal primarily with launch conditions at Cape Kennedy 28°27' N latitude. None of the data nor any of the stratifications of the data discussed below apply specifically to this site. However, the major portion of data used in this study is associated with the subtropical latitude belt (22.5° to 37.5°). Thus, the results derived from these data are believed to be directly relatable to conditions at Cape Kennedy.

The reentry requirements generally deal with atmospheric conditions over a wide range of latitudes unless a particular mission permits the reentry to be confined to a plane parallel with the plane of the earth's equator. Thus, for the general case all latitudes must be considered. This need is met by a consideration of data observed at sites ranging from the tropics to the arctic.

This report summarizes the results from a program of research on model atmospheres conducted for the National Aeronautics and Space Administration under Contract NAS8-20098 in an effort to satisfy some of these requirements. The work consisted of two distinct parts. The first part dealt with a study on the time and space variability of atmospheric density in the height interval 30 to 120 km. These statistical calculations were based on a collection of 211 upper-air soundings obtained by means of instrumented rockets. The results of these calculations were compared with the U.S. Standard Atmosphere [1]* and with the Patrick Reference Atmosphere. The findings from this work have been documented in a separate technical report [2], and are also included in Section II of this report.

The second part of the research program was concerned with investigating the validity and applicability of certain statistical models proposed by Buell [3,4] relating the mean values, and standard deviations of atmospheric density, temperature and pressure as well as certain correlation coefficients. The basic data set used for testing these models was considerably enlarged over that used in the first part; the number of soundings was more than doubled to 437 soundings. The densities, temperatures, and pressures of this expanded set of data have been published previously in a separate technical report [5] whereas this Section provides a detailed discussion of the analysis techniques used and presents the statistical results obtained.

*Numbers in [ ] represent reference numbers.

DEFINITION OF THE PROBLEM

The study reported below deals with the examination and verification of two statistical equations under the conditions to which they are subjected when various sets of observed data are used in their evaluation. The first of these equations will be referred to as the statistical form of the Gas Law, while the second will be called the statistical form of the Hydrostatic Equation. The statistical form of the Gas Law was first published by Buell [4] without any verification by means of numerical evaluation. The statistical form of the Hydrostatic Equation was also published by Buell [3] but in this instance the results of numerical evaluation were given for a limited data set extending from the surface to about 15 km altitude. No evaluation has heretofore been made for greater altitudes. The specific equations are given at the end of separate derivations which establish the theoretical validity of each equation.

Statistical Form of the Gas Law

It has been customary in the generation of recent model atmospheres [1,6-12] to use the following procedure:

(1) Determine a mean temperature-altitude profile for the model from available sounding data.

(2) Introduce this temperature-altitude profile and a single mean pressure value into the hypsometric equation to compute a pressure-altitude profile.

(3) Introduce corresponding values of temperature T and pressure p from steps (1) and (2) into the Gas Law (or equation of state) to compute density ρ for a density-altitude profile.

The equation of state is expressed by

$$p = \frac{R}{M} \rho T \tag{1}$$

where M is the mean molecular weight of air and R is the universal gas constant. Thus, while the model is based upon a mean temperature, deduced from a number of soundings, the density and pressure values are derived as if there had been but a single sounding. It may be demonstrated that the mean value of density and the mean value of pressure as deduced directly from the basic data, for a particular altitude, would not necessarily agree with the corresponding values of ρ and p as deduced by the above model-generation procedure. The implication of this situation is that while the simple Gas Law quite accurately relates the thermodynamic properties of the atmosphere for a single sounding it does not in general rigorously relate the corresponding mean values derived from a number of soundings.

If p, ρ and T are taken to be the corresponding values of the three thermodynamic properties for a single sounding, and if p', ρ', and T' are assumed to be the corresponding departures from the mean values $\bar{p}$, $\bar{\rho}$ and $\bar{T}$ deduced from a number of soundings we may write

$$p = \bar{p} + p' \tag{2}$$

$$\rho = \bar{\rho} + \rho' \tag{3}$$

$$T = \bar{T} + T' \tag{4}$$

Substituting Equations (2), (3) and (4) into Equation (1), and performing the indicated multiplications yields a second form of the Gas Law which, like Equation (1), is also applicable only to a single set of conditions, i.e., only to a single sounding;

$$\bar{p} + p' = \frac{R}{M} (\bar{\rho}\bar{T} + \bar{\rho}T' + \rho'\bar{T} + \rho'T') \tag{5}$$

The arithmetic average $\bar{x}$ of any group of n individual values x_i is derived by the mathematical operator

$$\bar{x} = \frac{1}{n} \sum_{i=1}^{n} x_i$$

Applying this operator to both sides of Equation (5) and noting that

$$\Sigma\, p' = \Sigma\, \rho' = \Sigma\, T' = 0$$

leads to one version of the statistical form of the Gas Law:

$$\bar{p} = \frac{R}{M} \bar{\rho}\bar{T} + \frac{R}{M} \frac{\Sigma\, \rho'T'}{n} \tag{6}$$

The quantity $(\Sigma\, \rho'T')/n$ in Equation (6) is commonly known as the covariance between variables ρ and T. The covariance is related to the correlation between ρ and T by the definition

$$\frac{\Sigma\, \rho'T'}{n} \equiv \sigma[\rho] \cdot \sigma[T] \cdot r[\rho,T] \tag{7}$$

where $r[\rho,T]$ is the correlation coefficient and $\sigma[\rho]$ and $\sigma[T]$ designate the standard deviation of ρ and T, respectively. Thus, the simple form of the Gas Law is satisfied exactly by the mean values of pressure, temperature and density only when the variations in ρ and T are <u>uncorrelated</u>.

Other versions of the statistical form of the Gas Law are:

$$\bar{p} = \frac{R}{M}\bar{\rho}\bar{T} + \frac{R}{M}\frac{n\,\Sigma\,\rho T - (\Sigma\rho)(\Sigma T)}{n^2} \tag{8}$$

$$100 = 100\,\frac{R}{M}\frac{\bar{\rho}\bar{T}}{\bar{p}} + 100\,\frac{R}{M}\frac{n\,\Sigma\,\rho T - (\Sigma\rho)(\Sigma T)}{n^2\,\bar{p}} \tag{9}$$

$$\bar{p} = \frac{R}{M}\bar{\rho}\bar{T} + \frac{R}{M}\sigma[\rho]\cdot\sigma[T]\cdot r[\rho,T] \tag{10}$$

$$100 = 100\,\frac{R}{M}\frac{\bar{\rho}\bar{T}}{\bar{p}} + 100\,\frac{R}{M}\frac{\bar{\rho}\bar{T}}{\bar{p}}\left(\frac{\sigma[\rho]}{\bar{\rho}}\cdot\frac{\sigma[T]}{\bar{T}}\cdot r[\rho,T]\right) \tag{11}$$

$$\bar{p} = \frac{R}{M}\bar{\rho}\bar{T}\left(1 + \frac{\sigma[\rho]}{\bar{\rho}}\cdot\frac{\sigma[T]}{\bar{T}}\cdot r[\rho,T]\right) \tag{12}$$

Each of these equations show one or another form of a correction which must be made to the simple form of the Gas Law, to make it rigorously applicable to the mean values of p, ρ, and T when the correlation is non-zero. The evaluation of one or more versions of this equation with observational data provides a means of determing the relative importance of the correction term at various altitudes.

Equations (8) and (9) are those versions of the Gas Law which have been evaluated term by term in this study, with values punched out according to the format given in Appendix C. Values of $\sigma[\rho]$, $\sigma[T]$, $\sigma[\rho]/\bar{\rho}$, $\sigma[T]/\bar{T}$, and $r[\rho,T]$ were also computed. The value of the covariance term of Equation (9) has been plotted as a function of altitude for each of 110 different groupings of data. These graphs are presented in Appendix A and show that the absolute value of this covariance term usually is small compared to 1 percent, and rarely exceeds 3 percent of the right-hand side of the equation. This implies that the value of the covariance term of Equation (10) is usually much smaller than 0.01 of $\bar{p}$ and rarely exceeds 0.03 of $\bar{p}$. One may imply that, to a first approximation, the value of the small quantity $\sigma[\rho]\cdot\sigma[T]\cdot r[\rho,T]$ in Equation (10) bears a similar relationship to the relatively large value of $\bar{\rho}\bar{T}$ in that equation.

For various reasons Equations (8) through (11) are not the most desirable forms to analyze for a determination of the dominant factors in any particular data set or altitude region. A more desirable form is arrived at by replacing $\bar{p}$ in the denominator of the covariance term of Equation (11) by its two-term equivalent in Equation (10). After rearranging terms, one obtains

$$1 = \frac{R}{M}\frac{\bar{\rho}\bar{T}}{\bar{p}} + \frac{\sigma[\rho] \cdot \sigma[T] \cdot r[\rho,T]}{\bar{\rho}\bar{T} + \sigma[\rho] \cdot \sigma[T] \cdot r[\rho,T]} \qquad (13)$$

The value of the covariance term of this equation is small compared with the value of the principal term in the same ratio as $\sigma[\rho] \cdot \sigma[T] \cdot r[\rho,T]$ is small compared to ρT. The denominator of this small convariance term, however, consists of the sum $\bar{\rho}\bar{T} + \sigma[\rho] \cdot \sigma[T] \cdot r[\rho,T]$, and only a very small error is introduced into this alrady small term if this denominator is simplified to the principal term alone; i.e., to $\bar{\rho}\bar{T}$. We may therefore rewrite Equation (13) as

$$1 \cong \frac{R}{M}\frac{\bar{\rho}\bar{T}}{\bar{p}} + \frac{\sigma[\rho]}{\bar{\rho}} \cdot \frac{\sigma[T]}{\bar{T}} \cdot r[\rho,T] \qquad (14)$$

This form more readily shows the contribution to the correction term provided by the variability of ρ, T, and by $r[\rho,T]$. For the purposes of this study the graphs of Appendix A may be considered to be an evaluation of the convariance term of Equation (14) expressed as a percent. The analysis of these graphs is the subject of a separate paper in preparation [13].

Statistical Form of the Hydrostatic Equation

From statistical considerations a rigorous version of the Gas Law for the mean values of p, ρ, and T was found to involve $\sigma[\rho]$, $\sigma[T]$, and $r[\rho,T]$. A statistical version of the Hydrostatic Equation; i.e., one involving $\sigma[\rho]$, $\sigma[p]$, and $r[\rho,p]$ may also be developed. We begin with the standard form of the Hydrostatic Equation; i.e., the form applying only to the data of a single sounding:

$$\partial p = - g\rho \, \partial Z \qquad (15)$$

where g is the acceleration of gravity, and Z is geometric altitude. Introducing Equations (2) and (3) into (15) yields

$$\frac{\partial \bar{p}}{\partial Z} + \frac{\partial p'}{\partial Z} = -g\bar{\rho} - g\rho' \qquad (16)$$

Applying the averaging operator to Equation (16) yields

$$\frac{\partial \bar{p}}{\partial Z} = -g\bar{\rho} \tag{17}$$

Subtracting Equation (17) from Equation (16) leaves

$$\frac{\partial p'}{\partial Z} = -g\rho' \tag{18}$$

The variance of pressure may be stated as

$$(\sigma[p])^2 = \frac{\Sigma(p')^2}{n} \tag{19}$$

Differentiation with respect to Z gives

$$\sigma[p]\,\frac{\partial \sigma[p]}{\partial Z} = \frac{1}{n}\,\Sigma\left[p'\,\frac{\partial p'}{\partial Z}\right] \tag{20}$$

Substituting Equation (18) into Equation (20) yields

$$\sigma[p]\,\frac{\partial \sigma[p]}{\partial Z} = \frac{-\Sigma\, g\rho' p'}{n} \tag{21}$$

If the summation in Equation (21) is performed at a single altitude and at a single site, g is constant and can be taken out of the summation leaving the covariance of ρ and p as a factor. Using the relationship between covariance and the coefficient of correlation in the form expressed in Equation (7), we may rewrite Equation (21) as

$$\frac{\partial \sigma[p]}{\partial Z} = -g\,\sigma[\rho]\cdot r[\rho,p] \tag{22}$$

Equation (22) is the particular statistical form of the Hydrostatic Equation which we evaluated.* In order to show how well this equation is satisfied by the observed data we also evaluated the percent difference between the two sides of Equation (22); i.e., we evaluated the quantity

---

*This equation is analogous to a relationship derived by Stidd [14] for the vertical gradient of the standard deviation of the height of a constant pressure surface.

$$\text{PlHY} \equiv \frac{100\left\{\frac{\partial\sigma[p]}{\partial Z} - g\,\sigma[\rho]\cdot r[\rho,p]\right\}}{\frac{\partial\sigma[p]}{\partial Z}} \qquad (23)$$

In the evaluation of Equations (22) and (23), the value of the standard deviation was obtained for each integer altitude while the value of $r[\rho,p]$ was obtained, also for each integer altitude, from the value of the covariance of ρ and p, and from $\sigma[T]$ after the manner of Equation (7). The value of $\partial\sigma[p]/\partial Z$, however, cannot be obtained for a single altitude. Rather, one must use data for three or more altitudes in a numerical-differentiation process to obtain a mean value averaged over several kilometers. The numerical differentation scheme used in evaluating this term was Stirling's central-difference formula [15],

$$\frac{\partial\sigma[p]}{\partial Z} \cong \frac{1}{\Delta Z}\left[\frac{f[Z_1]-f[Z_{-1}]}{2} - \frac{f[Z_2]-2f[Z_1]+2f[Z_{-1}]-f[Z_{-2}]}{12} + \ldots\right] \qquad (24)$$

In this expression $f[Z]$ refers to $\sigma[p]$ at the various altitudes. The subscripts refer to the kilometer altitudes of the measurement points relative to the central altitude for which the evaluation is being made, and ΔZ is the altitude increment. A minimum of three points (one point on either side of the central value) and a maximum of five points, (two points on either side of the central value) were used to evaluate the derivative.

It was initially intended to plot the quantity PlHY expressed by Equation (23) as a function of altitude for various sets of data. The value of PlHY, however, was found to be a very erratic function of altitude. The graphs would have been very difficult to read and of questionable value. It was decided, therefor to plot only an envelope of successive positive and negative maxima of PlHY as a function of altitude. Graphs containing such envelopes of percent differences for various sets of data are presented in Appendix B. These same figures also contain graphs of $\ell n\,\sigma[p]$ as a function of altitude.

In retrospect it appears that it may have been more meaningful to examine an integrated form of Equation (22); i.e.,

$$\sigma[p]_i = \sigma[p]_o + g\int_{Z_i}^{Z_o}\sigma[\rho]\cdot r[\rho,p]\,dZ \qquad (25)$$

or

$$\frac{\sigma[p]_i}{\bar{p}_i} = \frac{\sigma[p]_o}{\bar{p}_o} \cdot \frac{\bar{p}_o}{\bar{p}_i} + \frac{g}{\bar{p}_i} \int_{Z_i}^{Z_o} \sigma[\rho] \cdot r[\rho,p]\, dZ \qquad (26)$$

where g is assumed to be constant. In these equations the subscript, o, is associated with the greatest altitude of the set of data and with the corresponding values of $\sigma[p]$ and $\bar{p}$. The subscript, i, is associated with successive integer-kilometer altitudes below Z_o, and with the corresponding values of $\sigma[p]$ and $\bar{p}$. For Z_i sufficiently below Z_o the quantity $\bar{p}_o/\bar{p}_i$ becomes very small so that the term involving this ratio may be neglected. We may then write

$$\frac{\sigma[p]_i}{\bar{p}_i} \cong \frac{g}{\bar{p}_i} \int_{Z_i}^{Z_o} \sigma[\rho] \cdot r[\rho,p]\, dZ \qquad (27)$$

or simply

$$\sigma[p]_i \cong g \int_{Z_i}^{Z_o} \sigma[\rho] \cdot r[\rho,p]\, dZ \qquad (28)$$

The percentage difference between the two sides of Equations (27) or (28) may be expressed as

$$P2HY \cong 100 \left\{ 1 - \frac{g \int_{Z_i}^{Z_o} \sigma[\rho] \cdot r[\rho,p]\, dZ}{\sigma[p]_i} \right\} \qquad (29)$$

No numerical evaluation of this expression has been made under the contract being reported. A subsequent investigation by Minzner and Morgenstern [16] indicates that a much smaller and smoother difference would have been found in the evaluation of Equation (25) than was found in the evaluation of Equation (22).

Equation (28) suggests that the altitude profile of $\sigma[p]$ may be computed from the related altitude profile of $\sigma[\rho]$. This is true only if one knows simultaneously the altitude profile of $r[\rho,p]$, but this is generally not known. For altitudes above 30 km, however, the value of $r[\rho,p]$ has been found to remain within the limited range of about +0.5 to +0.98. Hence, using these values and known values of $\sigma[\rho]$ one obtains upper and lower bounds on the value of $\sigma[p]$.

The fact that g is not constant for varying altitudes may be compensated for in the numerical integration process. When the above equations are applied to sets of data made up of soundings from various latitudes, however, the value of g is not the same even for identical geometric altitudes. In this instance Z may be consider to be geopotential in which case g is truly a constant for all altitudes and all latitudes. To apply the data to equations expressed in terms of geopotential, however, the data must be grouped according to equal values of geopotential altitude. This was <u>not</u> done in the present study.

MEASUREMENT TECHNIQUES

In the altitude region 30 to 200 km, atmospheric data have been obtained primarily by vertical sounding rockets, although vertical light probes have also been used. In many instances only one of the three basic thermodynamic properties is determined at any time-space point. If this property is determined over an extended altitude region at essentially the same time, as in a near-vertical rocket-probe flight, this altitude profile of a single property leads to altitude profiles of the other two thermodynamic properties. If the basic data are for pressure versus altitude, the temperature-versus-height profiles may be deduced in principal from the slope of the semi-log graph of pressure versus altitude, that is

$$T(h) = \frac{GM}{R} \frac{1}{\frac{d\ \ell n\ p(h)}{dh}} \tag{30}$$

where G is a constant numerically equal to the sea-level value of the acceleration of gravity at about 45° latitude with dimensions depending on those of geopotential [6], and h is geopotential altitude. Thus, with p(h) and T(h) determined, ρ(h) is determined from Equation (1). Actually, the temperature determined is the mean temperature for the altitude interval between successive pressure measurements. Unfortunately, for practical pressure gauges, the temperature uncertainty becomes very large when the altitude interval is decreased to values less than 5 km, and this method has not been used extensively in the reduction of rocket sounding data.

If the primary data are values of density versus altitude of a specified accuracy without an independent knowledge of temperature at the top of the density-altitude profile, one may determine a temperature-altitude profile for all but the upper 10 to 15 km of the altitude region of the density data [17]. This is done using a numerical integration form of the expression

$$T_2 = T_1 \frac{\rho_1}{\rho_2} + \frac{GM}{R\rho_2} \int_{h_2}^{h_1} \rho(h)\ dh \tag{31}$$

where h_1 is the geopotential of the greatest height for which a density value exists, i.e., ρ_1, and h_2 is the geopotential associated with successive values of densities ρ at successively lower heights, for which heights of the successive values of T_2 is determined. When h_2 is sufficiently below h_1 so that the value $T_1(\rho_1/\rho_2)$ becomes small compared with T_2 for some reasonable value for T_1, T_2 is determined essentially by the integral term of Equation (31). Thus, for altitudes of 10 to 15 km below h_1 down to the lowest altitude of density data, temperature-altitude profile may be determined from density-altitude

data alone. The percentage uncertainty in T_2 is comparable with the percentage uncertainty of ρ_2.

If the observed data consist of an altitude profile of temperature, an additional piece of information consisting of a reference-level value of pressure or of density is required to develop a related pressure-altitude profile or a density-altitude profile. When this additional piece of information is a pressure-height value, p_o at h_o, a complete pressure-altitude profile may be determined.

If the temperature-altitude profile consists of a series of discrete temperature-altitude values so that the segments between these successive values may be taken as linear, the following equations may be used.

$$p = p_o \left[\frac{T_o}{T_o + (h - h_o)L} \right]^{\frac{GM}{RL}}, \quad \text{for } L = \frac{dt}{dh} \neq 0 \tag{32}$$

and

$$p = p_o \exp \left[- \frac{GM}{R} \frac{(h - h_o)}{T_o} \right], \quad \text{for } \frac{dt}{dh} = 0 \ . \tag{33}$$

These are the equations which were employed in the calculation of various standard and model atmospheres, Diehl [18]; Minzner and Ripley [6]; Minzner et al. [7]; Minzner et al. [8]; U.S. Standard Atmosphere [1]. Other suitable series-expansion equations of the type discussed by Minzner [19] are not limited to zero or nonzero values of temperature-altitude gradients, and are far more desirable when values of L may approach zero yet are not equal to zero.

The pressure equation of this latter type is

$$P = P_o \exp \left\{ - \left[\frac{GM}{R} \frac{(h - h_o)}{(1/2)(T + T_o)} \right] \left[\left(\frac{T - T_o}{T + T_o} \right) + \frac{1}{3} \left(\frac{T - T_o}{T + T_o} \right) + \frac{1}{5} \left(\frac{T - T_o}{T + T_o} \right) \right] \right\} \tag{34}$$

When the additional piece of information is a density-height value, ρ_o at h_o, the appropriate equations commonly used for a linearly segmented temperature-altitude profile are:

$$\rho = \rho_o \left[\frac{T_o}{T_o + (h - h_o)L} \right]^{1 + \frac{GM}{RL}}, \quad \text{for } L = \frac{dt}{dh} \neq 0 \tag{35}$$

and

$$\rho = \rho_o \exp\left[-\frac{GM}{R}\frac{(h - h_o)}{T_o}\right], \quad \text{for } \frac{dt}{dh} = 0 \quad . \tag{36}$$

In the case of digital data, where dt/dh may be any realistic value, including values near zero as well as zero, Minzner [20] has shown that the following rapidly converging series expansion is very convenient:

$$\rho = \rho_o \exp\left\{-\left[\frac{GM(h - h_o)}{1/2\,(T - T_o)R} + 1\right]\left[\left(\frac{T - T_o}{T + T_o}\right) + \frac{1}{3}\left(\frac{T - T_o}{T + T_o}\right)^3 + \frac{1}{5}\left(\frac{T - T_o}{T + T_o}\right)^5 + \ldots\right]\right\} \tag{37}$$

Both Equations (34) and (37) are related to equations derived earlier by Nicolet [21].

Following the use of Equations (32), (33), or (34) in conjunction with the single pressure-altitude point, the density-altitude profile may be determined from Equation (1), or from combinations of Equation (1) and one of Equations (35), (36), or (37). If Equation (35), (36), or (37) are first used in conjunction with an initial density-altitude point, the related pressure-altitude profile may be deduced using Equation (1) or a combination of Equation (1), (32), (33), and (34).

In the above methods, altitude was observed along with pressure, temperature, or density. Altitude need not be one of the fundamental observations, however; it may be inferred. A corresponding pair of values of pressure p_2 and and temperature T_2 at unknown altitude h_2, where the altitude increment h_2-h_1 is small relative to some initially known reference altitude h_1, leads to the determination of the value of h_2 the altitude of these observations:

$$h_2 = h_1 + \frac{R\bar{T}}{GM}\left[\ell n\, p_1 - \ell n\, p_2\right] \tag{38}$$

where $\bar{T}$ is the mean value of temperature between T_1 and T_2. Successive pairs of values of p_2 and T_2 thus lead to altitude profiles of pressure and temperature provided the altitude of the first observation is known.

The various high-altitude rocketborne experiments measure parameters which lead to one or the other of the thermodynamic properties, and rarely are these measured "directly" as with a thermometer, thermocouple system, or thermistor system for temperature determination, or as with an aneroid or mercurial barometer in the case of pressure or by some inertial device in the case of density. On the contrary they are all measured indirectly. Thus, for these observations it is meaningless to consider which is the independent and which is the dependent observation as is done by Buell [3]. Typical examples of the types of upper atmosphere observation follow.

In the grenade experiment, the mean velocity of sound is determined for a series of successive atmospheric layers. This is accomplished by a ground-based microphone array which measures the phase velocity of the wave system generated by each of a series of grenade bursts. These observations lead to values of mean temperatures for the altitude layers between successive grenade bursts.

In the falling-sphere experiment, the drag acceleration a_d experienced by the falling sphere is measured, either directly by an accelerometer or indirectly from radar tracking data. These same radar data or the results of single and double integration of the net acceleration (gravity minus drag) lead to velocity v and altitude h. These values of a_d and v when combined with the appropriate value of drag coefficient c_d and the area-to-mass ratio lead to density at altitude h. While the only thermodynamic property measured is density, this measurement can hardly be considered a direct or independent one.

In the pitot-tube experiment, ratios of impact pressures to cone-wall pressures or to ambient pressures are measured, sometimes with aneroid type pressure gauges, but more likely by some form of ionization gauge which actually measures particle number density. These pressure ratios lead to Mach numbers as well as to ambient pressure. The Mach number along with rocket velocity from some form of radar observation leads to sound speed and then to temperature.

In various ionization gauges experiments, measurements lead to the number density, mass density, or pressure depending upon calibration of the location of the gauge on the rocket, the rocket altitude and wall-temperature considerations.

In none of the above methods may the temperatures, densities or pressures be considered directly independent observations. While some of the measurement techniques have smaller errors than others, for various reasons, there appears to be no other inherent advantage to having measured one or another of the thermodynamic properties at various altitudes. With each method, altitude profiles of p, T, and ρ may be obtained ultimately for each of the individual soundings considered provided the correct initial conditions are met.

The investigators involved in the various atmospheric sounding experiments do not always derive all three of the thermodynamic properties p, T, and ρ from their observed data, and in some instances, the methods employed by one investigator may lead to greater uncertainties than that used by another. The study being herein reported used only the results of those soundings for which there existed a published set of density-altitude values, and only these data were used regardless of what other data may also have been published. Thus, in one sense, density-altitude data may be considered as the independent data in this study. The related temperatures for each sounding is used in this study were determined in all cases by a numerical integration form of Equation (31) and the pressures were then determined using Equation (1).

DATA SOURCES AND PRELIMINARY STEPS

A total of 437 soundings covering the period 1947 to early 1965 were assembled for analysis. This basic data was collected from 45 different sources including journal articles, institutional reports and private communications. Table 1 gives an inventory of the soundings showing the number available from each of 25 different launch sites. With the exception of three flights, data published in the reports of the Meteorological Rocket Network (MRN) [22] were not taken as the basic source of data in this study. MRN reports do, however, contain the same or revised forms of data for a considerable number of soundings used by us. The originally published forms of the soundings used had the common feature of density-altitude profiles $\rho(Z)$ in one of a number of systems of units. Temperatures or pressures were frequently not published with the basic density data in the original sources, and when published, were arrived at by a variety of methods. Consequently, to obtain uniformity, all temperature-altitude data used in this study were recomputed by us from the density-altitude data for each sounding using Equation (31); i.e., the principle of downward integration of the density-altitude data. The perfect integral of Equation (31) was replaced by a numerical-integration procedure using a semi-logarithmic trapezoidal rule described by Minzner and Sauermann [23]. The resulting temperatures, the original densities, and the Gas Law were then used to calculate the pressure-altitude profile. These data were compiled and published in a separate scientific technical report by Minzner, Morgenstern and Mello [5].

Checking and Editing

The calculated temperatures served as a basis for checking the quality of the density data and for verifying the key-punching accuracy. The computed temperatures were compared with interpolated values of the temperatures of the U.S. Standard Atmosphere [1] and with the originally published temperatures when these were available. The machine listings of the resulting temperature differences were then reviewed noting any large temperature differences or any abrupt change in differences from one level to the next. Such situations result from abnormal increments in the value of $\Delta \ell n \rho/\Delta Z$ versus altitude, and suggested key-punch errors or other difficulties in the basic data cards. The related data cards and the basic data were then checked and corrected when necessary. In at least two instances, this test indicated errors in the basic publication from which our data had been taken. Corrections of the basic data were made in these instances. At least six cases were found where one investigator in each of four different reports in the same year, had smoothed one or more extreme temperature values within a sounding without smoothing the density values which generated them.

TABLE 1

INVENTORY OF ATMOSPHERIC DATA BY SITE

Site Name	Code	Lat.	Long.	LST Hrs.	Number of Soundings
Albuquerque, N. Mexico	AQ	35.05N	106.40W	GMT-07.0	26
Ascension I., Atl. O.	AI	07.98S	014.42W	GMT-00.0	44
Barking Sands, Hawaii	BS	22.05N	159.78W	GMT-10.0	6
Carnarvon, W. Australia	CA	24.82S	113.87E	GMT+08.0	9
Eglin AF Base, Florida	EG	30.38N	086.70W	GMT-06.0	74
Ft. Churchill, Manitoba	FC	58.73N	093.82W	GMT-06.0	49
Guam, Mariana I., Pac. O	GM	13.62N	144.85E	GMT+10.0	7
Heiss I., Franz Jos. L.	HI	80.62N	058.13E	GMT+05.0	25
Holloman AFB, N. Mexico	HA	32.85N	106.10W	GMT-07.0	6
Kapustin Yar, Eur. USSR	KY	48.6 N	045.8 E	GMT+04.0	2
Kwajalein, Marshall I., P.	KW	08.73N	167.73E	GMT+12.0	23
McMurdo Sound, Antarctica	MC	77.88S	166.73E	GMT+11.0	20
Point Mugu, California	PM	34.12N	119.12W	GMT-08.0	3
Ship A, Eq. Pacific Ocean	SA	00.18N	161.42W	GMT-11.0	1
Ship B, N. Atlantic Ocean	SB	62.06N	063.92W	GMT-04.0	1
Ship C, Lancaster SND.	SC	74.57N	094.48W	GMT-05.0	1
Ship D, N. Atlantic Ocean	SD	54.0 N	053.33W	GMT-04.0	2
Ship E, N. Atlantic Ocean	SE	58.43N	055.06W	GMT-04.0	2
Ship F, N. Atlantic Ocean	SF	49.0 N	048.4 W	GMT-03.0	2
Ship G, N. Atlantic Ocean	SG	57.8 N	046.7 W	GMT-03.0	2
Ship H, N. Atlantic Ocean	SH	65.6 N	058. W	GMT-04.0	2
Thule, Greenland	TH	76.55N	068.82W	GMT-04.0	5
Wallops I., Virginia	WI	37.83N	075.48W	GMT-05.0	59
White Sands, New Mexico	WS	32.28N	106.48W	GMT-07.0	25
Woomera S. Australia	WO	31.11S	136.97E	GMT+09.5	41

Some observed density data were shown by this test to have a very erratic behavior, which most likely was not real but which probably represented the uncertainty in some phase of the measurement. Where such erratic observations resulted in density inversions; i.e., density increasing with increasing altitude, the data were either eliminated or smoothed in one of two ways: (1) in a selective smoothing process, individual data points were adjusted to eliminate isolated density inversions, and (2) in a number of other instances where many inversions existed within a sounding, a third order root-mean-square fit was made of the entire sounding. Soundings containing identical densities for two successive levels yielded impossible temperatures at the lowest of these levels, and these cases were eliminated by selective adjustment of density-data pairs. The pressure-altitude profiles, which in some instances were published in the original data source, were universally disregarded in the checking and editing procedures.

Soundings of which the data have been adjusted in one of several ways have been given appropriate code designations in the separate data report. In spite of the very large effort expended in editing the density-altitude data, at least four soundings containing uncorrected density inversions have been found since the publication of this data [5].

Normalizing the Data to Integer Altitudes

The values of density temperature and pressure published in the data report are given for the same altitudes cited in the basic source of the data. In the current statistical study, however, the data for the various soundings must all be normalized to a common set of altitudes. The set chosen is the series of successive integer geometric kilometer altitudes between the greatest and lowest altitude of the sounding. (It has since been determined that integer geopotential kilometer altitudes would have been preferable.) The adjustment of the data to this common set of altitudes were performed by a series of steps, the first of which was a semilogarithmic interpolation of the density-altitude data. The interpolated densities then served as the basis for a calculation of a temperature-altitude profile at the integer altitudes using the same method previously described. This temperature calculation, as in the case of that used for the data report, accounted for the variation of the acceleration of gravity with latitude of the site, as well as with altitude over the site. The temperature calculation also effectively accounted for possible diffusive separation (or change in molecular weight of air) at high altitudes by yielding a result which is commonly called molecular scale temperature [6]. This refinement, accounting for variations in molecular weight, is insignificant for data below 110 or 120 km altitude, but its influence at higher altitudes can be considerable. The molecular scale temperature was then used in the Gas Law equation with the related density values and with the appropriate constants to yield rigorously correct pressures at the integer altitudes.

The corresponding values of density, temperature and pressure at successive integer altitudes for each of 437 soundings, comprises the set of data hereinafter designated as the interpolated data. These data have an internal consistency and homogeneity in basic editing and method of generation which we believe adds considerably to the validity of the statistical results of this study. These data have not been separately published, but exist as a set of 17,000 IBM cards. In addition to the values of the three altitude-dependent parameters, density, temperature, and pressure, each card also contains a number of other pieces of information which are fixed for any particular sounding. This other information includes the following: (1) the date and time of the sounding in Greenwich or universal time, (2) the site of the launching, (3) the solar flux for the day preceeding and for the day of the launching, and (4) three sets of codes designating seasonal groupings, diurnal groupings, and a latitude grouping. The Greenwich time was assigned to each sounding on the basis of local standard time, plus or minus a time-zone correction. The solar flux was taken from the recordings of the 10.7-cm radiation at Ottawa, Canada [24,25]. The seasonal, diurnal and latitudinal codes were assigned in a manner described in the following sections.

STRATIFICATION OF THE DATA

Seasonal, Diurnal and Latitudinal Coding of the Data

The four basic types of seasonal divisions and one special seasonal division are determined and coded. These divisions are based on various numbers of days relative to the vernal equinox as shown in Table 2. They include a 16-season division, an 8-season division, a 4-season division, a 2-season division, and an extreme-season division.

Two kinds of diurnal divisions have been coded; a six-period division and a three-period division. These are based on the following criteria: (1) subsolar angle or zenith angle of the sun during daylight hours, (2) local apparent noon and midnight, and (3) height of earth's shadow during nighttime periods. These divisions are shown in Table 3 and in Figure 1.

Only one kind of latitude-belt division was coded, that shown in Table 4. This division allows for 7 latitude belts in a single hemisphere, each belt being 15 degrees wide with the exception of the tropical and polar belts which are only 7.5 degrees in one hemisphere. Data from a particular latitude belt in the southern hemisphere are combined with data in the corresponding latitude belt in the northern hemisphere after the southern hemisphere data have had a 183-day phase shift applied prior to the seasonal designation. A second type of latitude-belt division was considered. In this one, adjacent pairs of those belts designated in Table 4 would have been combined. Thus belts 0 plus 1, 2 plus 3, and 4 plus 5 form three wider belts. No coding was developed specifically for this division, although some initial calculations were made on the basis of such a division.

Four-Season Stratification of the Data

The four types of seasonal divisions, two types of diurnal divisions and two types of latitudinal division lead to 16 possible types of stratifications of the data in regard to the three variables; season, diurnal period, and latitude band. The system of codes greatly facilitated the process of trying various combinations of divisions and of sorting the data into homogeneous stratifications. Several different sortings were made to study the variation of sample size for different degrees of space and time resolution. For the number of soundings available (437) the maximum usable resolution of the three variables was judged after several trials to be four seasons, three diurnal periods (daytime, nighttime and diurnal transition), and six latitude belts. This leads to 72 possible basic cells. The distribution of maximum sample size (maximum number of soundings per cell) for such resolution is shown in Figure 2.

TABLE 2

DEFINING CONDITIONS OF SEASONAL CODING FOR NON-LEAP YEARS

Date	Day of Year	Days in Season	Sixteen-Season Code	Eight-Season Code	Four-Season Code	Two-Season Code	Extreme-Season Code
Feb 26	57		---	---	---		
		23	16		S		
Mar 21	80		---	7	P		
		23	1		R		
Apr 13	103		---	---	I 1	---	
		23	2		N		
May 06	126		---	0	G		
		23	3			S	
May 29	149		---	---	---	U	
		23	4		S	M	
Jun 21	172		---	1	U	M	---
		23	5		M	E	S
Jul 14	195		---	---	M 2	R 2	U 8
		23	6		E		X
Aug 06	218		---	2	R	H	---
		23	7			A	
Aug 29	241		---	---	---	L	
		23	8		A	F	
Sep 21	264		---	3	U		
		23	9		T		
Oct 14	287		---	---	U 3	---	
		23	10		M		
Nov 06	310		---	4	N		
		22	11			W	
Nov 28	332		---	---	---	I	
		23	12		W	N	
Dec 21	355		---	5	I	T	---
		22	13		N	E	W
Jan 12	12		---	---	T 4	R 1	I 9
		23	14		E		X
Feb 04	35		---	6	R	H	---
		22	15			A	
Feb 26	57		---	---	---	L	
		23	16			F	
Mar 21	80		---	7			
		23	1				
Apr 13	103		---	---		---	

For Southern Hemisphere sites the seasons are inverted by subtracting 183 from the number of the day of the year when that number is equal to or greater than 183, or by adding 183 when that number is less than 183.

For leap years, one day is added to the day of the year for months March through December. Correspondingly no correction is made for the accumulated quarter-day errors in successive members of the remainder of the four year cycle, insofar as the seasonal division is concerned.

Abbreviations: SUX - Summer Extreme, WIX - Winter Extreme,

TABLE 3

DIURNAL CODING AS RELATED TO RANGES OF
LOCAL APPARENT TIME, SUBSOLAR ANGLE, AND SHADOW HEIGHT

Shadow Height	Subsolar Angle	Local Apparent Time	Diurnal Classes 6-Period 6-Class Code	Diurnal Classes 3-Period 3-Class Code
$\geq$ 300 km	> 60 Deg	- - - - - - -	- - - -	2 Nighttime
			6	
- - - - -			- - - -	- - - - - - -
		< 12.00 Hr	1	0 Transition
	- - - - -		- - - -	- - - - - - -
			2	
< 300 km	$\leq$ 60 Deg	- - - - - - -	- - - -	1 Daytime
			3	
	- - - - -		- - - -	- - - - - - -
		$\geq$ 12.00 Hr	4	0 Transition
- - - - -			- - - -	- - - - - - -
			5	
$\geq$ 300 km	> 60 Deg	- - - - - - -	- - - -	2 Nighttime

Midnight is never designated as 24.00 Hours of the just-ending day.
Rather it is designated as 00.00 hours of the just-beginning day.

TABLE 4

LATITUDE CODING

Range of Latitude Increments	Latitude Code	Name of Band of Latitude	Sites Included
Degrees			
0.00 to +07.50	0	Equatorial	SA
0.00 to -07.50	0	Equatorial	
+7.51 to +22.50	1	Tropical	BS,GM,KW
-7.51 to -22.50	1	Tropical	AI
-22.51 to -37.50	2	Subtropical	CA,WO
+22.51 to +37.50	2	Subtropical	AQ,EG,HA,PM,WS
+37.51 to +52.50	3	Midlatitude	KY,SF,WI
-37.51 to -52.50	3	Midlatitude	
+52.51 to +67.50	4	Subarctic	FC,SB,SD,SE,SG,SH
-52.51 to -67.50	4	Subarctic	
+67.51 to +82.50	5	Arctic	HI,SC,TH
-67.51 to -82.50	5	Arctic	MS
+82.51 to +90.00	6	Polar	
-82.51 to -90.00	6	Polar	

Latitudes in the Northern Hemisphere are designated positive.
Latitudes in the Southern Hemisphere are designated negative.

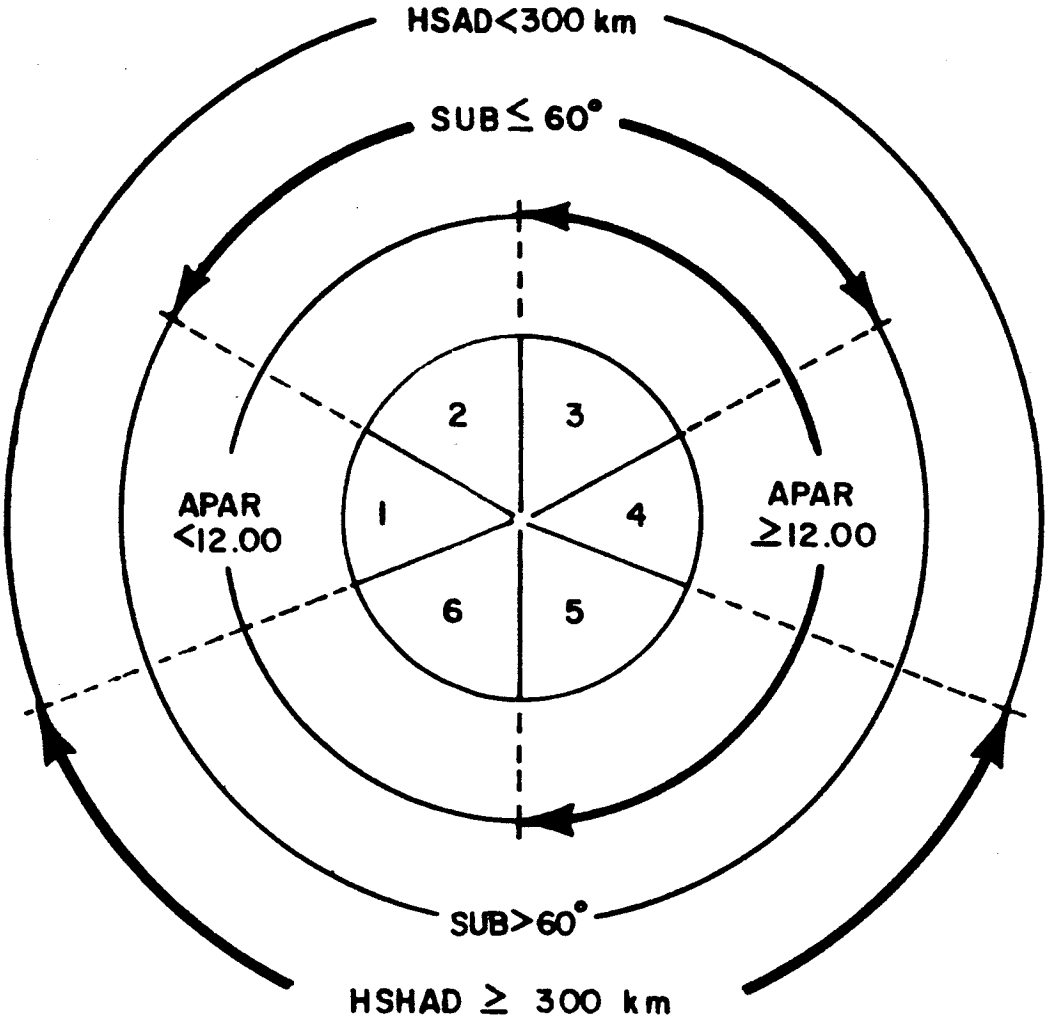

DEFINITIONS OF SYMBOLS AS USED IN THE COMPUTER CODING PROGRAM

SUB	-	sub-solar angle
APAR	-	local apparent time
HSHAD	-	height of earth's shadow
1	-	morning-transition period
2	-	early-day period
3	-	late-day period
4	-	evening-transition period
5	-	early-night period
6	-	late-night period

Figure 1. Definitions of symbols as used in the computer coding program.

	DAY	NIGHT	TRAN	TOTAL
SPRING	-	-	1	1
SUMMER	-	-	-	-
AUTUMN	-	-	-	-
WINTER	-	-	-	-
TOTAL	-	-	1	

EQUATORIAL, BELT 0

	DAY	NIGHT	TRAN	TOTAL
SPRING	13	3	5	21
SUMMER	8	10	2	20
AUTUMN	4	19	6	29
WINTER	6	1	3	10
TOTAL	31	33	16	

TROPICAL, BELT 1

	DAY	NIGHT	TRAN	TOTAL
SPRING	17	6	22	45
SUMMER	12	15	14	41
AUTUMN	9	37	29	75
WINTER	13	2	8	23
TOTAL	51	60	73	

SUBTROPICAL, BELT 2

	DAY	NIGHT	TRAN	TOTAL
SPRING	2	2	10	14
SUMMER	5	3	13	21
AUTUMN	1	3	9	13
WINTER	-	7	8	15
TOTAL	8	15	40	

MIDLATITUDE, BELT 3

	DAY	NIGHT	TRAN	TOTAL
SPRING	1	-	6	7
SUMMER	8	-	8	16
AUTUMN	-	2	14	16
WINTER	-	9	10	19
TOTAL	9	11	38	

SUBARCTIC, BELT 4

	DAY	NIGHT	TRAN	TOTAL
SPRING	1	-	11	12
SUMMER	3	-	14	17
AUTUMN	-	1	7	8
WINTER	-	6	8	14
TOTAL	4	7	40	

ARCTIC, BELT 5

Figure 2. Distribution of soundings into a three-dimensional array of cells distinguishing three diurnal periods, four seasons, and six latitude belts, when the indicated layers are stacked normal to the plane of the paper in ascending order of belt number.

Figure 2 represents a partial disection of a six-layer, three-dimensional array of cells in which each layer is shown as a separate part of the figure. Each layer is associated with a particular latitude belt and represents a two-dimensional array of 12 cells stemming from four seasonal units and three diurnal-period units.

A comparison of statistical results associated with any horizontal row of three cells (left to right in the plane of the paper) should indicate any influence of diurnal variability within a particular season and latitude belt. A comparison of results associated with any column of three cells, top to bottom in the plane of the paper should indicate any influence of seasonal variability within a particular diurnal period and latitude belt. A comparison of results associated with any column of six cells normal to the plane of the paper in the three-dimensional view (i.e., cells of corresponding season and diurnal period, one from each of the six latitude belts) should indicate any influence of latitudinal variability within a particular season or diurnal period.

The numbers within the 72 different cells represent the numbers of soundings (from our data set) which are associated with the particular cells. The most populous latitude belt is the subtropical belt with 184 soundings. This number accounts for over 40 percent of the total sample. The remainder of the data are distributed somewhat uniformly across the other latitude belts, with the exception of the equitorial belt for which there is but a single sounding in our sample.

Figure 2 shows the 184 soundings of latitude belt 2 (in which Patrick Air Force Base is located) to be reasonably well distributed among the four seasons and three diurnal periods. This situation is fortunate since it permits the examination of the associated data for seasonal and diurnal variability which could then be used as a predictor of conditions at Patrick Air Force Base.

Little reliance could be placed upon any atmospheric variability between latitude bands 0 and 1 which might be demonstrated by the data of the single sounding in belt 0 when compared with the data of the 80 soundings in belt 1. Consequently, for this study, the data from the single belt-0 sounding were combined with the data in the corresponding cell of latitude belt 1, thereby eliminating latitude belt 0, and reducing the number of basic cells under consideration to 60. (Therefore all subsequent discussion of Figure 2 will refer to only latitude belts 1 through 5).

The four totals in the right-hand column of each of the two-dimensional arrays of cells in Figure 2 represent the sums of soundings in each of the associated four seasons disregarding diurnal periods. Each of these sums is associated with what we call a compressed cell, wherein the number of soundings is increased at the expense of losing the opportunity of discerning the influence of one of the variables, in

this instance the diurnal period. The stacked three-dimensional array of cells of Figure 2, when viewed from the right, shows a set of 20 first-compression cells in the latitude-season plane as presented in Figure 3. A comparison of statistical results associated with any horizontal row of 4 cells in Figure 3 should indicate any influence of seasonal variability within a given latitude belt, provided it is not masked by the unresolved diurnal variability. Similarly, a comparison of results associated with any vertical column should indicate any influence of a latitudinal variability within a given season, without regard to diurnal period.

The three totals in the bottom row of each of the five latitude sections in Figure 2 represent the sums of the number of soundings in the four seasons for any one diurnal period. These numbers are associated with a set of 15 first-compression cells within which the number of soundings is increased at the expense of losing the seasonal resolution. As viewed from the front of the stacked array of Figure 2, this set of first-compression cells lies in the plane defined by latitude and diurnal periods as shown in Figure 4. A comparison of statistical results associated with any horizontal row of these cells permits the examination of diurnal variability at a fixed latitude, without regard for season. Similarly, a comparison of results of any vertical column of these cells permits the examination of latitudinal variability for a fixed diurnal period, provided that the unresolved seasonal variability does not obscure the results.

The first four totals in the bottom row of the array of Figure 3 represent the totals of the corresponding columns. Each of these numbers is associated with one member of a set of four second-compression cells within which neither diurnal period nor latitude belt is resolved. These cells constitute a one-dimensional array in which only the season is resolved. The first five totals in the right-hand column of the array of Figure 3 are each associated with a corresponding member of a set of five second-compression cells. In this instance, neither the four seasons nor the three-diurnal periods are resolved. Hence, these five cells constitute a one-dimensional array in which latitude belt is the only resolved variable.

Similarly, the three totals in the bottom row of the array of Figure 4 are each associated with corresponding members of a set of three second-compression cells. In this instance, however, it is the four seasons and six latitude belts which are not resolved. Thus, these cells constitute a one-dimensional array in which only diurnal period is resolved.

The number on the lower right-hand corner of the array of Figure 3 is the identical sum of the corresponding column and row. This number is

		WINTER	AUTUMN	SUMMER	SPRING	TOTAL
ARCTIC,	BELT 5	14	8	17	12	51
SUBARCTIC,	BELT 4	19	16	16	7	58
MIDLATITUDE,	BELT 3	15	13	21	14	63
SUBTROPICAL,	BELT 2	23	75	41	45	184
TROPICAL,	BELT 1	10	29	20	22	81
	TOTAL	81	141	115	100	437

Figure 3. Distribution of soundings into four distinct sets of cells — one first-compression set, two different second-compression sets, and one third-compression set — where the four sets of cells distinguish respectively the following seasonal and latitudinal divisions: four seasonal periods and five latitude belts — four seasonal periods only — five latitude belts only, and neither seasonal periods nor latitude belts.

		DAY	NIGHT	TRANS
ARCTIC,	BELT 5	4	7	50
SUBARCTIC,	BELT 4	9	11	38
MIDLATITUDE,	BELT 3	8	15	40
SUBTROPICAL,	BELT 2	51	60	73
TROPICAL,	BELT 1	31	23	17
	TOTAL	103	126	208

Figure 4. Distribution of soundings into two distinct sets of cells — one first-compression set, and one second-compression set — where the two sets of cells distinguish respectively the following diurnal and latitudinal divisions. Three diurnal periods and five latitude belts, and three diurnal periods only.

associated with a single third-compression cell in which none of the three variables, season, diurnal period, or latitude belt is resolved. The number in this cell is, of course, the size of the total sample. The total number of cells defined in the four-season classifications described above is 108.

Extreme-Season Stratification

In addition to the four-season classification scheme shown in Figures 2, 3, and 4, the data were also stratified according to a two extreme-season classification. One of these extreme seasons consists of a summer extreme which is half the length of the previously defined summer season, and covers the 46-day period following the summer solstice. The second extreme season consists of a winter extreme which covers the 46-day period following the winter solstice. These two subsets were designed to aid in the detection of extremes of any statistical model which depends upon the annual heating and cooling cycle.

As in the four-season classification, the sounding data in the summer-extreme and winter-extreme classes were further stratified into three times-of-day periods, and five latitude belts. This stratification leads to 30 basic cells for which the sample sizes are shown in the basic portions of the five layers of the three-dimensional array in Figure 5. Each horizontal row of these basic cells was compressed across diurnal periods yielding first-compression cells with numbers of soundings shown in the columns entitled total in each section of Figure 5. These ten, first-compression, extreme-season cells are shown grouped in the season-latitude plane in Figure 6. Here the results of a second compression, this one across latitude belts, is shown as two cells with sounding numbers given in the totals of Figure 6. Figure 6 bears the same relationship to Figure 5 as Figure 3 bears to Figure 2.

No second-compression, extreme-season cells were obtained by compressing across seasons. This is because the annual mean value so obtained would not be as valid as one obtained from the four, quarter-year periods. There is, therefore, no extreme-season, second-compression diagram comparable to the basic second-compression diagram of Figure 4. There are also no corresponding data cells for analysis.

In the extreme-season category, a total of 12 compressed cells and 30 basic cells yield a sum of 42 extreme-season cells. These cells added to the 60 basic cells and the 48 compressed cells in the four-season category yield a total of 90 basic cells and 60 compressed cells or a grand total of 150 defined data cells.

Sample-Size Distribution Within the Data Cells

A review of the 150 possible data cells shows that a wide range of sample size exists particularly in the 90 basic cells; i.e., 0 to 37

	NIGHT			
	DAY			TOTAL
SUMMER EXTREME	-	3	2	5
WINTER EXTREME	1	1	1	3

TROPICAL, BELT 1

	NIGHT			
	DAY			TOTAL
SUMMER EXTREME	2	8	6	16
WINTER EXTREME	7	1	1	9

SUBTROPICAL, BELT 2

	NIGHT			
	DAY			TOTAL
SUMMER EXTREME	5	1	2	8
WINTER EXTREME	-	2	1	3

MIDLATITUDE, BELT 3

	NIGHT			
	DAY			TOTAL
SUMMER EXTREME	5	-	3	8
WINTER EXTREME	-	2	6	8

SUBARCTIC, BELT 4

	NIGHT			
	DAY			TOTAL
SUMMER EXTREME	3	-	5	8
WINTER EXTREME	-	-	4	4

ARCTIC, BELT 5

Figure 5. Distribution of soundings into a three-dimensional array of cells distinguishing three diurnal periods. Two extreme-season periods, and five latitude belts, when the indicated layers are stacked normal to the plane of the paper in ascending order of the belt number.

		WINTER MEMBER	SUMMER MEMBER
ARCTIC,	BELT 5	4	8
SUBARCTIC,	BELT 4	8	8
MIDLATITUDE,	BELT 3	3	8
SUBTROPICAL,	BELT 2	9	16
TROPICAL,	BELT 1	3	5
	TOTAL	23	33

Figure 6. Distribution of soundings into two distinct sets of cells — one first compression set, and one second-compression set — where the two sets of cells distinguish respectively the following diurnal and latitudinal divisions. Two extreme-season periods and five latitude belts, and two extreme-season periods only.

soundings. Sixteen basic cells contain no soundings from our sample, 14 contain soundings such that there is one and only one data point at any altitude, while 10 additional cells contain soundings such that the greatest concentration of data points at any particular altitude is two. Since our programs made statistical analyses only for sample sizes of 3 or more, no computations were made for 40 of the basic cells. Hence, results exist for only 110 data cells.

There are at least four general factors which contribute to the disproportionate distribution of the sample size; these factors involve geographical, sociological, psycological and astronomical considerations. Of these, only the latter can be specifically defined, but some subjective comments appear to be applicable to the others. The more remote areas, and hence the subarctic and arctic belts, have fewer soundings merely because of the logistical problems involved. The first half of the winter-extreme period between December 21 and mid-January have very few soundings in any latitude belt largely because of the holidays. Arctic and subarctic regions are most uncomfortable during the winter, and field parties tend to avoid discomfort by avoiding extreme conditions. These reasons are largely responsible for the fact that only 37 percent of all extreme-season soundings occurred during the winter-extreme period.

In retrospect it is apparent that defined astronomical conditions for day and night divisions in our study are responsible for a large amount of the disproportionate distribution of sample size, particularly in latitude belts 4 and 5, although these reasons also apply to a lesser degree to latitude belt 3. Our definition of daytime required the local elevation angle of the sun to be greater than 30 degrees. It may be demonstrated, therefore, that no winter or winter-extreme daytime conditions are possible in latitude belts 4 and 5 and that only a few hours of such daytime conditions exist in latitude belt 3. In particular, on the day of the winter solstice no such daytime conditions exist at latitudes greater than 36.56° and even at the summer solstice, the northern boundary of the arctic belt is just within the latitude which satisfies the condition. Similarly, autumn daytime conditions are almost non-existent in the arctic belt with the total number of daytime hours per autumn season gradually increasing as the latitude decreases.

Our definition of nighttime required an earth's shadow height of 300 km. It may be shown that this condition is met at local midnight when the sum of the latitude and the declination angle is equal to or less than 71.43 degrees (atmospheric refraction being considered). Taking the value of the sun's declination angle for those dates which serve as boundaries to the several seasons as defined by us, one may readily estimate the periods when no nighttime conditions exists at the various latitudes. One sees that there is no summer night in the arctic and almost none in the subarctic. Even at the more northerly portions of latitude belt 3, summer nighttime as defined by us does not exist for some

days around the summer solstice. Spring and autumn nighttimes are severely curtailed in the arctic and partly curtailed in the subarctic and mid-latitudes by our definition.

High-Resolution Stratifications

A finer resolution of the three variables, season, diurnal period and latitude was also considered during the early part of this study. This resolution involved eight seasons, six diurnal periods and five latitude bands. It leads consequently to a total of 240 basic cells without considering any compression cells. The basic three-dimensional array of cells for this resolution, with the number of sounding of our basic data in each cell is given in Figure 7. The many cells in such an array which have fewer than three soundings make it obvious that our basic data set is too small for such resolution.

Special Stratifications

In addition to the uniform sequency of data stratifications described above, several special data groupings were used. The objective here was to obtain increased sample sizes by selectively grouping some of the higher resolution cells. The three special stratifications were:

(1) Division of the annual cycle into winter half and summer half seasons (see Table 2). This grouping was made only for the data in the tropical and arctic latitude belts.

(2) All data from the subtropical and mid-latitude belts were combined into a single 30^{o} latitude belt class.

EQUATORIAL, BELT 0

SEASON	DIURNAL PERIODS 1	2	3	4	5	6	TOTAL
0				1			1
S 1							
E 2							
A 3							
S 4							
O 5							
N 6							
S 7							
TOTAL				1			1

TROPICAL, BELT 1

SEASON	DIURNAL PERIODS 1	2	3	4	5	6	TOTAL
0			5	1	3		9
S 1			8	2	3	2	15
E 2						5	5
A 3	1			3	2	1	7
S 4			4	2	7	9	22
O 5			2			1	3
N 6	3	1	3				7
S 7	2		8	2			12
TOTAL	6	1	30	10	15	18	80

SUBTROPICAL, BELT 2

SEASON	DIURNAL PERIODS 1	2	3	4	5	6	TOTAL
0	4	2	11	12	3	3	35
S 1	3	2	2	4	6	1	18
E 2	6	4	4	1	4	4	23
A 3	1	2	5	12	19	3	42
S 4	4	2		12	8	7	33
O 5	1		3	4	1		9
N 6		4	6	3	1		14
S 7	3	1	3	3			10
TOTAL	22	17	34	51	42	18	184

MIDLATITUDE, BELT 3

SEASON	DIURNAL PERIODS 1	2	3	4	5	6	TOTAL
0	1	1	1	2	1		6
S 1	1		4	8	1		14
E 2	1	1		3	2		7
A 3				1		1	2
S 4	1		1	7	1	1	11
O 5	3			2		1	6
N 6	1			2	6		9
S 7	2			5	1		8
TOTAL	10	2	6	30	12	3	63

SUBARCTIC, BELT 4

SEASON	DIURNAL PERIODS 1	2	3	4	5	6	TOTAL
0				1			1
S 1							
E 2	1	1	7	7			16
A 3				1			1
S 4	5			8	1	1	15
O 5				1	2	1	4
N 6				9	4	2	15
S 7		1		5			6
TOTAL	6	2	7	32	7	4	58

ARCTIC, BELT 5

SEASON	DIURNAL PERIODS 1	2	3	4	5	6	TOTAL
0	2		1				3
S 1	1		2	2			5
E 2	4		1	7			12
A 3	1						1
S 4	4			2	1		7
O 5				3	1	3	7
N 6	2			3		2	7
S 7	3			6			9
TOTAL	17		4	23	2	5	51

Figure 7. Distribution of soundings according to six diurnal periods, eight seasons, and six latitude belts.

REFERENCES

1. U.S. Standard Atmosphere, 1962, National Aeronautics and Space Administration, U.S. Air Force and U.S. Weather Bureau, Government Printing Office, Washington, D.C.

2. Minzner, R.A., and S. Mello, Range and Structure of Ambient Density from 0 to 120 Km Altitude, GCA-TR-67-16-N, GCA Corporation, Bedford, Mass.(1967) (In preparation).

3. Buell, C.E., Some Relations Among Atmospheric Statistics, J. Meteor., 11(6), 238-244 (June, 1954).

4. Buell, C.E., Statistical Relations in a Perfect Gas Atmosphere, Kaman Aircraft Corp., Colorado Springs, Colorado, Internal Report (March 1965).

5. Minzner, R.A., P. Morgenstern, and S. Mello, Tabulations of Atmospheric Density, Temperature and Pressure from 437 Rocket and Optical-Probe Soundings During the Period 1947 to Early 1965, GCA Corp., Bedford, Mass., GCA-TR-67-10-N, Contracts NASW-1463 and NASW-1225.

6. Minzner, R.A., and W.S. Ripley, The ARDC Model Atmosphere, 1956. Air Force Surveys in Geophysics No. 86, AFCRC IN-56-204 (Dec. 1956).

7. Minzner, R.A., W.S. Ripley, and T.P. Condron, U.S. Extension to the ICAO Standard Atmosphere, U.S. Government Printing Office, Washington, D.C. (1958).

8. Minzner, R.A., K.S. Champion, and H.L. Pond, The ARDC Model Atmosphere 1959, Air Force Surveys in Geophysics, No. 115, AFCRC-TR-59-267 (1959).

9. Smith, O.E., A Reference Atmosphere for Patrick Air Force Base, Florida, (Ann.) NASA -TN-D-595 (July 1960).

10. Smith, O.E., and D.K. Weidner, A Reference Atmosphere for Patrick Air Force Base, Florida Annual (1963 Rev.), NASA-TM X-53139 (Sept. 1964).

11. Court, A., A.J. Kantor, and A.E. Cole, Supplemental Atmospheres, Research Note AFCRL-62-899, (Sept. 1962).

12. Cole, A.E. and A.J. Kantor, Air Force Interim Supplemental Atmospheres to 90 Km., Air Force Surveys in Geophysics, No. 153, AFCRL-63-936 (Dec. 1963).

13. Minzner, R.A., and P. Morgenstern, (1968a) (In preparation).

14. Stidd, C.K., A Note on the Application of the Hydrostatic Equation to Atmospheric Statistics. J. Meteor., 11(4), 165-166 (April 1954).

REFERENCES (Cont.)

15. Scarborough, J.B., Numerical Mathematical Analysis, 2nd Edition, John Hopkins Press, Baltimore, Md. (1950).

16. Minzner, R.A., and P. Morgenstern,(1968b), (In preparation).

17. Minzner, R A., G.O. Sauermann, and G.A Faucher, Low Mesopause Temperatures over Eglin Test Range Deduced from Density Data, GCA Tech. Rpt. 65-1-N, Contract NASW-976 (1965). Also J. Geophys. Res., 70(3), 739-742 (1965).

18. Diehl, W.S, Standard Atmosphere Tables and Data, NACA Report 218 (October 1925, Reprinted 1948).

19. Minzner, R A., Pressure and Density Scale Heights Defining Atmospheric Models, GCA Tech. Rpt. 64-6-A, AFCRL 64-450, Sci. Rpt. 5, Contract AF19(628)-1633 (April 1964).

20. Minzner, R.A., Critical Examination of Equations for Atmospheric Number-Density Calculations - Computed Values Compared with Observations. GCA Tech. Rpt. 65-27-N, Contract NASW-1225, (1965)(Submitted to J. Geo. Res.).

21. Nicolet, M., Density of the Heterosphere Related to Temperature. Smithsonian Astrophys. Obs. Spec. Rpt. 75, 30pp., Republished in Smithsonian Contributions to Astrophysics, Vol. 6, 175-187.

22. Meteorological Rocket Network Committee, Editors, 1962-1966, Data Report of the Meteorological Rocket Network Firings Document 109-62.

23. Minzner, R.A., and G.O. Sauermann, Temperature Determination of Planetary Atmospheres - Optimum Boundary Conditions for Both Low and High Solar Activity - Equation Analysis and Error Analysis, GCA Tech. Rpt. 66-6-N, Contract NASW-1225.

24. Smith, R.S., Private communication (Sept. 1965).

25. Smithsonian Astrophys. Observatory, Listing of 10.7 cm Solar Flux.

APPENDIX A

STATISTICAL GAS LAW GRAPHS

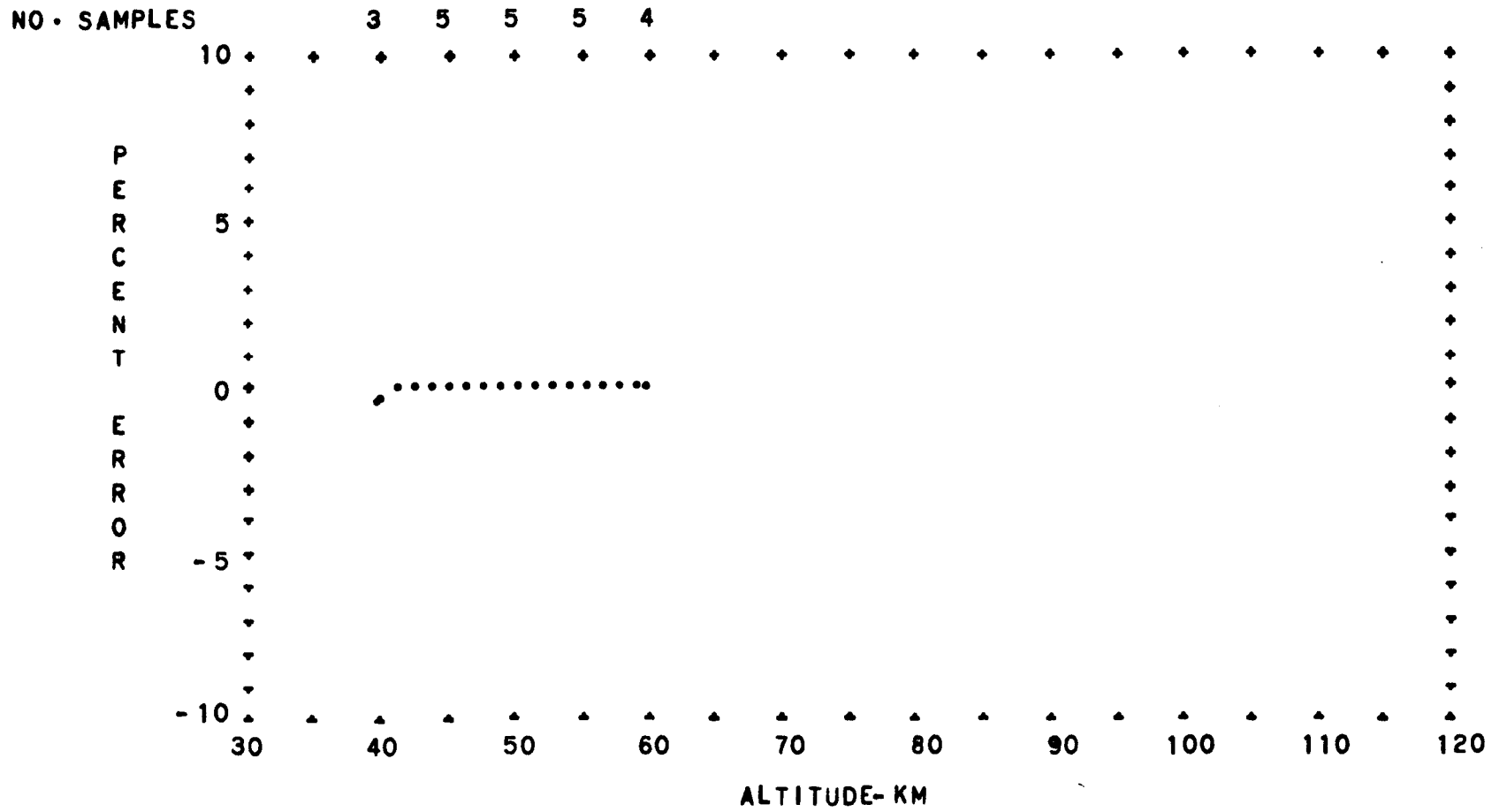

FIG. A-1 PERCENT CONTRIBUTION OF THE COVARIANCE TO THE MEAN PRESSURE OF THE BUELL GAS LAW EQUATION AS A FUNCTION OF ALTITUDE

TROPICAL SPRING DIURNAL TRANSITION

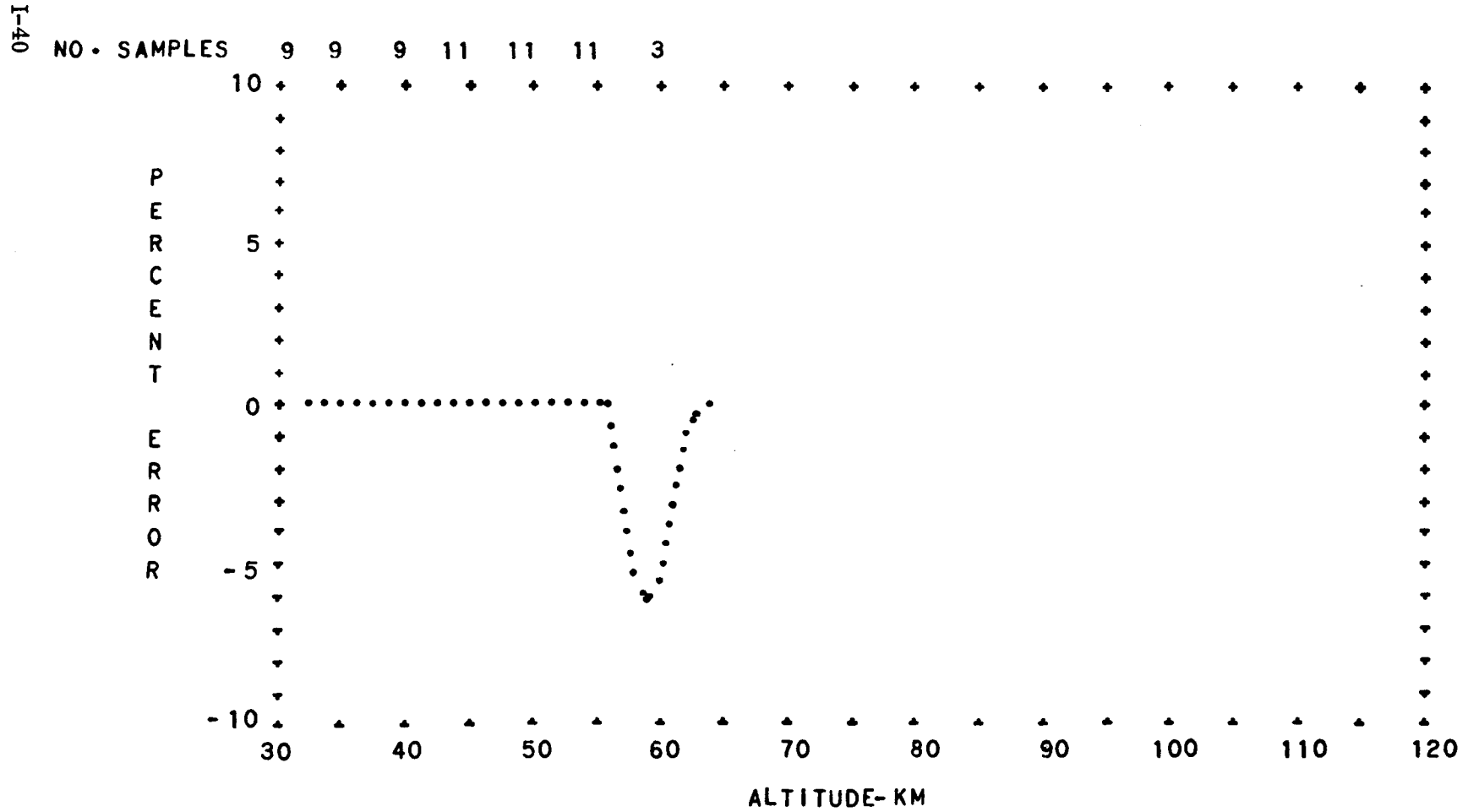

FIG. A-2 PERCENT CONTRIBUTION OF THE COVARIANCE TO THE MEAN PRESSURE OF THE BUELL GAS LAW EQUATION AS A FUNCTION OF ALTITUDE

TROPICAL SPRING DAYTIME

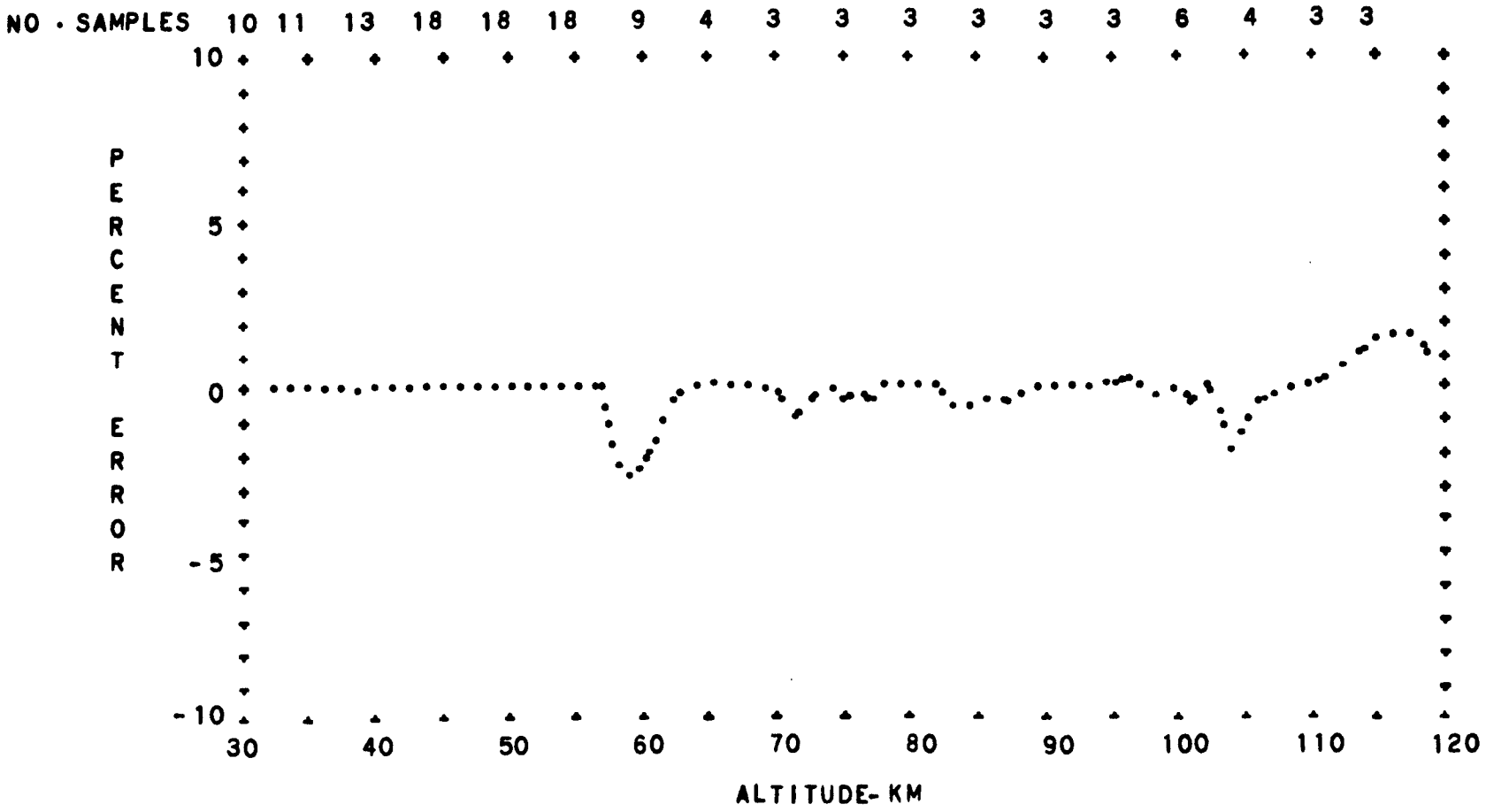

FIG. A-3 PERCENT CONTRIBUTION OF THE COVARIANCE TO THE MEAN PRESSURE OF THE BUELL GAS LAW EQUATION AS A FUNCTION OF ALTITUDE

TROPICAL SPRING DIURNAL MEAN

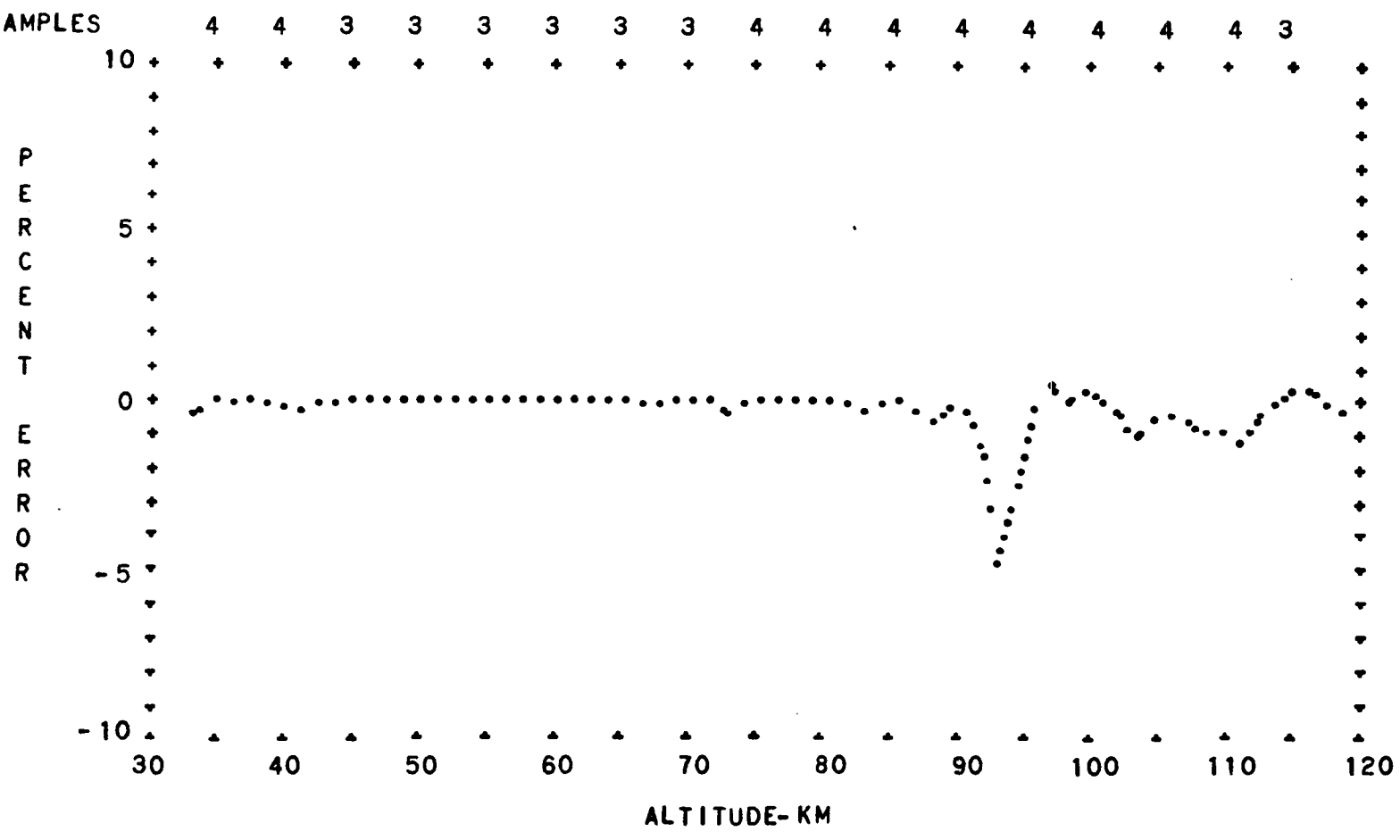

FIG. A-4 PERCENT CONTRIBUTION OF THE COVARIANCE TO THE MEAN PRESSURE OF THE BUELL GAS LAW EQUATION AS A FUNCTION OF ALTITUDE

TROPICAL SUMMER DAYTIME

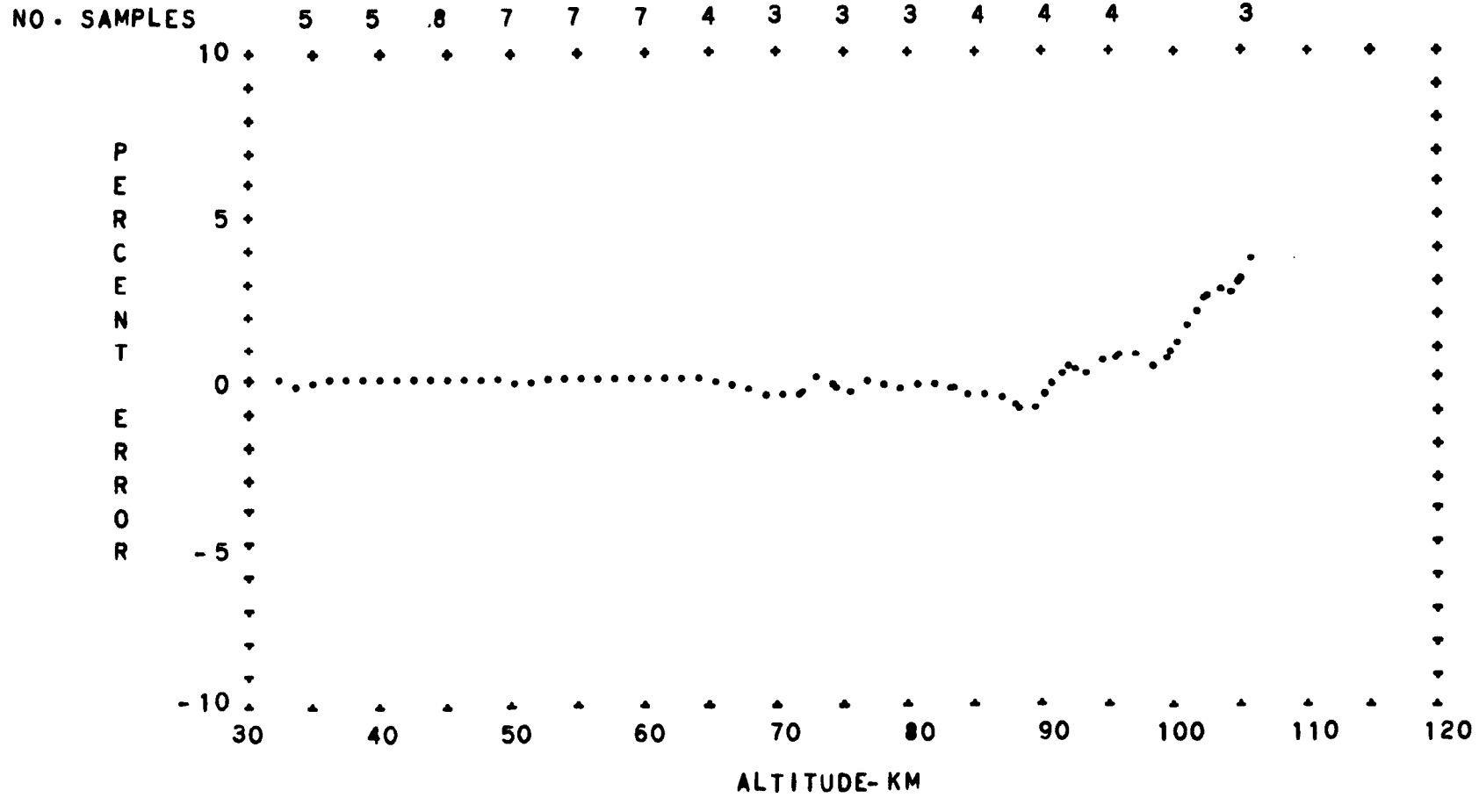

FIG. A-5 PERCENT CONTRIBUTION OF THE COVARIANCE TO THE MEAN PRESSURE OF THE BUELL GAS LAW EQUATION AS A FUNCTION OF ALTITUDE

TROPICAL SUMMER NIGHTTIME

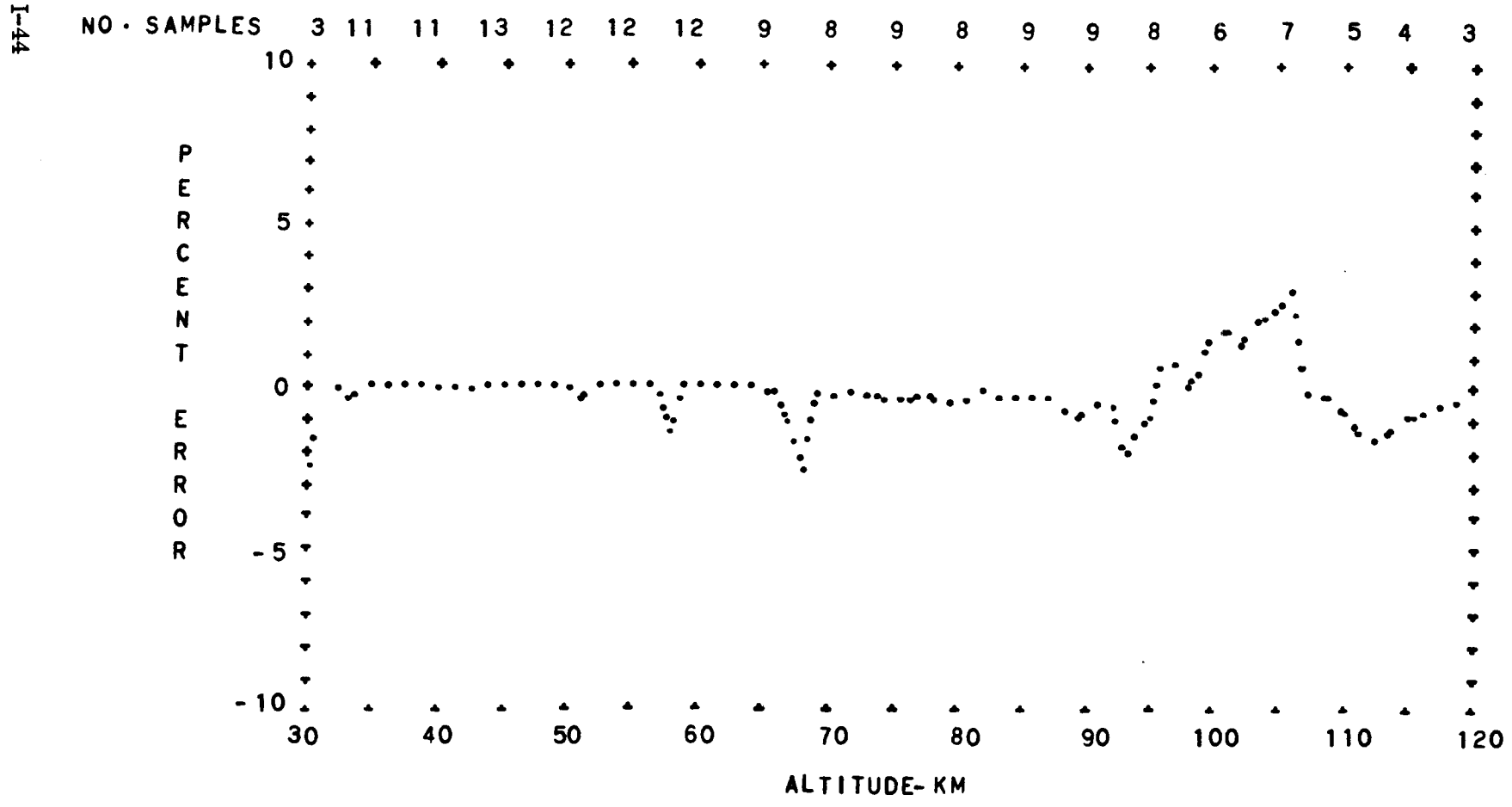

FIG. A-6 PERCENT CONTRIBUTION OF THE COVARIANCE TO THE MEAN PRESSURE OF THE BUELL GAS LAW EQUATION AS A FUNCTION OF ALTITUDE

TROPICAL SUMMER DIURNAL MEAN

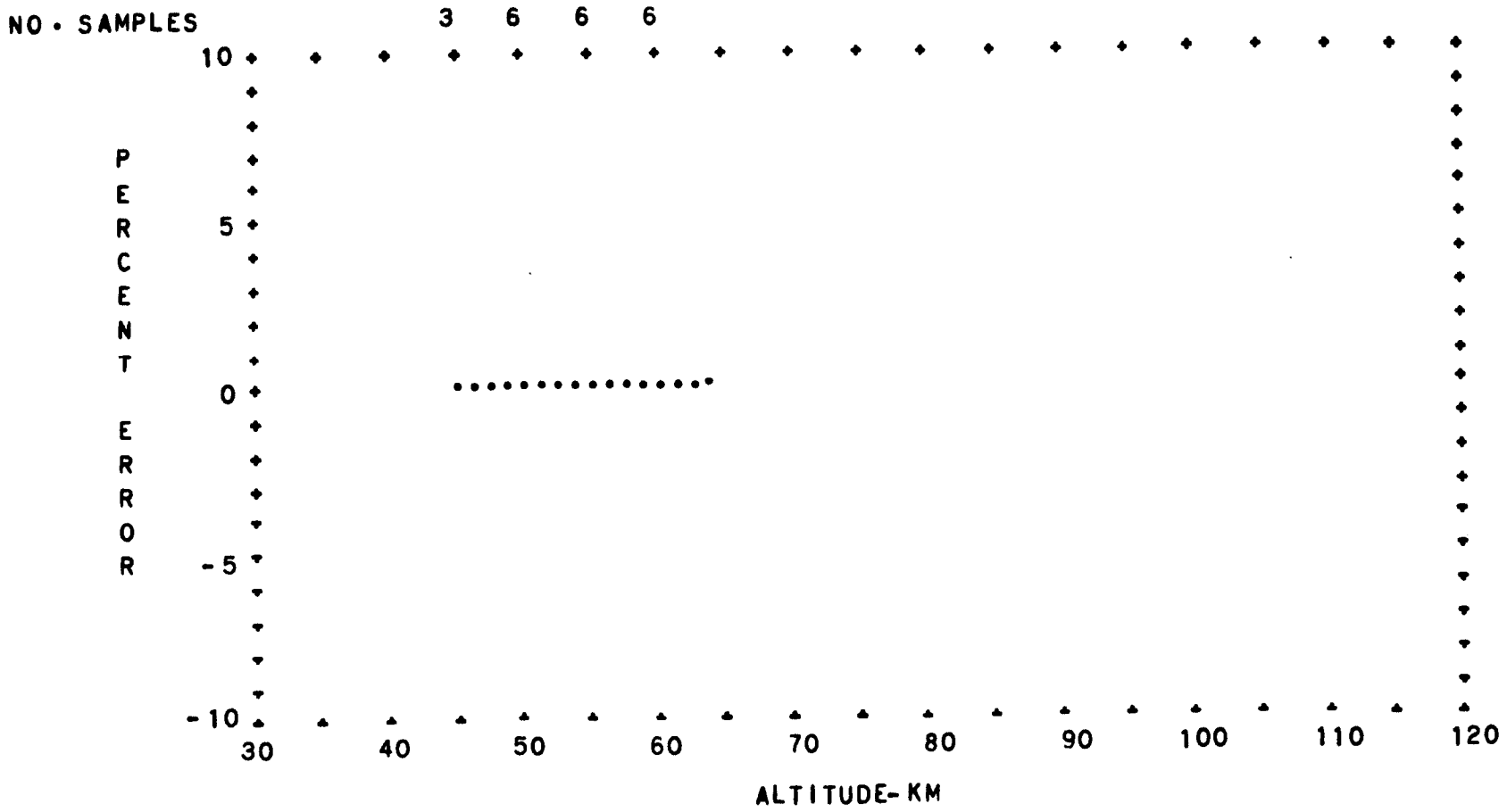

FIG. A-7 PERCENT CONTRIBUTION OF THE COVARIANCE TO THE MEAN PRESSURE OF THE BUELL GAS LAW EQUATION AS A FUNCTION OF ALTITUDE

TROPICAL AUTUMN DIURNAL TRANSITION

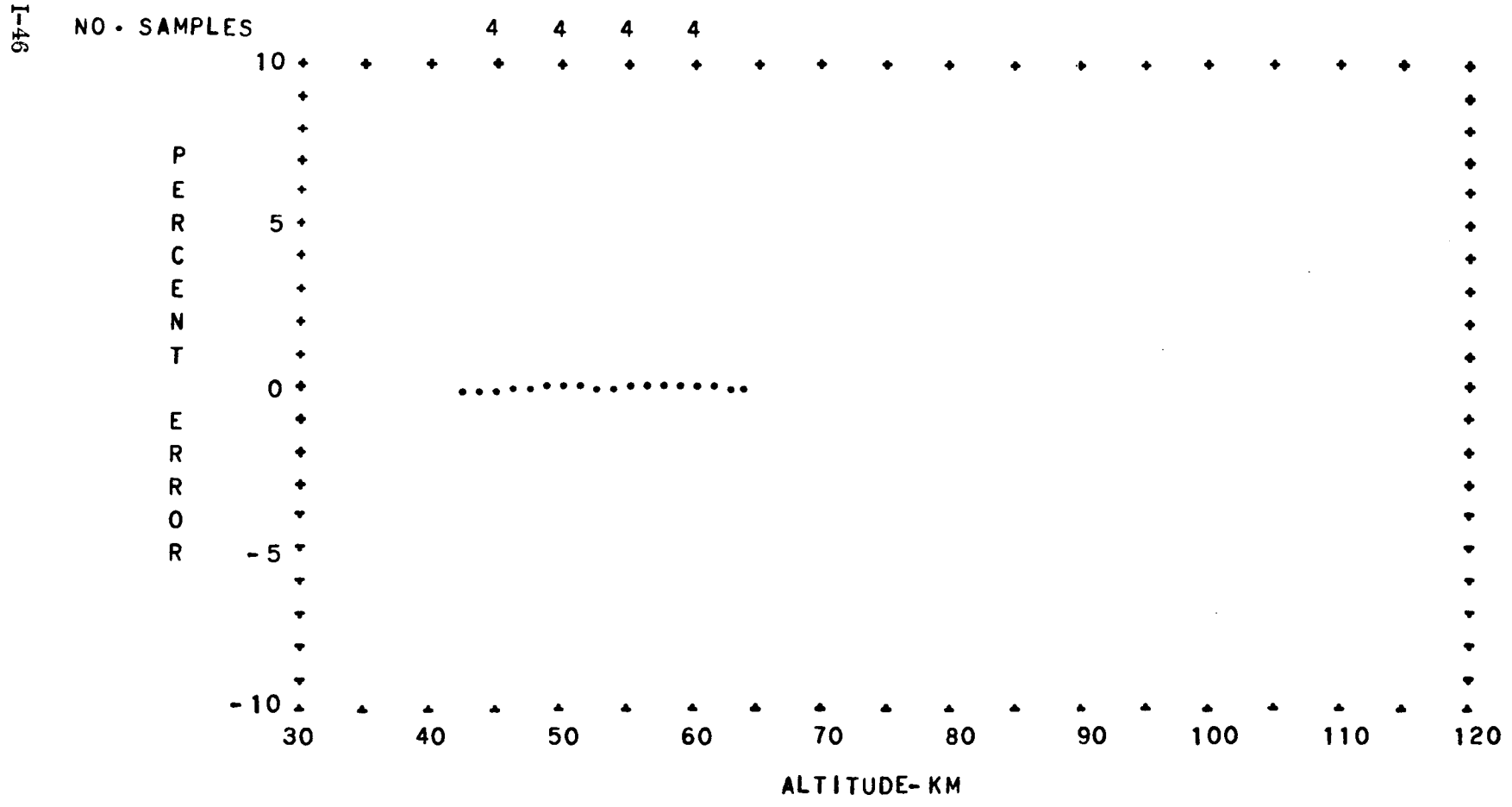

FIG. A-8 PERCENT CONTRIBUTION OF THE COVARIANCE TO THE MEAN PRESSURE OF THE BUELL GAS LAW EQUATION AS A FUNCTION OF ALTITUDE

TROPICAL AUTUMN DAYTIME

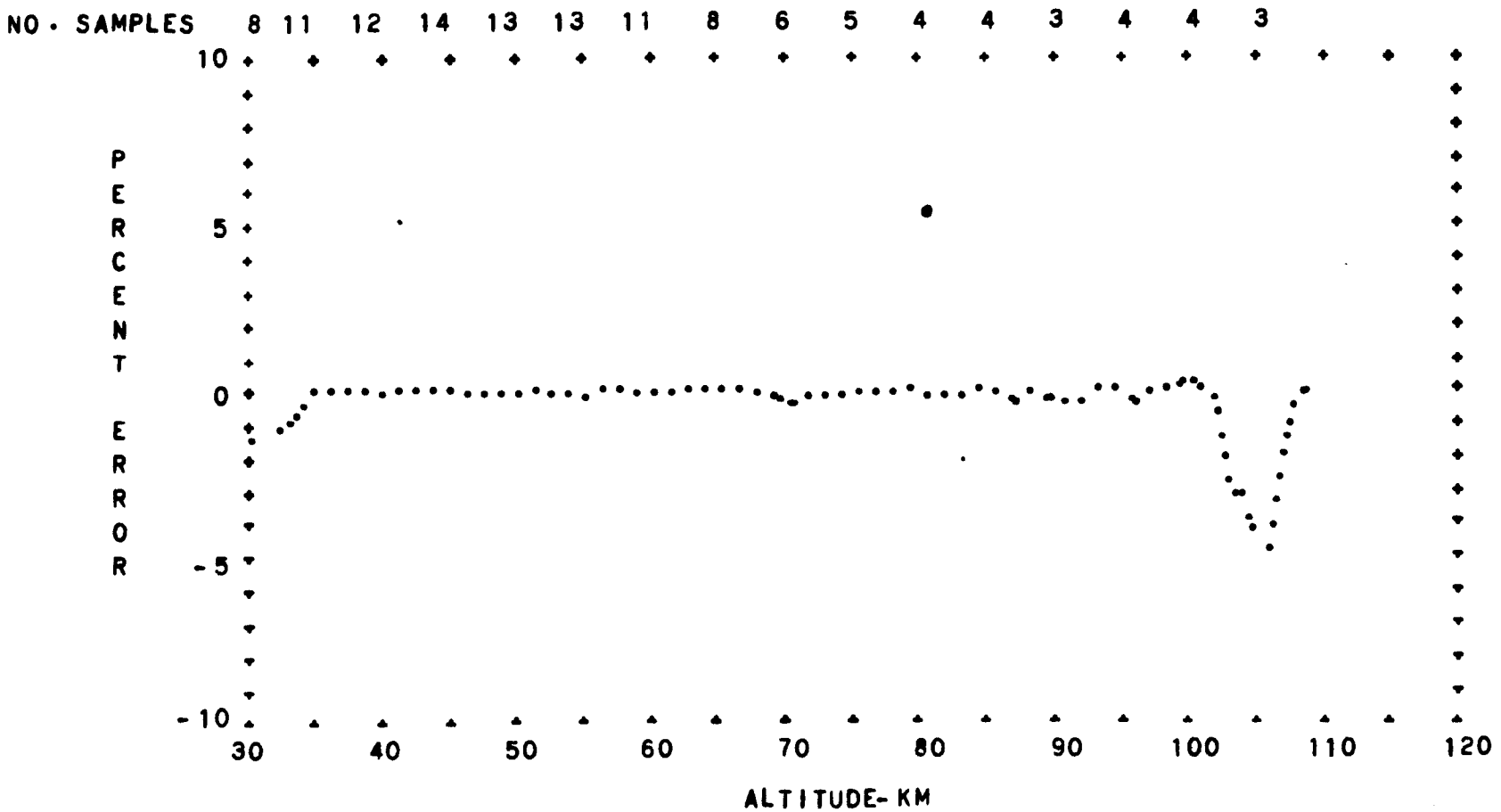

FIG. A-9 PERCENT CONTRIBUTION OF THE COVARIANCE TO THE MEAN PRESSURE OF THE BUELL GAS LAW EQUATION AS A FUNCTION OF ALTITUDE

TROPICAL AUTUMN NIGHTTIME

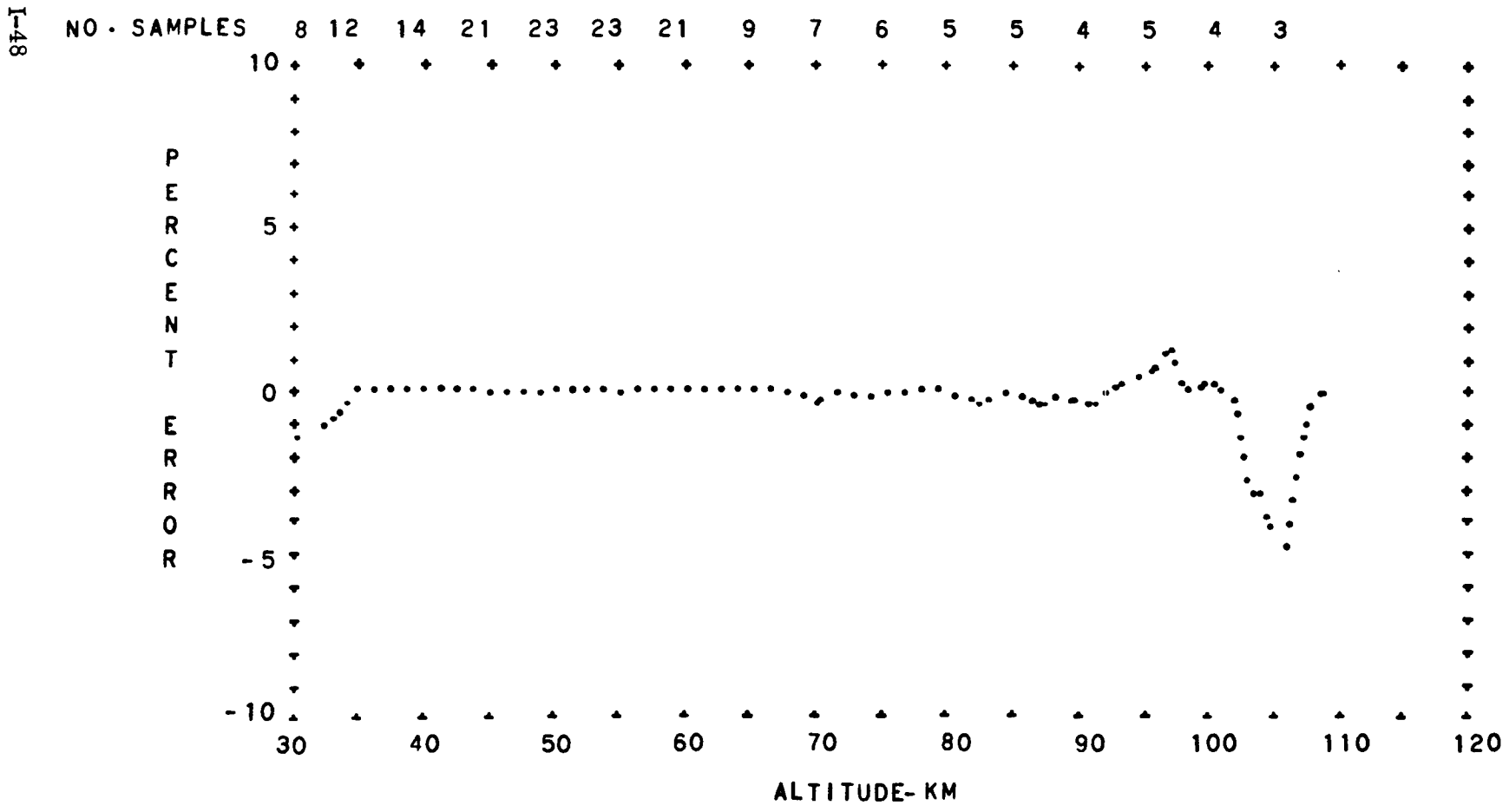

FIG. A-10 PERCENT CONTRIBUTION OF THE COVARIANCE TO THE MEAN PRESSURE OF THE BUELL GAS LAW EQUATION AS A FUNCTION OF ALTITUDE

TROPICAL AUTUMN DIURNAL MEAN

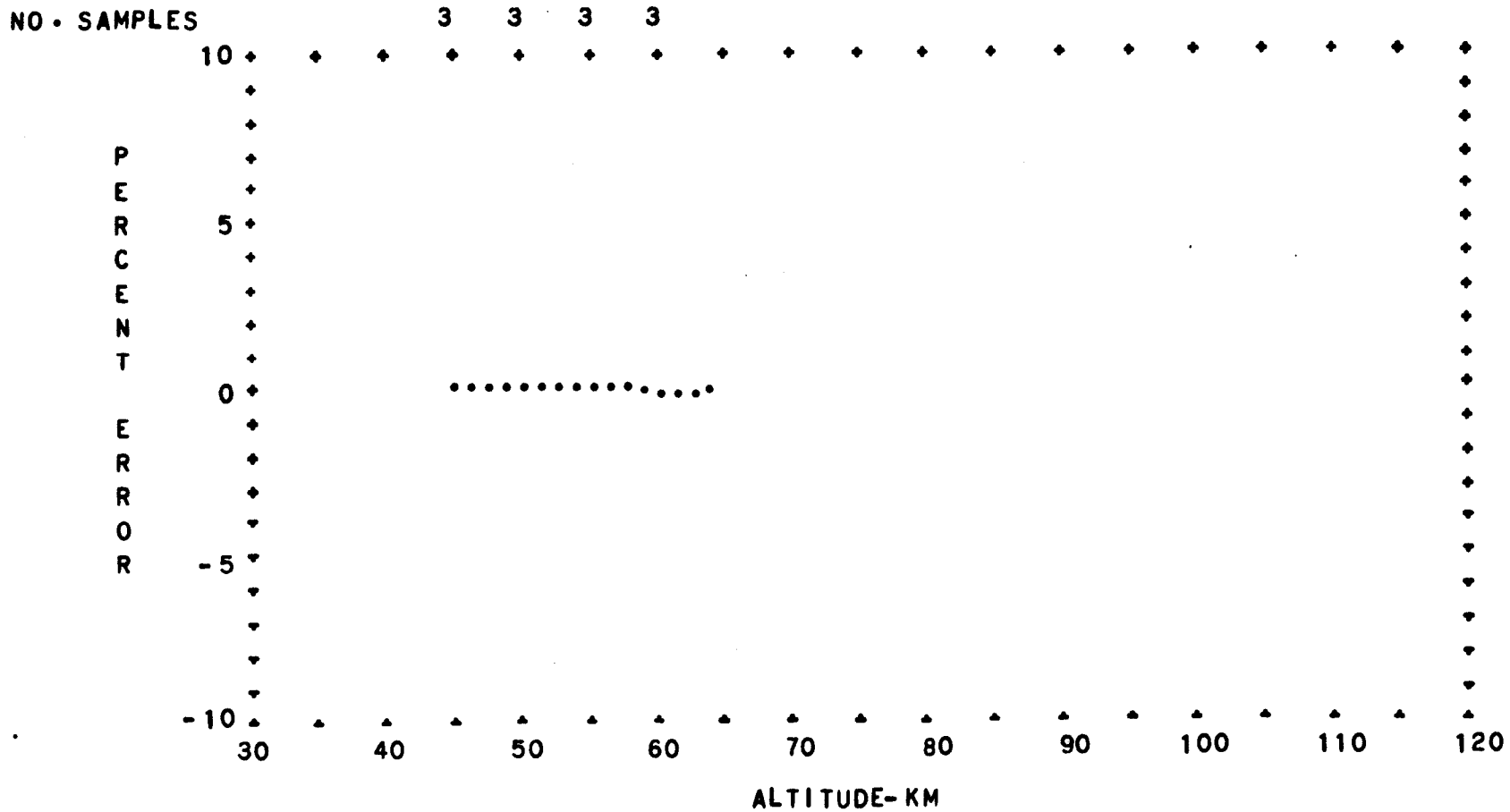

FIG. A-11 PERCENT CONTRIBUTION OF THE COVARIANCE TO THE MEAN PRESSURE OF THE BUELL GAS LAW EQUATION AS A FUNCTION OF ALTITUDE TROPICAL WINTER DIURNAL TRANSITION

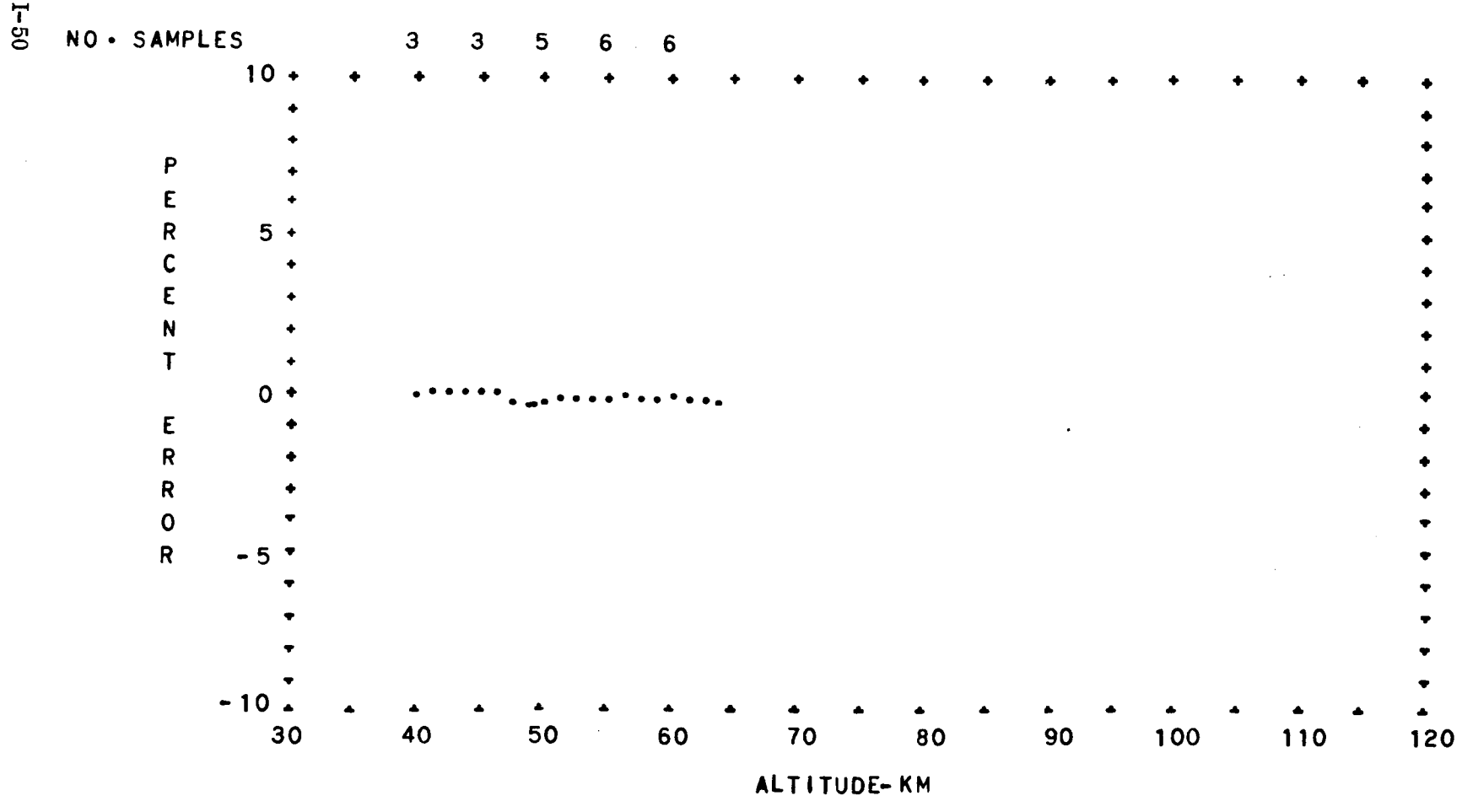

FIG. A-12 PERCENT CONTRIBUTION OF THE COVARIANCE TO THE MEAN PRESSURE OF THE BUELL GAS LAW EQUATION AS A FUNCTION OF ALTITUDE

TROPICAL WINTER DAYTIME

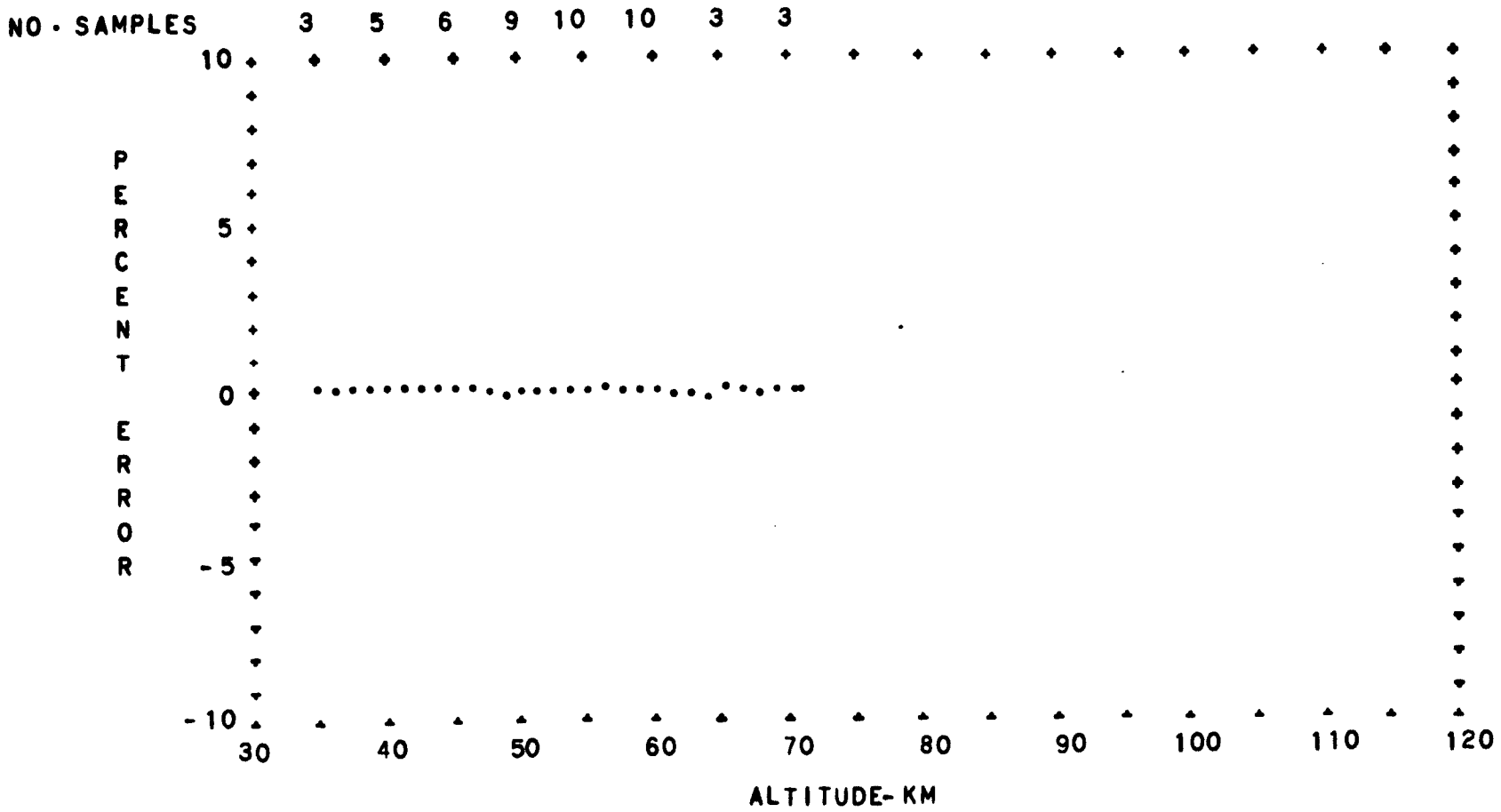

FIG. A-13 PERCENT CONTRIBUTION OF THE COVARIANCE TO THE MEAN PRESSURE OF THE BUELL GAS LAW EQUATION AS A FUNCTION OF ALTITUDE

TROPICAL WINTER DIURNAL MEAN

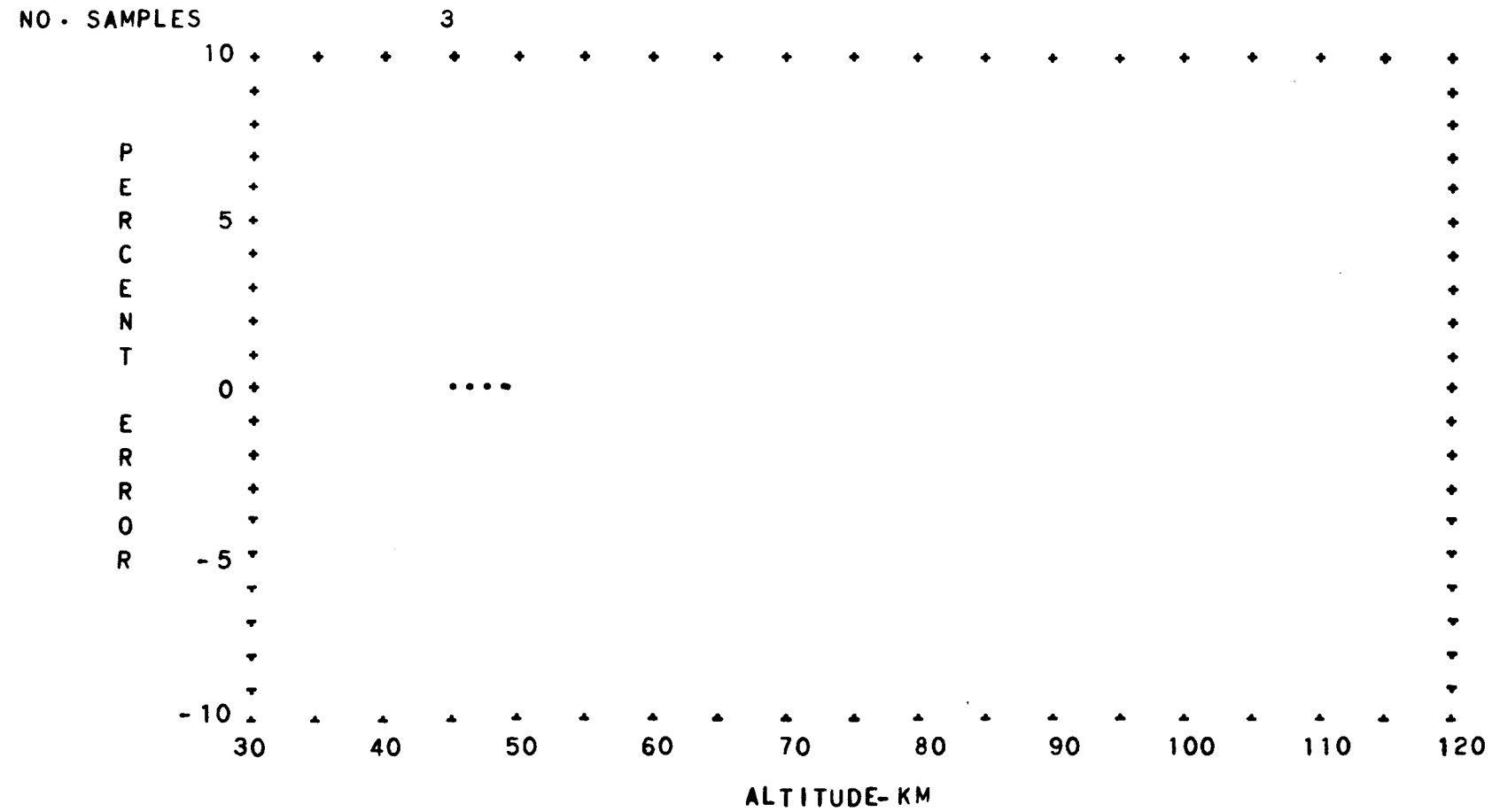

FIG. A-14 PERCENT CONTRIBUTION OF THE COVARIANCE TO THE MEAN PRESSURE OF THE BUELL GAS LAW EQUATION AS A FUNCTION OF ALTITUDE

TROPICAL SUMMER EXTREME NIGHTTIME

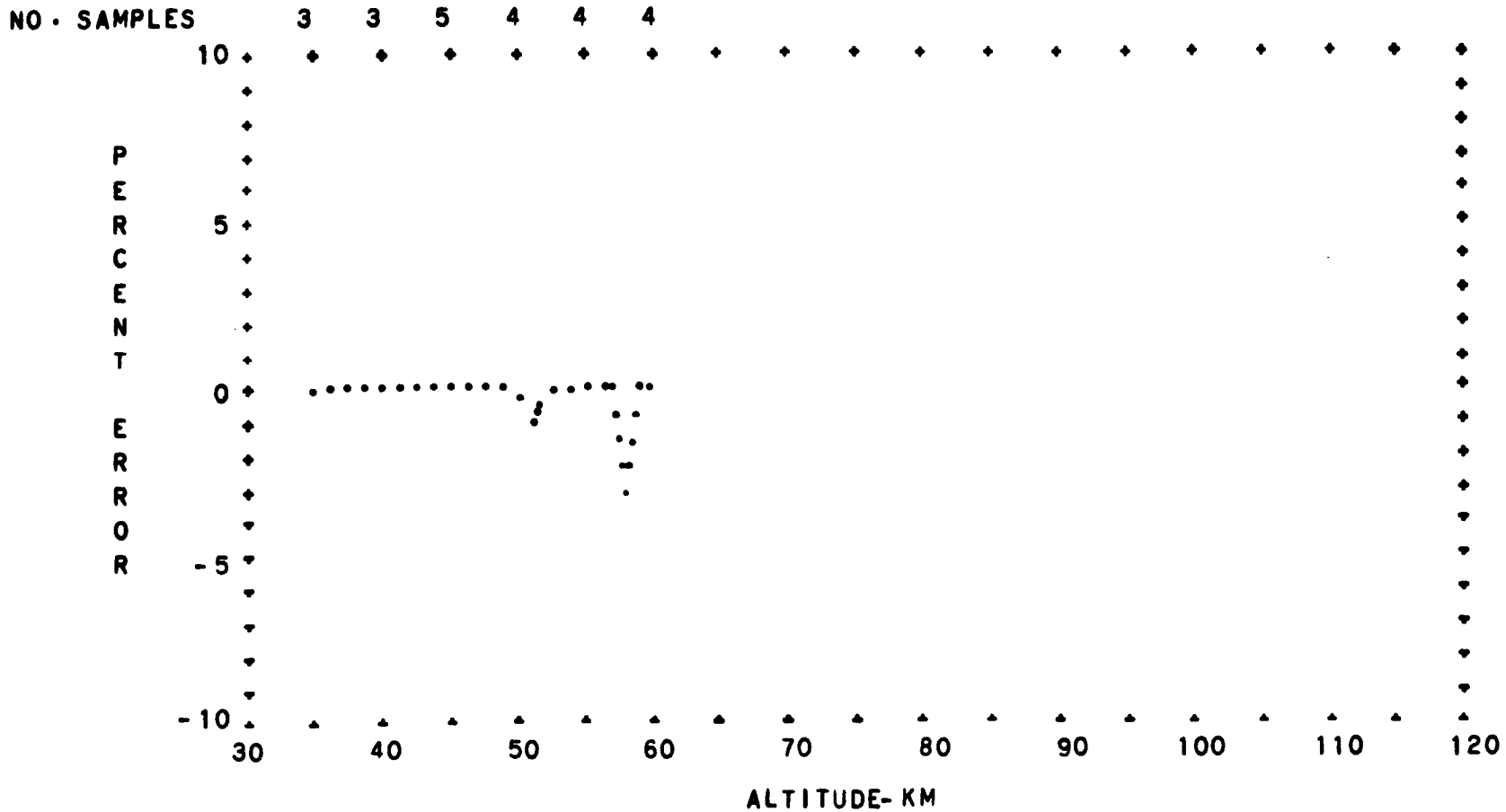

FIG. A-15 PERCENT CONTRIBUTION OF THE COVARIANCE TO THE MEAN PRESSURE OF THE BUELL GAS LAW EQUATION AS A FUNCTION OF ALTITUDE

TROPICAL SUMMER EXTREME DIURNAL MEAN

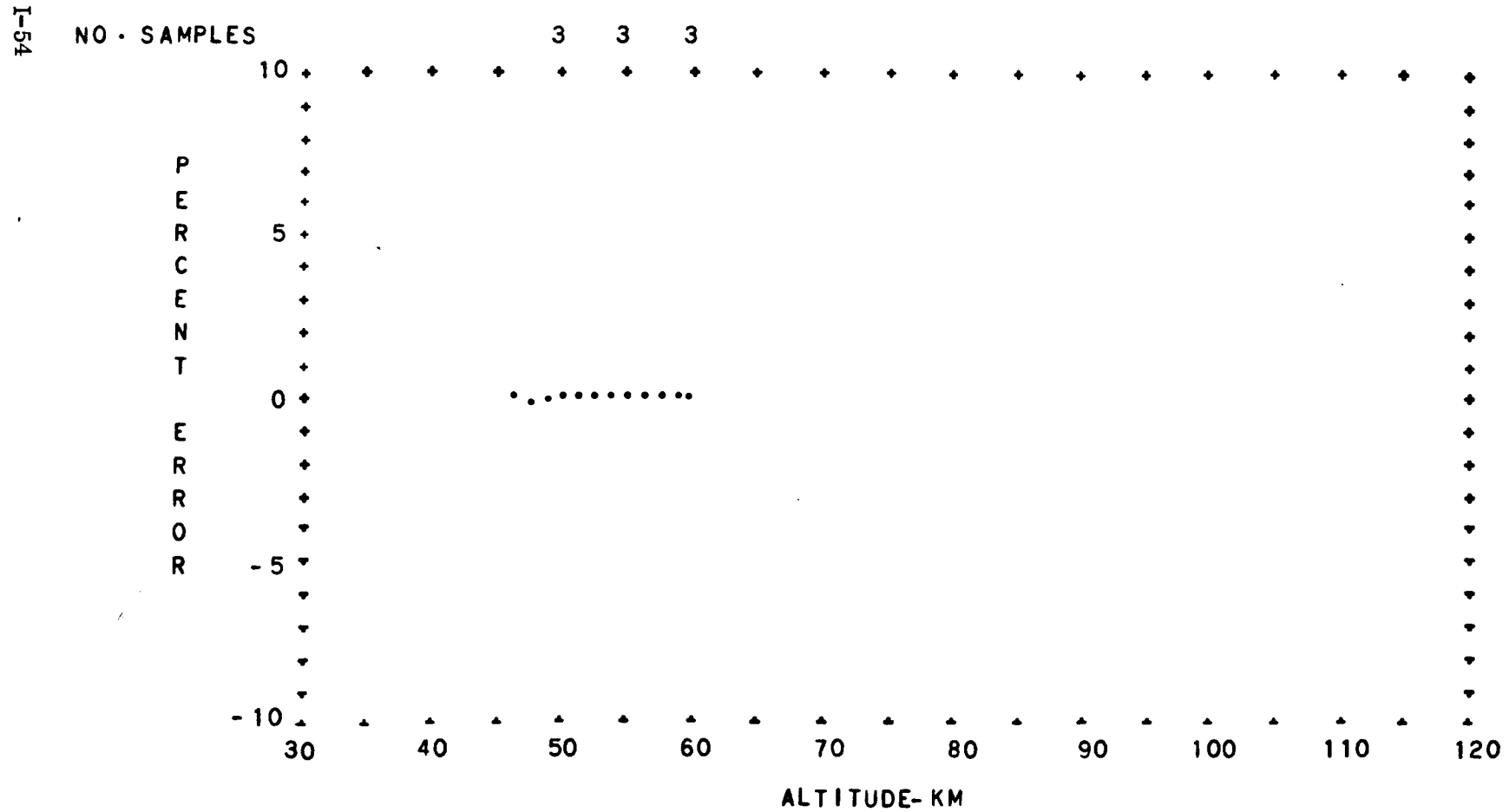

FIG. A-16 PERCENT CONTRIBUTION OF THE COVARIANCE TO THE MEAN PRESSURE OF THE BUELL GAS LAW EQUATION AS A FUNCTION OF ALTITUDE

TROPICAL WINTER EXTREME DIURNAL MEAN

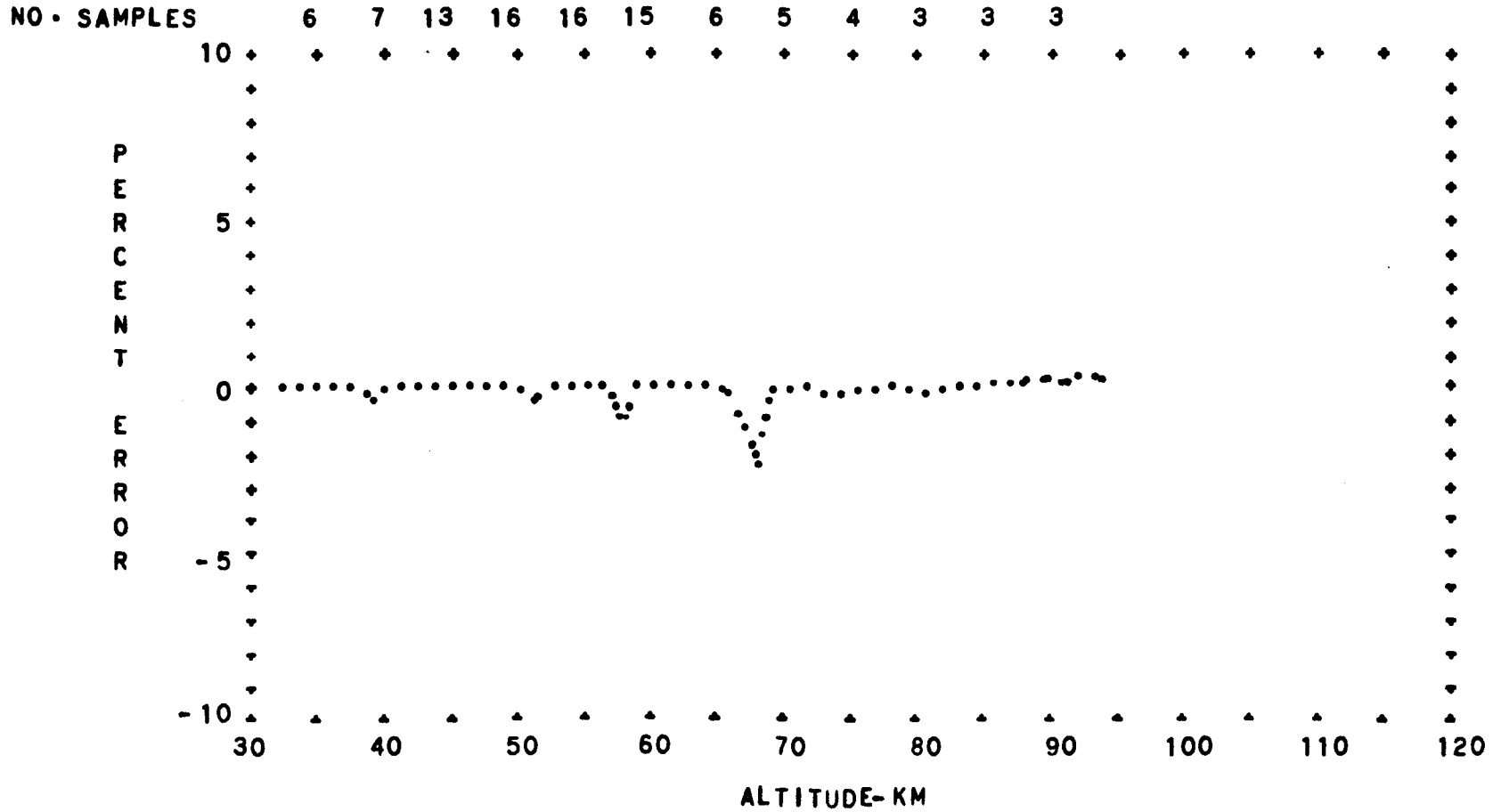

FIG. A-17 PERCENT CONTRIBUTION OF THE COVARIANCE TO THE MEAN PRESSURE OF THE BUELL GAS LAW EQUATION AS A FUNCTION OF ALTITUDE

TROPICAL ANNUAL MEAN DIURNAL TRANSITION

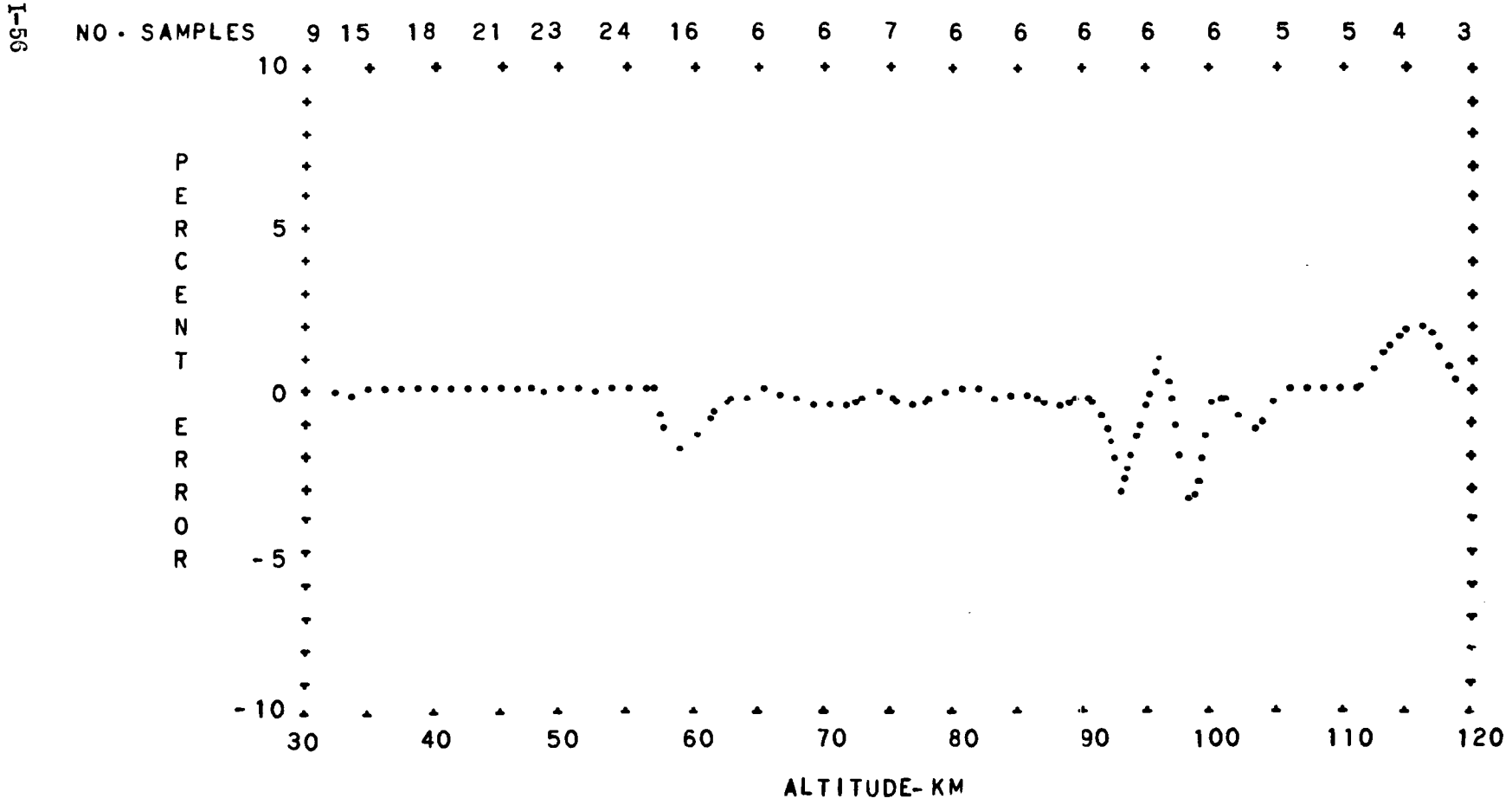

FIG. A-18 PERCENT CONTRIBUTION OF THE COVARIANCE TO THE MEAN PRESSURE OF THE BUELL GAS LAW EQUATION AS A FUNCTION OF ALTITUDE

TROPICAL ANNUAL MEAN DAYTIME

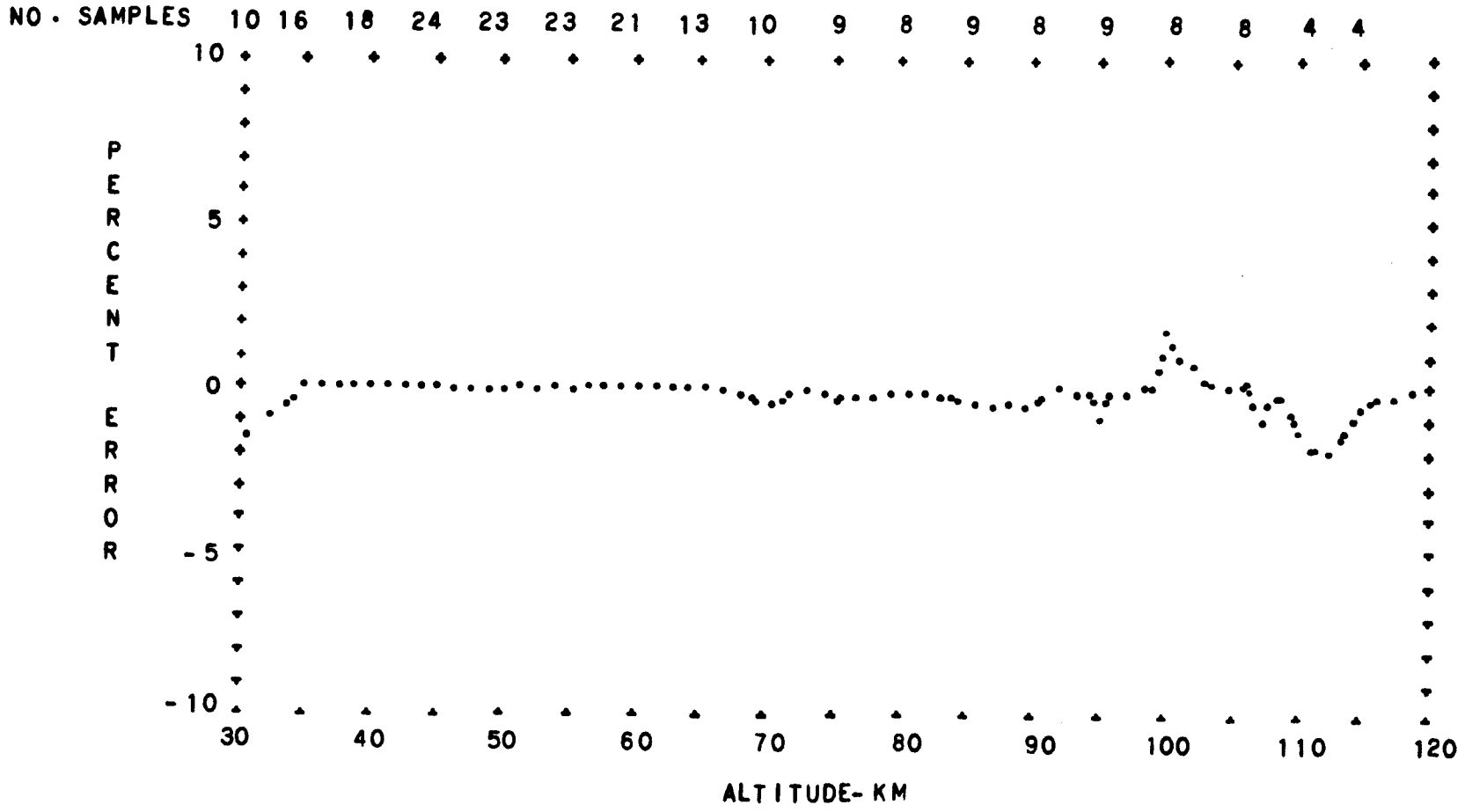

FIG. A-19 PERCENT CONTRIBUTION OF THE COVARIANCE TO THE MEAN PRESSURE OF THE BUELL GAS LAW EQUATION AS A FUNCTION OF ALTITUDE

TROPICAL ANNUAL MEAN NIGHTTIME

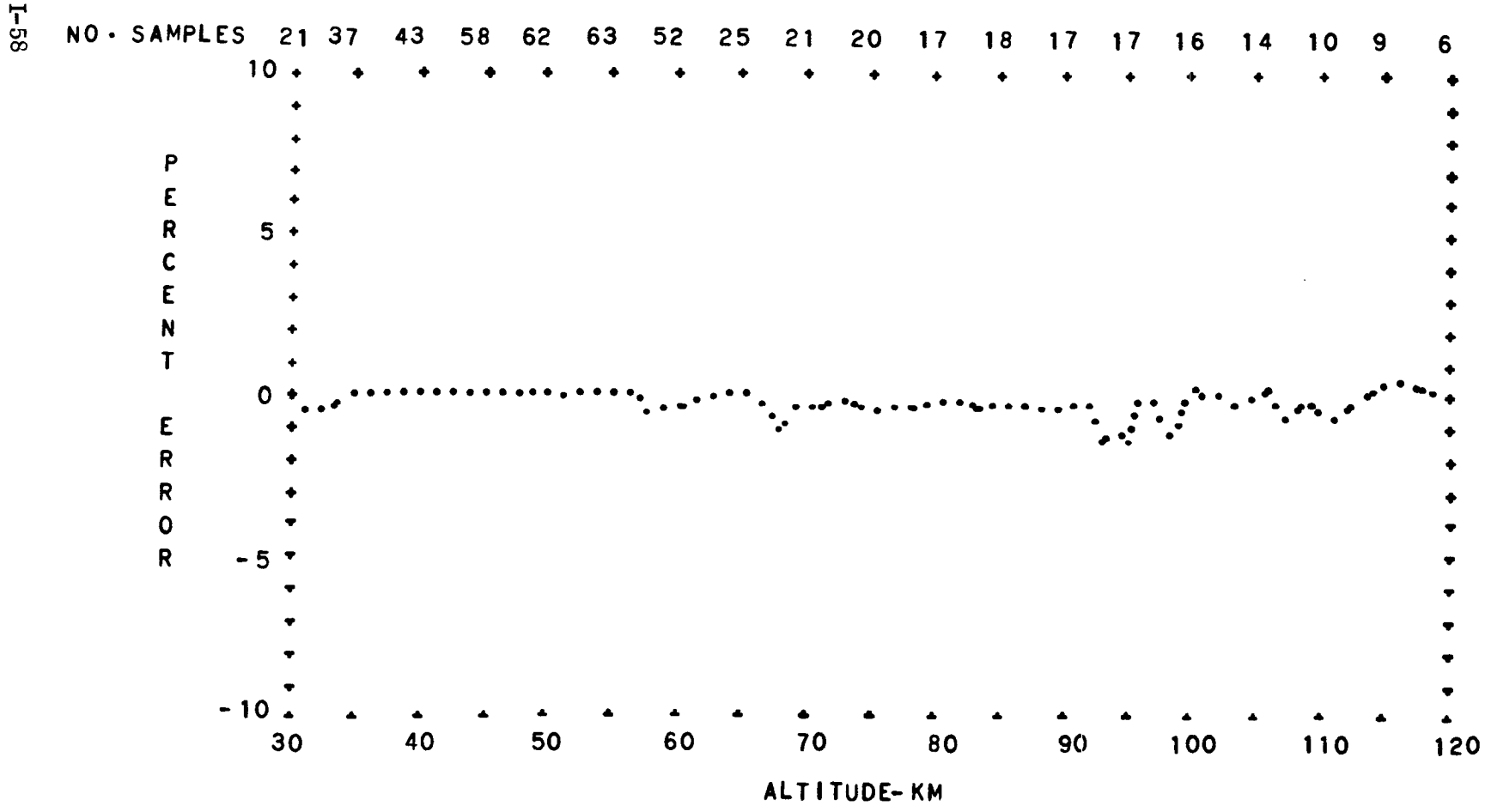

FIG. A-20 PERCENT CONTRIBUTION OF THE COVARIANCE TO THE MEAN PRESSURE OF THE BUELL GAS LAW EQUATION AS A FUNCTION OF ALTITUDE

TROPICAL ANNUAL MEAN DIURNAL MEAN

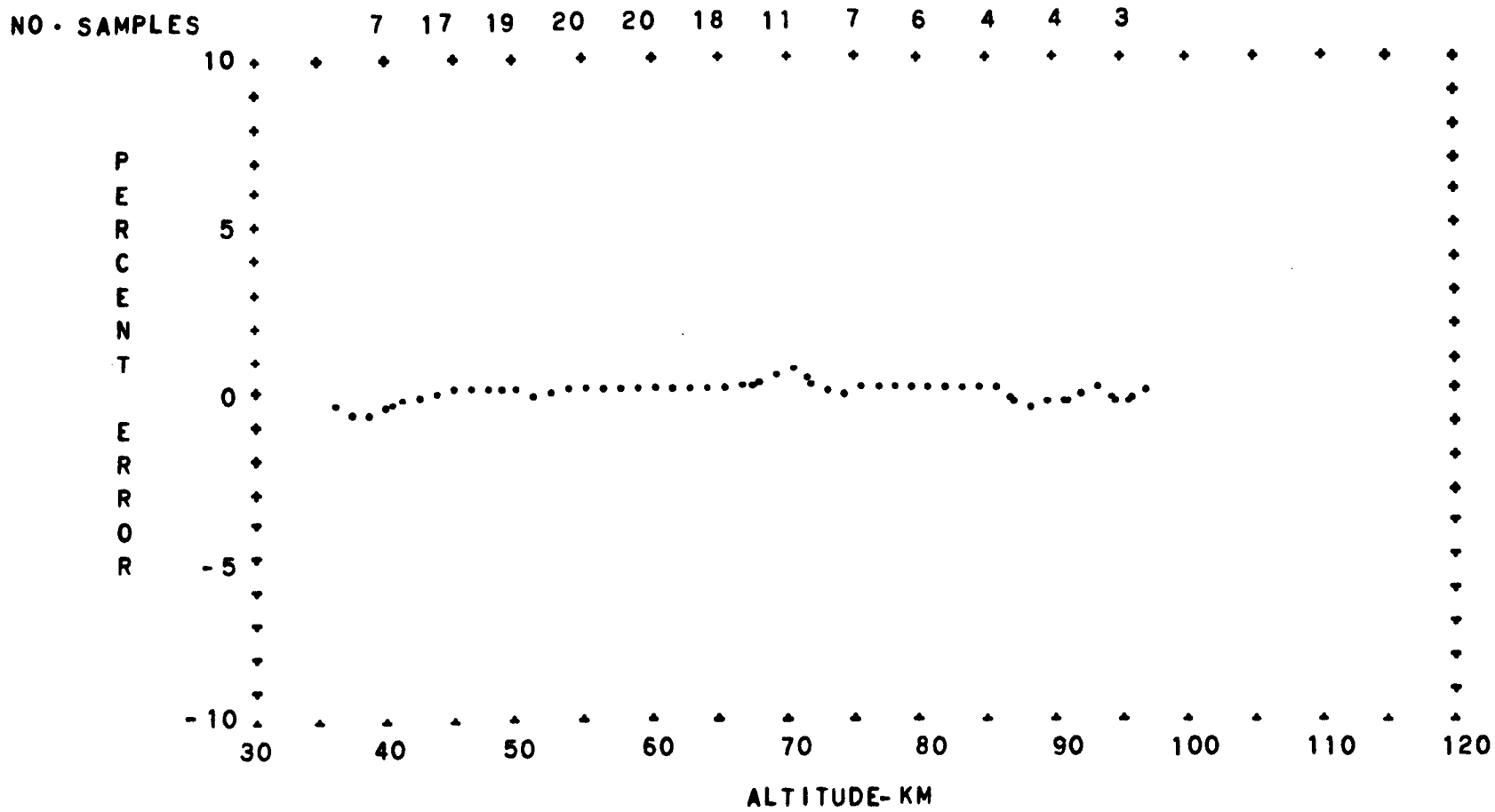

FIG. A-21 PERCENT CONTRIBUTION OF THE COVARIANCE TO THE MEAN PRESSURE OF THE BUELL GAS LAW EQUATION AS A FUNCTION OF ALTITUDE SUBTROPICAL SPRING DIURNAL TRANSITION

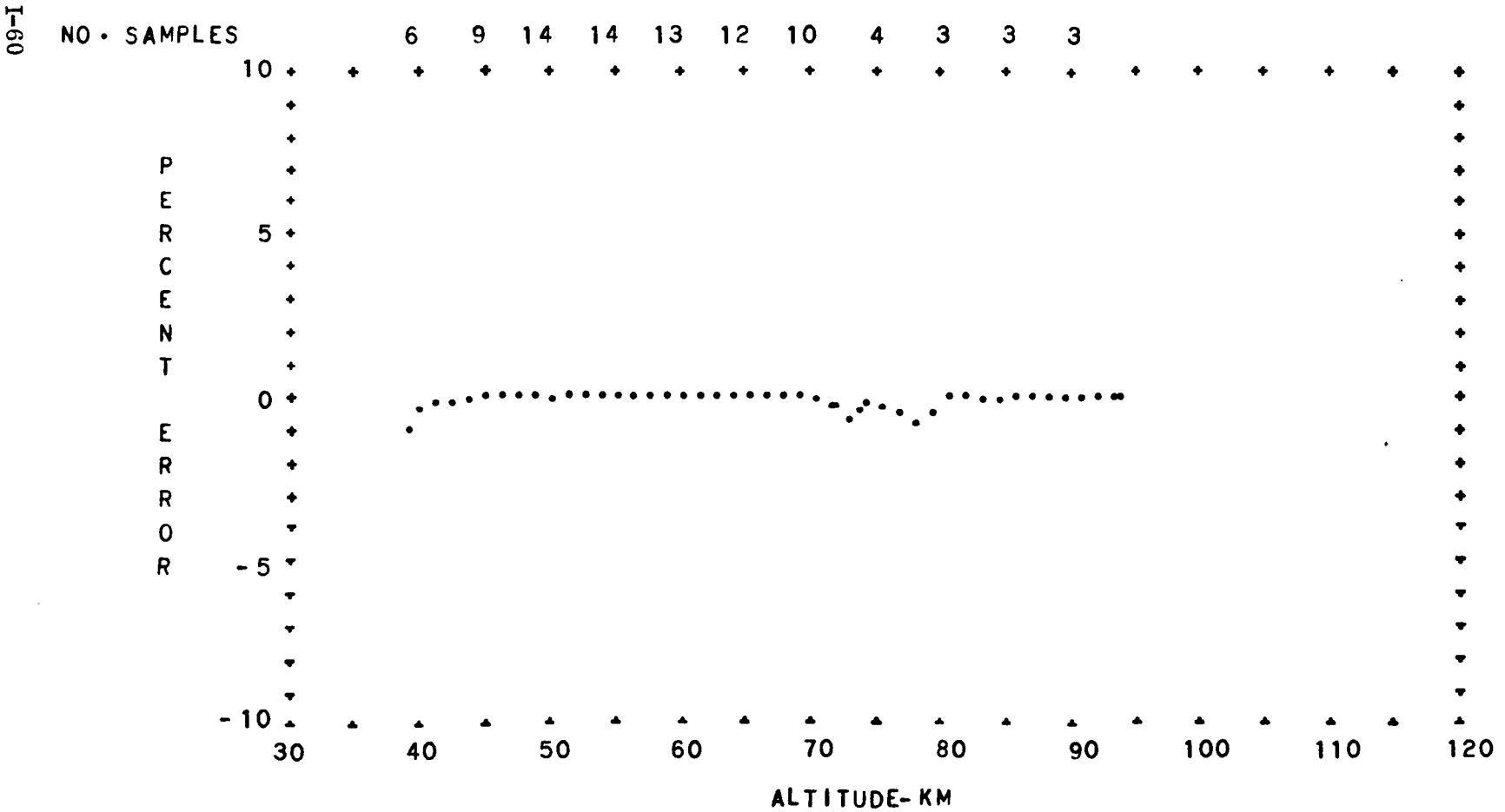

FIG. A-22 PERCENT CONTRIBUTION OF THE COVARIANCE TO THE MEAN PRESSURE OF THE BUELL GAS LAW EQUATION AS A FUNCTION OF ALTITUDE

SUBTROPICAL SPRING DAYTIME

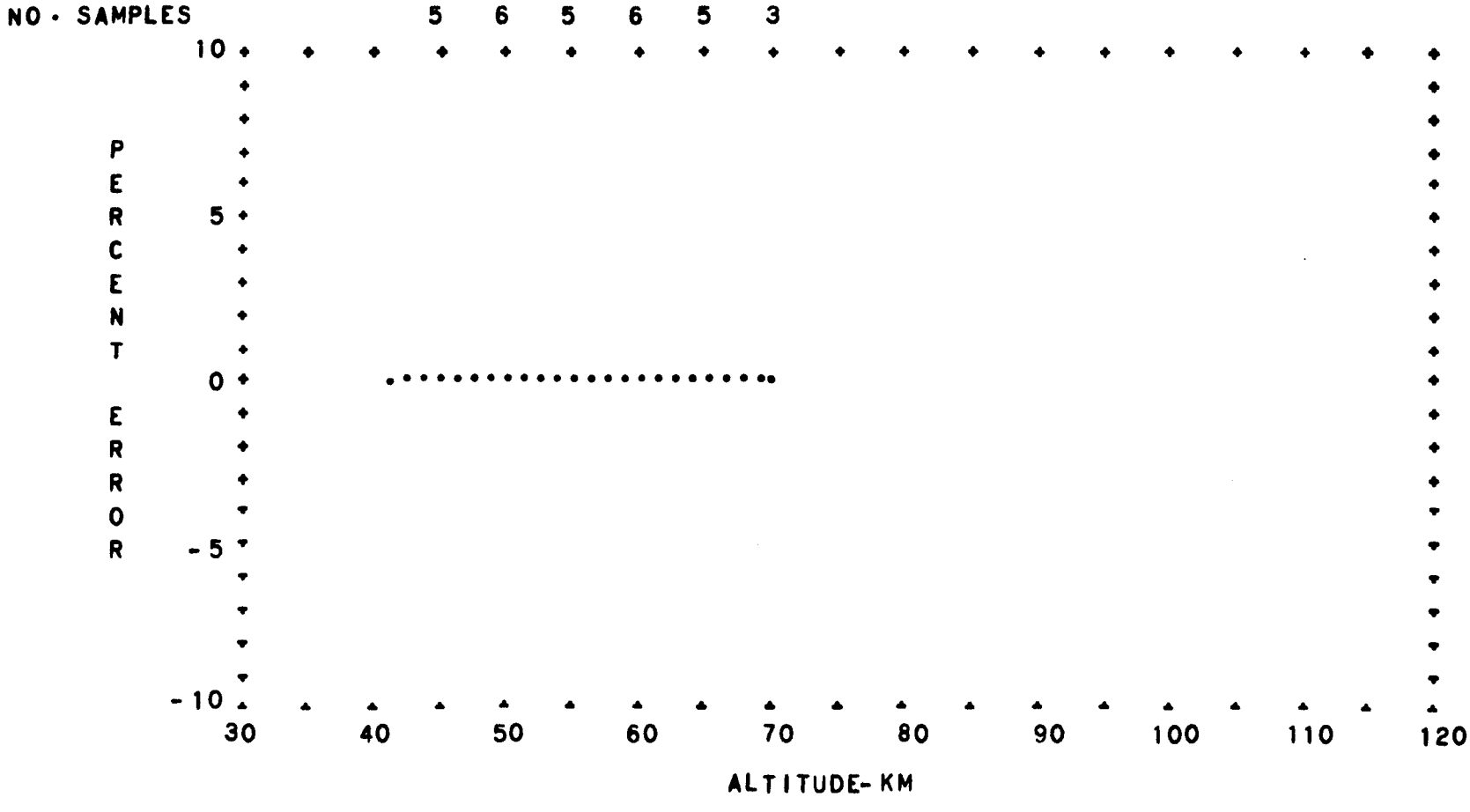

FIG. A-23 PERCENT CONTRIBUTION OF THE COVARIANCE TO THE MEAN PRESSURE OF THE BUELL GAS LAW EQUATION AS A FUNCTION OF ALTITUDE SUBTROPICAL SPRING NIGHTTIME

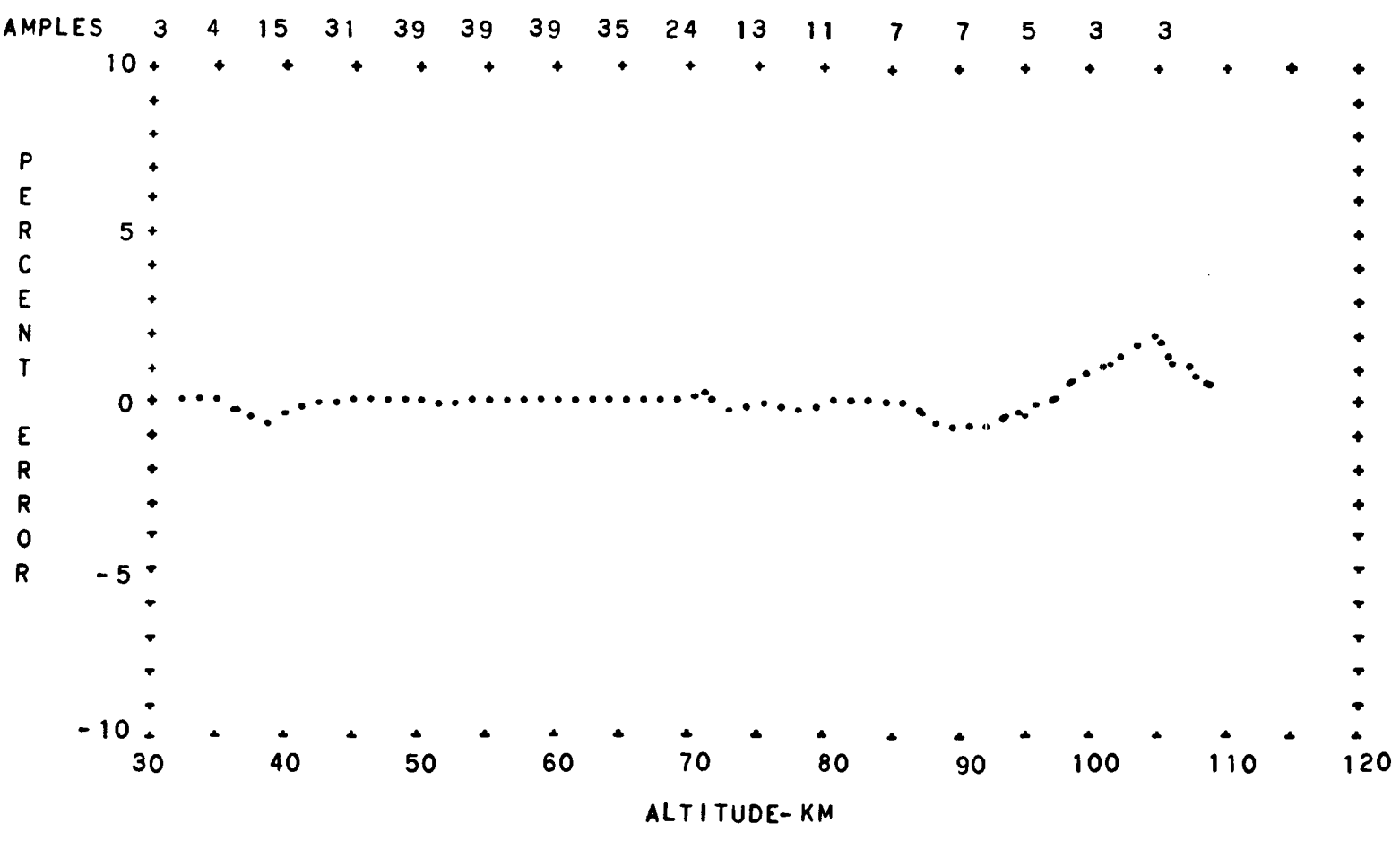

FIG. A-24 PERCENT CONTRIBUTION OF THE COVARIANCE TO THE MEAN PRESSURE OF THE BUELL GAS LAW EQUATION AS A FUNCTION OF ALTITUDE

SUBTROPICAL SPRING DIURNAL MEAN

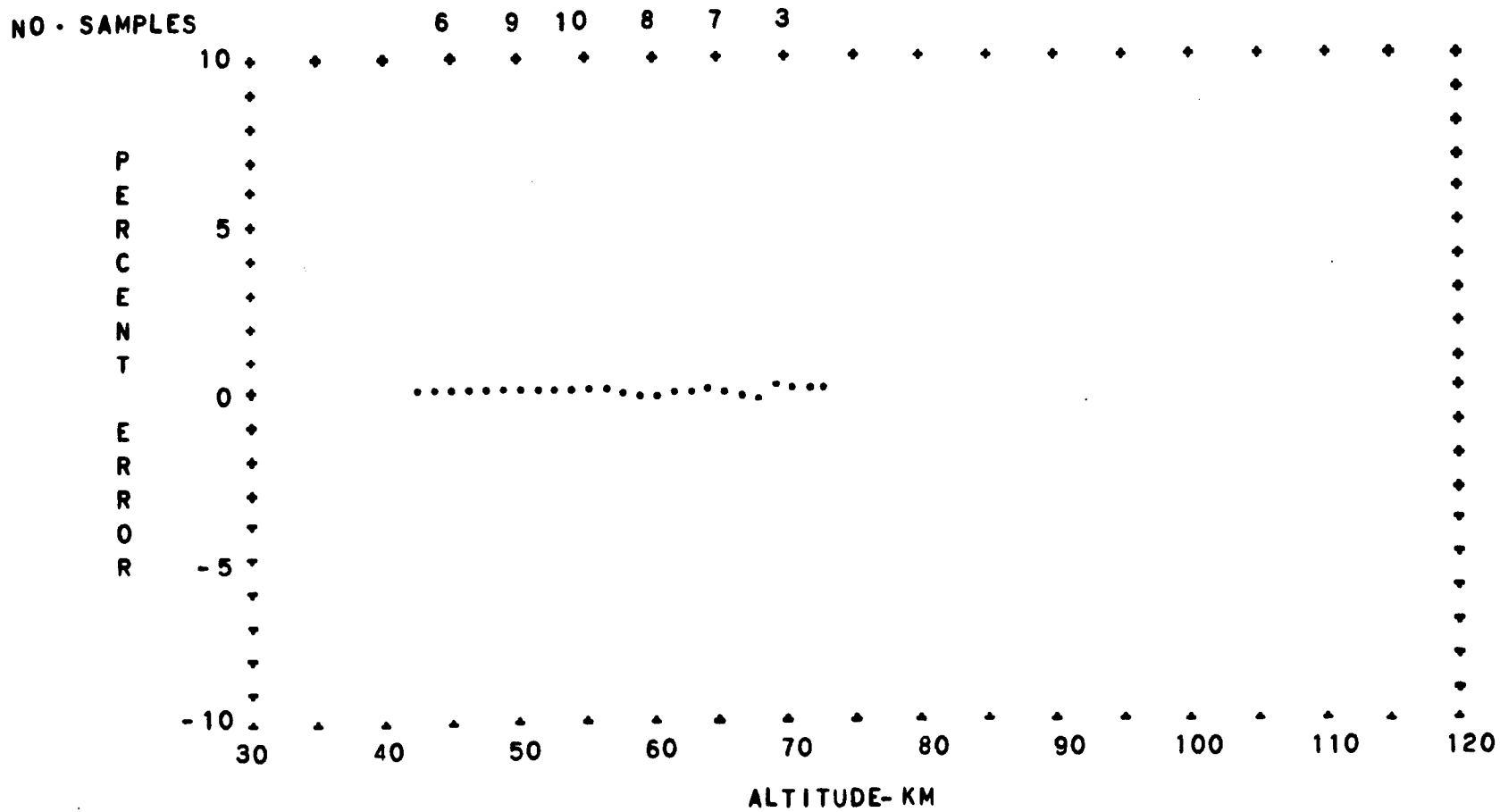

FIG. A-25 PERCENT CONTRIBUTION OF THE COVARIANCE TO THE MEAN PRESSURE OF THE BUELL GAS LAW EQUATION AS A FUNCTION OF ALTITUDE SUBTROPICAL SUMMER DIURNAL TRANSITION

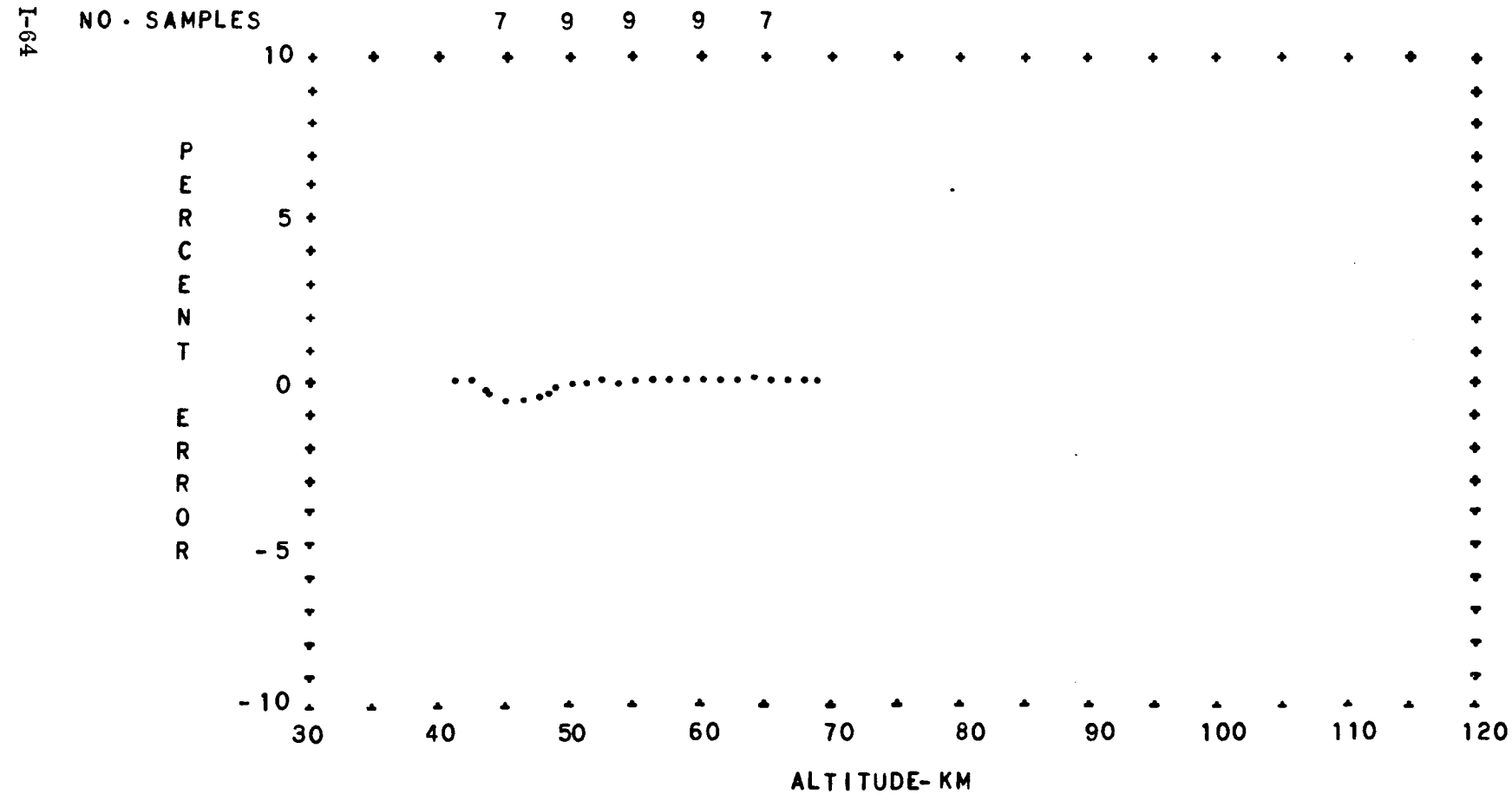

FIG. A-26 PERCENT CONTRIBUTION OF THE COVARIANCE TO THE MEAN PRESSURE OF THE BUELL GAS LAW EQUATION AS A FUNCTION OF ALTITUDE

SUBTROPICAL SUMMER DAYTIME

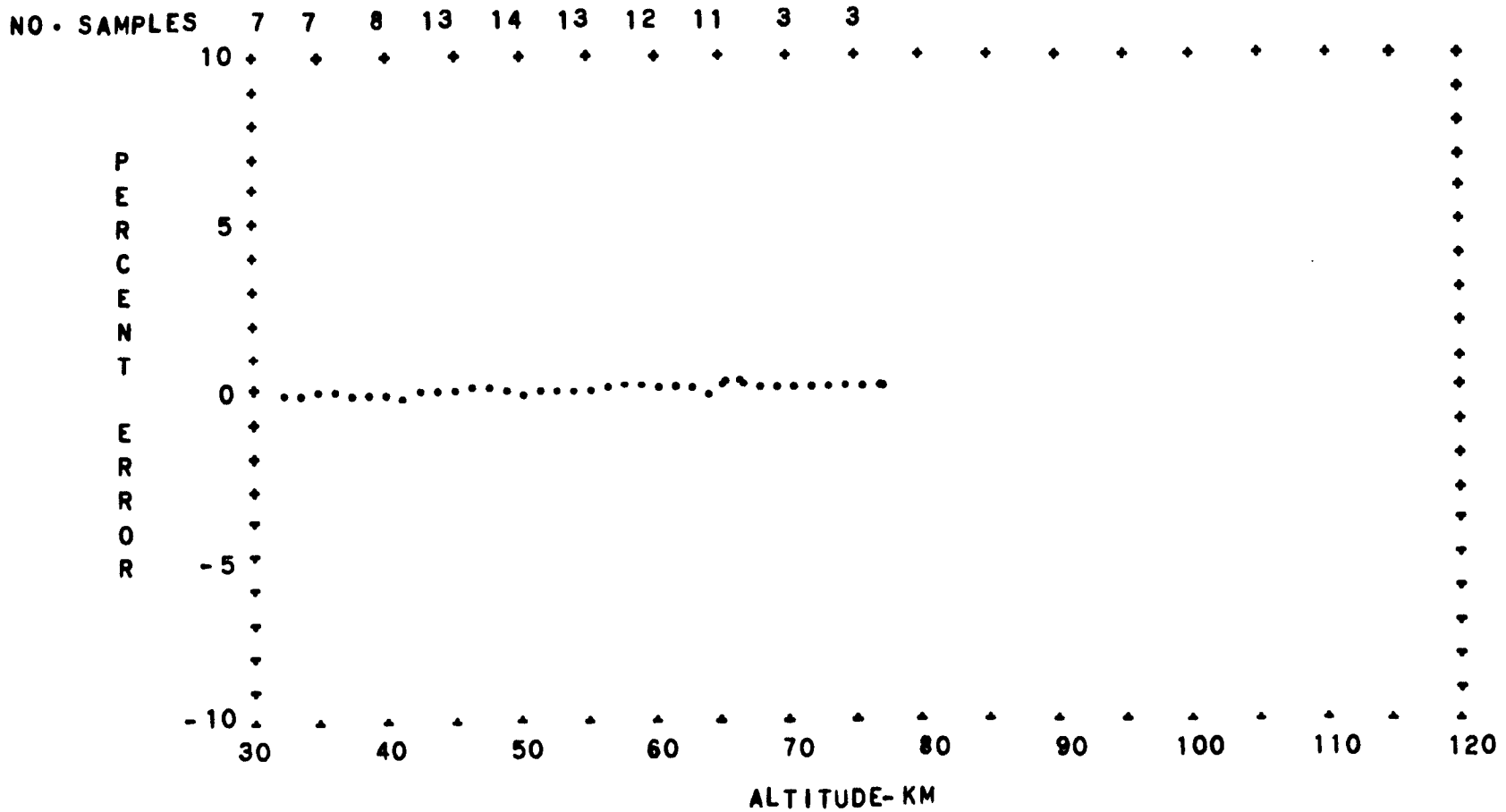

FIG. A-27 PERCENT CONTRIBUTION OF THE COVARIANCE TO THE MEAN PRESSURE OF THE BUELL GAS LAW EQUATION AS A FUNCTION OF ALTITUDE

SUBTROPICAL SUMMER NIGHTTIME

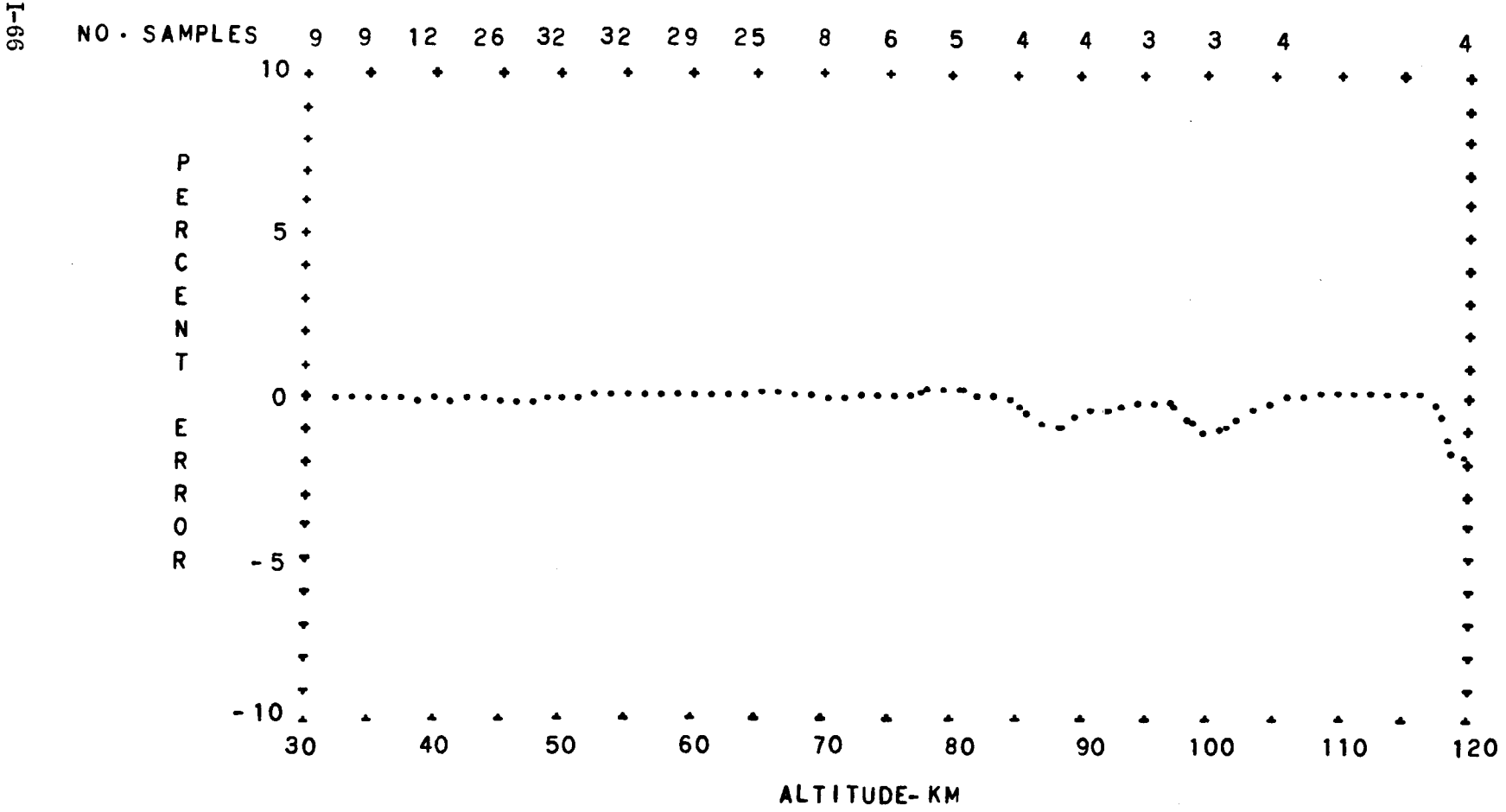

FIG. A-28 PERCENT CONTRIBUTION OF THE COVARIANCE TO THE MEAN PRESSURE OF THE BUELL GAS LAW EQUATION AS A FUNCTION OF ALTITUDE

SUBTROPICAL SUMMER DIURNAL MEAN

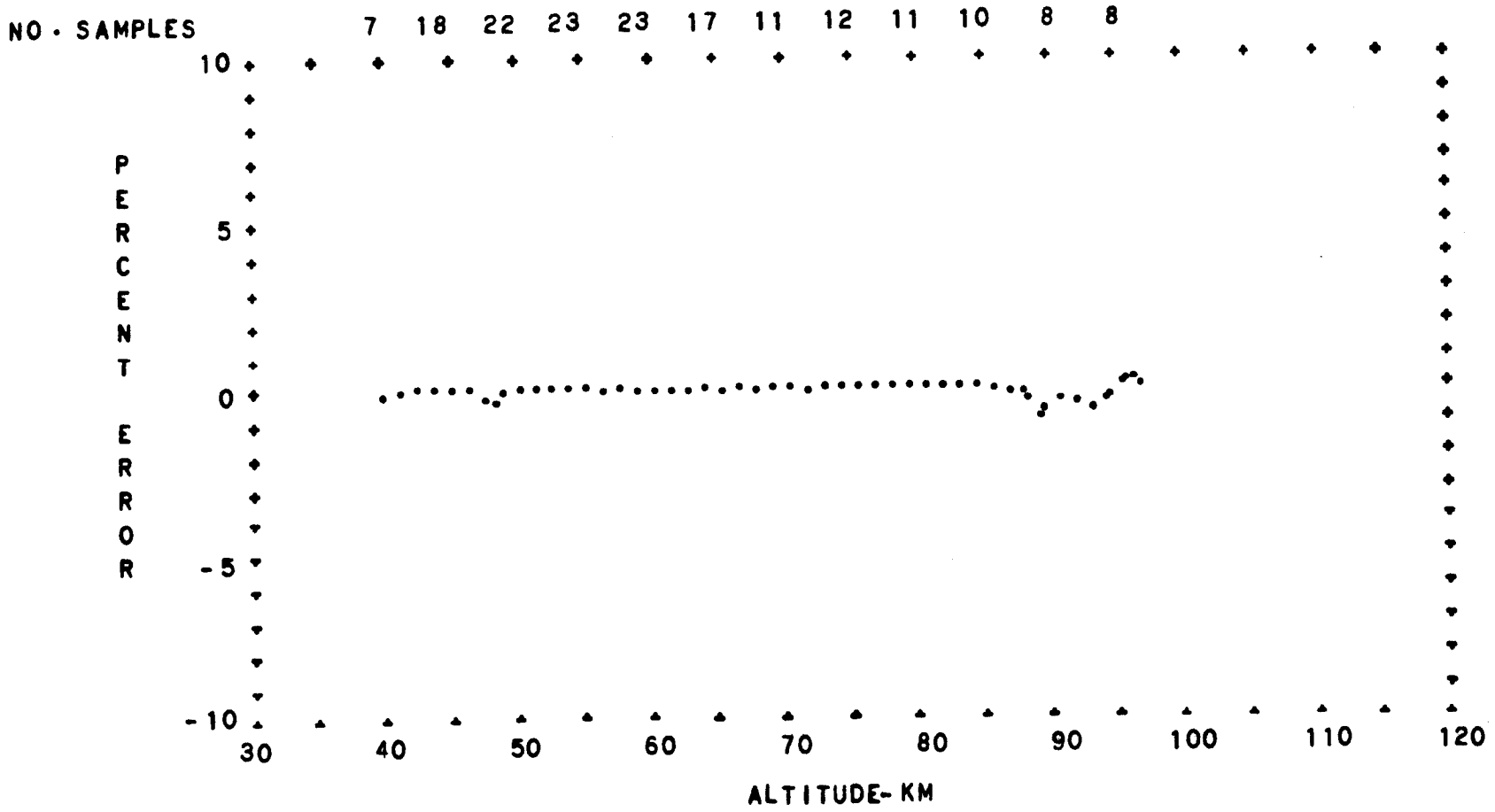

FIG. A-29 PERCENT CONTRIBUTION OF THE COVARIANCE TO THE MEAN PRESSURE OF THE BUELL GAS LAW EQUATION AS A FUNCTION OF ALTITUDE

SUBTROPICAL AUTUMN DIURNAL TRANSITION

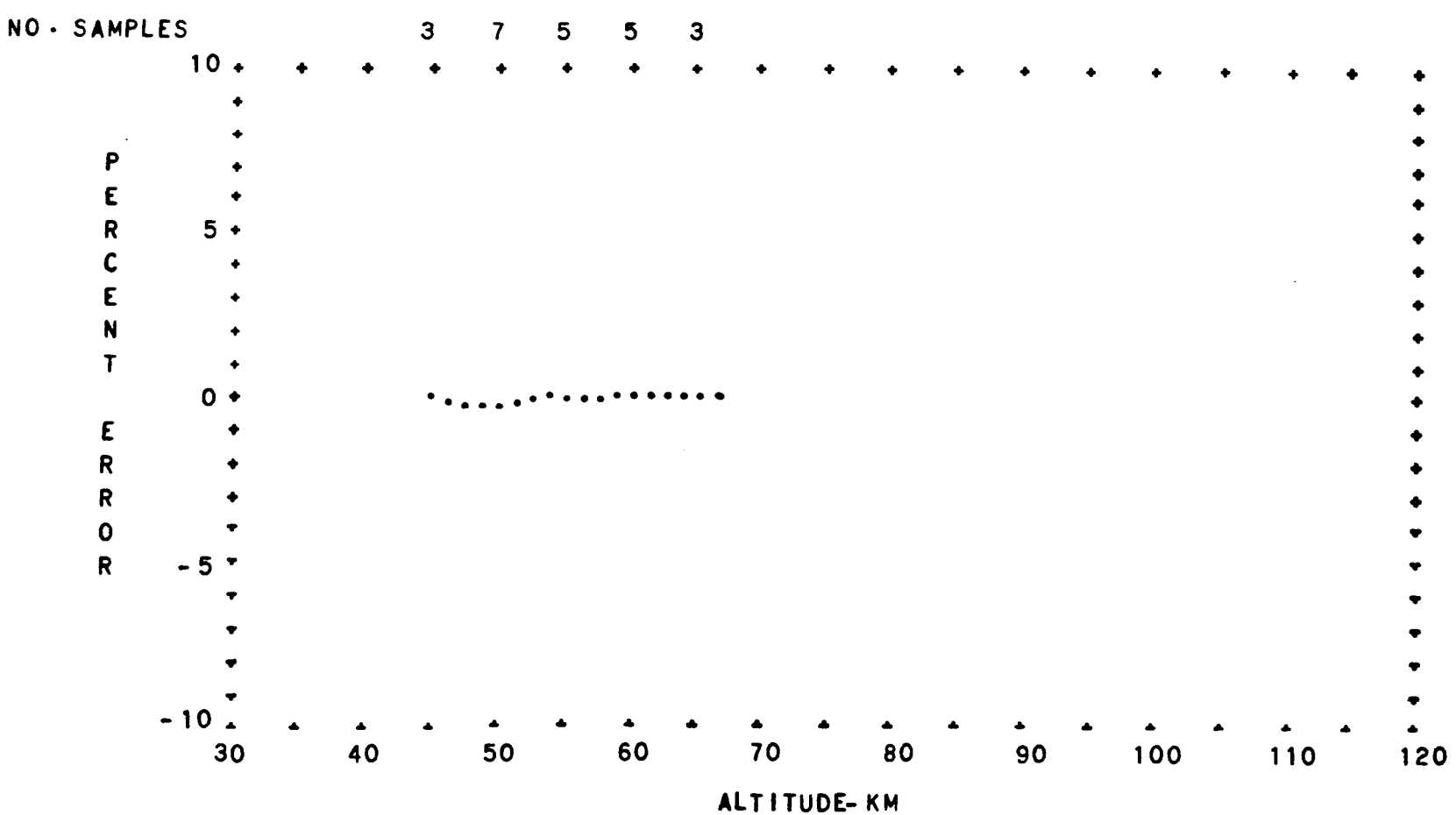

FIG. A-30 PERCENT CONTRIBUTION OF THE COVARIANCE TO THE MEAN PRESSURE OF THE BUELL GAS LAW EQUATION AS A FUNCTION OF ALTITUDE

SUBTROPICAL AUTUMN DAYTIME

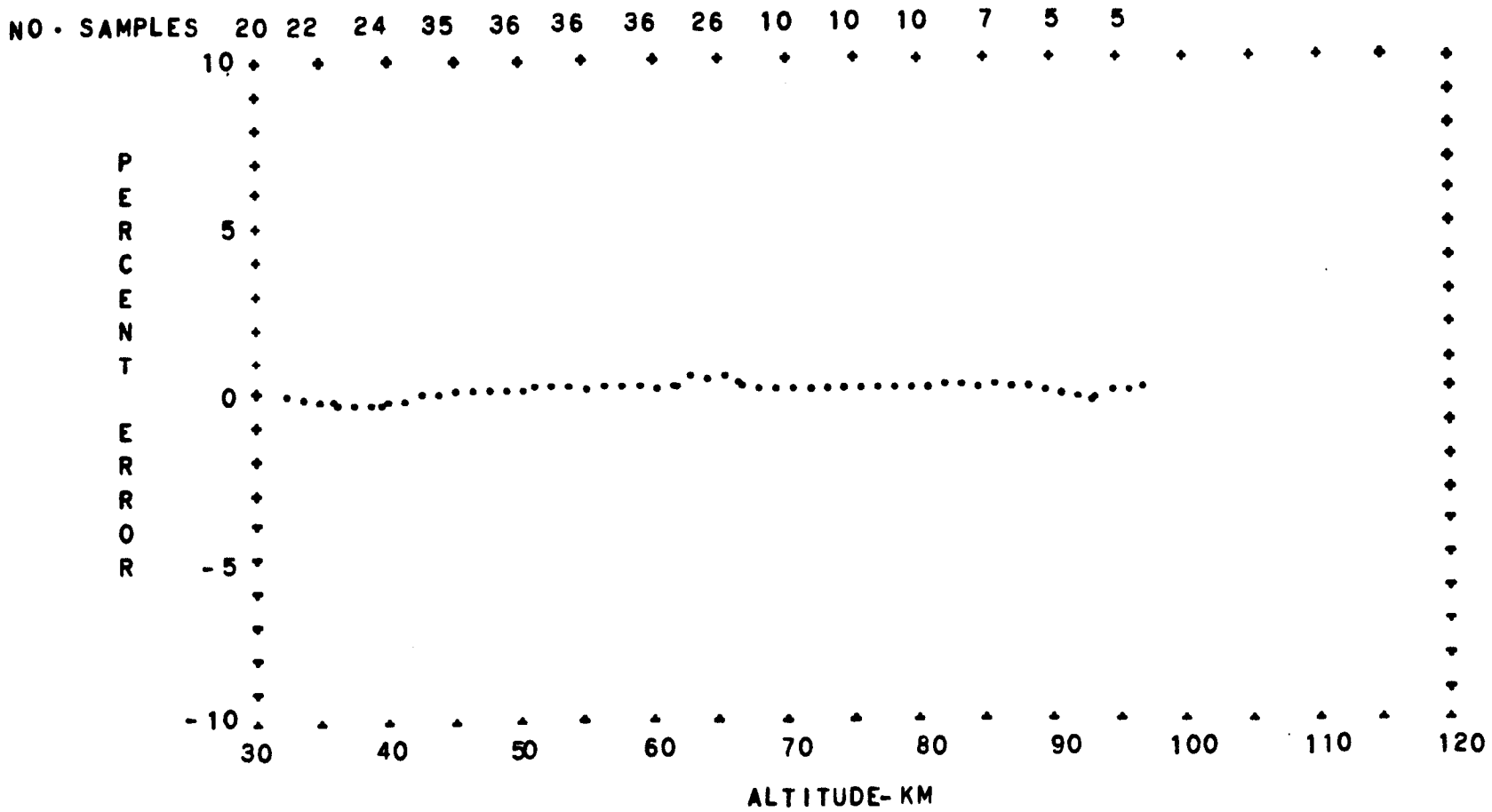

FIG. A-31 PERCENT CONTRIBUTION OF THE COVARIANCE TO THE MEAN PRESSURE OF THE BUELL GAS LAW EQUATION AS A FUNCTION OF ALTITUDE

SUBTROPICAL AUTUMN NIGHTTIME

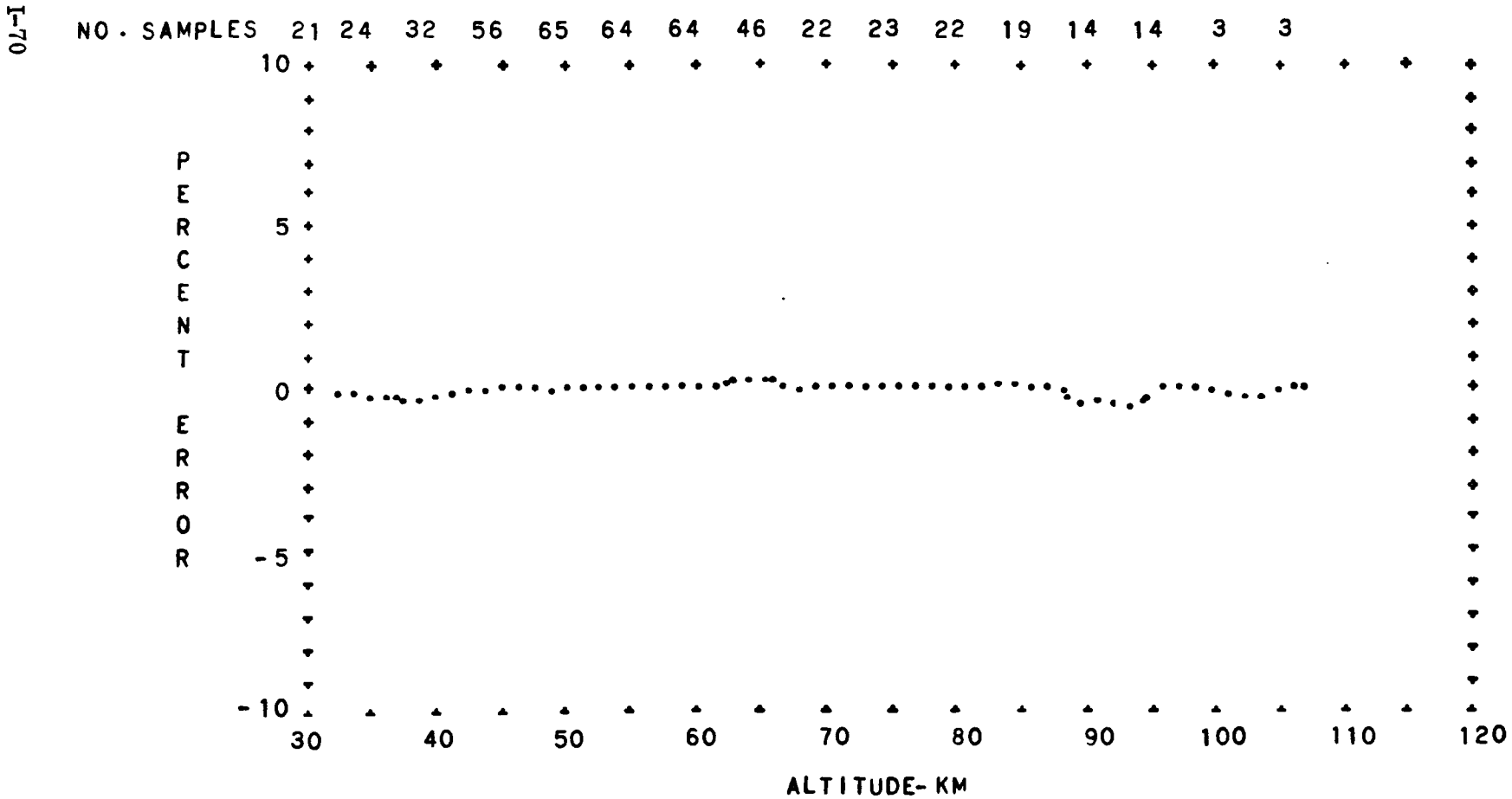

FIG. A-32 PERCENT CONTRIBUTION OF THE COVARIANCE TO THE MEAN PRESSURE OF THE BUELL GAS LAW EQUATION AS A FUNCTION OF ALTITUDE

SUBTROPICAL AUTUMN DIURNAL MEAN

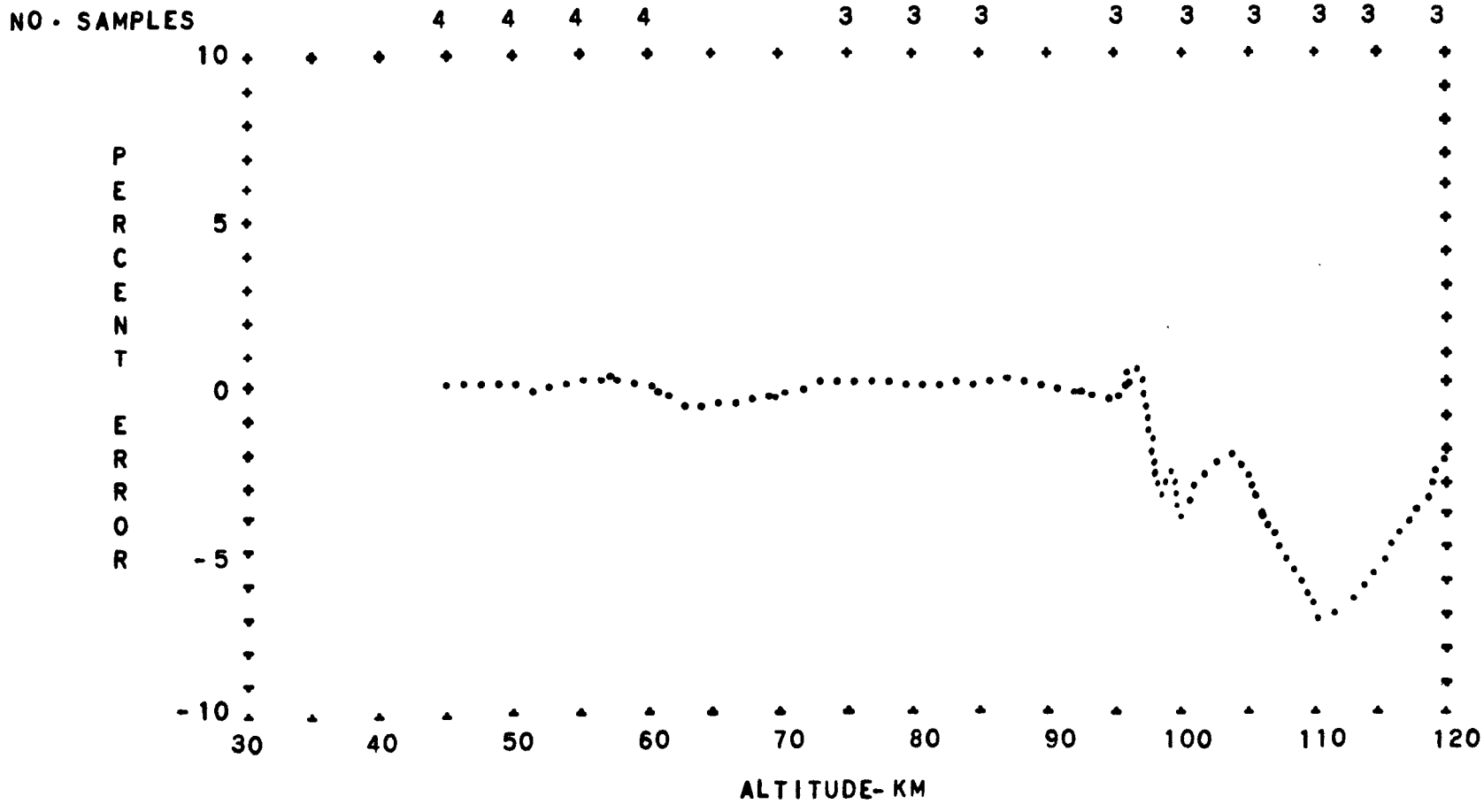

FIG. A-33 PERCENT CONTRIBUTION OF THE COVARIANCE TO THE MEAN PRESSURE OF THE BUELL GAS LAW EQUATION AS A FUNCTION OF ALTITUDE SUBTROPICAL WINTER . DIURNAL TRANSITION

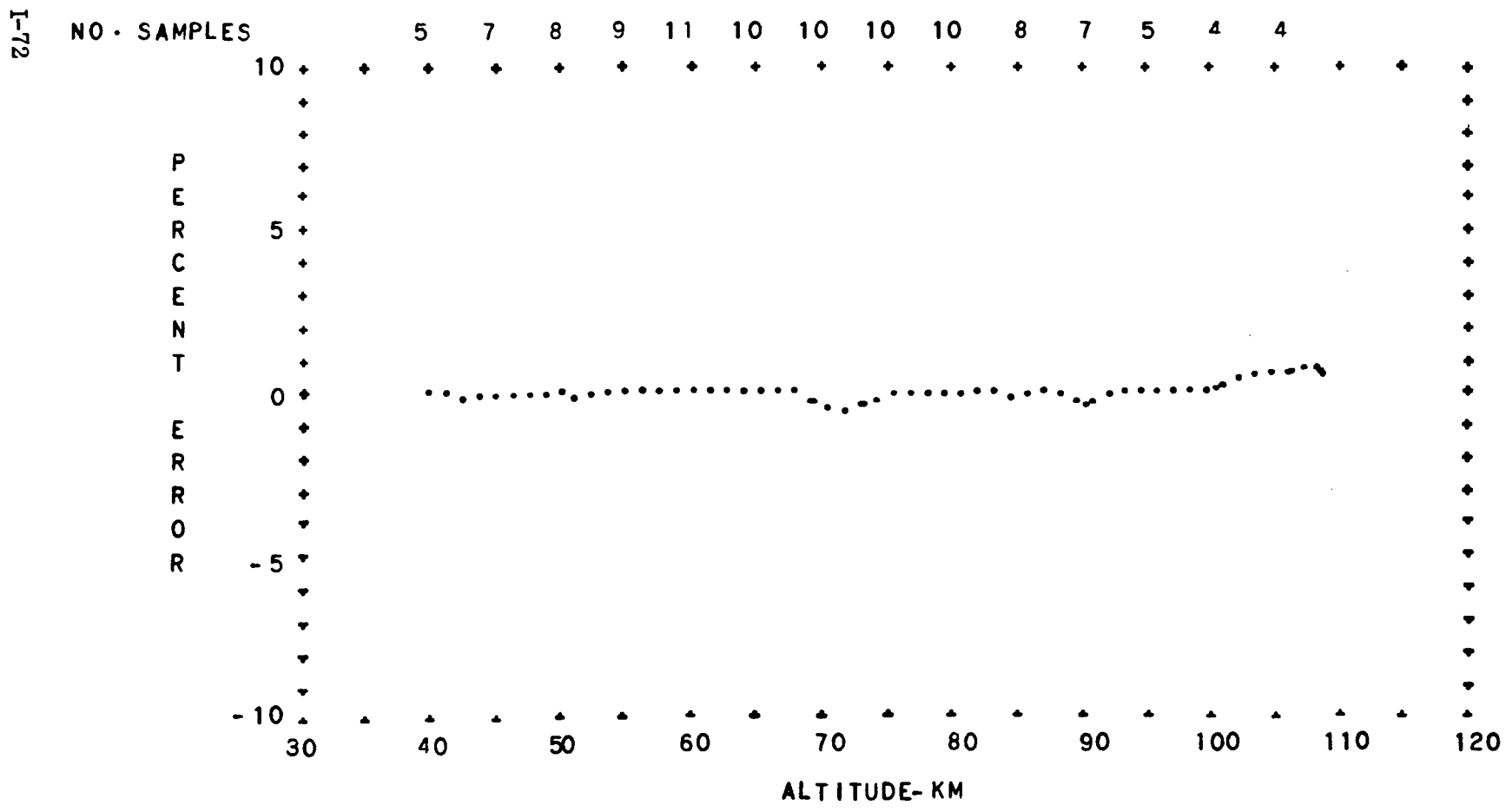

FIG. A-34 PERCENT CONTRIBUTION OF THE COVARIANCE TO THE MEAN PRESSURE OF THE BUELL GAS LAW EQUATION AS A FUNCTION OF ALTITUDE

SUBTROPICAL WINTER DAYTIME

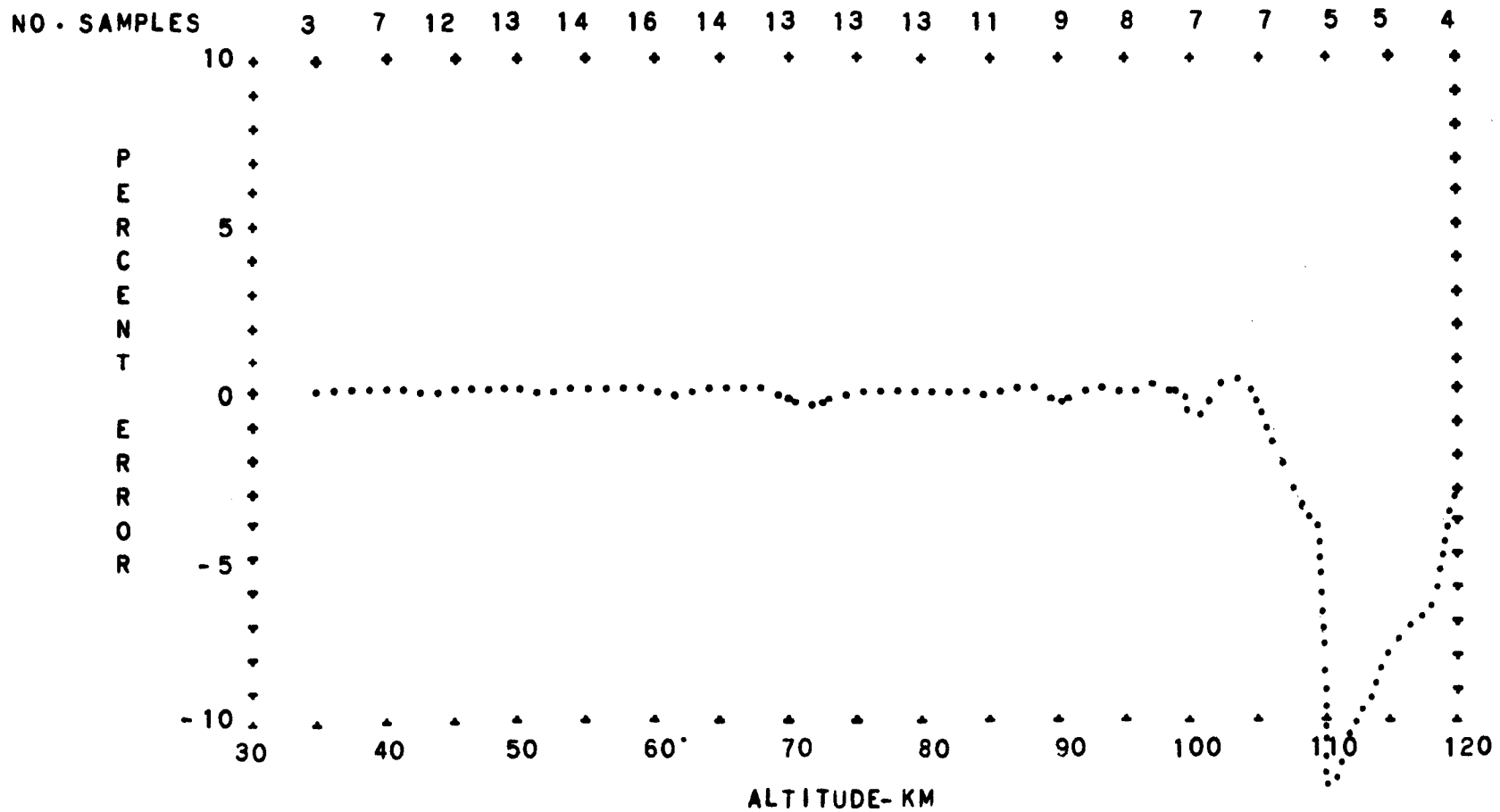

FIG. A-35 PERCENT CONTRIBUTION OF THE COVARIANCE TO THE MEAN PRESSURE OF THE BUELL GAS LAW EQUATION AS A FUNCTION OF ALTITUDE

SUBTROPICAL WINTER DIURNAL MEAN

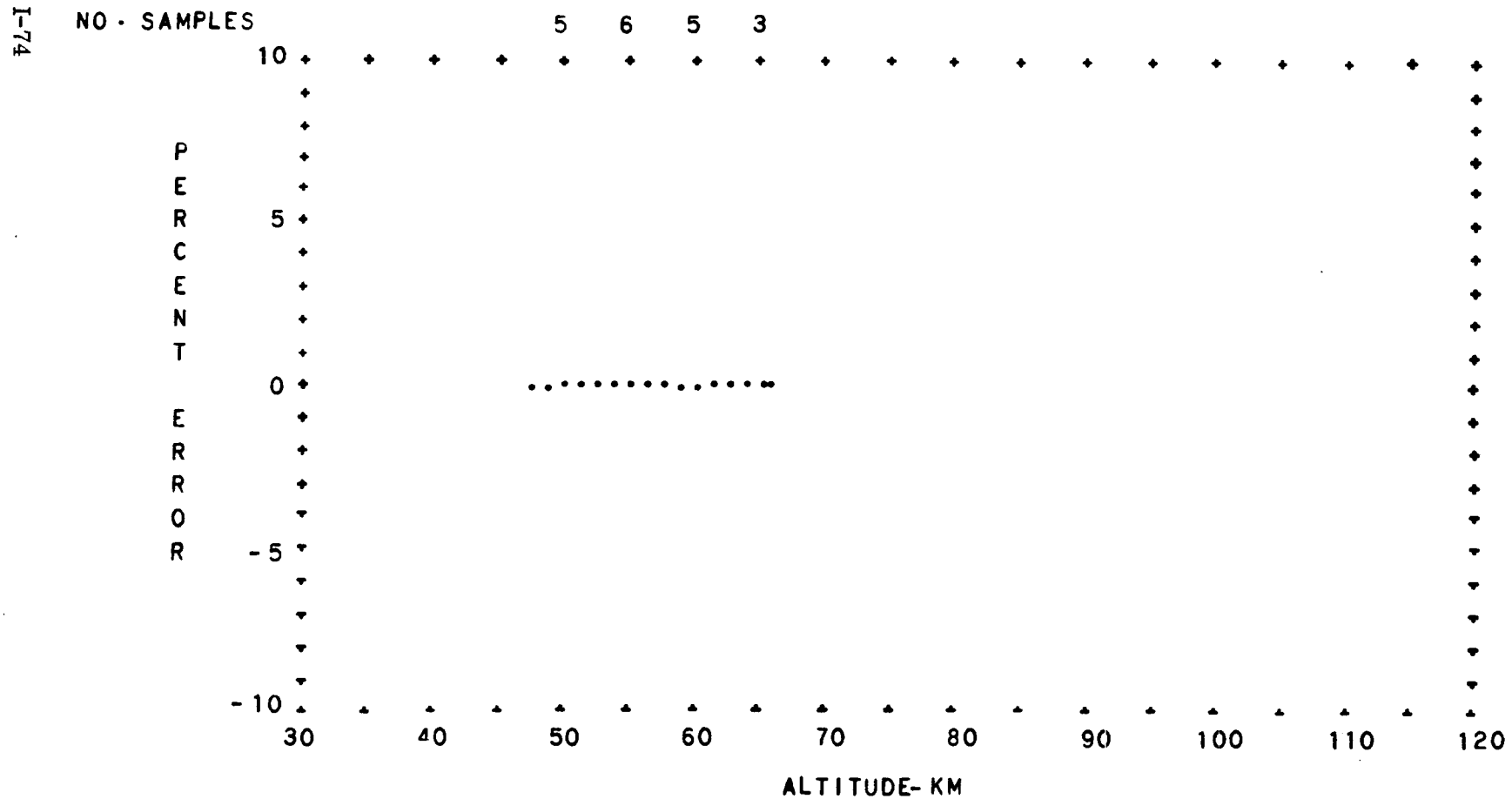

FIG. A-36 PERCENT CONTRIBUTION OF THE COVARIANCE TO THE MEAN PRESSURE OF THE BUELL GAS LAW EQUATION AS A FUNCTION OF ALTITUDE

SUBTROPICAL SUMMER EXTREME DIURNAL TRANSITION

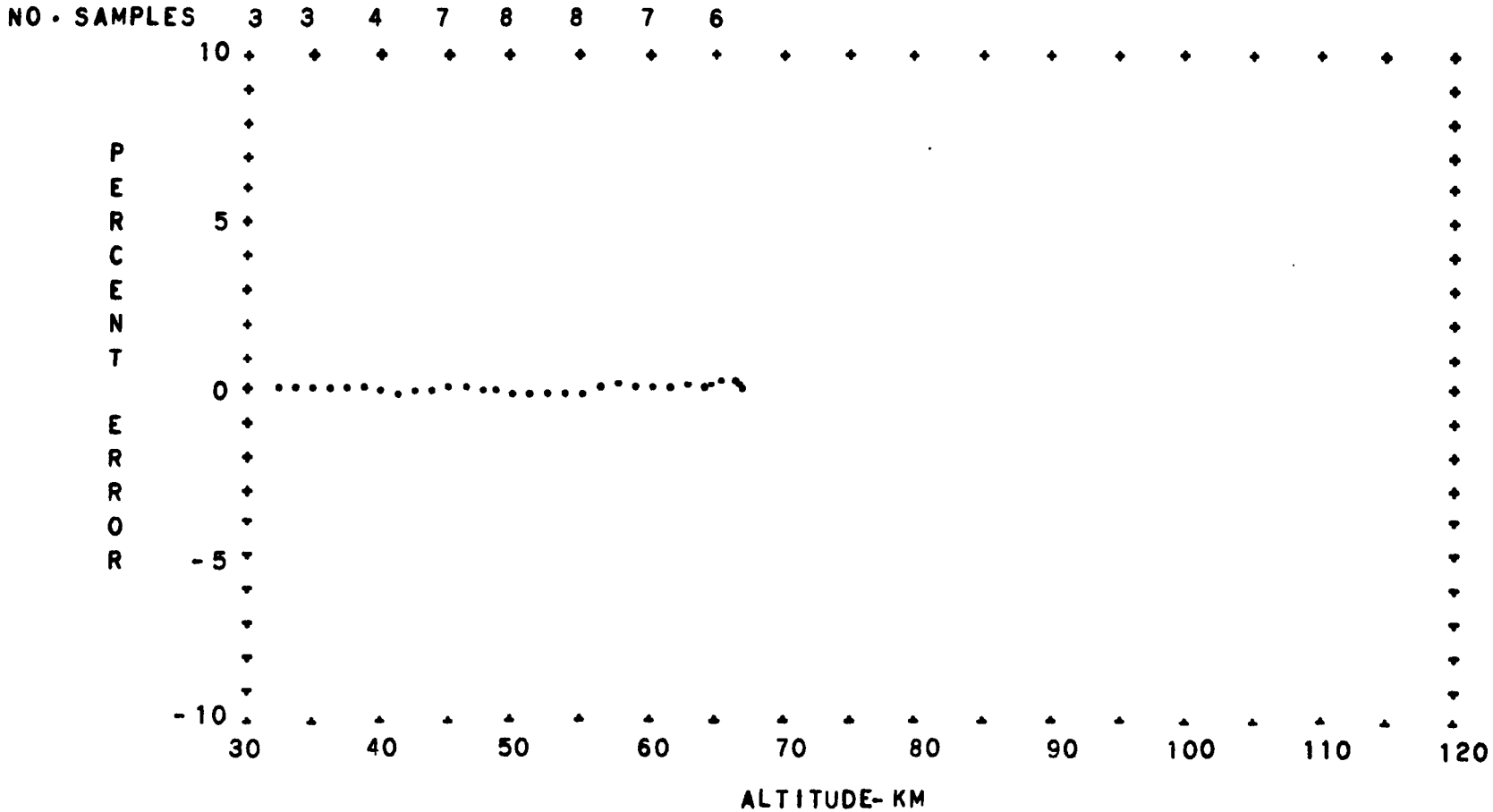

FIG. A-37 PERCENT CONTRIBUTION OF THE COVARIANCE TO THE MEAN PRESSURE OF THE BUELL GAS LAW EQUATION AS A FUNCTION OF ALTITUDE

SUBTROPICAL SUMMER EXTREME NIGHTTIME

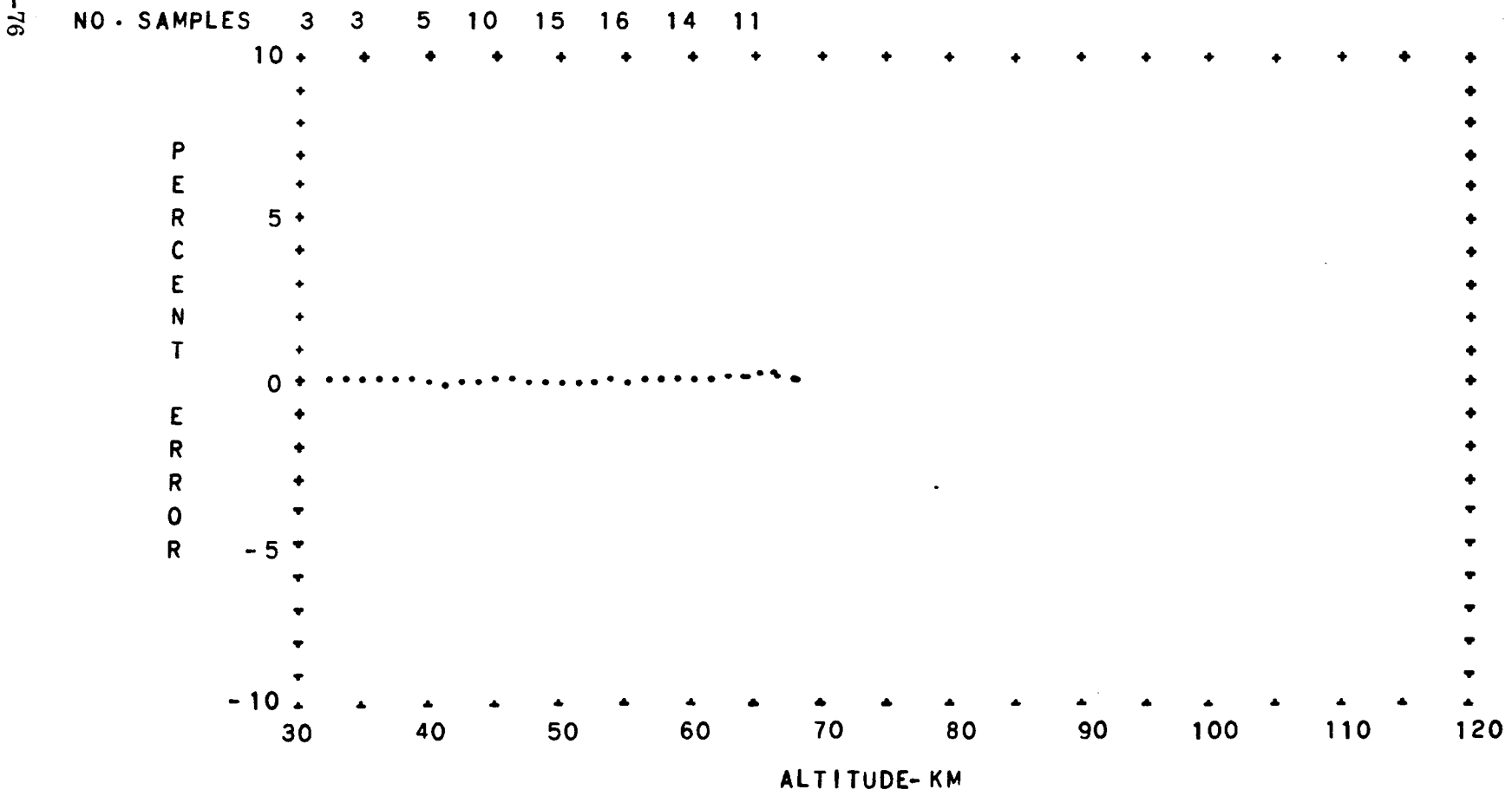

FIG. A-38 PERCENT CONTRIBUTION OF THE COVARIANCE TO THE MEAN PRESSURE OF THE BUELL GAS LAW EQUATION AS A FUNCTION OF ALTITUDE

SUBTROPICAL SUMMER EXTREME DIURNAL MEAN

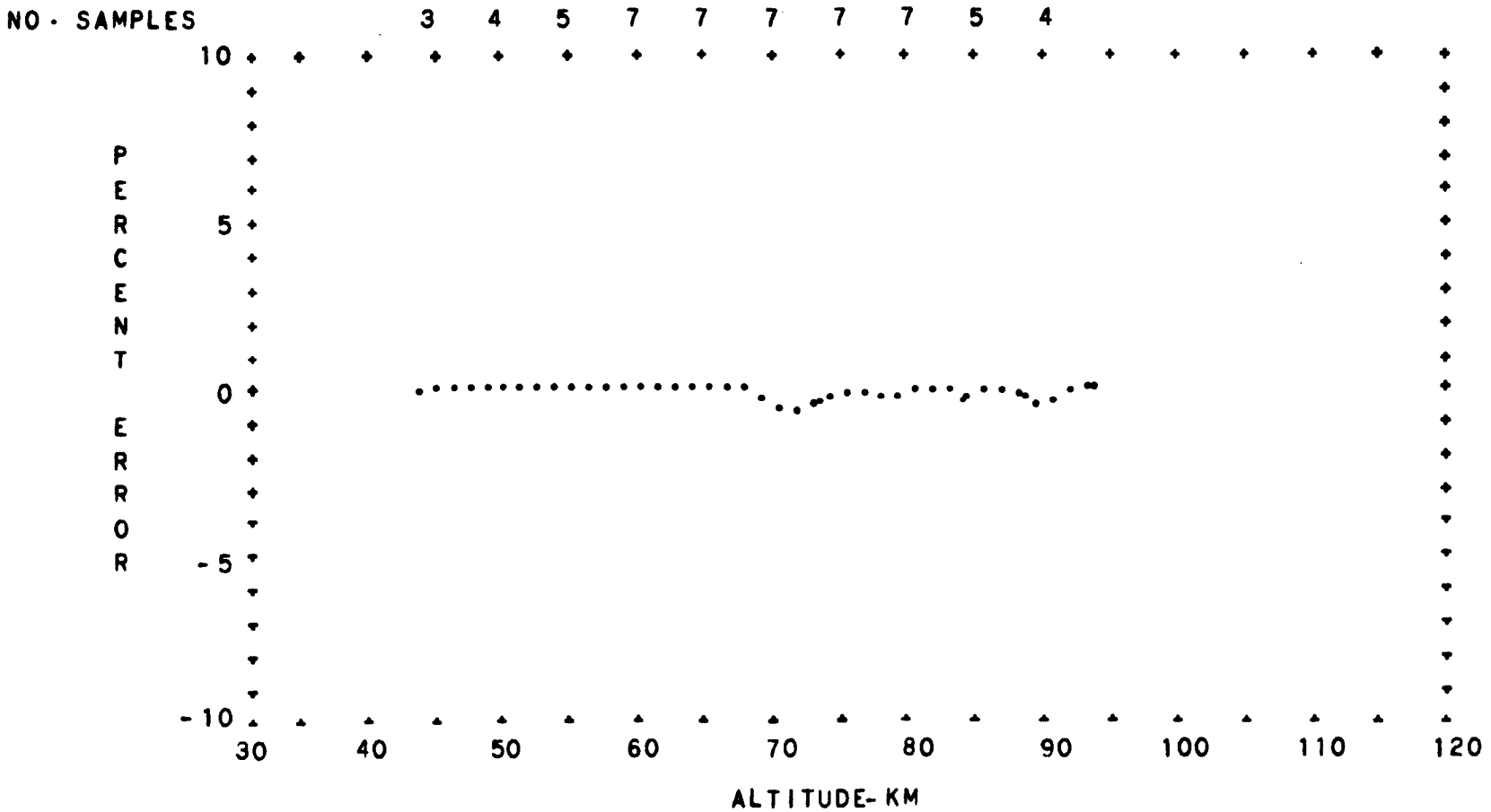

FIG. A-39 PERCENT CONTRIBUTION OF THE COVARIANCE TO THE MEAN PRESSURE OF THE BUELL GAS LAW EQUATION AS A FUNCTION OF ALTITUDE

SUBTROPICAL WINTER EXTREME DAYTIME

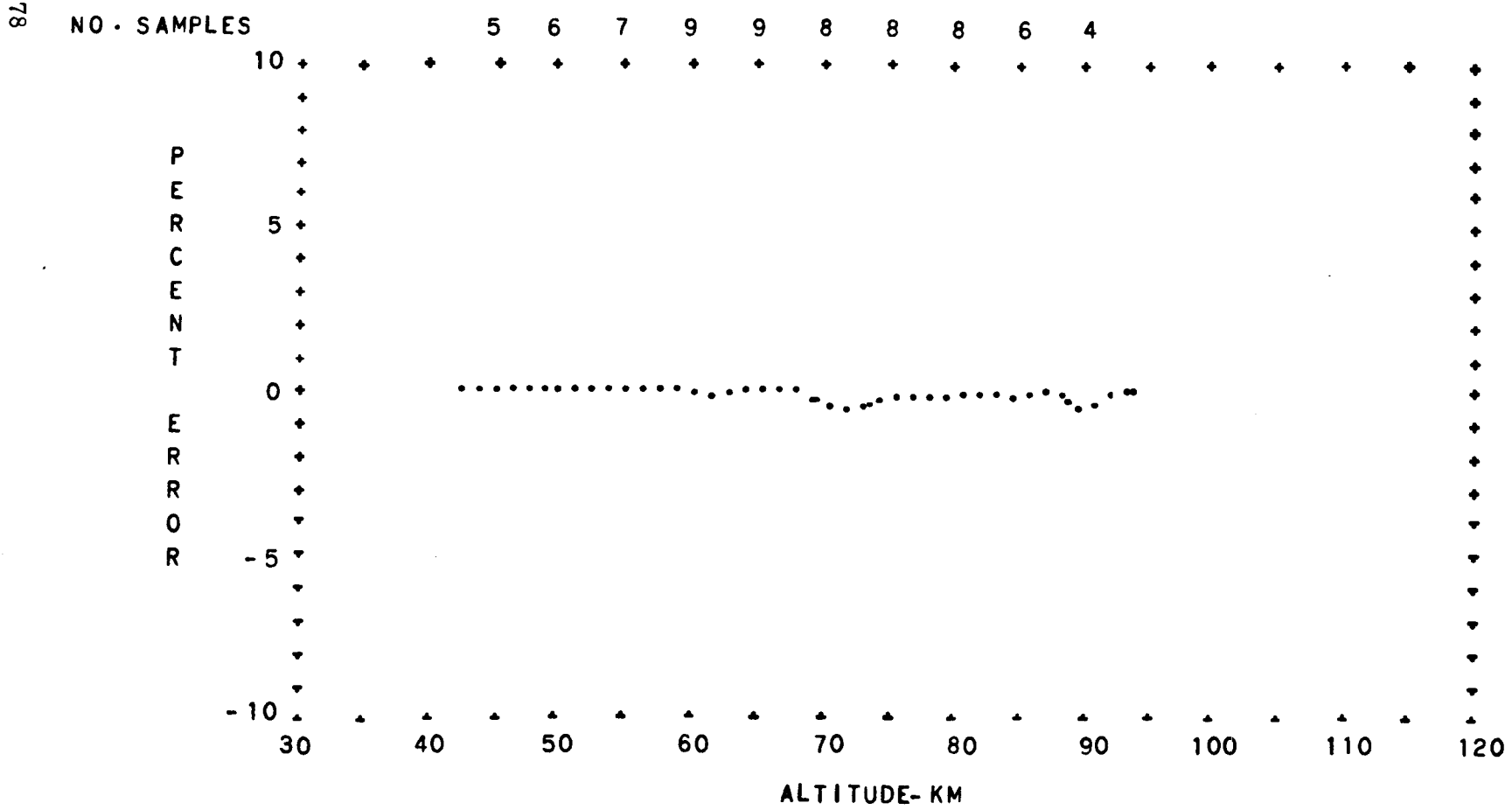

FIG. A-40 PERCENT CONTRIBUTION OF THE COVARIANCE TO THE MEAN PRESSURE OF THE BUELL GAS LAW EQUATION AS A FUNCTION OF ALTITUDE

SUBTROPICAL WINTER EXTREME DIURNAL MEAN

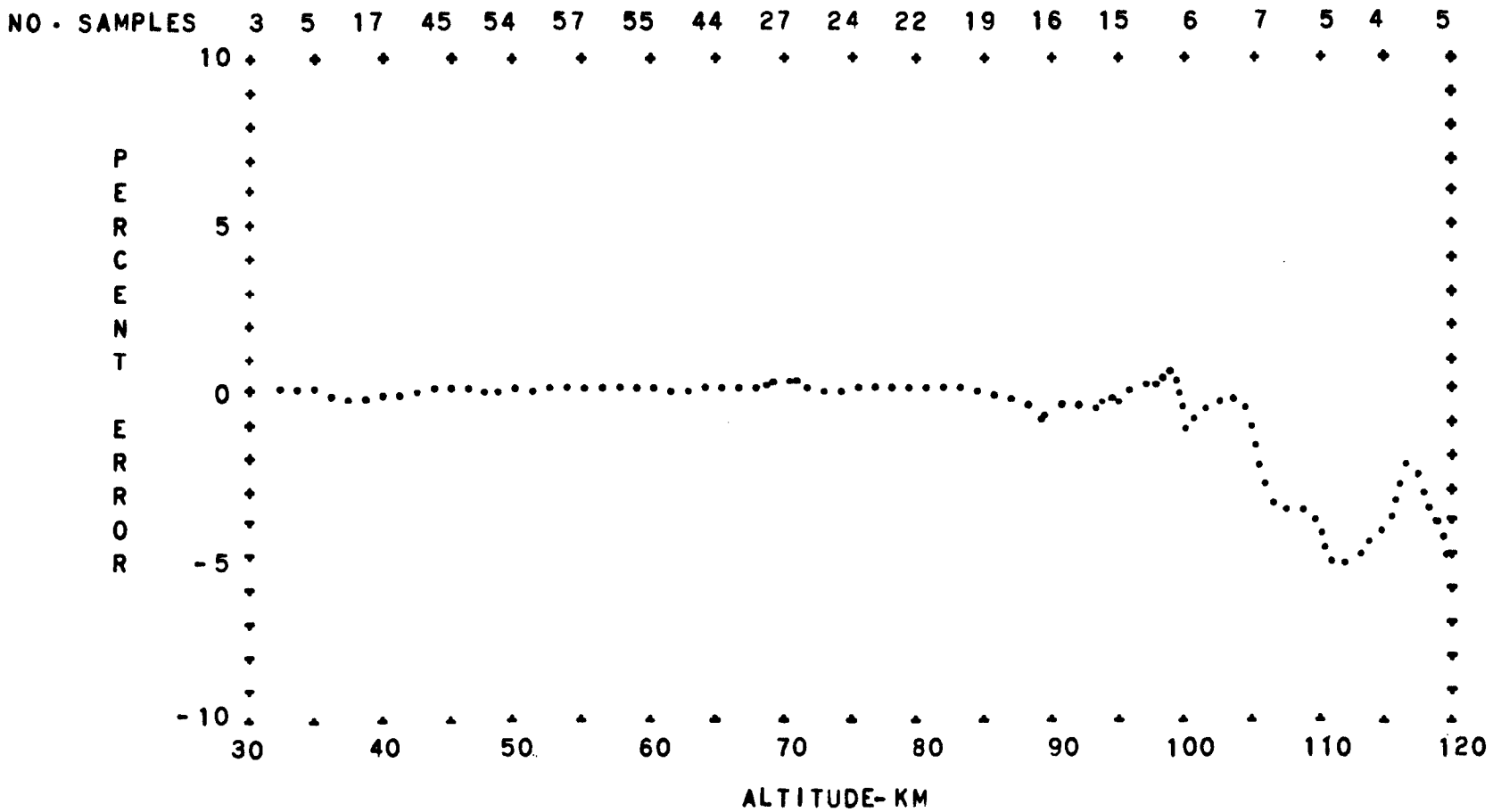

FIG. A-41 PERCENT CONTRIBUTION OF THE COVARIANCE TO THE MEAN PRESSURE OF THE BUELL GAS LAW EQUATION AS A FUNCTION OF ALTITUDE SUBTROPICAL ANNUAL MEAN DIURNAL TRANSITION

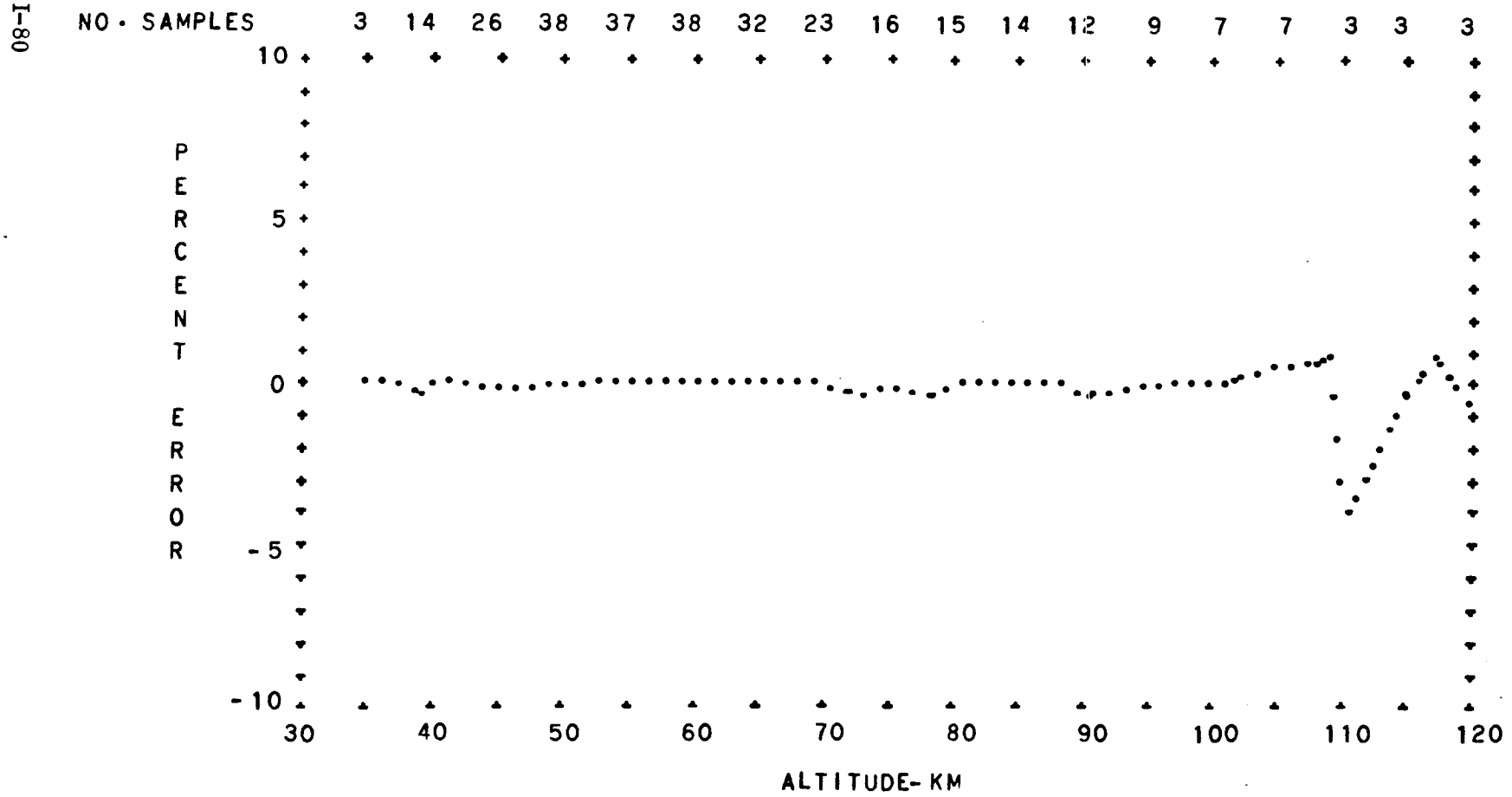

FIG. A-42 PERCENT CONTRIBUTION OF THE COVARIANCE TO THE MEAN PRESSURE OF THE BUELL GAS LAW EQUATION AS A FUNCTION OF ALTITUDE

SUBTROPICAL ANNUAL MEAN DAYTIME

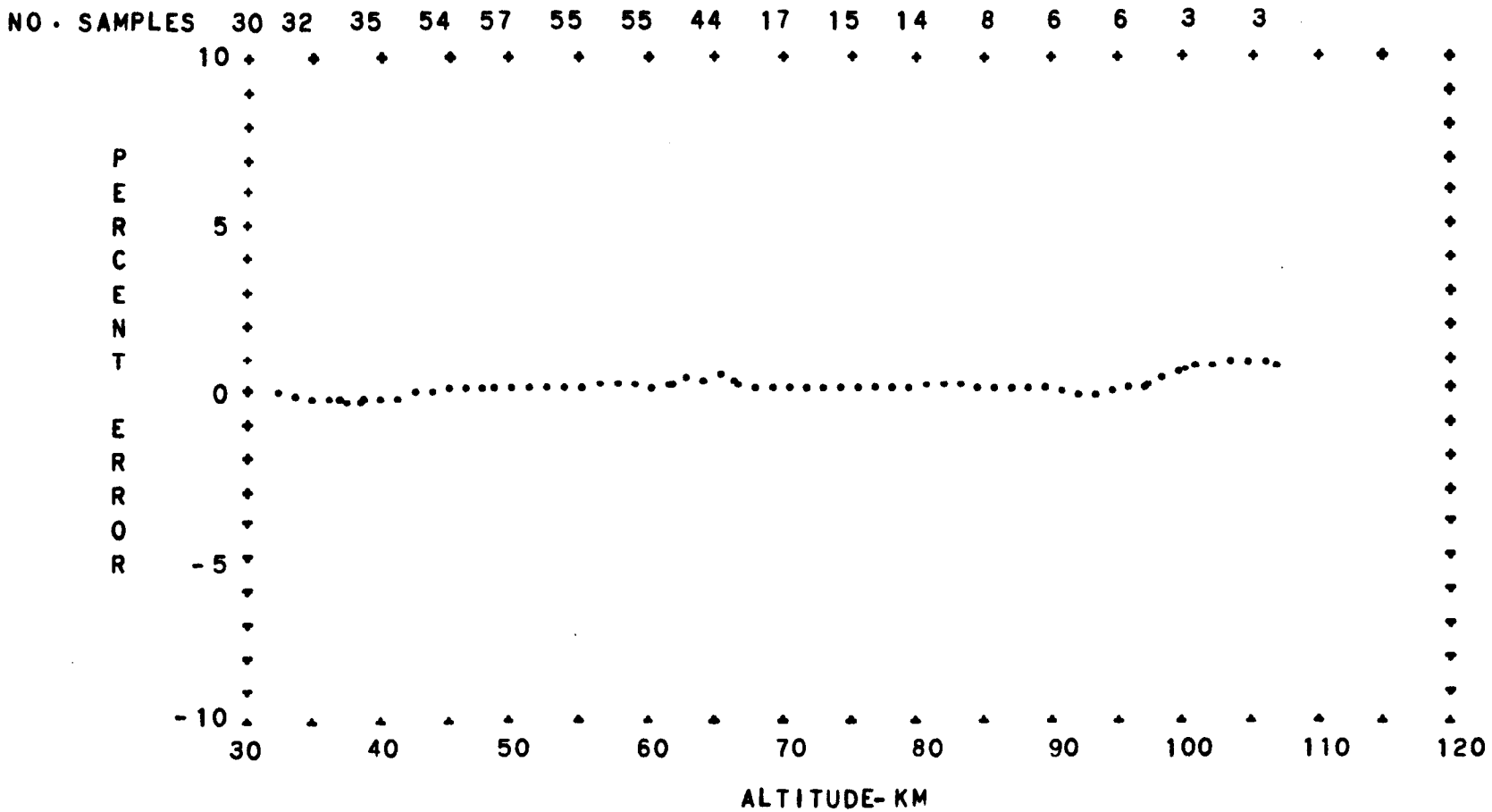

FIG. A-43 PERCENT CONTRIBUTION OF THE COVARIANCE TO THE MEAN PRESSURE OF THE BUELL GAS LAW EQUATION AS A FUNCTION OF ALTITUDE SUBTROPICAL ANNUAL MEAN NIGHTTIME

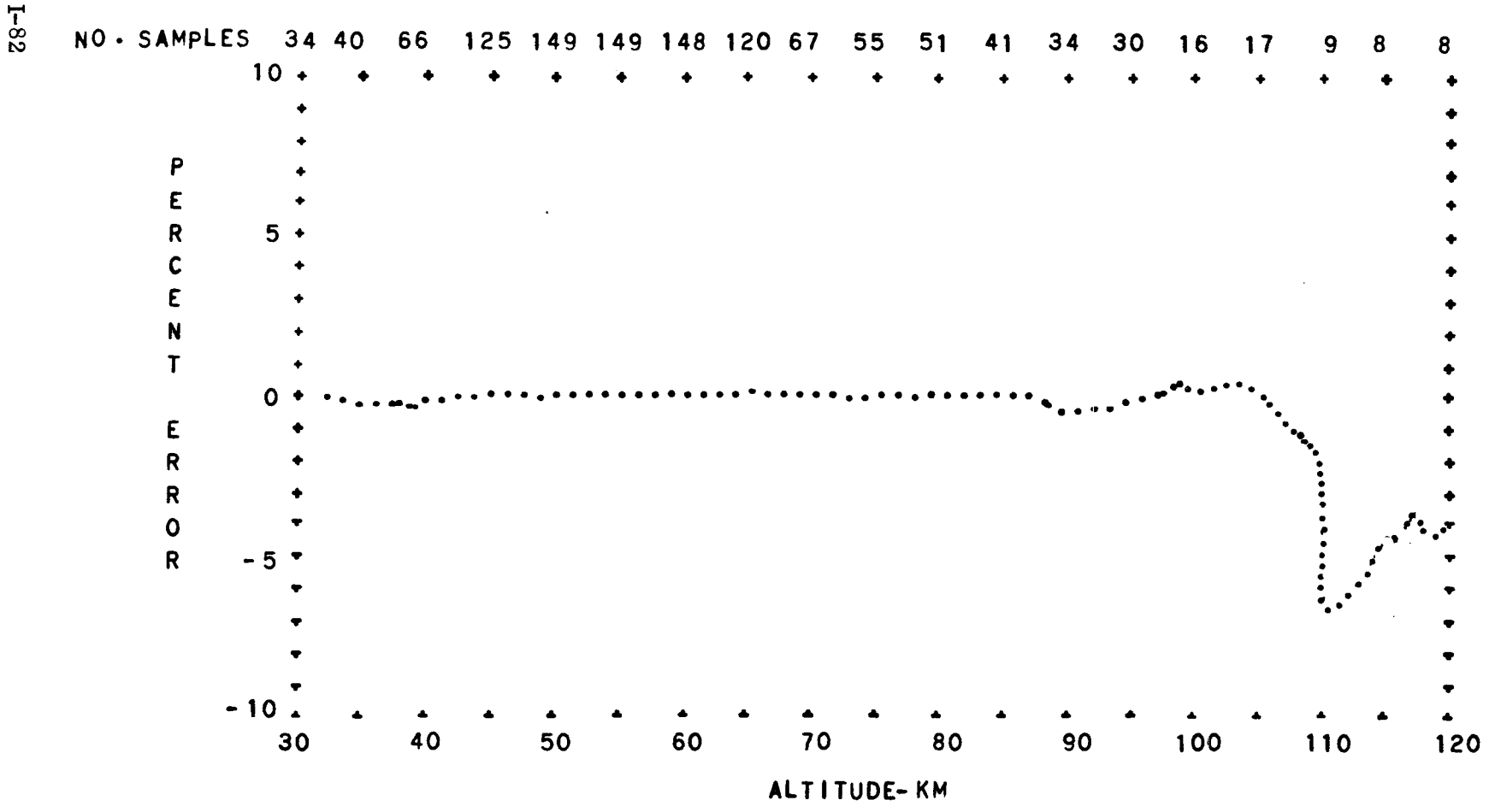

FIG. A-44 PERCENT CONTRIBUTION OF THE COVARIANCE TO THE MEAN PRESSURE OF THE BUELL GAS LAW EQUATION AS A FUNCTION OF ALTITUDE

SUBTROPICAL ANNUAL MEAN DIURNAL MEAN

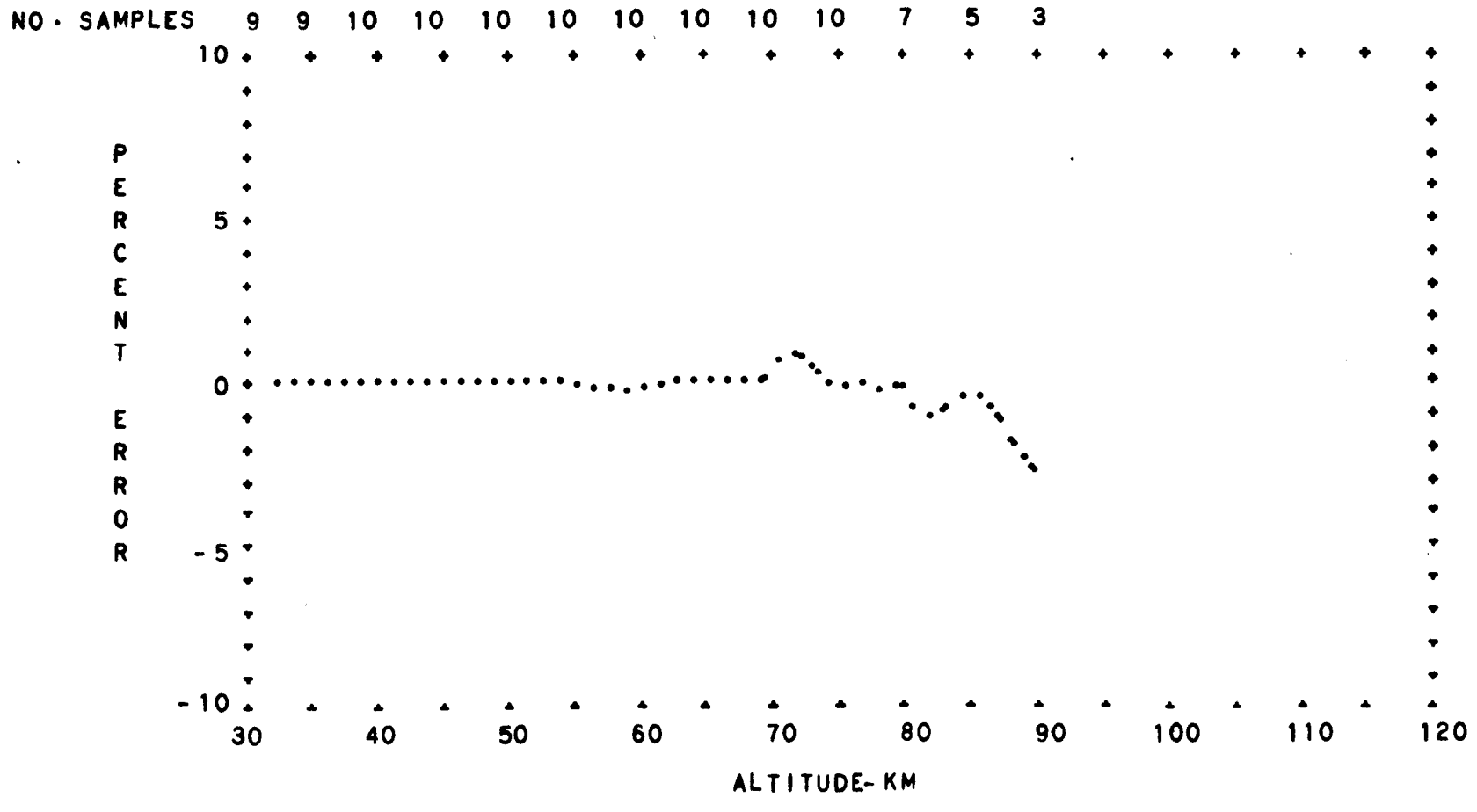

FIG. A-45 PERCENT CONTRIBUTION OF THE COVARIANCE TO THE MEAN PRESSURE OF THE BUELL GAS LAW EQUATION AS A FUNCTION OF ALTITUDE MIDLATITUDE SPRING DIURNAL TRANSITION

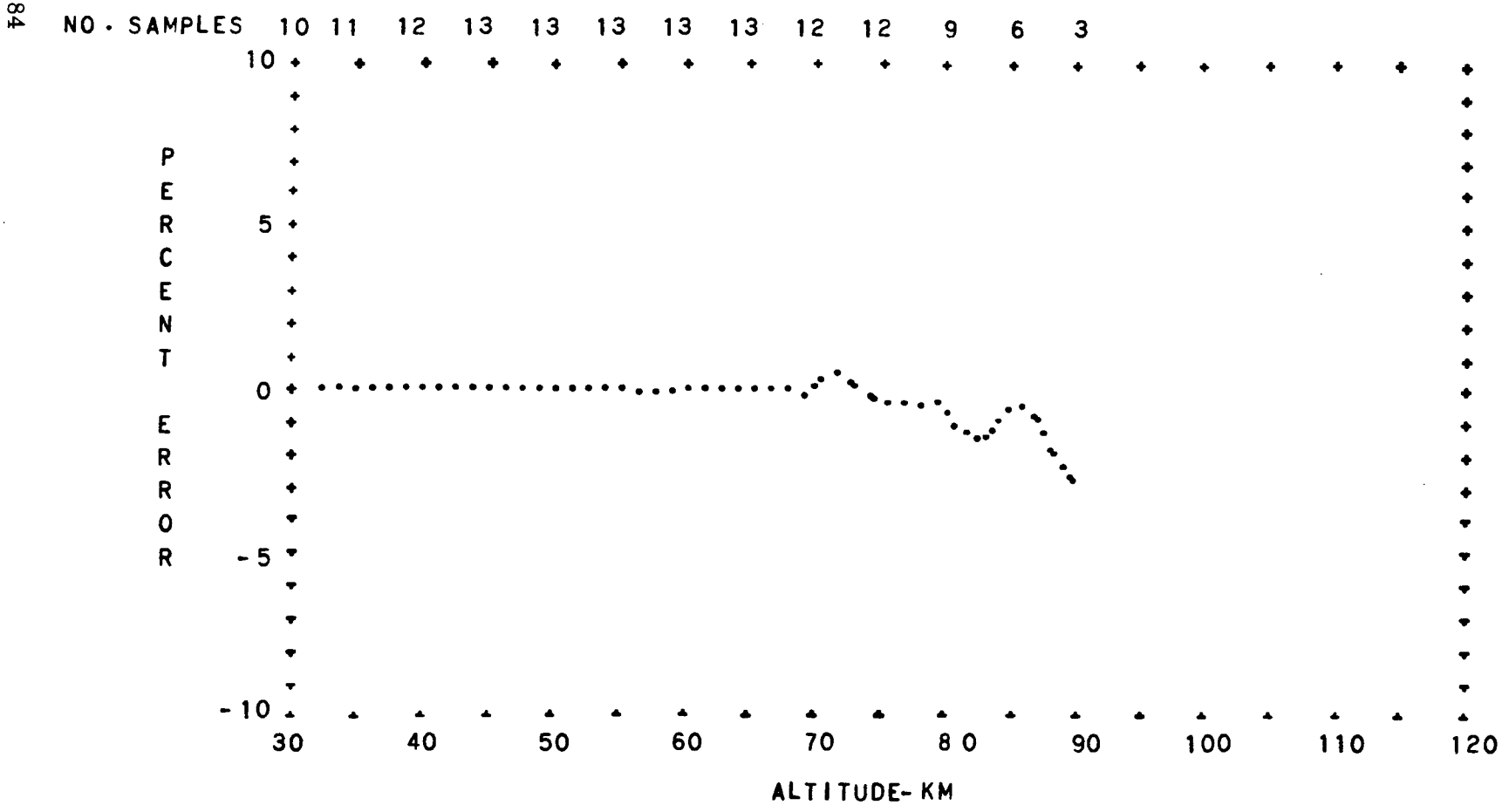

FIG. A-46 PERCENT CONTRIBUTION OF THE COVARIANCE TO THE MEAN PRESSURE OF THE BUELL GAS LAW EQUATION AS A FUNCTION OF ALTITUDE

MIDLATITUDE SPRING DIURNAL MEAN

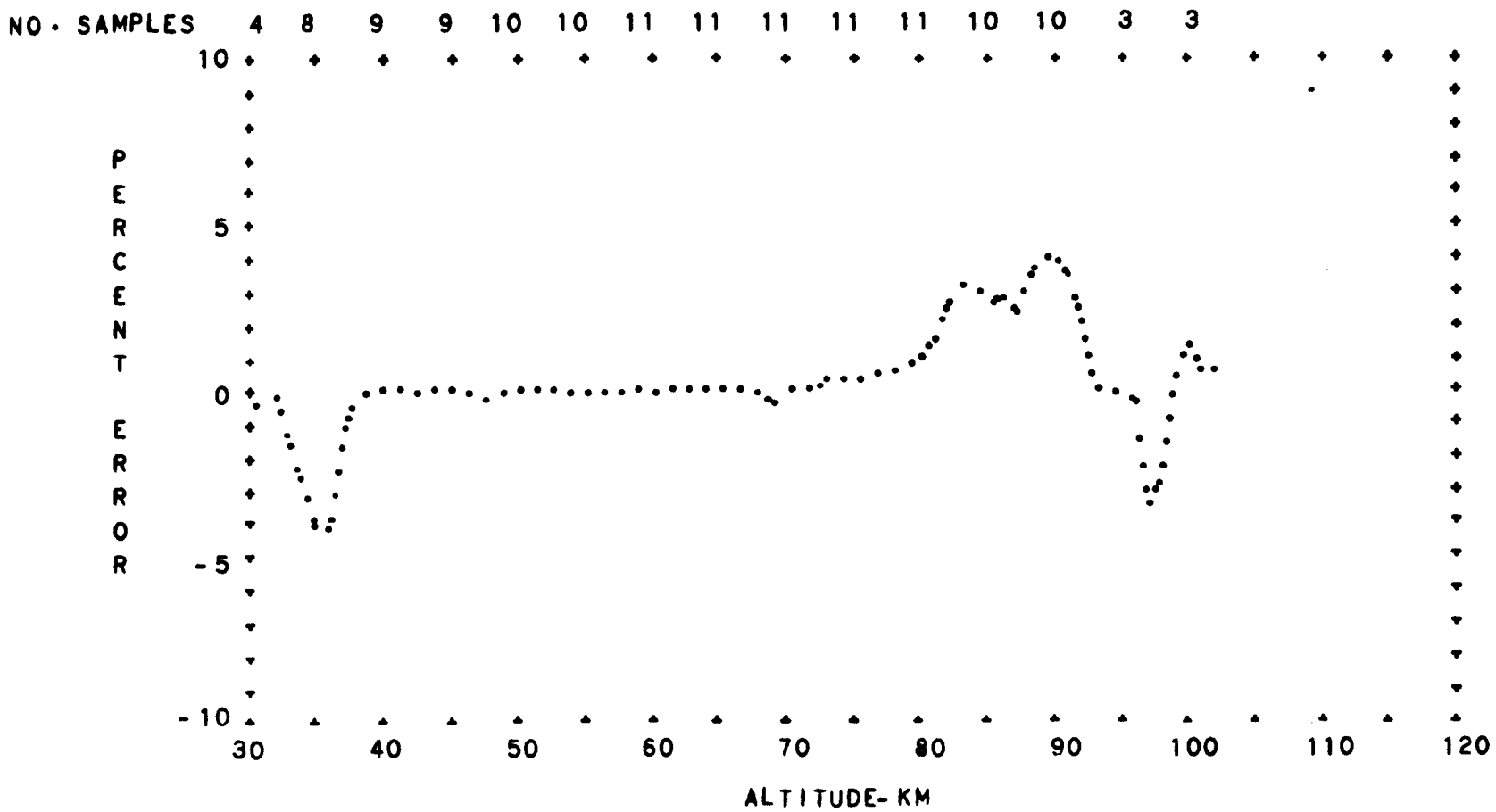

FIG. A-47 PERCENT CONTRIBUTION OF THE COVARIANCE TO THE MEAN PRESSURE OF THE BUELL GAS LAW EQUATION AS A FUNCTION OF ALTITUDE MIDLATITUDE SUMMER DIURNAL TRANSITION

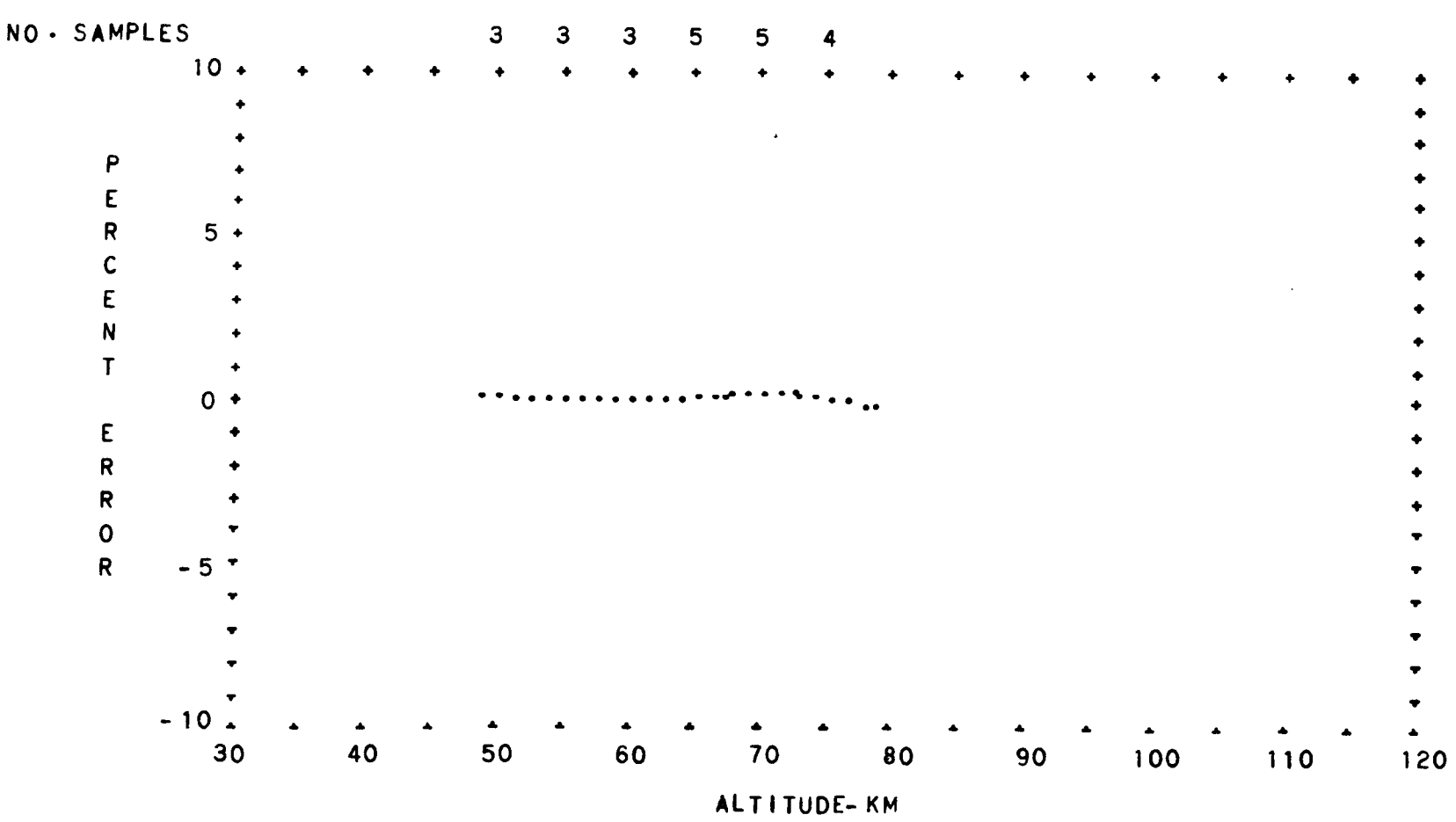

FIG. A-48 PERCENT CONTRIBUTION OF THE COVARIANCE TO THE MEAN PRESSURE OF THE BUELL GAS LAW EQUATION AS A FUNCTION OF ALTITUDE

MIDLATITUDE SUMMER DAYTIME

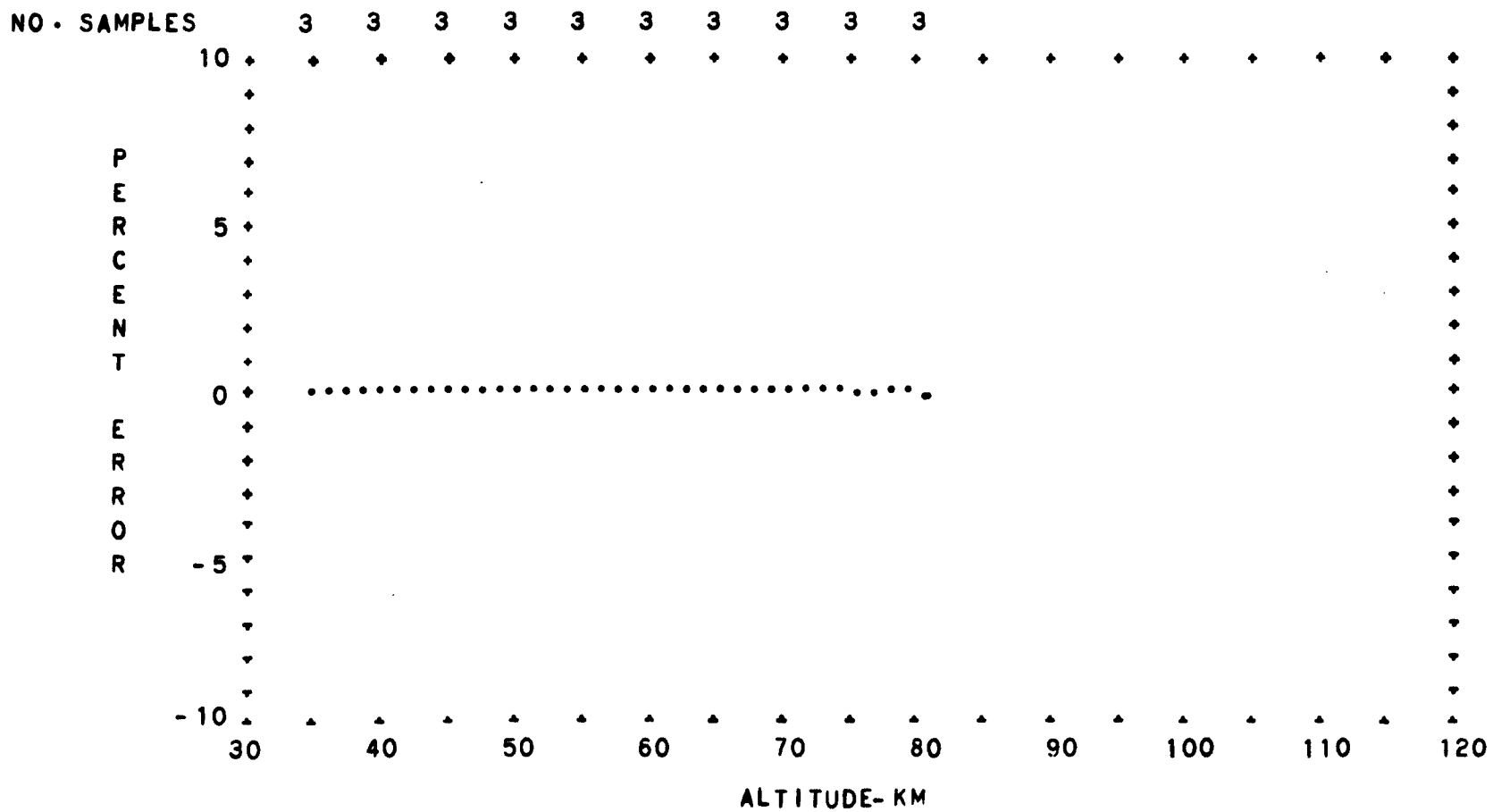

FIG. A-49 PERCENT CONTRIBUTION OF THE COVARIANCE TO THE MEAN PRESSURE OF THE BUELL GAS LAW EQUATION AS A FUNCTION OF ALTITUDE

MIDLATITUDE SUMMER NIGHTTIME

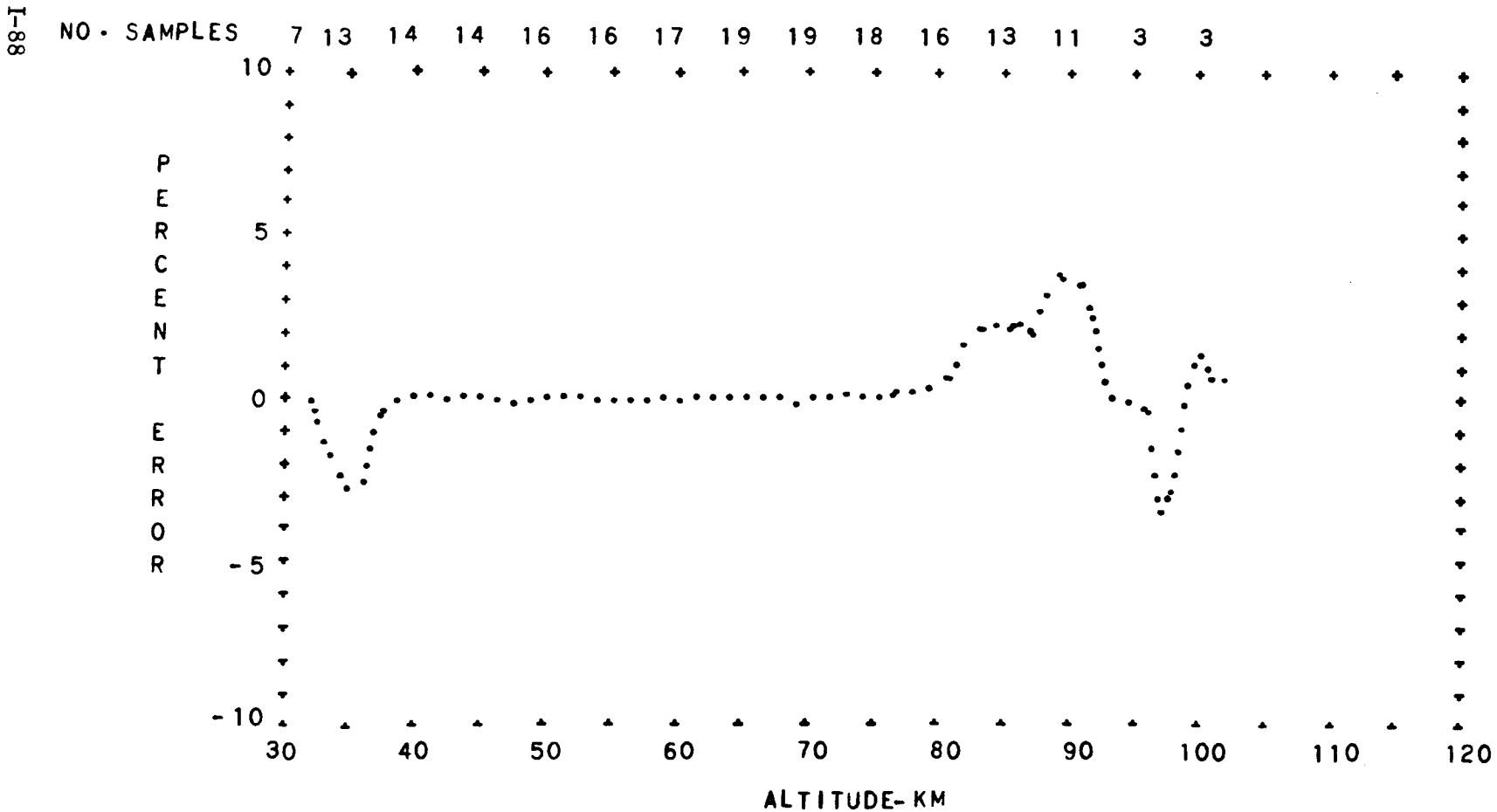

FIG. A-50 PERCENT CONTRIBUTION OF THE COVARIANCE TO THE MEAN PRESSURE OF THE BUELL GAS LAW EQUATION AS A FUNCTION OF ALTITUDE

MIDLATITUDE SUMMER DIURNAL MEAN

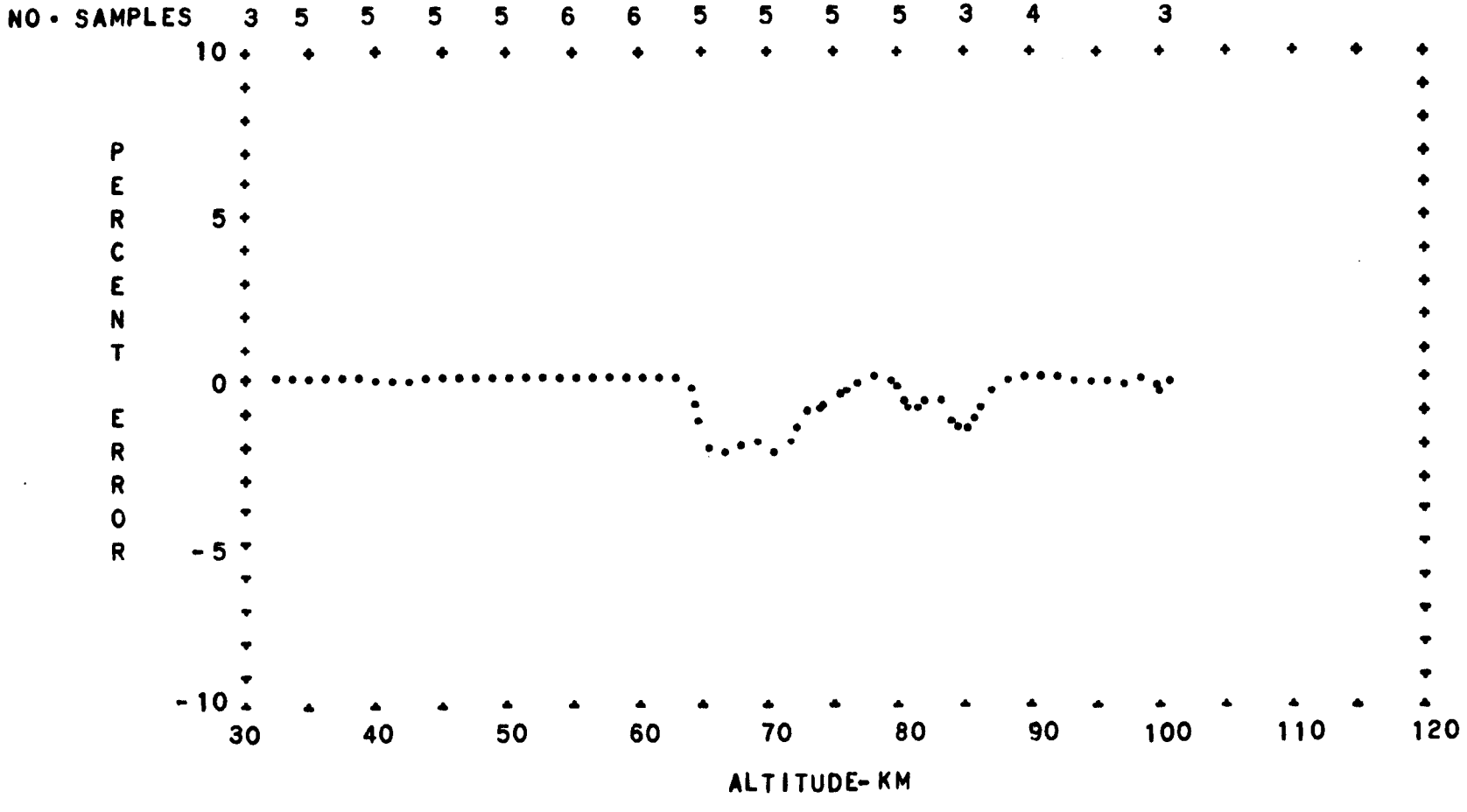

FIG. A-51 PERCENT CONTRIBUTION OF THE COVARIANCE TO THE MEAN PRESSURE OF THE BUELL GAS LAW EQUATION AS A FUNCTION OF ALTITUDE

MIDLATITUDE AUTUMN DIURNAL TRANSITION

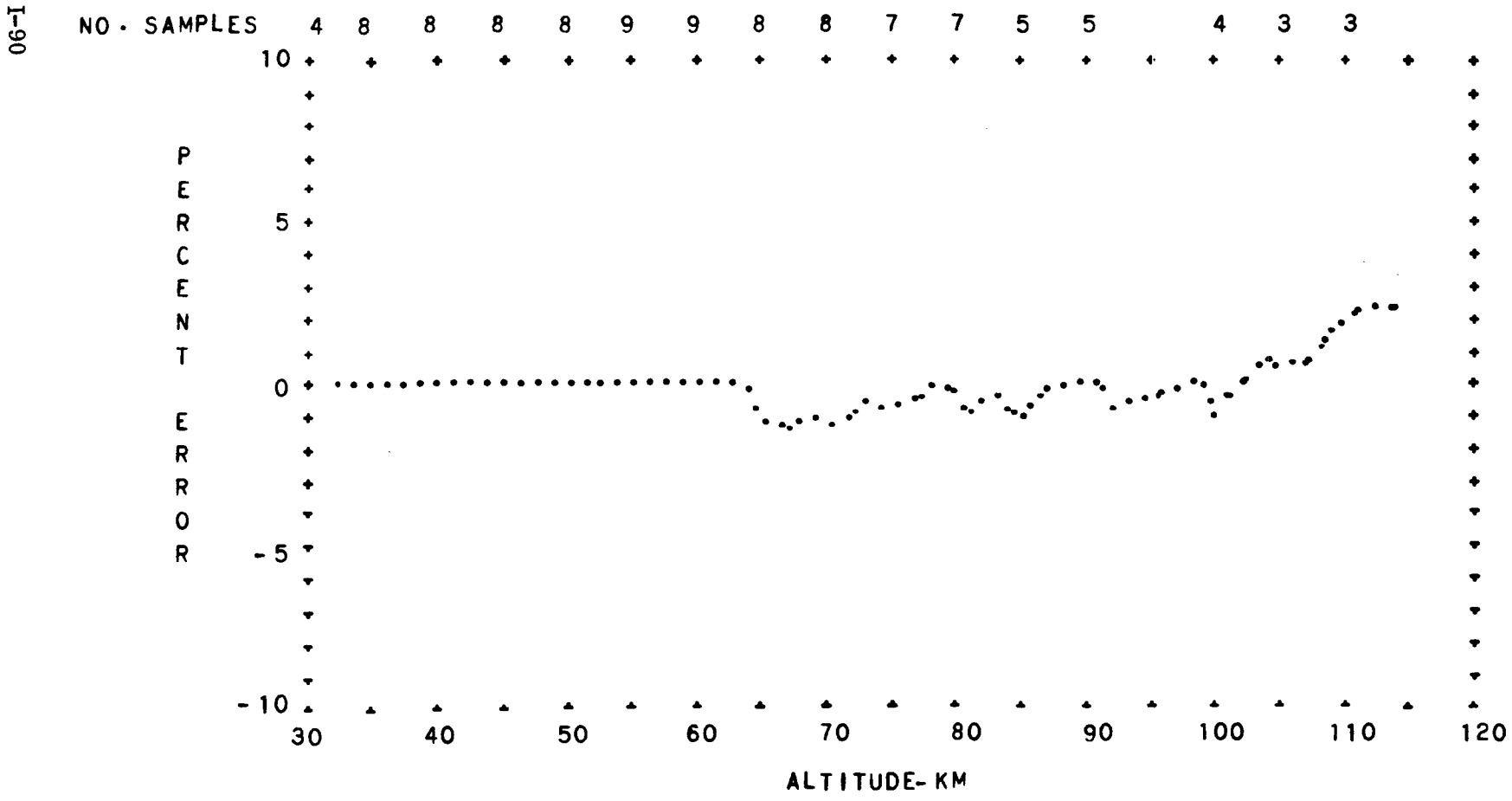

FIG. A-52 PERCENT CONTRIBUTION OF THE COVARIANCE TO THE MEAN PRESSURE OF THE BUELL GAS LAW EQUATION AS A FUNCTION OF ALTITUDE

MIDLATITUDE AUTUMN DIURNAL MEAN

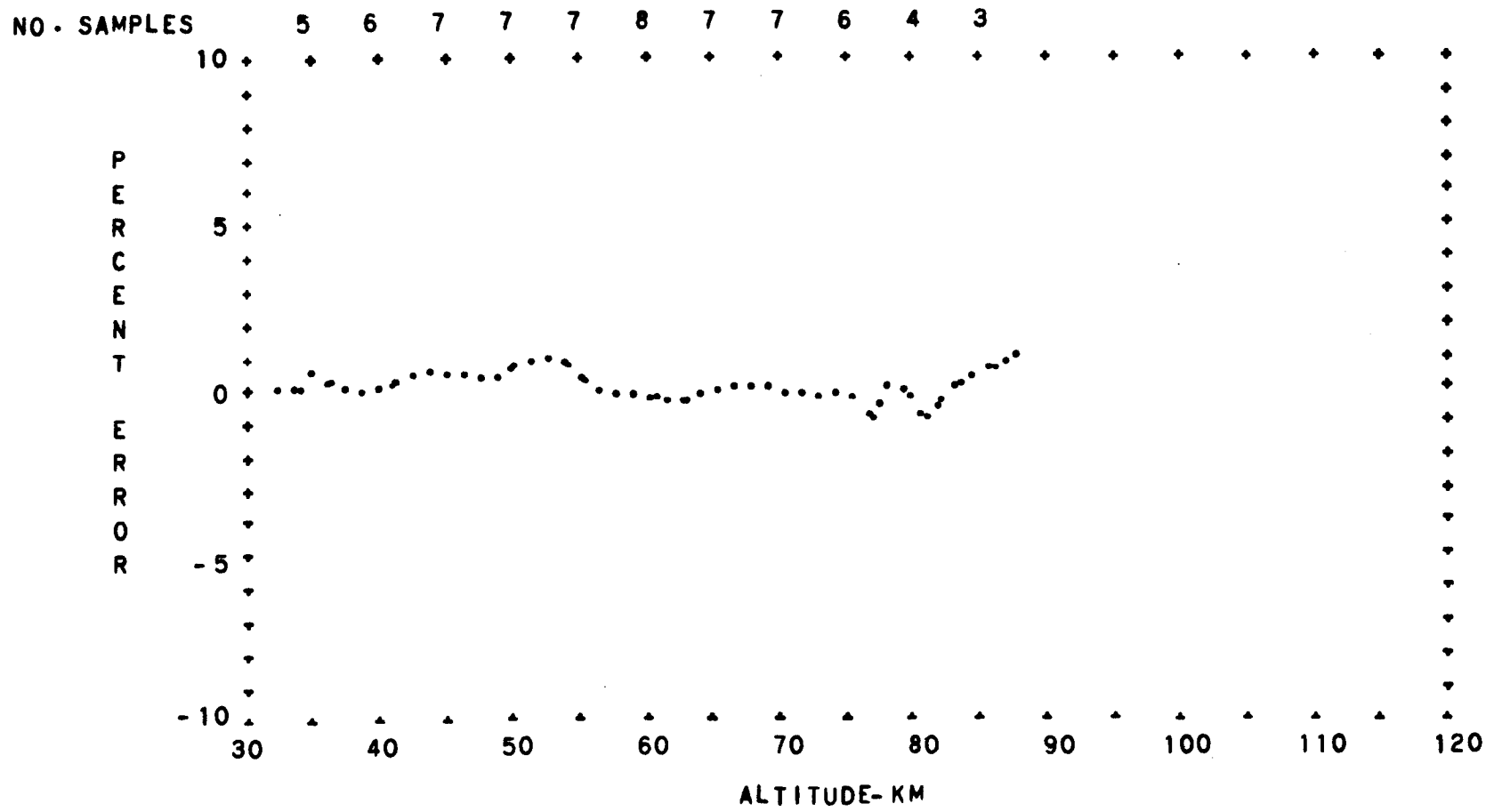

FIG. A-53 PERCENT CONTRIBUTION OF THE COVARIANCE TO THE MEAN PRESSURE OF THE BUELL GAS LAW EQUATION AS A FUNCTION OF ALTITUDE MIDLATITUDE WINTER DIURNAL TRANSITION

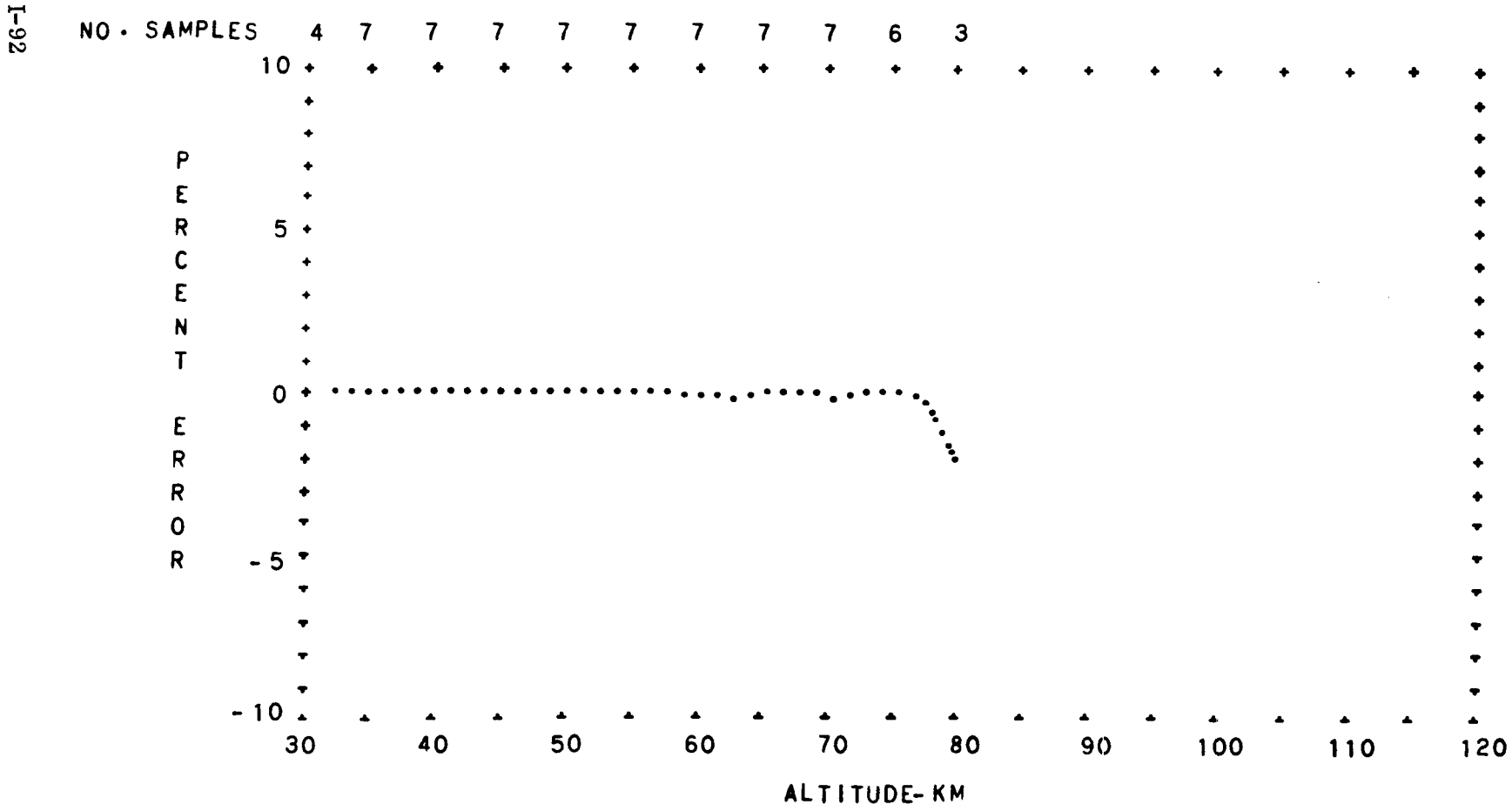

FIG. A-54 PERCENT CONTRIBUTION OF THE COVARIANCE TO THE MEAN PRESSURE OF THE BUELL GAS LAW EQUATION AS A FUNCTION OF ALTITUDE

MIDLATITUDE WINTER NIGHTTIME

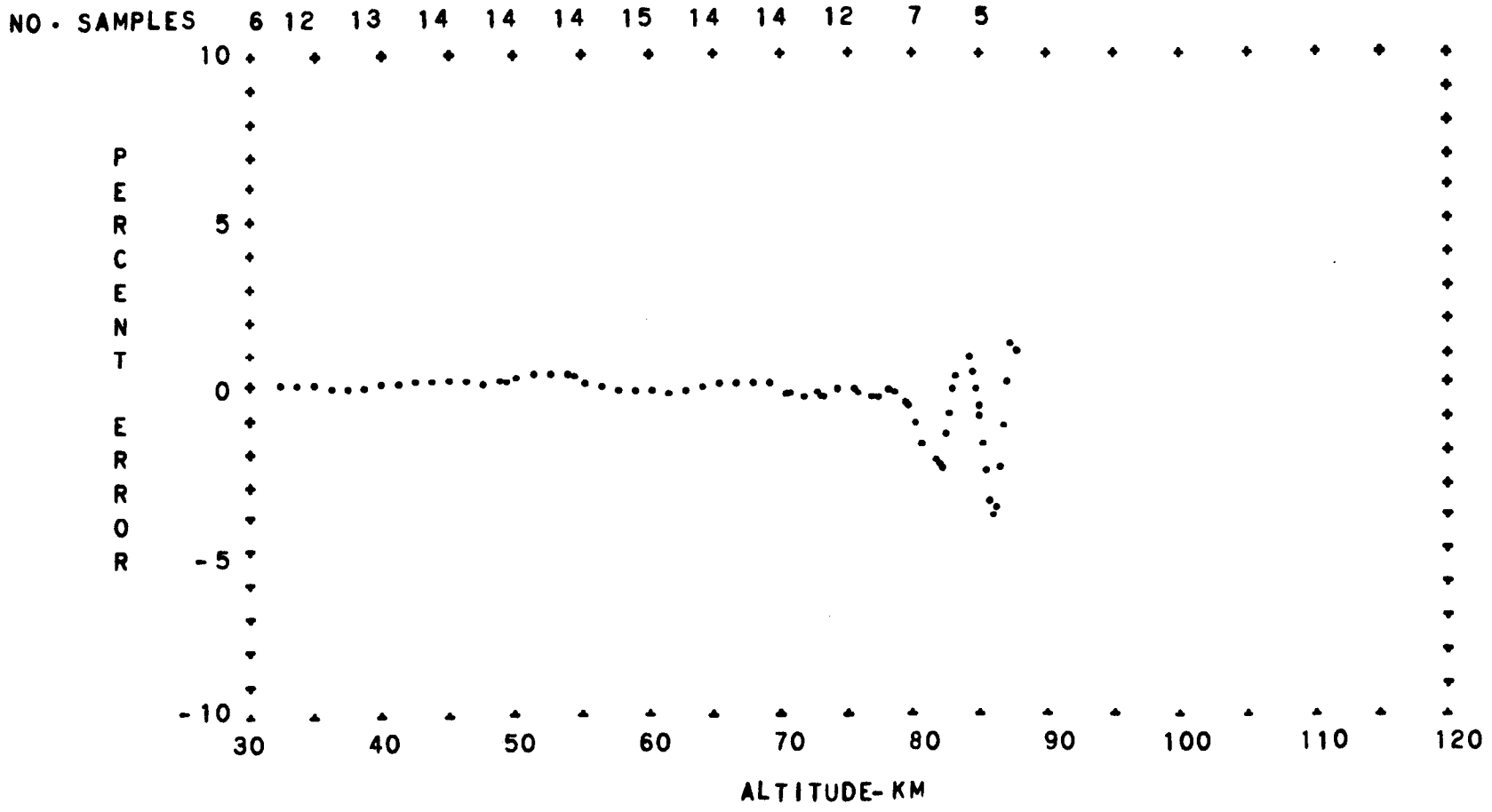

FIG. A-55 PERCENT CONTRIBUTION OF THE COVARIANCE TO THE MEAN PRESSURE OF THE BUELL GAS LAW EQUATION AS A FUNCTION OF ALTITUDE

MIDLATITUDE WINTER DIURNAL MEAN

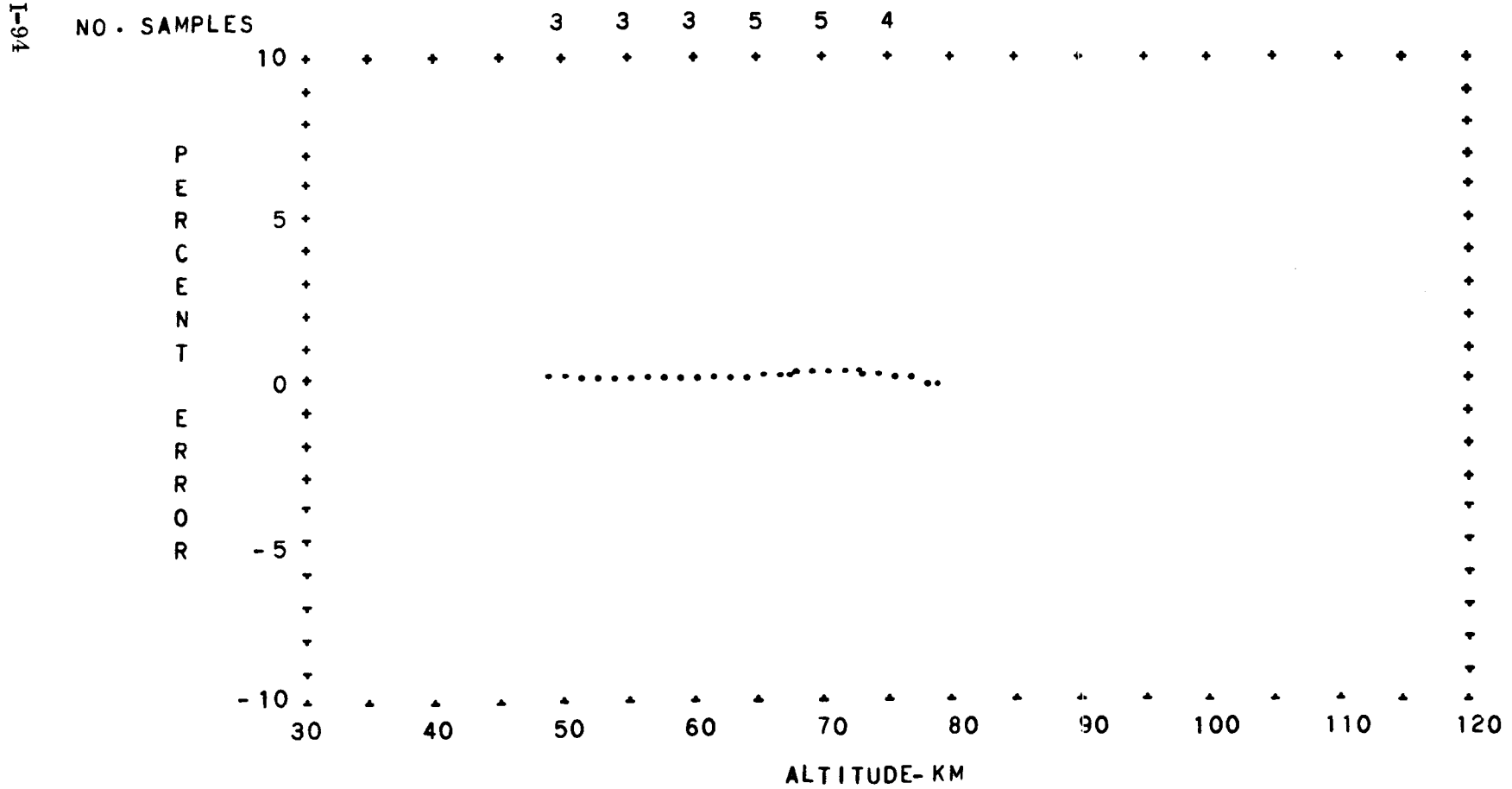

FIG. A-56 PERCENT CONTRIBUTION OF THE COVARIANCE TO THE MEAN PRESSURE OF THE BUELL GAS LAW EQUATION AS A FUNCTION OF ALTITUDE

MIDLATITUDE SUMMER EXTREME DAYTIME

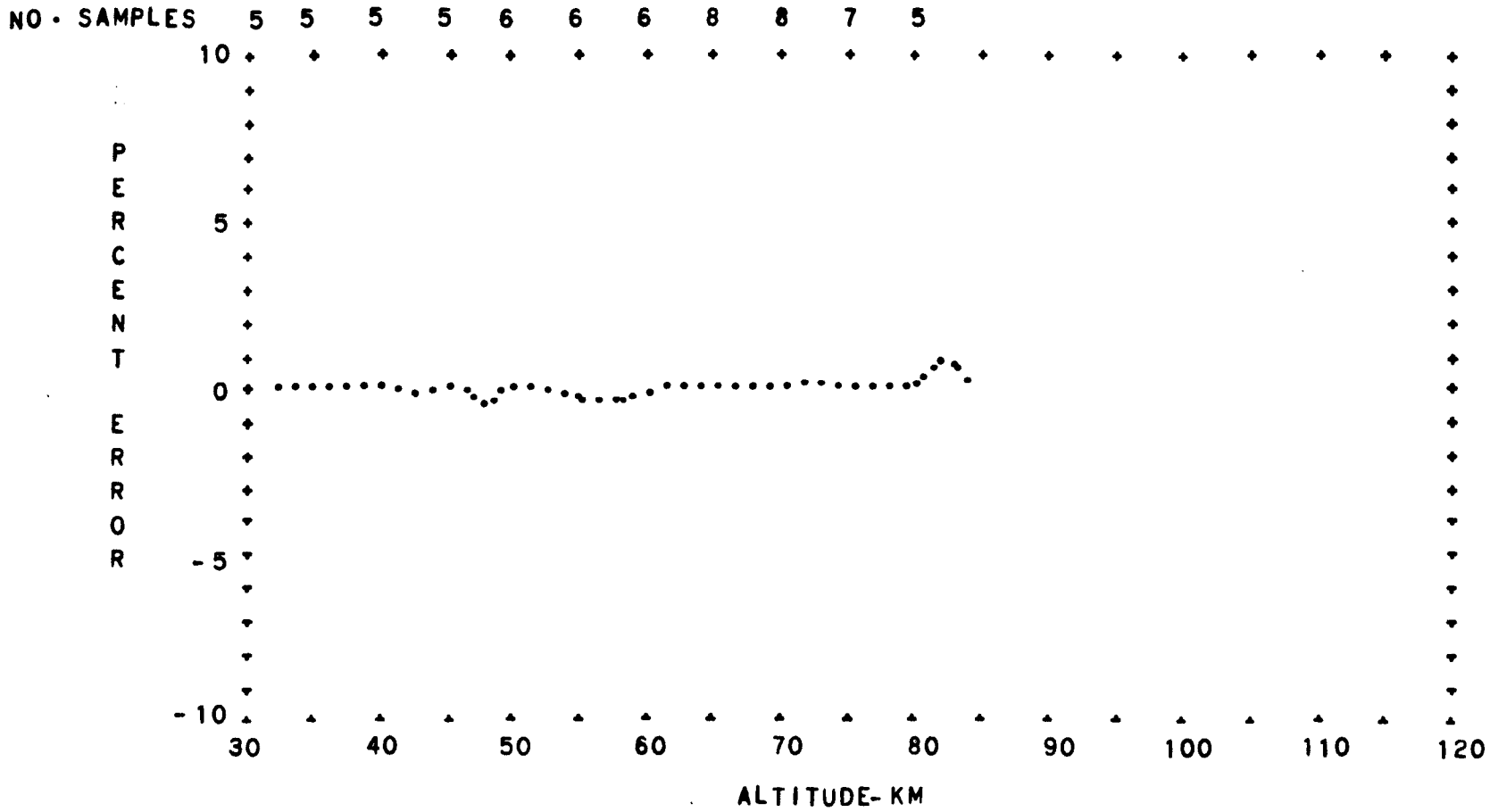

FIG. A-57 PERCENT CONTRIBUTION OF THE COVARIANCE TO THE MEAN PRESSURE OF THE BUELL GAS LAW EQUATION AS A FUNCTION OF ALTITUDE

MIDLATITUDE SUMMER EXTREME DIURNAL MEAN

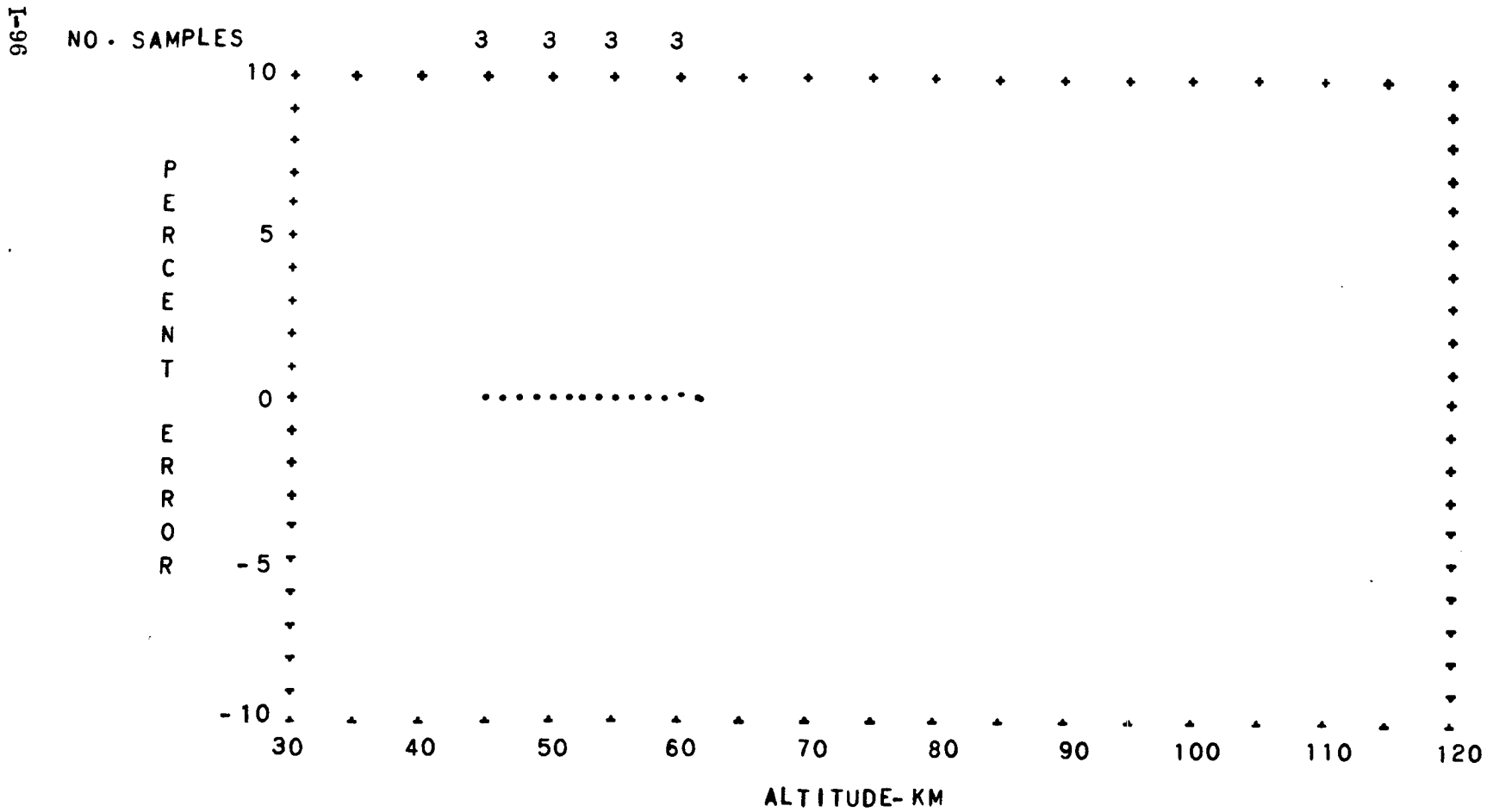

FIG. A-58 PERCENT CONTRIBUTION OF THE COVARIANCE TO THE MEAN PRESSURE OF THE BUELL GAS LAW EQUATION AS A FUNCTION OF ALTITUDE

MIDLATITUDE WINTER EXTREME DIURNAL MEAN

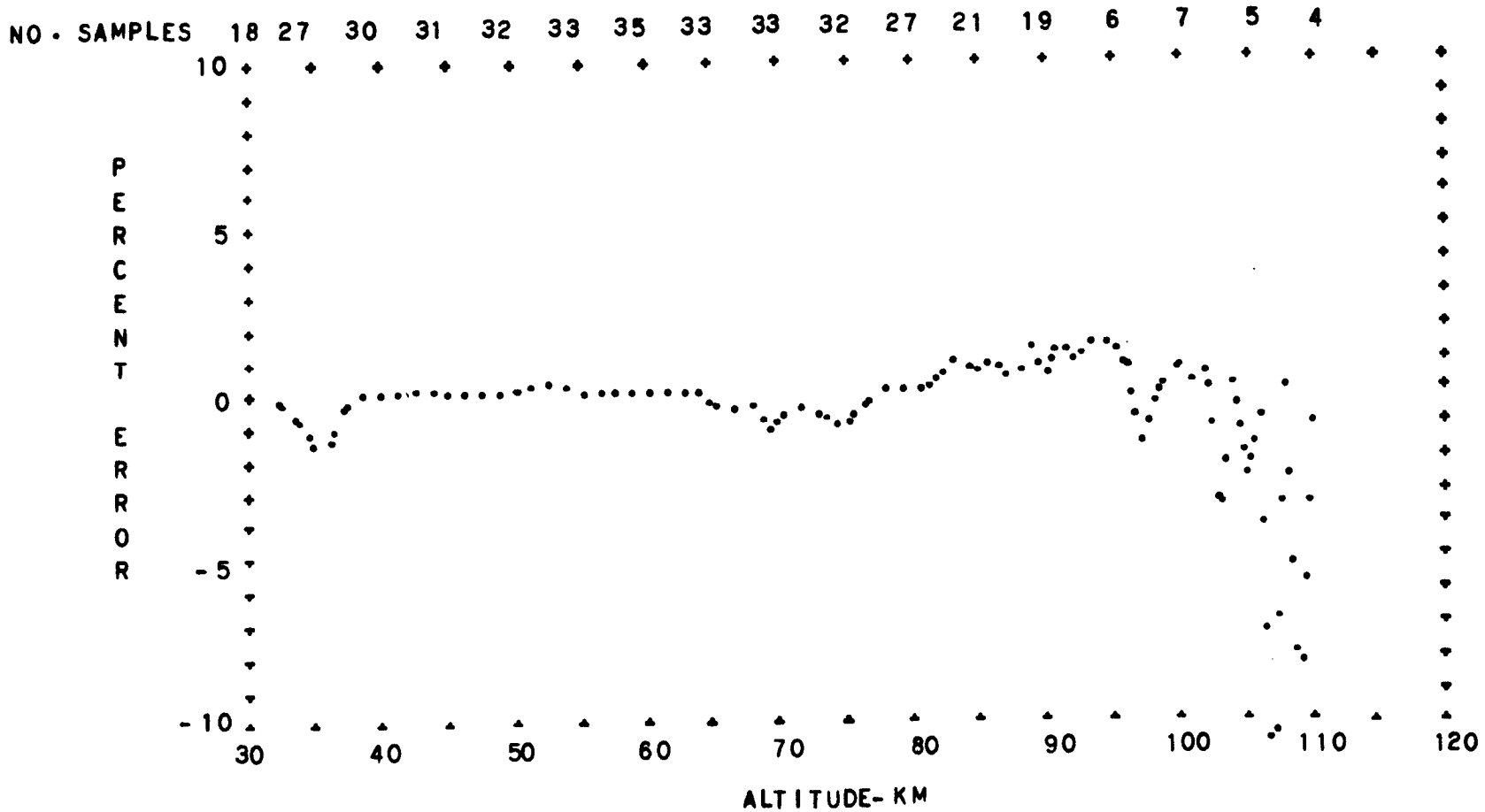

FIG. A-59 PERCENT CONTRIBUTION OF THE COVARIANCE TO THE MEAN PRESSURE OF THE BUELL GAS LAW EQUATION AS A FUNCTION OF ALTITUDE

MIDLATITUDE ANNUAL MEAN DIURNAL TRANSITION

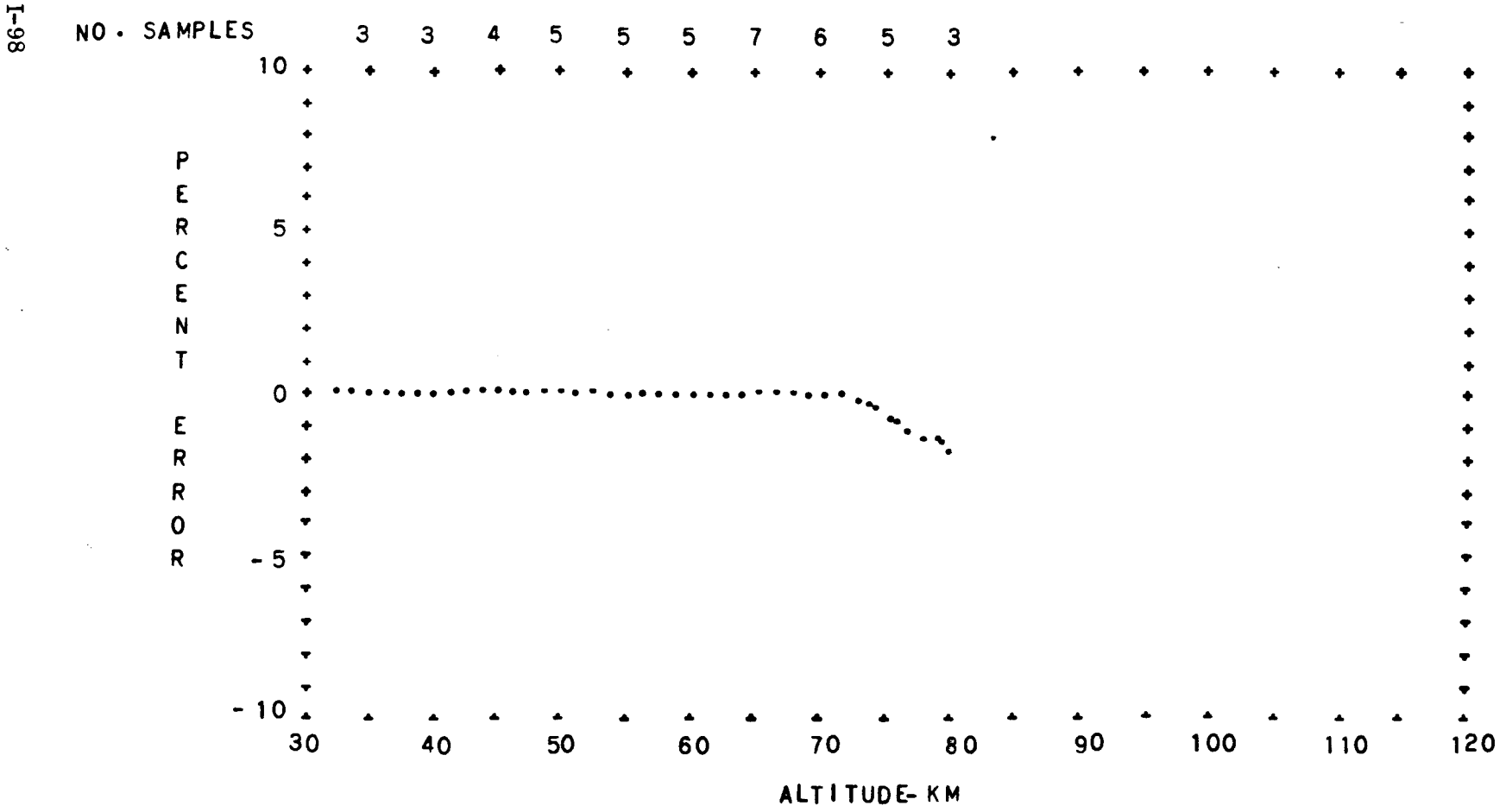

FIG. A-60 PERCENT CONTRIBUTION OF THE COVARIANCE TO THE MEAN PRESSURE OF THE BUELL GAS LAW EQUATION AS A FUNCTION OF ALTITUDE

MIDLATITUDE ANNUAL MEAN DAYTIME

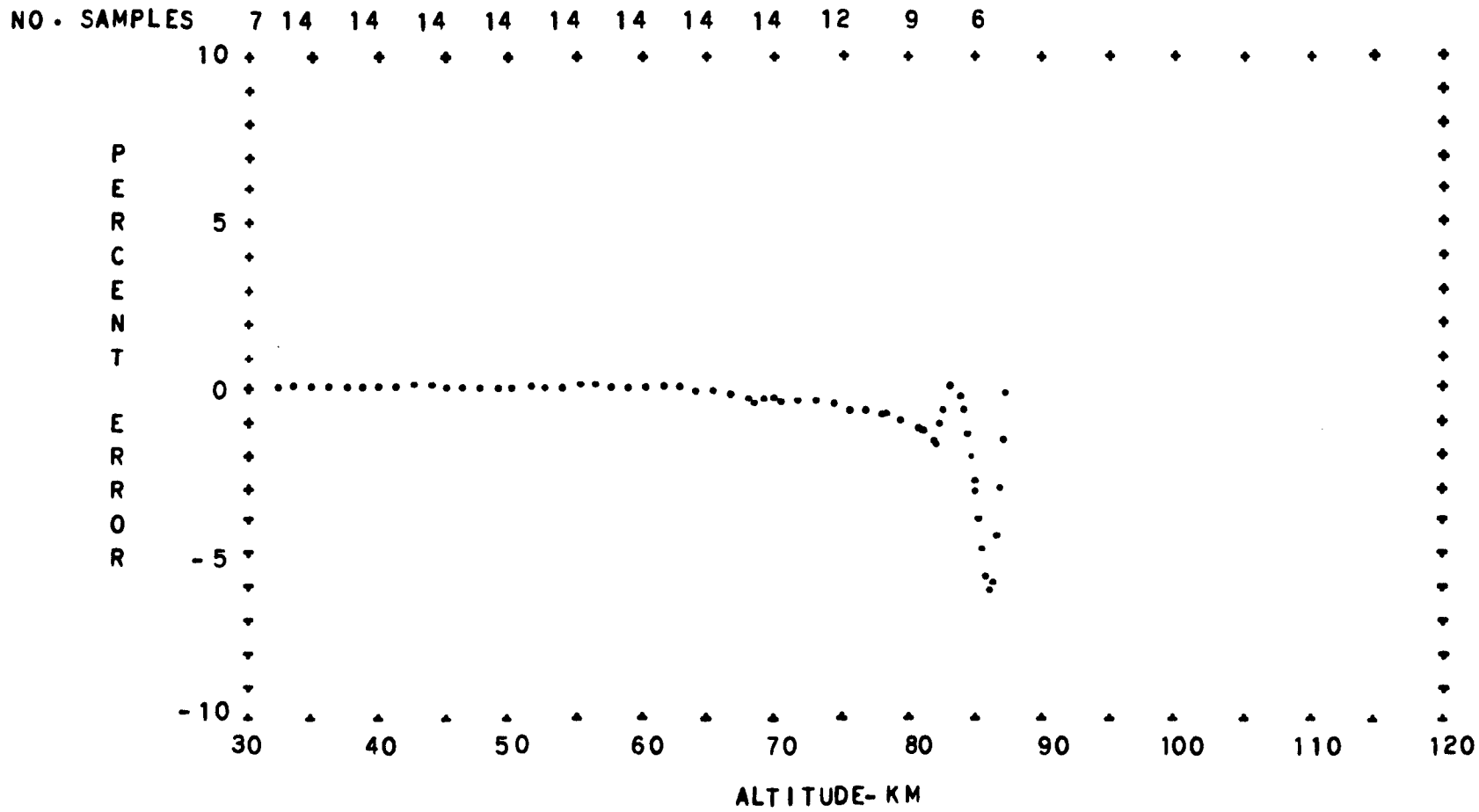

FIG. A-61 PERCENT CONTRIBUTION OF THE COVARIANCE TO THE MEAN PRESSURE OF THE BUELL GAS LAW EQUATION AS A FUNCTION OF ALTITUDE

MIDLATITUDE ANNUAL MEAN NIGHTTIME

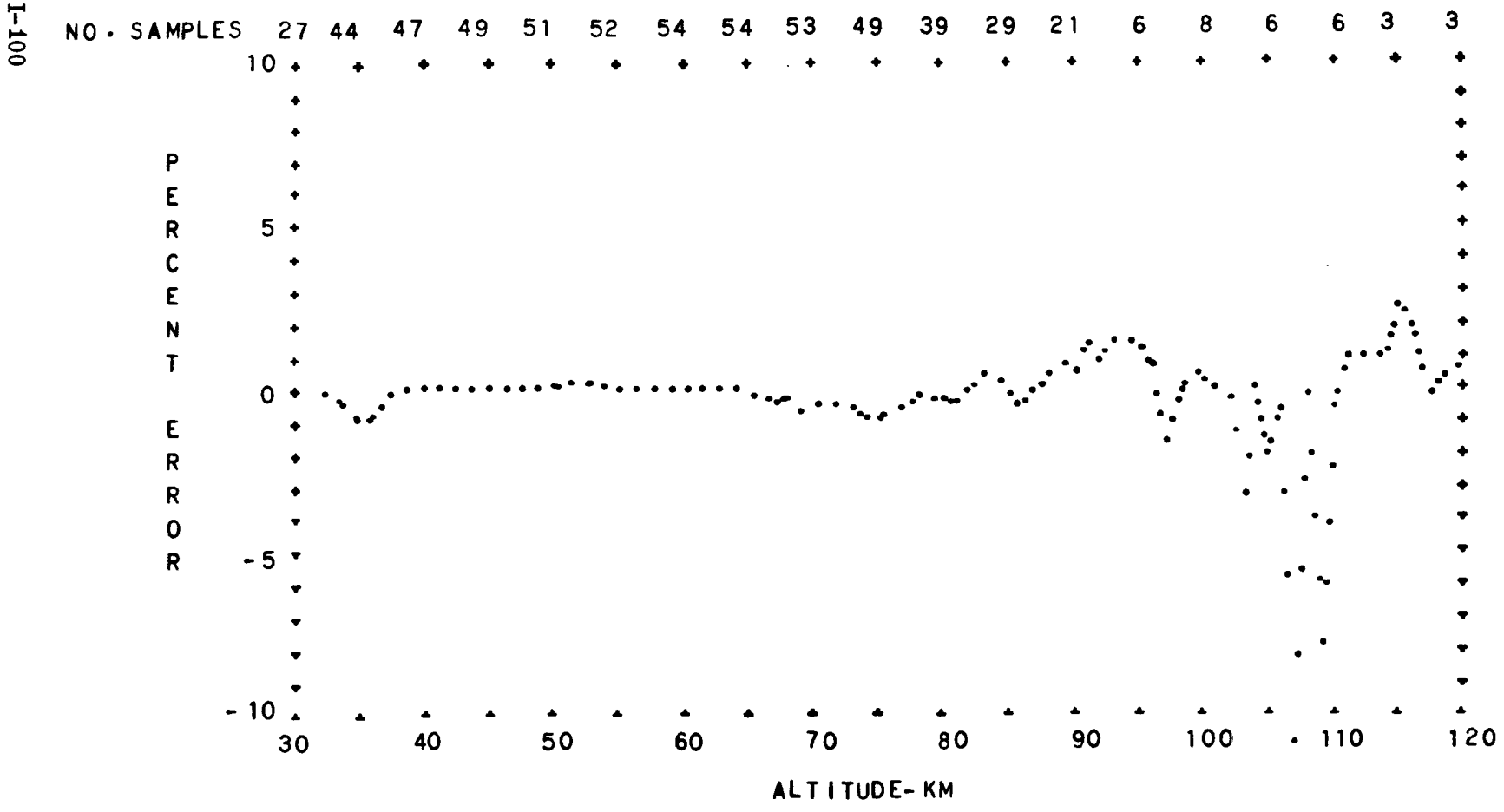

FIG. A-62 PERCENT CONTRIBUTION OF THE COVARIANCE TO THE MEAN PRESSURE OF THE BUELL GAS LAW EQUATION AS A FUNCTION OF ALTITUDE

MIDLATITUDE ANNUAL MEAN DIURNAL MEAN

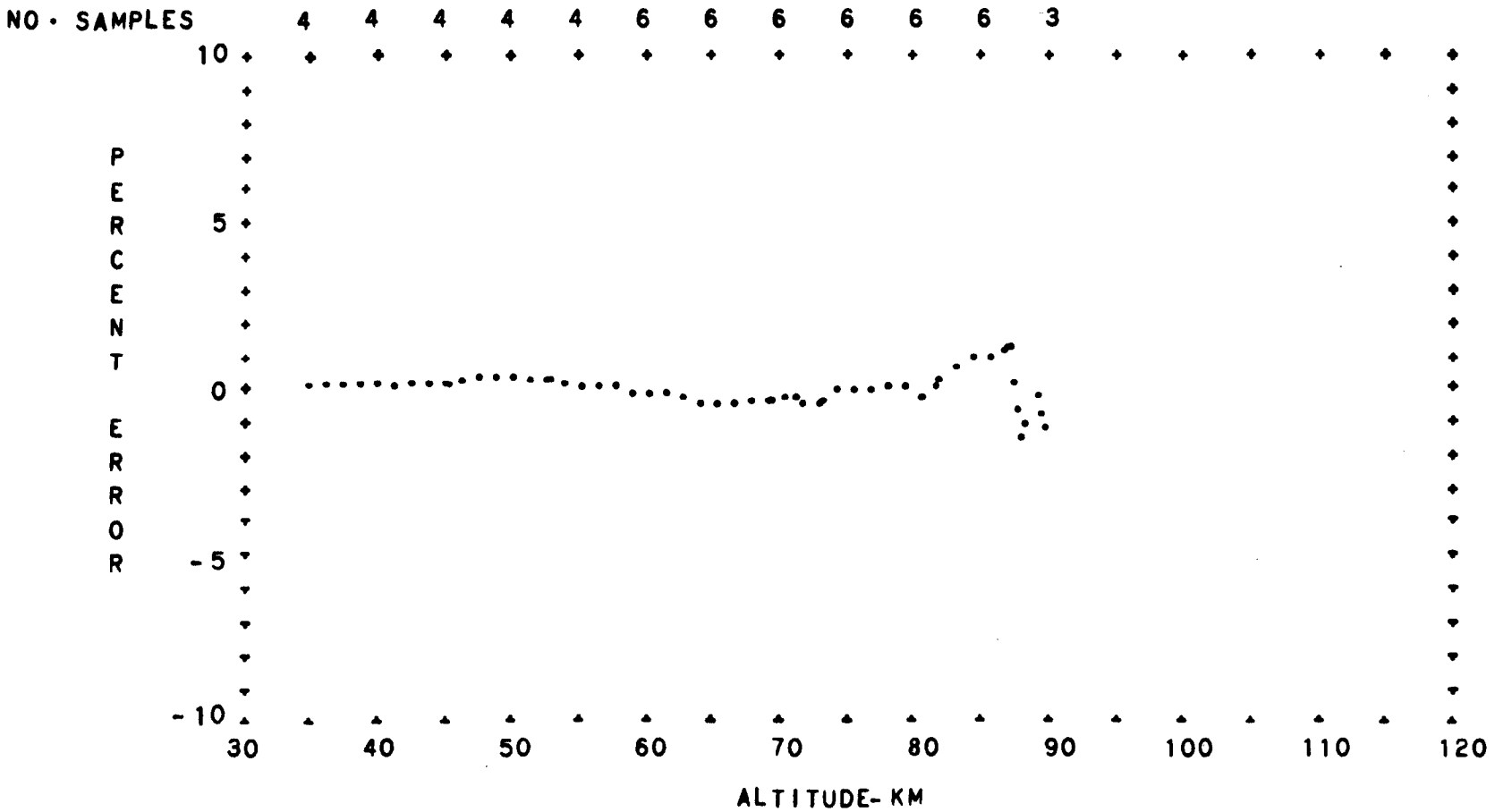

FIG. A-63 PERCENT CONTRIBUTION OF THE COVARIANCE TO THE MEAN PRESSURE OF THE BUELL GAS LAW EQUATION AS A FUNCTION OF ALTITUDE SUBARCTIC SPRING DIURNAL TRANSITION

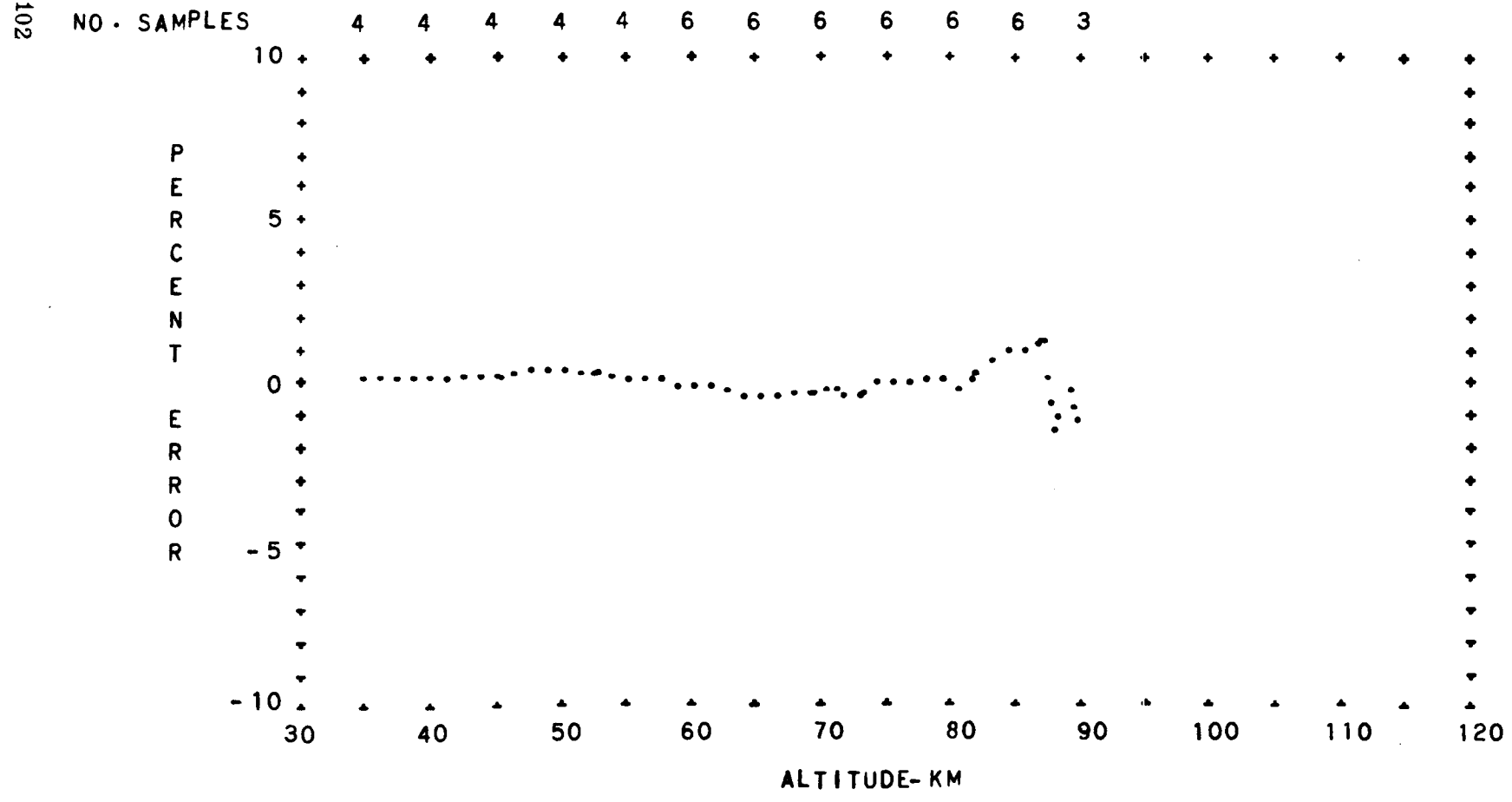

FIG. A-64 PERCENT CONTRIBUTION OF THE COVARIANCE TO THE MEAN PRESSURE OF THE BUELL GAS LAW EQUATION AS A FUNCTION OF ALTITUDE

SUBARCTIC SPRING DIURNAL MEAN

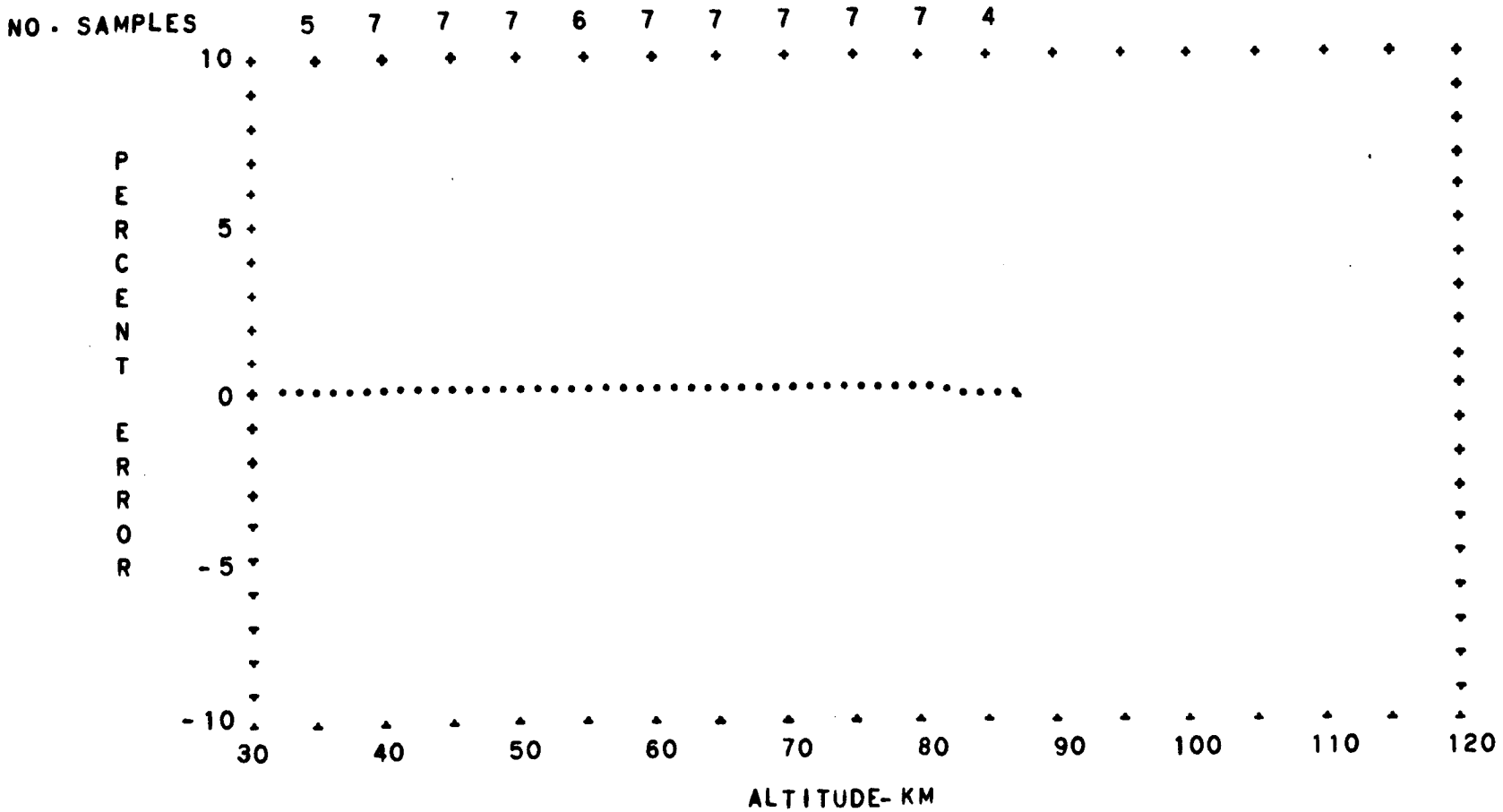

FIG. A-65 PERCENT CONTRIBUTION OF THE COVARIANCE TO THE MEAN PRESSURE OF THE BUELL GAS LAW EQUATION AS A FUNCTION OF ALTITUDE

SUBARCTIC SUMMER DIURNAL TRANSITION

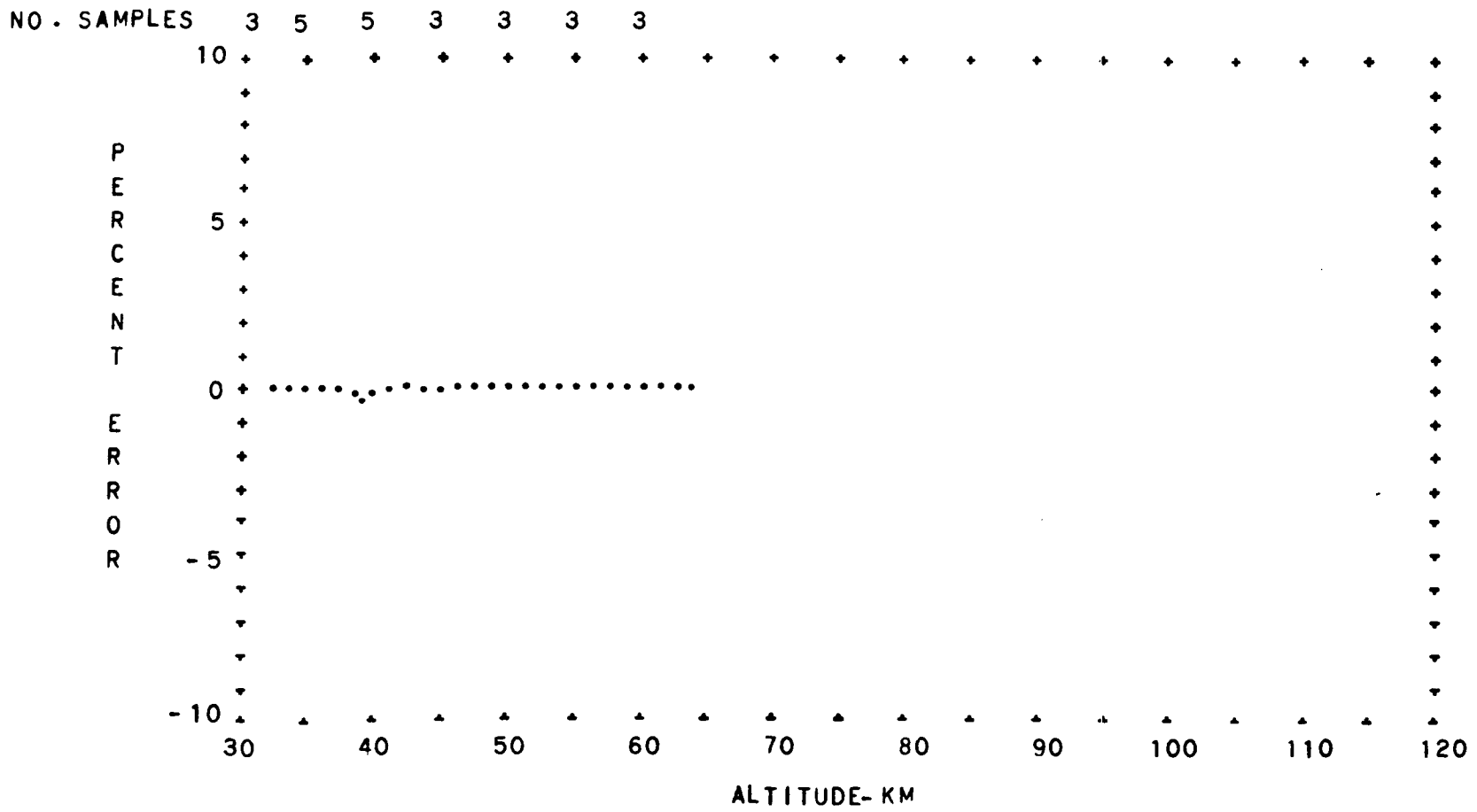

FIG. A-66 PERCENT CONTRIBUTION OF THE COVARIANCE TO THE MEAN PRESSURE OF THE BUELL GAS LAW EQUATION AS A FUNCTION OF ALTITUDE

SUBARCTIC SUMMER DAYTIME

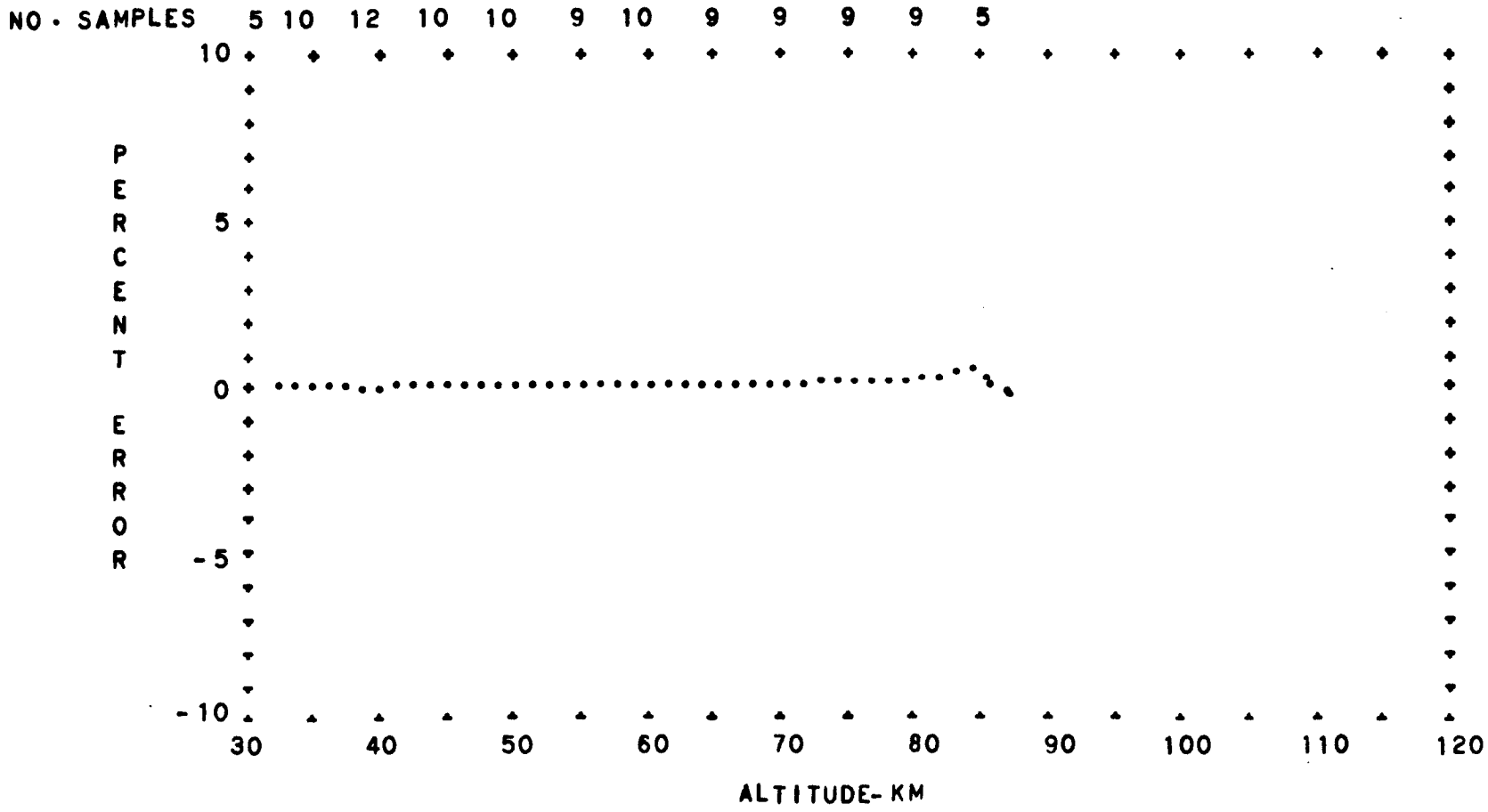

FIG. A-67 PERCENT CONTRIBUTION OF THE COVARIANCE TO THE MEAN PRESSURE OF THE BUELL GAS LAW EQUATION AS A FUNCTION OF ALTITUDE

SUBARCTIC SUMMER DIURNAL MEAN

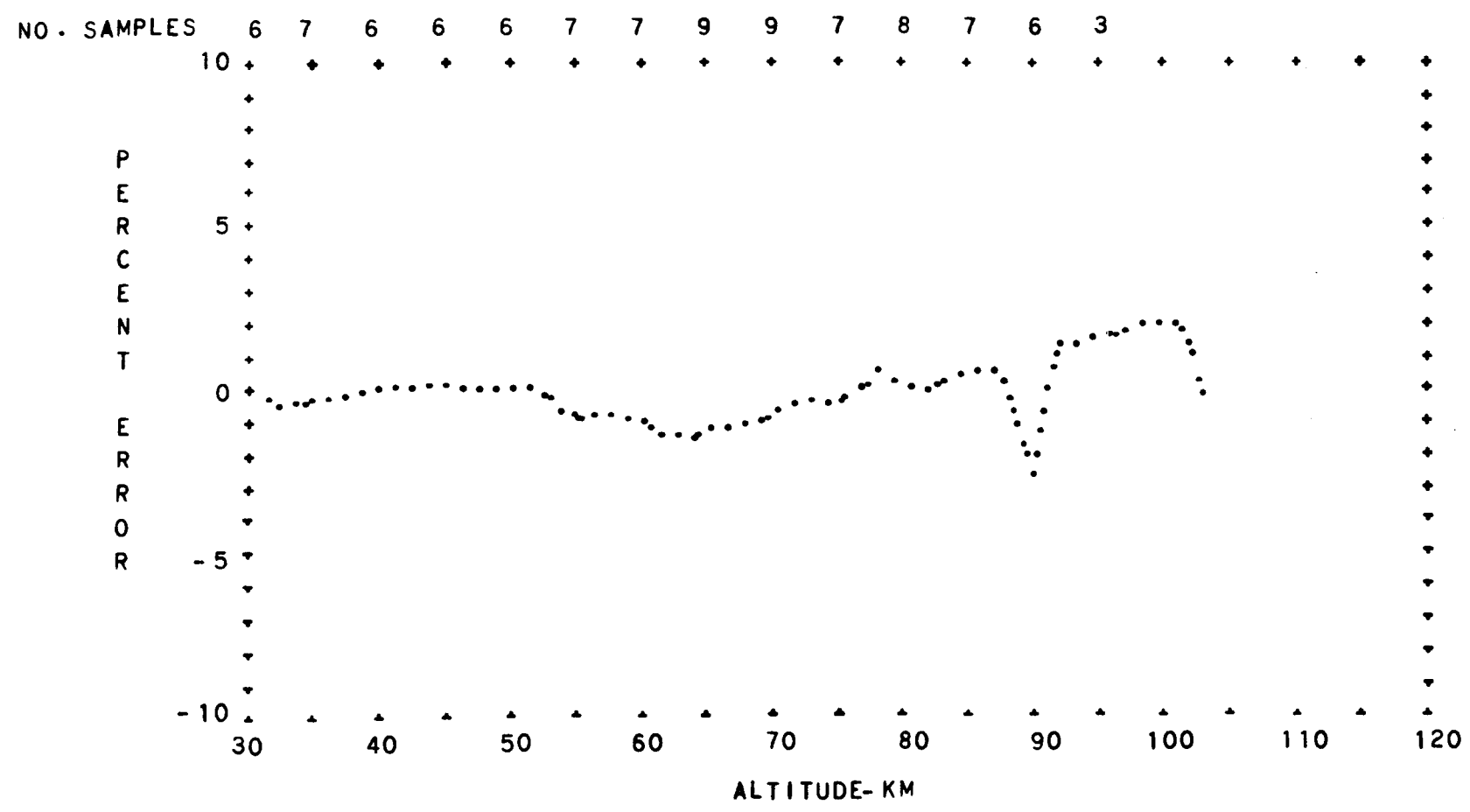

FIG. A-68 PERCENT CONTRIBUTION OF THE COVARIANCE TO THE MEAN PRESSURE OF THE BUELL GAS LAW EQUATION AS A FUNCTION OF ALTITUDE

SUBARCTIC AUTUMN DIURNAL TRANSITION

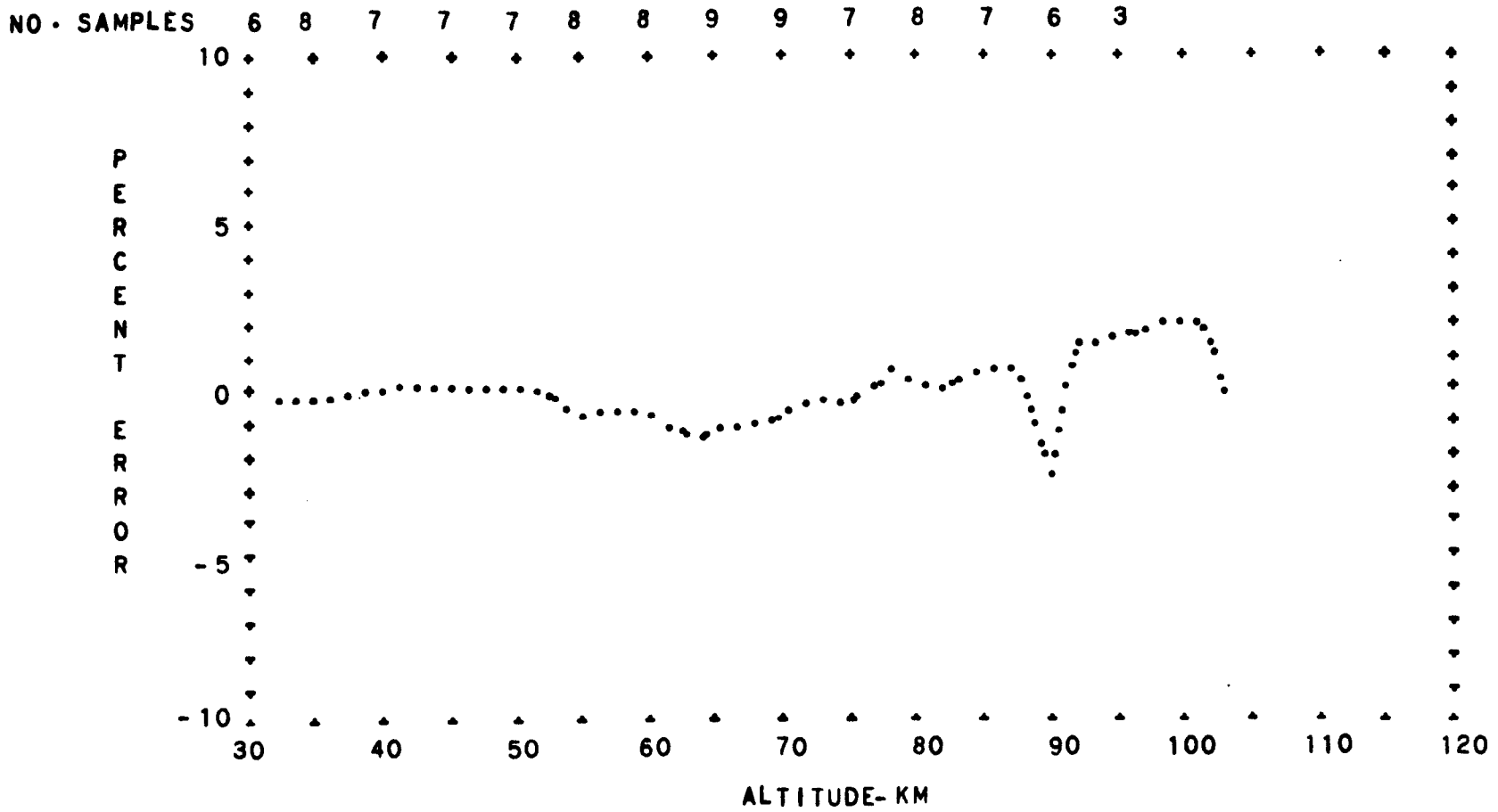

FIG. A-69 PERCENT CONTRIBUTION OF THE COVARIANCE TO THE MEAN PRESSURE OF THE BUELL GAS LAW EQUATION AS A FUNCTION OF ALTITUDE

SUBARCTIC AUTUMN DIURNAL MEAN

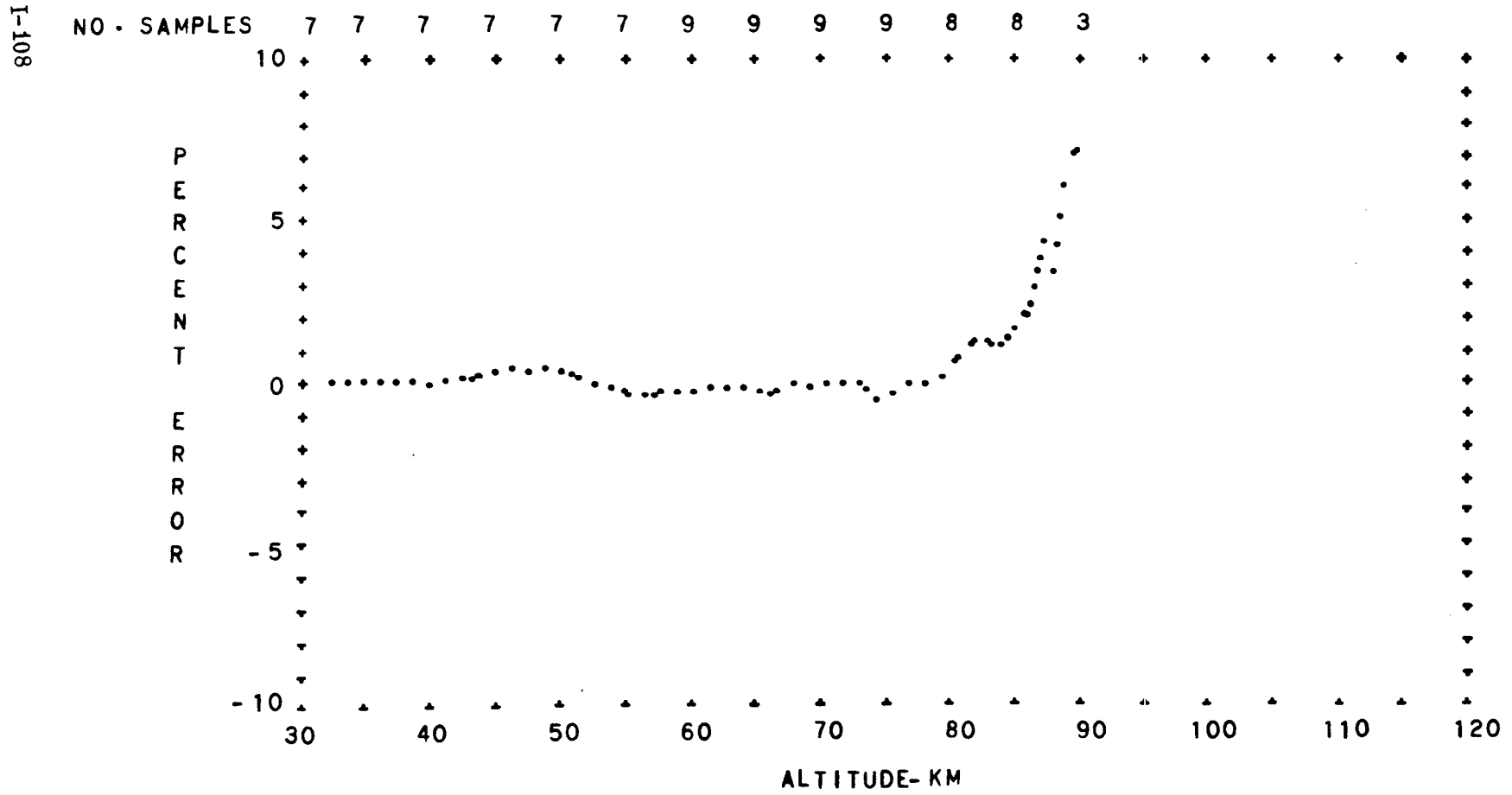

FIG. A-70 PERCENT CONTRIBUTION OF THE COVARIANCE TO THE MEAN PRESSURE OF THE BUELL GAS LAW EQUATION AS A FUNCTION OF ALTITUDE

SUBARCTIC WINTER DIURNAL TRANSITION

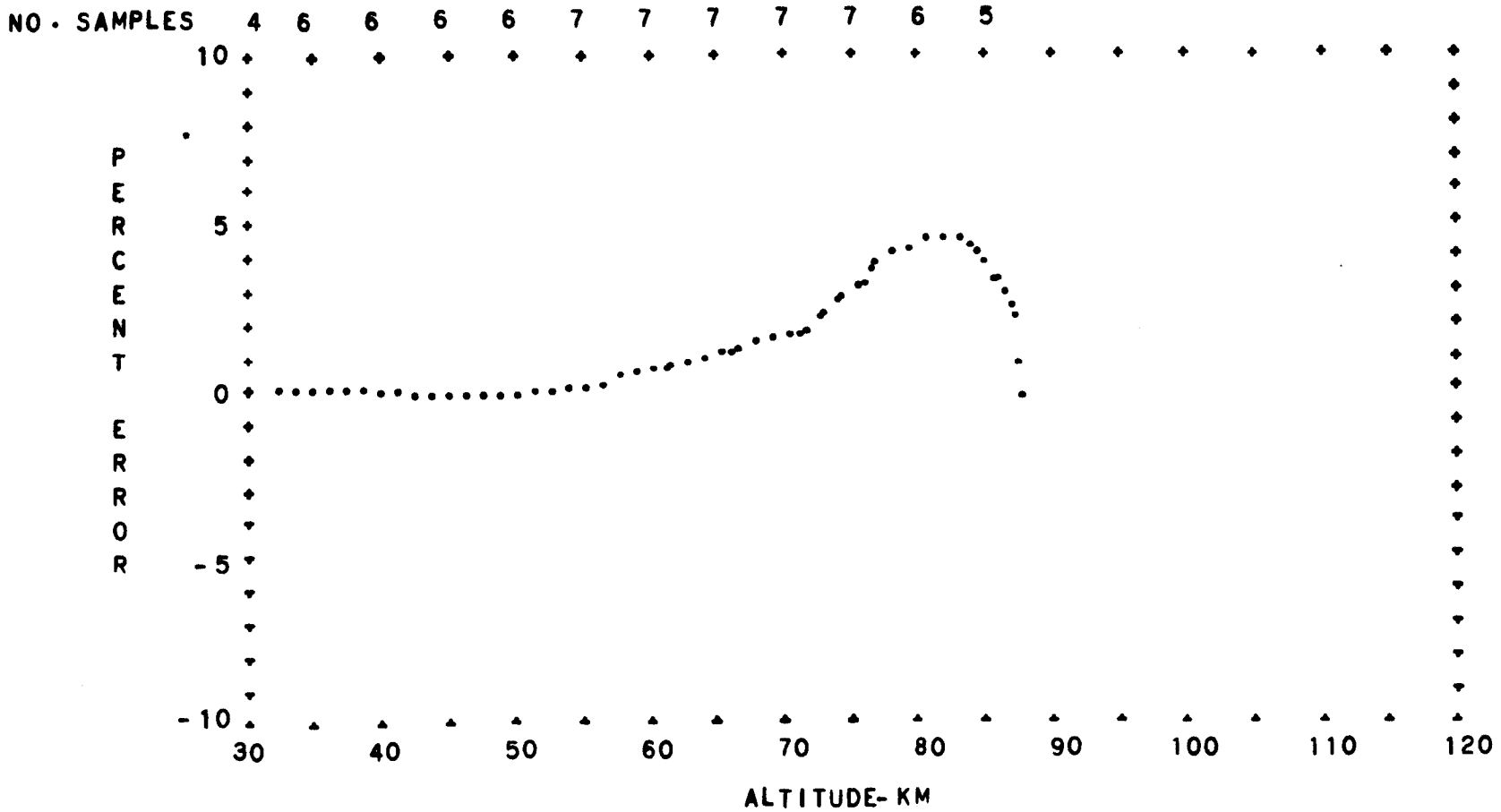

FIG. A-71 PERCENT CONTRIBUTION OF THE COVARIANCE TO THE MEAN PRESSURE OF THE BUELL GAS LAW EQUATION AS A FUNCTION OF ALTITUDE

SUBARCTIC WINTER NIGHTTIME

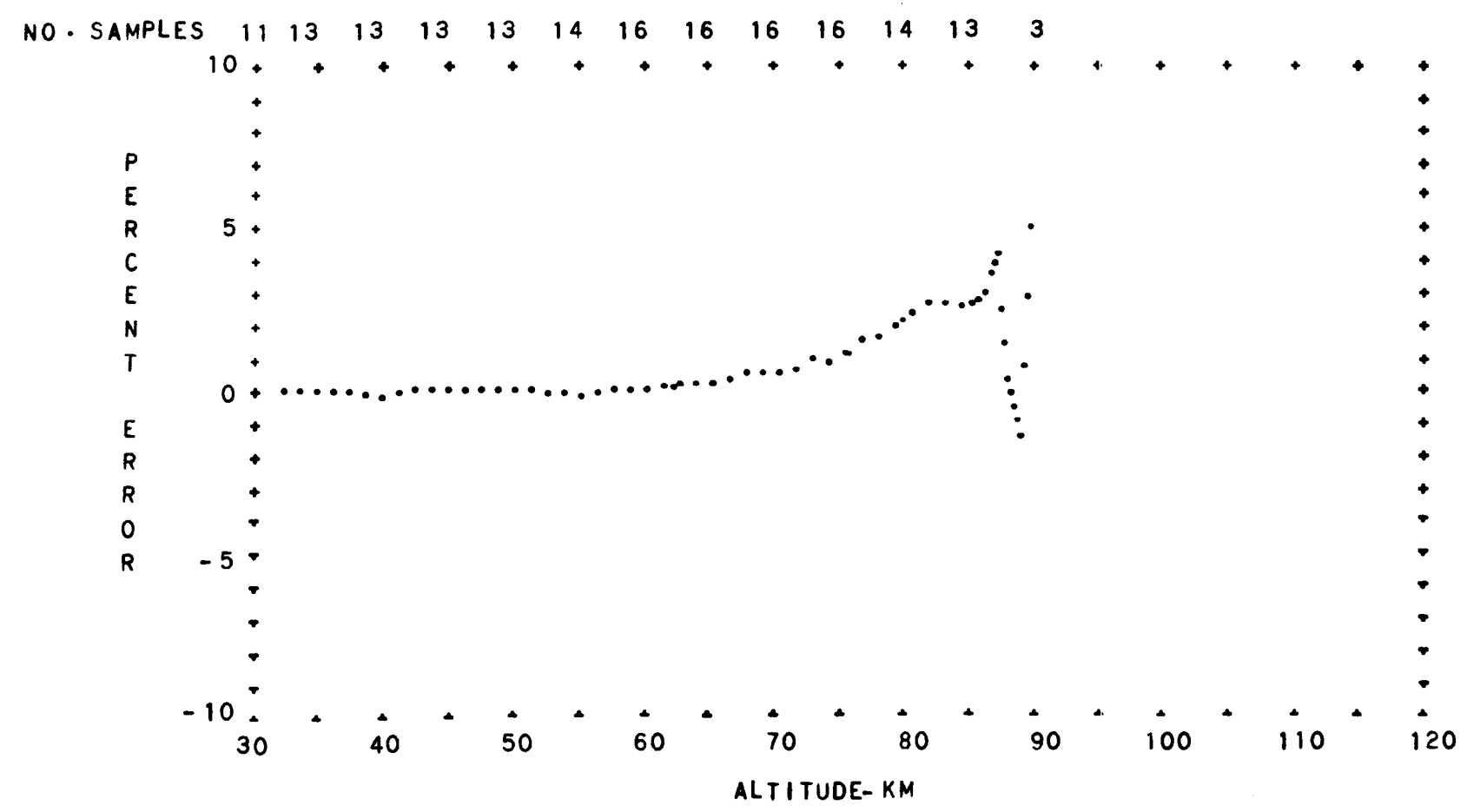

FIG. A-72 PERCENT CONTRIBUTION OF THE COVARIANCE TO THE MEAN PRESSURE OF THE BUELL GAS LAW EQUATION AS A FUNCTION OF ALTITUDE

SUBARCTIC WINTER DIURNAL MEAN

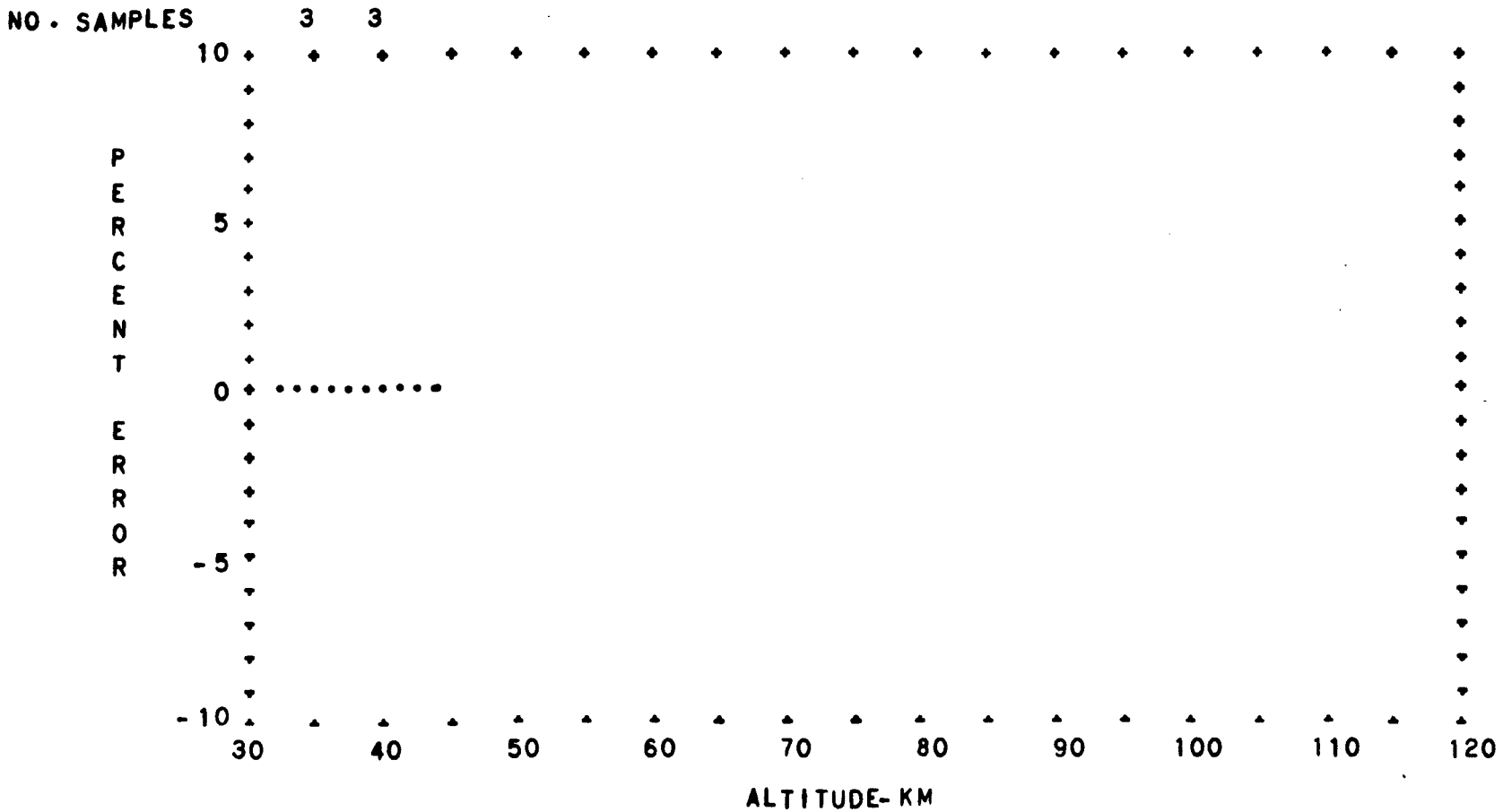

FIG. A-73 PERCENT CONTRIBUTION OF THE COVARIANCE TO THE MEAN PRESSURE OF THE BUELL GAS LAW EQUATION AS A FUNCTION OF ALTITUDE

SUBARCTIC SUMMER EXTREME DIURNAL TRANSITION

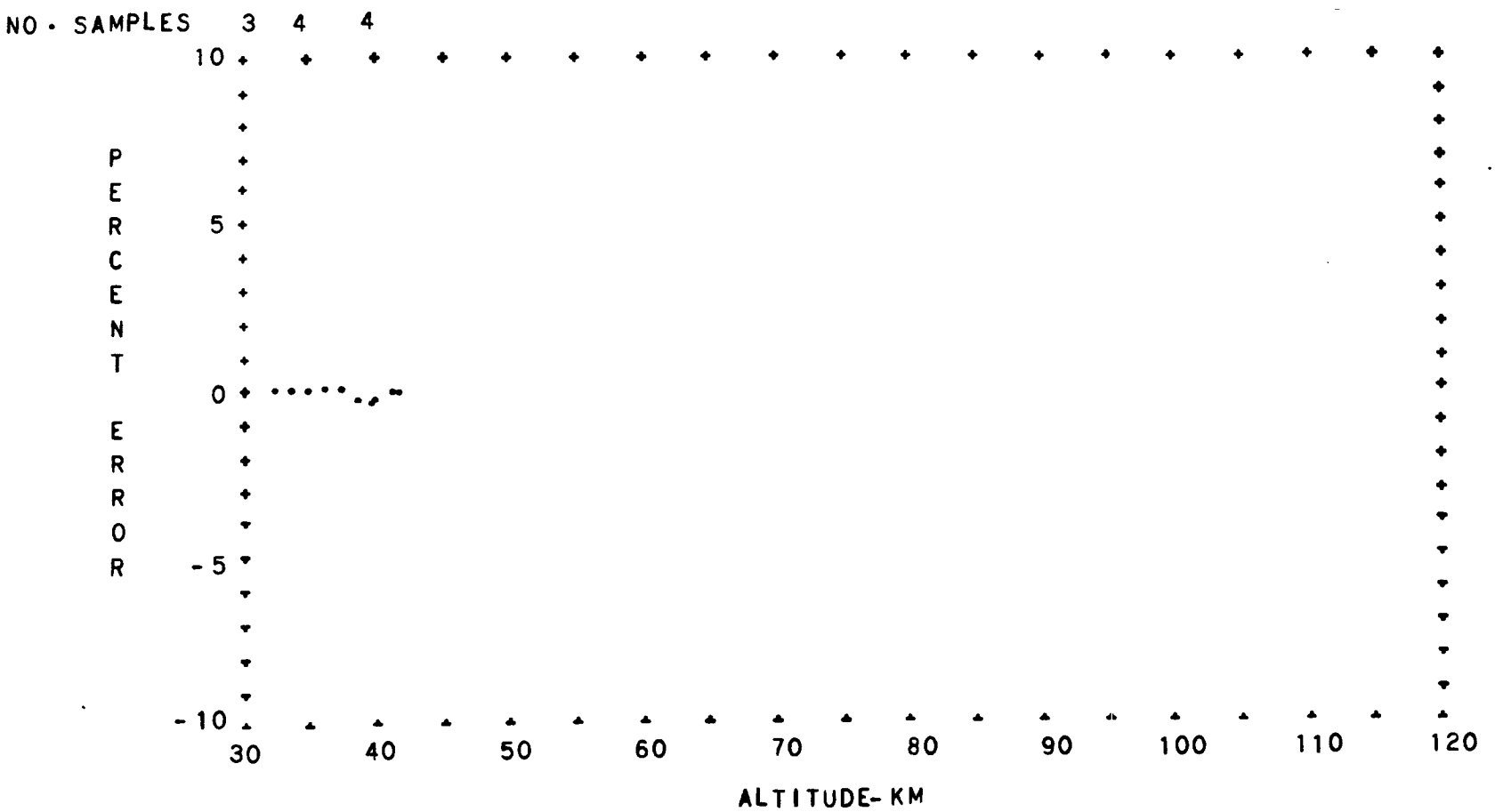

FIG. A-74 PERCENT CONTRIBUTION OF THE COVARIANCE TO THE MEAN PRESSURE OF THE BUELL GAS LAW EQUATION AS A FUNCTION OF ALTITUDE

SUBARCTIC SUMMER EXTREME DAYTIME

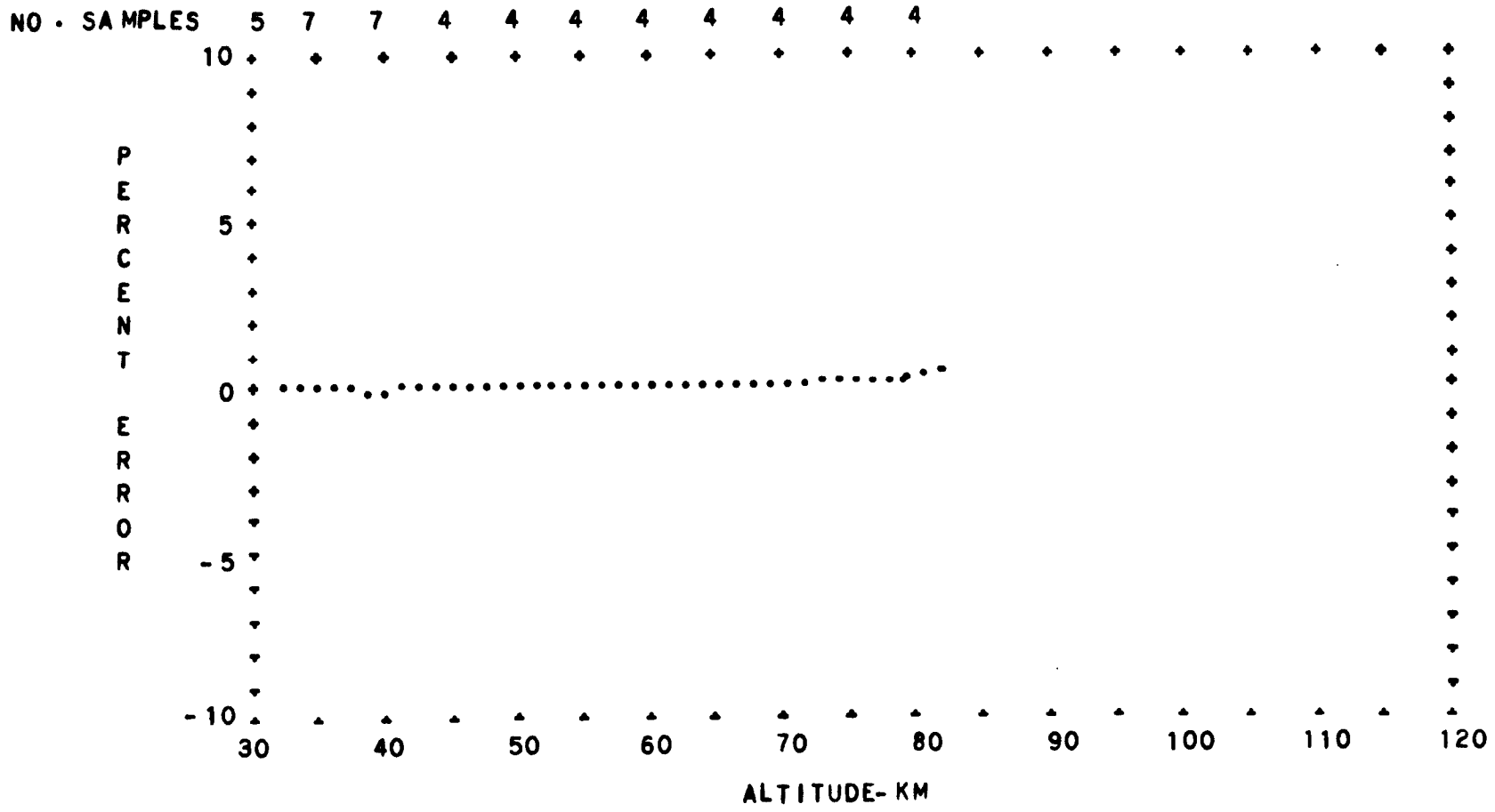

FIG. A-75 PERCENT CONTRIBUTION OF THE COVARIANCE TO THE MEAN PRESSURE OF THE BUELL GAS LAW EQUATION AS A FUNCTION OF ALTITUDE

SUBARCTIC SUMMER EXTREME DIURNAL MEAN

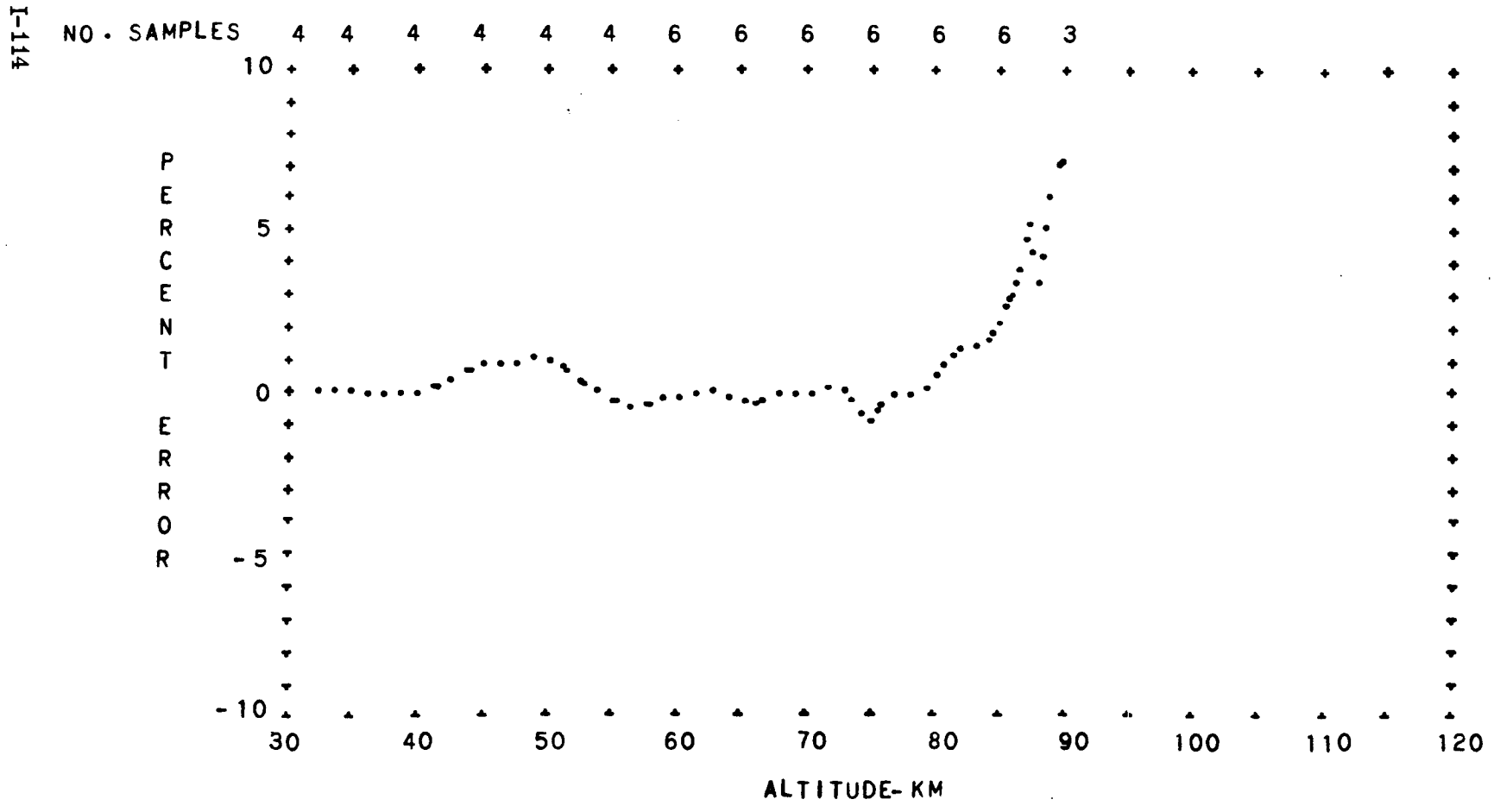

FIG. A-76 PERCENT CONTRIBUTION OF THE COVARIANCE TO THE MEAN PRESSURE OF THE BUELL GAS LAW EQUATION AS A FUNCTION OF ALTITUDE

SUBARCTIC WINTER EXTREME DIURNAL TRANSITION

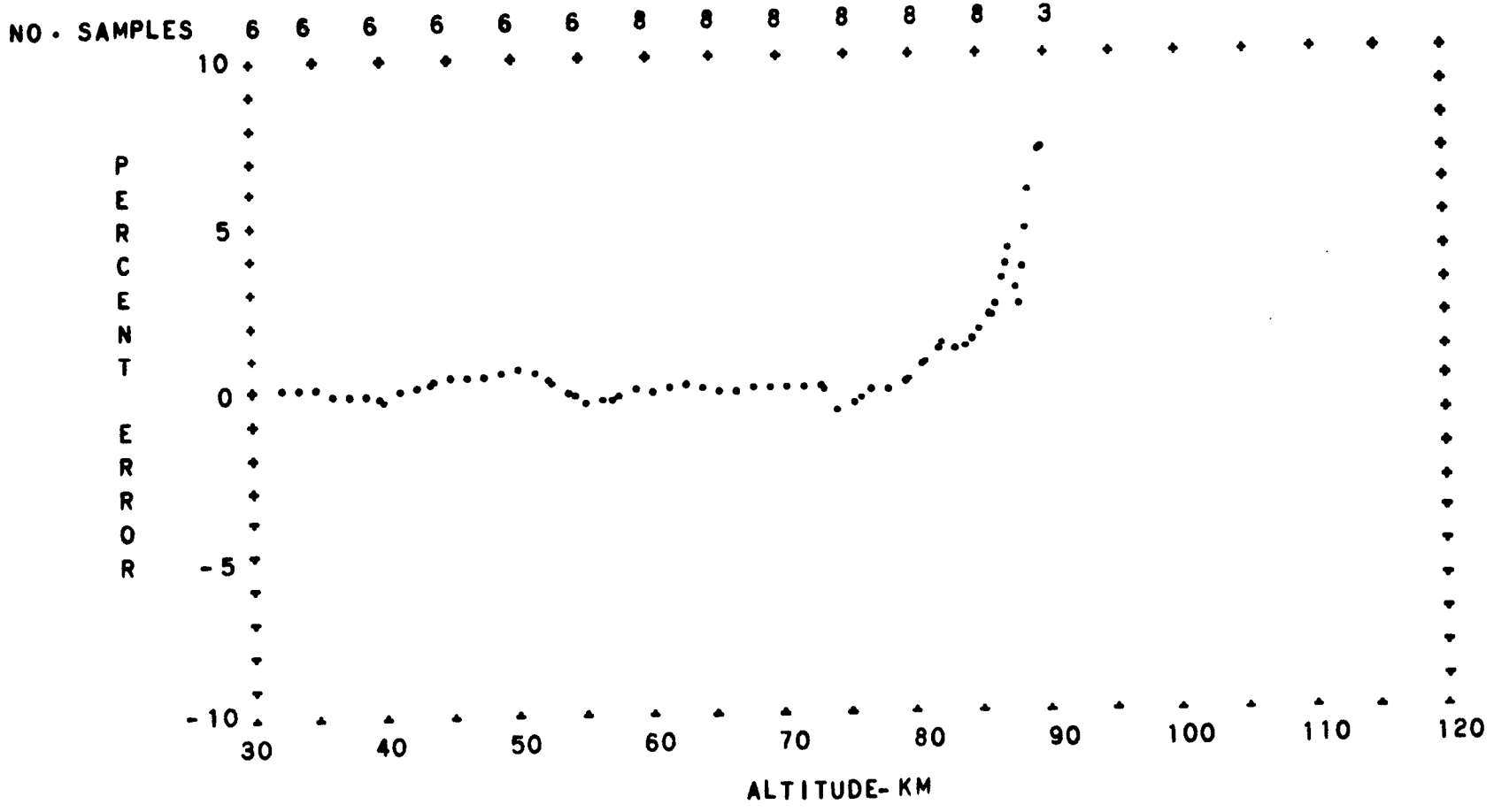

FIG. A-77 PERCENT CONTRIBUTION OF THE COVARIANCE TO THE MEAN PRESSURE OF THE BUELL GAS LAW EQUATION AS A FUNCTION OF ALTITUDE

SUBARCTIC WINTER EXTREME DIURNAL MEAN

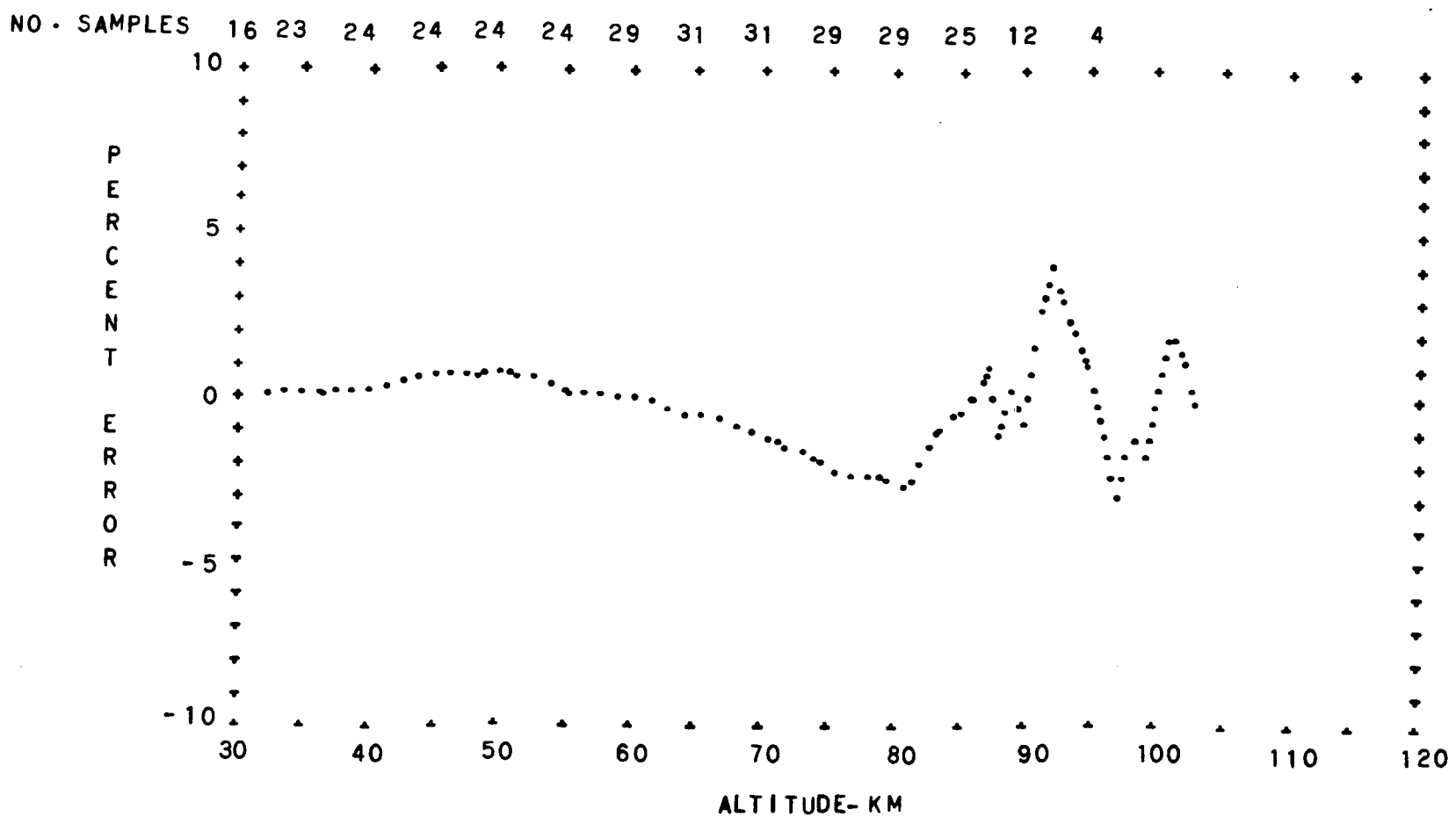

FIG. A-78 PERCENT CONTRIBUTION OF THE COVARIANCE TO THE MEAN PRESSURE OF THE BUELL GAS LAW EQUATION AS A FUNCTION OF ALTITUDE

SUBARCTIC ANNUAL MEAN DIURNAL TRANSITION

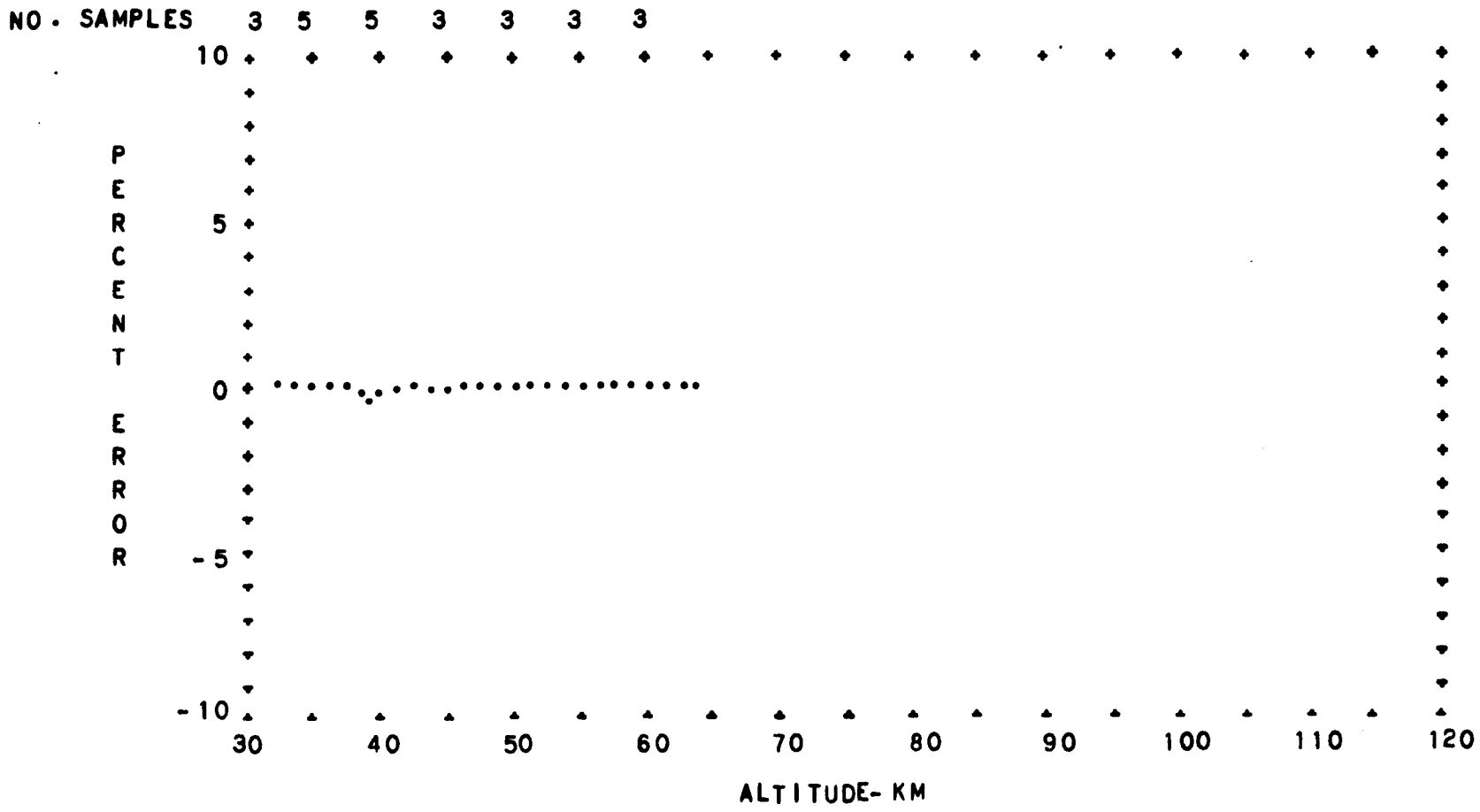

FIG. A-79 PERCENT CONTRIBUTION OF THE COVARIANCE TO THE MEAN PRESSURE OF THE BUELL GAS LAW EQUATION AS A FUNCTION OF ALTITUDE

SUBARCTIC ANNUAL MEAN DAYTIME

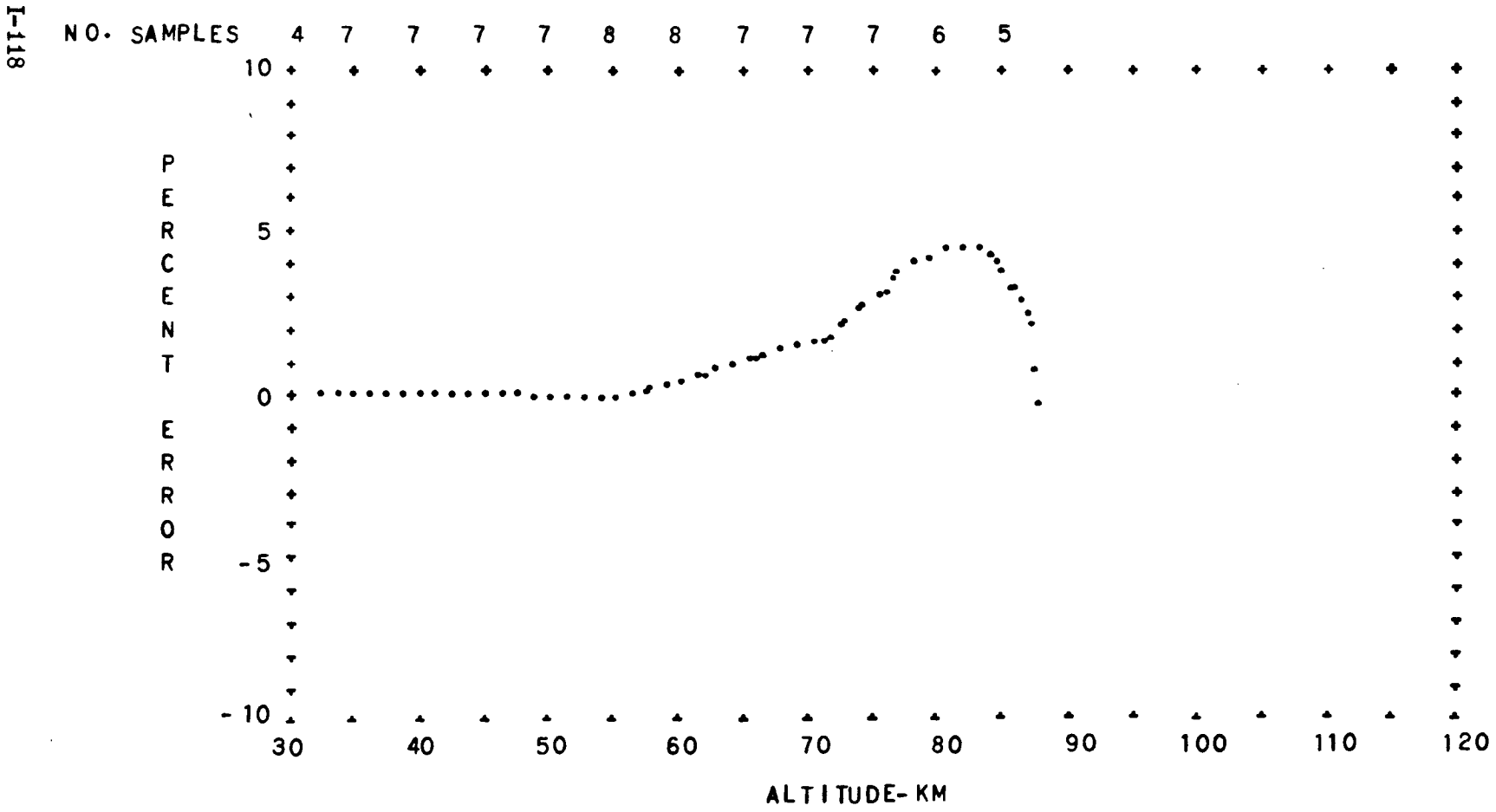

FIG. A-80 PERCENT CONTRIBUTION OF THE COVARIANCE TO THE MEAN PRESSURE OF THE BUELL GAS LAW EQUATION AS A FUNCTION OF ALTITUDE

SUBARCTIC ANNUAL MEAN NIGHTTIME

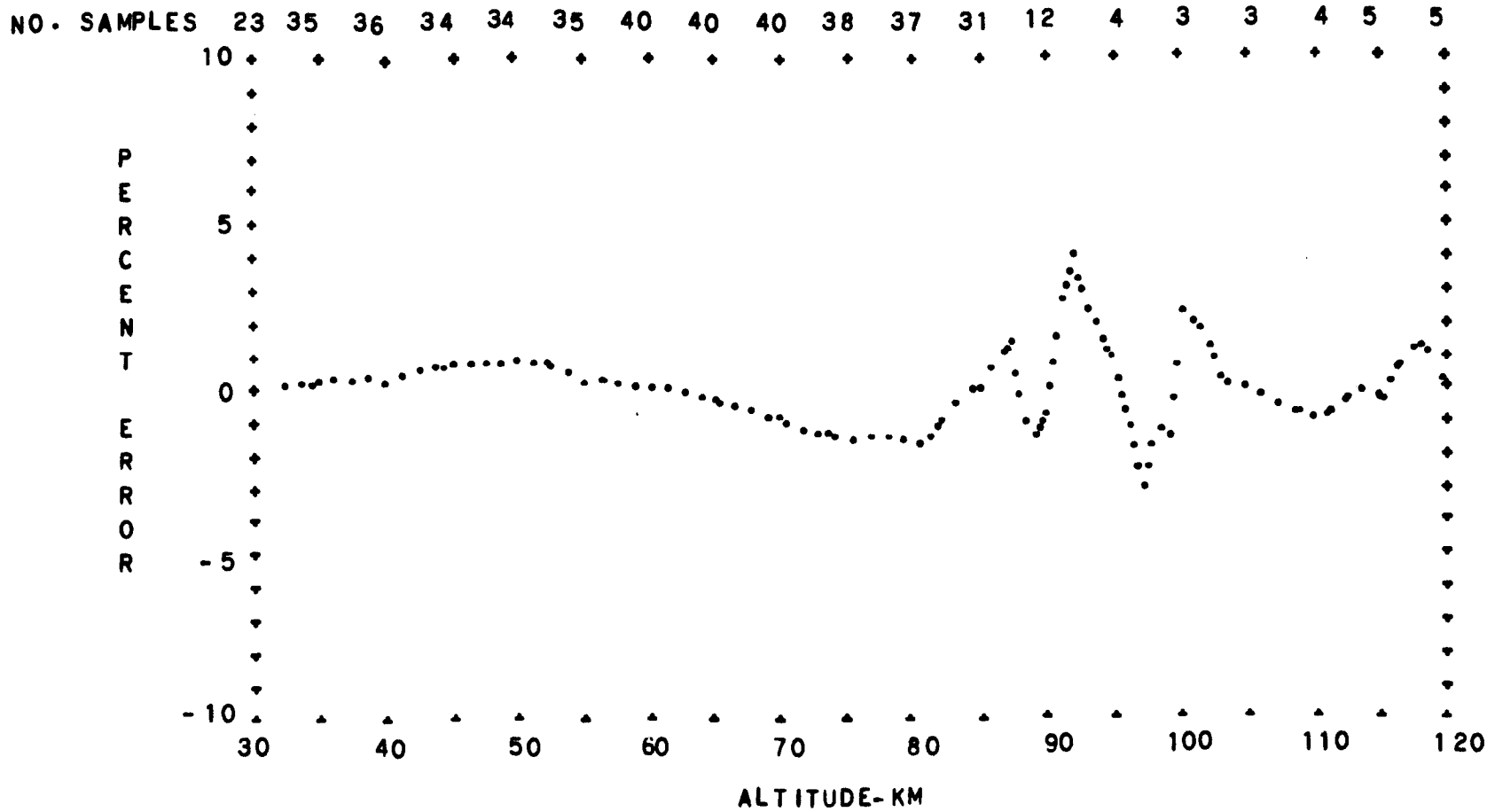

FIG. A-81 PERCENT CONTRIBUTION OF THE COVARIANCE TO THE MEAN PRESSURE OF THE BUELL GAS LAW EQUATION AS A FUNCTION OF ALTITUDE

SUBARCTIC ANNUAL MEAN DIURNAL MEAN

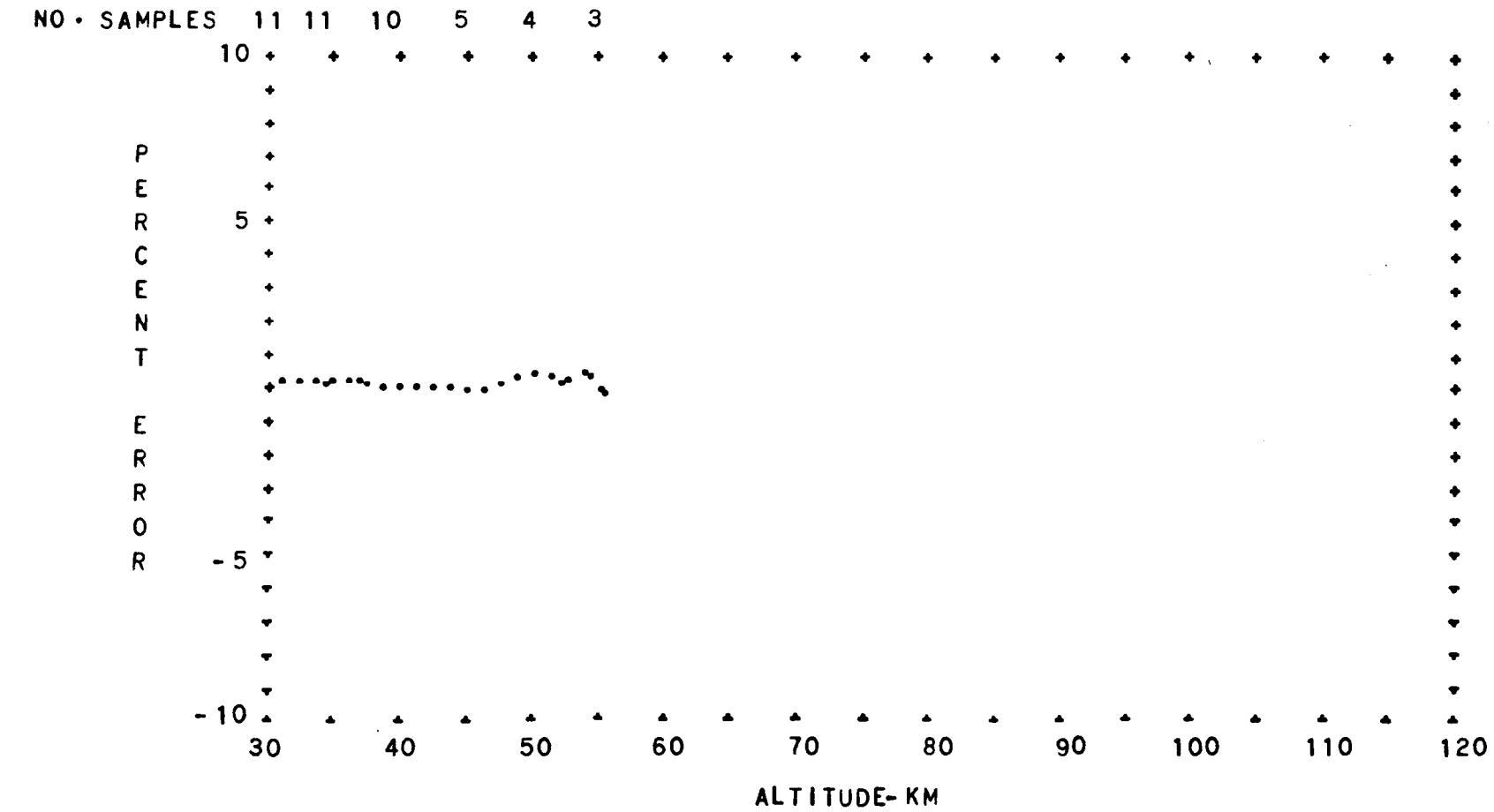

FIG. A-82 PERCENT CONTRIBUTION OF THE COVARIANCE TO THE MEAN PRESSURE OF THE BUELL GAS LAW EQUATION AS A FUNCTION OF ALTITUDE

ARCTIC SPRING DIURNAL TRANSITION

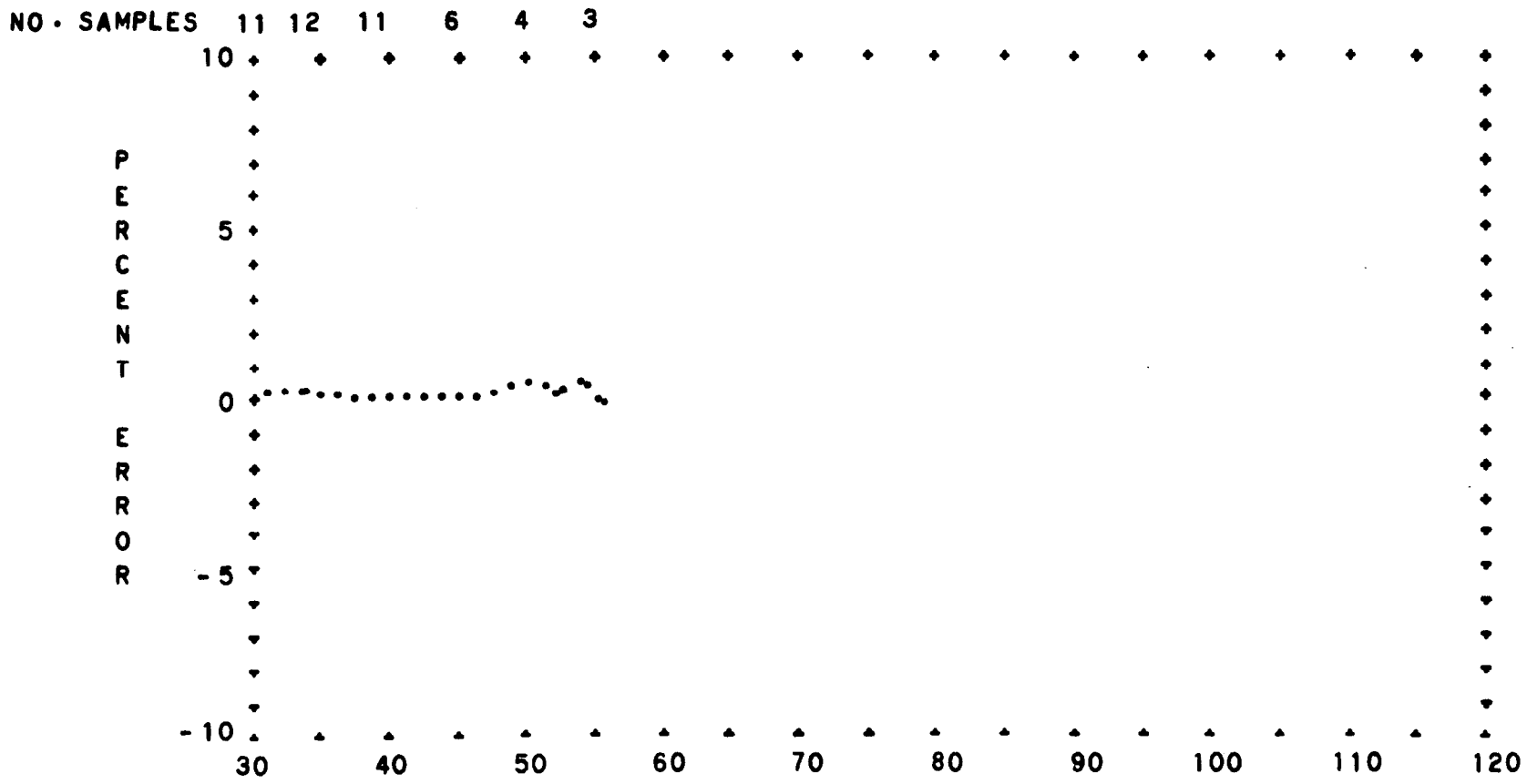

FIG. A-83 PERCENT CONTRIBUTION OF THE COVARIANCE TO THE MEAN PRESSURE OF THE BUELL GAS LAW EQUATION AS A FUNCTION OF ALTITUDE

ARCTIC SPRING DIURNAL MEAN

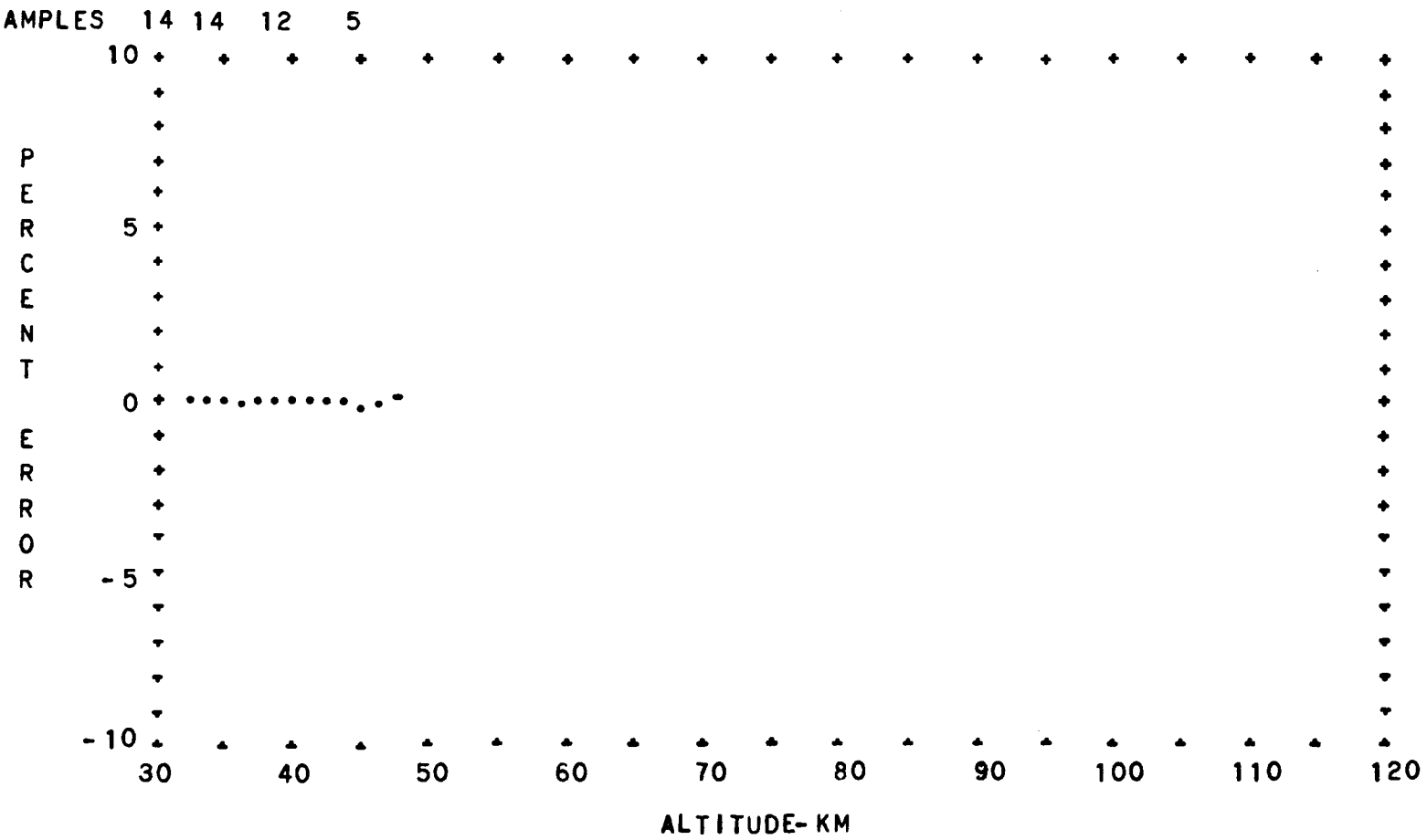

FIG. A-84 PERCENT CONTRIBUTION OF THE COVARIANCE TO THE MEAN PRESSURE OF THE BUELL GAS LAW EQUATION AS A FUNCTION OF ALTITUDE

ARCTIC SUMMER DIURNAL TRANSITION

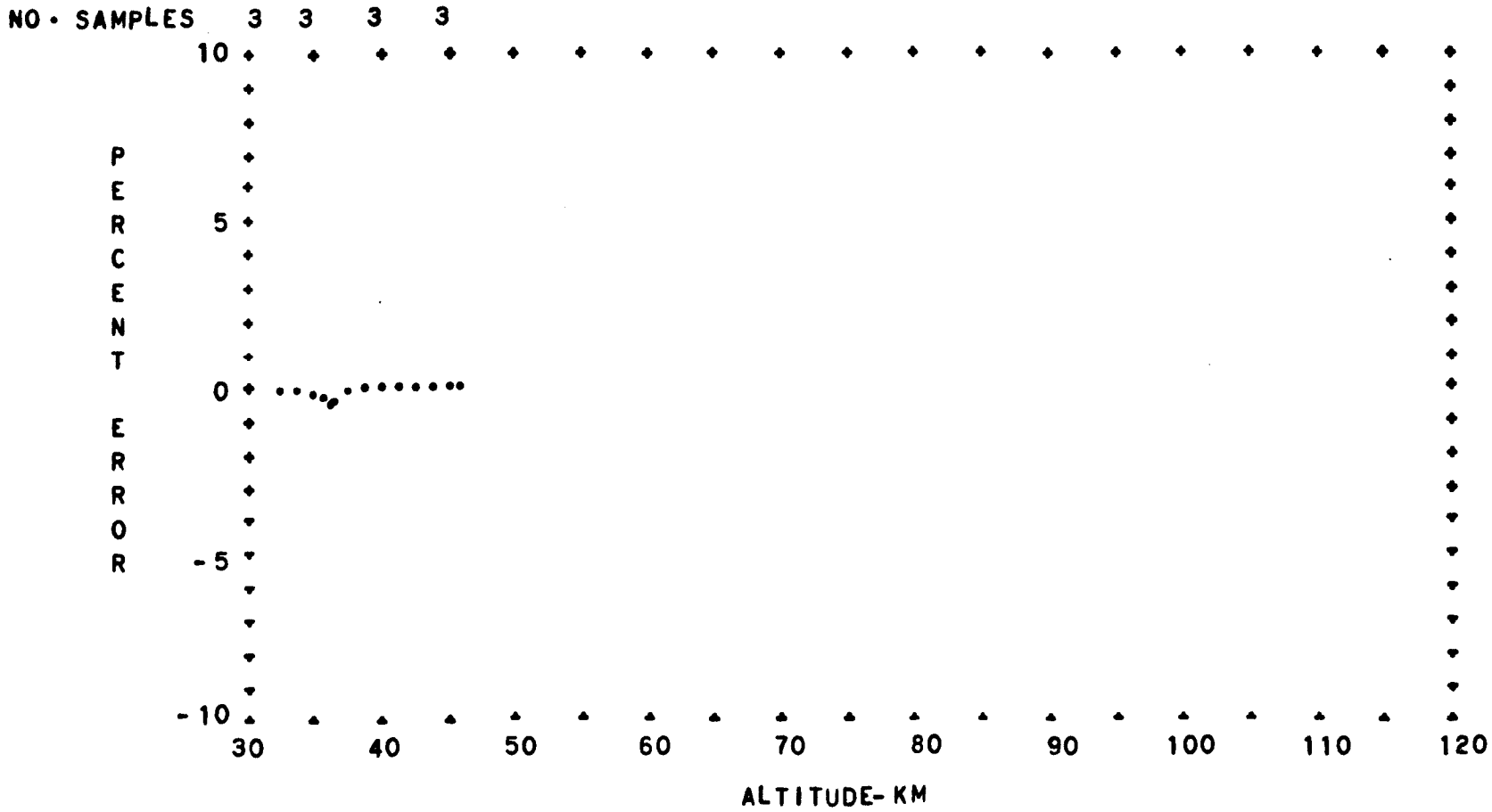

FIG. A-85 PERCENT CONTRIBUTION OF THE COVARIANCE TO THE MEAN PRESSURE OF THE BUELL GAS LAW EQUATION AS A FUNCTION OF ALTITUDE

ARCTIC SUMMER DAYTIME

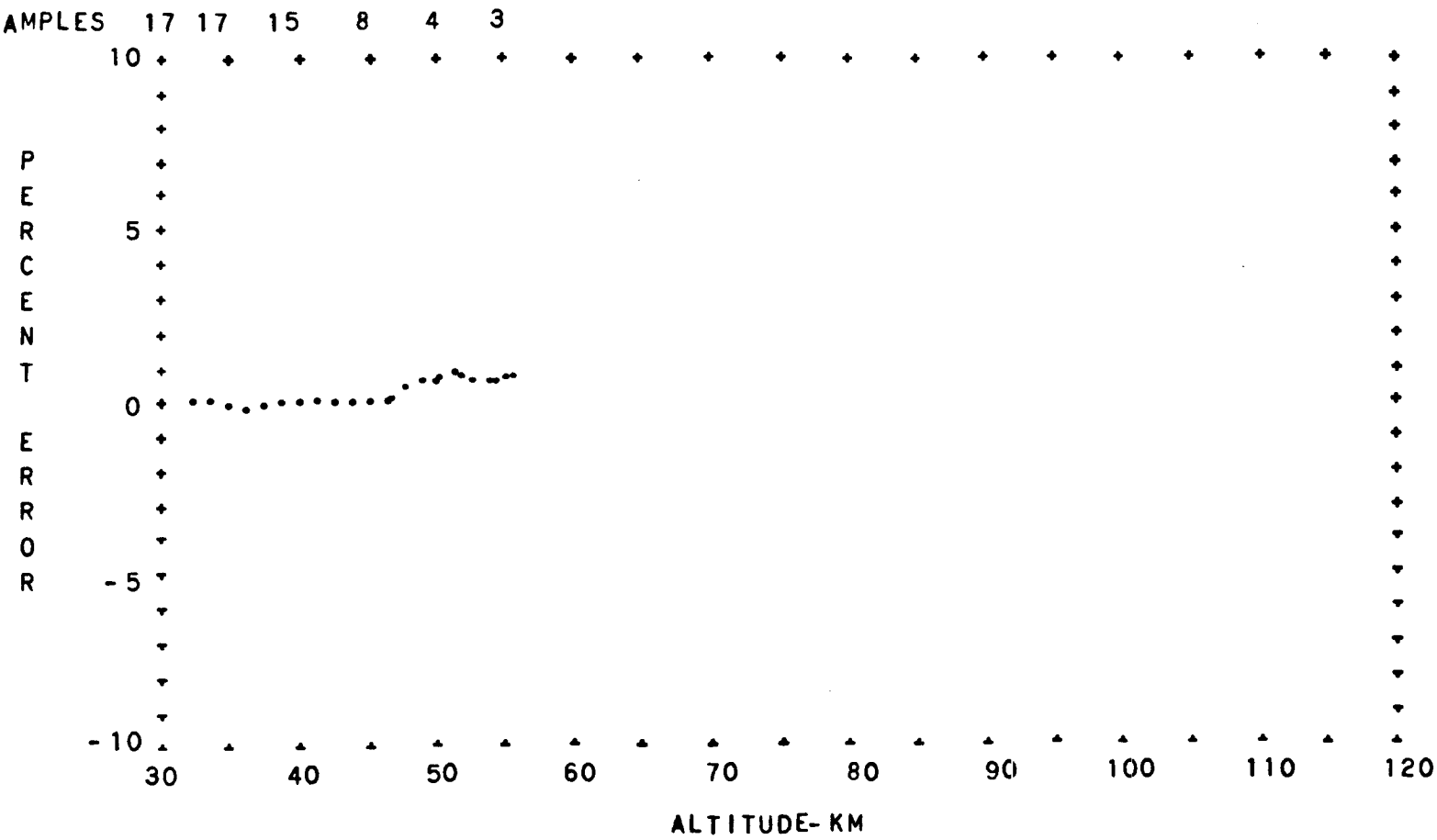

FIG. A-86 PERCENT CONTRIBUTION OF THE COVARIANCE TO THE MEAN PRESSURE OF THE BUELL GAS LAW EQUATION AS A FUNCTION OF ALTITUDE

ARCTIC SUMMER DIURNAL MEAN

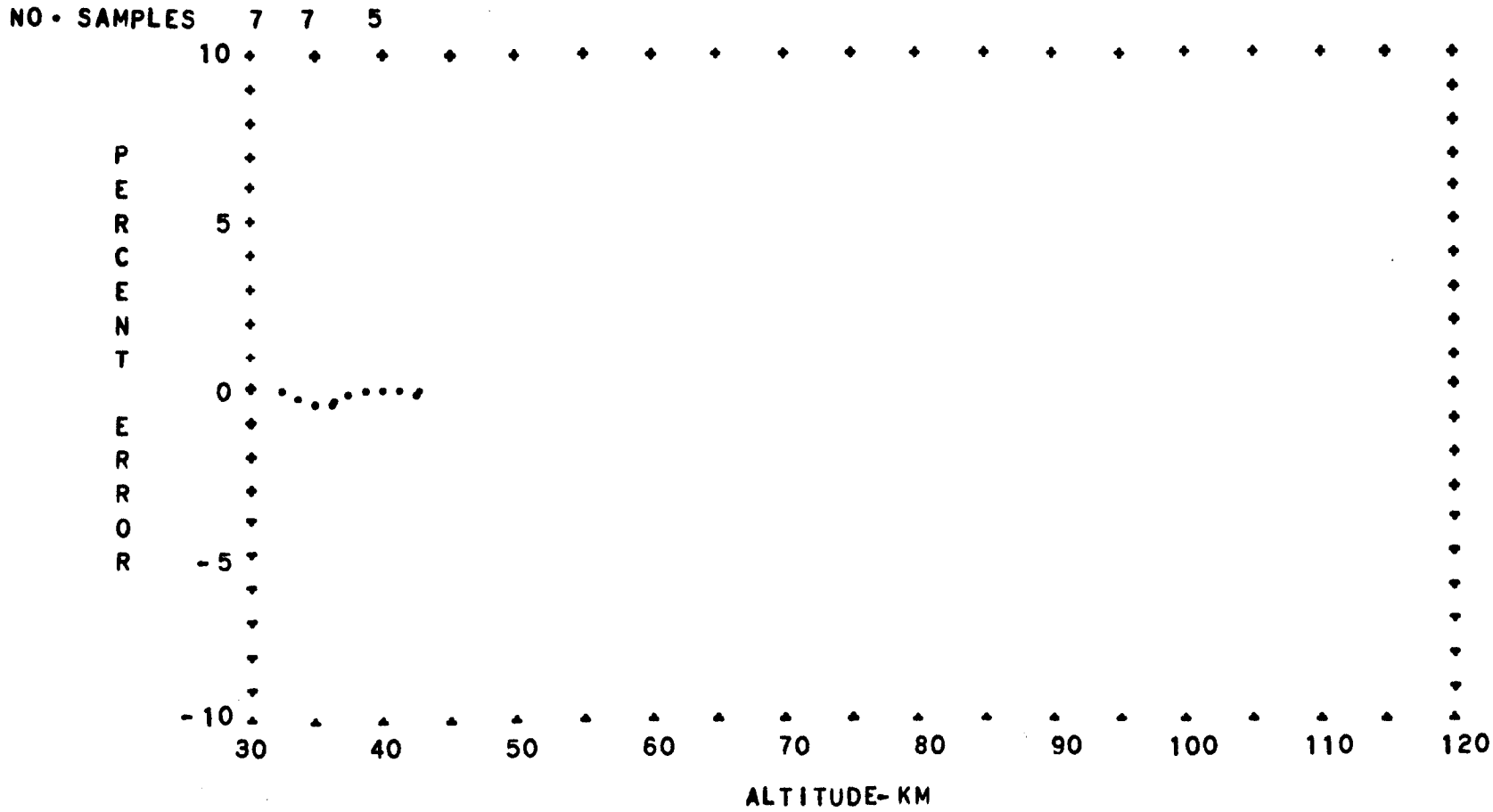

FIG. A-87 PERCENT CONTRIBUTION OF THE COVARIANCE TO THE MEAN PRESSURE OF THE BUELL GAS LAW EQUATION AS A FUNCTION OF ALTITUDE

ARCTIC AUTUMN DIURNAL TRANSITION

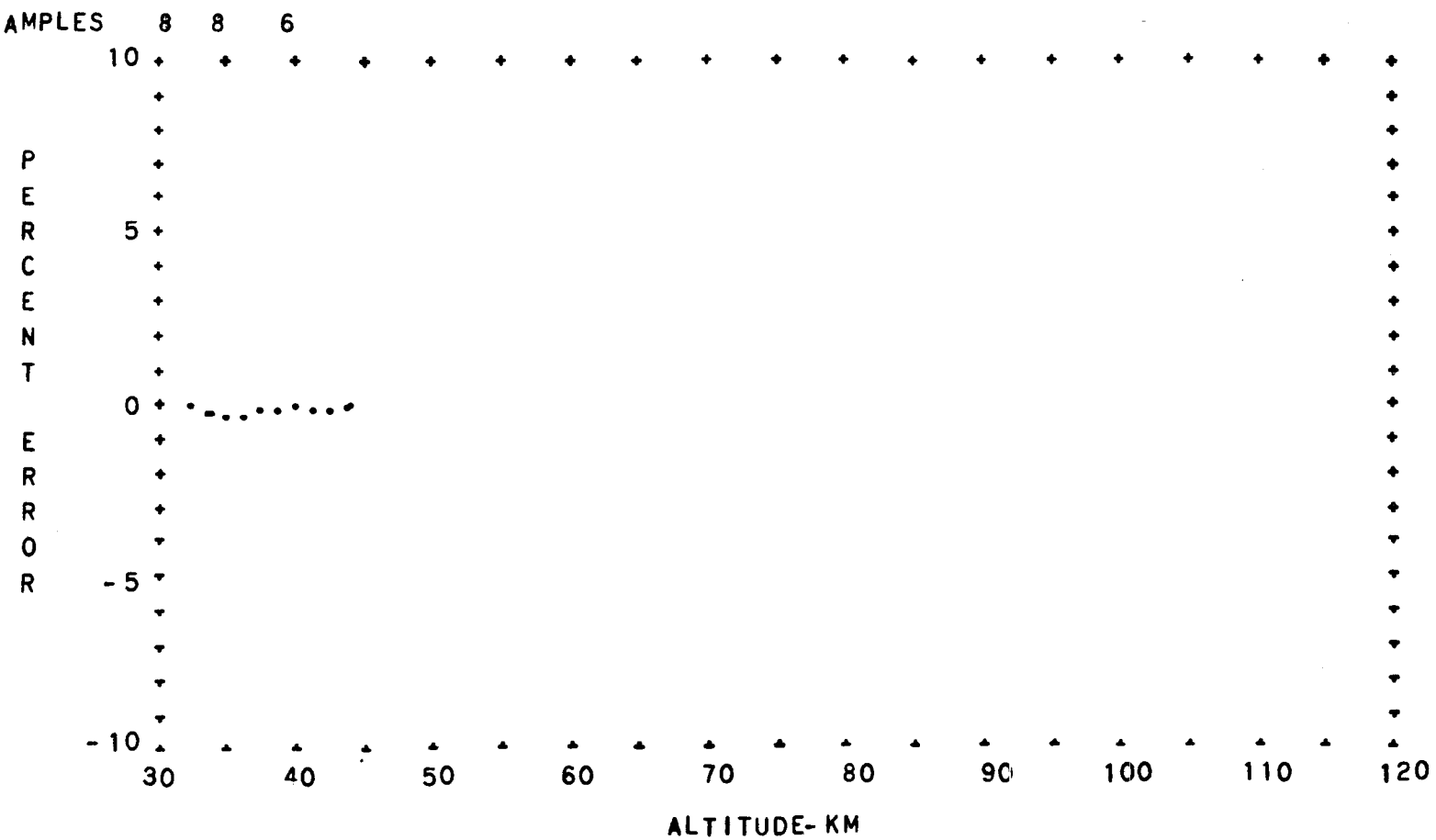

FIG. A-88 PERCENT CONTRIBUTION OF THE COVARIANCE TO THE MEAN PRESSURE OF THE BUELL GAS LAW EQUATION AS A FUNCTION OF ALTITUDE

ARCTIC AUTUMN DIURNAL MEAN

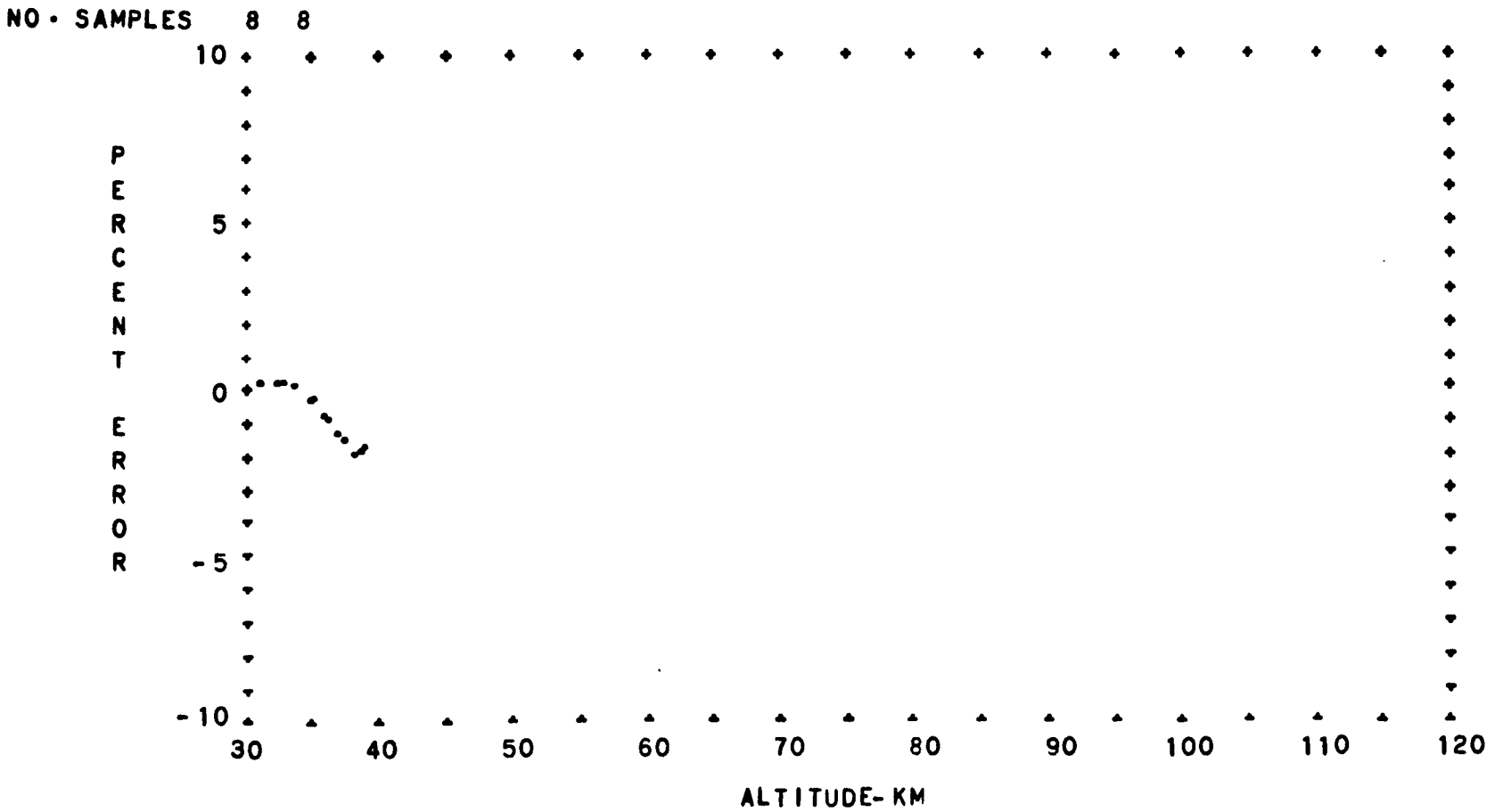

FIG. A-89 PERCENT CONTRIBUTION OF THE COVARIANCE TO THE MEAN PRESSURE OF THE BUELL GAS LAW EQUATION AS A FUNCTION OF ALTITUDE

ARCTIC WINTER DIURNAL TRANSITION

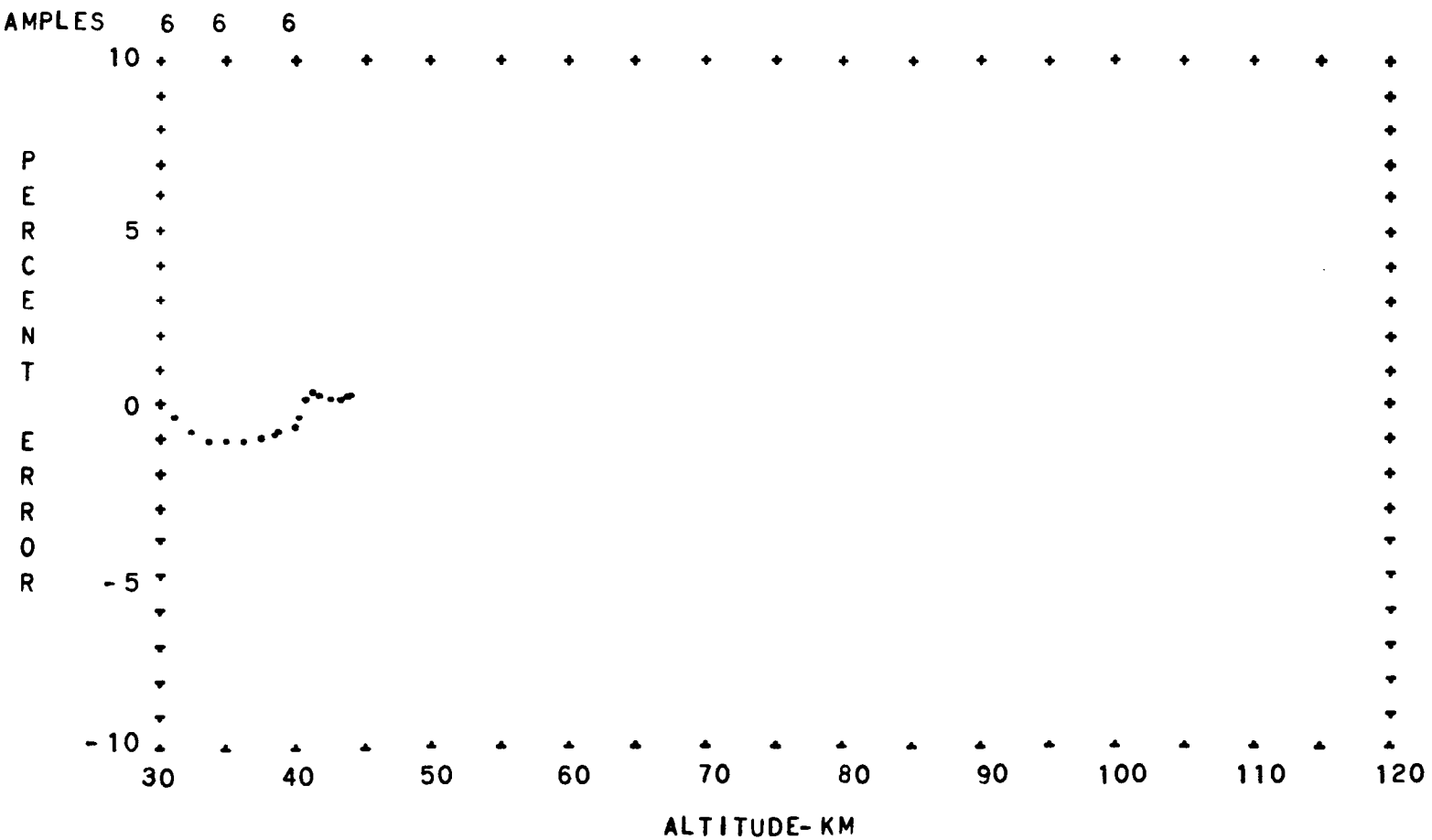

FIG. A-90 PERCENT CONTRIBUTION OF THE COVARIANCE TO THE MEAN PRESSURE OF THE BUELL GAS LAW EQUATION AS A FUNCTION OF ALTITUDE

ARCTIC WINTER NIGHTTIME

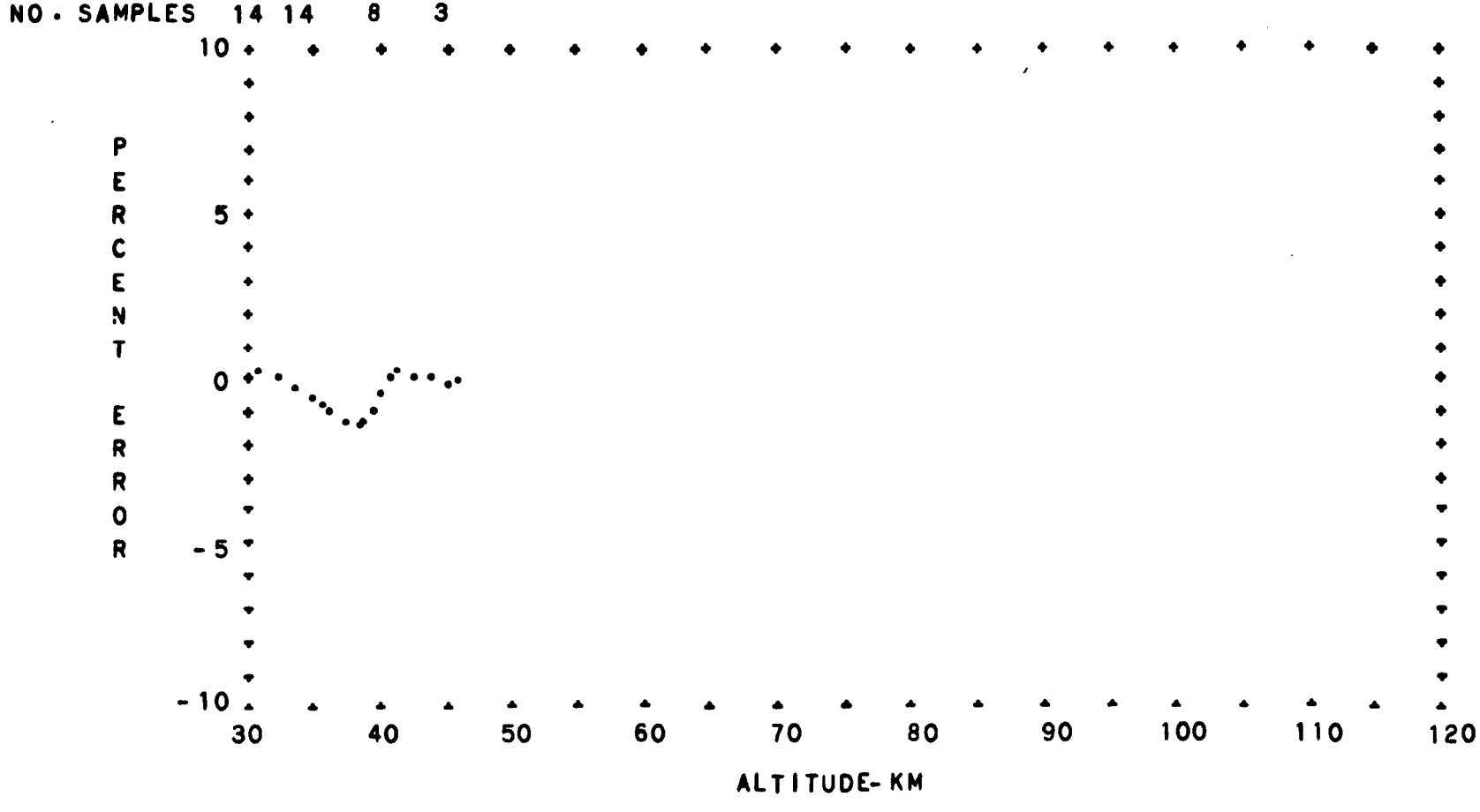

FIG. A-91 PERCENT CONTRIBUTION OF THE COVARIANCE TO THE MEAN PRESSURE OF THE BUELL GAS LAW EQUATION AS A FUNCTION OF ALTITUDE

ARCTIC WINTER DIURNAL MEAN

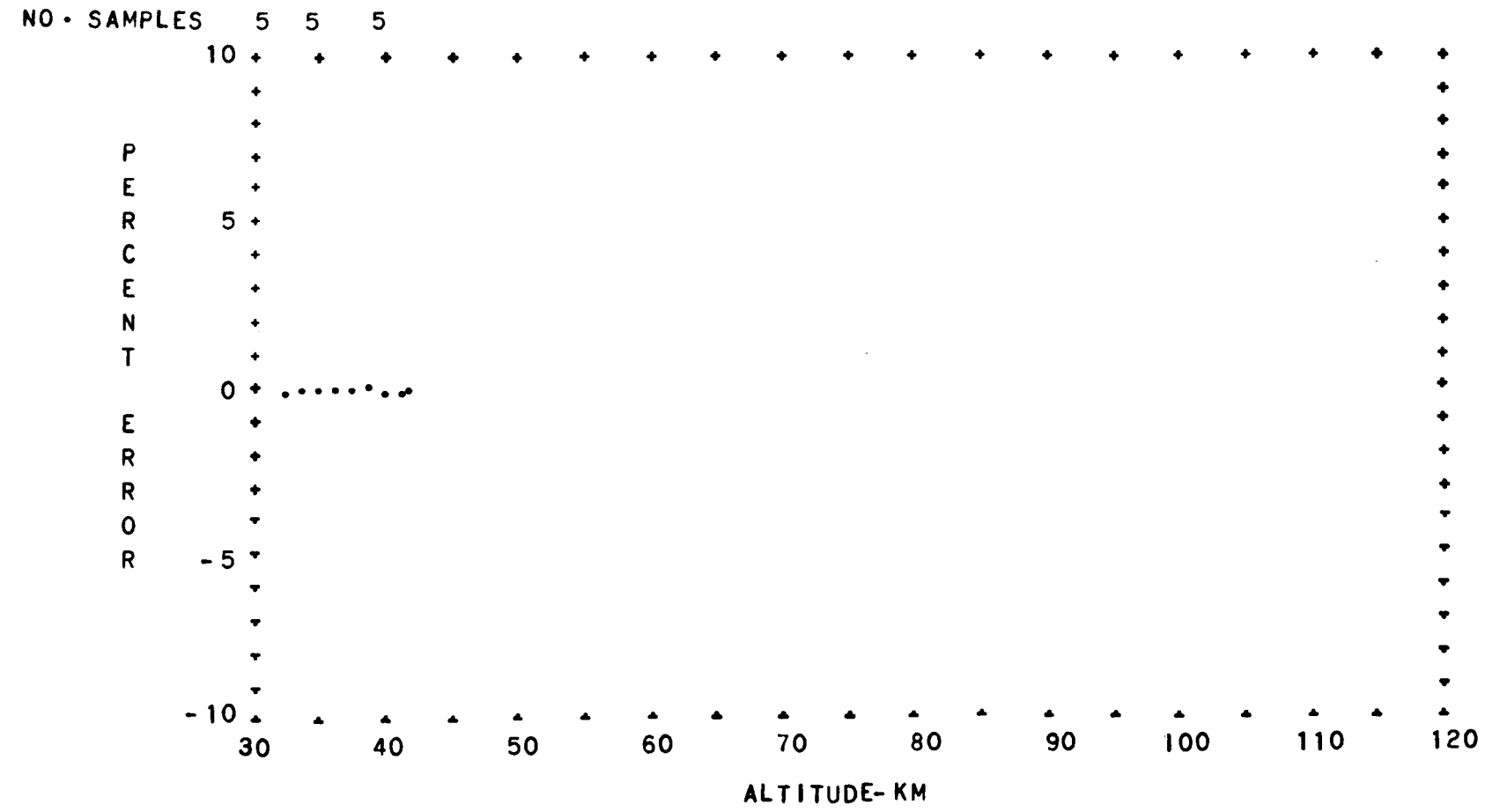

FIG. A-92 PERCENT CONTRIBUTION OF THE COVARIANCE TO THE MEAN PRESSURE OF THE BUELL GAS LAW EQUATION AS A FUNCTION OF ALTITUDE

ARCTIC SUMMER EXTREME DIURNAL TRANSITION

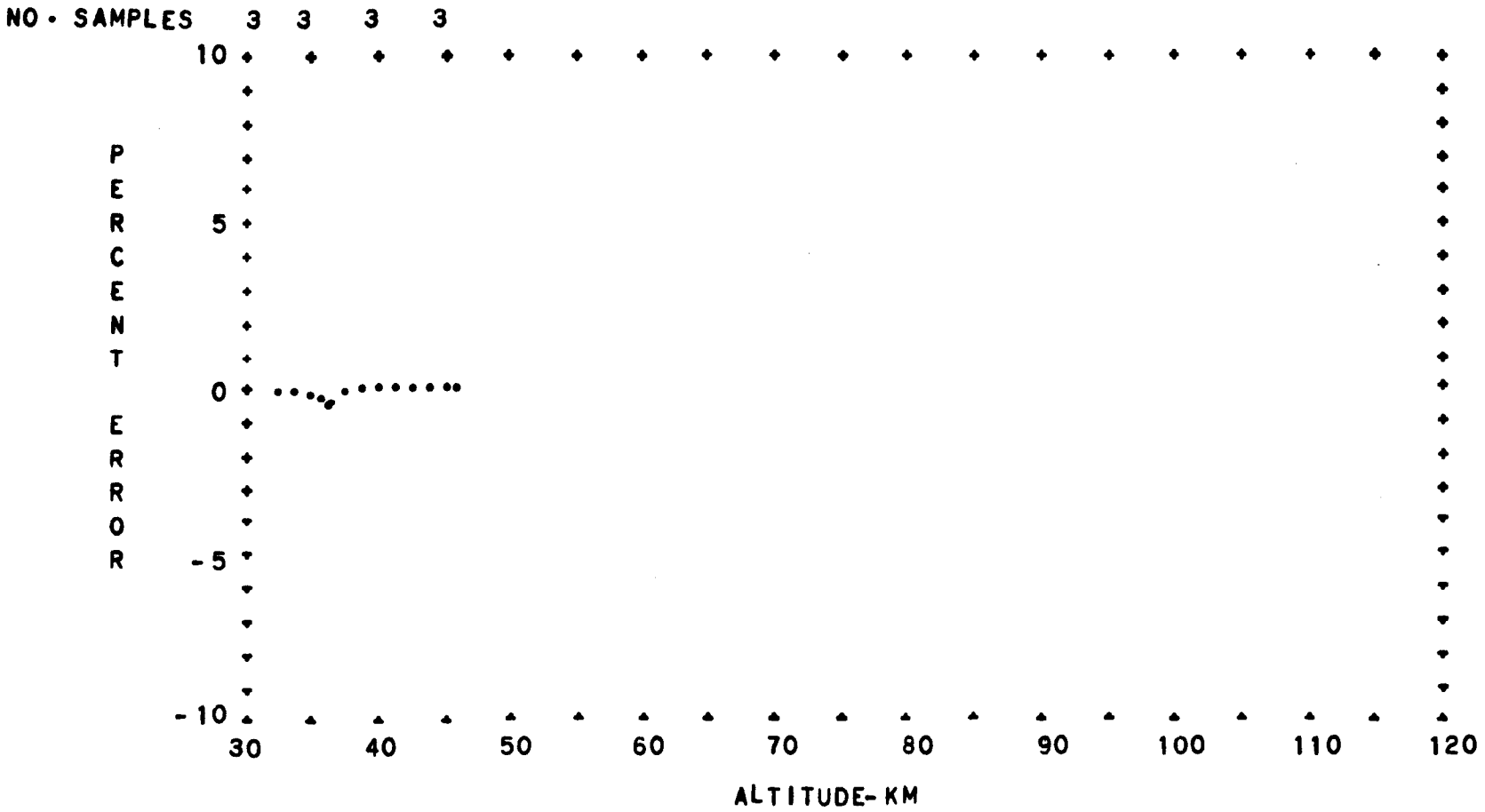

FIG. A-93 PERCENT CONTRIBUTION OF THE COVARIANCE TO THE MEAN PRESSURE OF THE BUELL GAS LAW EQUATION AS A FUNCTION OF ALTITUDE

ARCTIC SUMMER EXTREME DAYTIME

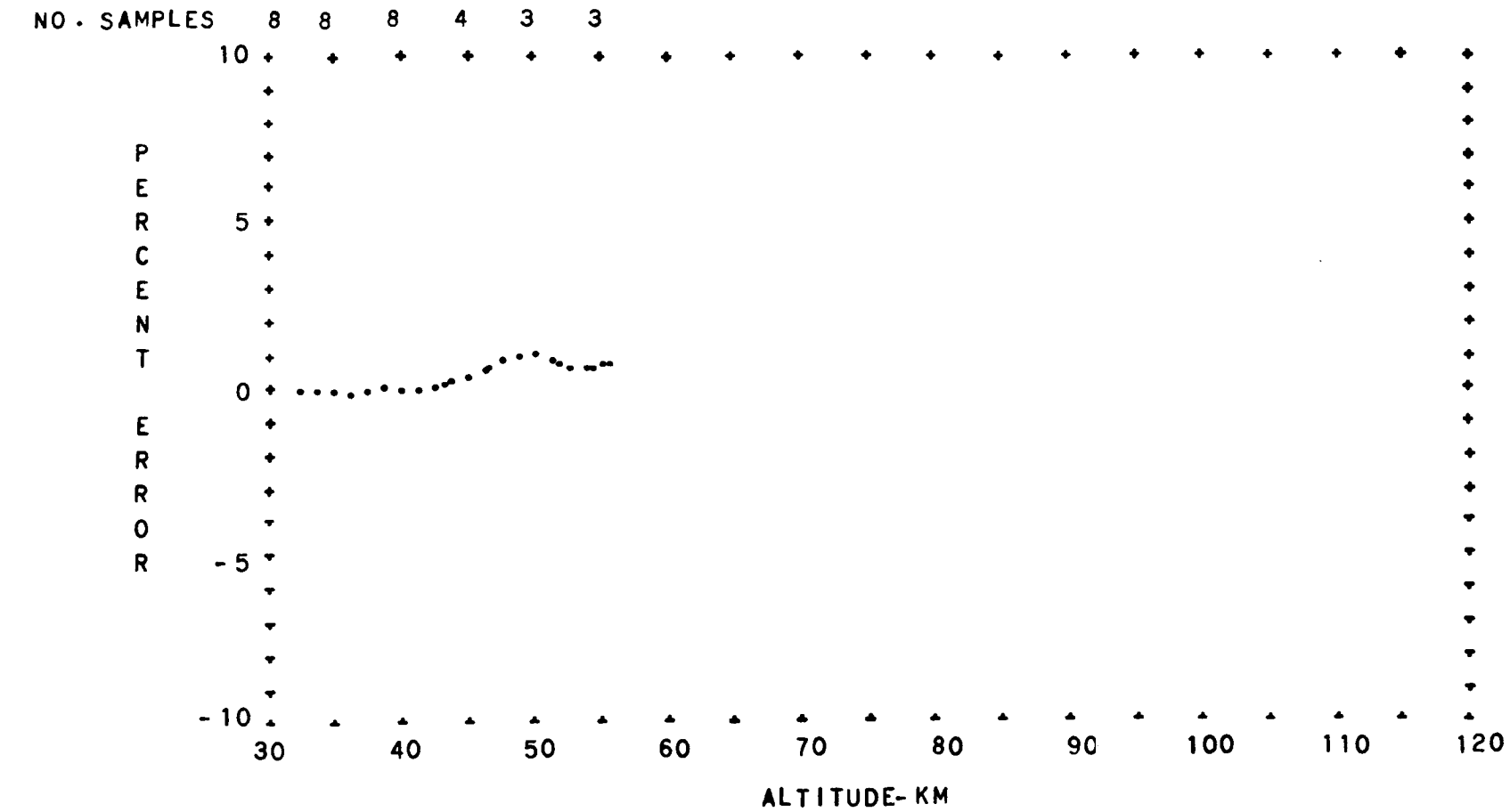

FIG. A-94 PERCENT CONTRIBUTION OF THE COVARIANCE TO THE MEAN PRESSURE OF THE BUELL GAS LAW EQUATION AS A FUNCTION OF ALTITUDE

ARCTIC SUMMER EXTREME DIURNAL MEAN

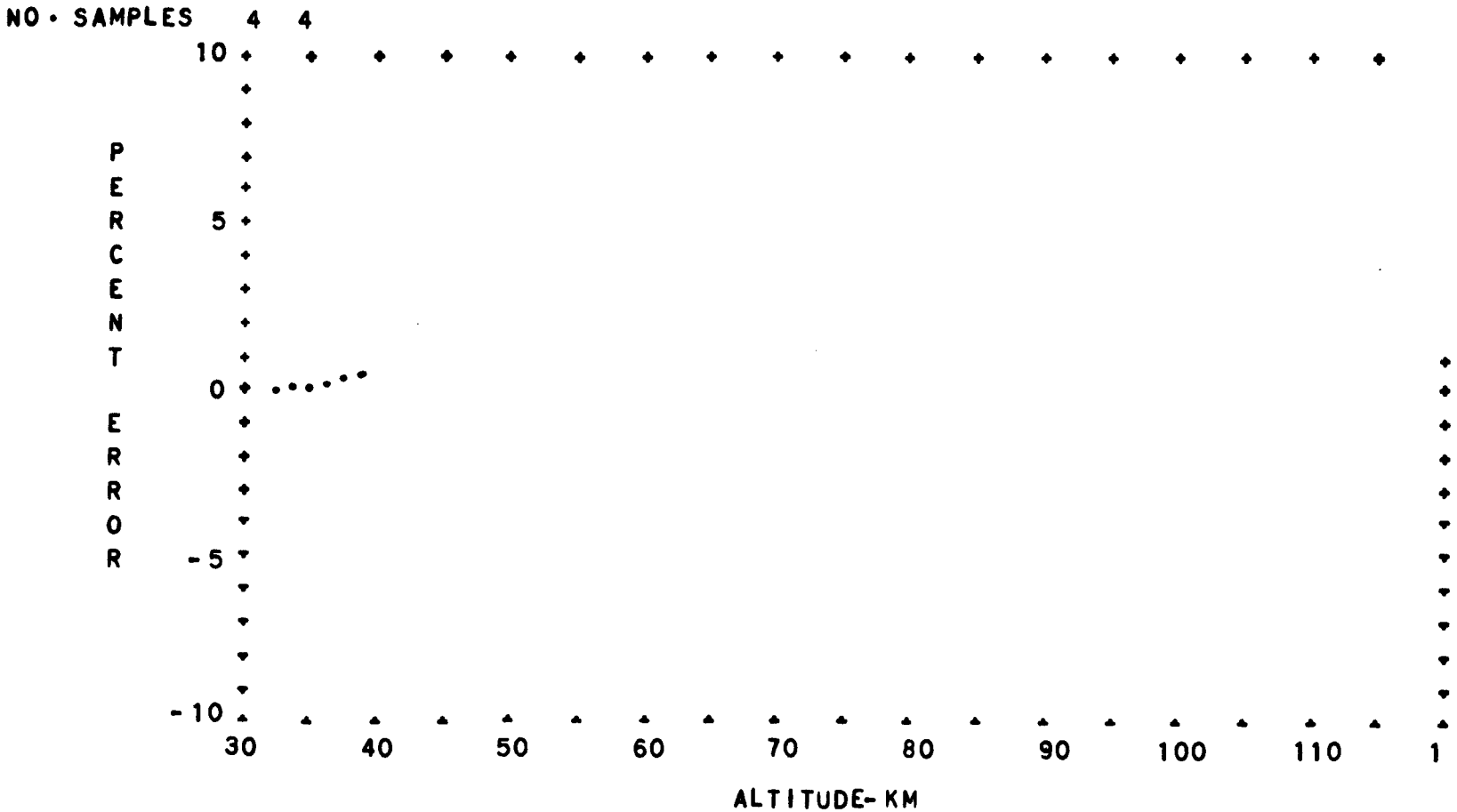

FIG. A-95 PERCENT CONTRIBUTION OF THE COVARIANCE TO THE MEAN PRESSURE OF THE BUELL GAS LAW EQUATION AS A FUNCTION OF ALTITUDE

ARCTIC WINTER EXTREME DIURNAL TRANSITION

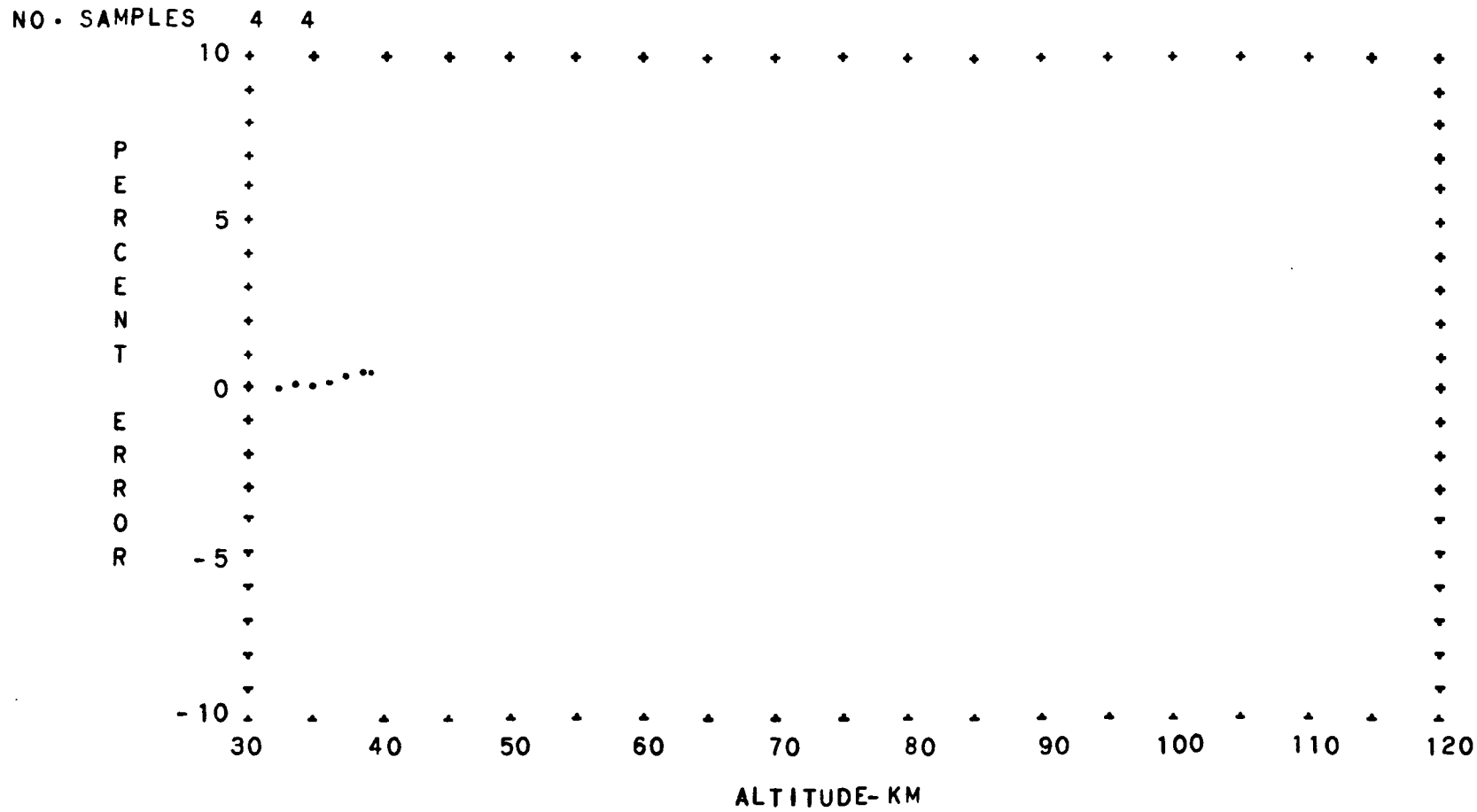

FIG. A-96 PERCENT CONTRIBUTION OF THE COVARIANCE TO THE MEAN PRESSURE OF THE BUELL GAS LAW EQUATION AS A FUNCTION OF ALTITUDE

ARCTIC WINTER EXTREME DIURNAL MEAN

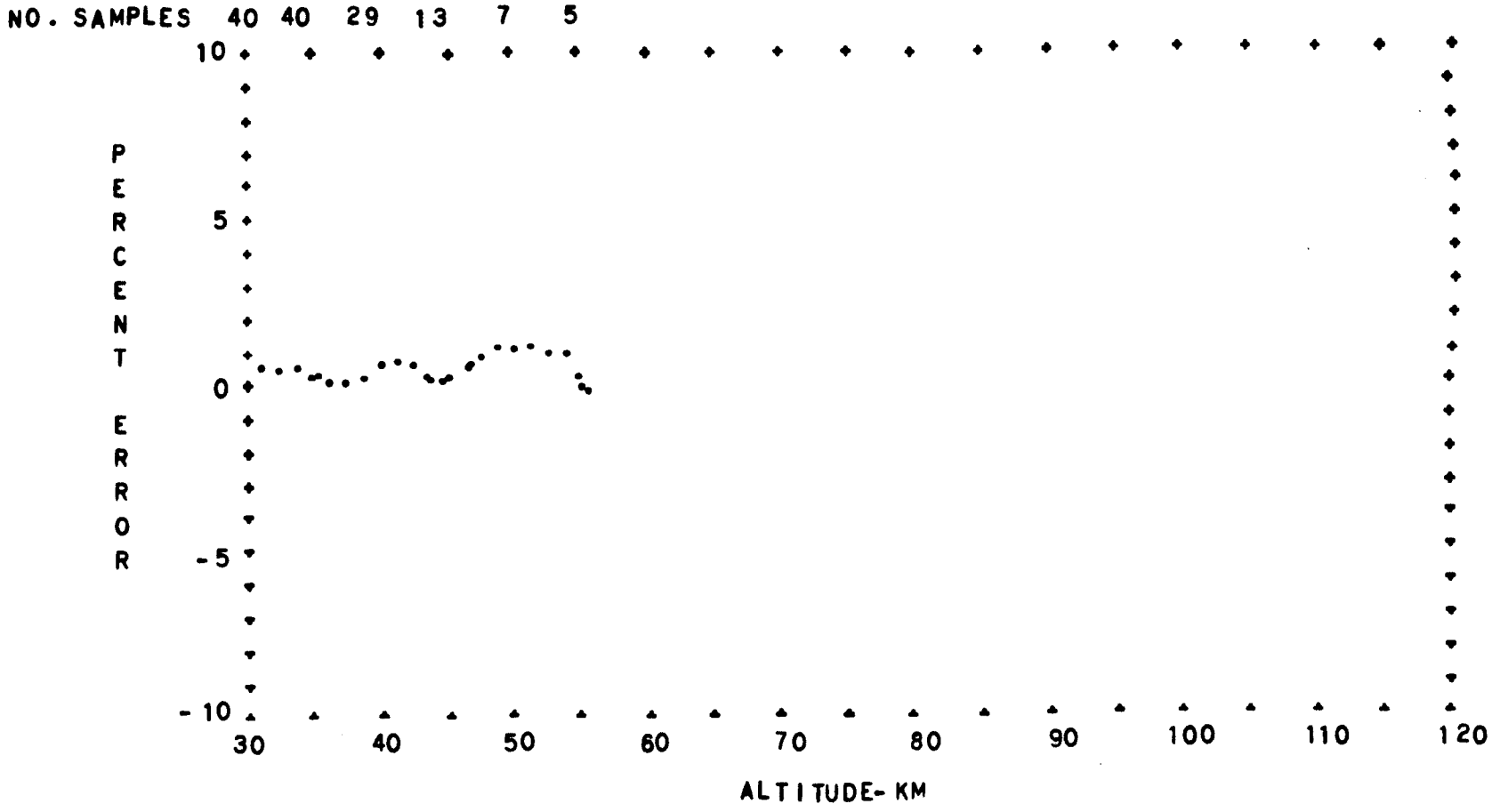

FIG. A-97 PERCENT CONTRIBUTION OF THE COVARIANCE TO THE MEAN PRESSURE OF THE BUELL GAS LAW EQUATION AS A FUNCTION OF ALTITUDE

ARCTIC ANNUAL MEAN DIURNAL TRANSITION

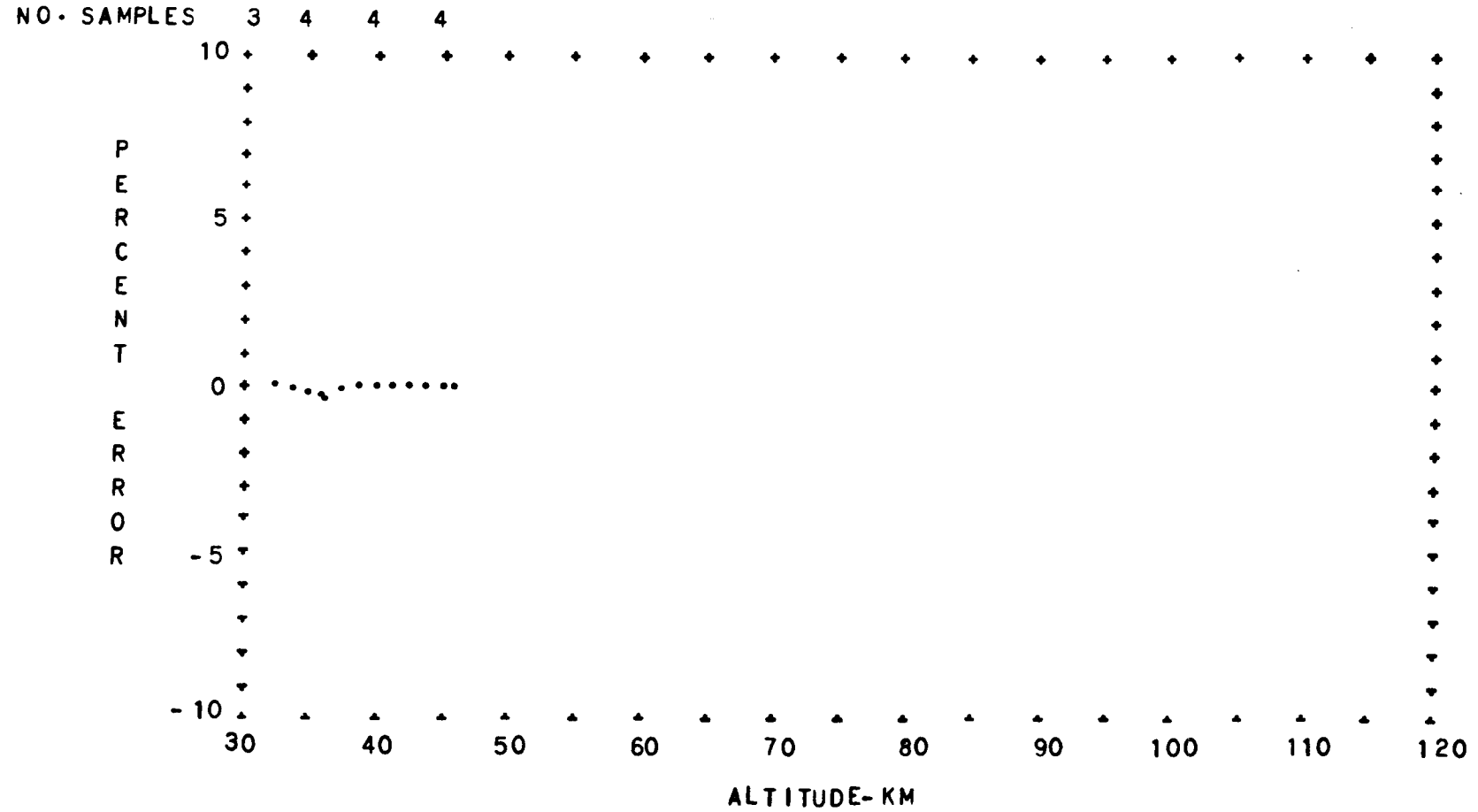

FIG. A-98 PERCENT CONTRIBUTION OF THE COVARIANCE TO THE MEAN PRESSURE OF THE BUELL GAS LAW EQUATION AS A FUNCTION OF ALTITUDE

ARCTIC ANNUAL MEAN DAYTIME

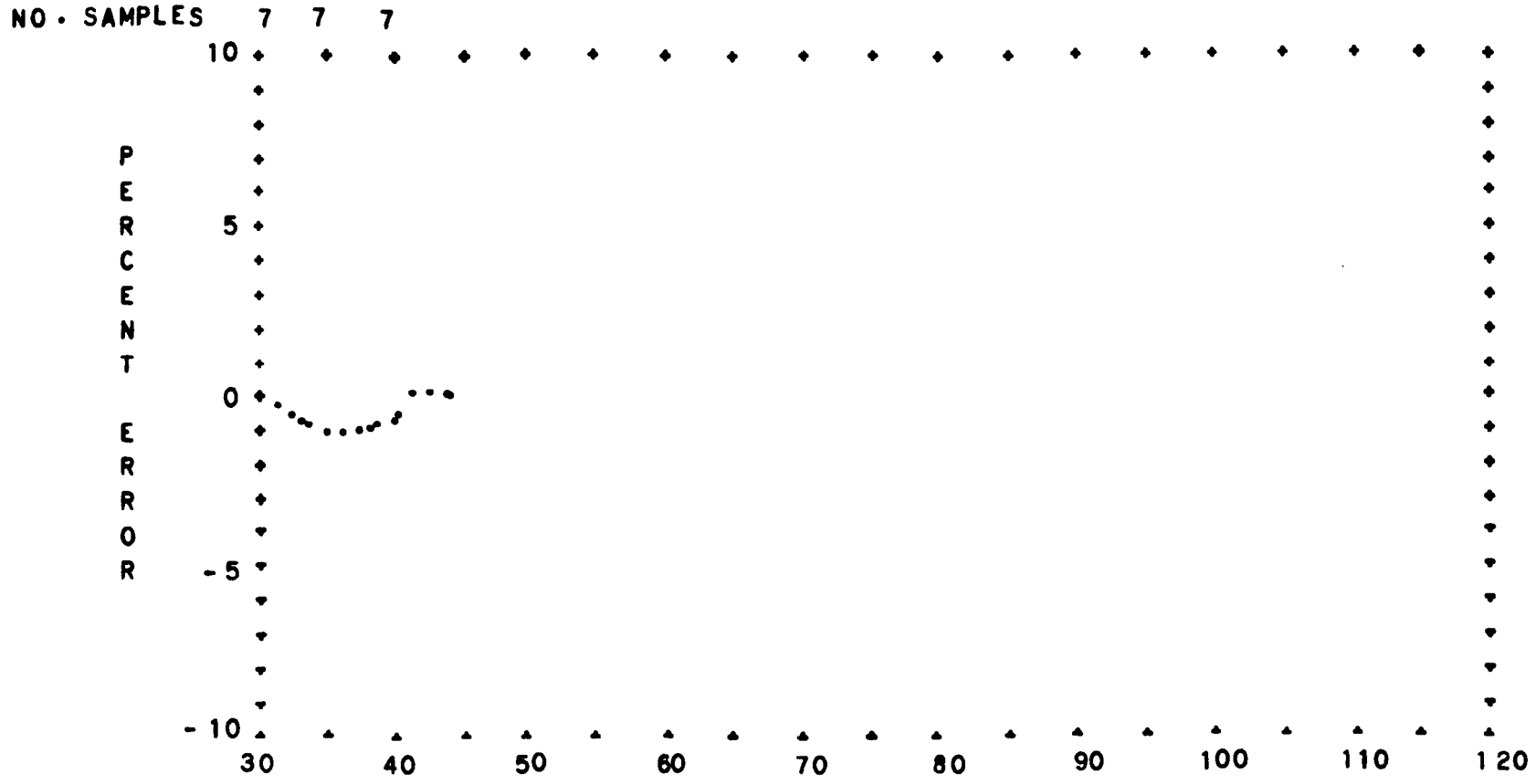

FIG. A-99 PERCENT CONTRIBUTION OF THE COVARIANCE TO THE MEAN PRESSURE OF THE BUELL GAS LAW EQUATION AS A FUNCTION OF ALTITUDE

ARCTIC ANNUAL MEAN NIGHTTIME

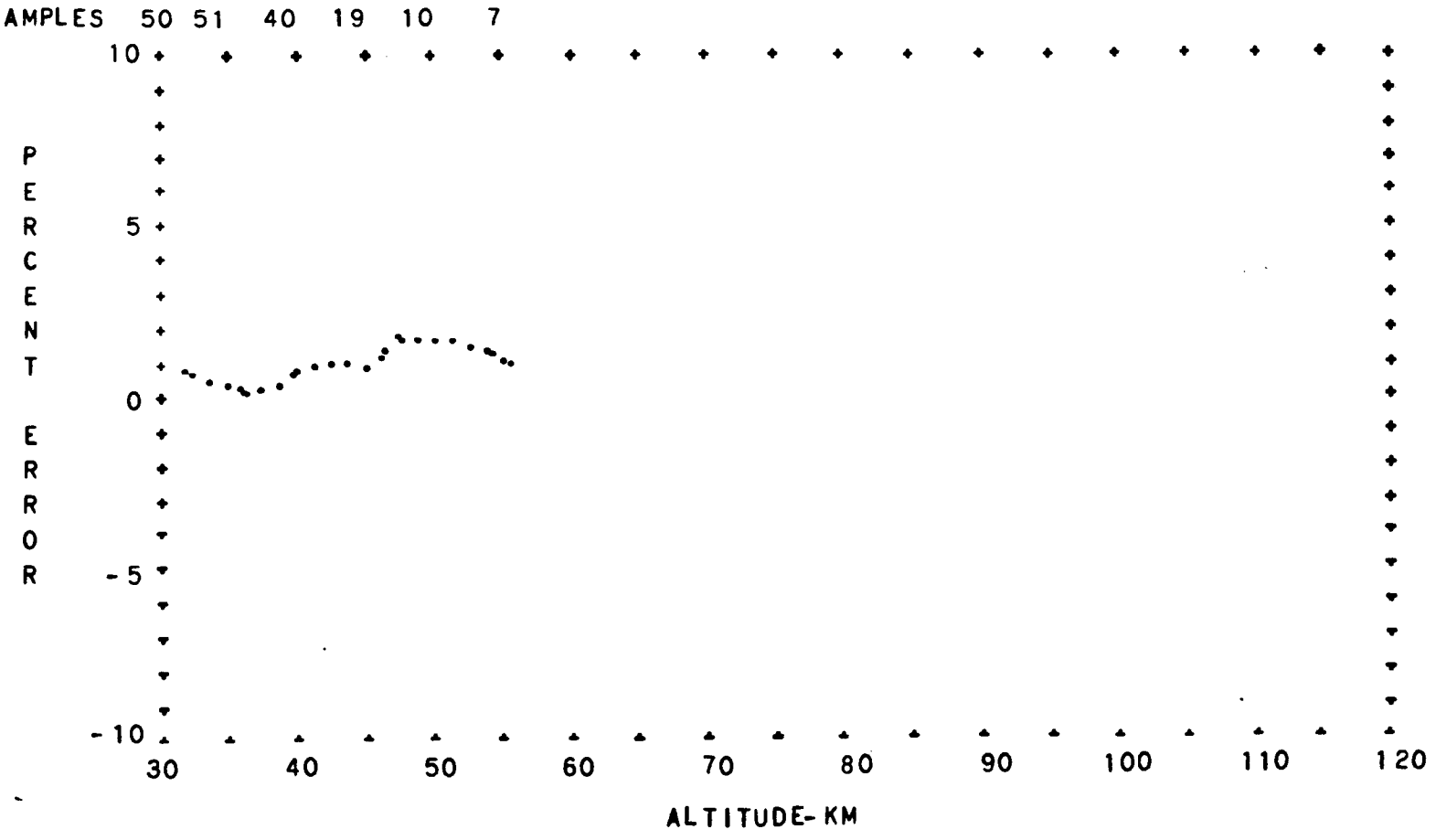

FIG. A-100 PERCENT CONTRIBUTION OF THE COVARIANCE TO THE MEAN PRESSURE OF THE BUELL GAS LAW EQUATION AS A FUNCTION OF ALTITUDE

ARCTIC ANNUAL MEAN DIURNAL MEAN

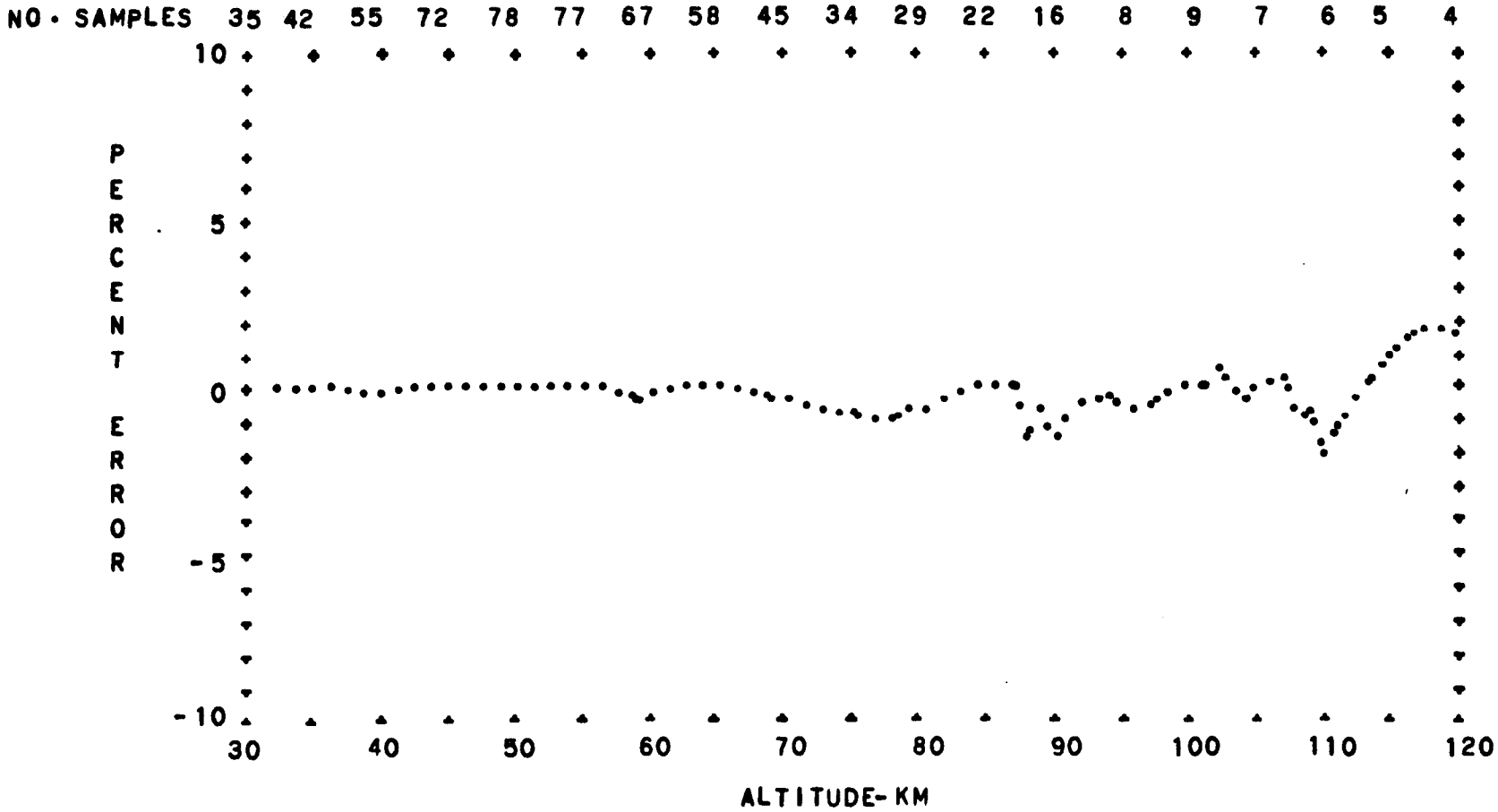

FIG. A-101 PERCENT CONTRIBUTION OF THE COVARIANCE TO THE MEAN PRESSURE OF THE BUELL GAS LAW EQUATION AS A FUNCTION OF ALTITUDE

HEMISPHERICAL MEAN SPRING DIURNAL MEAN

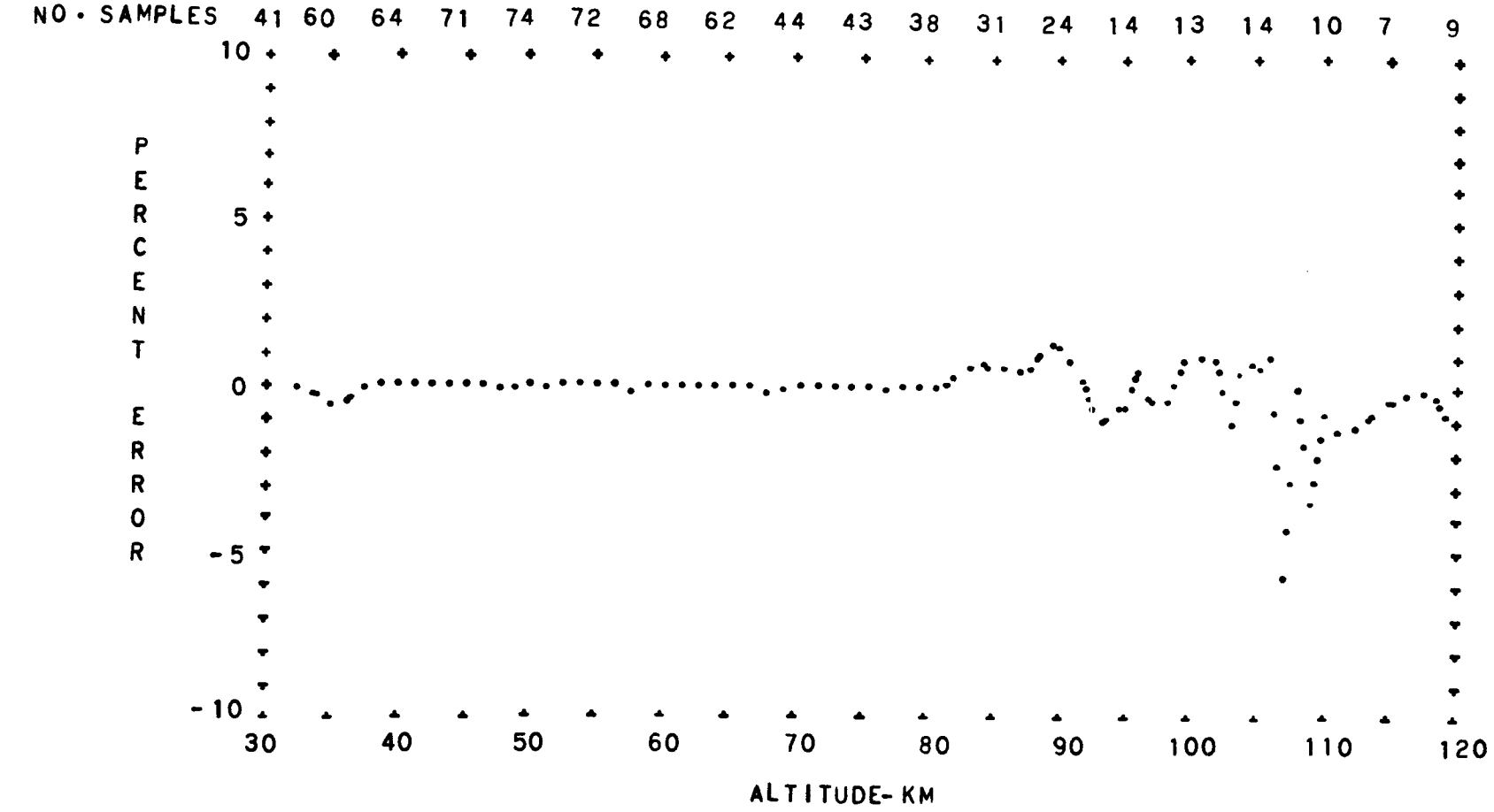

FIG. A-102 PERCENT CONTRIBUTION OF THE COVARIANCE TO THE MEAN PRESSURE OF THE BUELL GAS LAW EQUATION AS A FUNCTION OF ALTITUDE

HEMISPHERICAL MEAN SUMMER DIURNAL MEAN

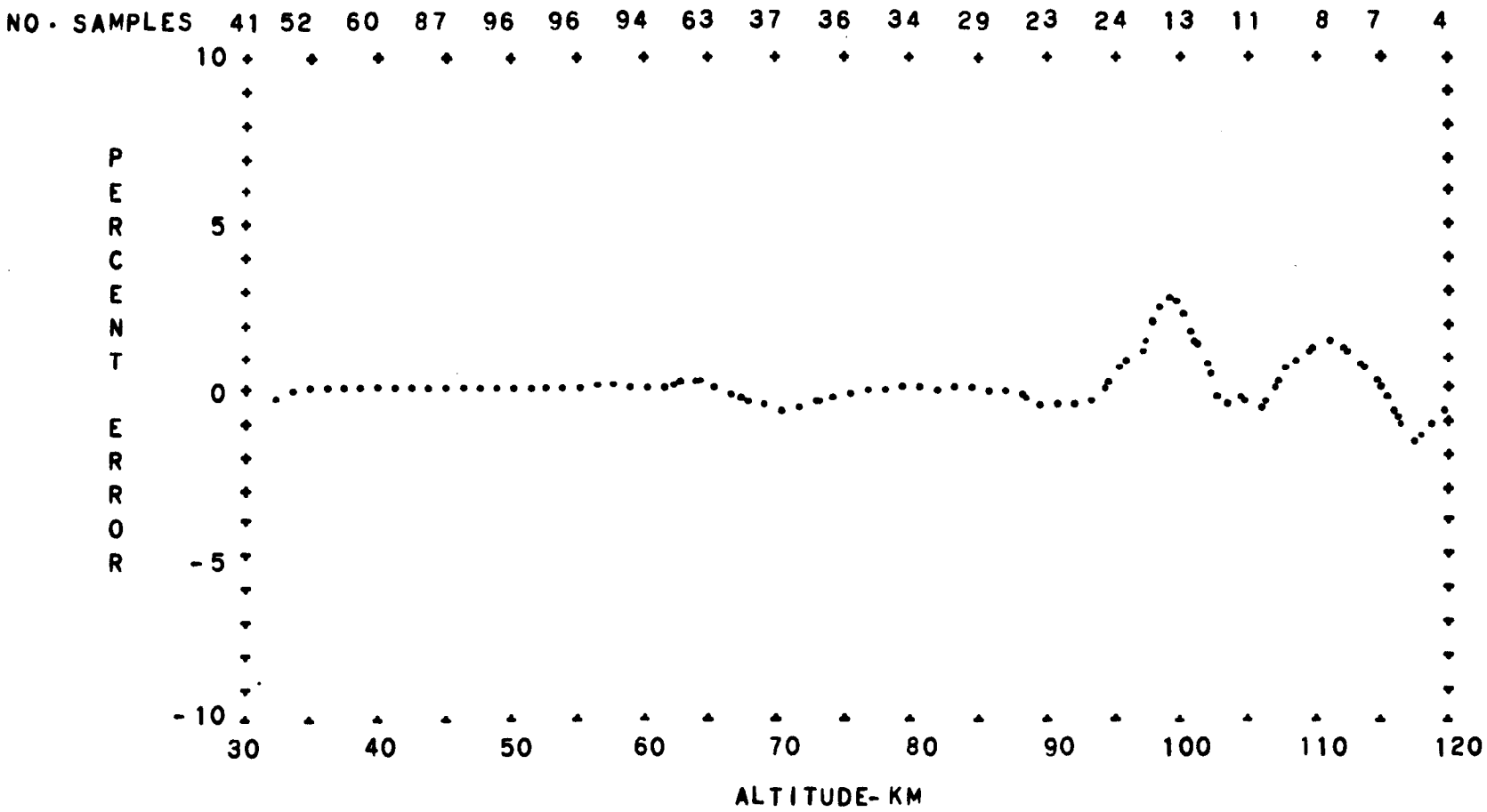

FIG. A-103 PERCENT CONTRIBUTION OF THE COVARIANCE TO THE MEAN PRESSURE OF THE BUELL GAS LAW EQUATION AS A FUNCTION OF ALTITUDE

HEMISPHERICAL MEAN AUTUMN DIURNAL MEAN

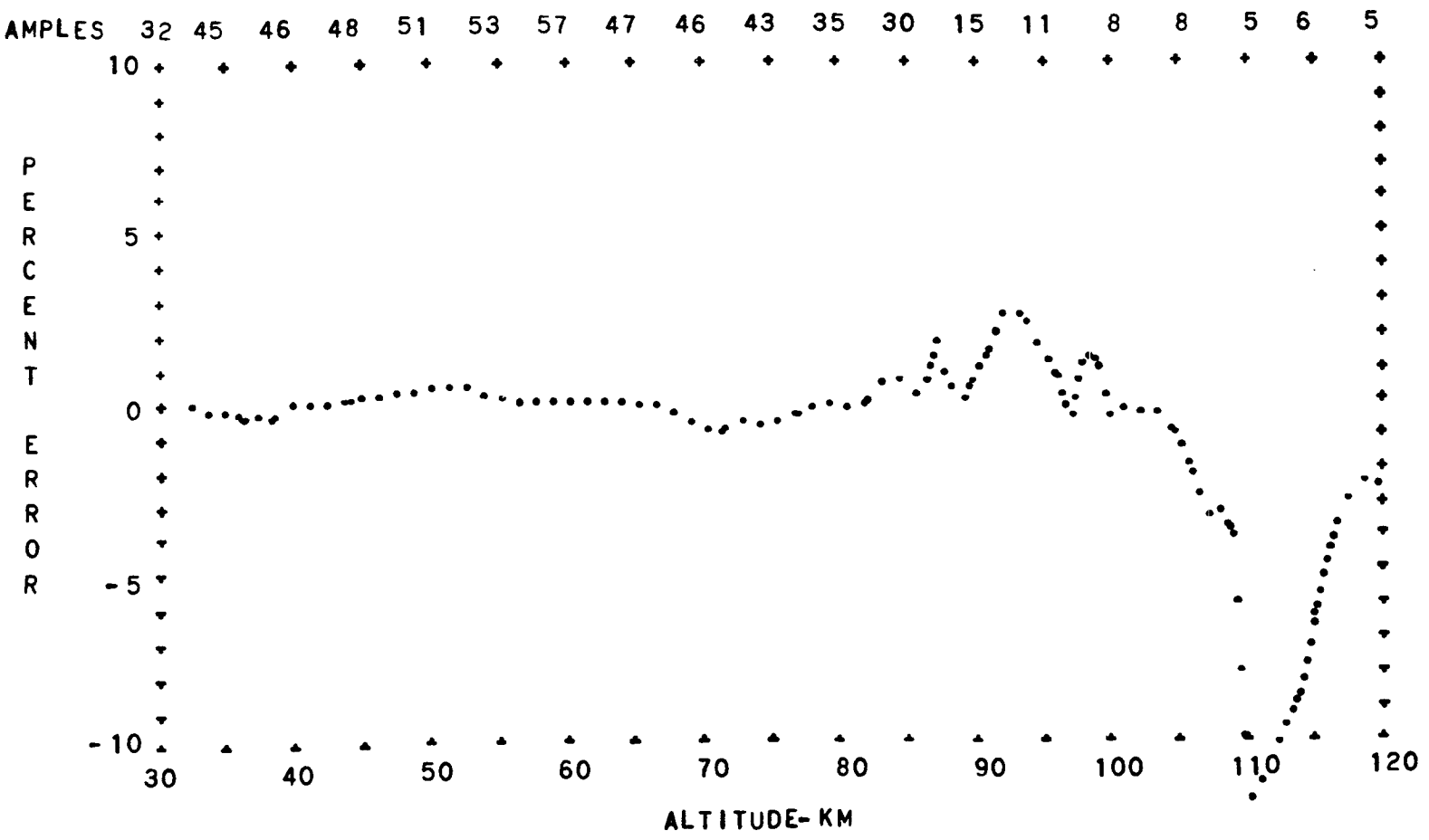

FIG. A-104 PERCENT CONTRIBUTION OF THE COVARIANCE TO THE MEAN PRESSURE OF THE BUELL GAS LAW EQUATION AS A FUNCTION OF ALTITUDE

HEMISPHERICAL MEAN WINTER DIURNAL MEAN

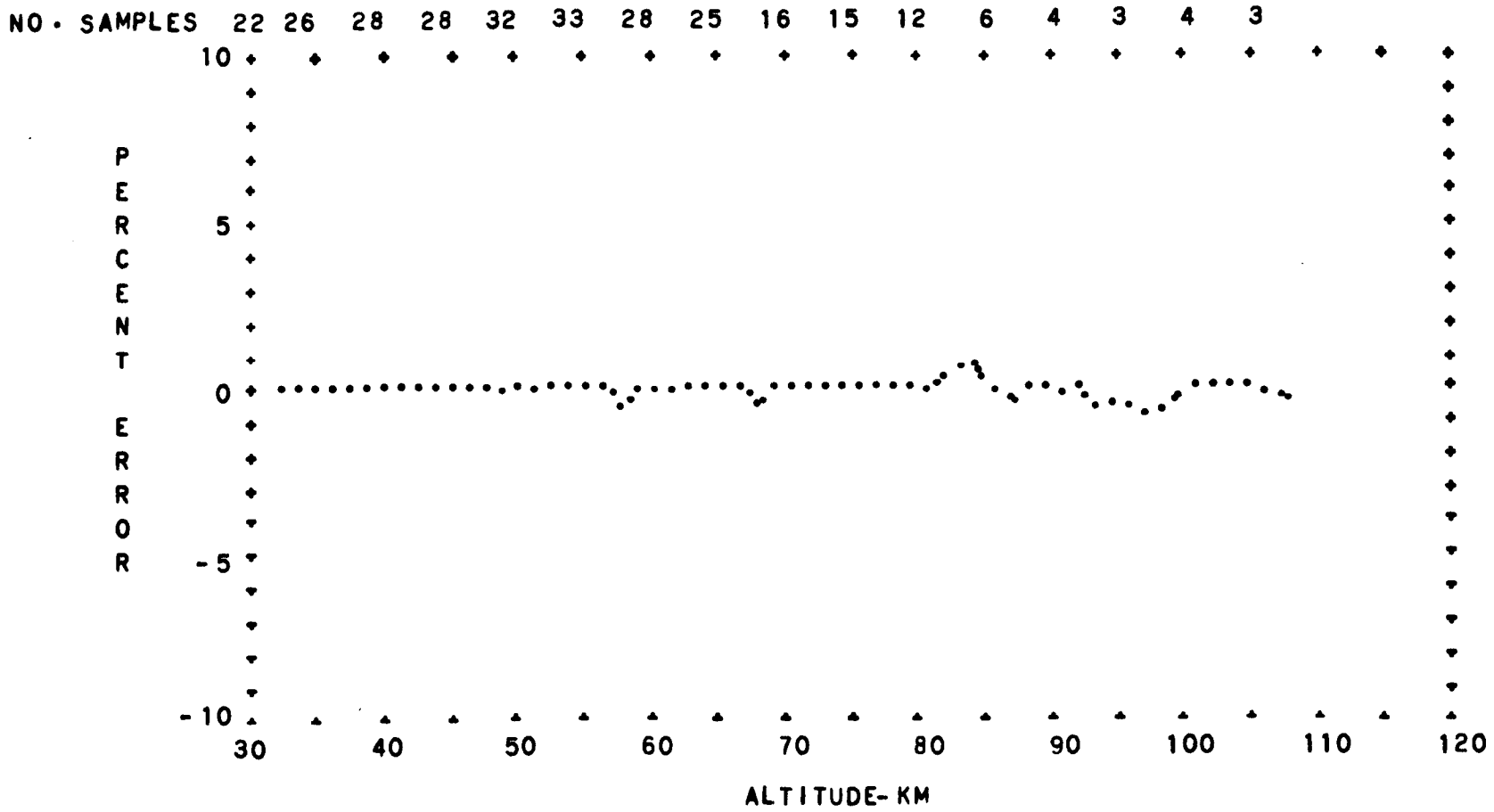

FIG. A-105 PERCENT CONTRIBUTION OF THE COVARIANCE TO THE MEAN PRESSURE OF THE BUELL GAS LAW EQUATION AS A FUNCTION OF ALTITUDE

HEMISPHERICAL MEAN SUMMER EXTREME DIURNAL MEAN

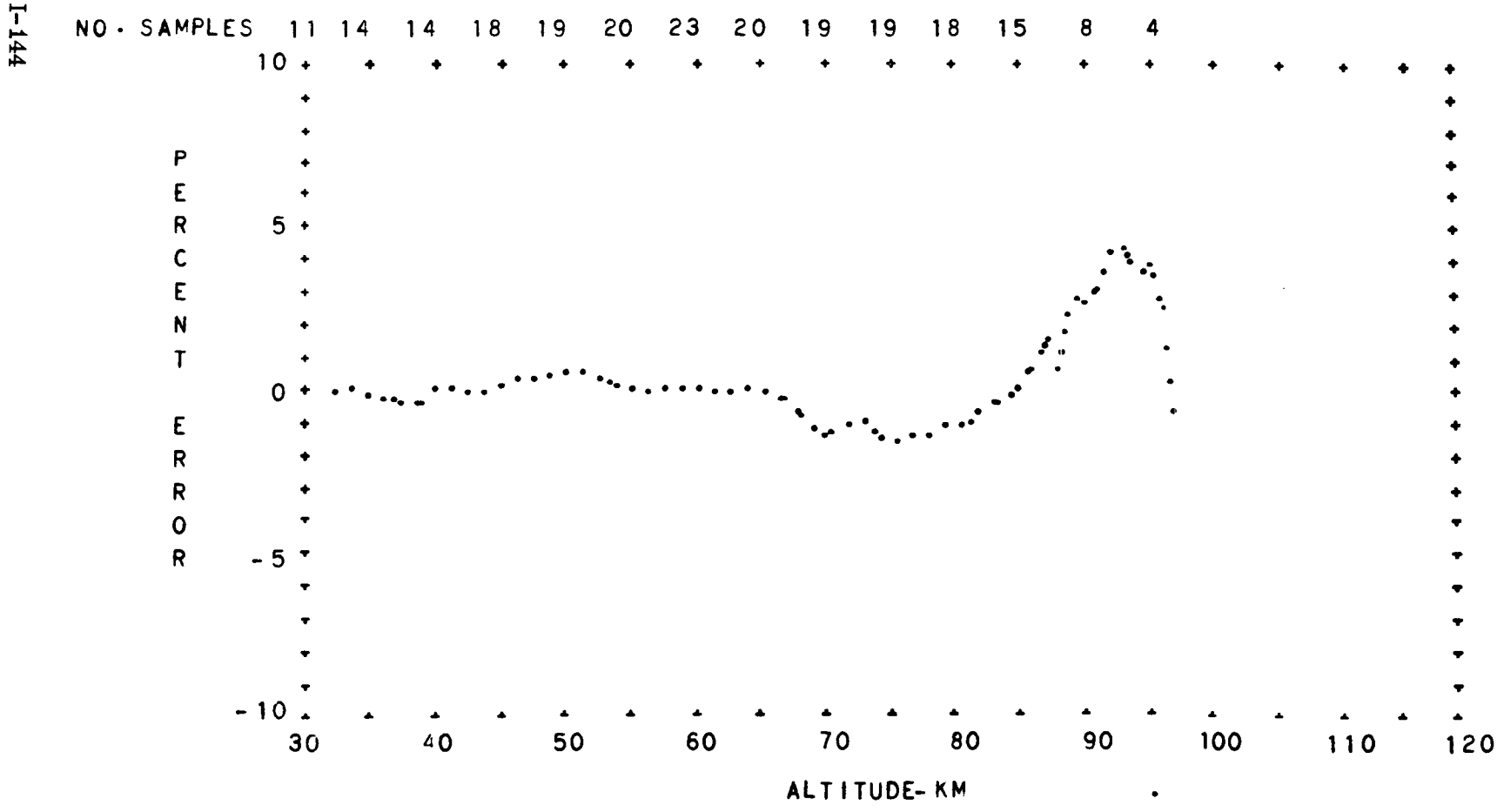

FIG. A-106 PERCENT CONTRIBUTION OF THE COVARIANCE TO THE MEAN PRESSURE OF THE BUELL GAS LAW EQUATION AS A FUNCTION OF ALTITUDE

HEMISPHERICAL MEAN WINTER EXTREME DIURNAL MEAN

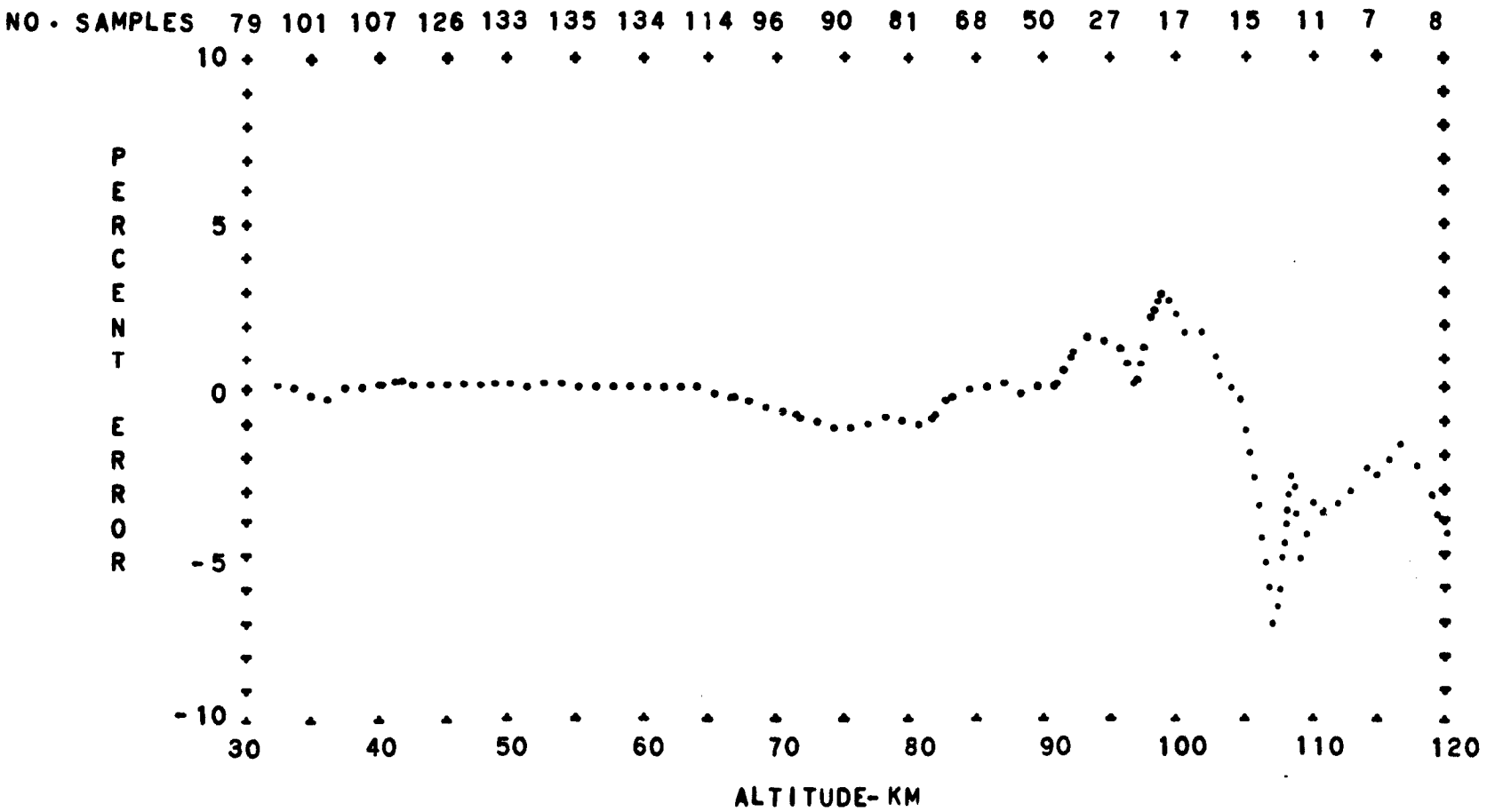

FIG. A-107 PERCENT CONTRIBUTION OF THE COVARIANCE TO THE MEAN PRESSURE OF THE BUELL GAS LAW EQUATION AS A FUNCTION OF ALTITUDE

HEMISPHERICAL MEAN ANNUAL MEAN DIURNAL TRANSITION

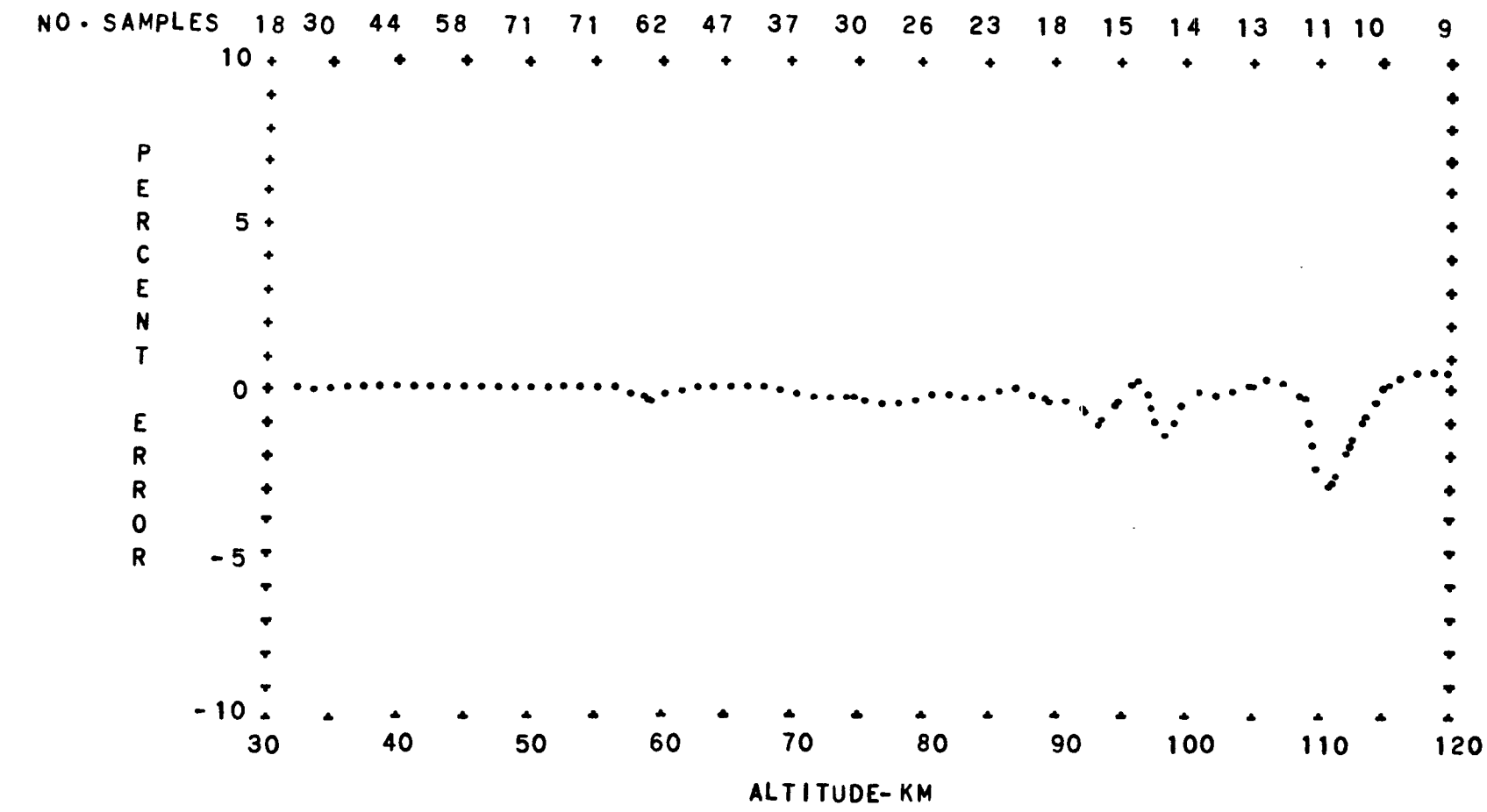

FIG. A-108 PERCENT CONTRIBUTION OF THE COVARIANCE TO THE MEAN PRESSURE OF THE BUELL GAS LAW EQUATION AS A FUNCTION OF ALTITUDE

HEMISPHERICAL MEAN ANNUAL MEAN DAYTIME

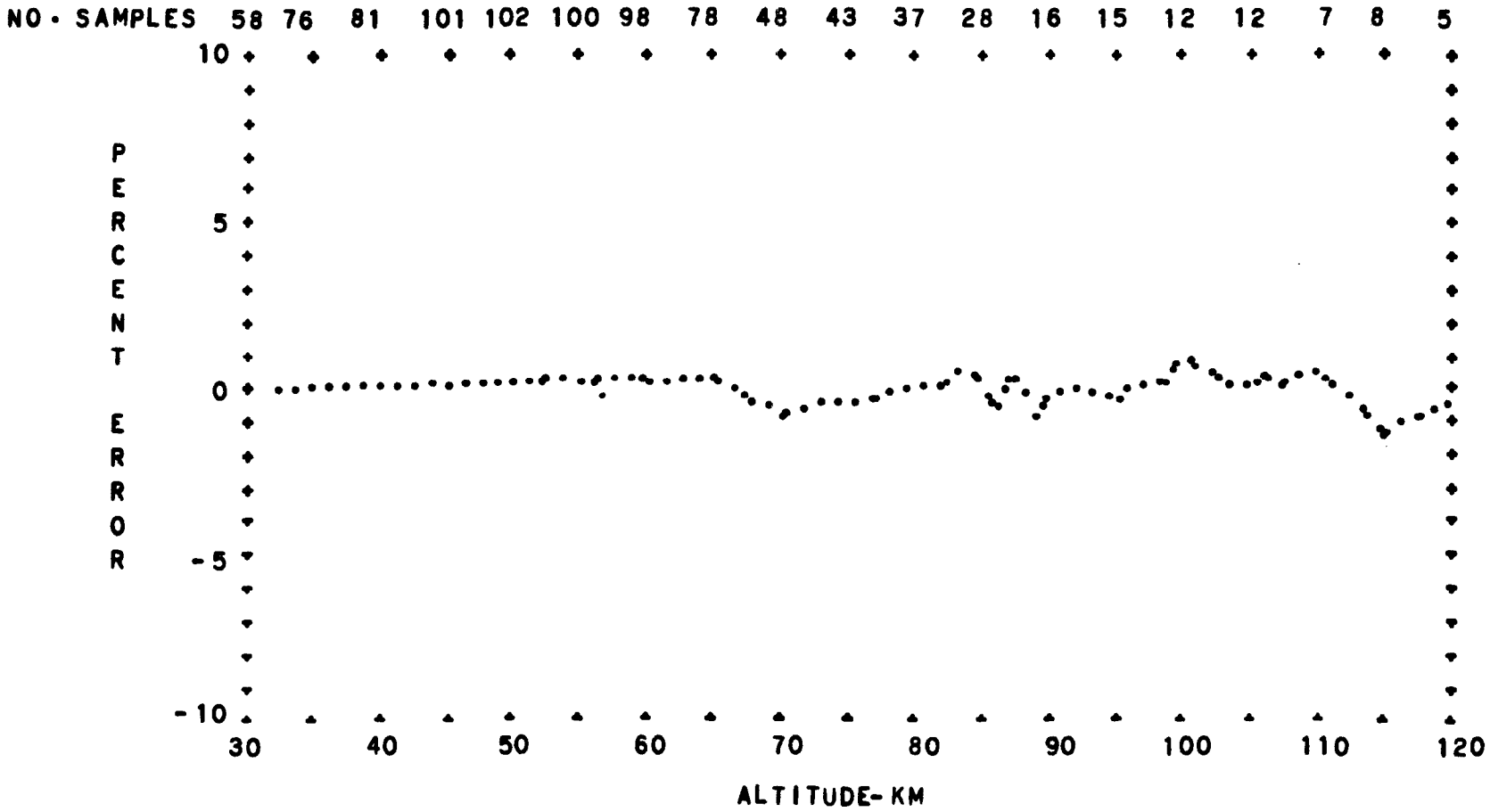

FIG. A-109 PERCENT CONTRIBUTION OF THE COVARIANCE TO THE MEAN PRESSURE OF THE BUELL GAS LAW EQUATION AS A FUNCTION OF ALTITUDE

HEMISPHERICAL MEAN ANNUAL MEAN NIGHTTIME

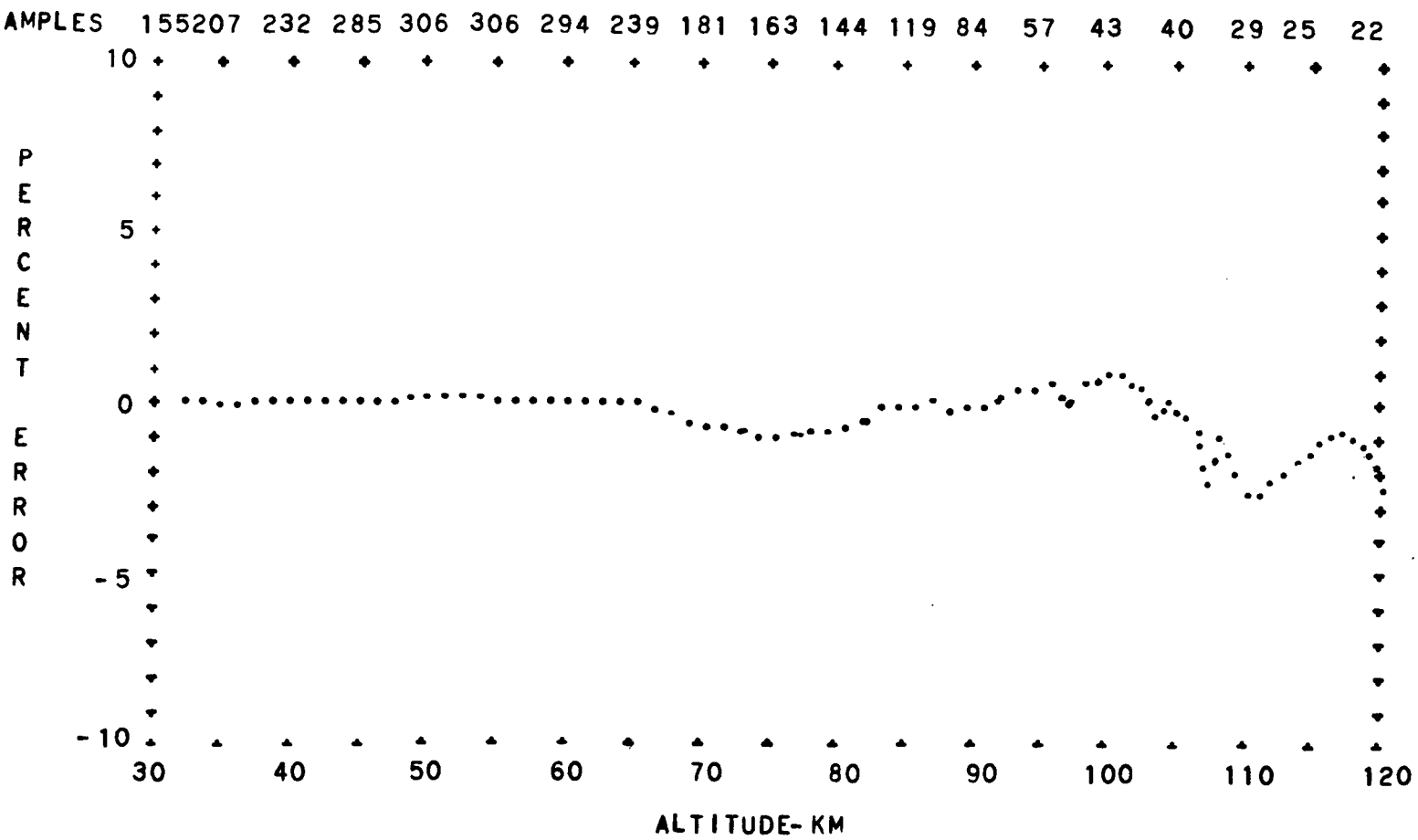

FIG. A-110 PERCENT CONTRIBUTION OF THE COVARIANCE TO THE MEAN PRESSURE OF THE BUELL GAS LAW EQUATION AS A FUNCTION OF ALTITUDE

HEMISPHERICAL MEAN ANNUAL MEAN DIURNAL MEAN

APPENDIX B

STATISTICAL HYDROSTATIC EQUATION GRAPHS

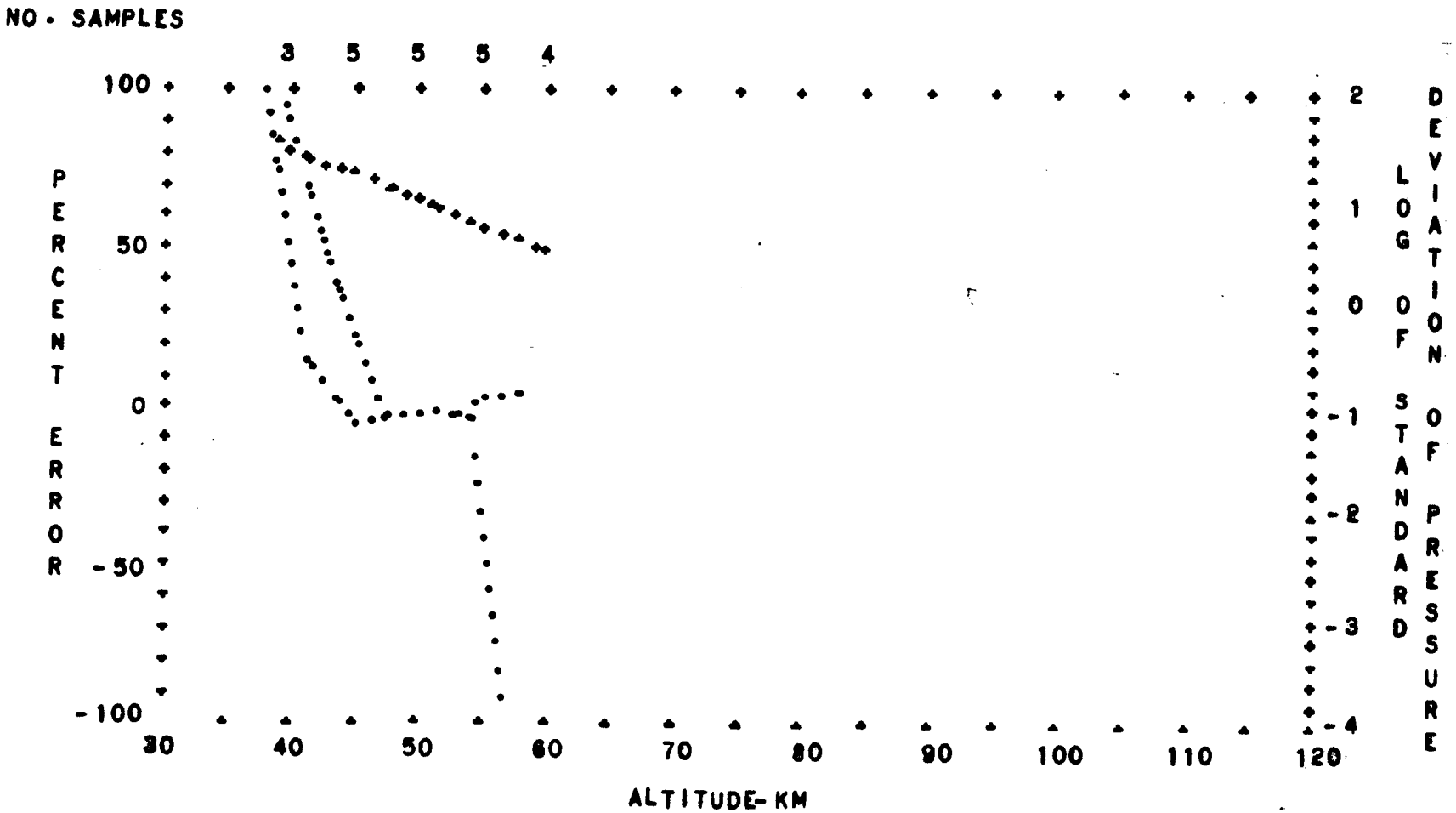

FIG. B-1. STANDARD DEVIATION OF PRESSURE AND PERCENT ERROR OF BUELL HYDROSTATIC EQUATION VERSUS ALTITUDE

TROPICAL SPRING DIURNAL TRANSITION

PERCENT ERROR--DOTS LOG DEVIATION--CROSSES

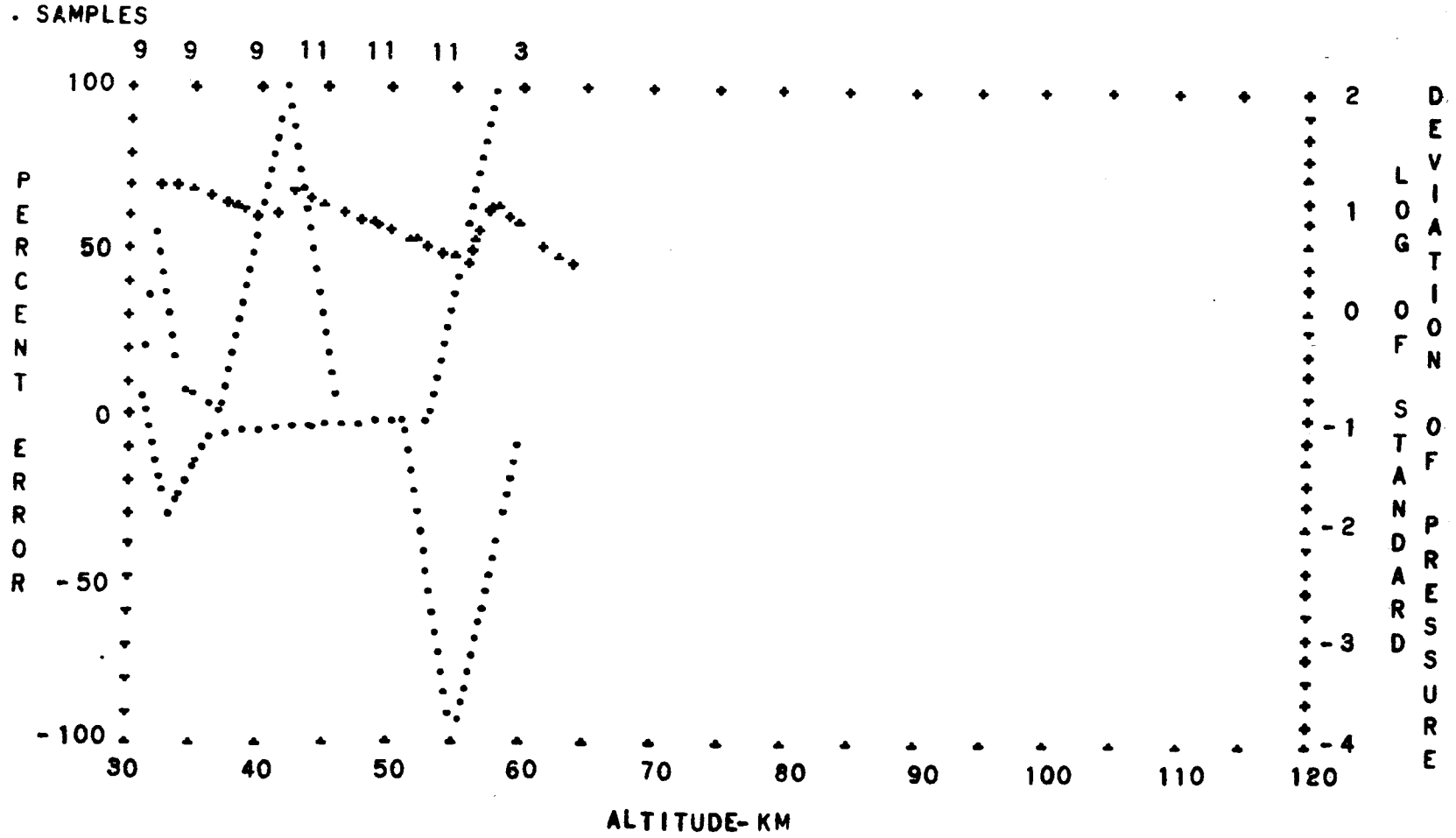

FIG. B-2. STANDARD DEVIATION OF PRESSURE AND PERCENT ERROR OF BUELL HYDROSTATIC EQUATION VERSUS ALTITUDE

TROPICAL SPRING DAYTIME

PERCENT ERROR--DOTS

LOG DEVIATION--CROSSES

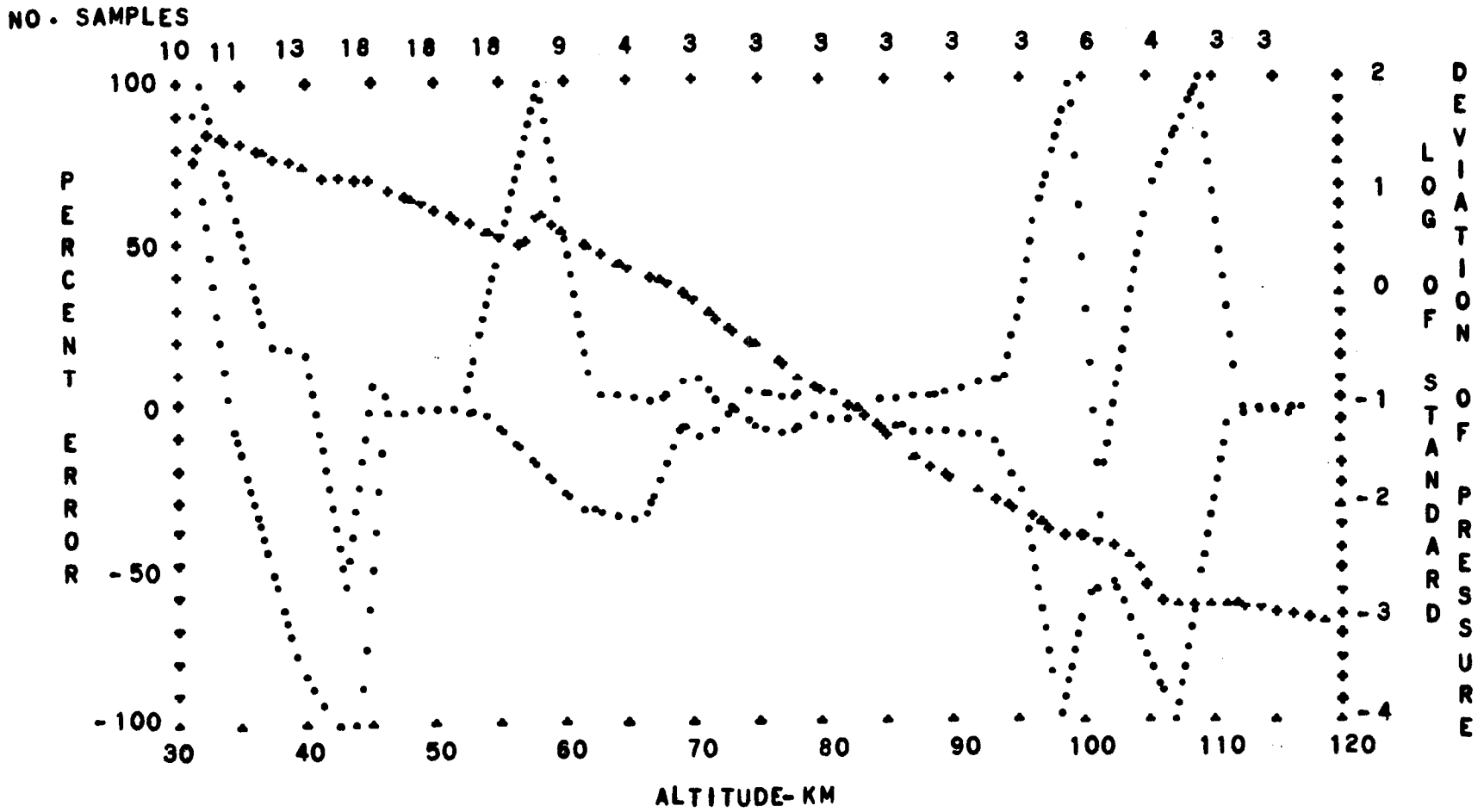

FIG. B-3. STANDARD DEVIATION OF PRESSURE AND PERCENT ERROR OF BUELL HYDROSTATIC EQUATION VERSUS ALTITUDE

TROPICAL SPRING DIURNAL MEAN

PERCENT ERROR--DOTS LOG DEVIATION--CROSSES

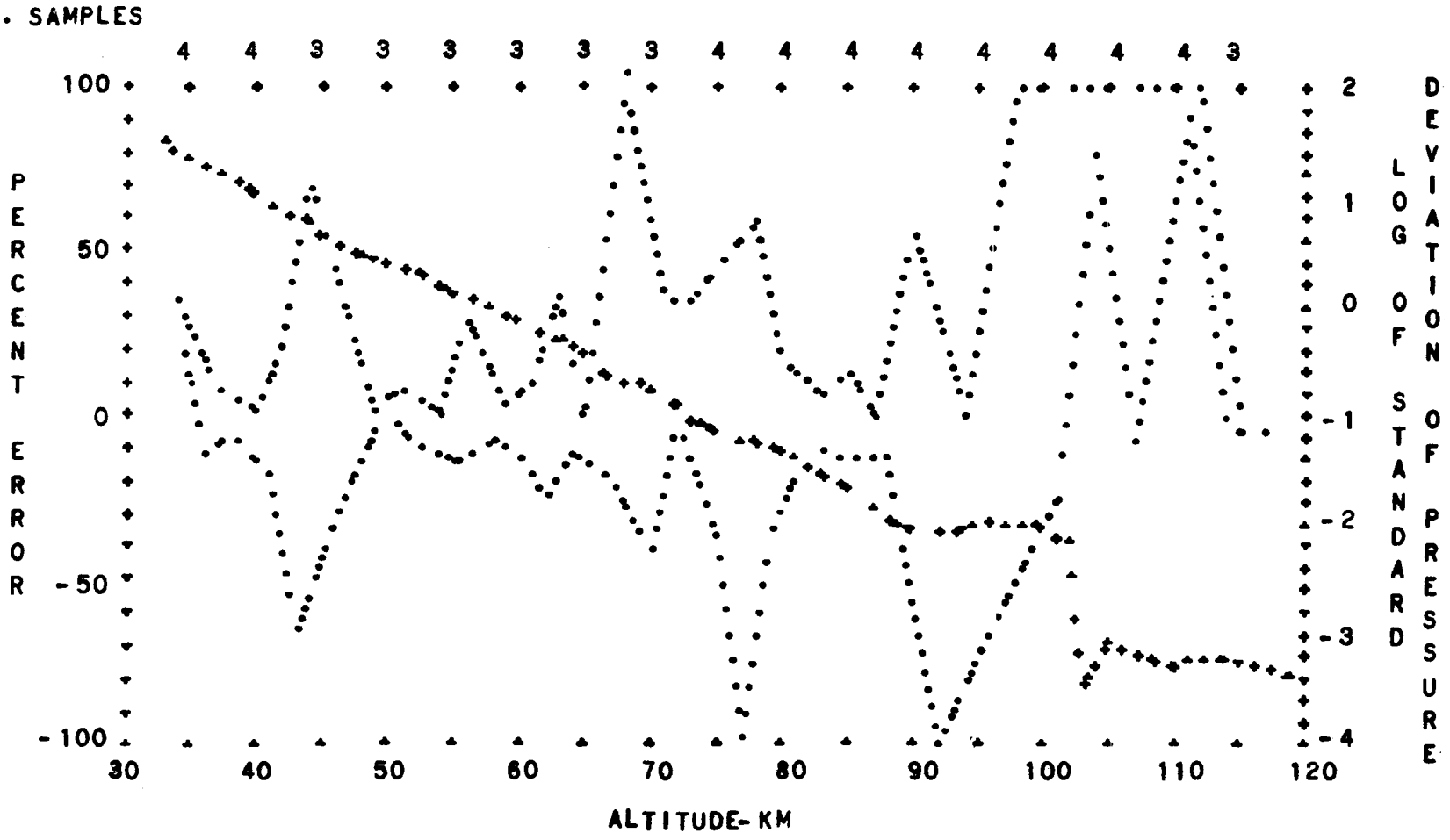

FIG. B-4. STANDARD DEVIATION OF PRESSURE AND PERCENT ERROR OF BUELL HYDROSTATIC EQUATION VERSUS ALTITUDE

TROPICAL SUMMER DAYTIME

PERCENT ERROR--DOTS LOG DEVIATION--CROSSES

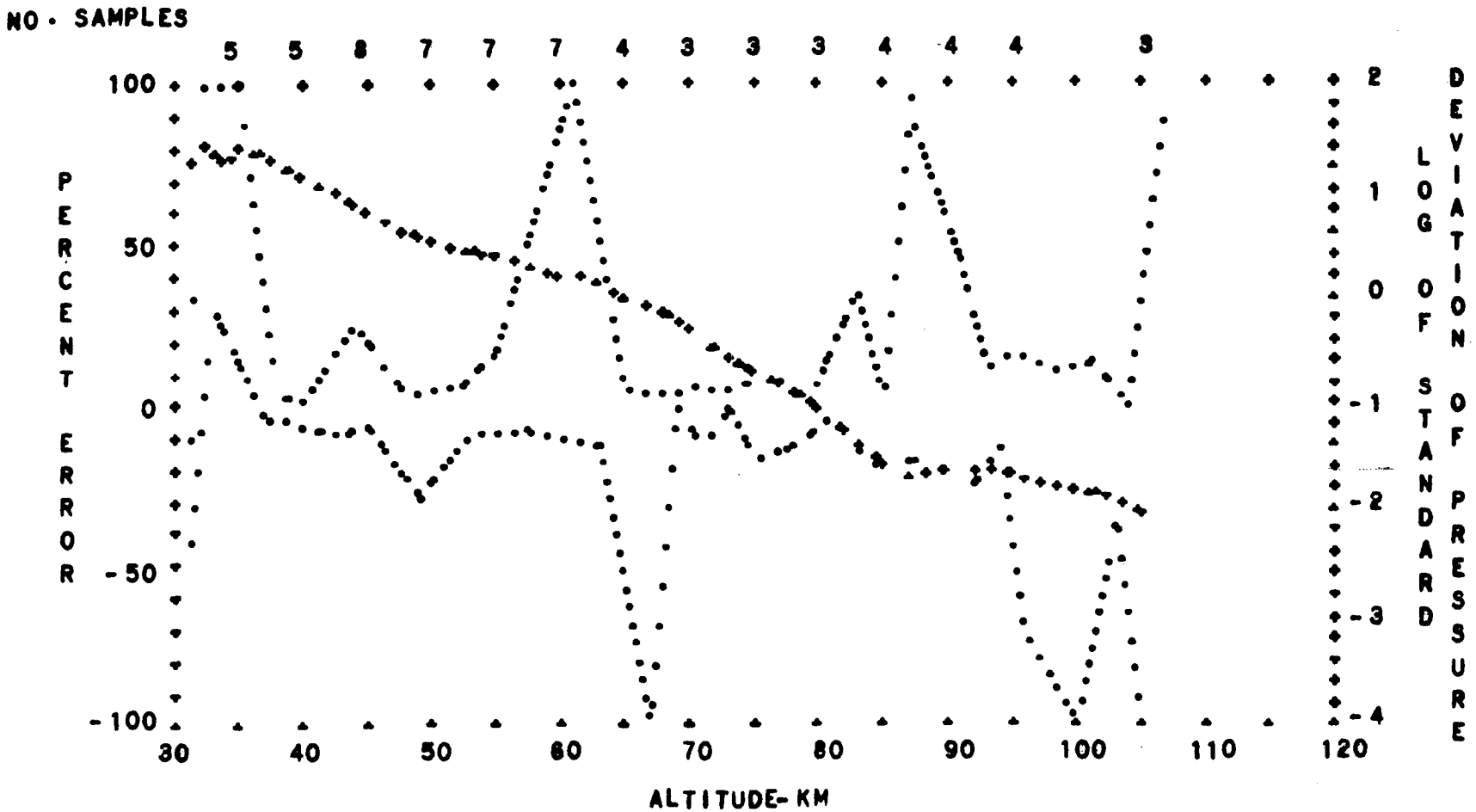

FIG. B-5. STANDARD DEVIATION OF PRESSURE AND PERCENT ERROR OF BUELL HYDROSTATIC EQUATION VERSUS ALTITUDE

TROPICAL SUMMER NIGHTTIME

PERCENT ERROR--DOTS LOG DEVIATION--CROSSES

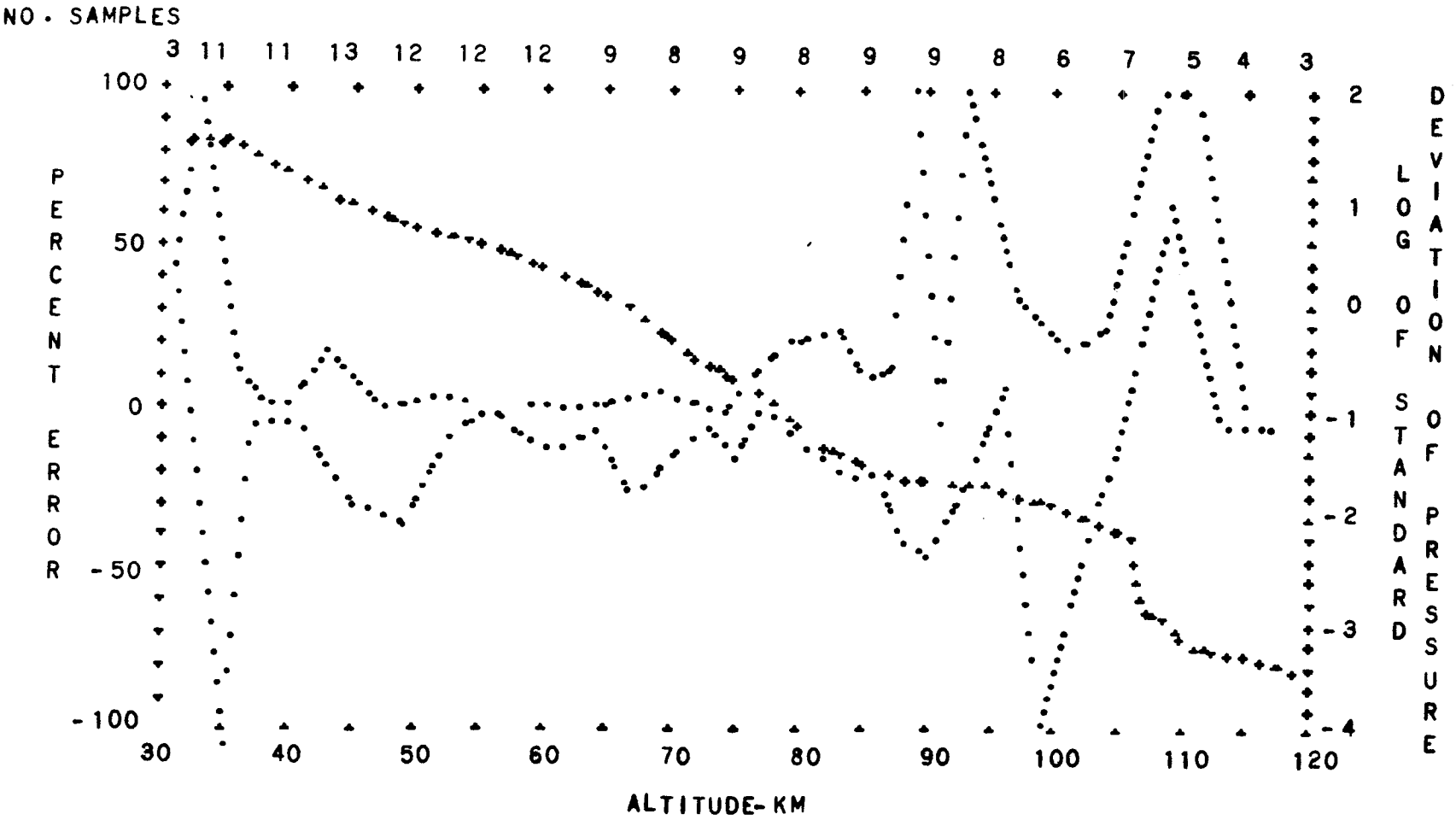

FIG. B-6. STANDARD DEVIATION OF PRESSURE AND PERCENT ERROR OF BUELL HYDROSTATIC EQUATION VERSUS ALTITUDE

TROPICAL SUMMER DIURNAL MEAN

PERCENT ERROR--DOTS LOG. DEVIATION--CROSSES

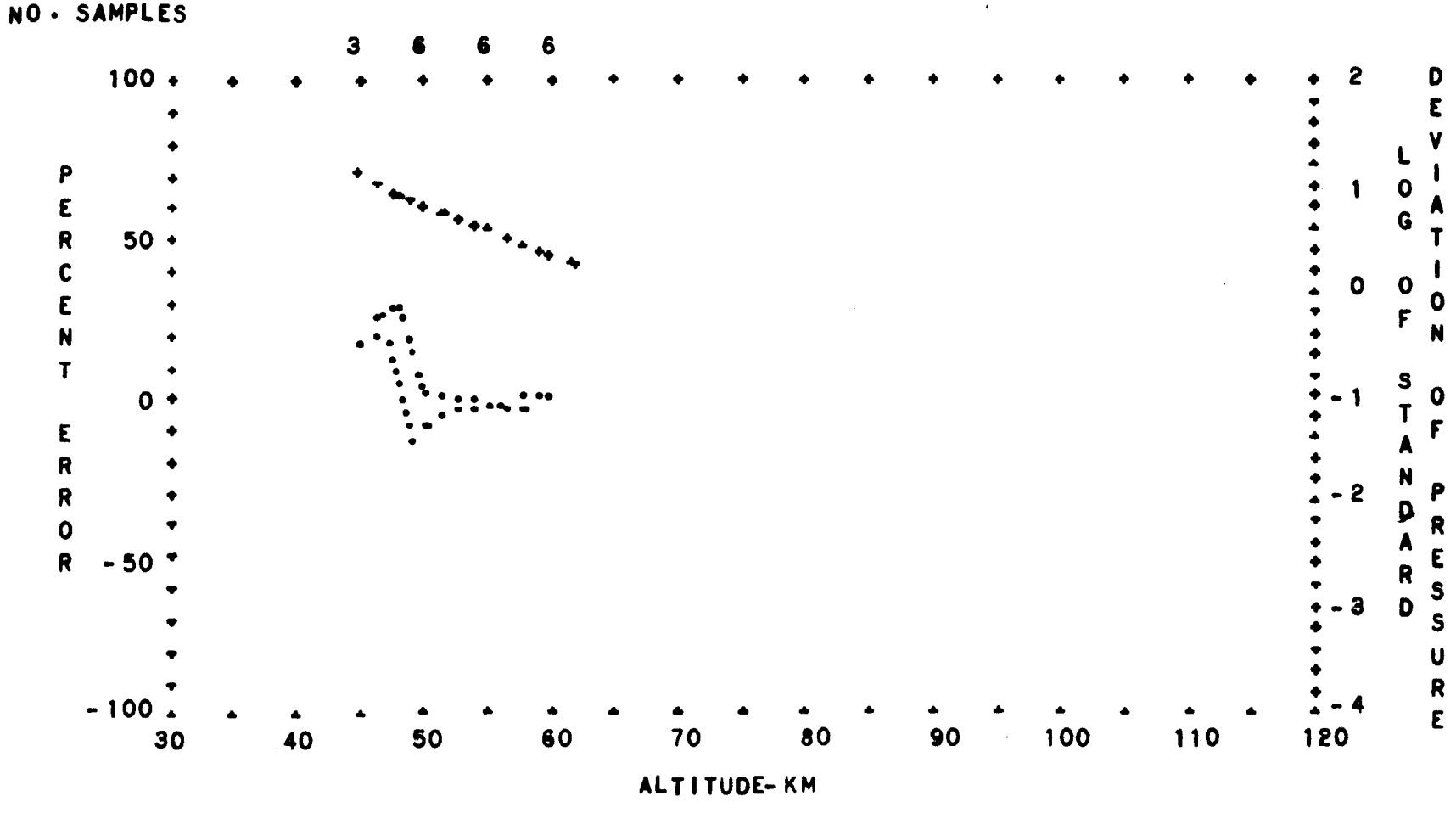

FIG. B-7. STANDARD DEVIATION OF PRESSURE AND PERCENT ERROR OF BUELL HYDROSTATIC EQUATION VERSUS ALTITUDE

TROPICAL AUTUMN DIURNAL TRANSITION

PERCENT ERROR--DOTS LOG DEVIATION--CROSSES

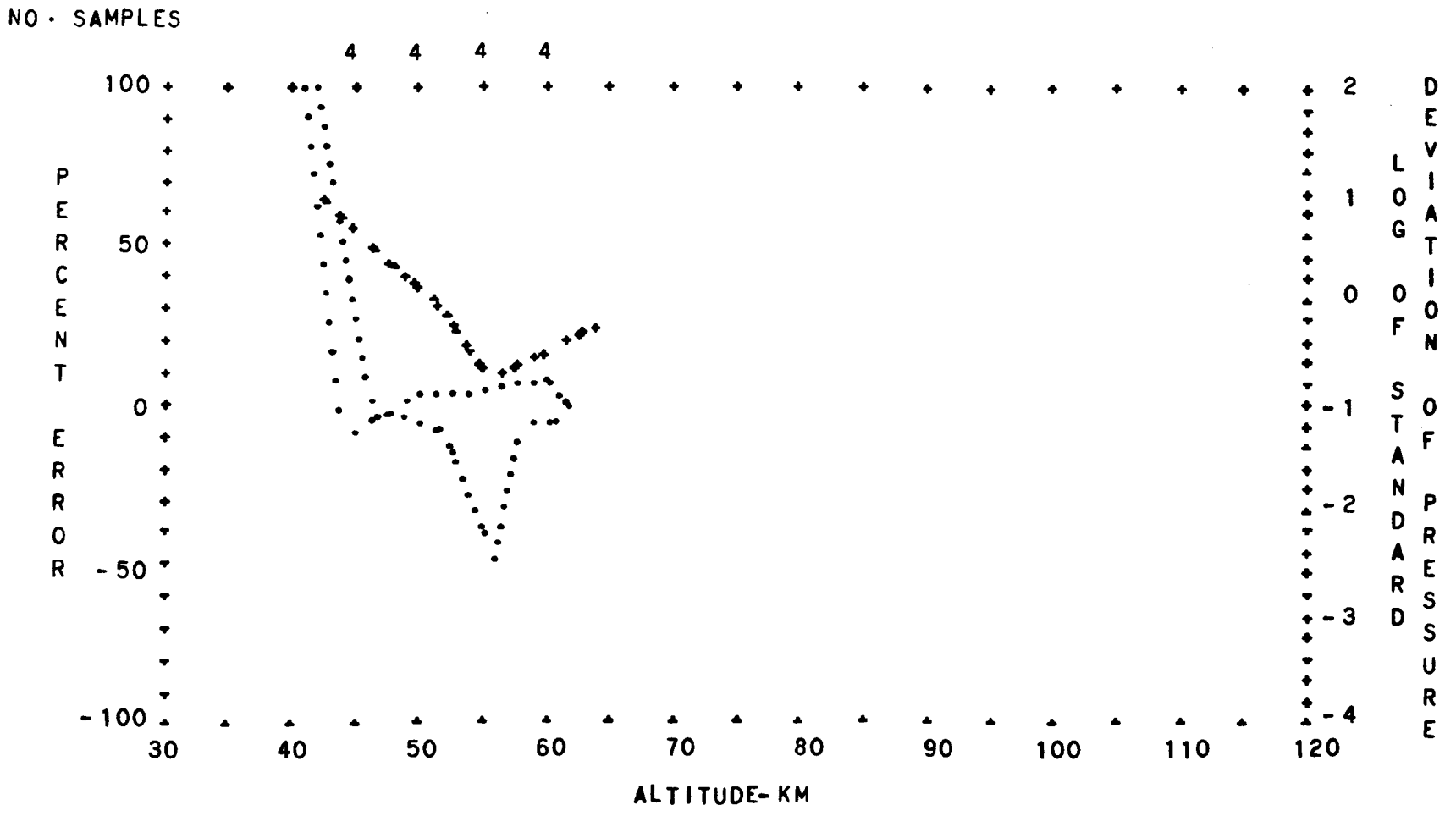

FIG. B-8. STANDARD DEVIATION OF PRESSURE AND PERCENT ERROR OF BUELL HYDROSTATIC EQUATION VERSUS ALTITUDE

TROPICAL AUTUMN DAYTIME

PERCENT ERROR--DOTS LOG DEVIATION--CROSSES

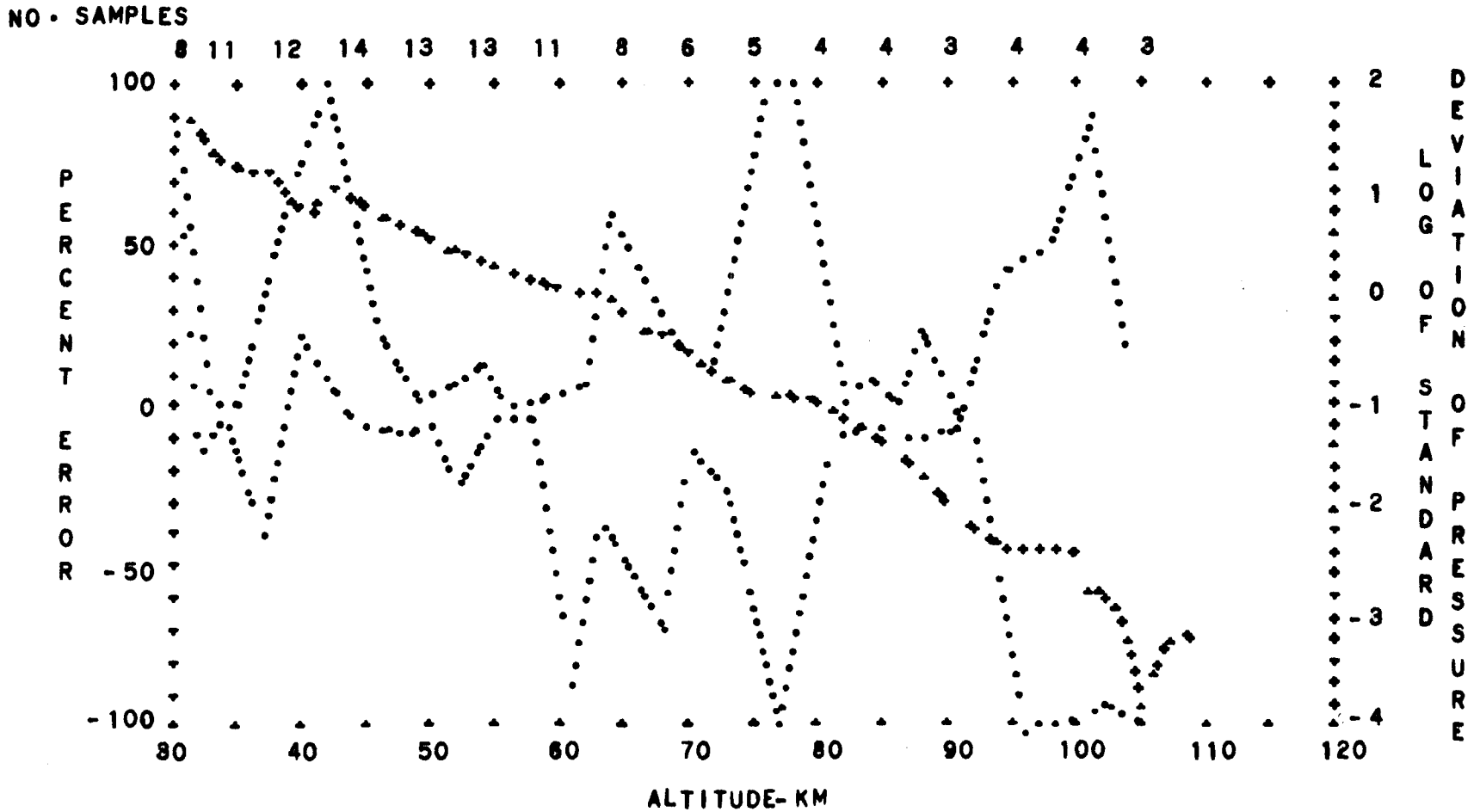

FIG. B-9. STANDARD DEVIATION OF PRESSURE AND PERCENT ERROR OF BUELL HYDROSTATIC EQUATION VERSUS ALTITUDE

TROPICAL AUTUMN NIGHTTIME

PERCENT ERROR--DOTS LOG DEVIATION--CROSSES

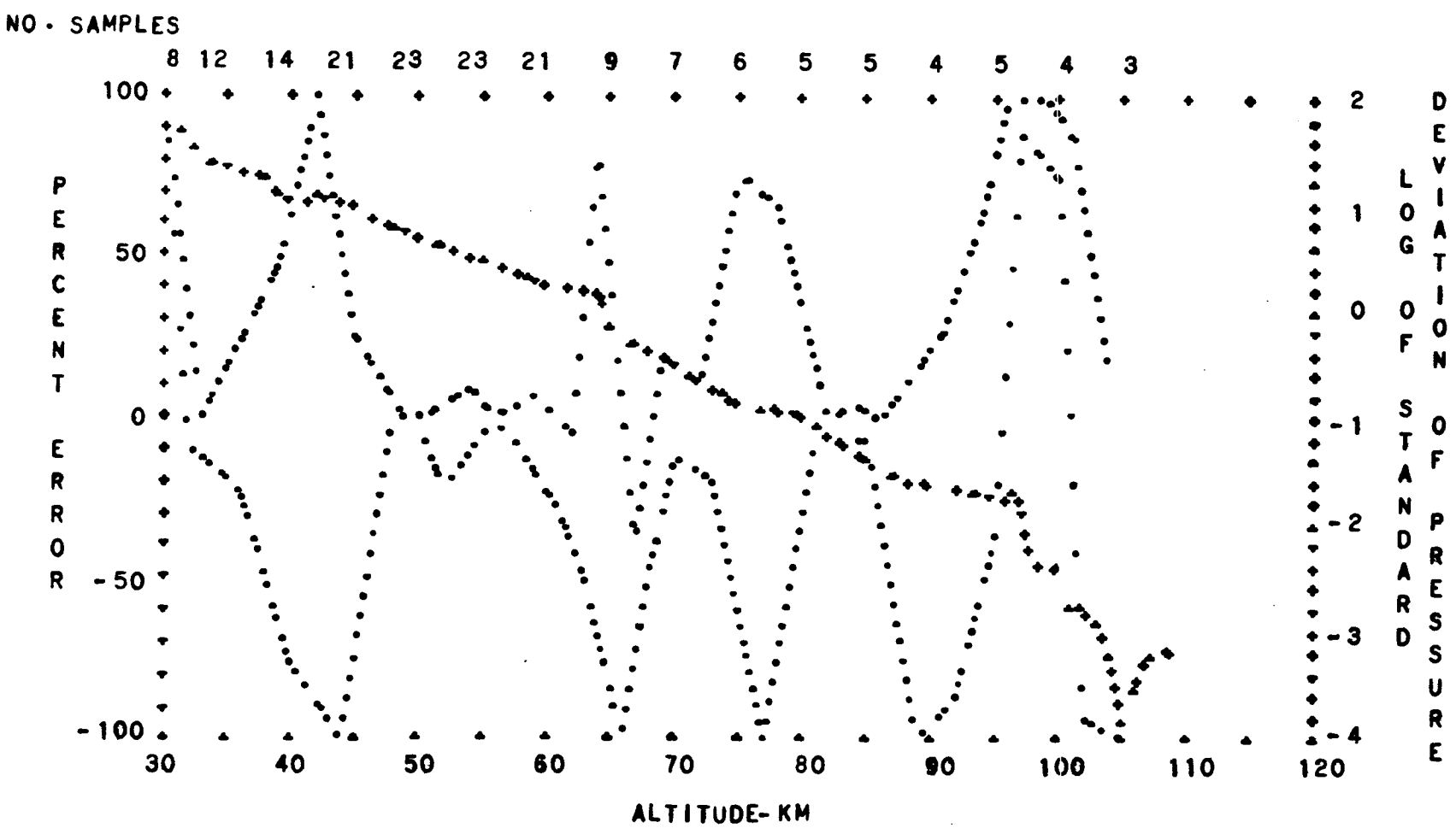

FIG. B-10. STANDARD DEVIATION OF PRESSURE AND PERCENT ERROR OF BUELL HYDROSTATIC EQUATION VERSUS ALTITUDE

TROPICAL AUTUMN DIURNAL MEAN

PERCENT ERROR--DOTS LOG DEVIATION--CROSSES

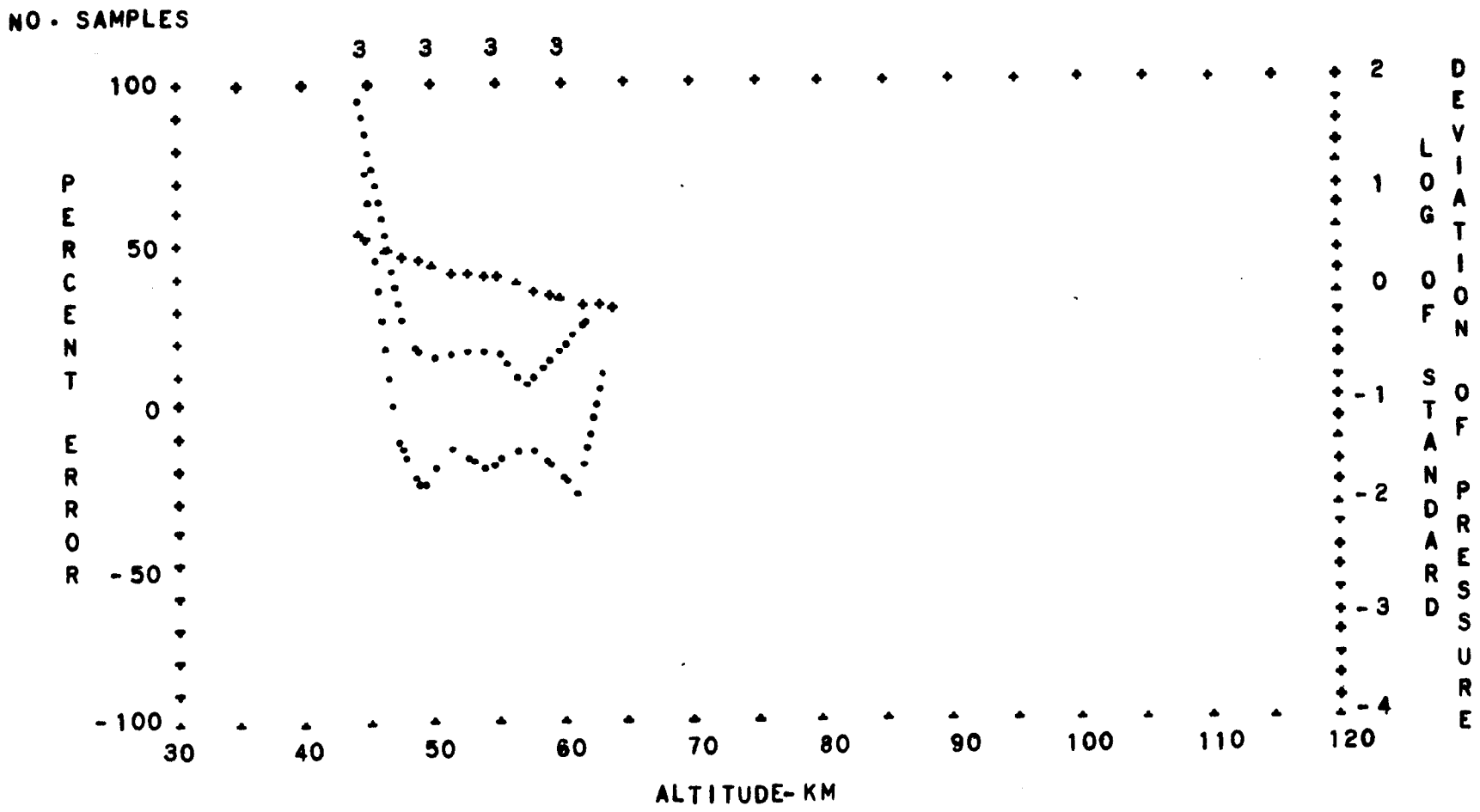

FIG. B-11. STANDARD DEVIATION OF PRESSURE AND PERCENT ERROR OF BUELL HYDROSTATIC EQUATION VERSUS ALTITUDE

TROPICAL WINTER DIURNAL TRANSITION

PERCENT ERROR--DOTS LOG DEVIATION--CROSSES

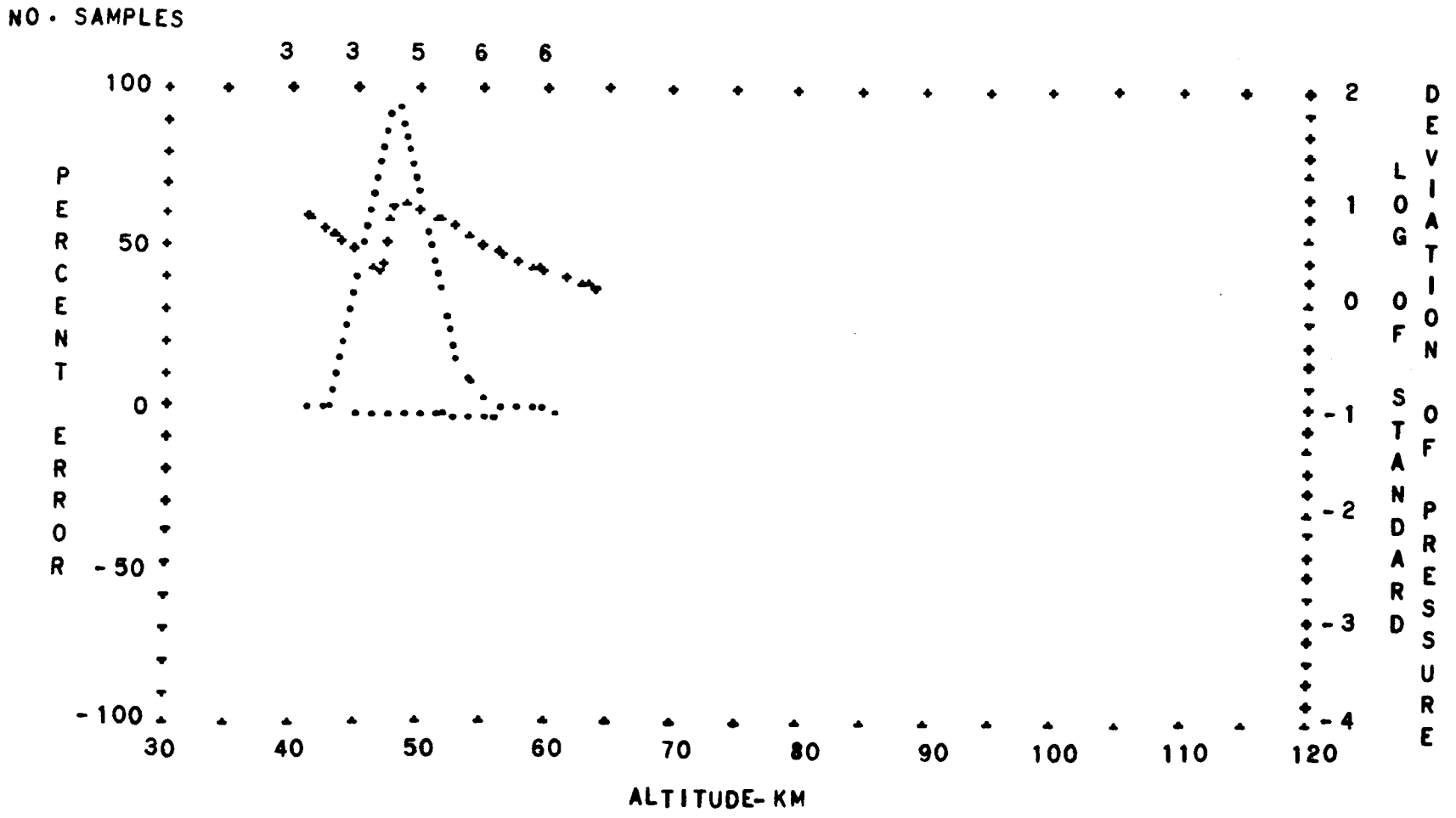

FIG. B-12. STANDARD DEVIATION OF PRESSURE AND PERCENT ERROR OF BUELL HYDROSTATIC EQUATION VERSUS ALTITUDE

TROPICAL WINTER DAYTIME

PERCENT ERROR--DOTS LOG DEVIATION--CROSSES

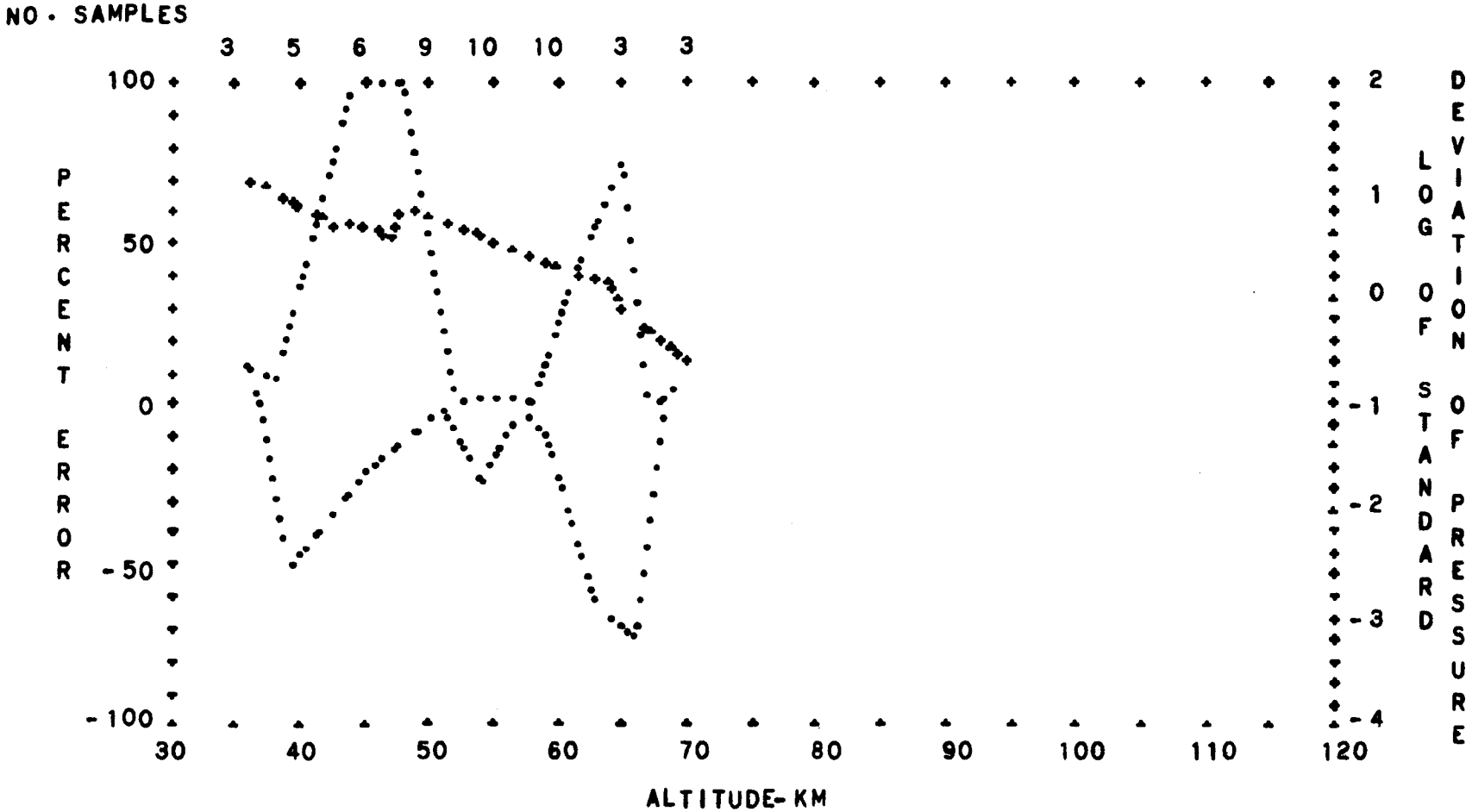

FIG. B-13. STANDARD DEVIATION OF PRESSURE AND PERCENT ERROR OF BUELL HYDROSTATIC EQUATION VERSUS ALTITUDE

TROPICAL WINTER DIURNAL MEAN

PERCENT ERROR--DOTS LOG DEVIATION--CROSSES

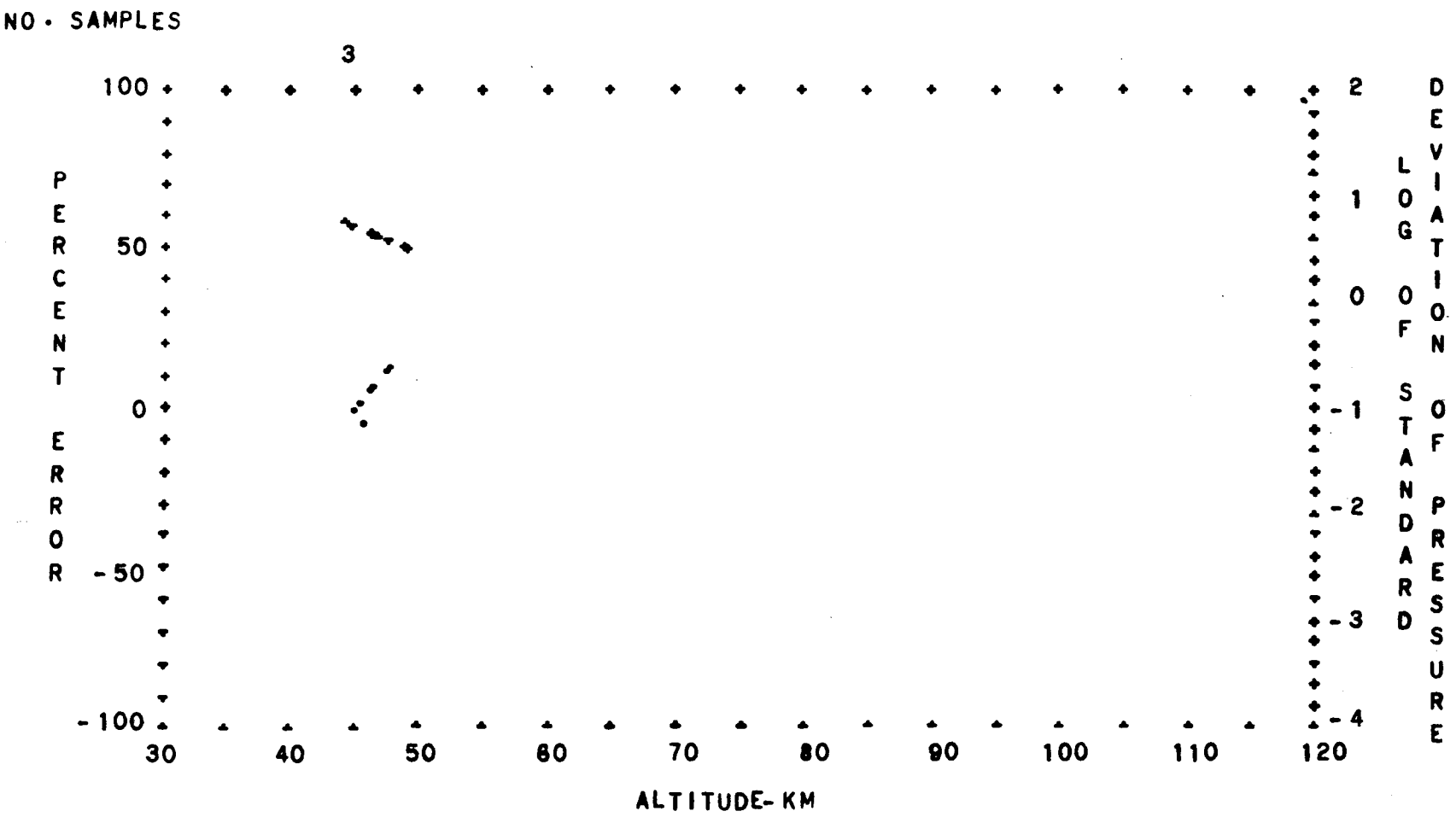

FIG. B-14. STANDARD DEVIATION OF PRESSURE AND PERCENT ERROR OF BUELL HYDROSTATIC EQUATION VERSUS ALTITUDE

TROPICAL SUMMER EXTREME NIGHTTIME

PERCENT ERROR--DOTS LOG DEVIATION--CROSSES

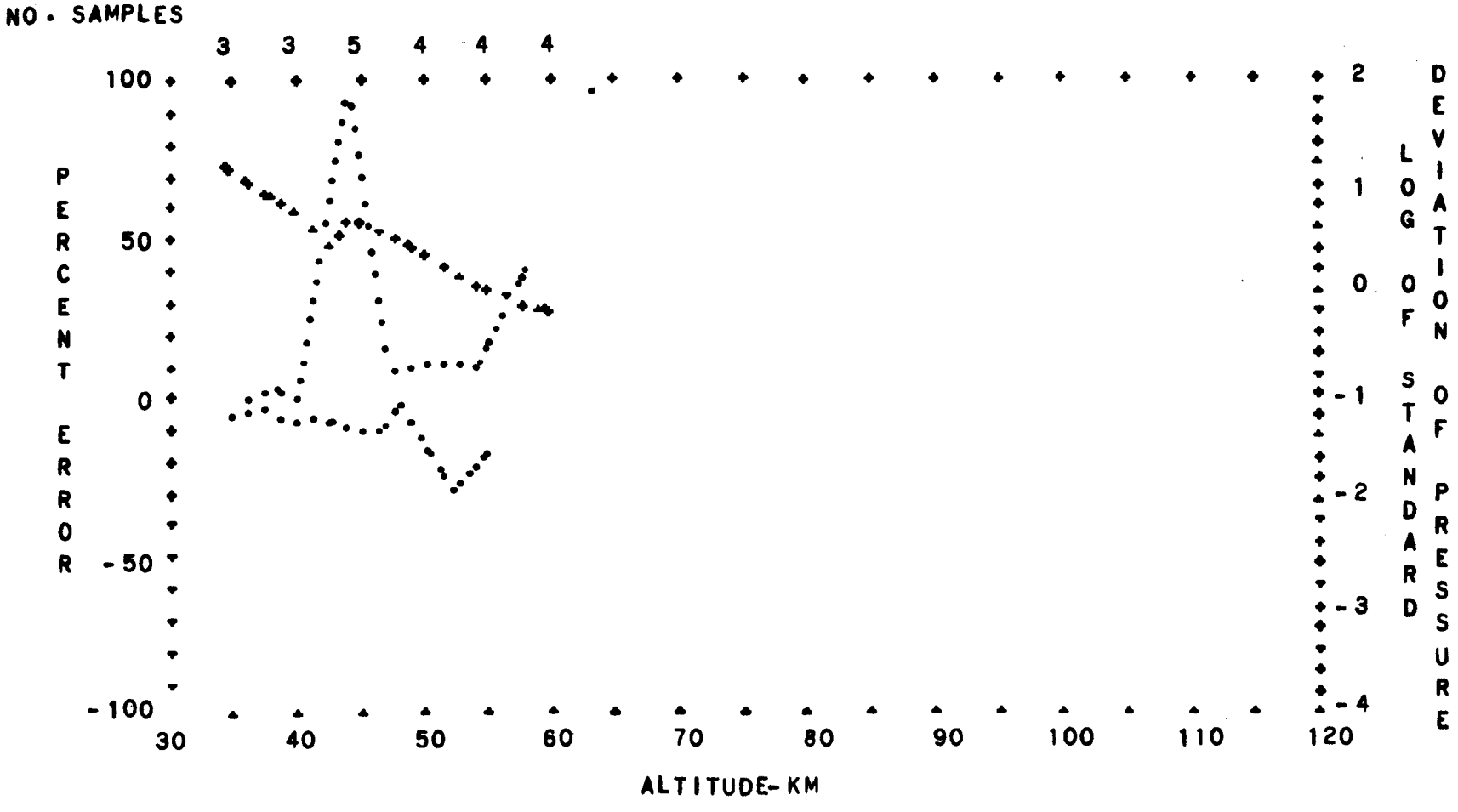

FIG. B-15. STANDARD DEVIATION OF PRESSURE AND PERCENT ERROR OF BUELL HYDROSTATIC EQUATION VERSUS ALTITUDE

TROPICAL SUMMER EXTREME DIURNAL MEAN

PERCENT ERROR--DOTS LOG DEVIATION--CROSSES

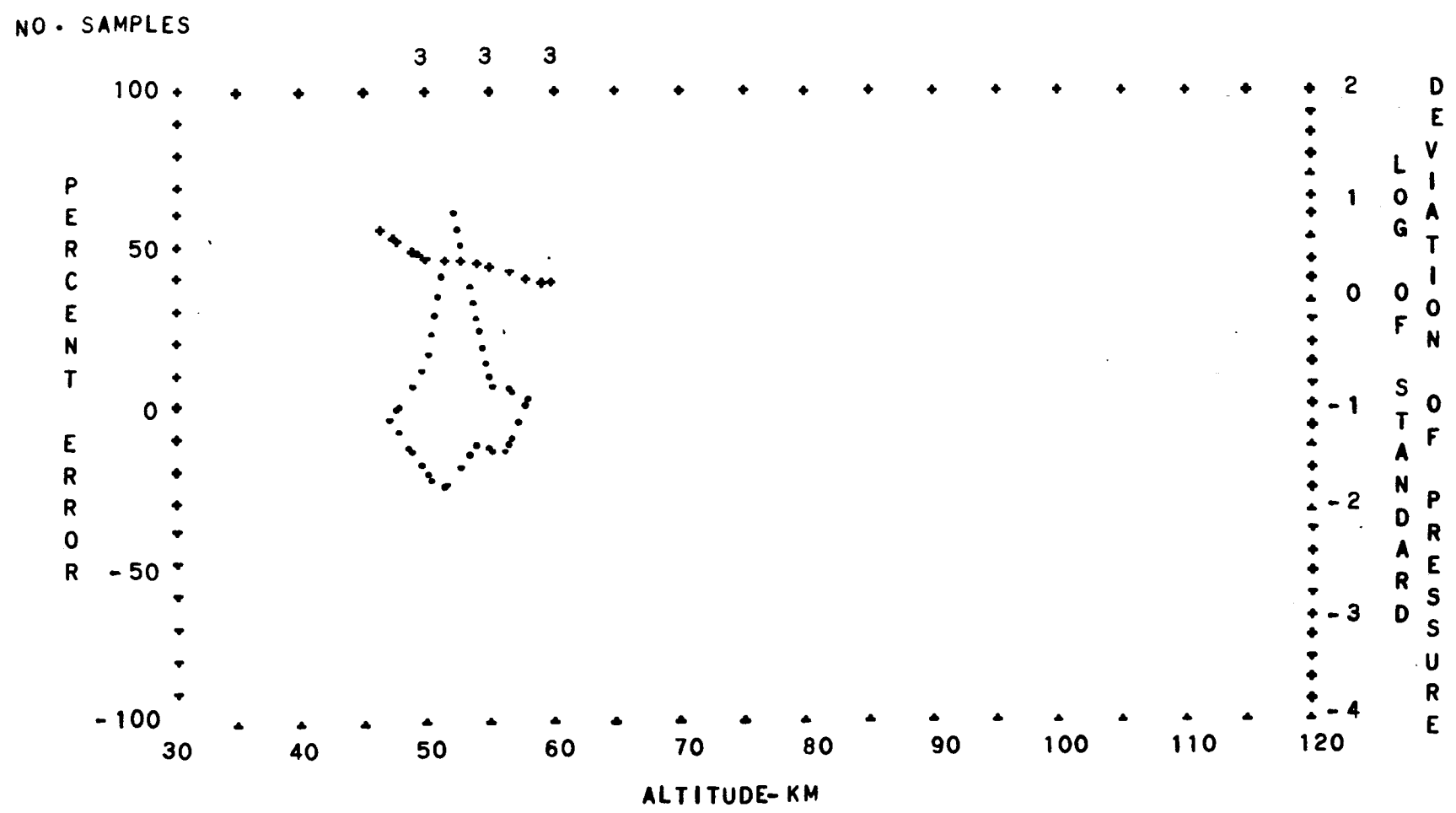

FIG. B-16. STANDARD DEVIATION OF PRESSURE AND PERCENT ERROR OF BUELL HYDROSTATIC EQUATION VERSUS ALTITUDE

TROPICAL WINTER EXTREME DIURNAL MEAN

PERCENT ERROR--DOTS LOG DEVIATION--CROSSES

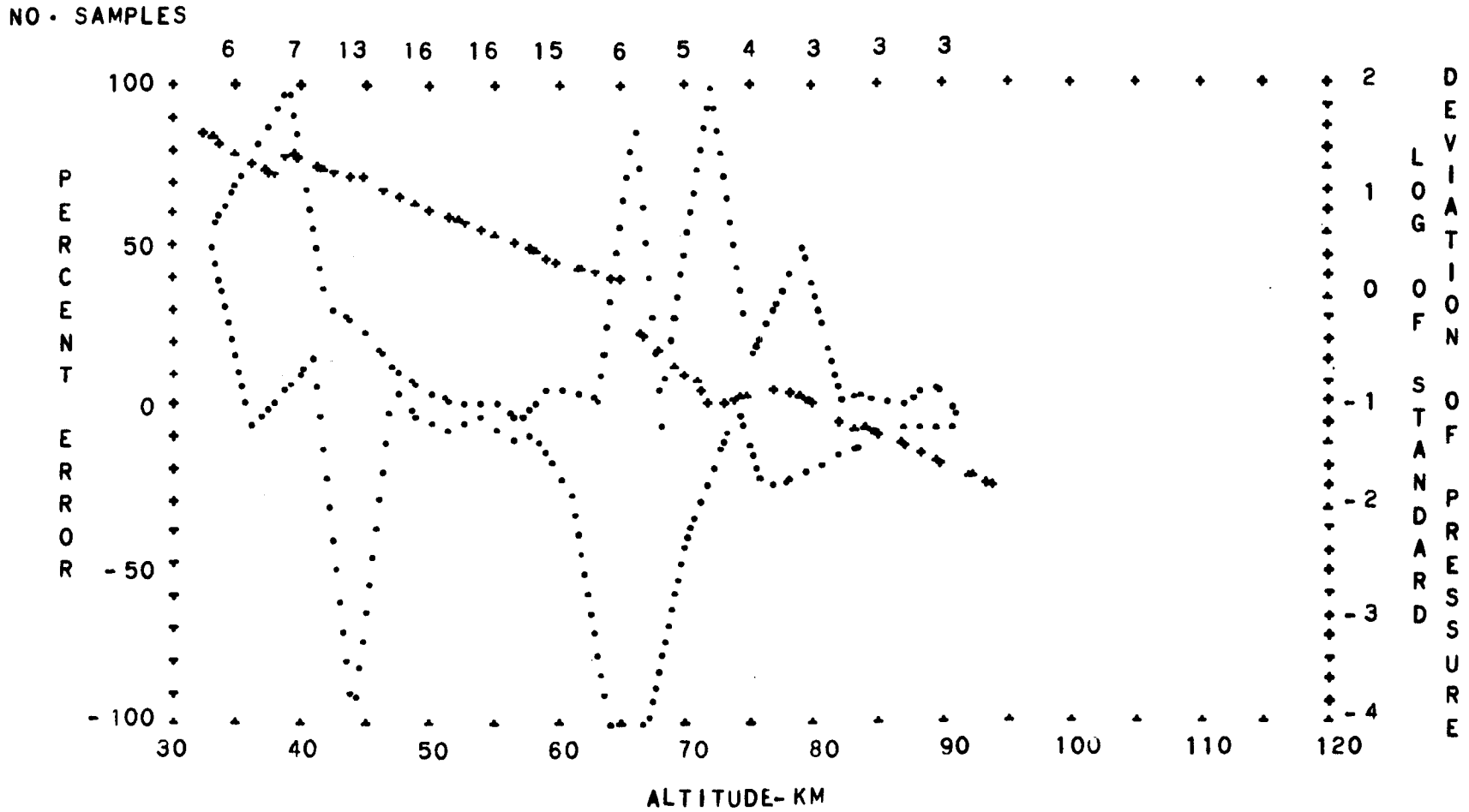

FIG B-17. STANDARD DEVIATION OF PRESSURE AND PERCENT ERROR OF BUELL HYDROSTATIC EQUATION VERSUS ALTITUDE

TROPICAL ANNUAL MEAN DIURNAL TRANSITION

PERCENT ERROR--DOTS LOG DEVIATION--CROSSES

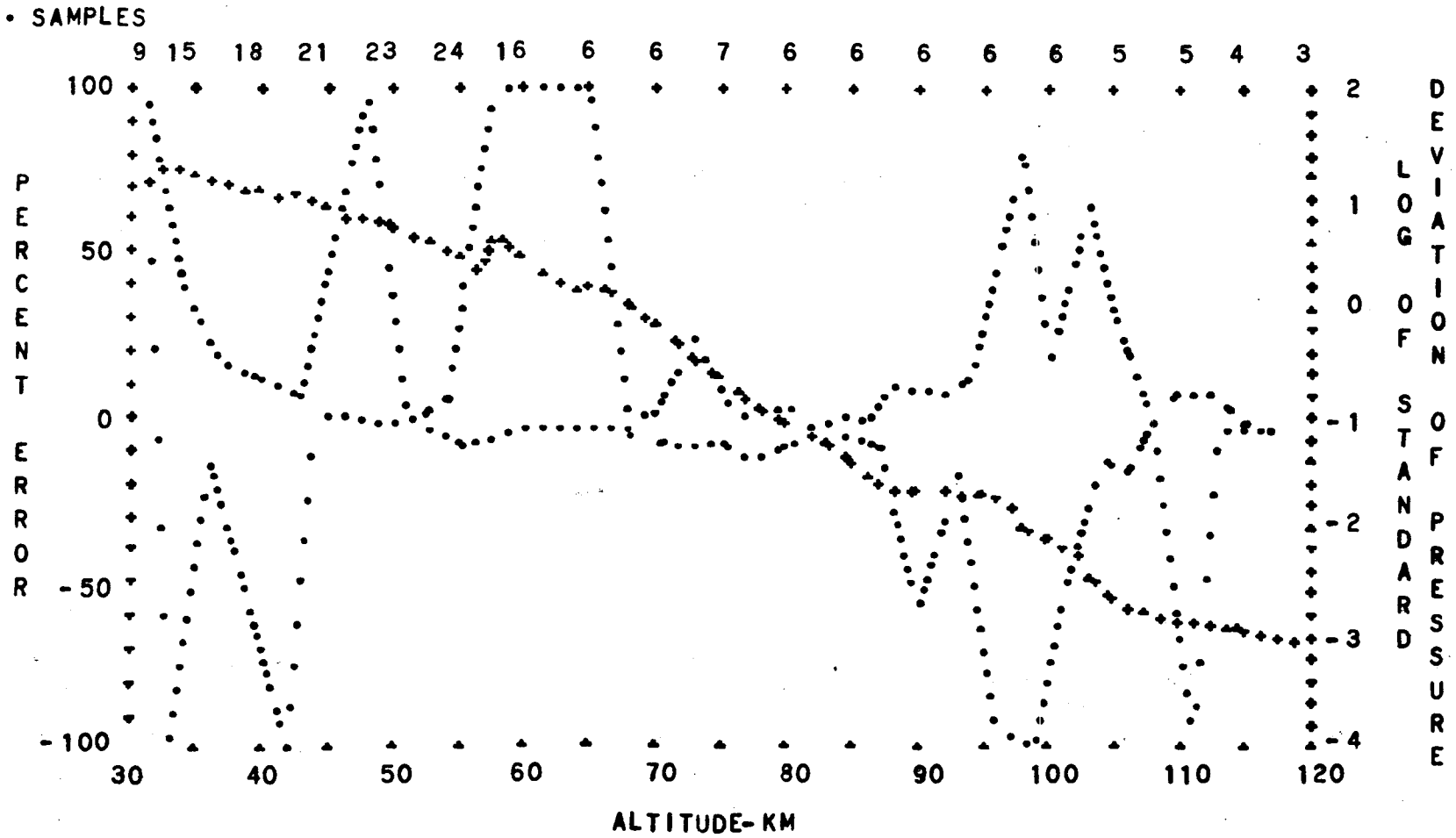

FIG. B-18. STANDARD DEVIATION OF PRESSURE AND PERCENT ERROR OF BUELL HYDROSTATIC EQUATION VERSUS ALTITUDE

TROPICAL ANNUAL MEAN DAYTIME

PERCENT ERROR--DOTS LOG DEVIATION--CROSSES

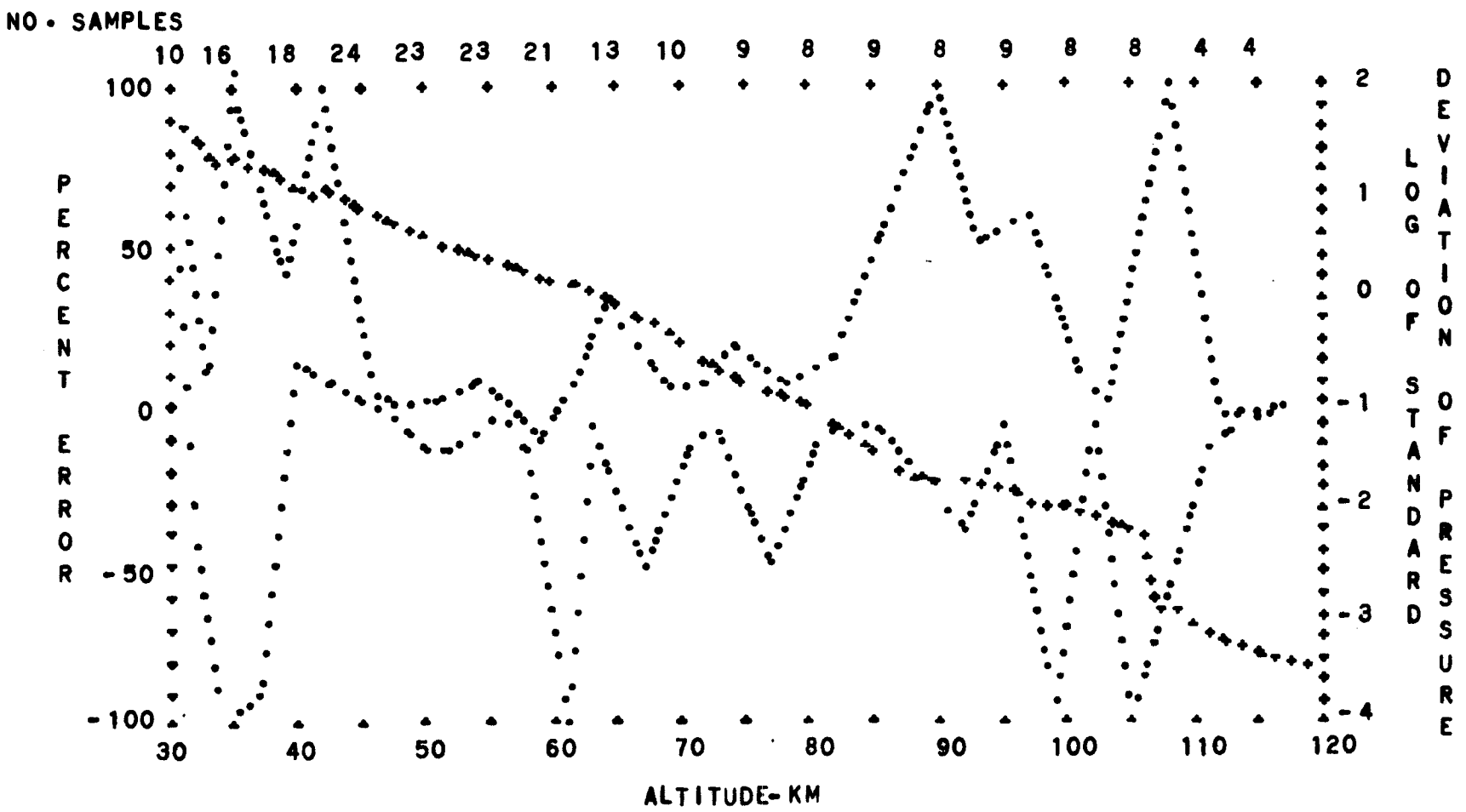

FIG. B-19. STANDARD DEVIATION OF PRESSURE AND PERCENT ERROR OF BUELL HYDROSTATIC EQUATION VERSUS ALTITUDE

TROPICAL ANNUAL MEAN NIGHTTIME

PERCENT ERROR--DOTS LOG DEVIATION--CROSSES

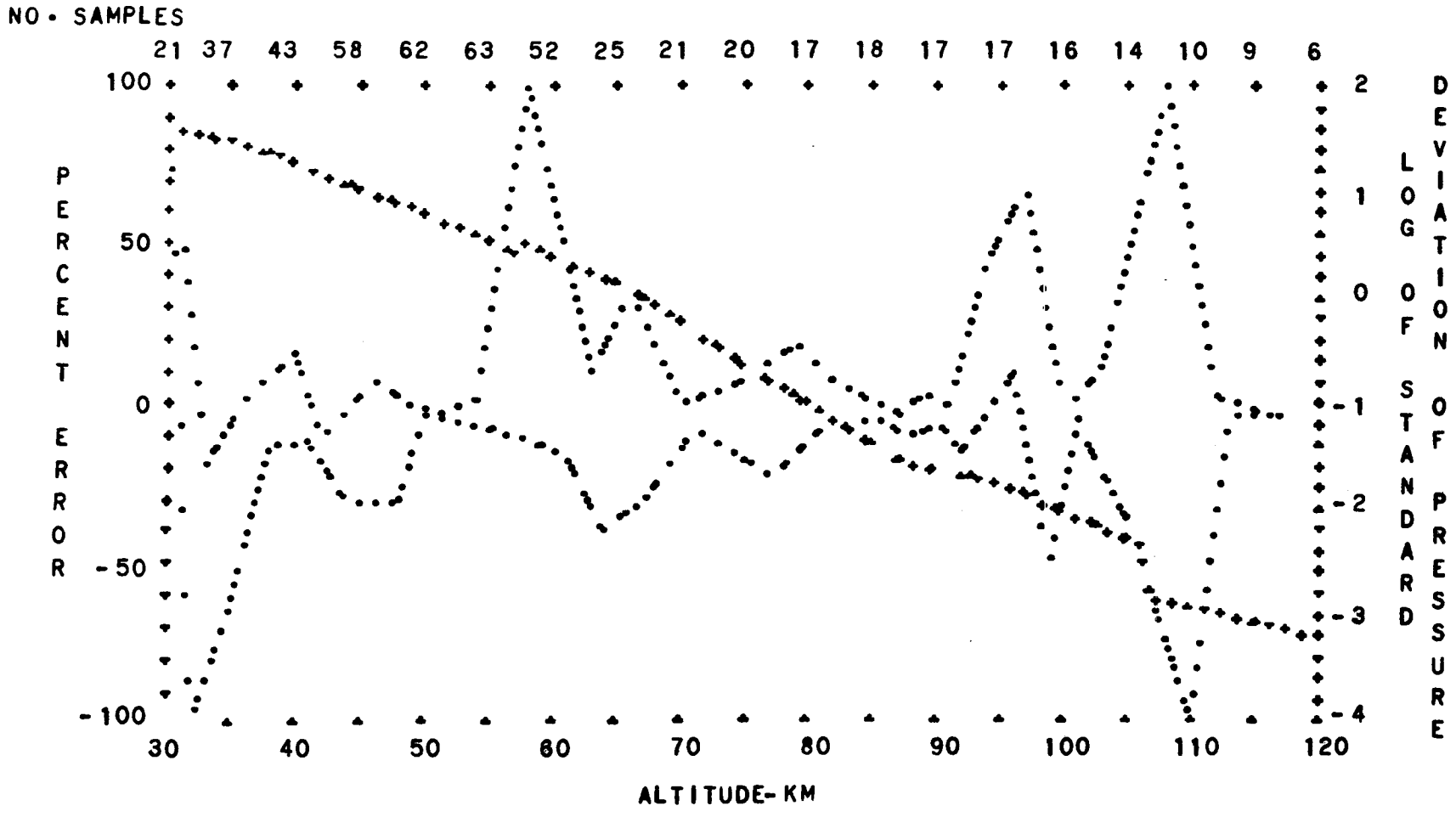

FIG. B-20. STANDARD DEVIATION OF PRESSURE AND PERCENT ERROR OF BUELL HYDROSTATIC EQUATION VERSUS ALTITUDE

TROPICAL ANNUAL MEAN DIURNAL MEAN

PERCENT ERROR--DOTS LOG DEVIATION--CROSSES

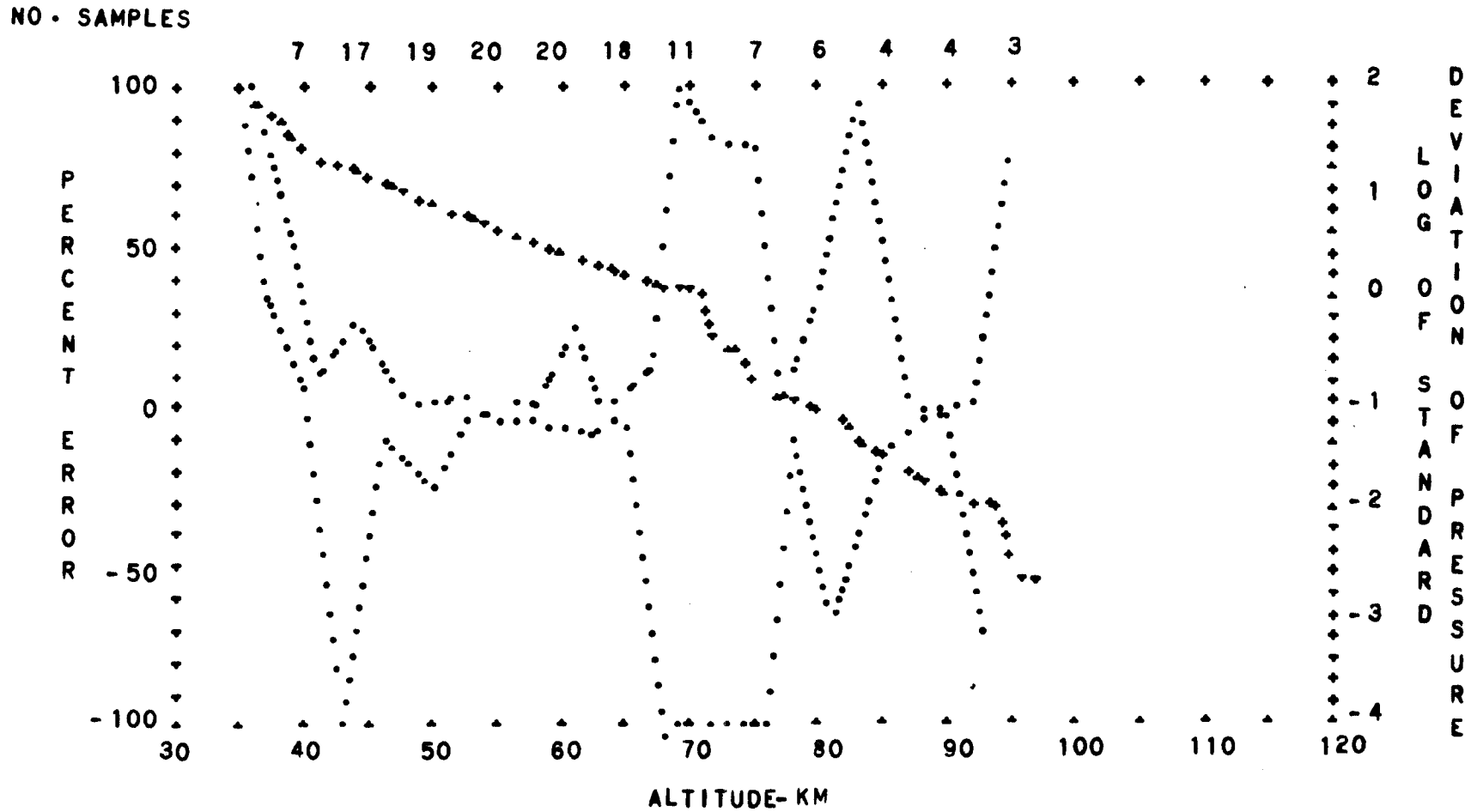

FIG. B-21. STANDARD DEVIATION OF PRESSURE AND PERCENT ERROR OF BUELL HYDROSTATIC EQUATION VERSUS ALTITUDE

SUBTROPICAL SPRING DIURNAL TRANSITION

PERCENT ERROR--DOTS LOG DEVIATION--CROSSES

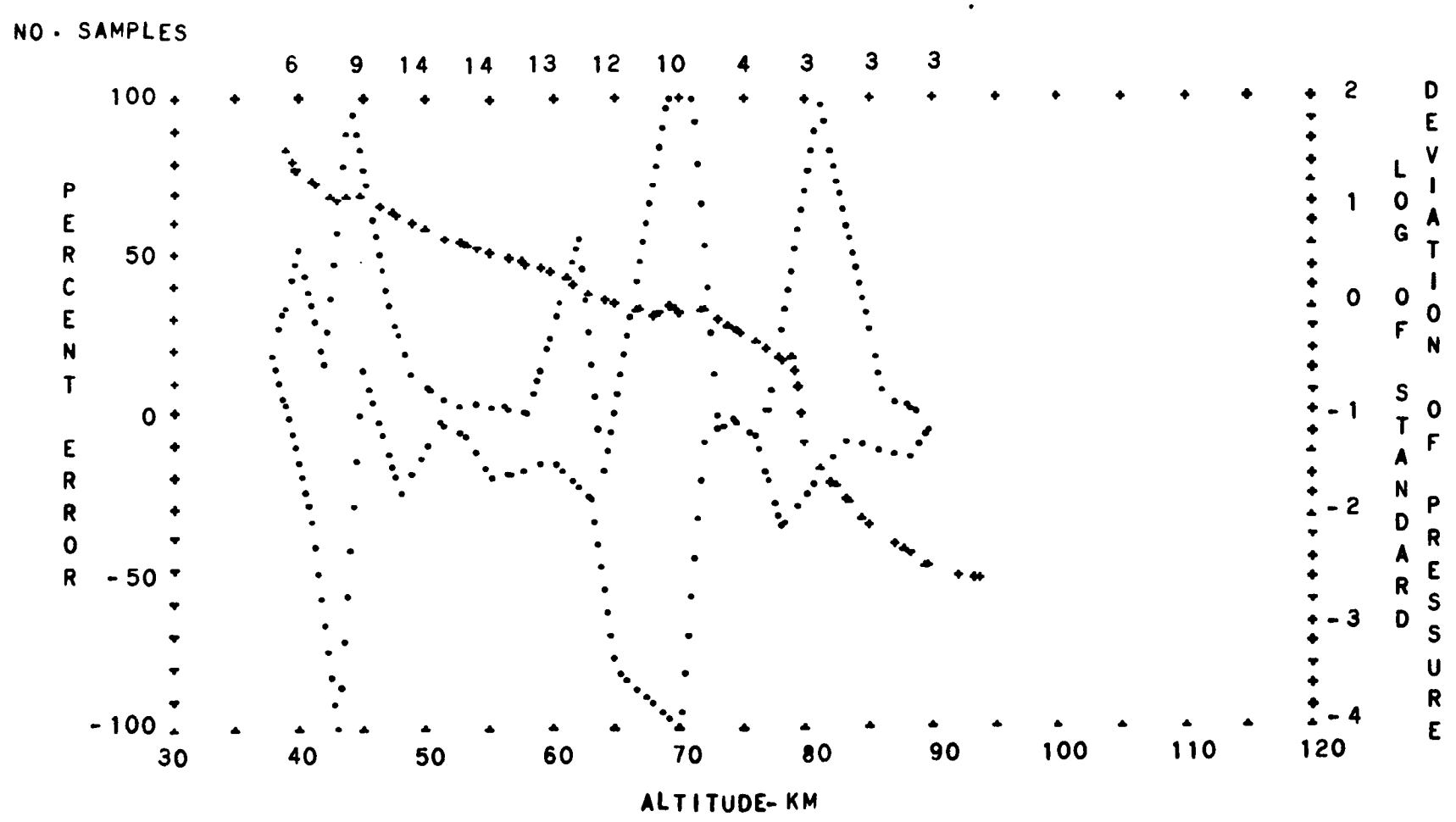

FIG. B-22. STANDARD DEVIATION OF PRESSURE AND PERCENT ERROR OF BUELL HYDROSTATIC EQUATION VERSUS ALTITUDE

SUBTROPICAL SPRING DAYTIME

PERCENT ERROR--DOTS LOG DEVIATION--CROSSES

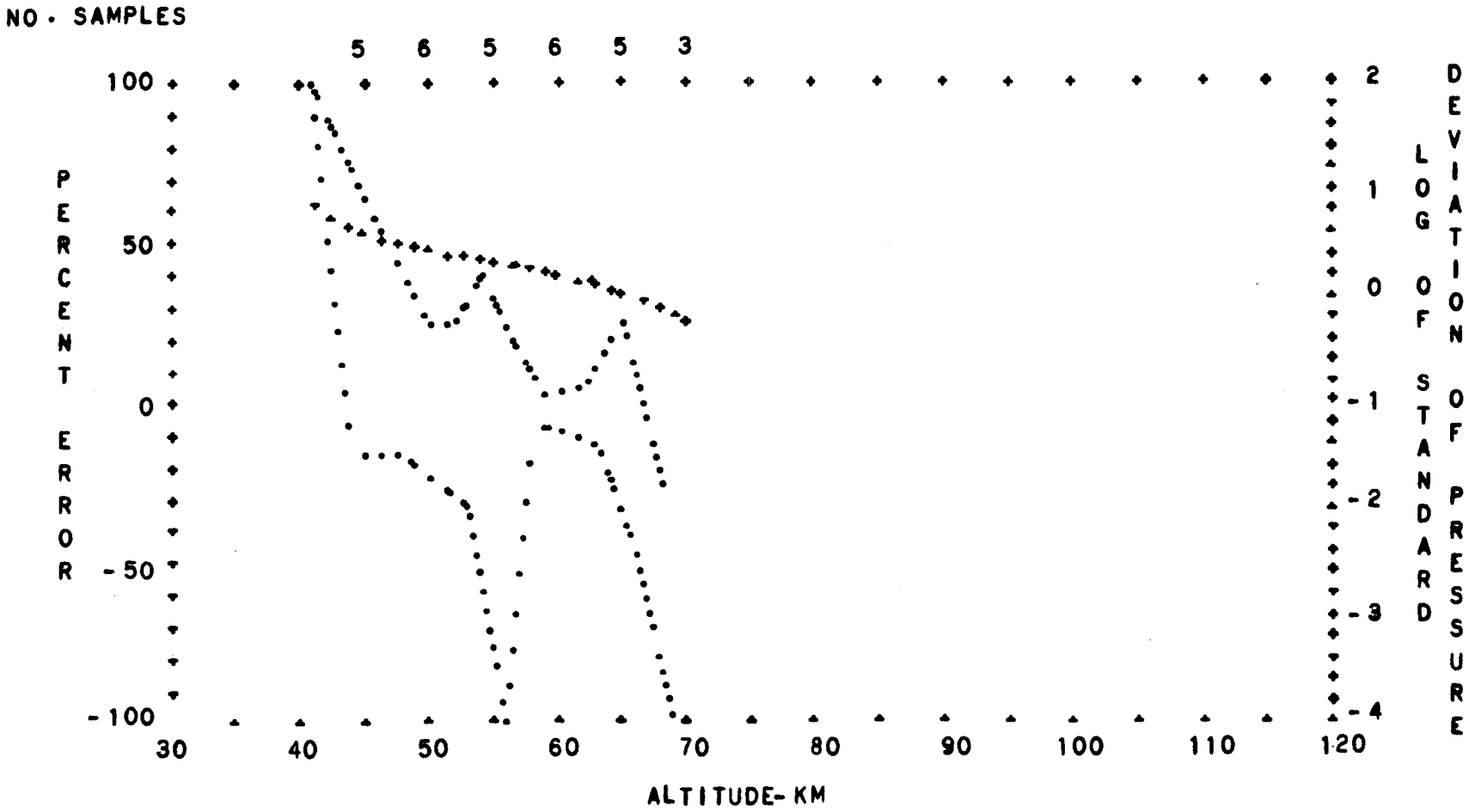

FIG. B-23. STANDARD DEVIATION OF PRESSURE AND PERCENT ERROR OF BUELL HYDROSTATIC EQUATION VERSUS ALTITUDE

SUBTROPICAL SPRING NIGHTTIME

PERCENT ERROR--DOTS LOG. DEVIATION--CROSSES

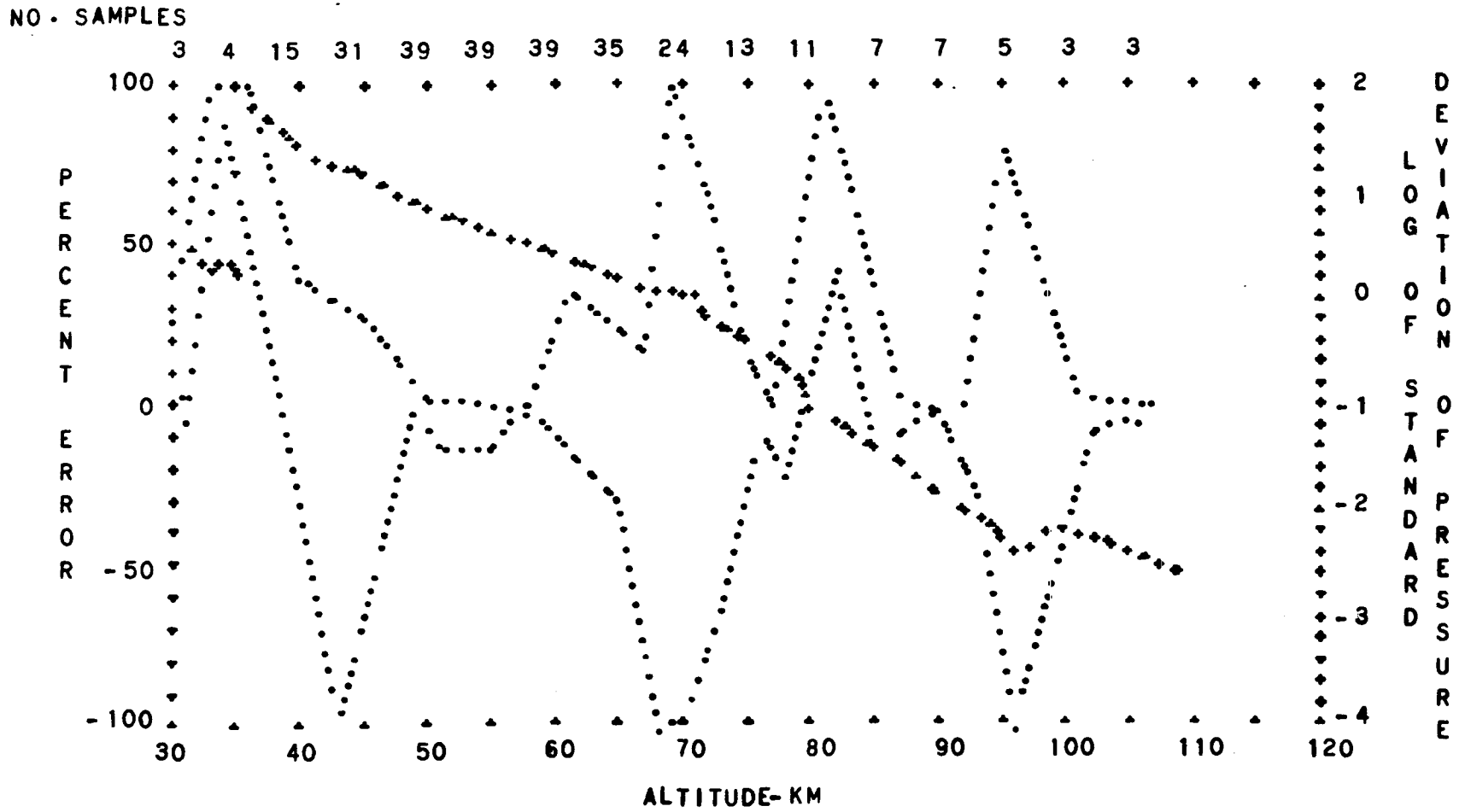

FIG. B-24. STANDARD DEVIATION OF PRESSURE AND PERCENT ERROR OF BUELL HYDROSTATIC EQUATION VERSUS ALTITUDE

SUBTROPICAL SPRING DIURNAL MEAN

PERCENT ERROR--DOTS LOG DEVIATION--CROSSES

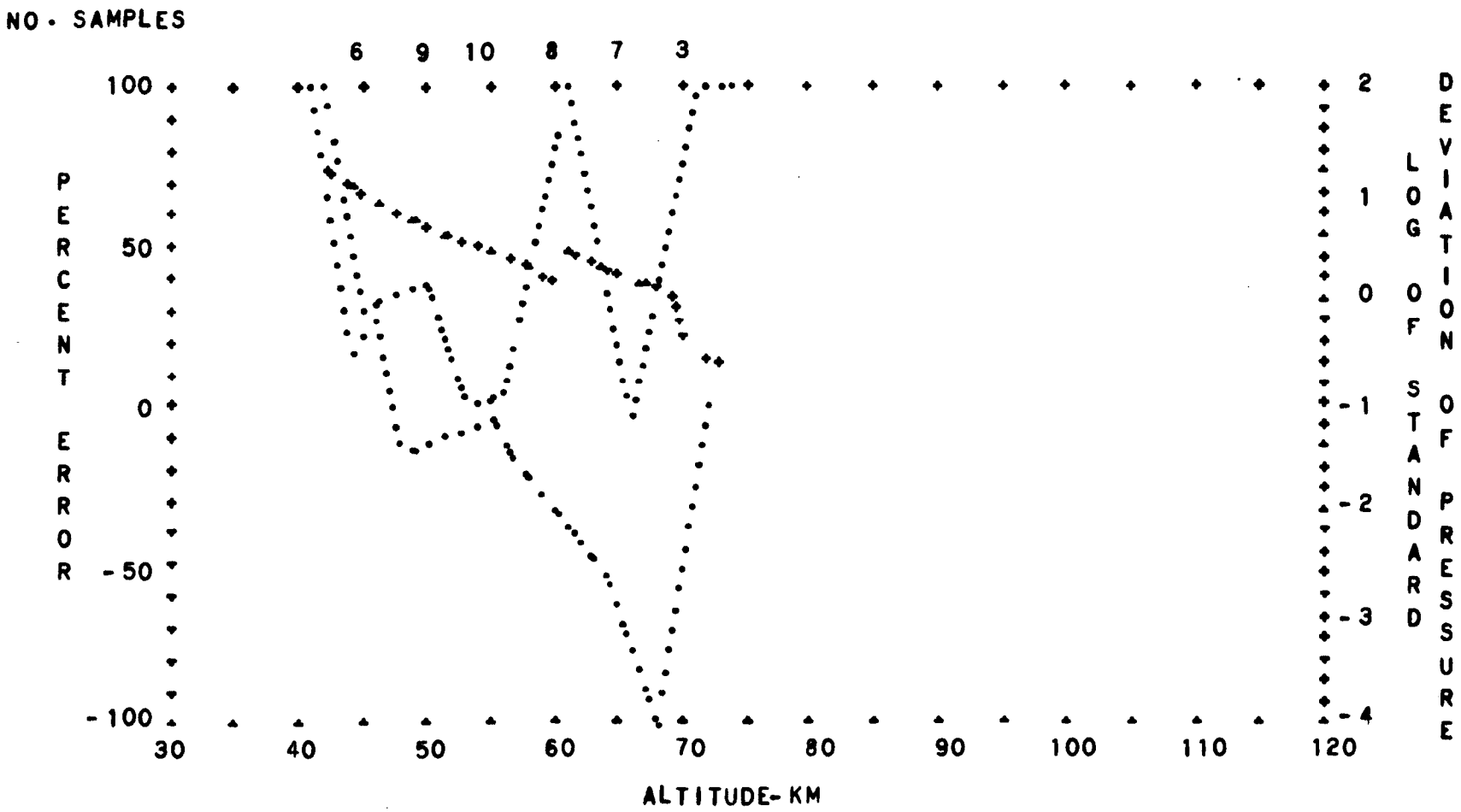

FIG. B-25. STANDARD DEVIATION OF PRESSURE AND PERCENT ERROR OF BUELL HYDROSTATIC EQUATION VERSUS ALTITUDE

SUBTROPICAL SUMMER DIURNAL TRANSITION

PERCENT ERROR--DOTS LOG DEVIATION--CROSSES

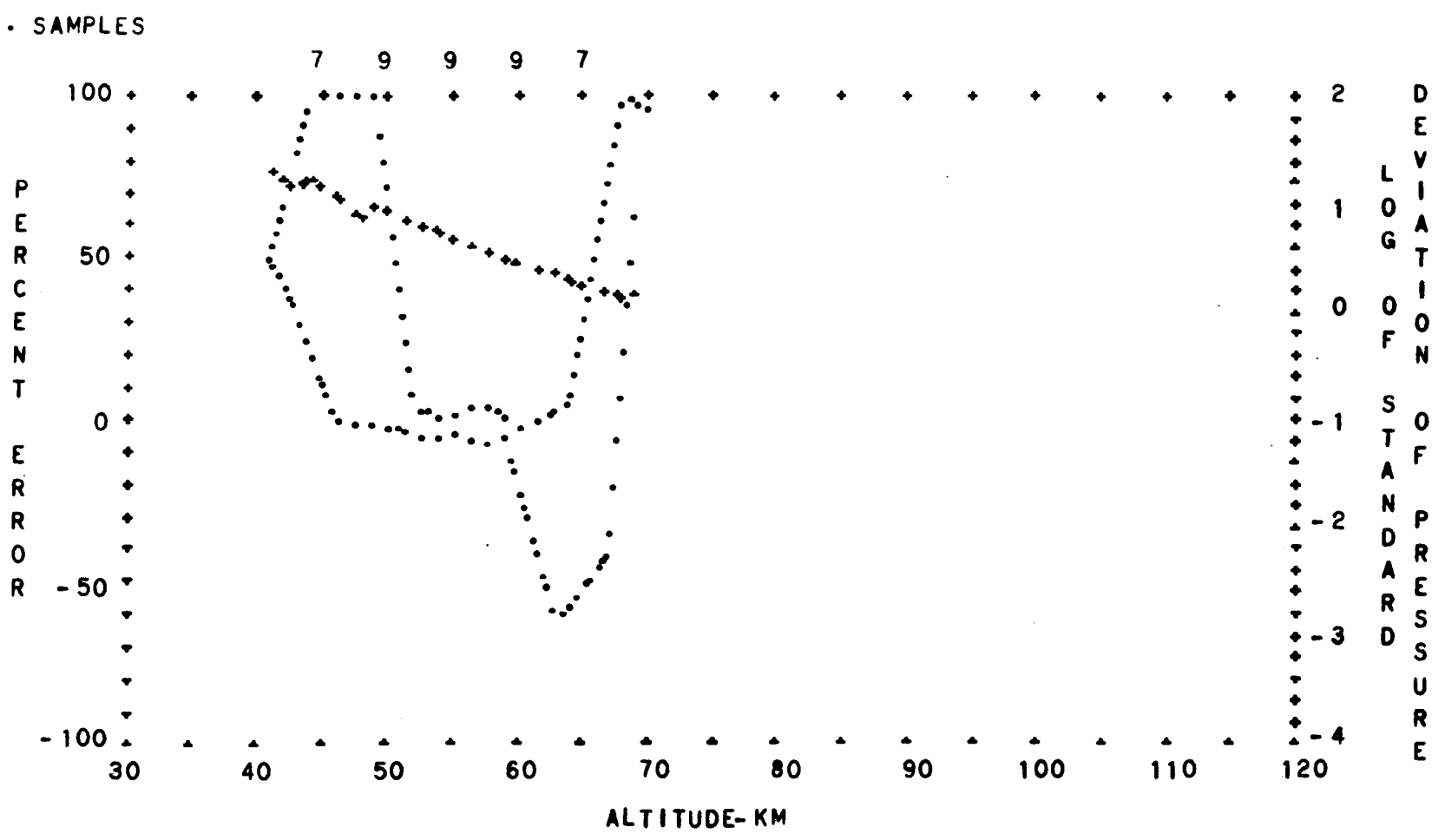

FIG. B-26. STANDARD DEVIATION OF PRESSURE AND PERCENT ERROR OF BUELL HYDROSTATIC EQUATION VERSUS ALTITUDE

SUBTROPICAL SUMMER DAYTIME

PERCENT ERROR--DOTS LOG DEVIATION--CROSSES

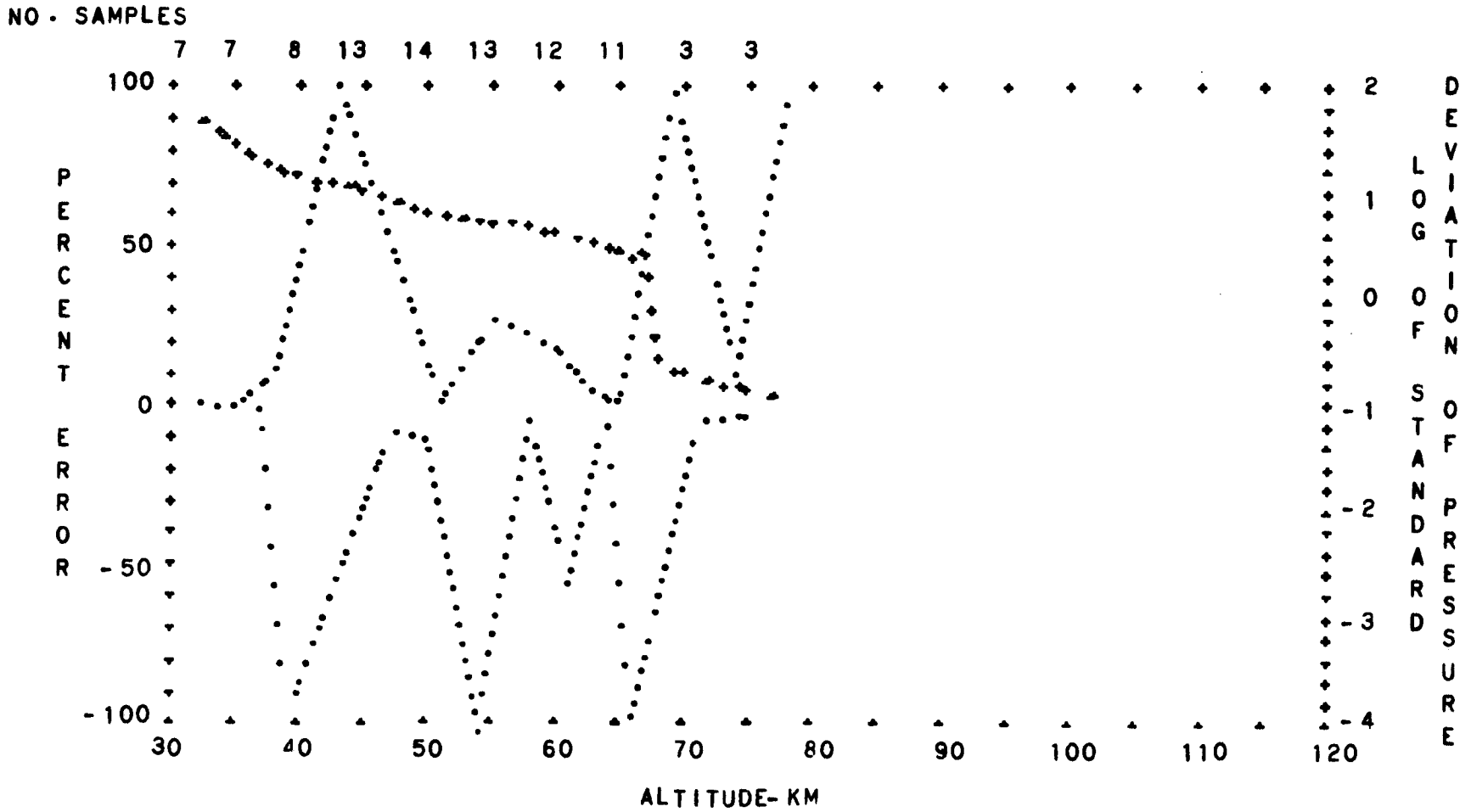

FIG. B-27. STANDARD DEVIATION OF PRESSURE AND PERCENT ERROR OF BUELL HYDROSTATIC EQUATION VERSUS ALTITUDE

SUBTROPICAL SUMMER NIGHTTIME

PERCENT ERROR--DOTS LOG DEVIATION--CROSSES

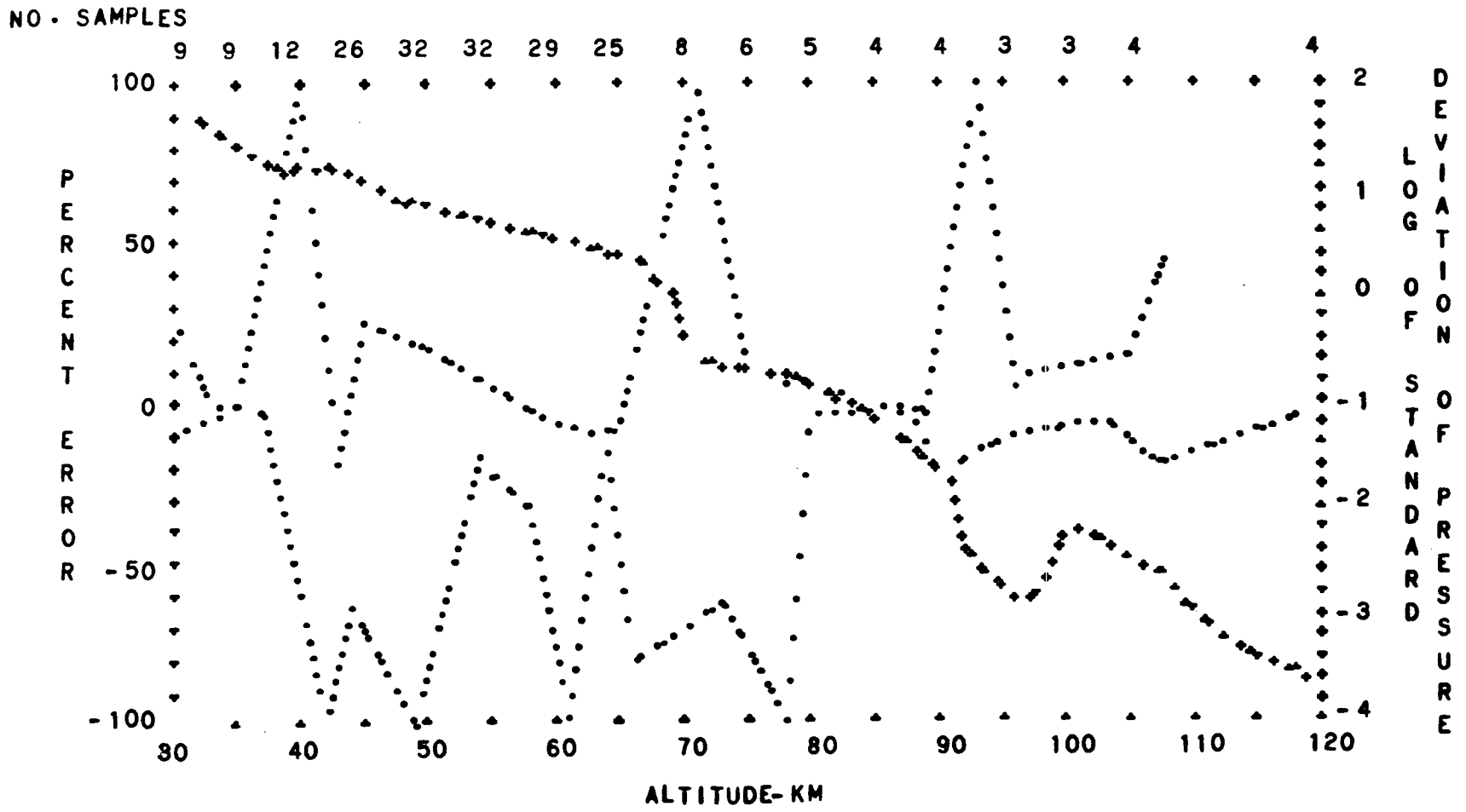

FIG. B-28. STANDARD DEVIATION OF PRESSURE AND PERCENT ERROR OF BUELL HYDROSTATIC EQUATION VERSUS ALTITUDE

SUBTROPICAL SUMMER DIURNAL MEAN

PERCENT ERROR--DOTS LOG. DEVIATION--CROSSES

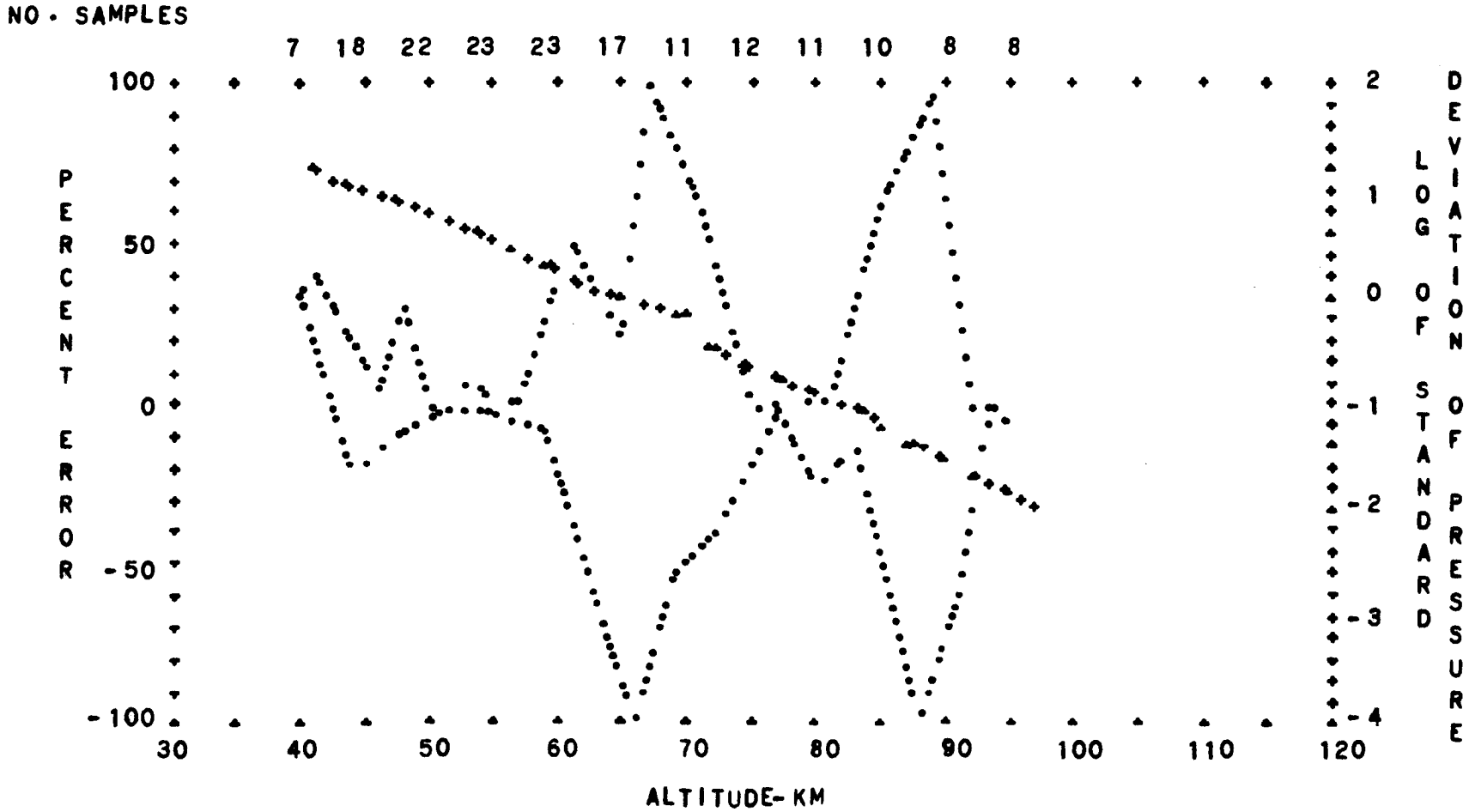

FIG. B-29. STANDARD DEVIATION OF PRESSURE AND PERCENT ERROR OF BUELL HYDROSTATIC EQUATION VERSUS ALTITUDE

SUBTROPICAL AUTUMN DIURNAL TRANSITION

PERCENT ERROR--DOTS LOG. DEVIATION--CROSSES

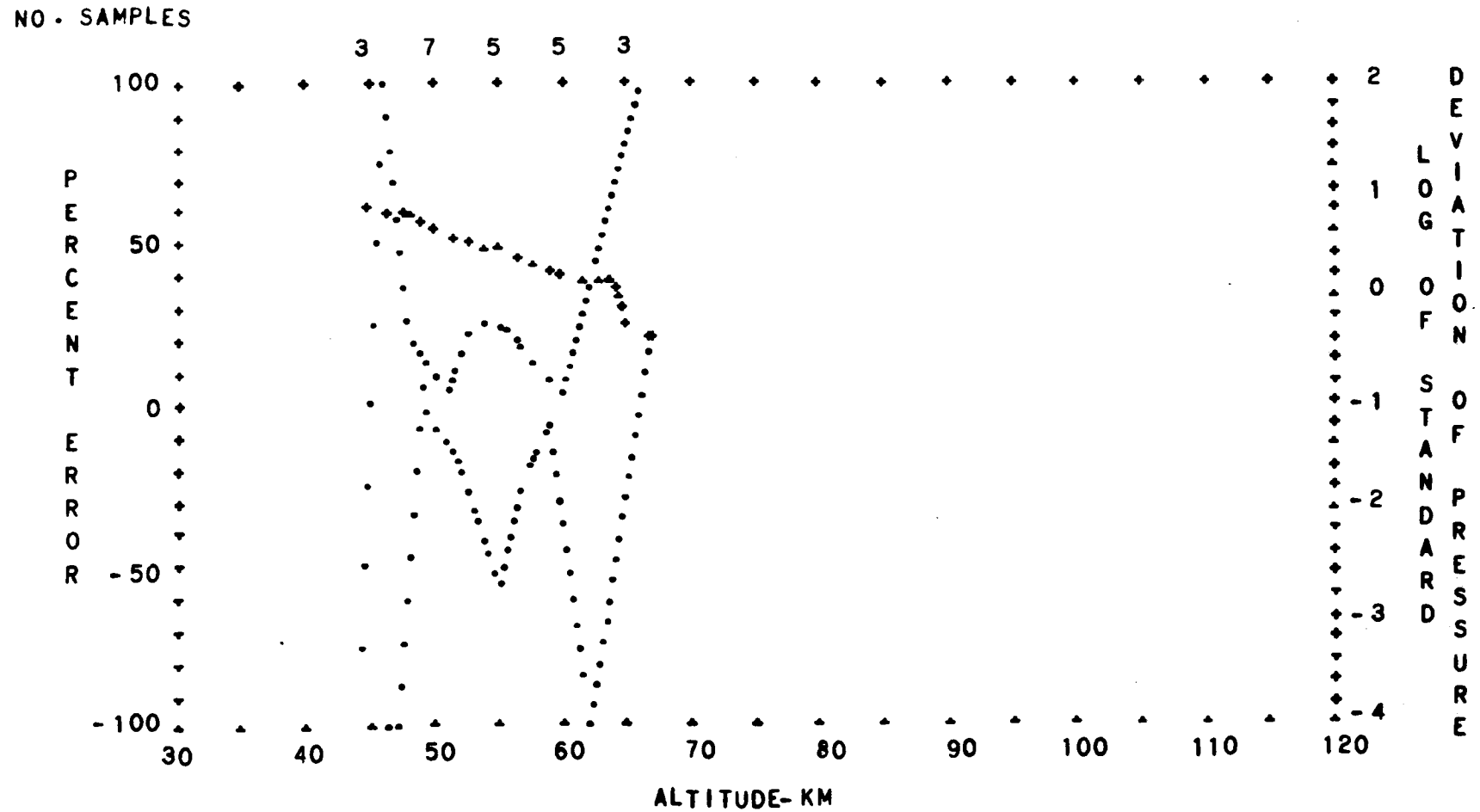

FIG.B-30. STANDARD DEVIATION OF PRESSURE AND PERCENT ERROR OF BUELL HYDROSTATIC EQUATION VERSUS ALTITUDE

SUBTROPICAL AUTUMN DAYTIME

PERCENT ERROR--DOTS LOG DEVIATION--CROSSES

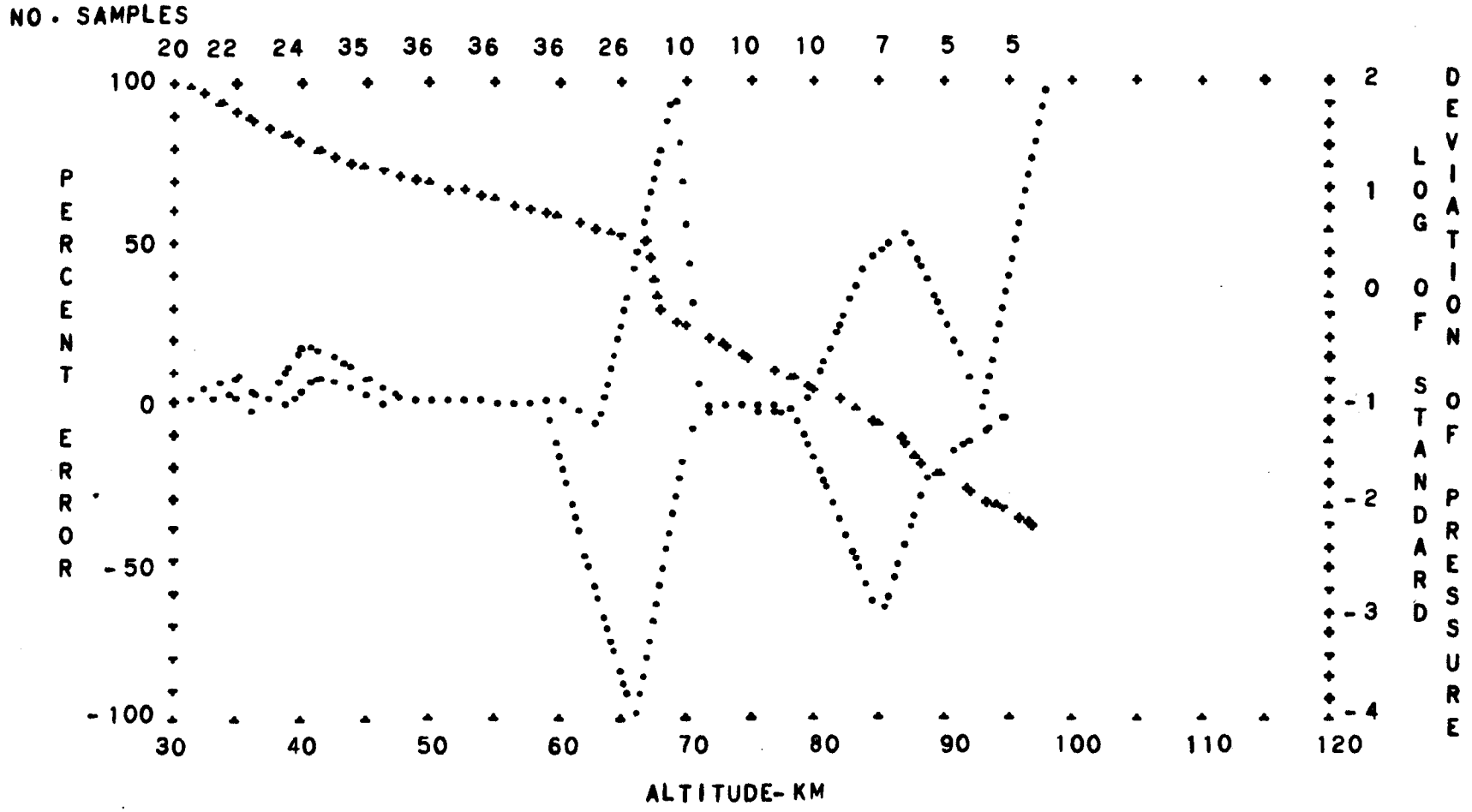

FIG. B-31. STANDARD DEVIATION OF PRESSURE AND PERCENT ERROR OF BUELL HYDROSTATIC EQUATION VERSUS ALTITUDE

SUBTROPICAL AUTUMN NIGHTTIME

PERCENT ERROR--DOTS LOG DEVIATION--CROSSES

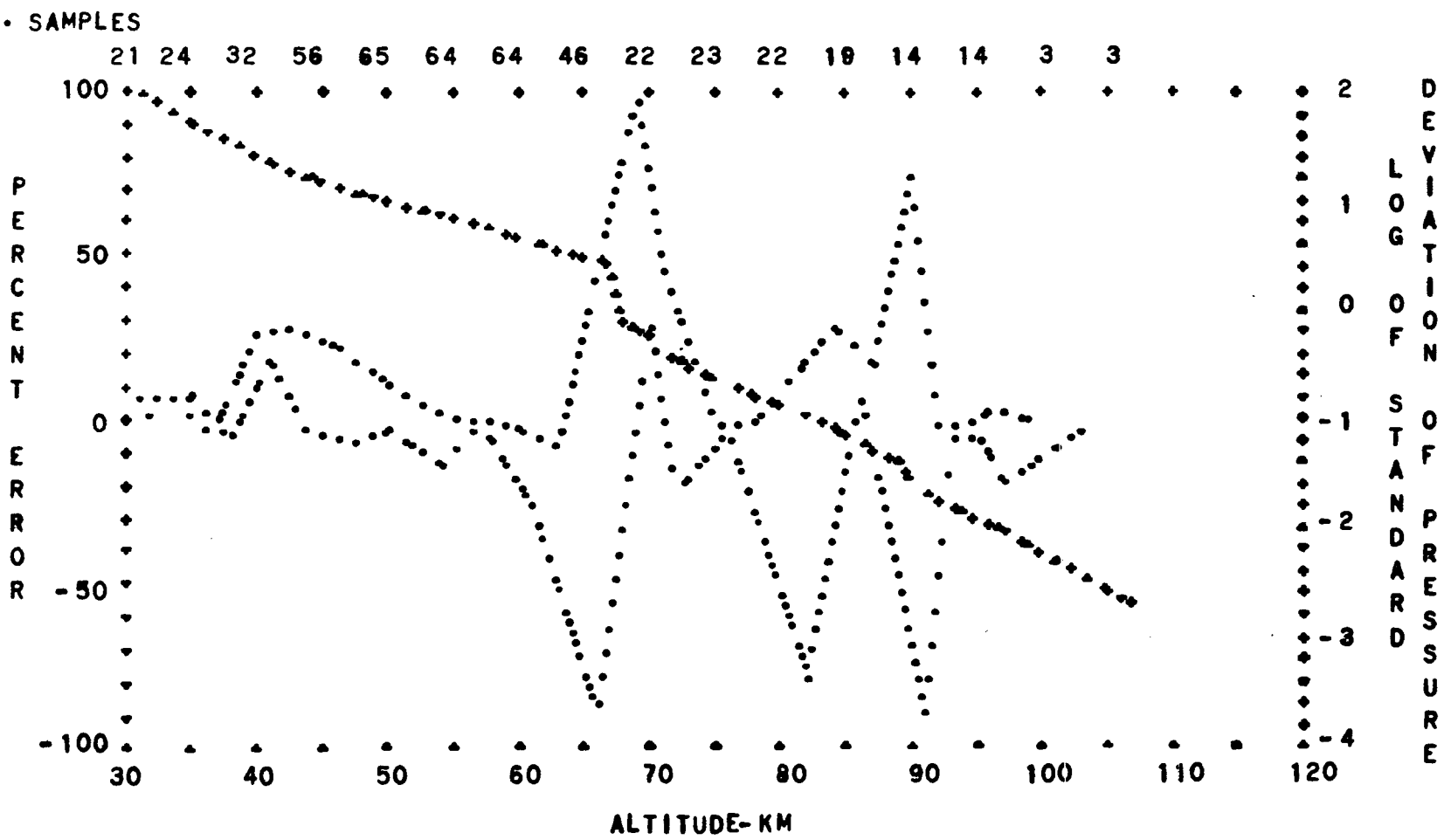

FIG. B-32. STANDARD DEVIATION OF PRESSURE AND PERCENT ERROR OF BUELL HYDROSTATIC EQUATION VERSUS ALTITUDE

SUBTROPICAL AUTUMN DIURNAL MEAN

PERCENT ERROR--DOTS LOG DEVIATION--CROSSES

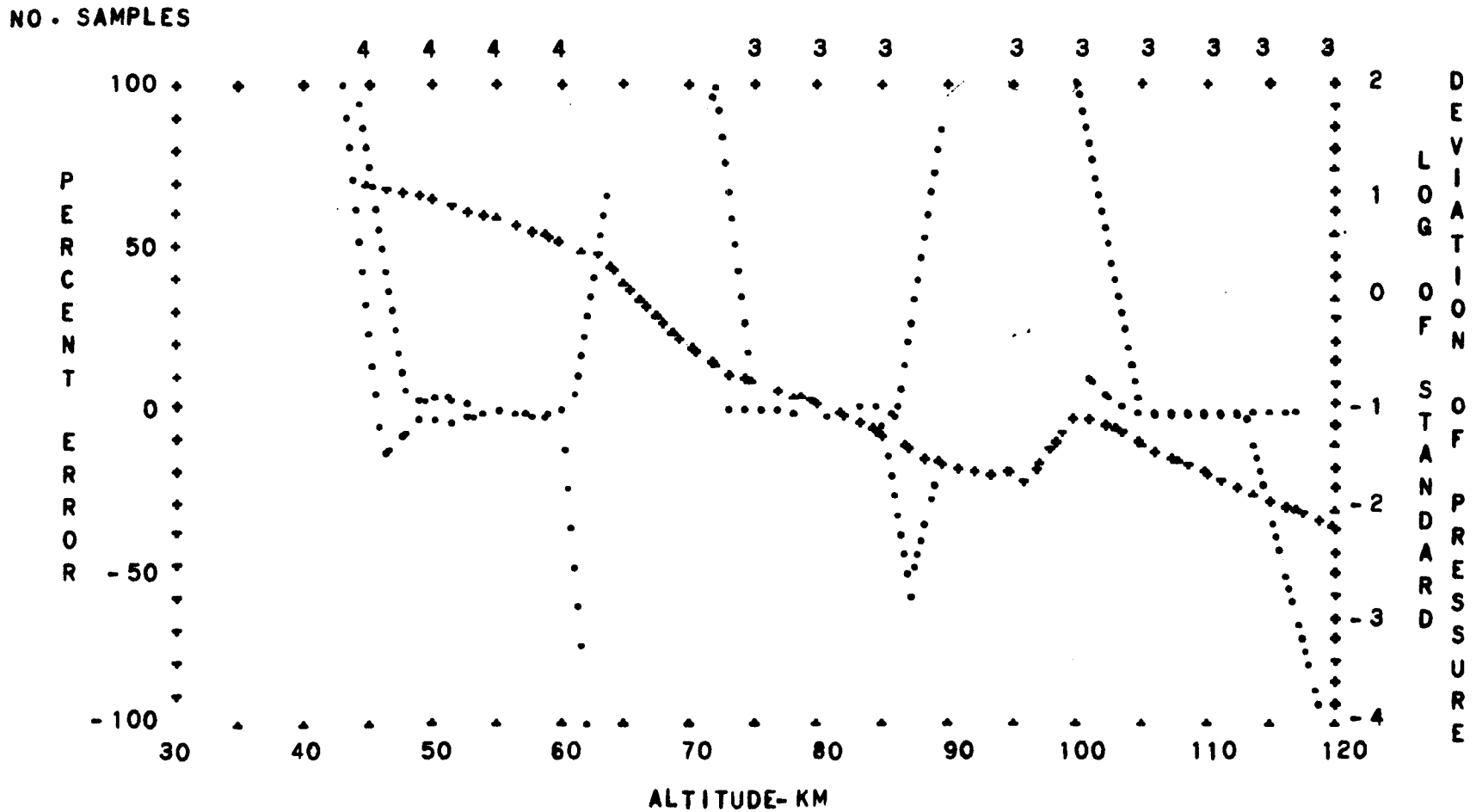

FIG. B-33. STANDARD DEVIATION OF PRESSURE AND PERCENT ERROR OF BUELL HYDROSTATIC EQUATION VERSUS ALTITUDE

SUBTROPICAL WINTER DIURNAL TRANSITION

PERCENT ERROR--DOTS LOG DEVIATION--CROSSES

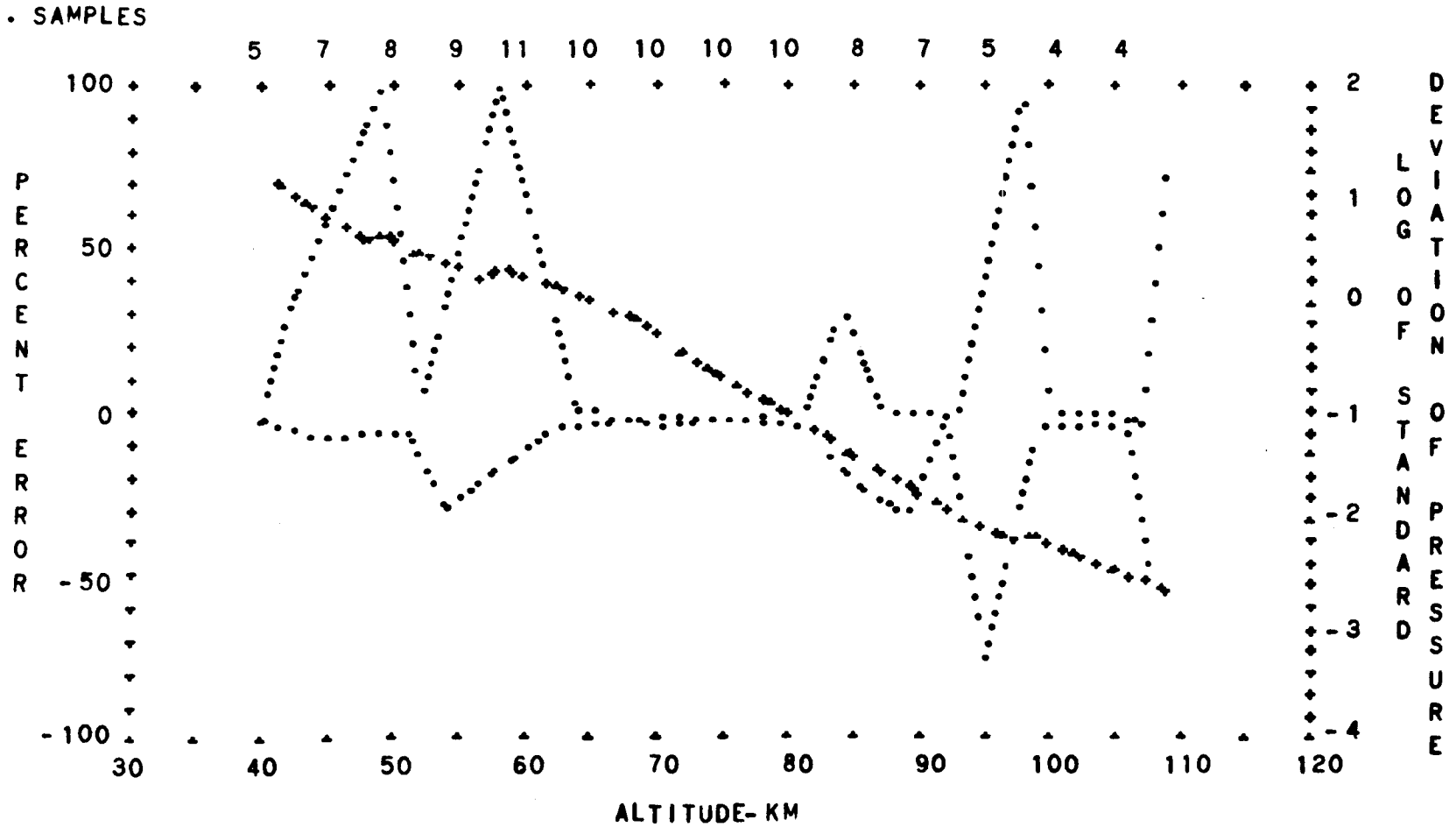

FIG. B-34. STANDARD DEVIATION OF PRESSURE AND PERCENT ERROR OF BUELL HYDROSTATIC EQUATION VERSUS ALTITUDE

SUBTROPICAL WINTER DAYTIME

PERCENT ERROR--DOTS LOG DEVIATION--CROSSES

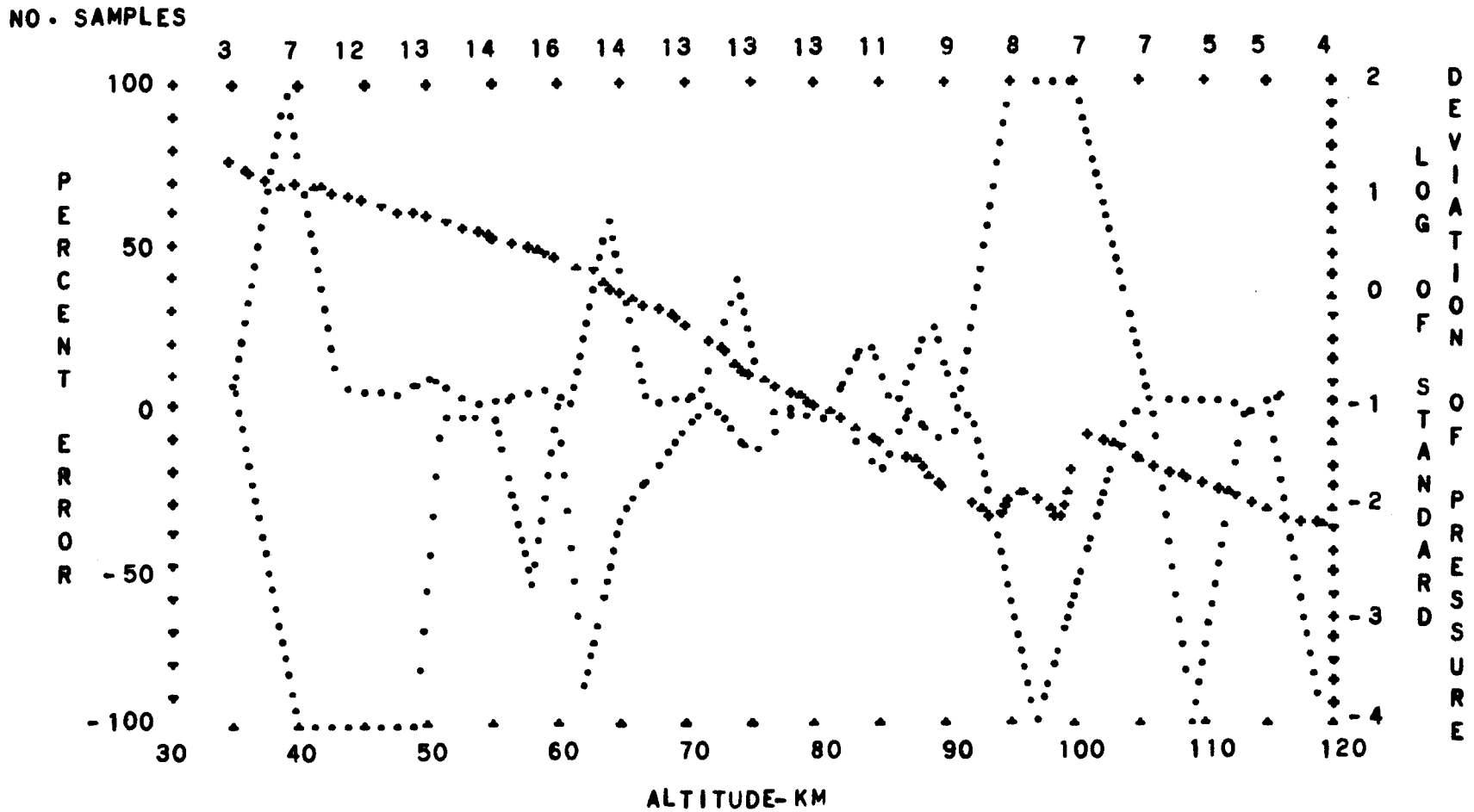

FIG. B-35. STANDARD DEVIATION OF PRESSURE AND PERCENT ERROR OF BUELL HYDROSTATIC EQUATION VERSUS ALTITUDE

SUBTROPICAL WINTER DIURNAL MEAN

PERCENT ERROR--DOTS LOG DEVIATION--CROSSES

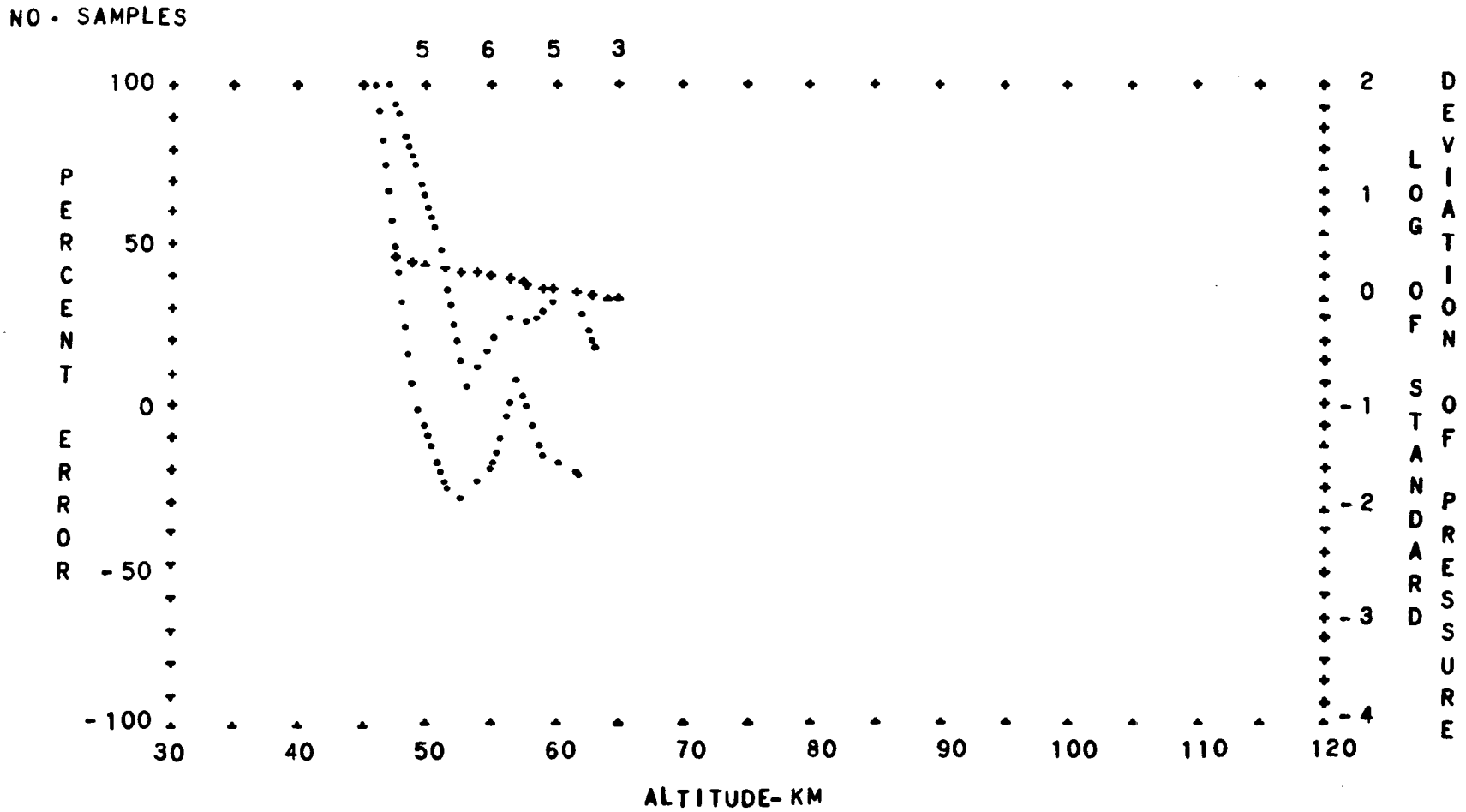

FIG. B-36. STANDARD DEVIATION OF PRESSURE AND PERCENT ERROR OF BUELL HYDROSTATIC EQUATION VERSUS ALTITUDE

SUBTROPICAL SUMMER EXTREME DIURNAL TRANSITION

PERCENT ERROR--DOTS LOG DEVIATION--CROSSES

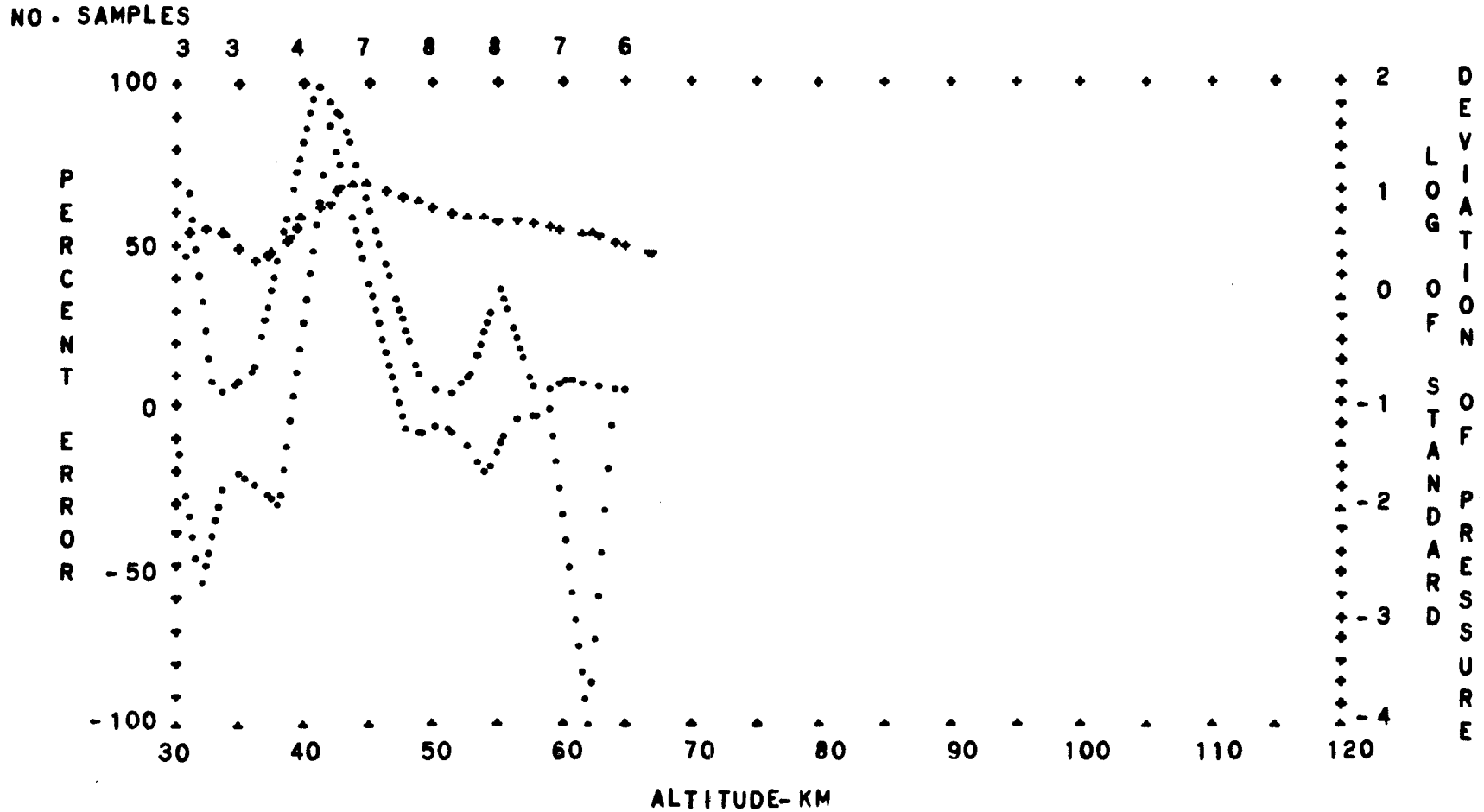

FIG. B-37. STANDARD DEVIATION OF PRESSURE AND PERCENT ERROR OF BUELL HYDROSTATIC EQUATION VERSUS ALTITUDE

SUBTROPICAL SUMMER EXTREME NIGHTTIME

PERCENT ERROR--DOTS LOG DEVIATION--CROSSES

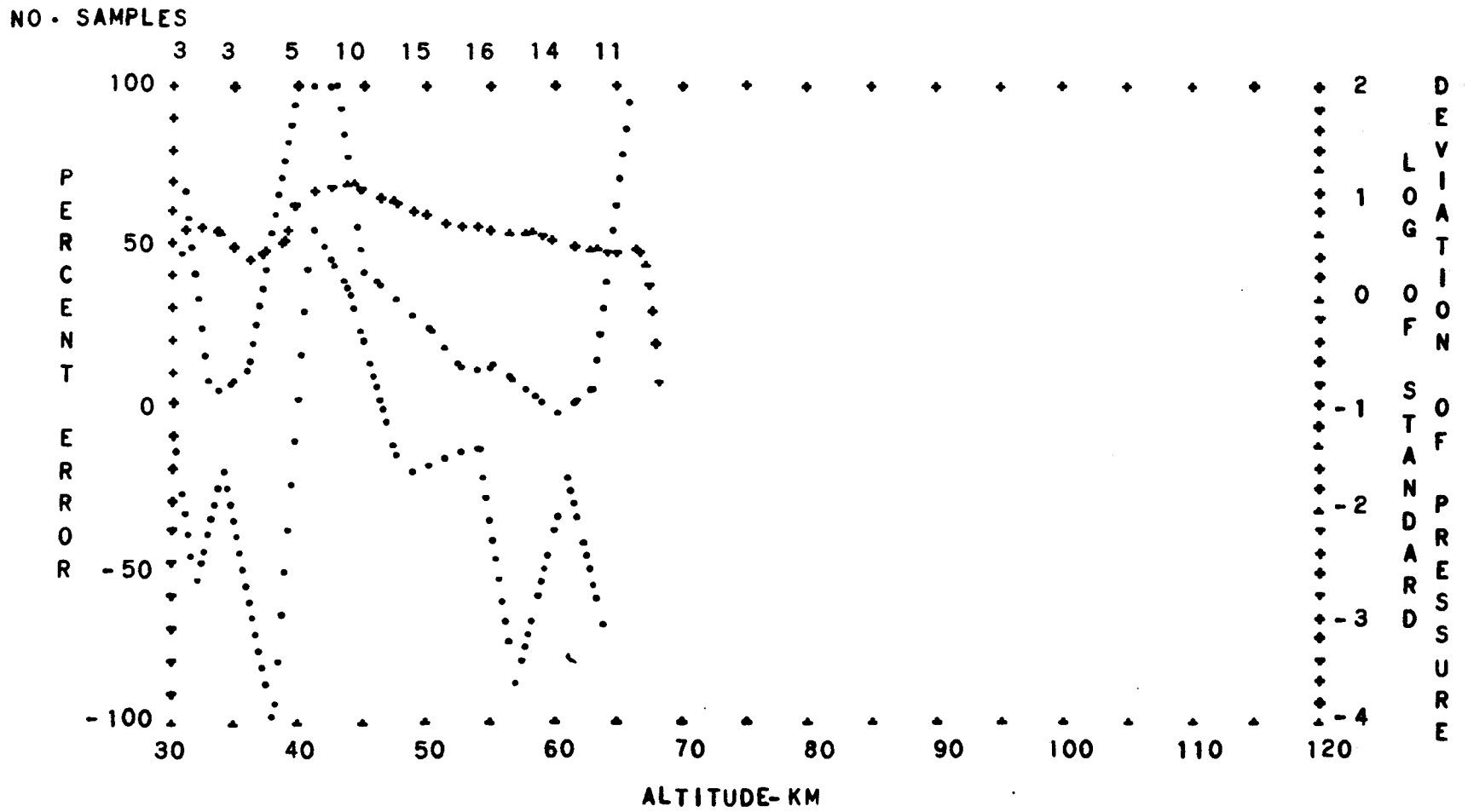

FIG. B-38. STANDARD DEVIATION OF PRESSURE AND PERCENT ERROR OF BUELL HYDROSTATIC EQUATION VERSUS ALTITUDE

SUBTROPICAL SUMMER EXTREME DIURNAL MEAN

PERCENT ERROR--DOTS LOG DEVIATION--CROSSES

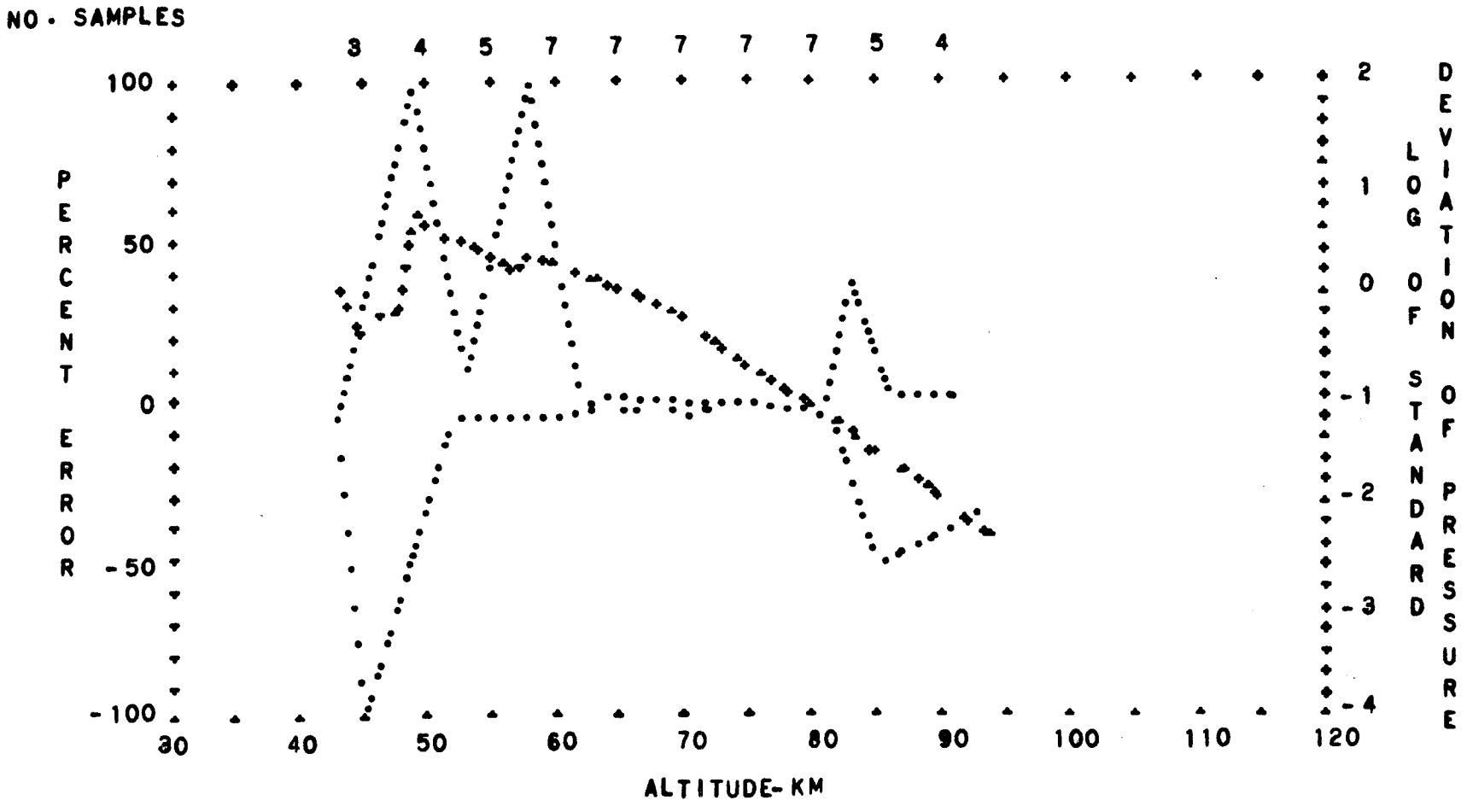

FIG. B-39. STANDARD DEVIATION OF PRESSURE AND PERCENT ERROR OF BUELL HYDROSTATIC EQUATION VERSUS ALTITUDE

SUBTROPICAL WINTER EXTREME DAYTIME

PERCENT ERROR--DOTS LOG DEVIATION--CROSSES

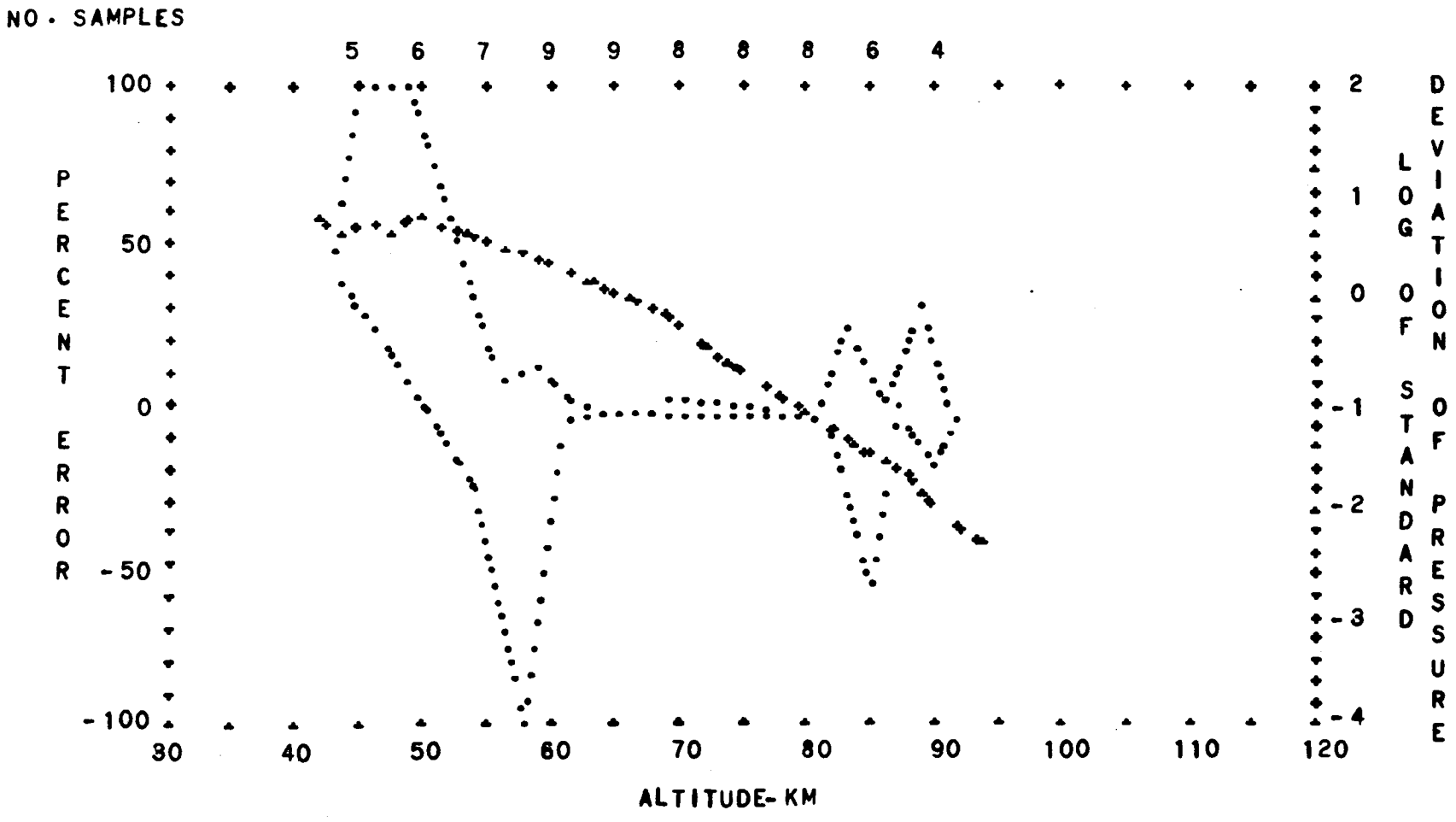

FIG. B-40. STANDARD DEVIATION OF PRESSURE AND PERCENT ERROR OF BUELL HYDROSTATIC EQUATION VERSUS ALTITUDE

SUBTROPICAL WINTER EXTREME DIURNAL MEAN

PERCENT ERROR--DOTS LOG. DEVIATION--CROSSES

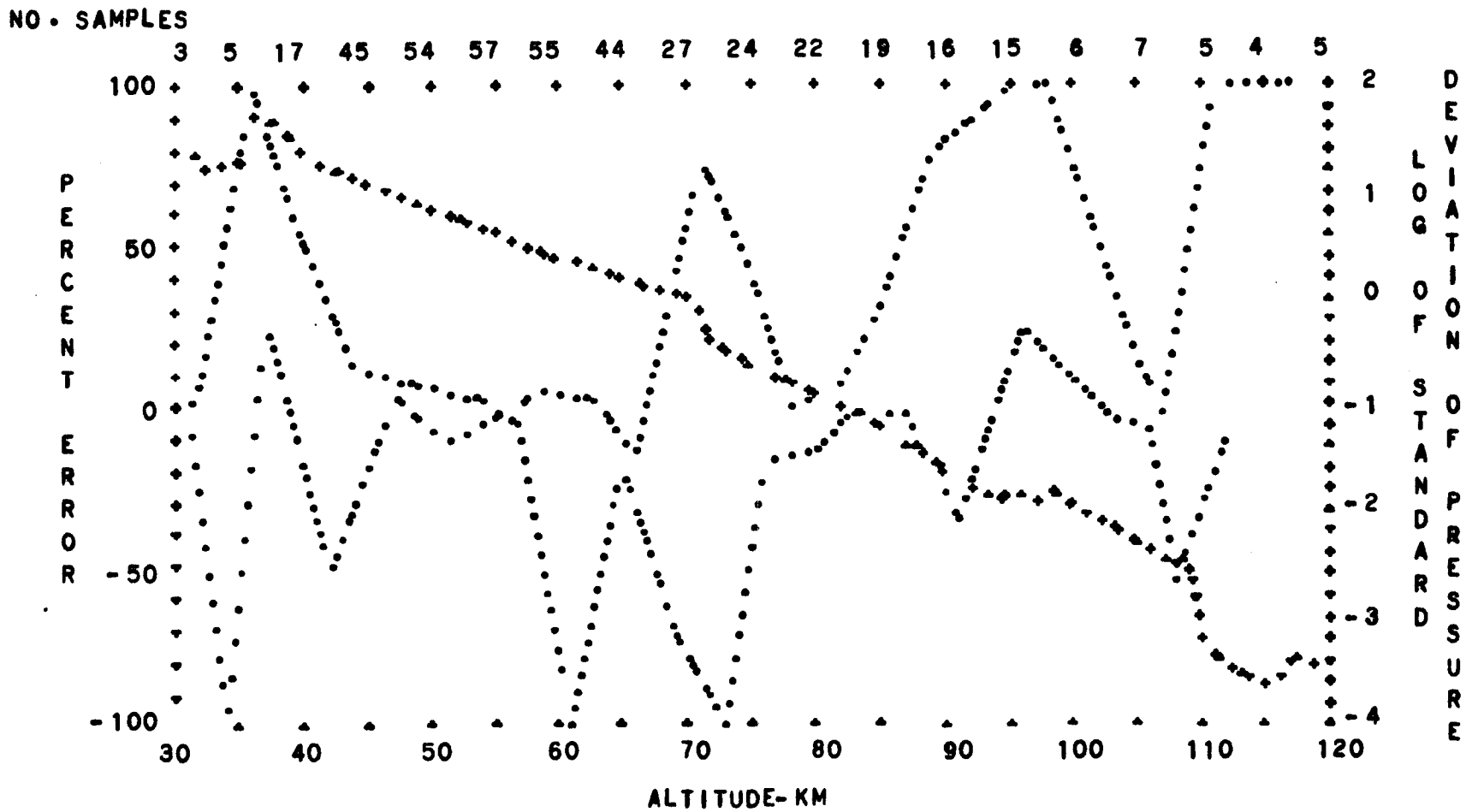

FIG. B-41. STANDARD DEVIATION OF PRESSURE AND PERCENT ERROR OF BUELL HYDROSTATIC EQUATION VERSUS ALTITUDE

SUBTROPICAL ANNUAL MEAN DIURNAL TRANSITION

PERCENT ERROR--DOTS LOG DEVIATION--CROSSES

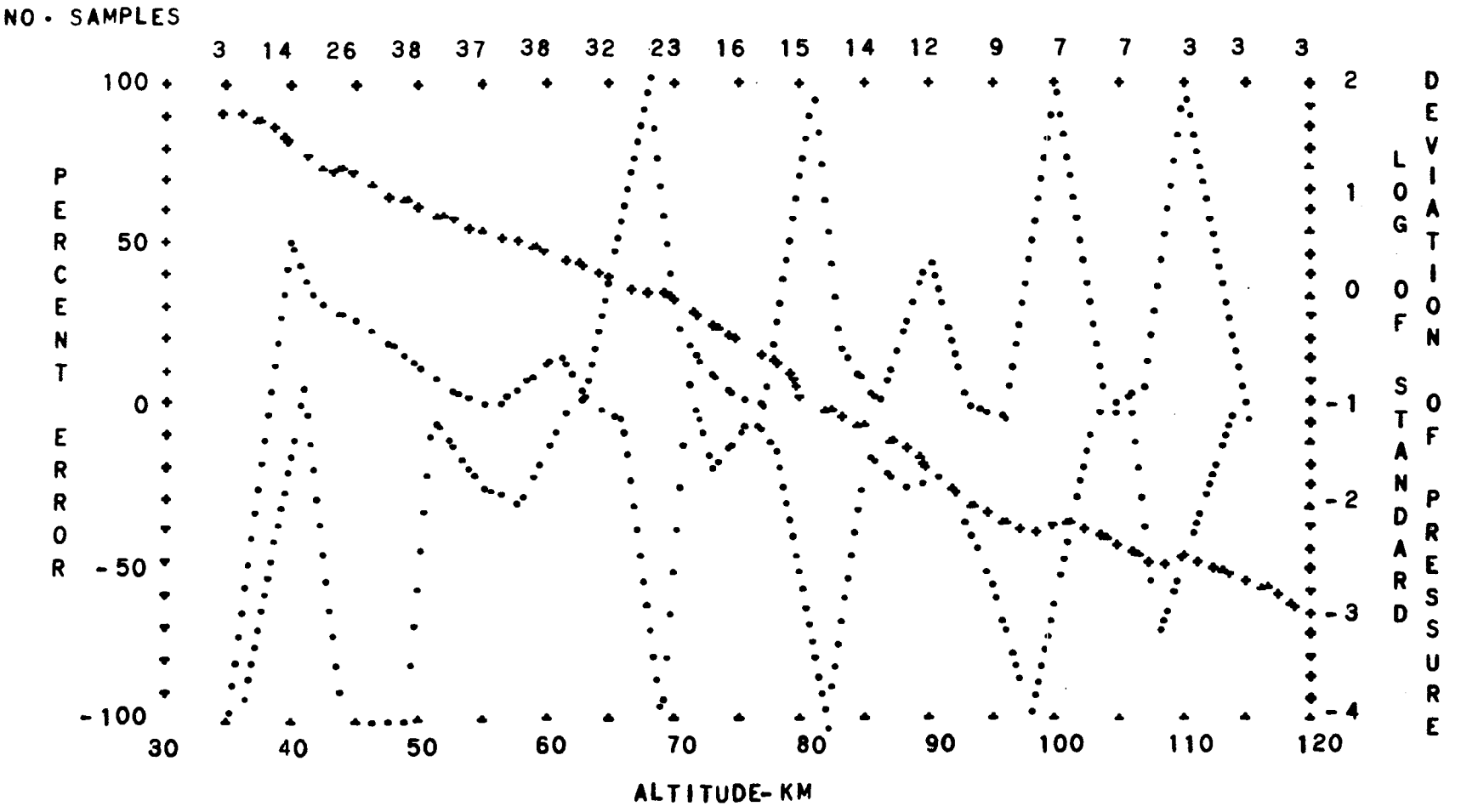

FIG. B-42. STANDARD DEVIATION OF PRESSURE AND PERCENT ERROR OF BUELL HYDROSTATIC EQUATION VERSUS ALTITUDE

SUBTROPICAL ANNUAL MEAN DAYTIME

PERCENT ERROR--DOTS LOG DEVIATION--CROSSES

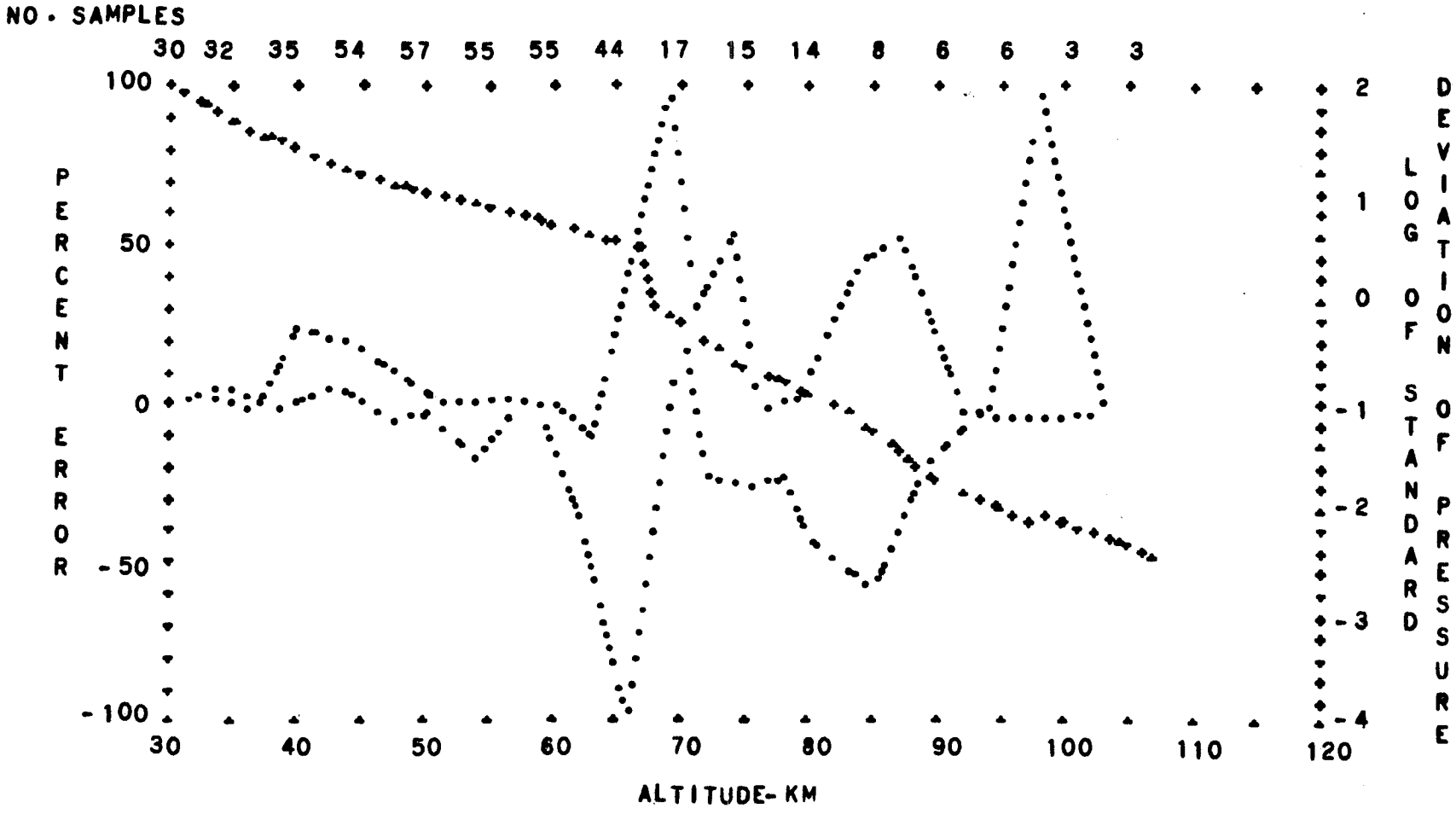

FIG. B-43. STANDARD DEVIATION OF PRESSURE AND PERCENT ERROR OF BUELL HYDROSTATIC EQUATION VERSUS ALTITUDE

SUBTROPICAL ANNUAL MEAN NIGHTTIME

PERCENT ERROR--DOTS LOG DEVIATION--CROSSES

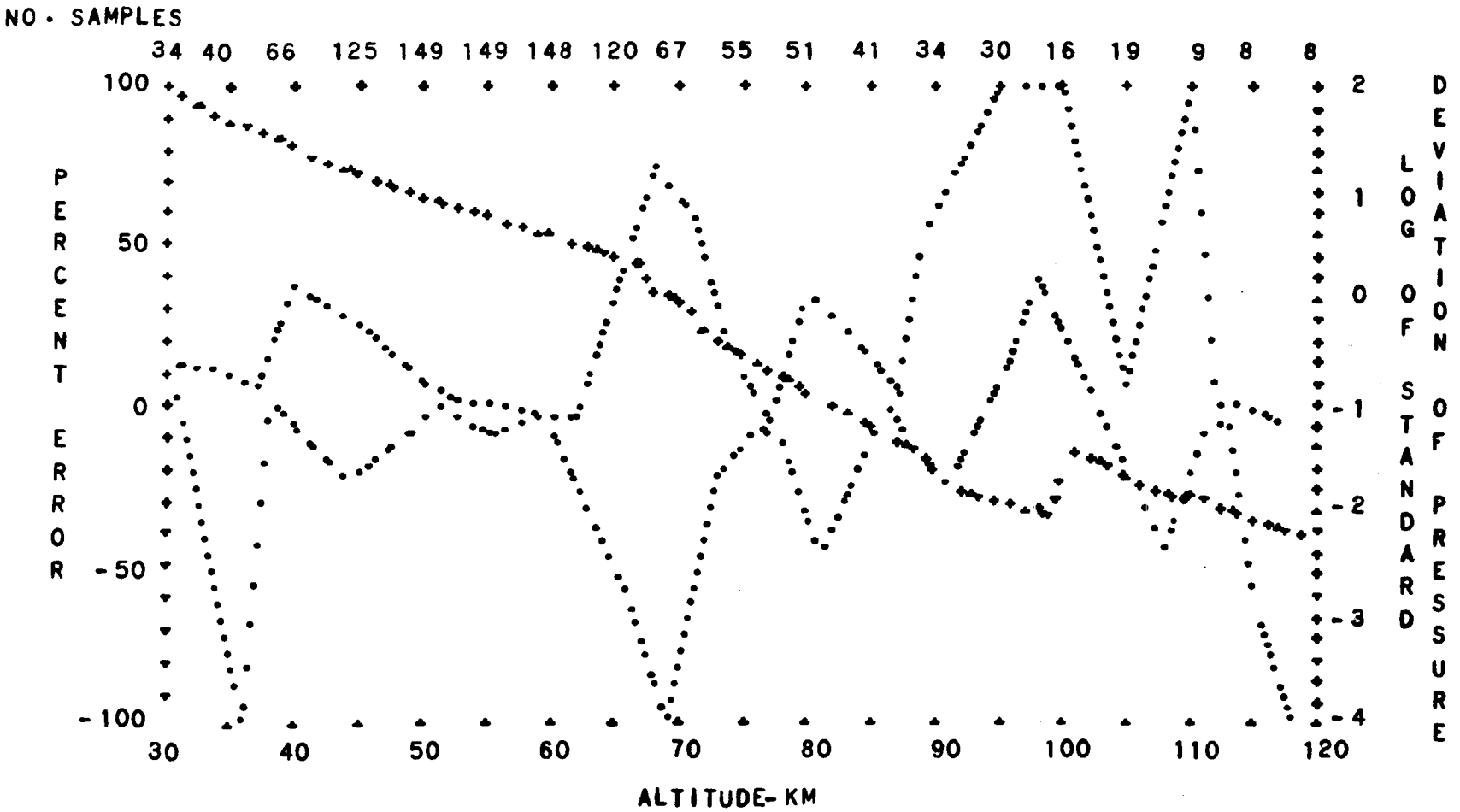

FIG. B-44. STANDARD DEVIATION OF PRESSURE AND PERCENT ERROR OF BUELL HYDROSTATIC EQUATION VERSUS ALTITUDE

SUBTROPICAL ANNUAL MEAN DIURNAL MEAN

PERCENT ERROR--DOTS LOG DEVIATION--CROSSES

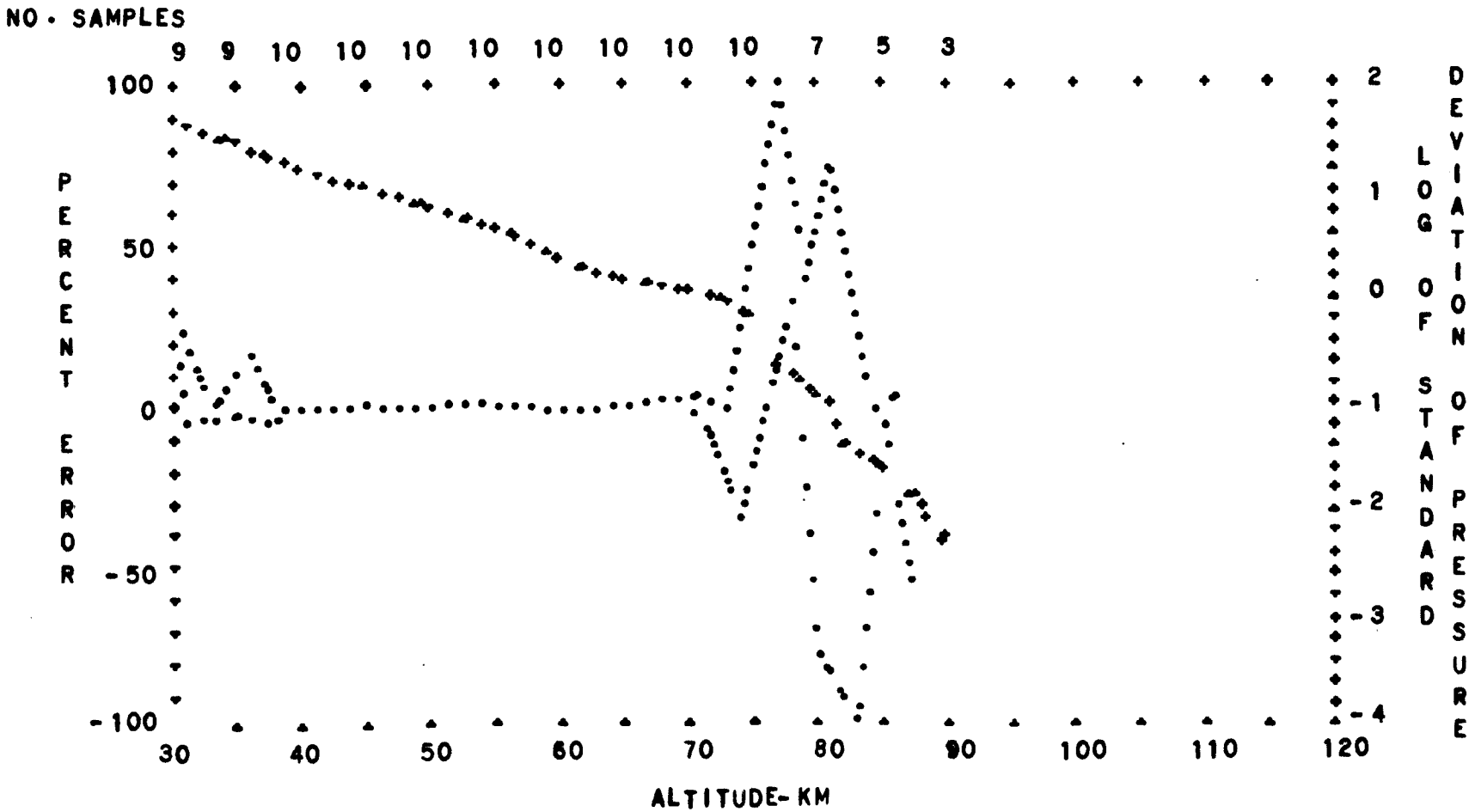

FIG. B-45. STANDARD DEVIATION OF PRESSURE AND PERCENT ERROR OF BUELL HYDROSTATIC EQUATION VERSUS ALTITUDE

MIDLATITUDE SPRING DIURNAL TRANSITION

PERCENT ERROR--DOTS LOG DEVIATION--CROSSES

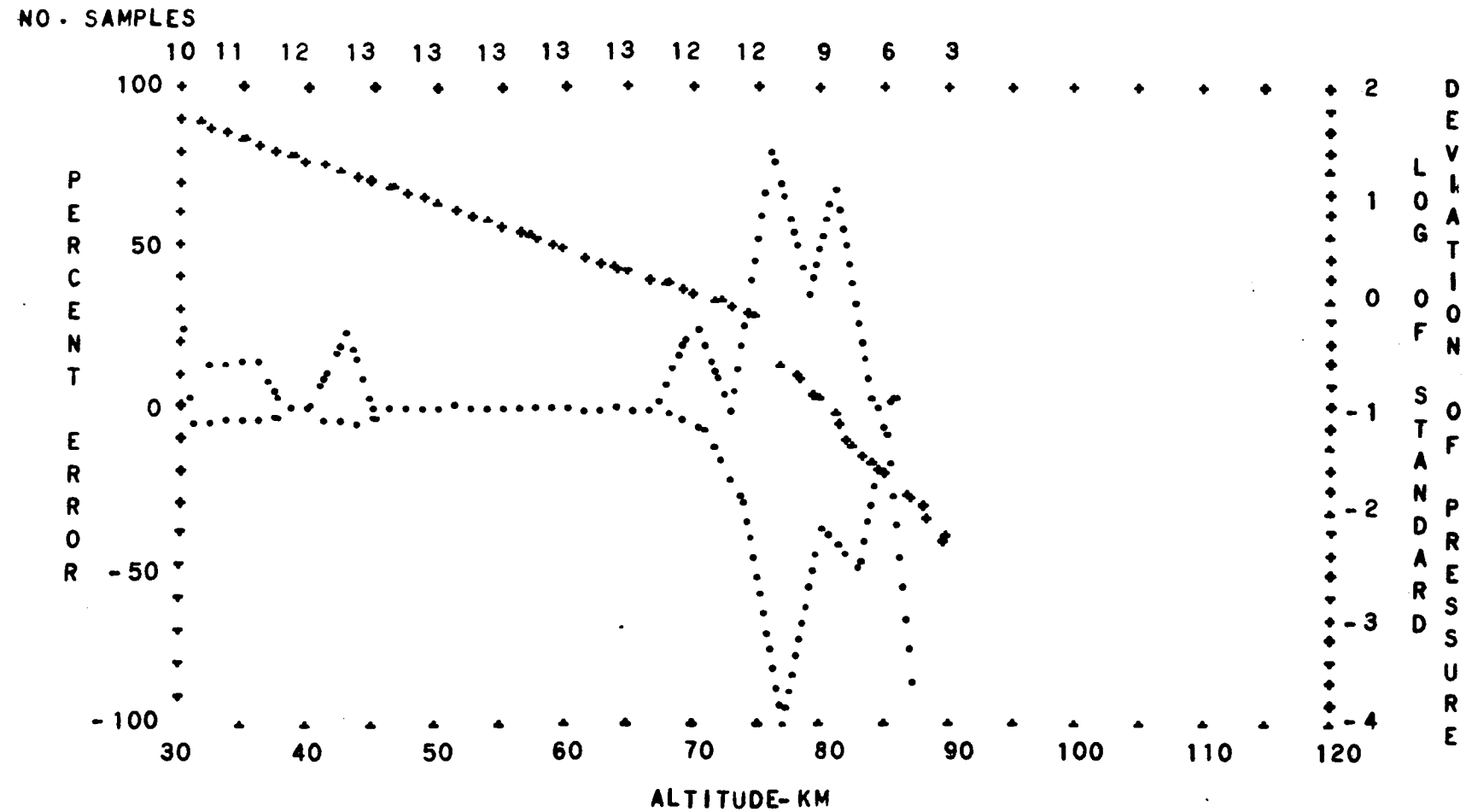

FIG. B-46. STANDARD DEVIATION OF PRESSURE AND PERCENT ERROR OF BUELL HYDROSTATIC EQUATION VERSUS ALTITUDE

MIDLATITUDE SPRING DIURNAL MEAN

PERCENT ERROR--DOTS LOG DEVIATION--CROSSES

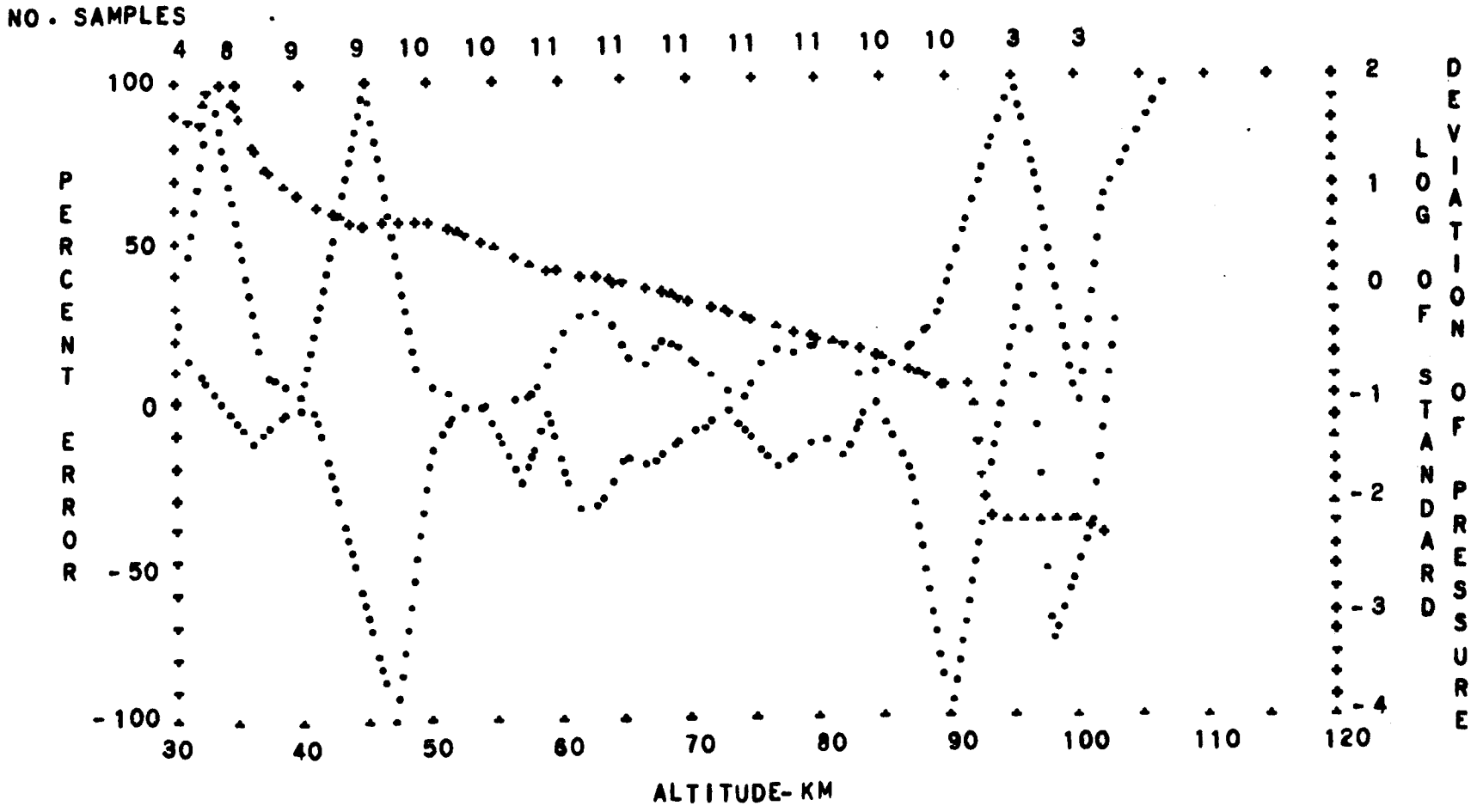

FIG. B-47. STANDARD DEVIATION OF PRESSURE AND PERCENT ERROR OF BUELL HYDROSTATIC EQUATION VERSUS ALTITUDE

MIDLATITUDE SUMMER DIURNAL TRANSITION

PERCENT ERROR--DOTS LOG DEVIATION--CROSSES

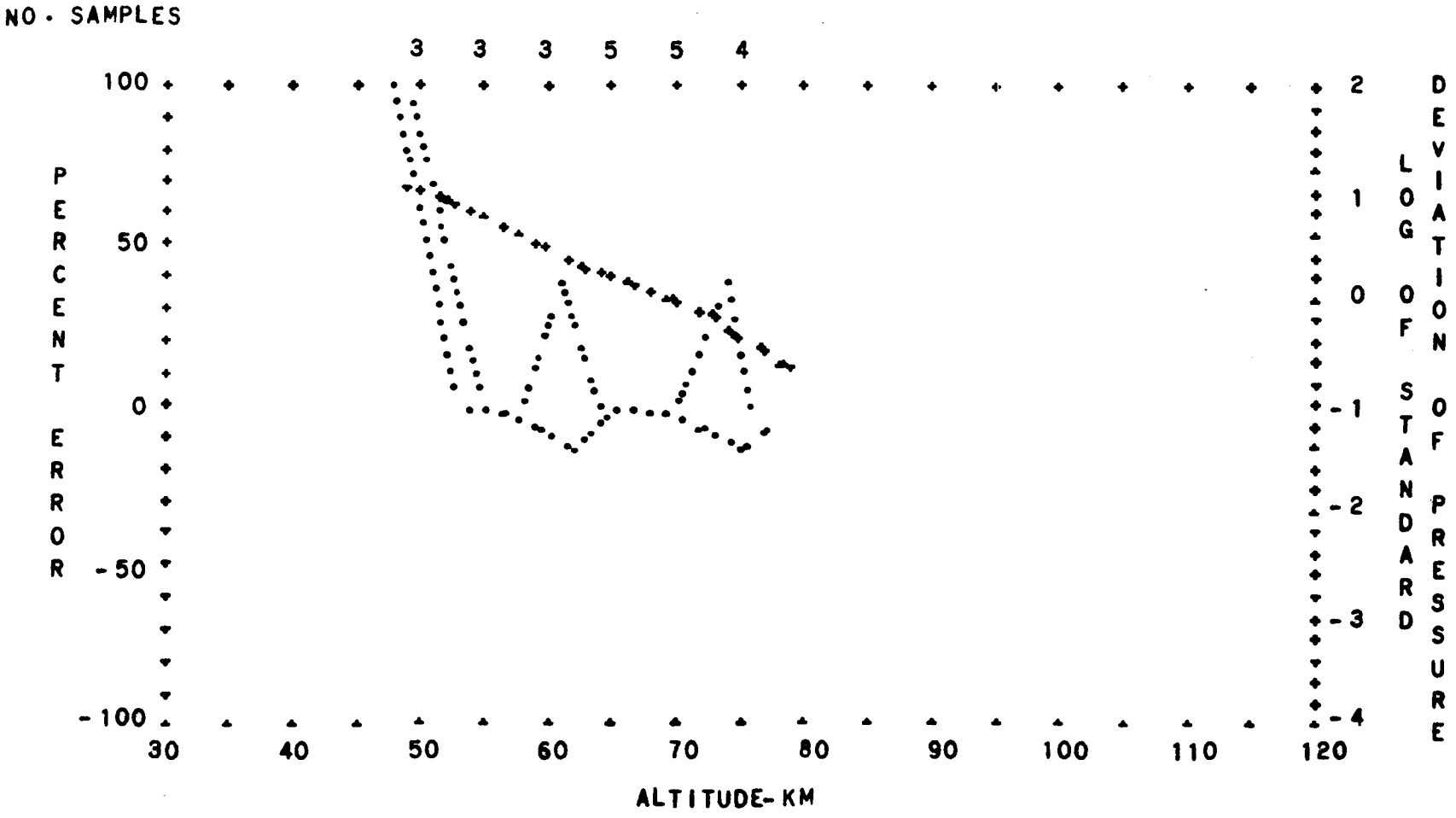

FIG. B-48. STANDARD DEVIATION OF PRESSURE AND PERCENT ERROR OF BUELL HYDROSTATIC EQUATION VERSUS ALTITUDE

MIDLATITUDE SUMMER DAYTIME

PERCENT ERROR--DOTS LOG DEVIATION--CROSSES

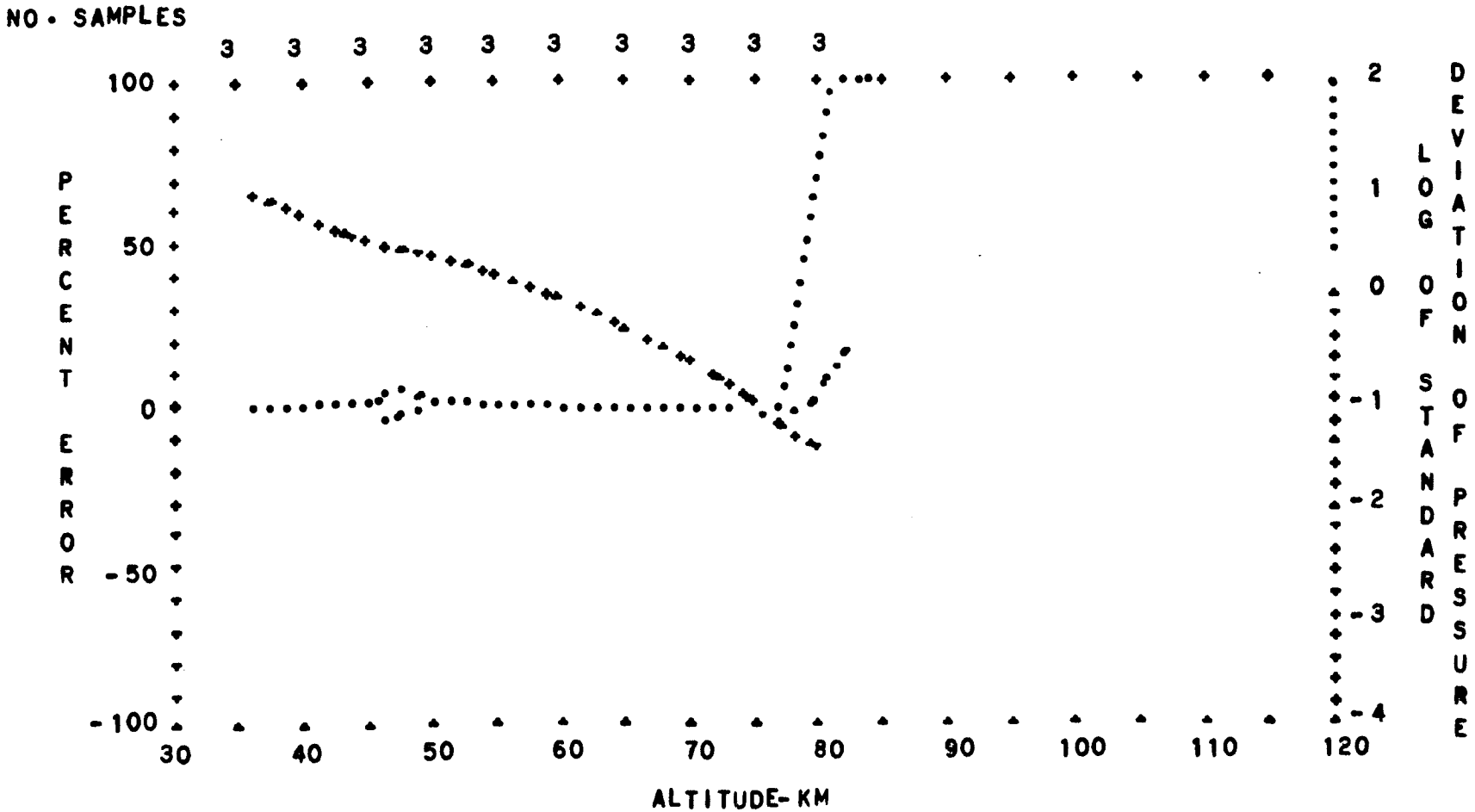

FIG. B-49. STANDARD DEVIATION OF PRESSURE AND PERCENT ERROR OF BUELL HYDROSTATIC EQUATION VERSUS ALTITUDE

MIDLATITUDE SUMMER NIGHTTIME

PERCENT ERROR--DOTS LOG DEVIATION--CROSSES

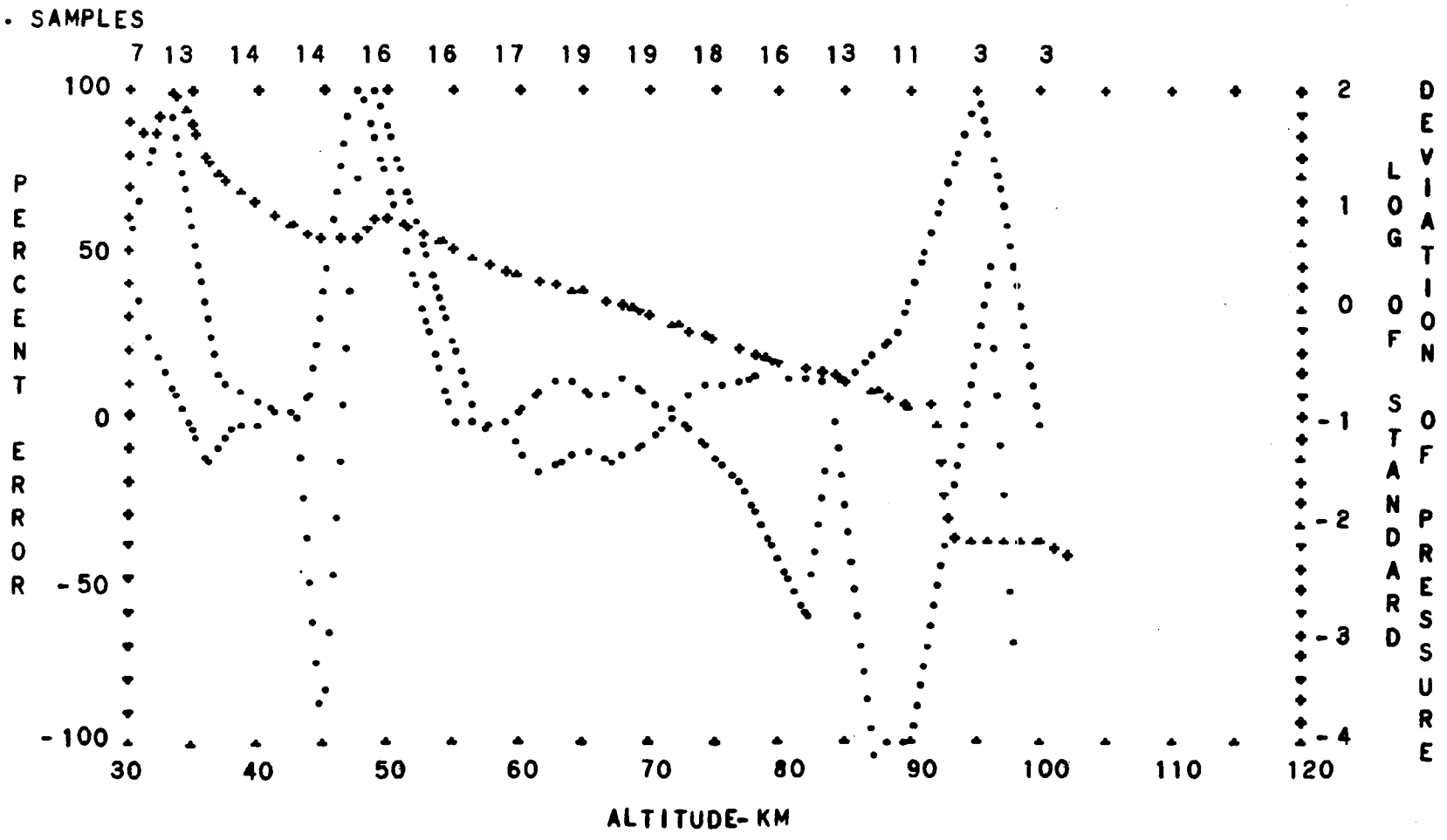

FIG. B-50. STANDARD DEVIATION OF PRESSURE AND PERCENT ERROR OF BUELL HYDROSTATIC EQUATION VERSUS ALTITUDE

MIDLATITUDE SUMMER DIURNAL MEAN

PERCENT ERROR--DOTS LOG DEVIATION--CROSSES

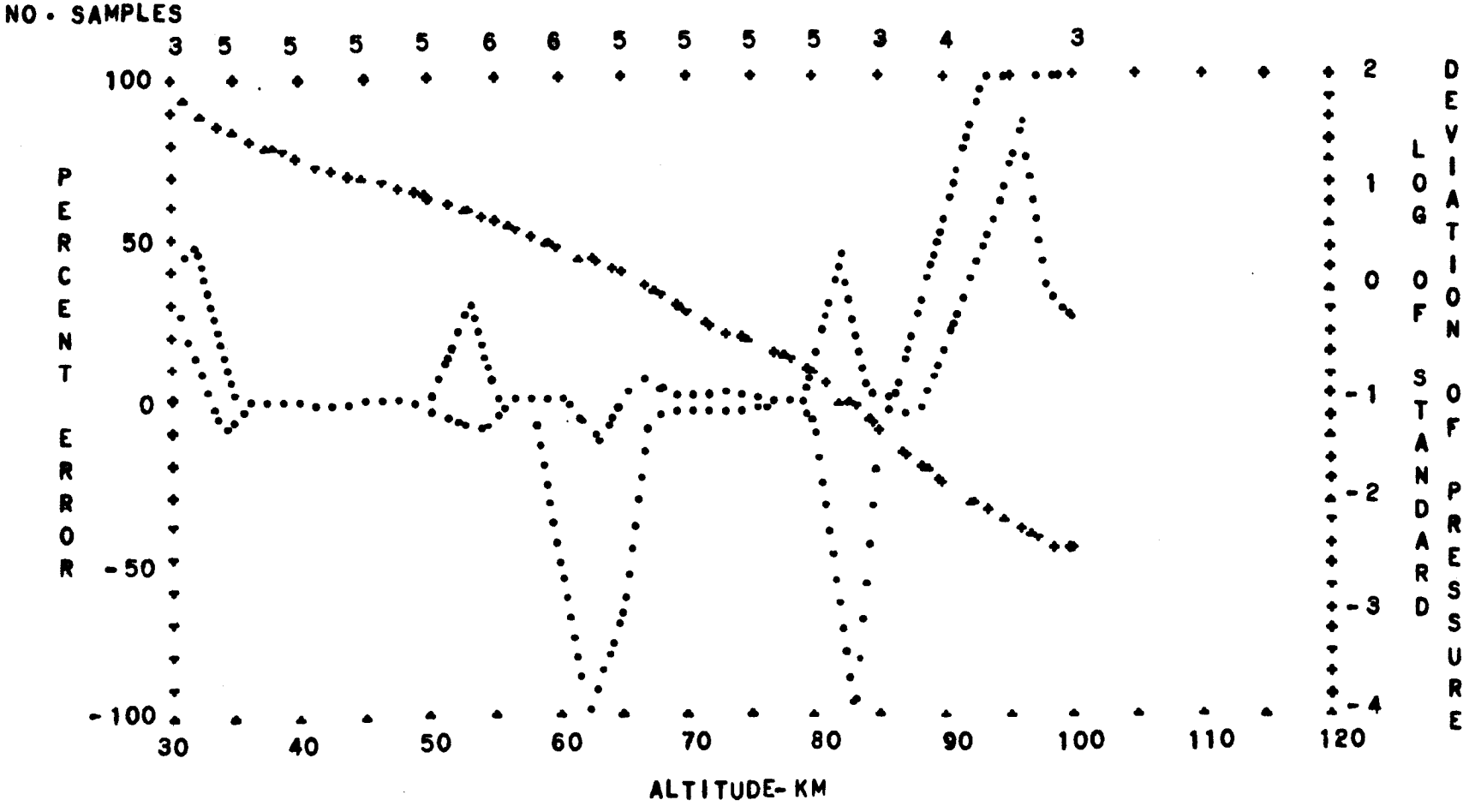

FIG. B-51. STANDARD DEVIATION OF PRESSURE AND PERCENT ERROR OF BUELL HYDROSTATIC EQUATION VERSUS ALTITUDE

MIDLATITUDE AUTUMN DIURNAL TRANSITION

PERCENT ERROR--DOTS LOG DEVIATION--CROSSES

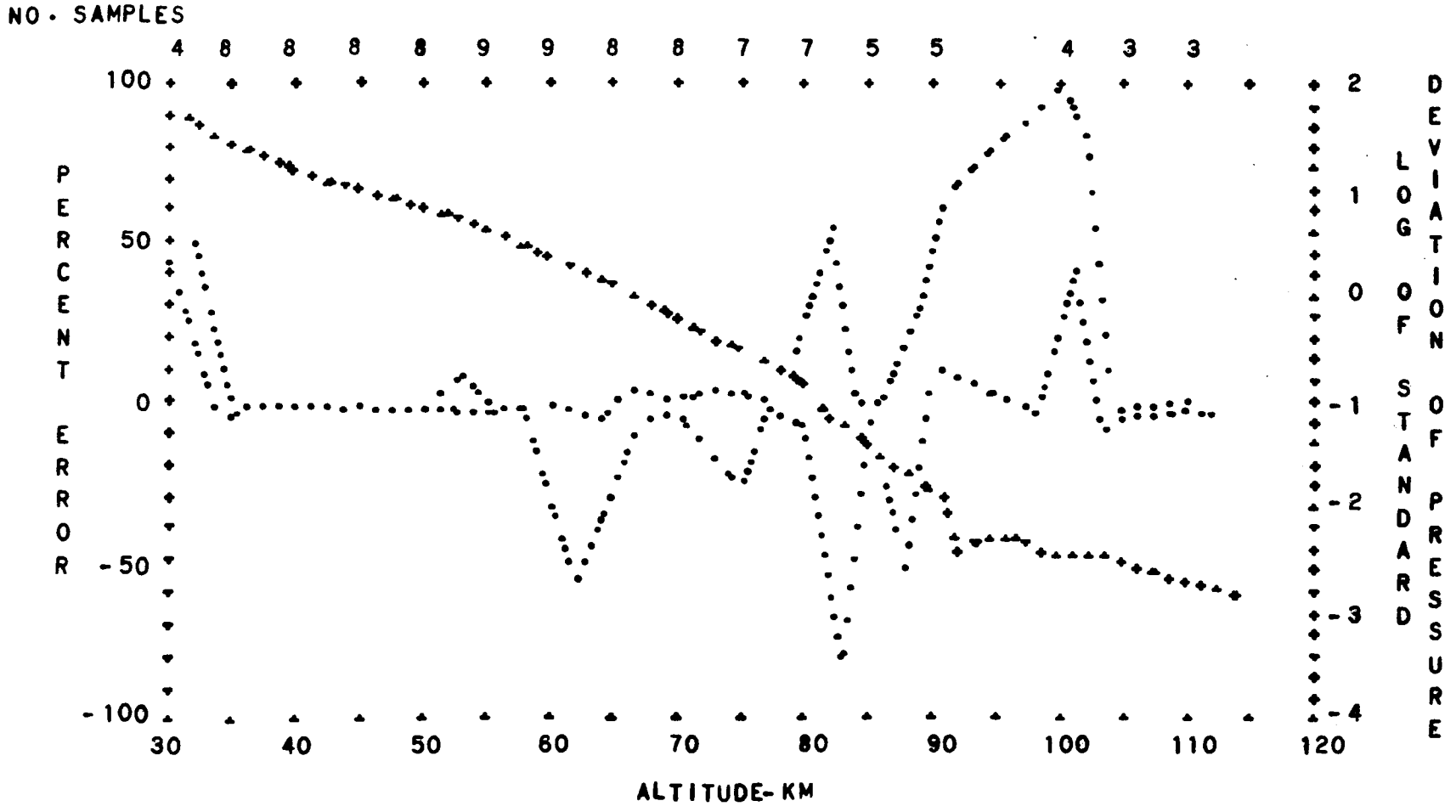

FIG. B-52. STANDARD DEVIATION OF PRESSURE AND PERCENT ERROR OF BUELL HYDROSTATIC EQUATION VERSUS ALTITUDE

MIDLATITUDE AUTUMN DIURNAL MEAN

PERCENT ERROR--DOTS LOG DEVIATION--CROSSES

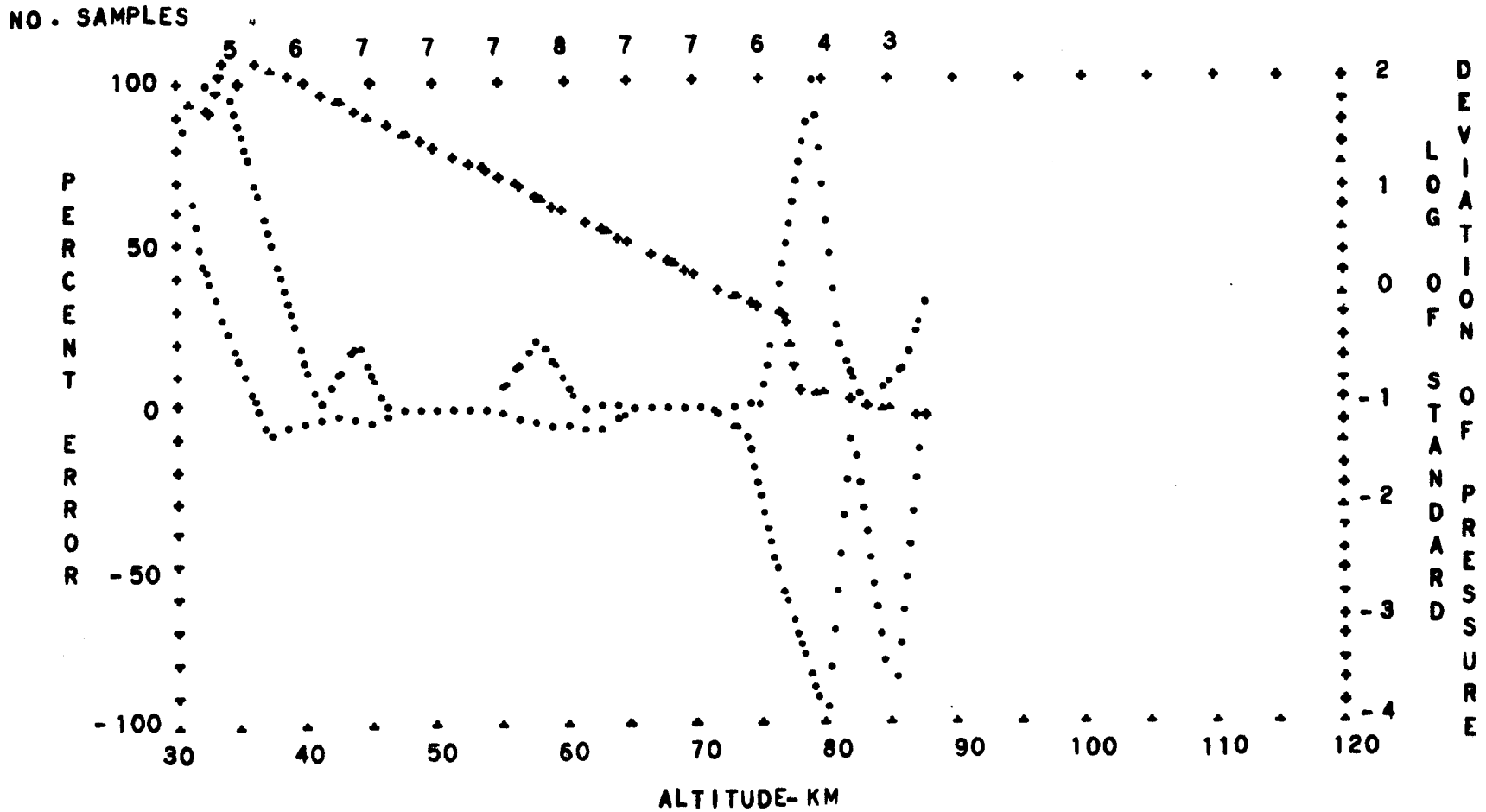

FIG. B-53. STANDARD DEVIATION OF PRESSURE AND PERCENT ERROR OF BUELL HYDROSTATIC EQUATION VERSUS ALTITUDE

MIDLATITUDE WINTER DIURNAL TRANSITION

PERCENT ERROR--DOTS LOG DEVIATION--CROSSES

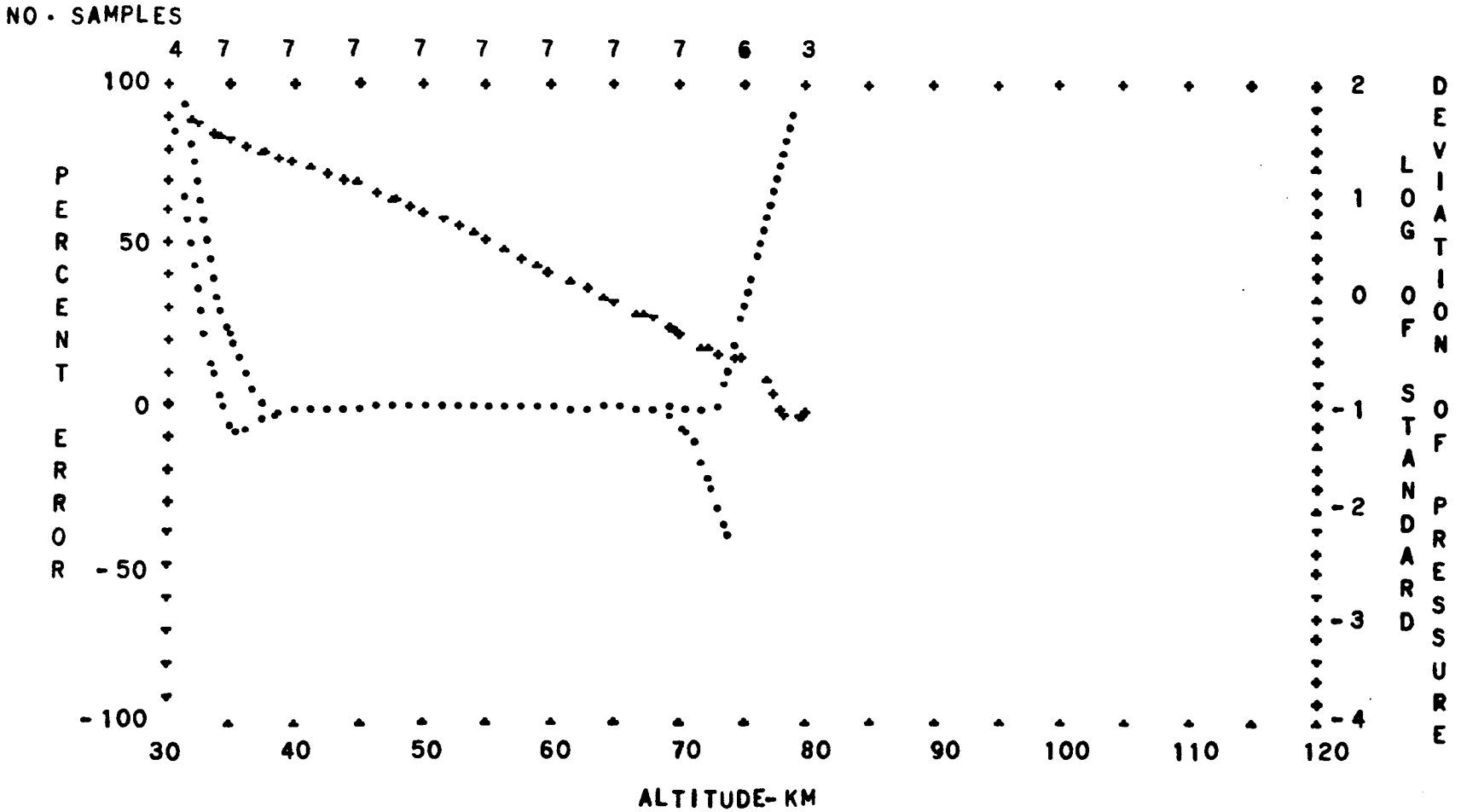

FIG. B-54: STANDARD DEVIATION OF PRESSURE AND PERCENT ERROR OF BUELL HYDROSTATIC EQUATION VERSUS ALTITUDE

MIDLATITUDE WINTER NIGHTTIME

PERCENT ERROR--DOTS LOG DEVIATION--CROSSES

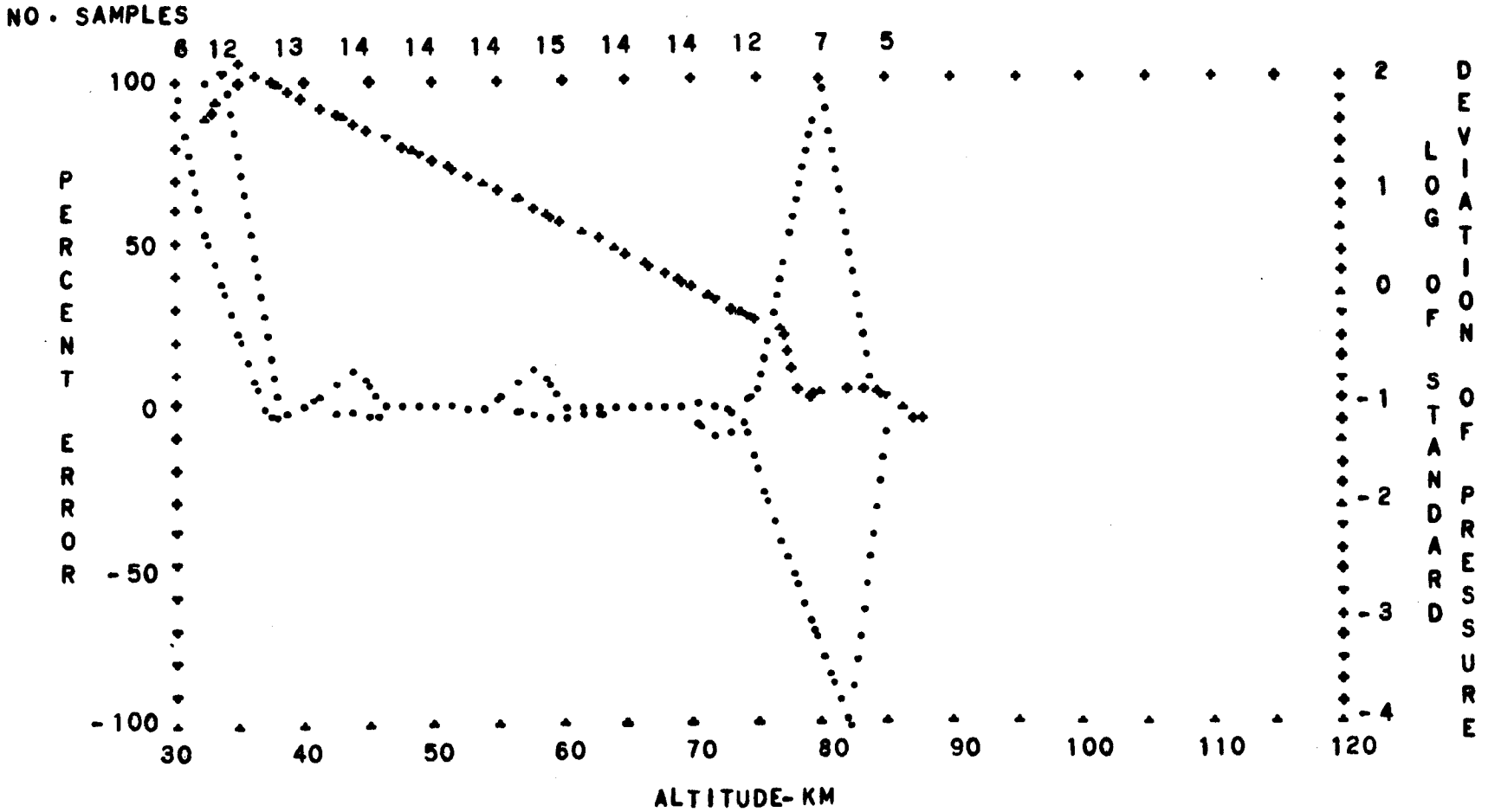

FIG. B-55. STANDARD DEVIATION OF PRESSURE AND PERCENT ERROR OF BUELL HYDROSTATIC EQUATION VERSUS ALTITUDE

MIDLATITUDE WINTER DIURNAL MEAN

PERCENT ERROR--DOTS LOG DEVIATION--CROSSES

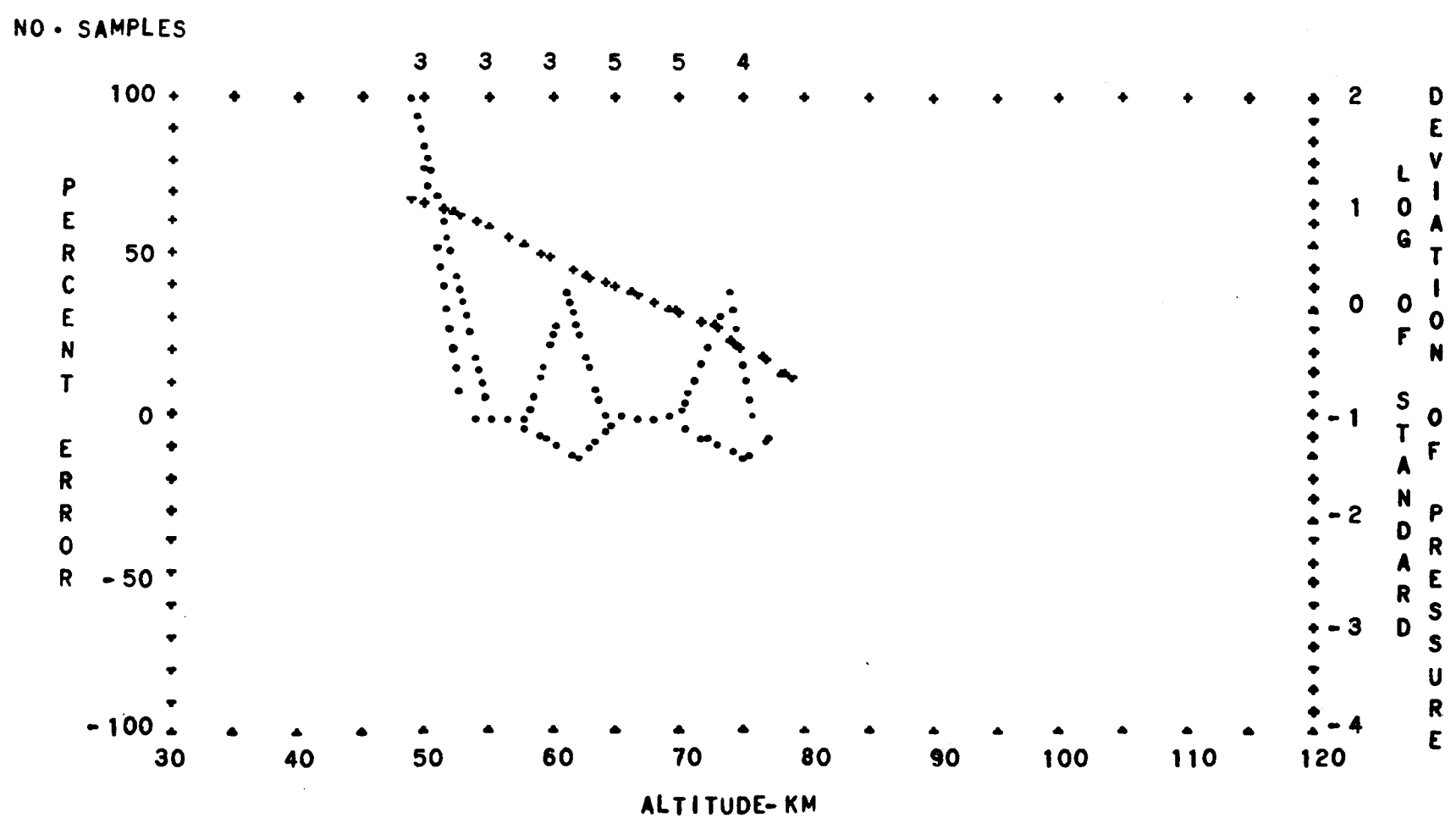

FIG. B-56. STANDARD DEVIATION OF PRESSURE AND PERCENT ERROR OF BUELL HYDROSTATIC EQUATION VERSUS ALTITUDE

MIDLATITUDE SUMMER EXTREME DAYTIME

PERCENT ERROR--DOTS LOG DEVIATION--CROSSES

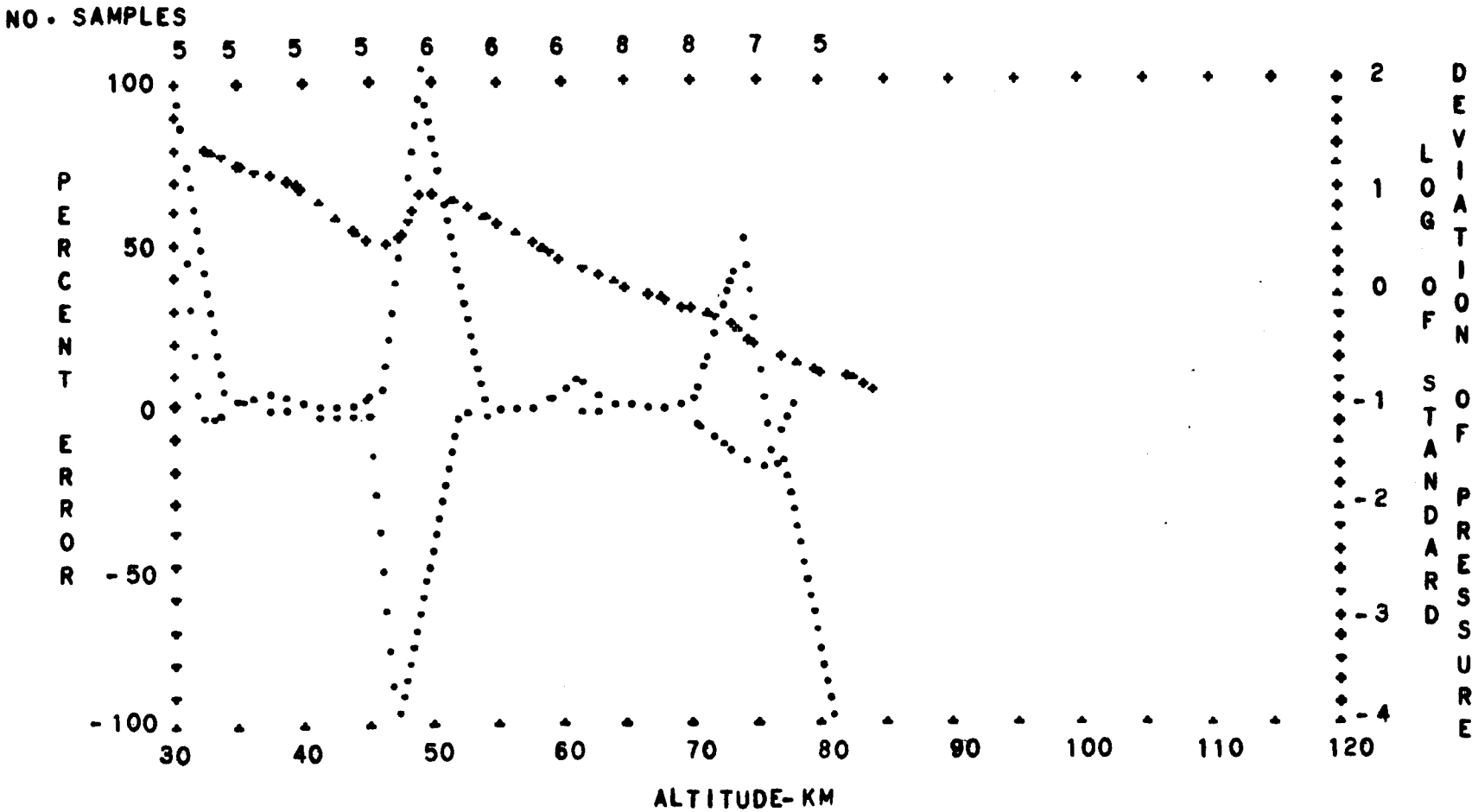

FIG. B-57. STANDARD DEVIATION OF PRESSURE AND PERCENT ERROR OF BUELL HYDROSTATIC EQUATION VERSUS ALTITUDE

MIDLATITUDE SUMMER EXTREME DIURNAL MEAN

PERCENT ERROR--DOTS LOG DEVIATION--CROSSES

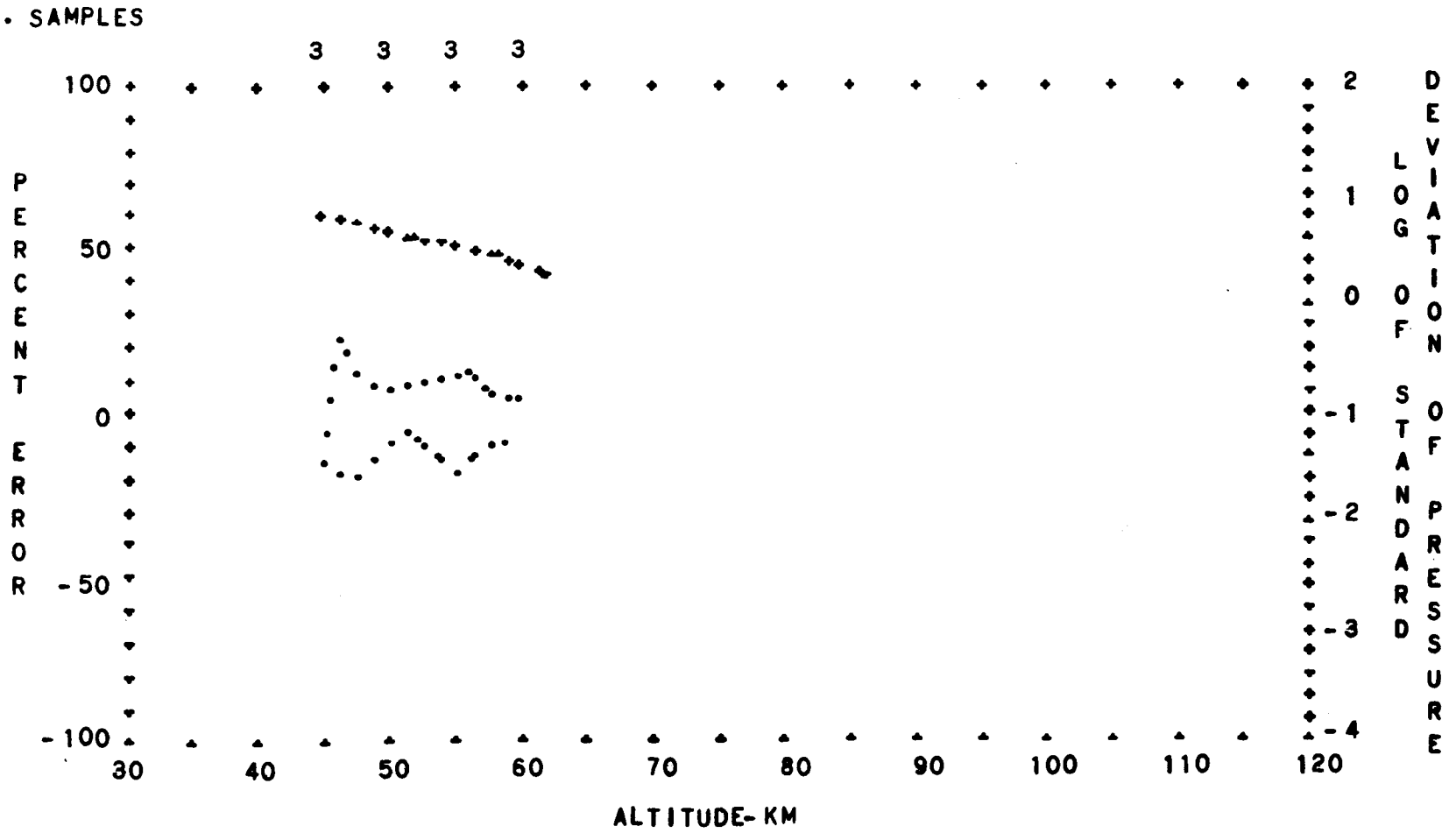

FIG. B-58. STANDARD DEVIATION OF PRESSURE AND PERCENT ERROR OF BUELL HYDROSTATIC EQUATION VERSUS ALTITUDE

MIDLATITUDE WINTER EXTREME DIURNAL MEAN

PERCENT ERROR--DOTS LOG DEVIATION--CROSSES

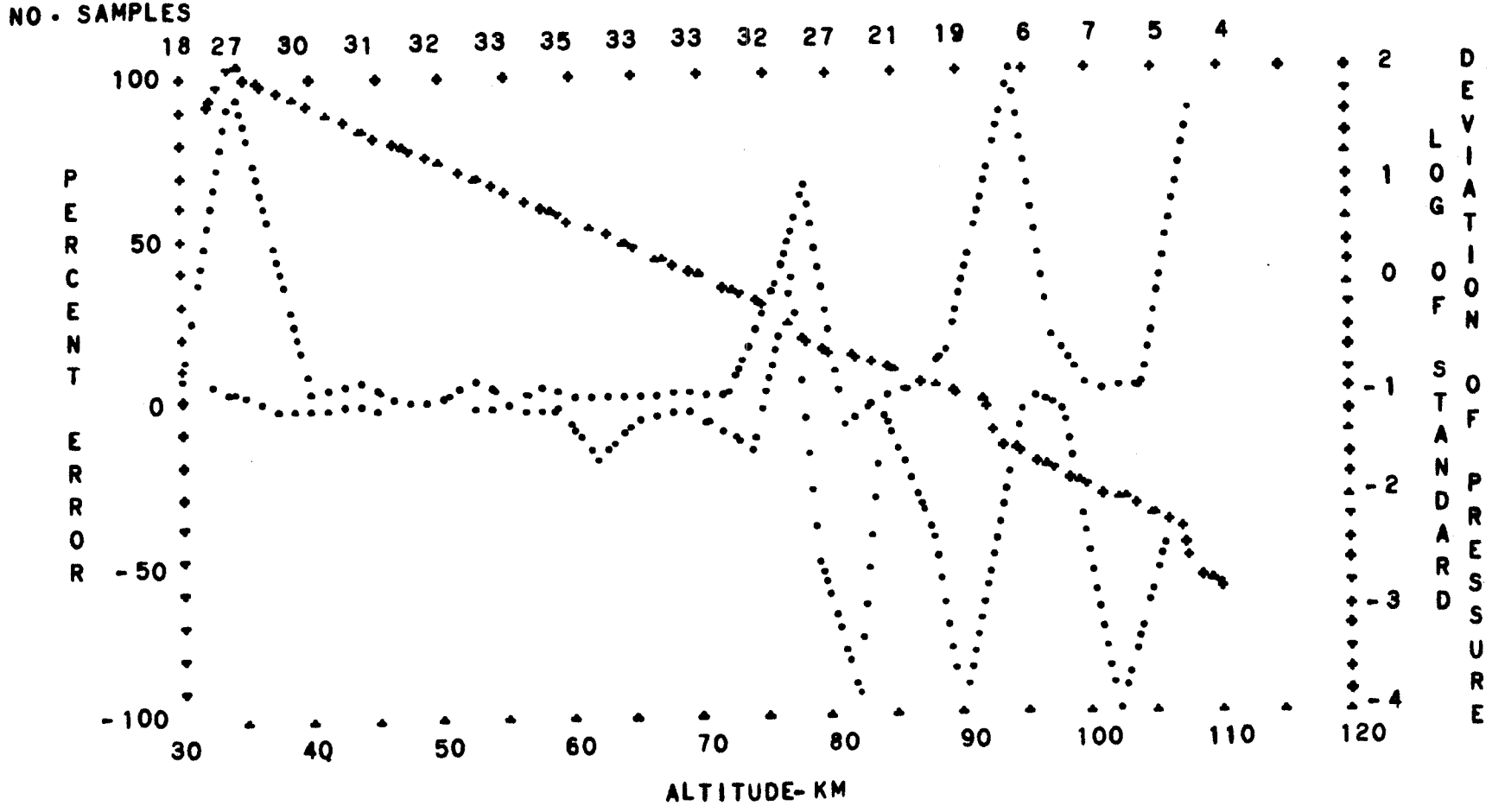

FIG. B-59. STANDARD DEVIATION OF PRESSURE AND PERCENT ERROR OF BUELL HYDROSTATIC EQUATION VERSUS ALTITUDE

MIDLATITUDE ANNUAL MEAN DIURNAL TRANSITION

PERCENT ERROR--DOTS LOG DEVIATION--CROSSES

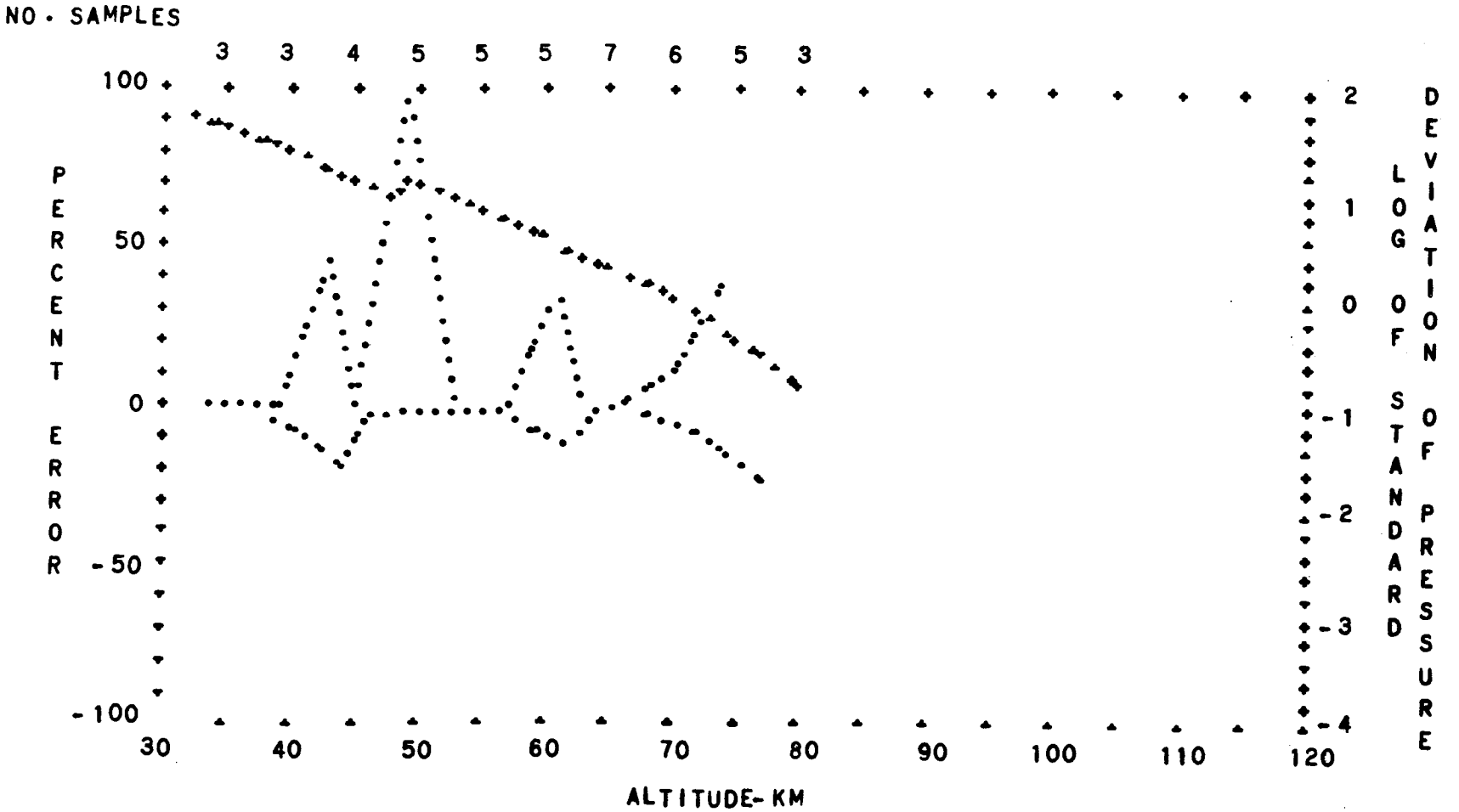

FIG. B-60. STANDARD DEVIATION OF PRESSURE AND PERCENT ERROR OF BUELL HYDROSTATIC EQUATION VERSUS ALTITUDE

MIDLATITUDE ANNUAL MEAN DAYTIME

PERCENT ERROR--DOTS LOG DEVIATION--CROSSES

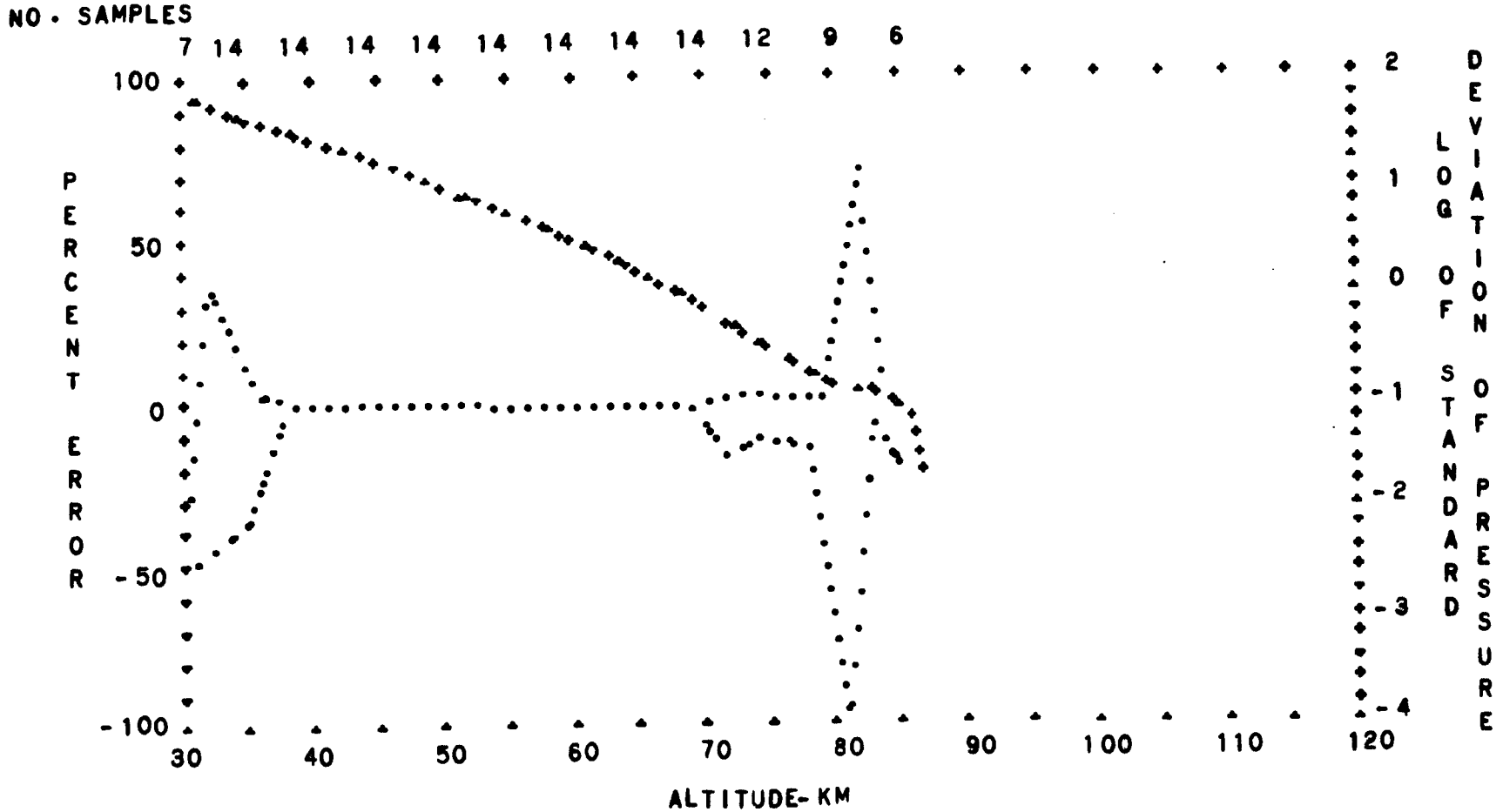

FIG. B-61. STANDARD DEVIATION OF PRESSURE AND PERCENT ERROR OF BUELL HYDROSTATIC EQUATION VERSUS ALTITUDE

MIDLATITUDE ANNUAL MEAN NIGHTTIME

PERCENT ERROR--DOTS LOG DEVIATION--CROSSES

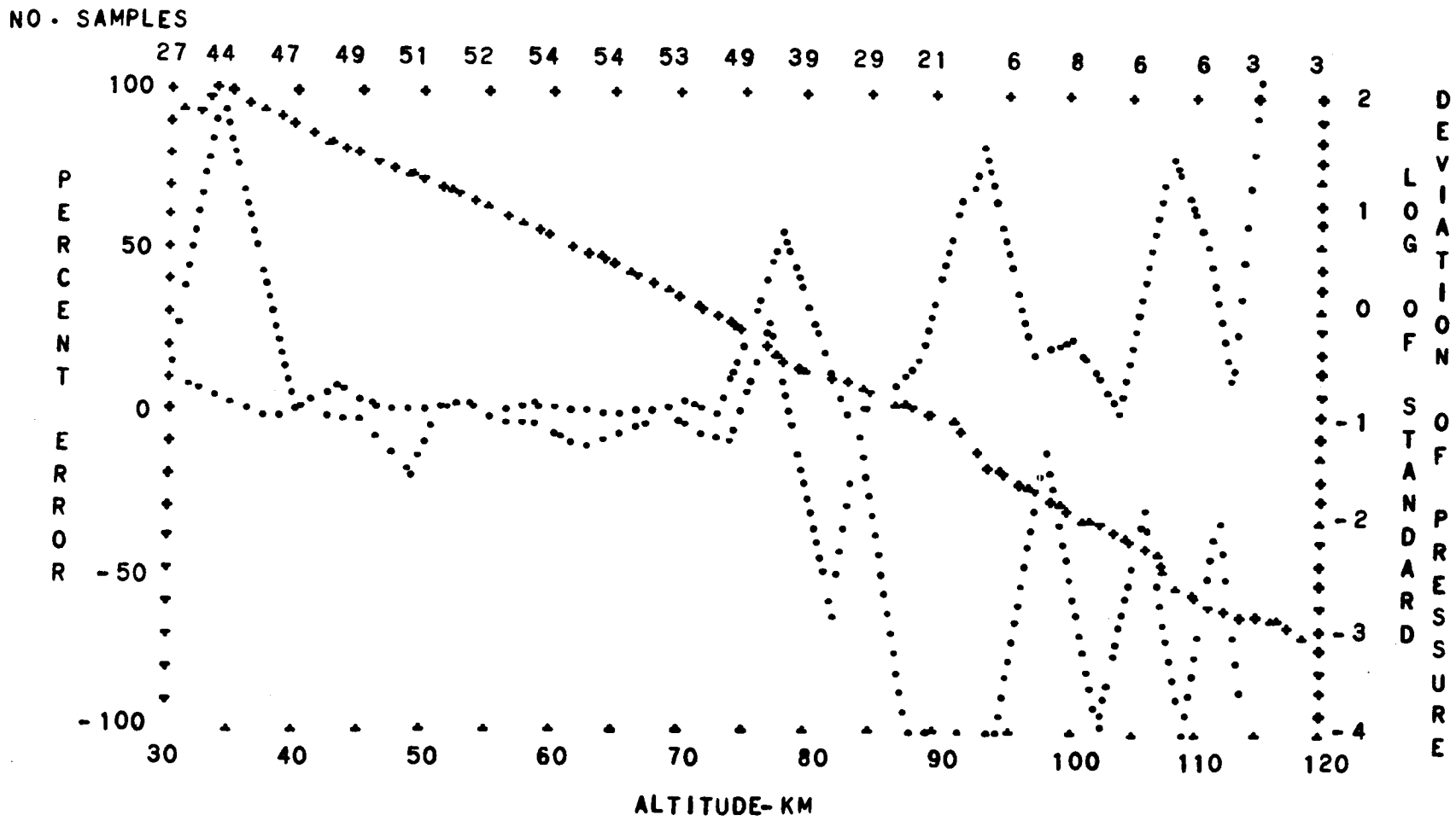

FIG. B-62. STANDARD DEVIATION OF PRESSURE AND PERCENT ERROR OF BUELL HYDROSTATIC EQUATION VERSUS ALTITUDE
MIDLATITUDE ANNUAL MEAN DIURNAL MEAN
PERCENT ERROR--DOTS LOG DEVIATION--CROSSES

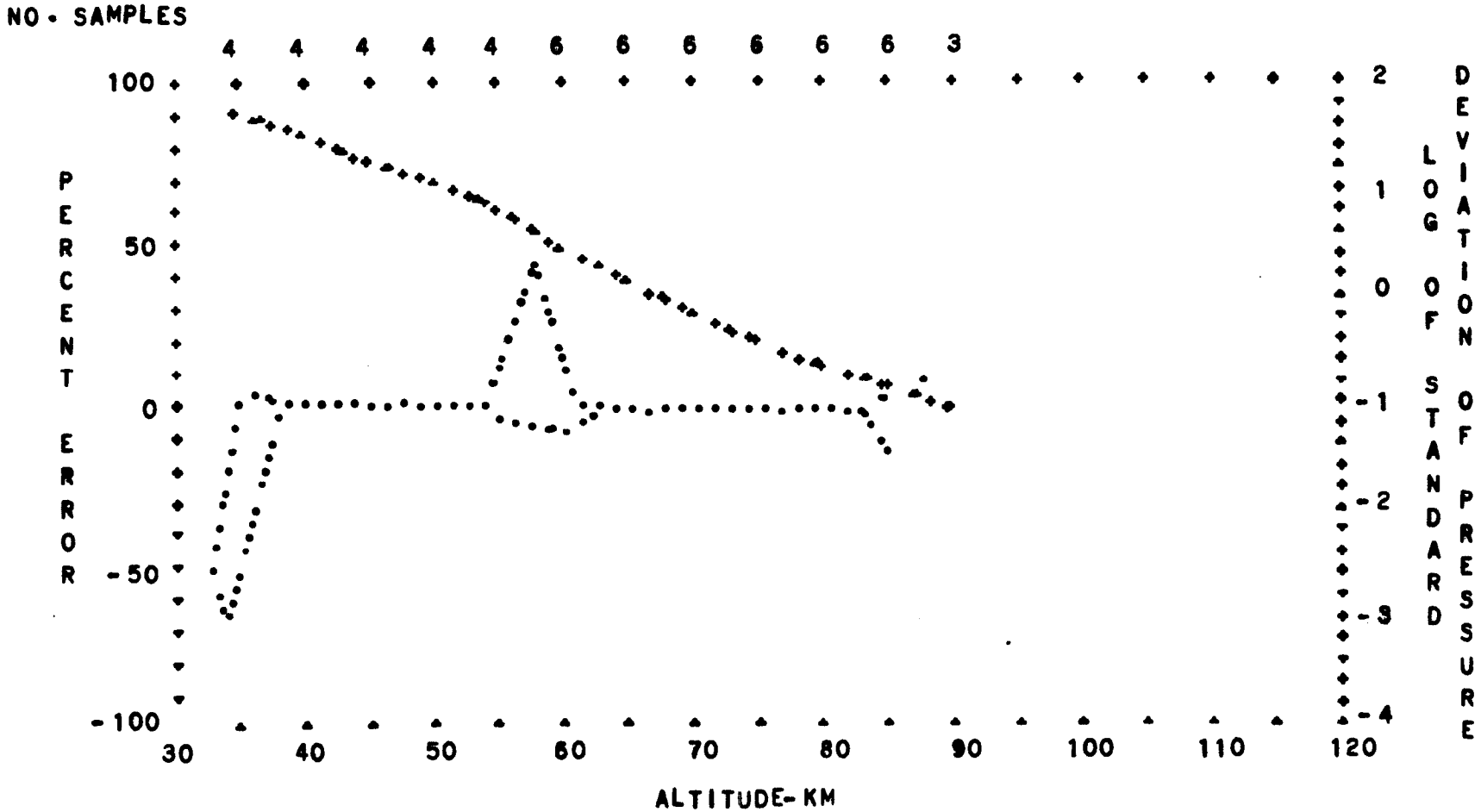

FIG. B-63. STANDARD DEVIATION OF PRESSURE AND PERCENT ERROR OF BUELL HYDROSTATIC EQUATION VERSUS ALTITUDE

SUBARCTIC SPRING DIURNAL TRANSITION

PERCENT ERROR--DOTS LOG DEVIATION--CROSSES

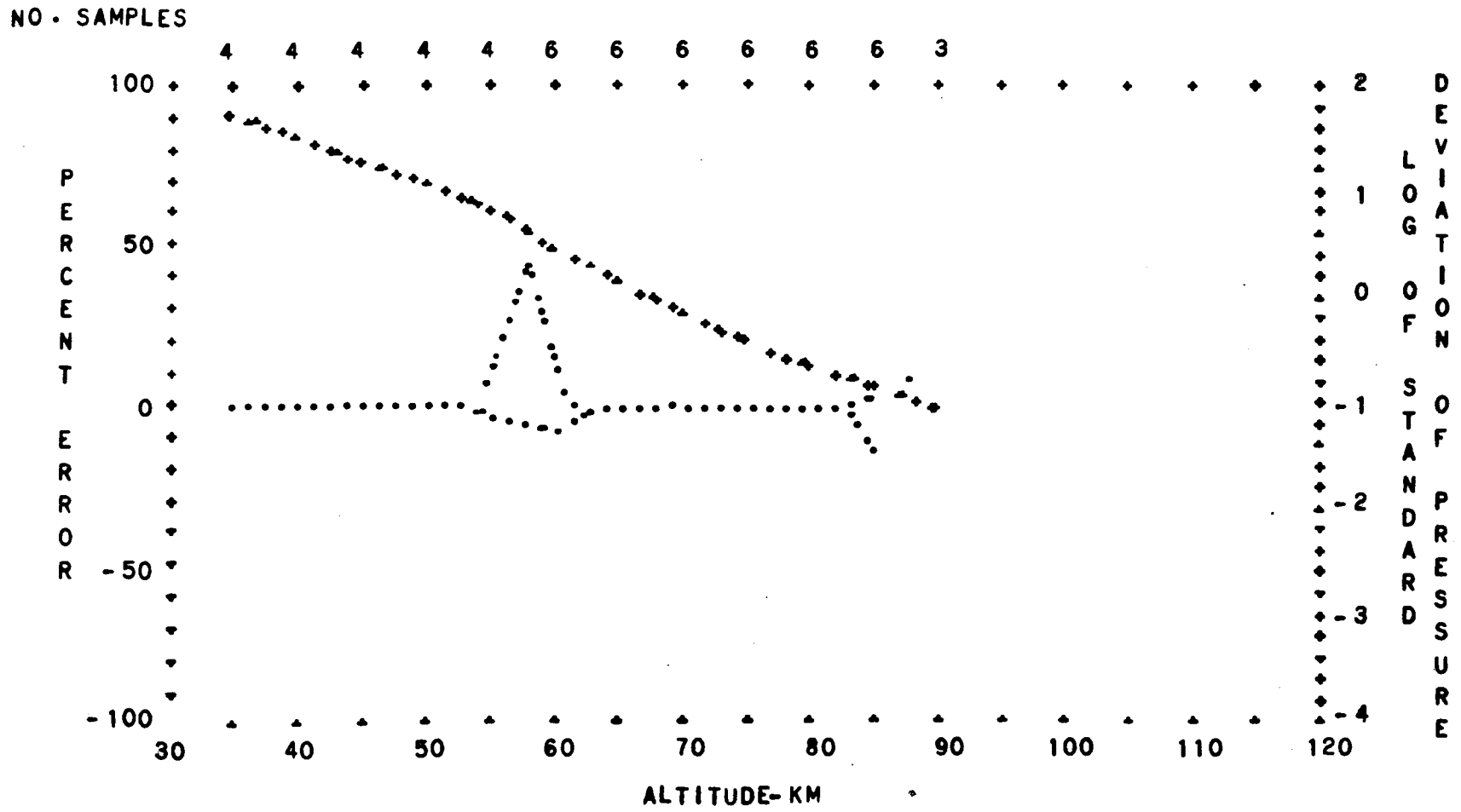

FIG. B-64. STANDARD DEVIATION OF PRESSURE AND PERCENT ERROR OF BUELL HYDROSTATIC EQUATION VERSUS ALTITUDE

SUBARCTIC SPRING DIURNAL MEAN

PERCENT ERROR--DOTS LOG DEVIATION--CROSSES

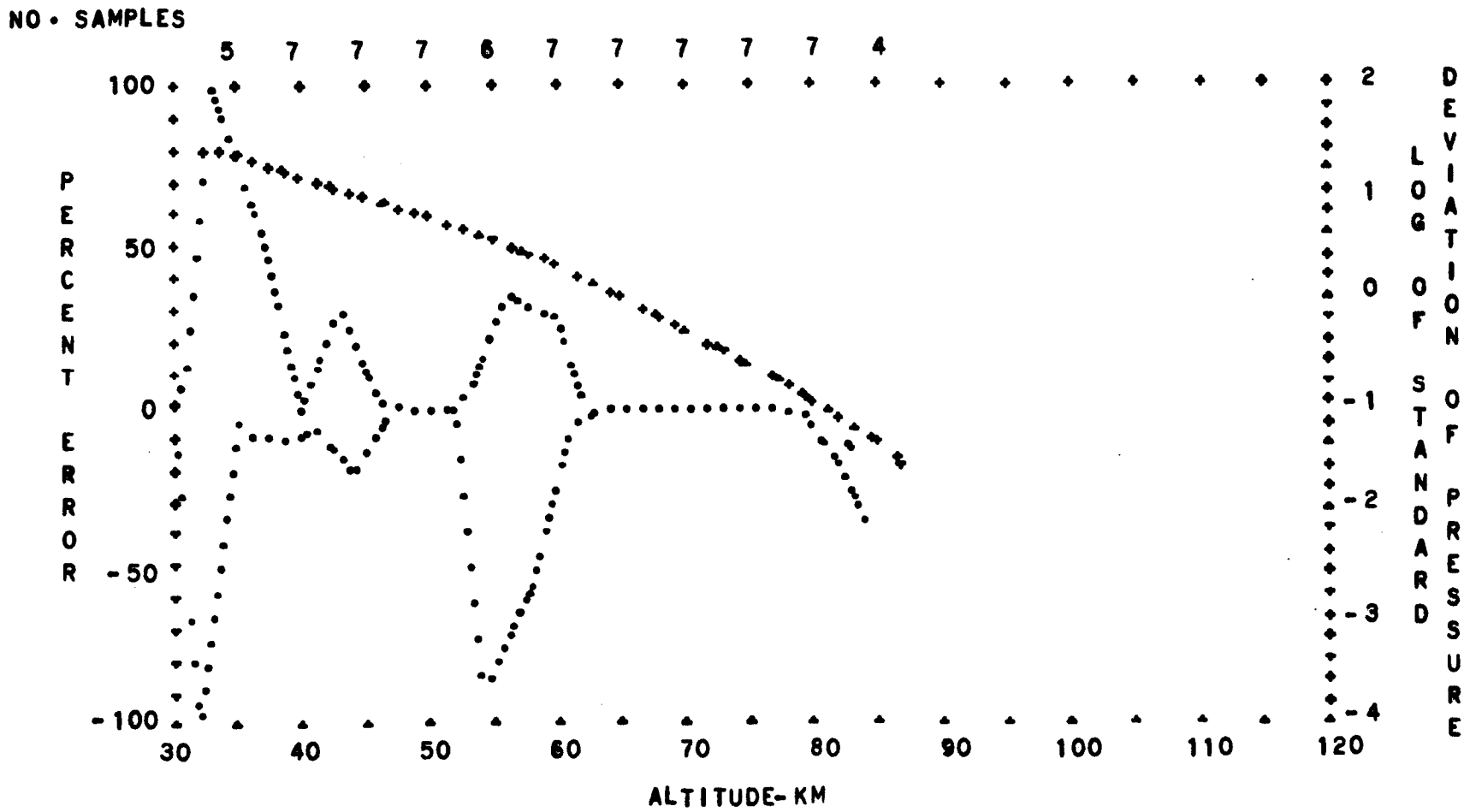

FIG. B-65. STANDARD DEVIATION OF PRESSURE AND PERCENT ERROR OF BUELL HYDROSTATIC EQUATION VERSUS ALTITUDE

SUBARCTIC SUMMER DIURNAL TRANSITION

PERCENT ERROR--DOTS LOG DEVIATION--CROSSES

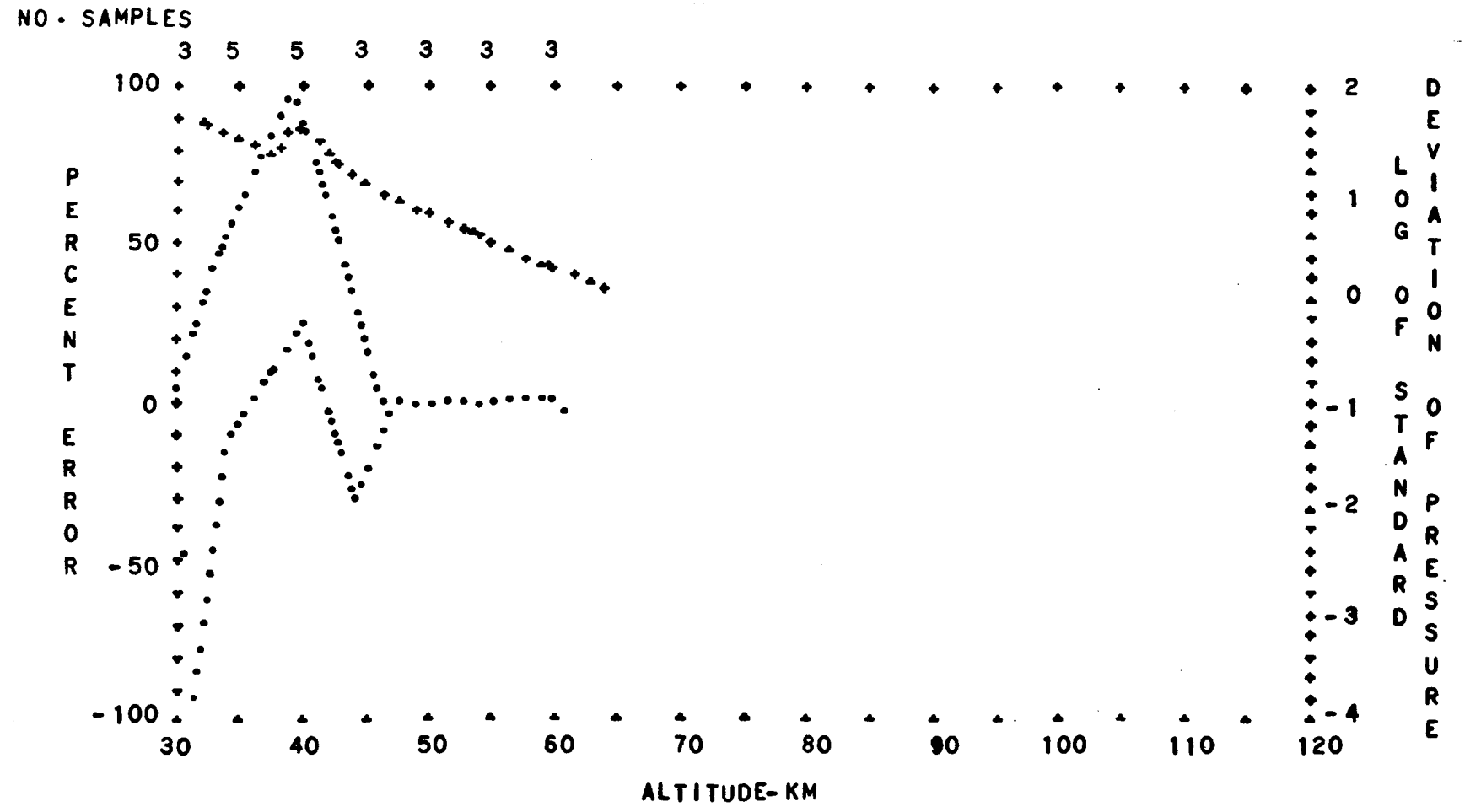

FIG. B-66. STANDARD DEVIATION OF PRESSURE AND PERCENT ERROR OF BUELL HYDROSTATIC EQUATION VERSUS ALTITUDE

SUBARCTIC SUMMER DAYTIME

PERCENT ERROR--DOTS LOG DEVIATION--CROSSES

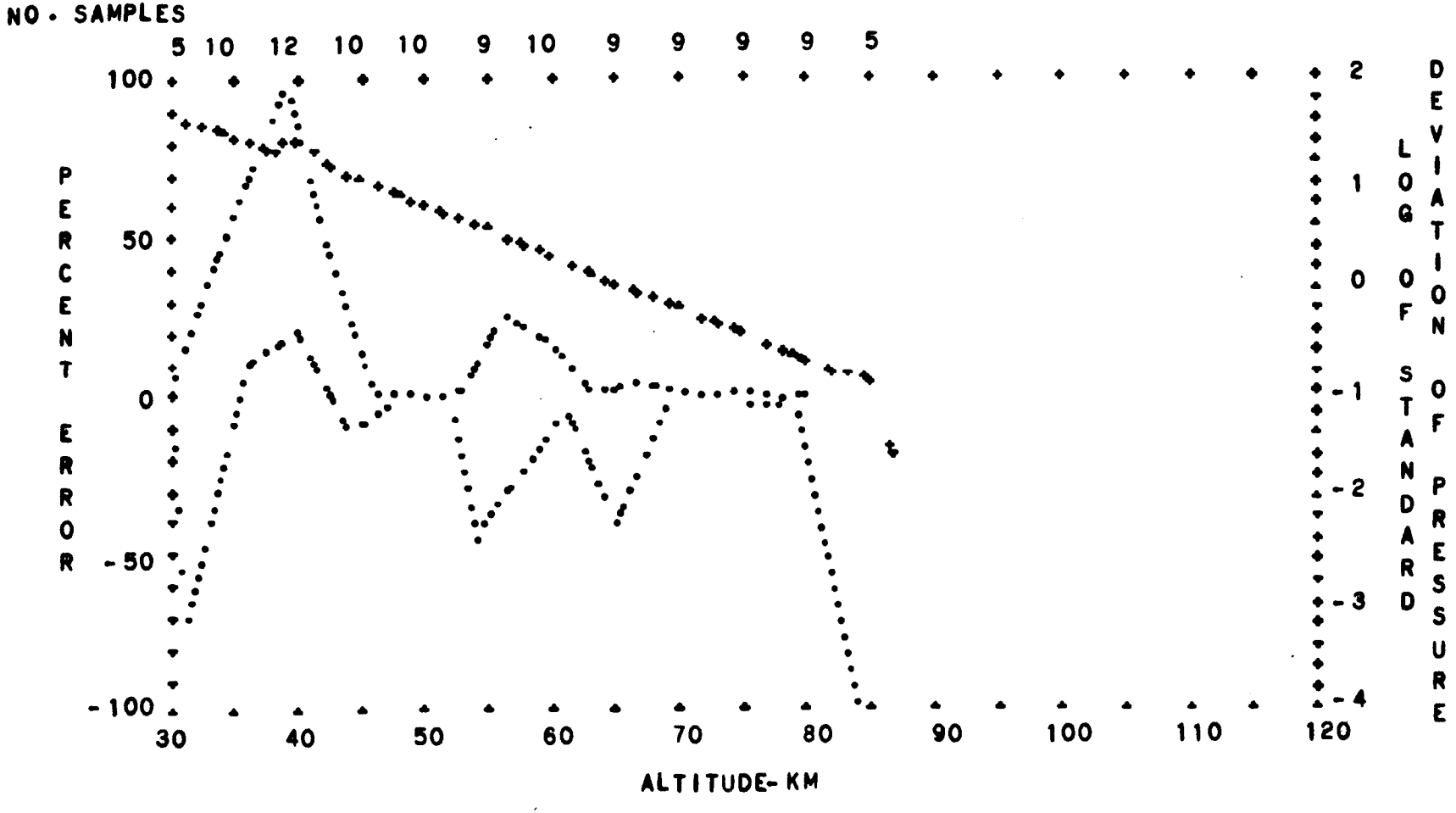

FIG. B-67. STANDARD DEVIATION OF PRESSURE AND PERCENT ERROR OF BUELL HYDROSTATIC EQUATION VERSUS ALTITUDE

SUBARCTIC SUMMER DIURNAL MEAN

PERCENT ERROR--DOTS LOG DEVIATION--CROSSES

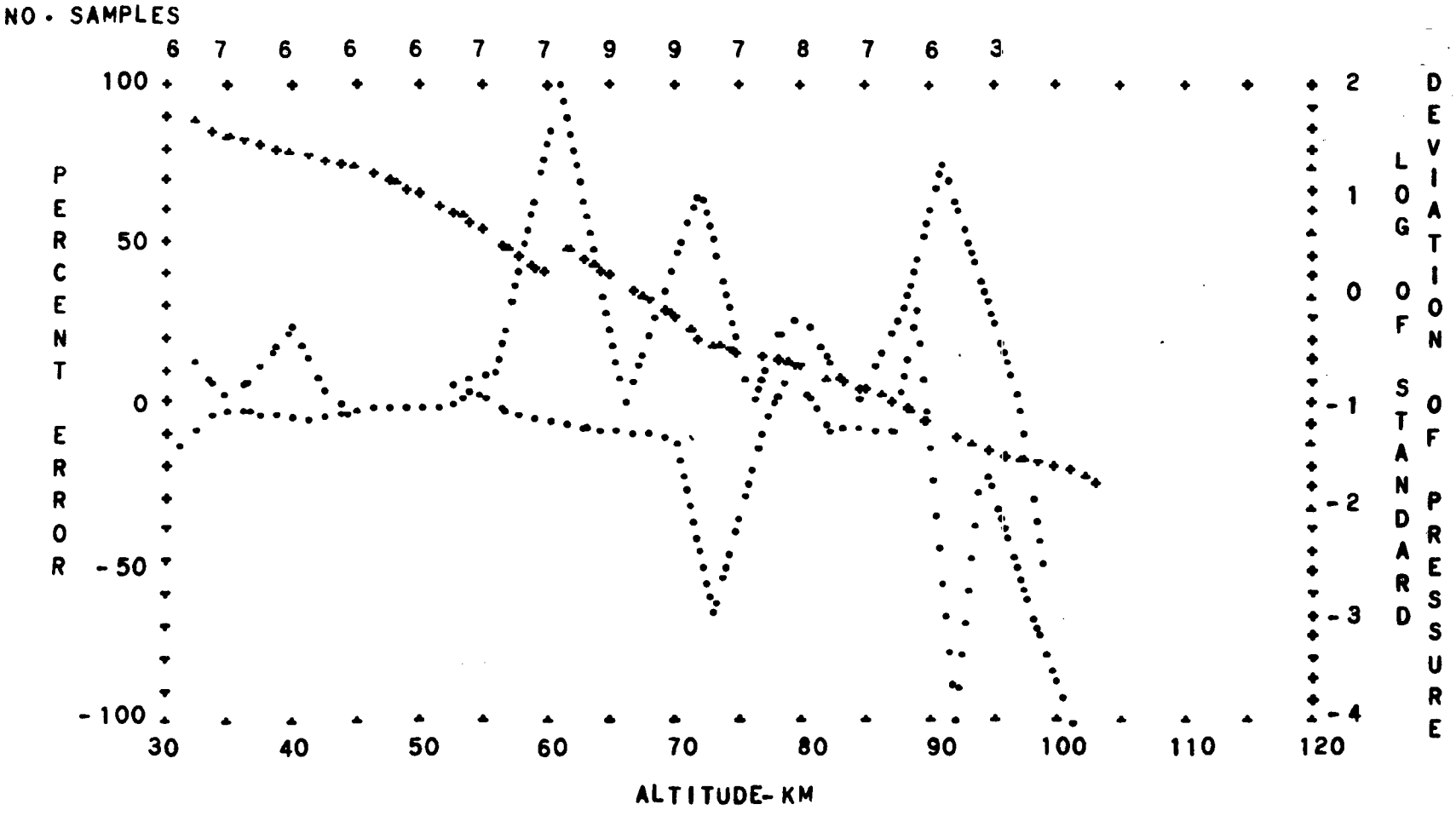

FIG. B-68. STANDARD DEVIATION OF PRESSURE AND PERCENT ERROR OF BUELL HYDROSTATIC EQUATION VERSUS ALTITUDE

SUBARCTIC AUTUMN DIURNAL TRANSITION

PERCENT ERROR--DOTS LOG DEVIATION--CROSSES

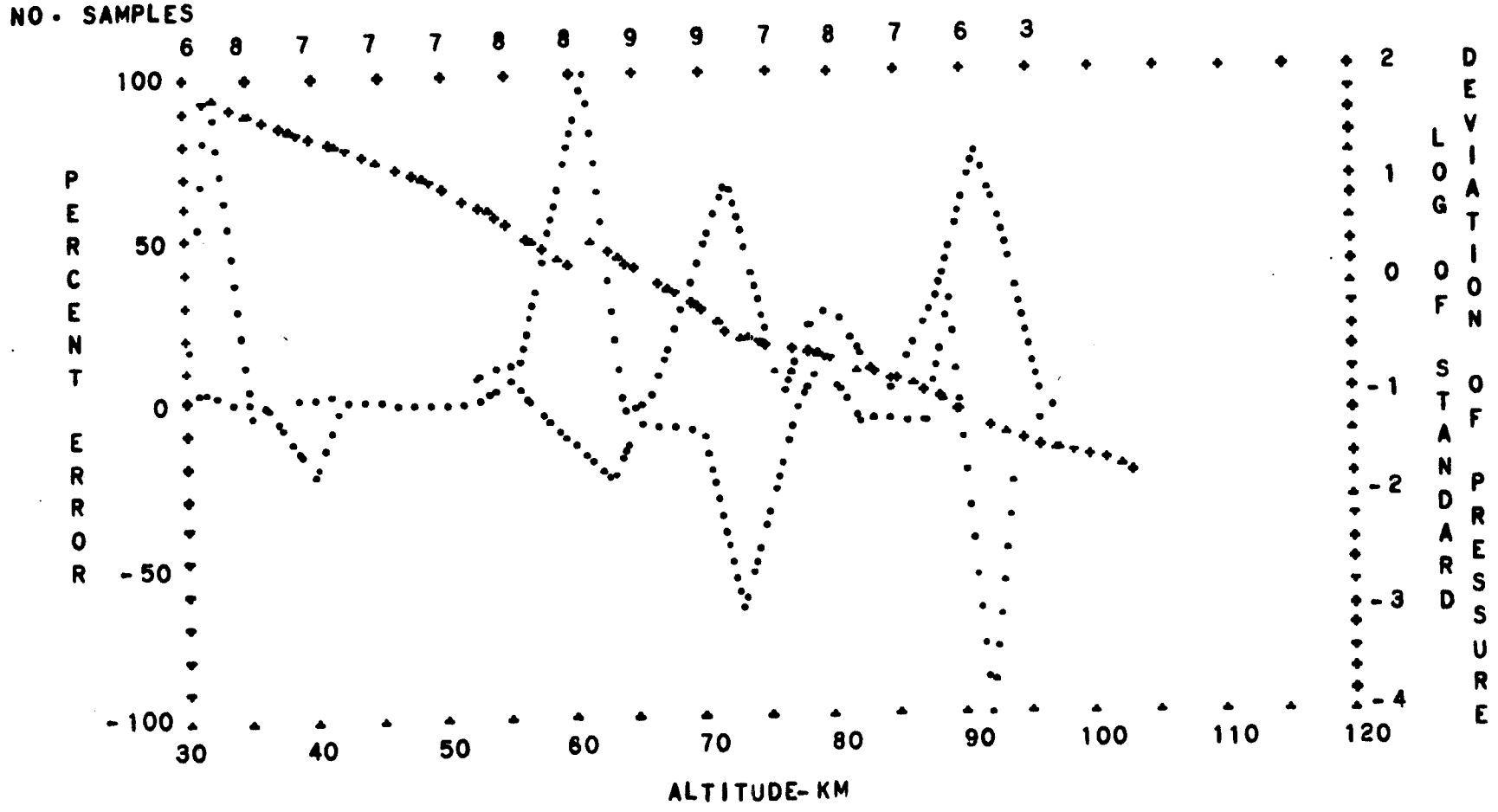

FIG. B-69. STANDARD DEVIATION OF PRESSURE AND PERCENT ERROR OF BUELL HYDROSTATIC EQUATION VERSUS ALTITUDE

SUBARCTIC AUTUMN DIURNAL MEAN

PERCENT ERROR--DOTS LOG DEVIATION--CROSSES

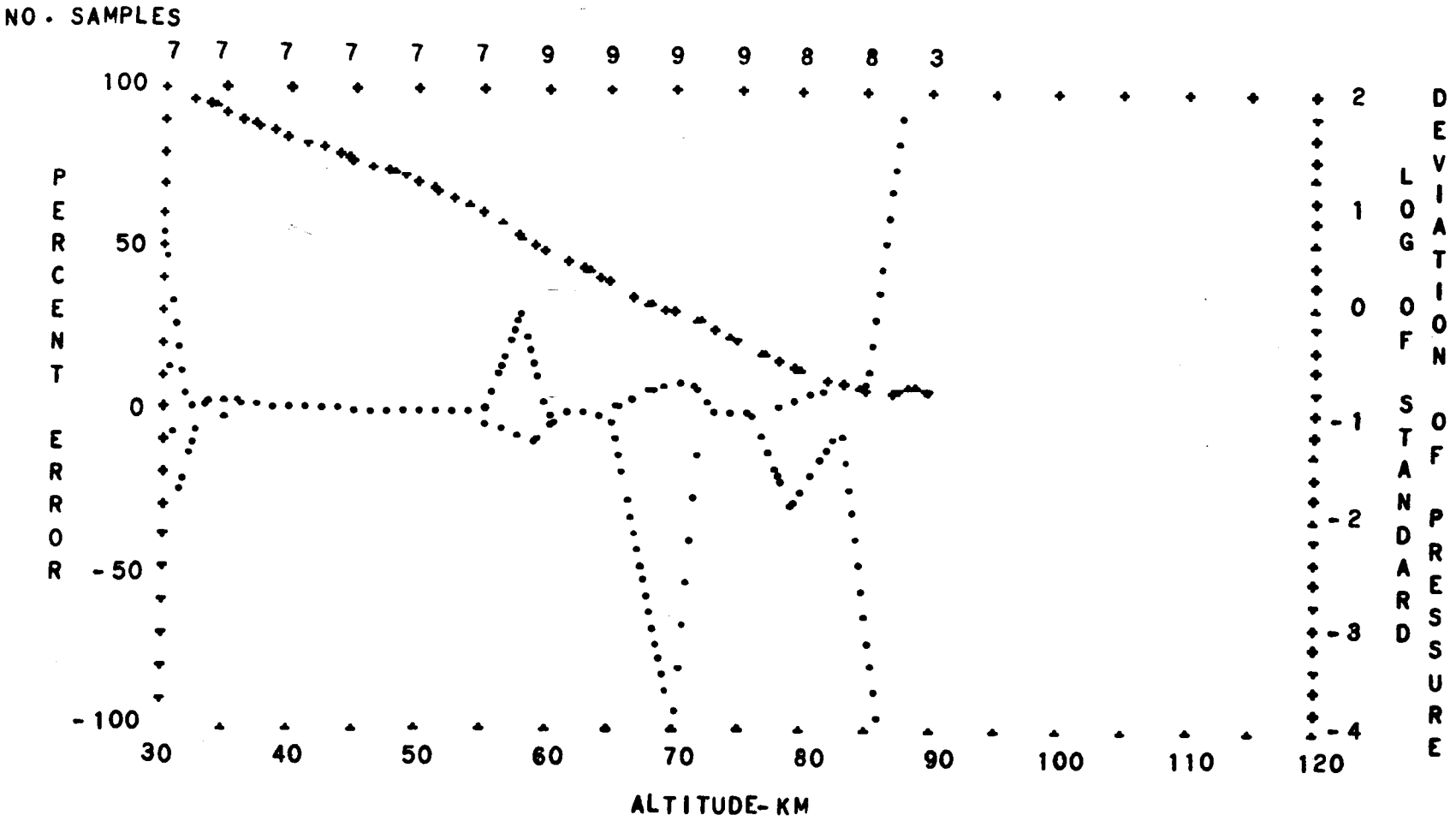

FIG. B-70. STANDARD DEVIATION OF PRESSURE AND PERCENT ERROR OF BUELL HYDROSTATIC EQUATION VERSUS ALTITUDE

SUBARCTIC WINTER DIURNAL TRANSITION

PERCENT ERROR--DOTS LOG DEVIATION--CROSSES

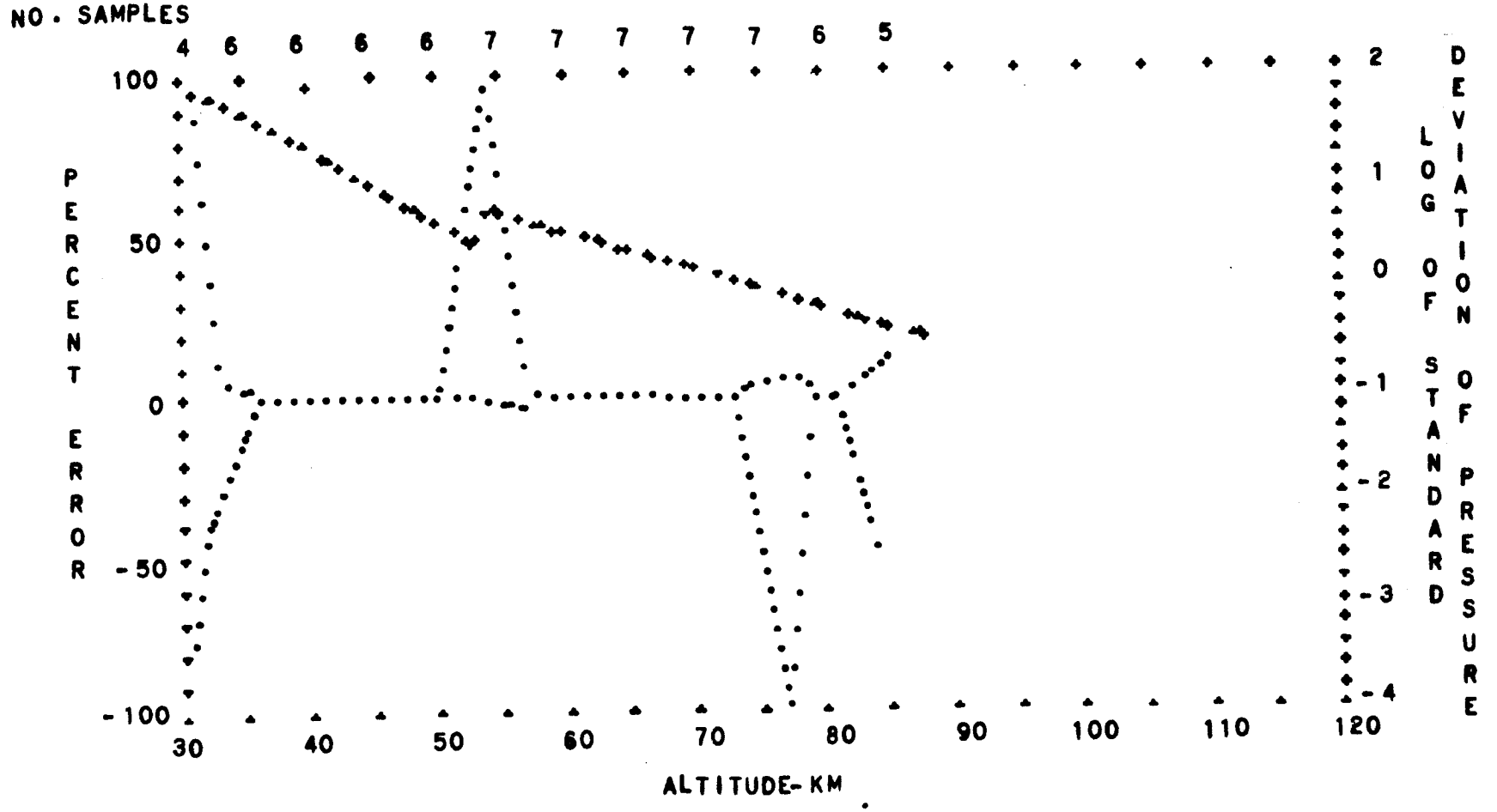

FIG. B-71. STANDARD DEVIATION OF PRESSURE AND PERCENT ERROR OF BUELL HYDROSTATIC EQUATION VERSUS ALTITUDE

SUBARCTIC WINTER NIGHTTIME

PERCENT ERROR--DOTS LOG DEVIATION--CROSSES

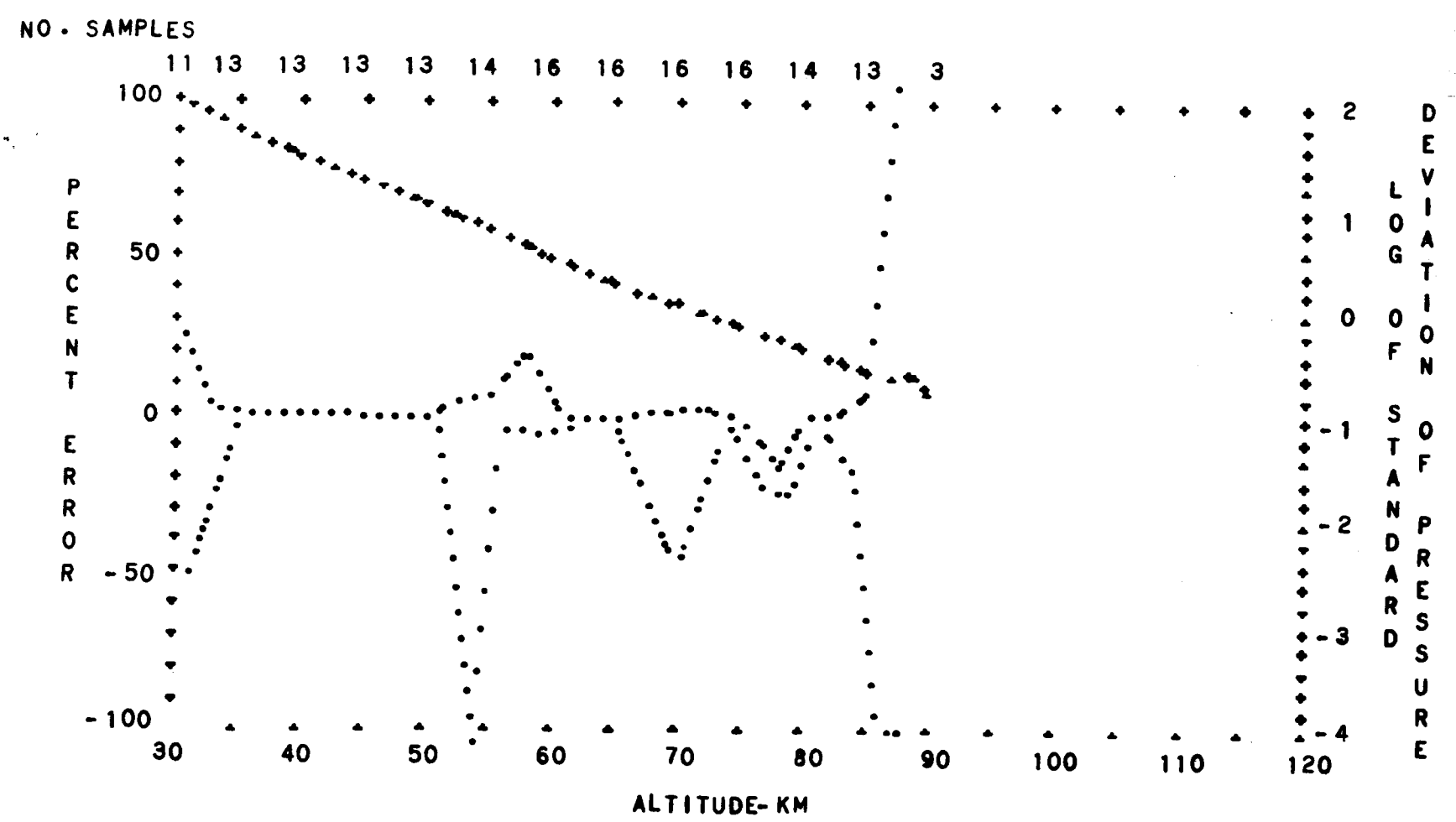

FIG. B-72. STANDARD DEVIATION OF PRESSURE AND PERCENT ERROR OF BUELL HYDROSTATIC EQUATION VERSUS ALTITUDE

SUBARCTIC WINTER DIURNAL MEAN

PERCENT ERROR--DOTS

LOG. DEVIATION--CROSSES

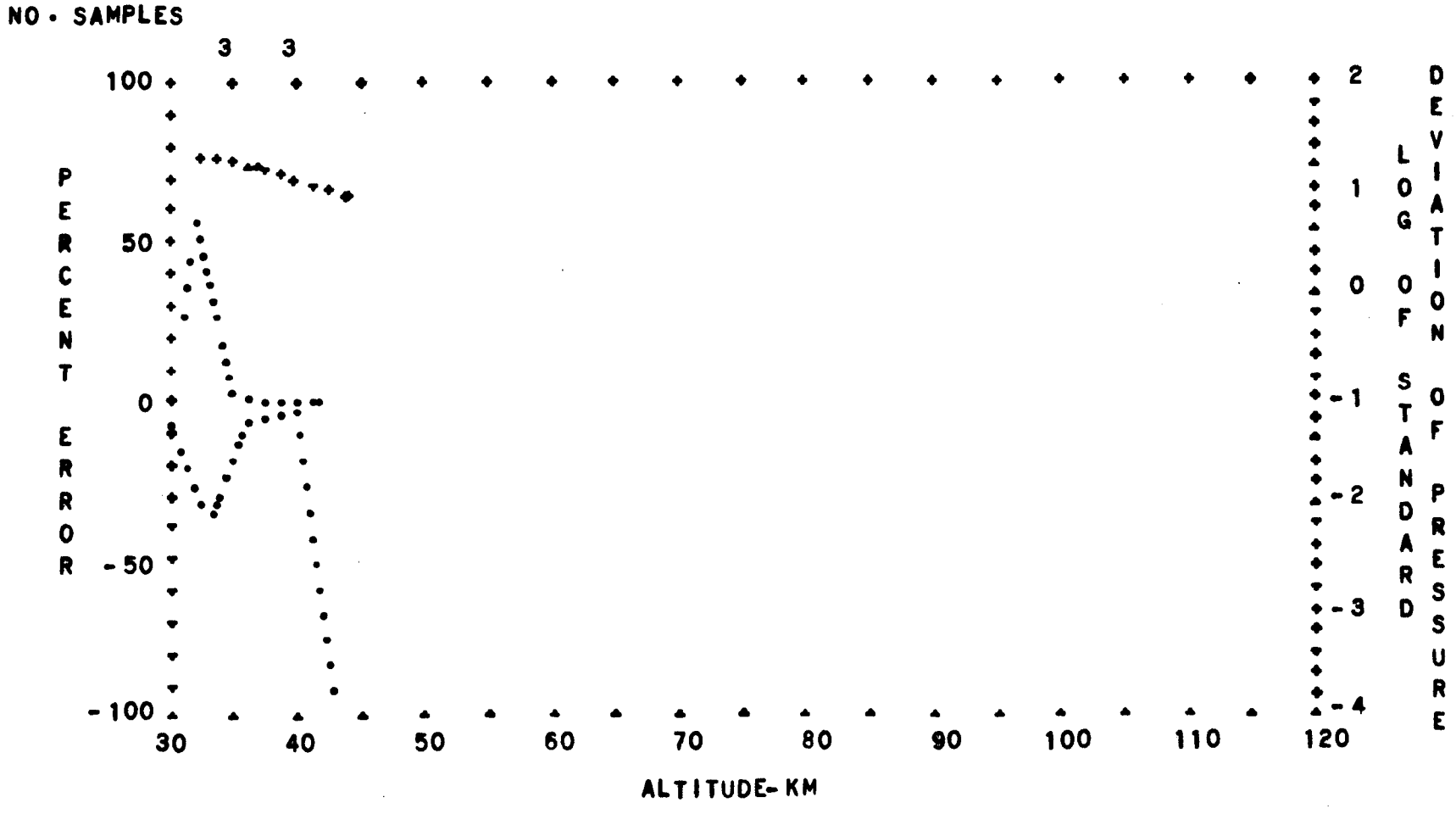

FIG. B-73. STANDARD DEVIATION OF PRESSURE AND PERCENT ERROR OF BUELL HYDROSTATIC EQUATION VERSUS ALTITUDE

SUBARCTIC SUMMER EXTREME DIURNAL TRANSITION

PERCENT ERROR--DOTS LOG. DEVIATION--CROSSES

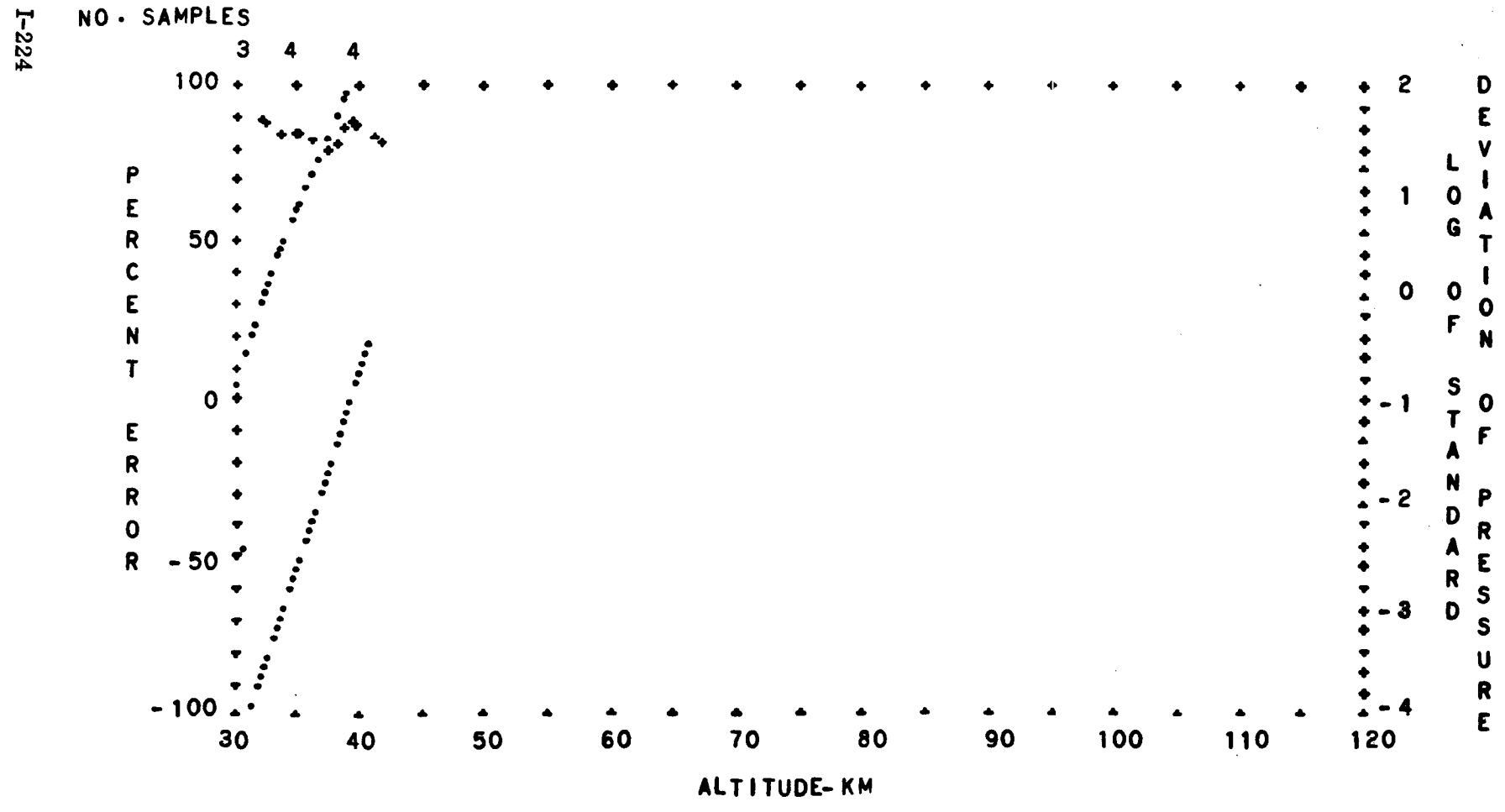

FIG. B-74. STANDARD DEVIATION OF PRESSURE AND PERCENT ERROR OF BUELL HYDROSTATIC EQUATION VERSUS ALTITUDE

SUBARCTIC SUMMER EXTREME DAYTIME

PERCENT ERROR--DOTS LOG DEVIATION--CROSSES

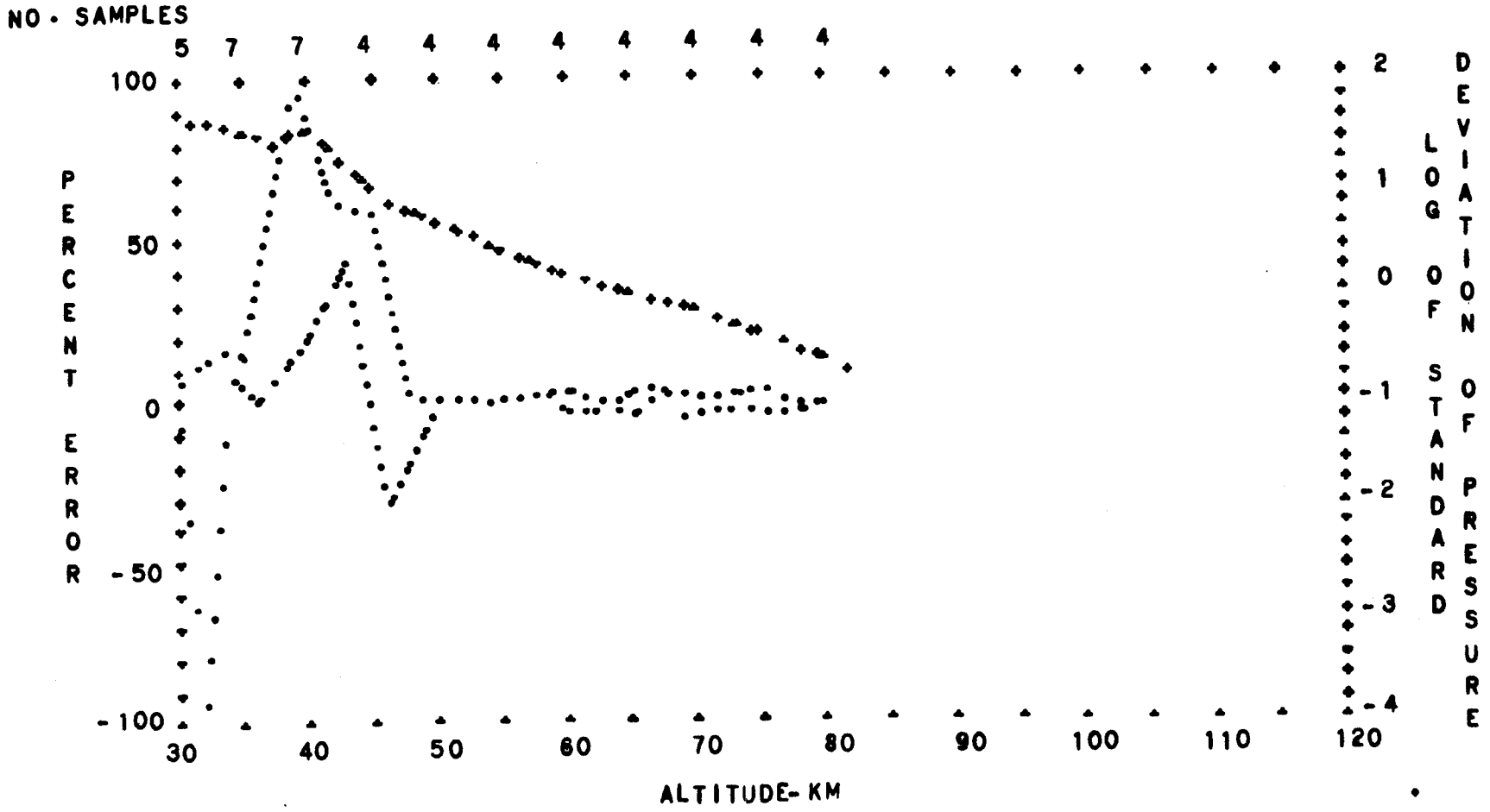

FIG. B-75. STANDARD DEVIATION OF PRESSURE AND PERCENT ERROR OF BUELL HYDROSTATIC EQUATION VERSUS ALTITUDE

SUBARCTIC SUMMER EXTREME DIURNAL MEAN

PERCENT ERROR--DOTS LOG DEVIATION--CROSSES

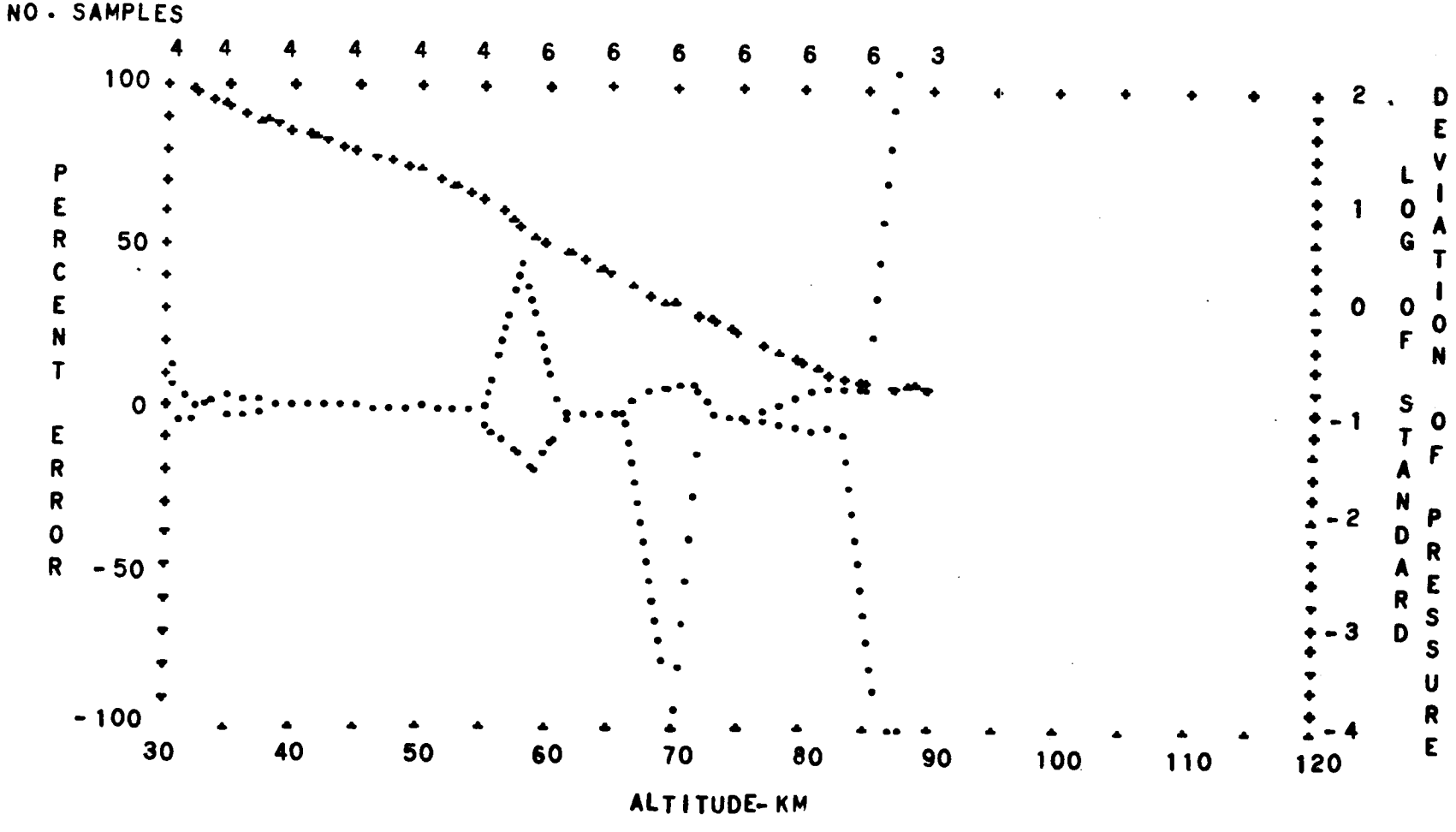

FIG. B-76. STANDARD DEVIATION OF PRESSURE AND PERCENT ERROR OF BUELL HYDROSTATIC EQUATION VERSUS ALTITUDE

SUBARCTIC WINTER EXTREME DIURNAL TRANSITION

PERCENT ERROR--DOTS LOG DEVIATION--CROSSES

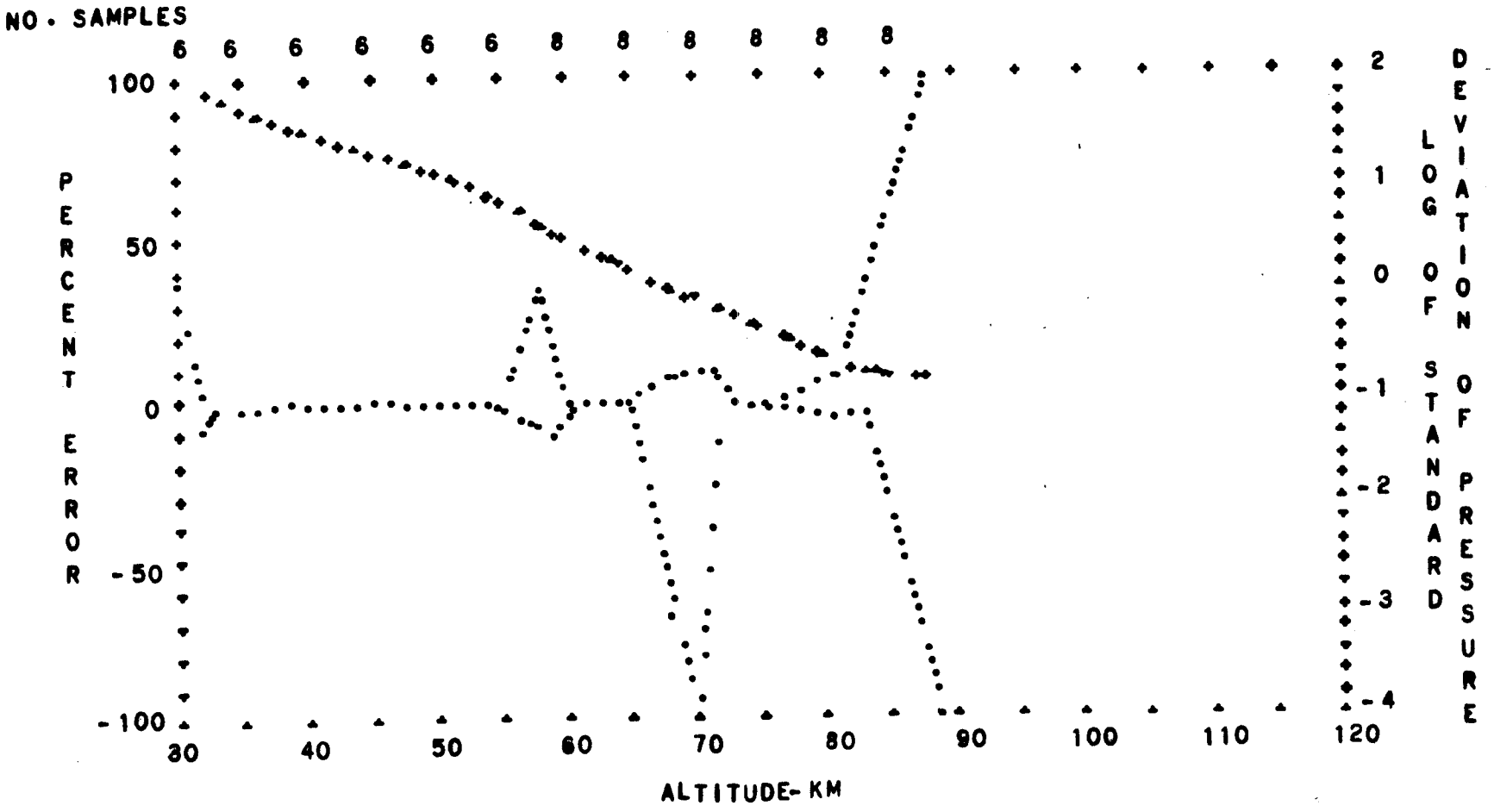

FIG. B-77. STANDARD DEVIATION OF PRESSURE AND PERCENT ERROR OF BUELL HYDROSTATIC EQUATION VERSUS ALTITUDE

SUBARCTIC WINTER EXTREME DIURNAL MEAN

PERCENT ERROR--DOTS LOG DEVIATION--CROSSES

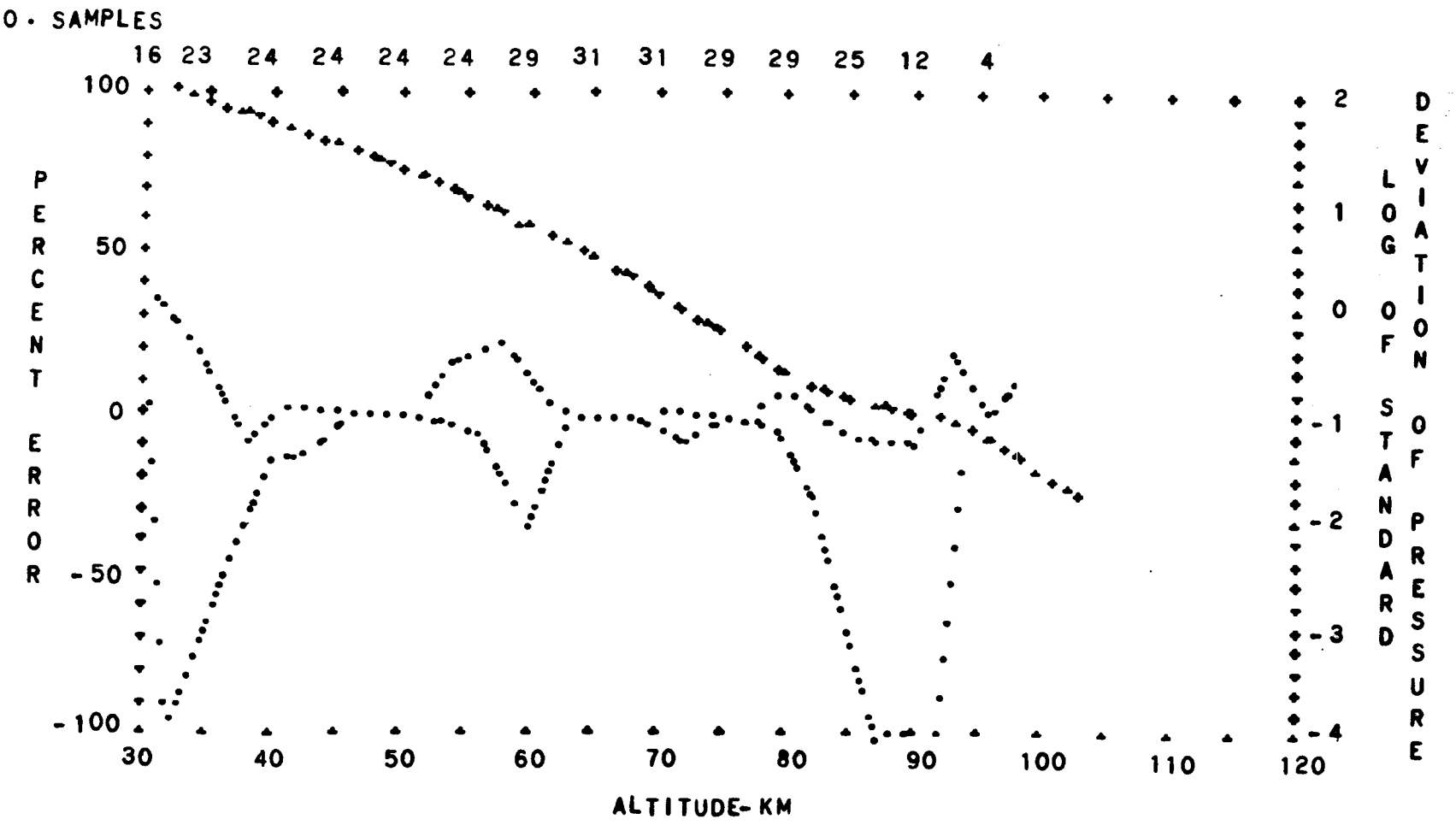

FIG. B-78. STANDARD DEVIATION OF PRESSURE AND PERCENT ERROR OF BUELL HYDROSTATIC EQUATION VERSUS ALTITUDE

SUBARCTIC ANNUAL MEAN DIURNAL TRANSITION

PERCENT ERROR--DOTS LOG DEVIATION--CROSSES

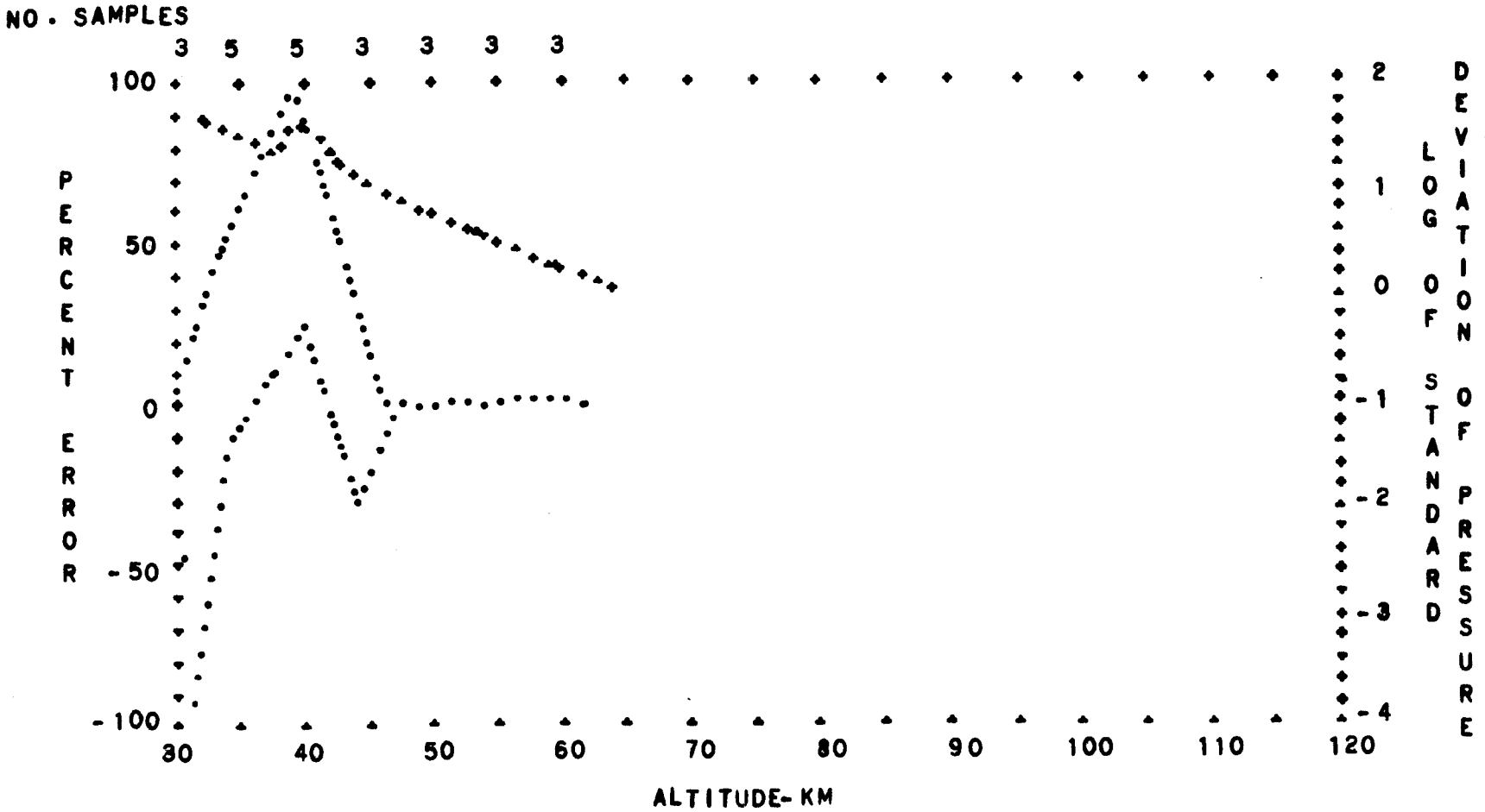

FIG. B-79. STANDARD DEVIATION OF PRESSURE AND PERCENT ERROR OF BUELL HYDROSTATIC EQUATION VERSUS ALTITUDE

SUBARCTIC ANNUAL MEAN DAYTIME

PERCENT ERROR--DOTS LOG DEVIATION--CROSSES

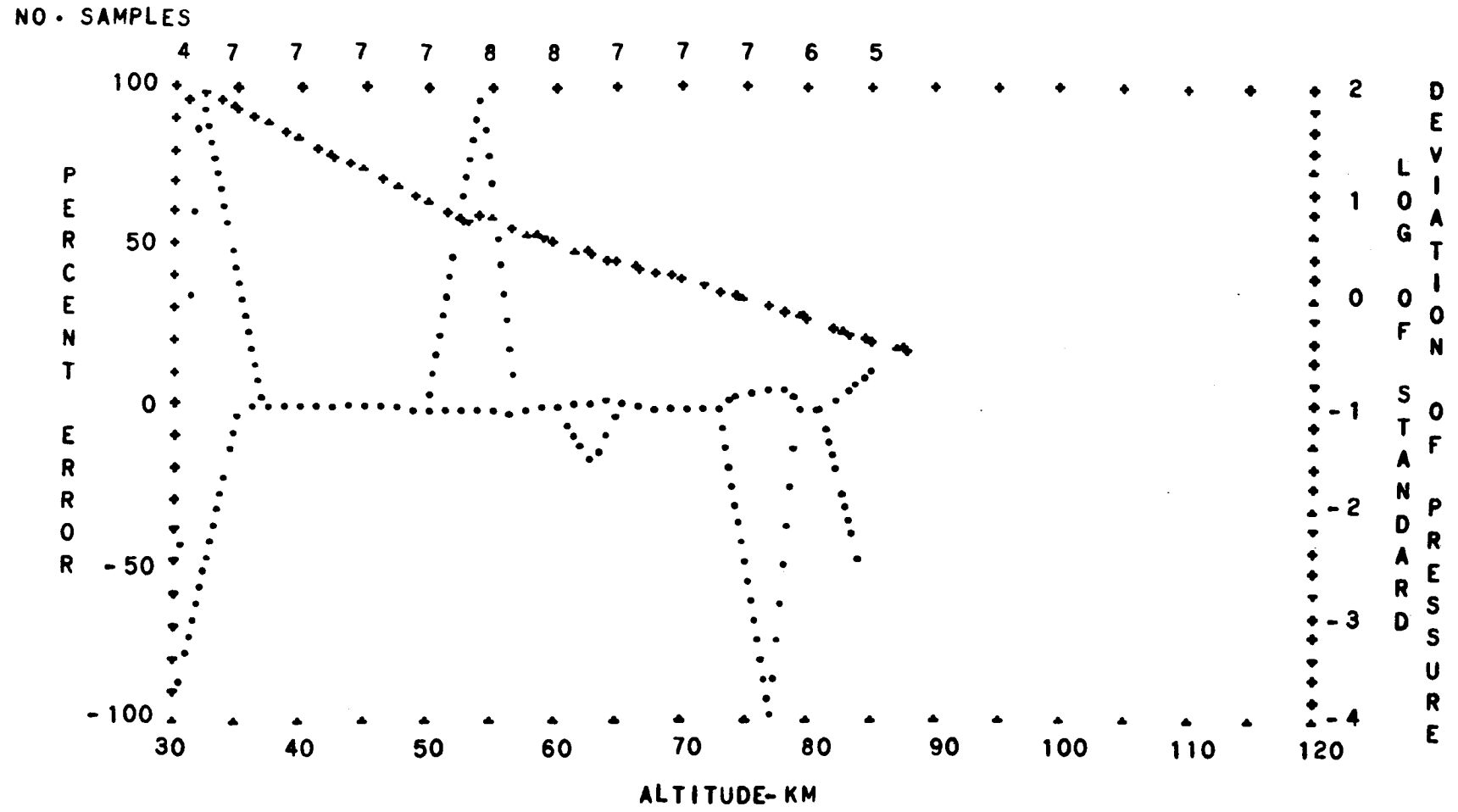

FIG. B-80. STANDARD DEVIATION OF PRESSURE AND PERCENT ERROR OF BUELL HYDROSTATIC EQUATION VERSUS ALTITUDE

SUBARCTIC ANNUAL MEAN NIGHTTIME

PERCENT ERROR--DOTS LOG. DEVIATION--CROSSES

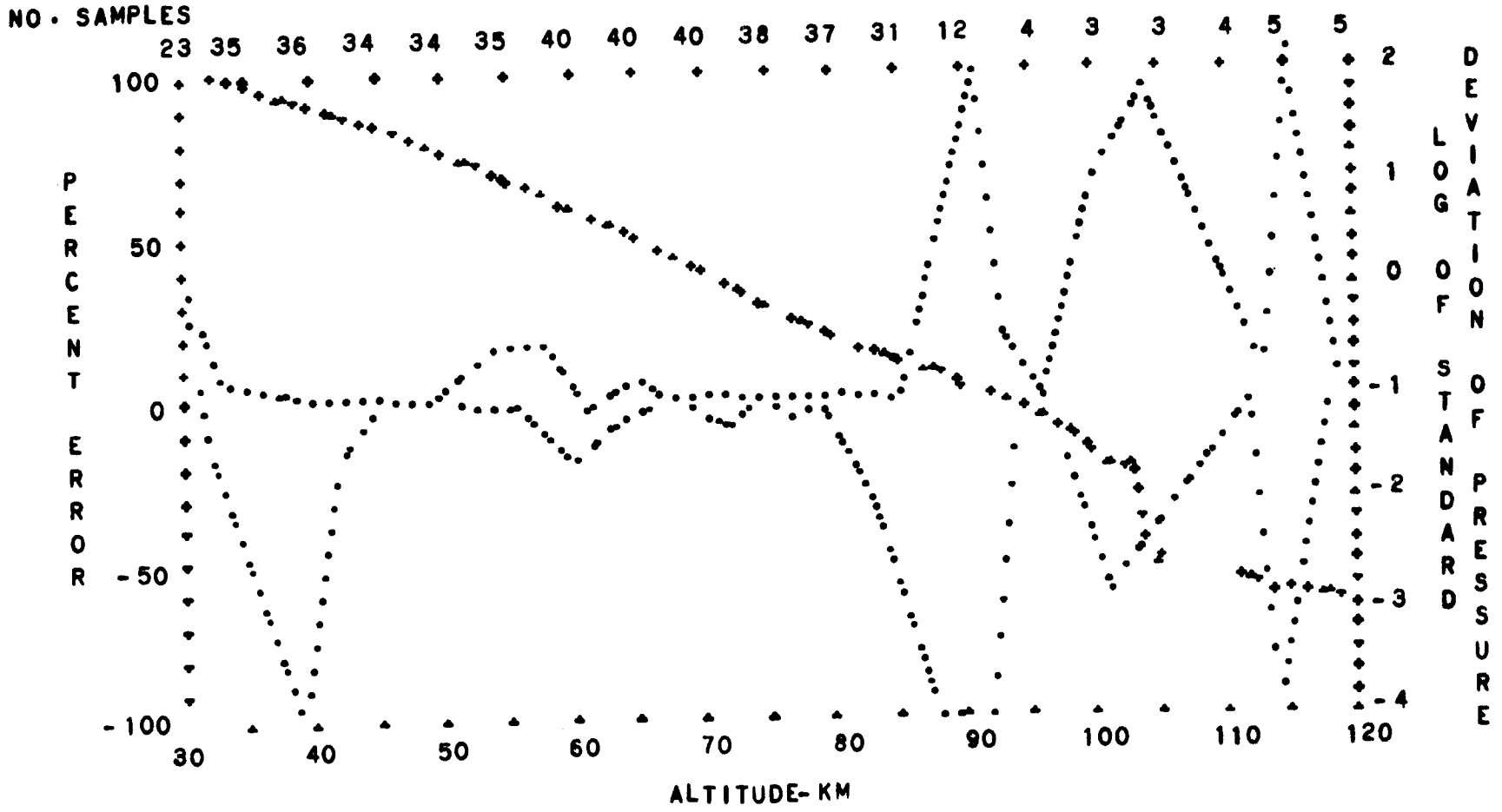

FIG. B-81. STANDARD DEVIATION OF PRESSURE AND PERCENT ERROR OF BUELL HYDROSTATIC EQUATION VERSUS ALTITUDE

SUBARCTIC ANNUAL MEAN DIURNAL MEAN

PERCENT ERROR--DOTS LOG. DEVIATION--CROSSES

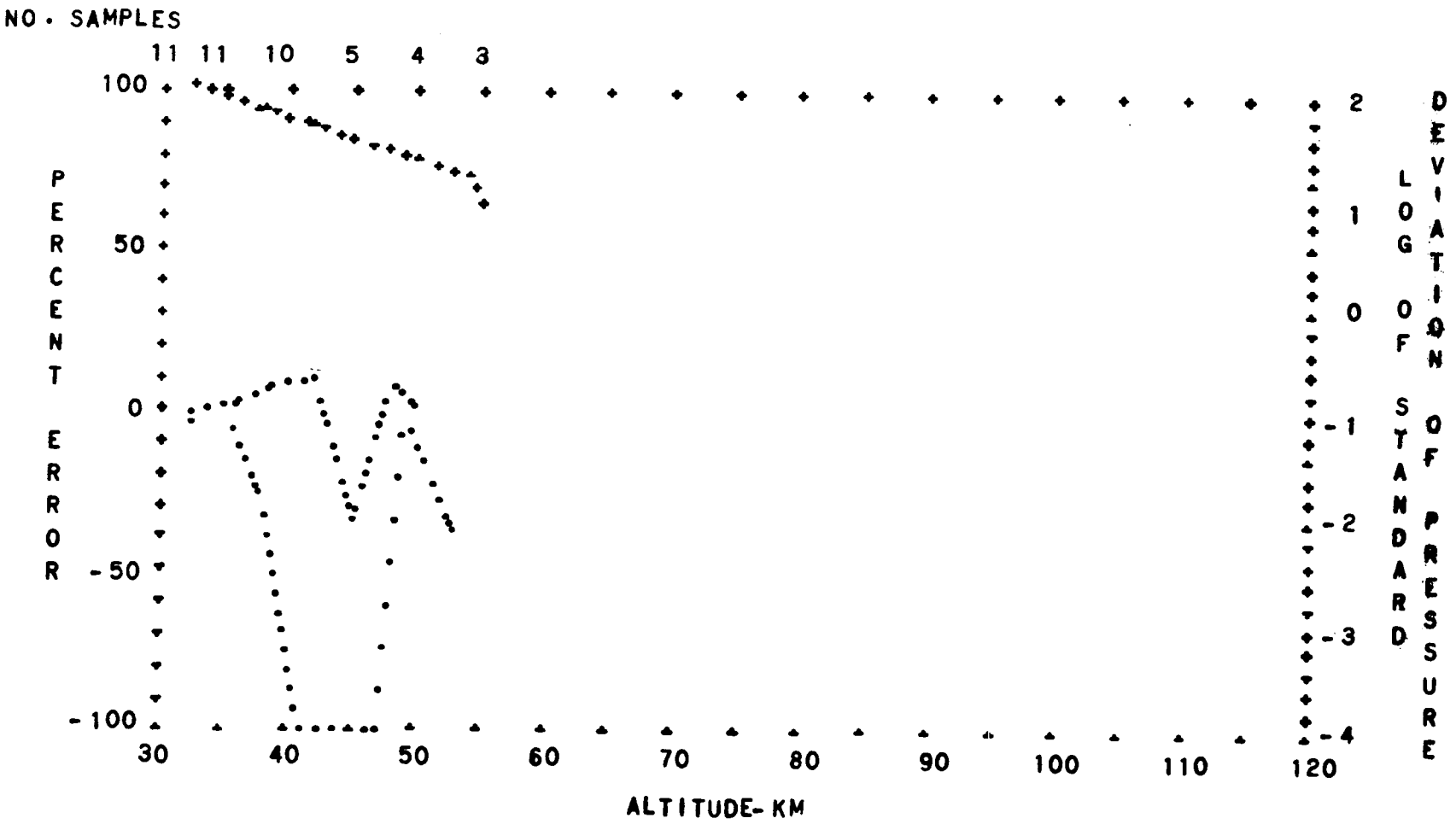

FIG. B-82. STANDARD DEVIATION OF PRESSURE AND PERCENT ERROR OF BUELL HYDROSTATIC EQUATION VERSUS ALTITUDE

ARCTIC SPRING DIURNAL TRANSITION

PERCENT ERROR--DOTS

LOG DEVIATION--CROSSES

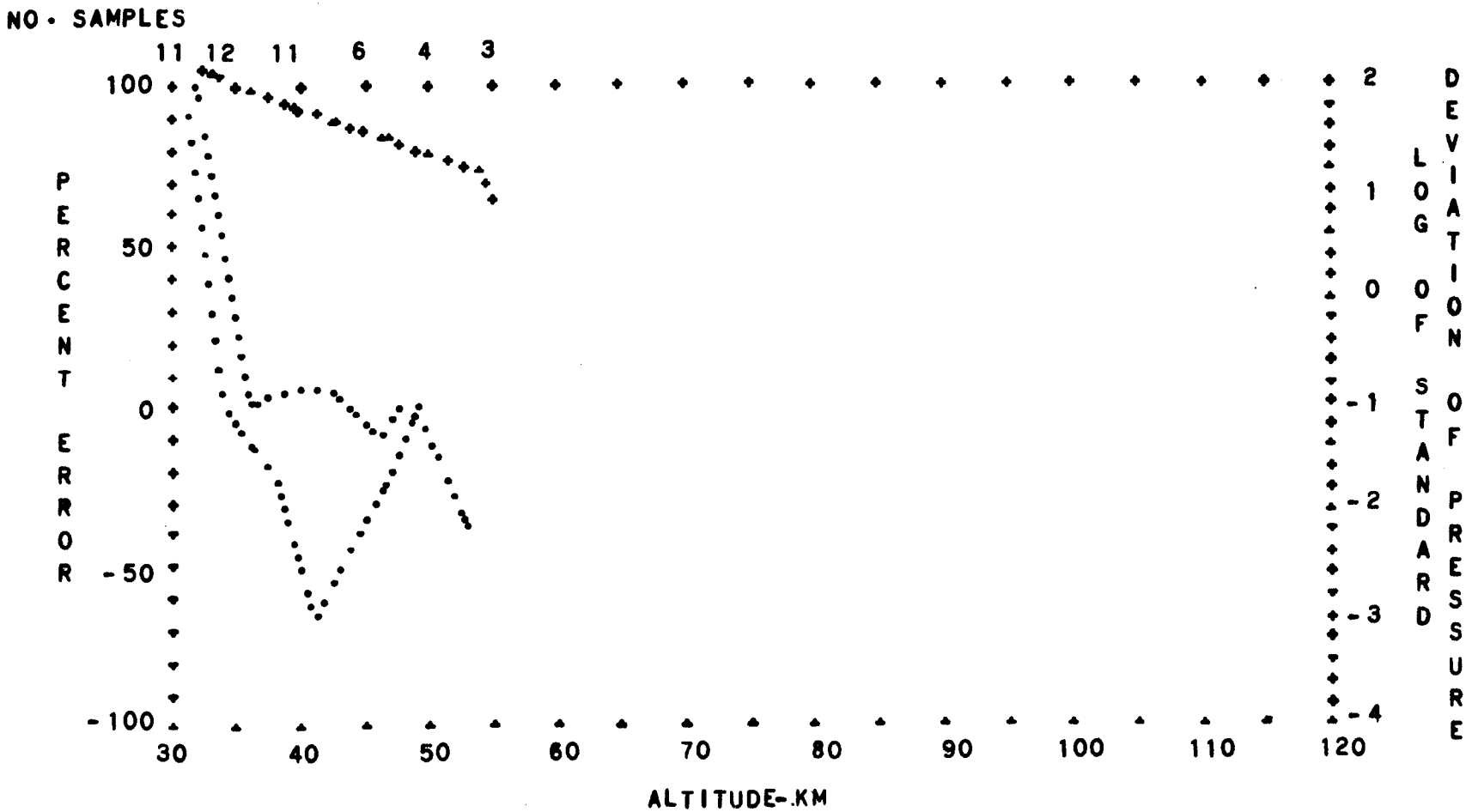

FIG. B-83. STANDARD DEVIATION OF PRESSURE AND PERCENT ERROR OF BUELL HYDROSTATIC EQUATION VERSUS ALTITUDE

ARCTIC SPRING DIURNAL MEAN

PERCENT ERROR--DOTS LOG DEVIATION--CROSSES

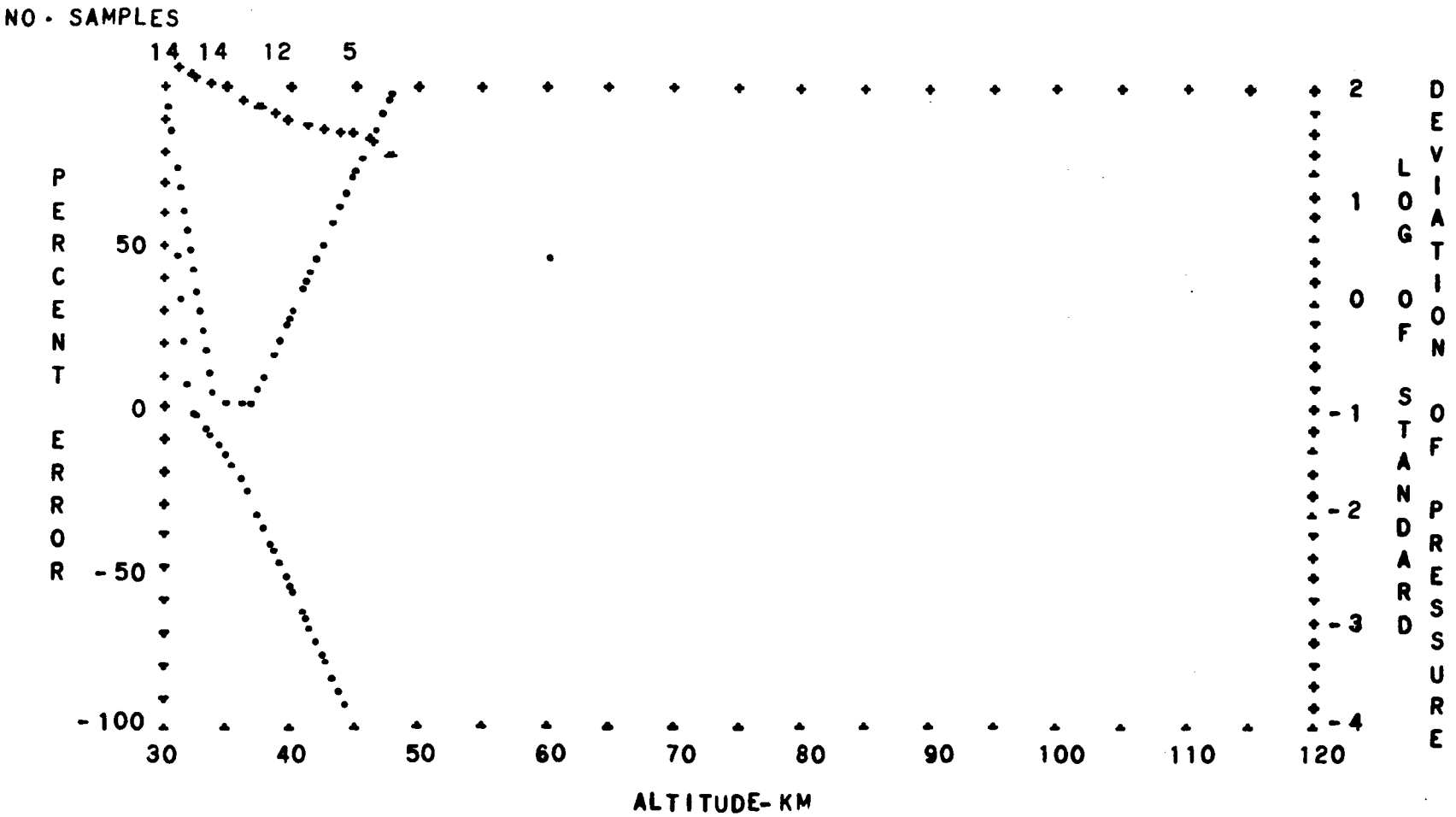

FIG. B-84. STANDARD DEVIATION OF PRESSURE AND PERCENT ERROR OF BUELL HYDROSTATIC EQUATION VERSUS ALTITUDE

ARCTIC SUMMER DIURNAL TRANSITION

PERCENT ERROR--DOTS LOG DEVIATION--CROSSES

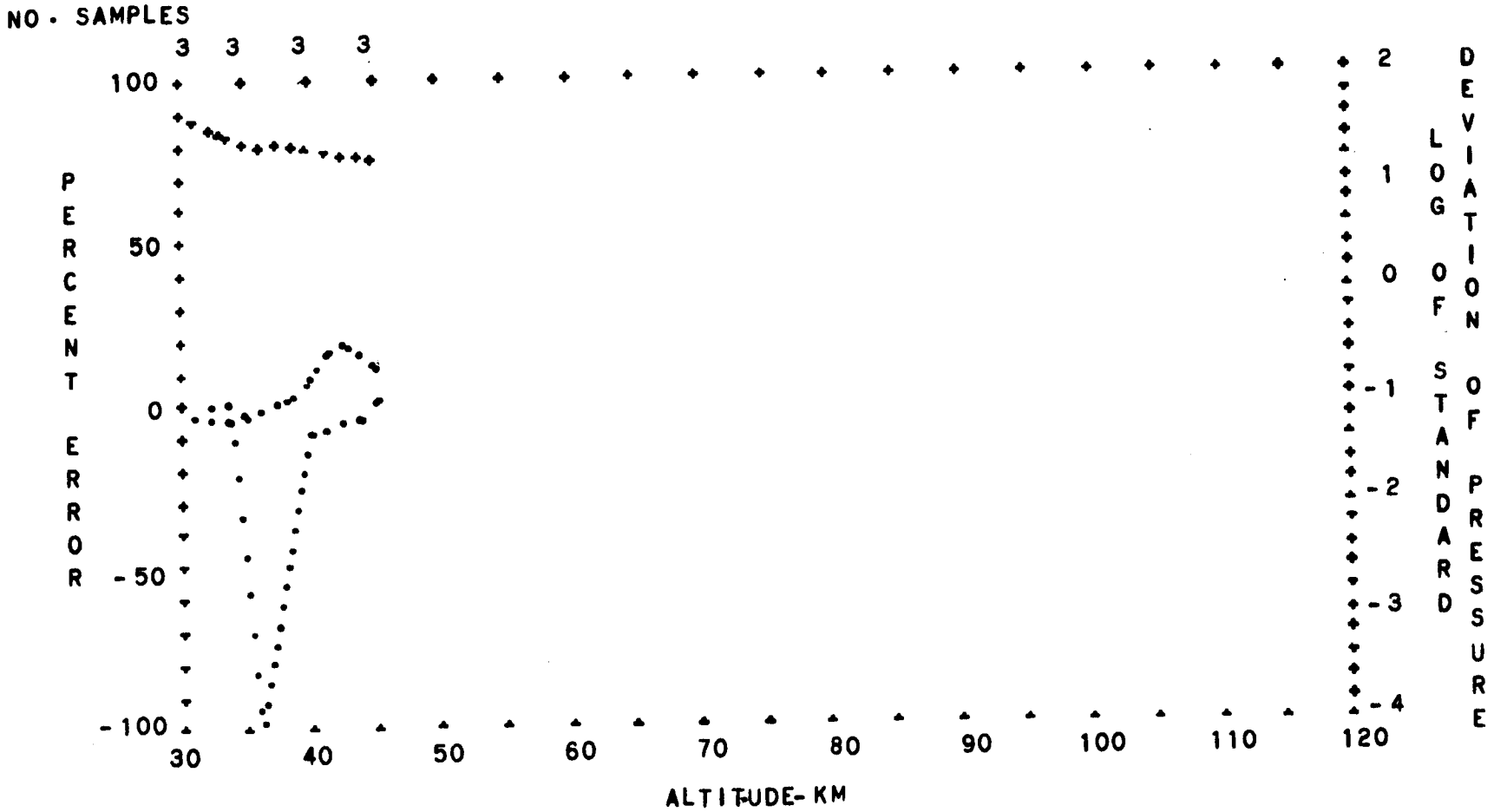

FIG. B-85. STANDARD DEVIATION OF PRESSURE AND PERCENT ERROR OF BUELL HYDROSTATIC EQUATION VERSUS ALTITUDE

ARCTIC SUMMER DAYTIME

PERCENT ERROR--DOTS LOG DEVIATION--CROSSES

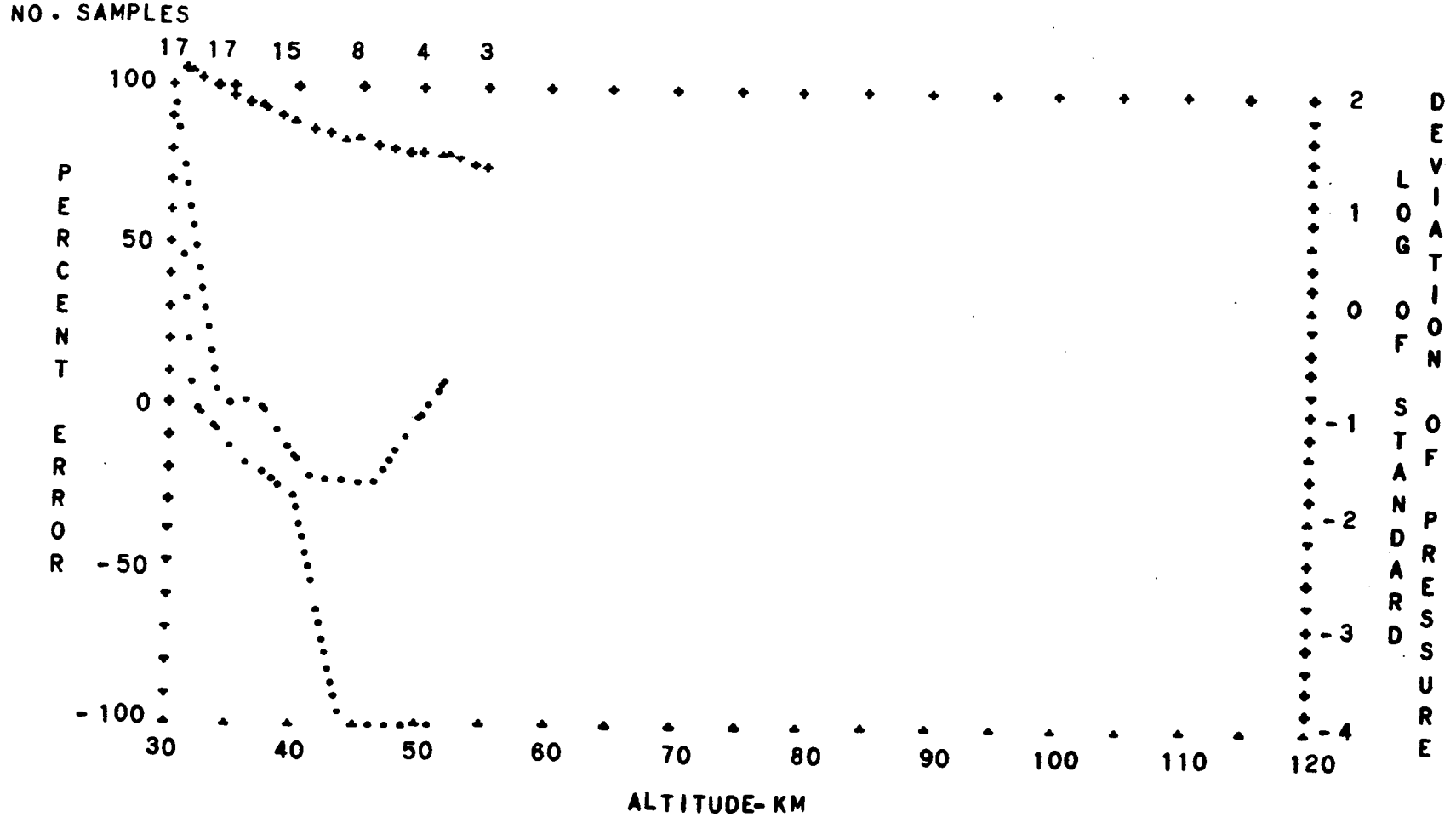

FIG. B-86. STANDARD DEVIATION OF PRESSURE AND PERCENT ERROR OF BUELL HYDROSTATIC EQUATION VERSUS ALTITUDE

ARCTIC SUMMER DIURNAL MEAN

PERCENT ERROR--DOTS

LOG DEVIATION--CROSSES

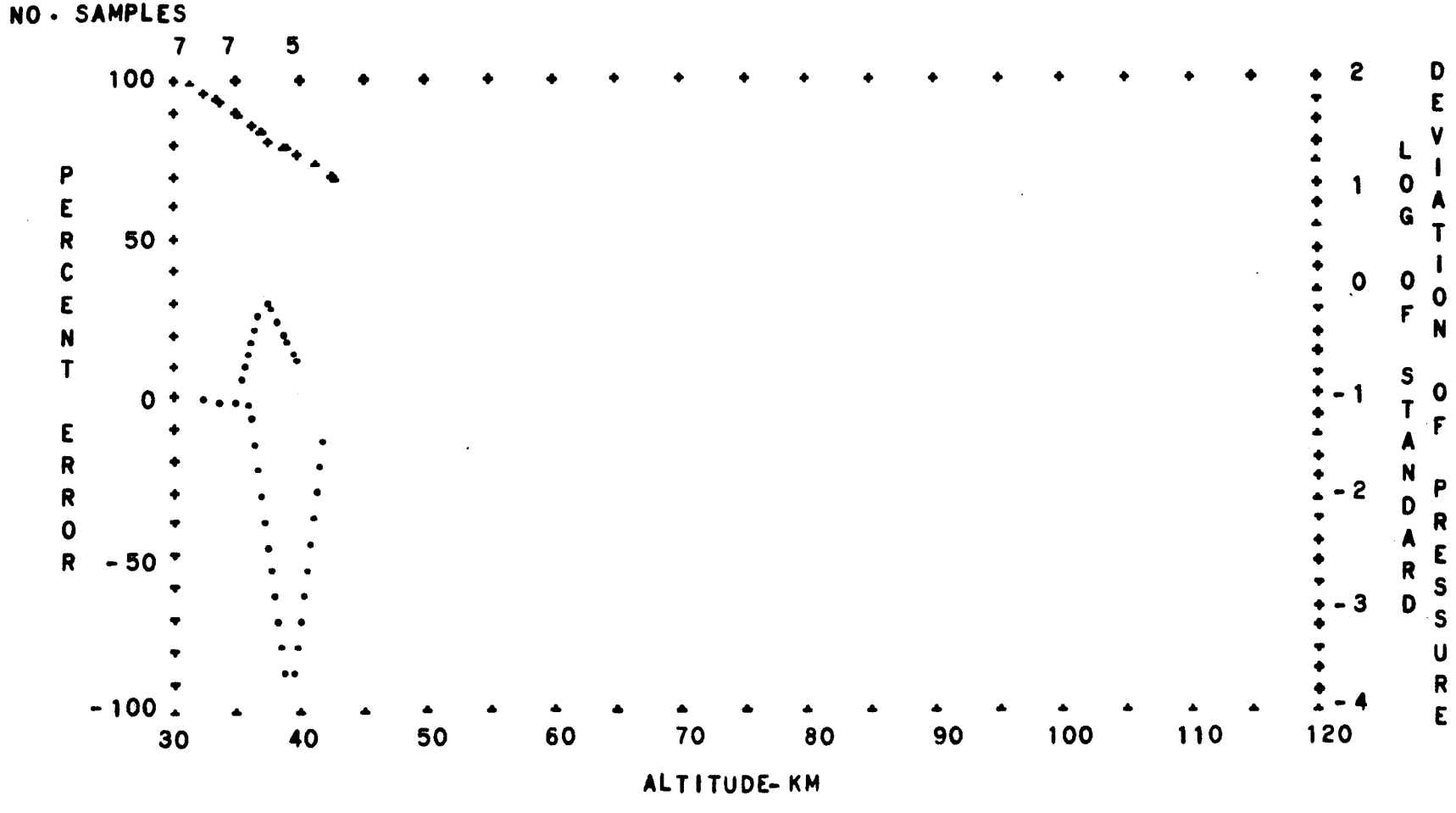

FIG. B-87. STANDARD DEVIATION OF PRESSURE AND PERCENT ERROR OF BUELL HYDROSTATIC EQUATION VERSUS ALTITUDE

ARCTIC AUTUMN DIURNAL TRANSITION

PERCENT ERROR--DOTS LOG DEVIATION--CROSSES

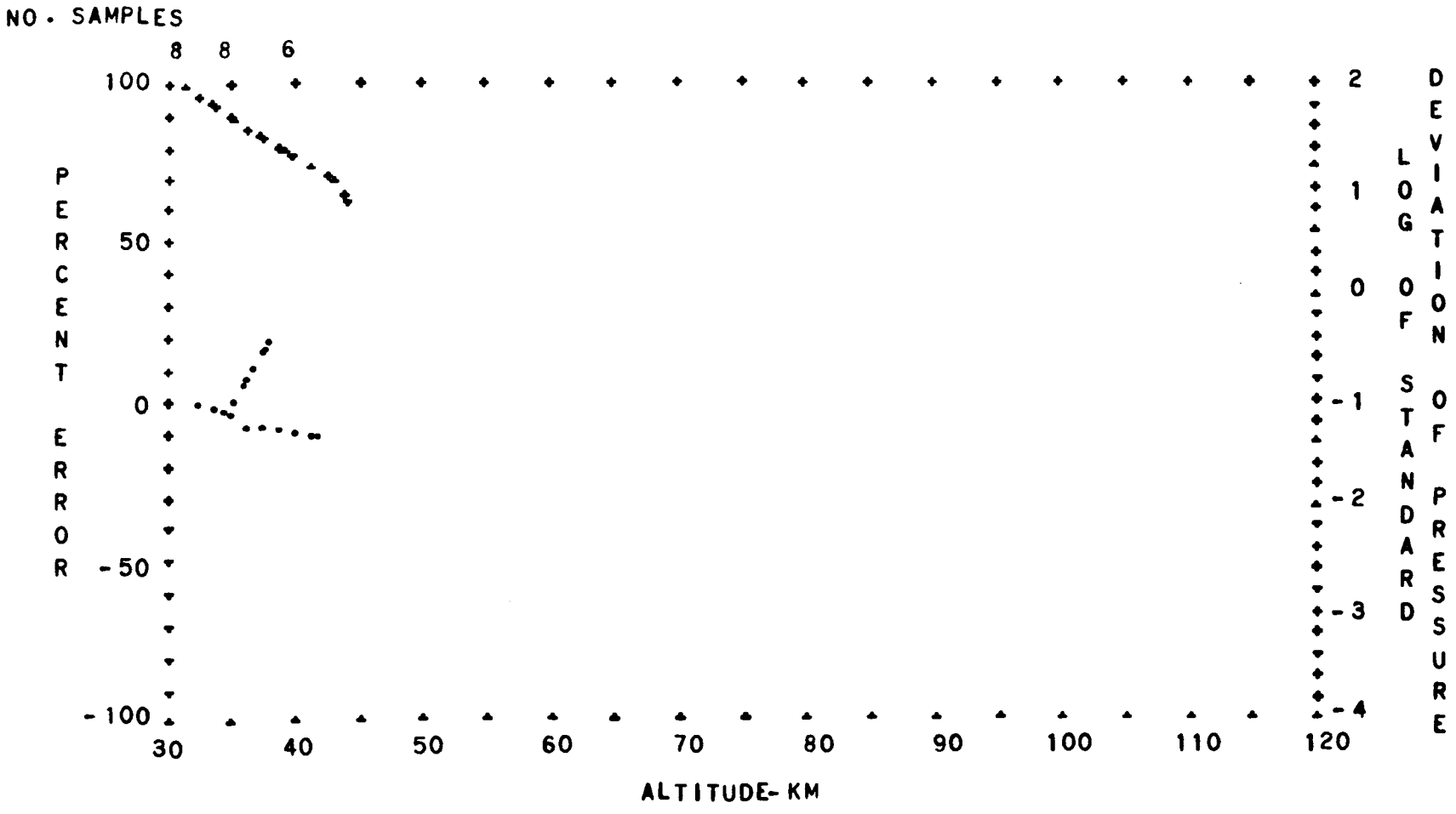

FIG. B-88. STANDARD DEVIATION OF PRESSURE AND PERCENT ERROR OF BUELL HYDROSTATIC EQUATION VERSUS ALTITUDE

ARCTIC AUTUMN DIURNAL MEAN

PERCENT ERROR--DOTS LOG. DEVIATION--CROSSES

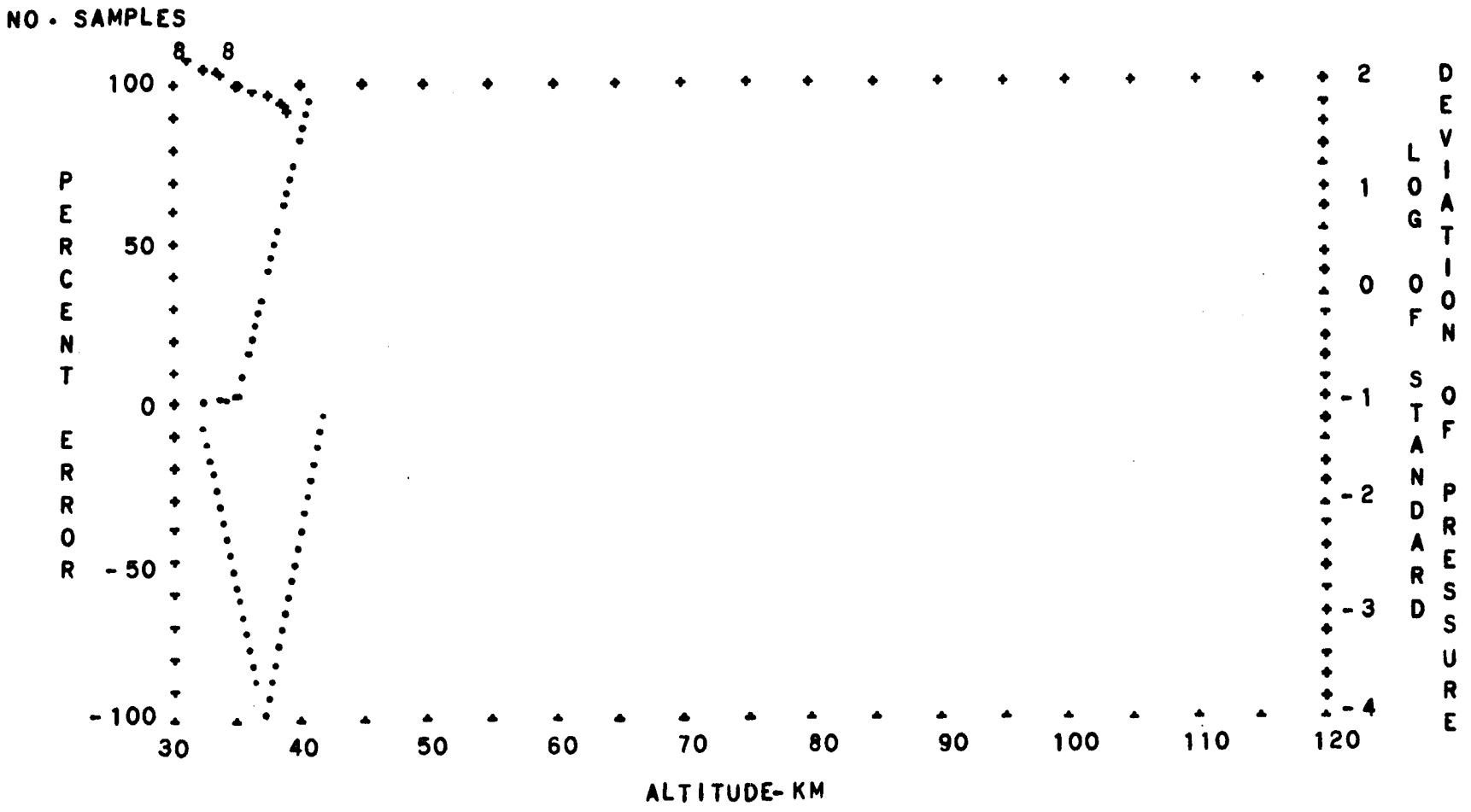

FIG. B-89. STANDARD DEVIATION OF PRESSURE AND PERCENT ERROR OF BUELL HYDROSTATIC EQUATION VERSUS ALTITUDE

ARCTIC WINTER DIURNAL TRANSITION

PERCENT ERROR--DOTS LOG DEVIATION--CROSSES

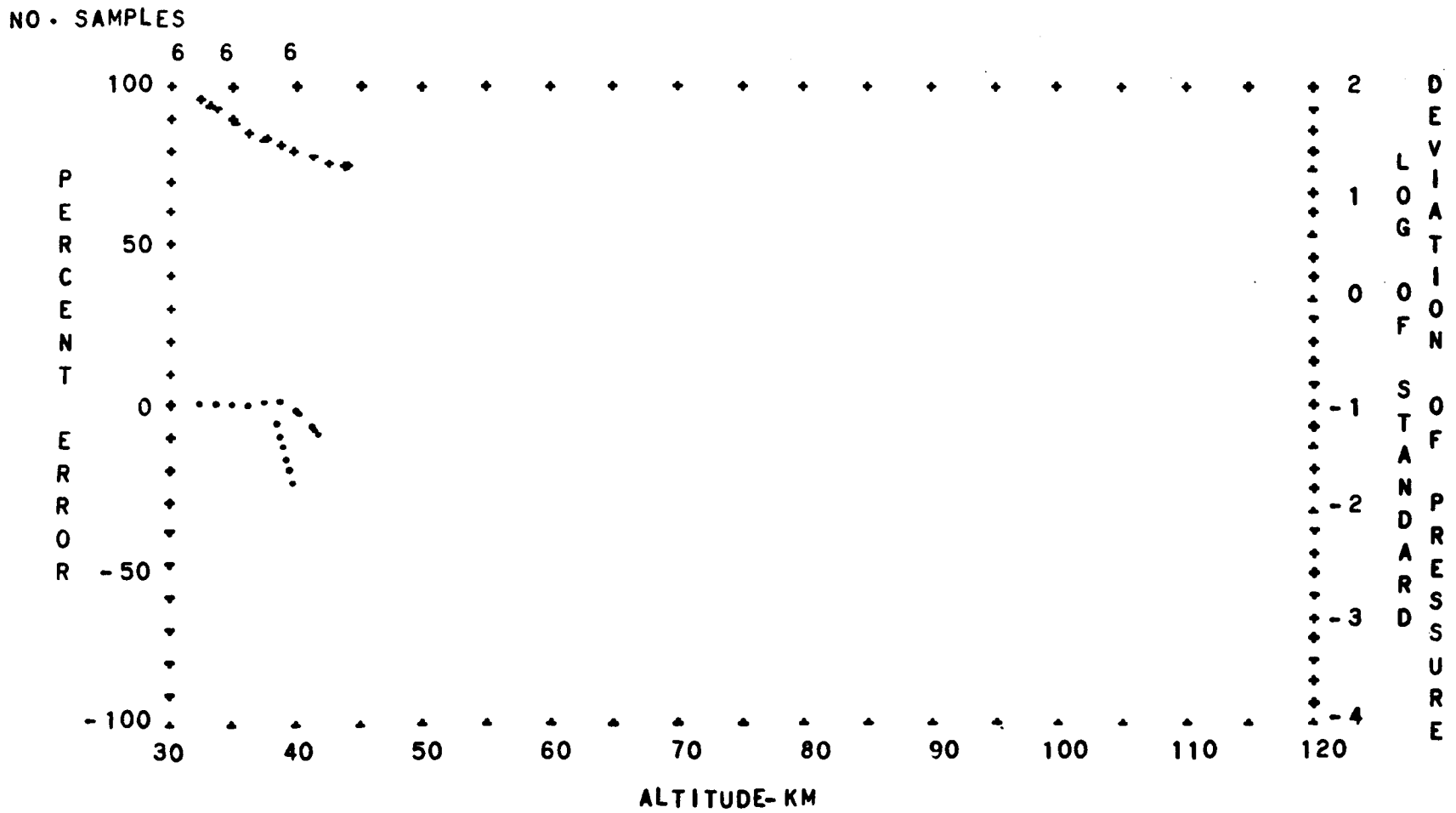

FIG. B-90. STANDARD DEVIATION OF PRESSURE AND PERCENT ERROR OF BUELL HYDROSTATIC EQUATION VERSUS ALTITUDE

ARCTIC WINTER NIGHTTIME

PERCENT ERROR--DOTS LOG DEVIATION--CROSSES

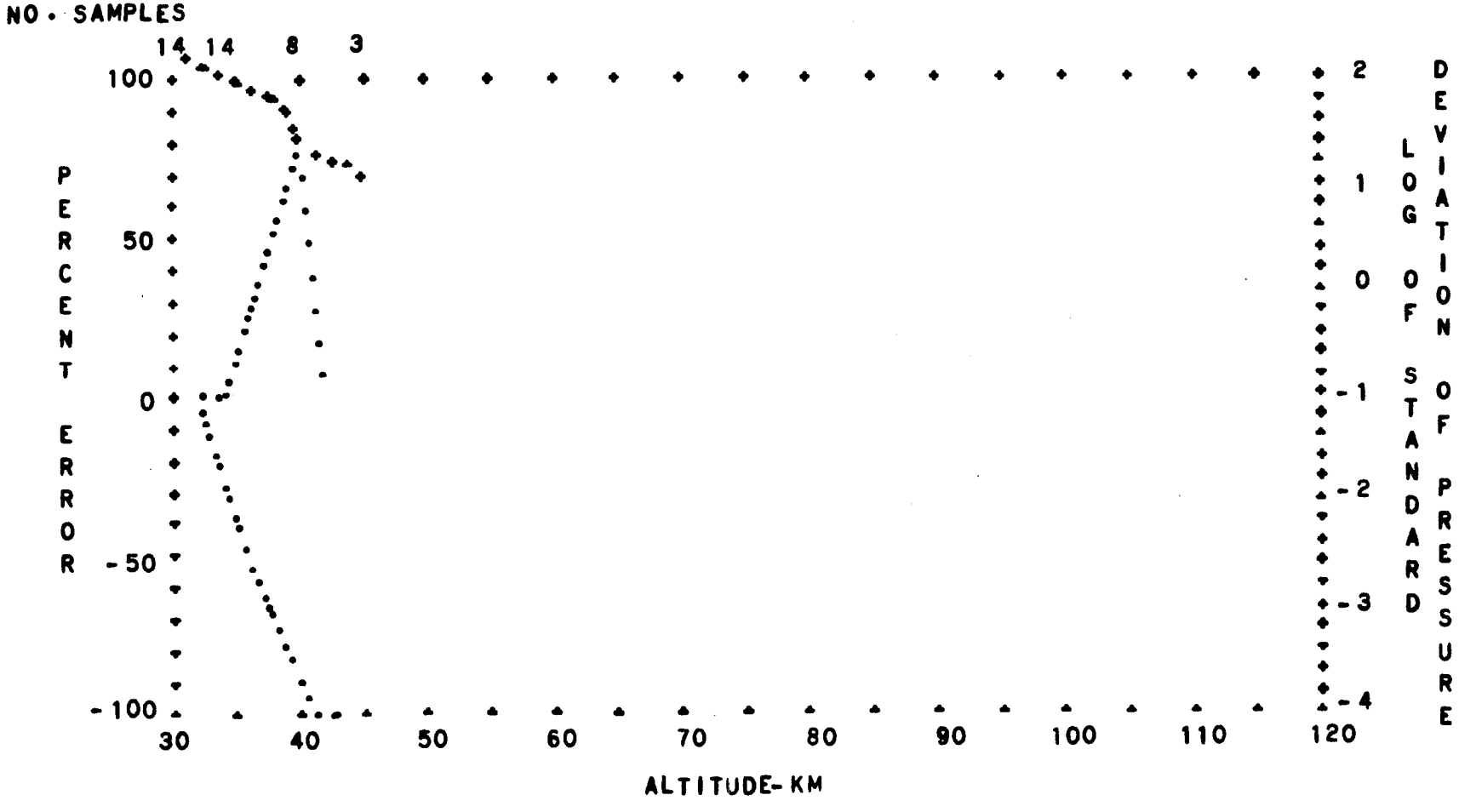

FIG. B-91. STANDARD DEVIATION OF PRESSURE AND PERCENT ERROR OF BUELL HYDROSTATIC EQUATION VERSUS ALTITUDE

ARCTIC WINTER DIURNAL MEAN

PERCENT ERROR--DOTS LOG. DEVIATION--CROSSES

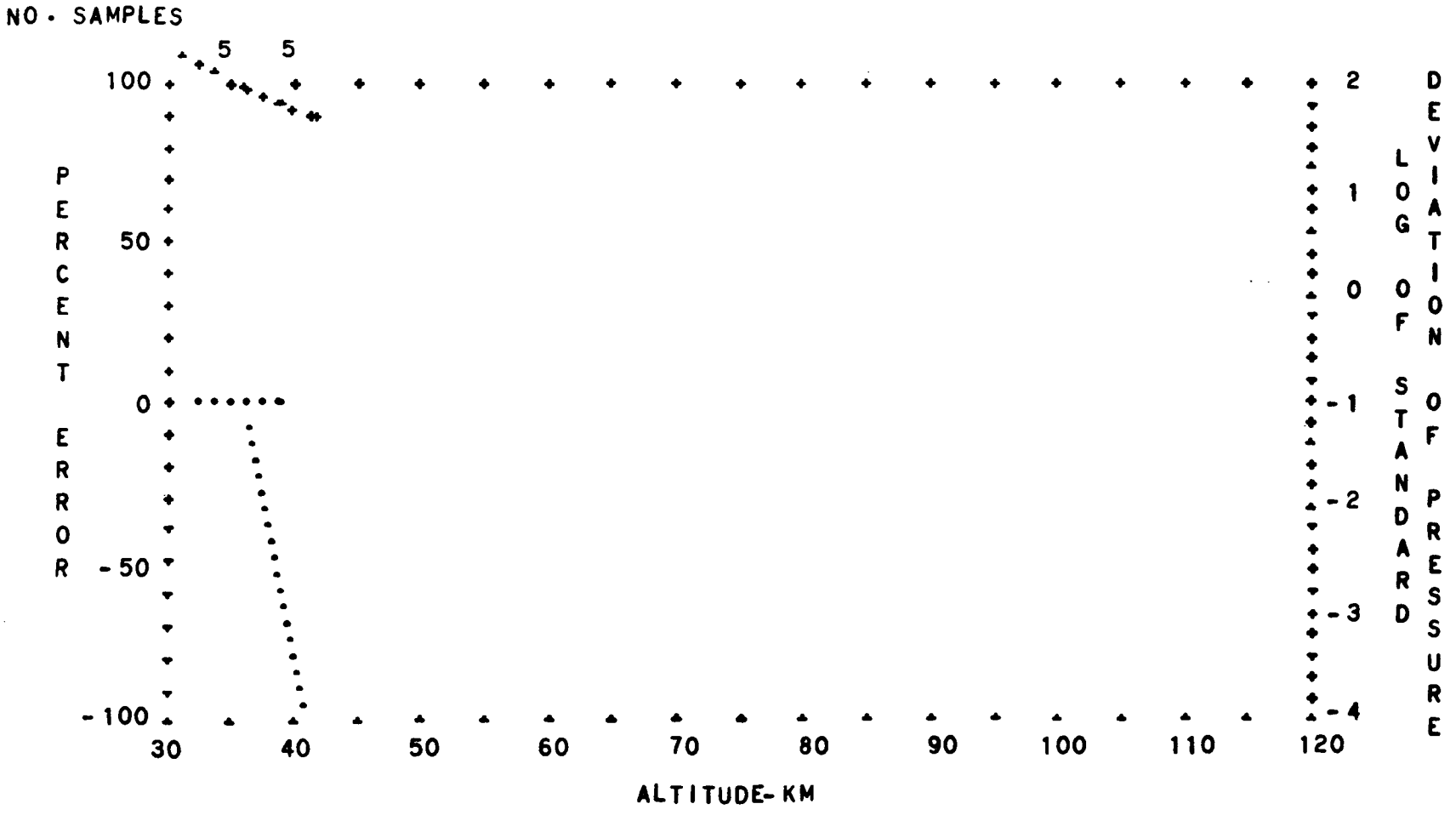

FIG. B-92. STANDARD DEVIATION OF PRESSURE AND PERCENT ERROR OF BUELL HYDROSTATIC EQUATION VERSUS ALTITUDE

ARCTIC SUMMER EXTREME DIURNAL TRANSITION

PERCENT ERROR--DOTS LOG DEVIATION--CROSSES

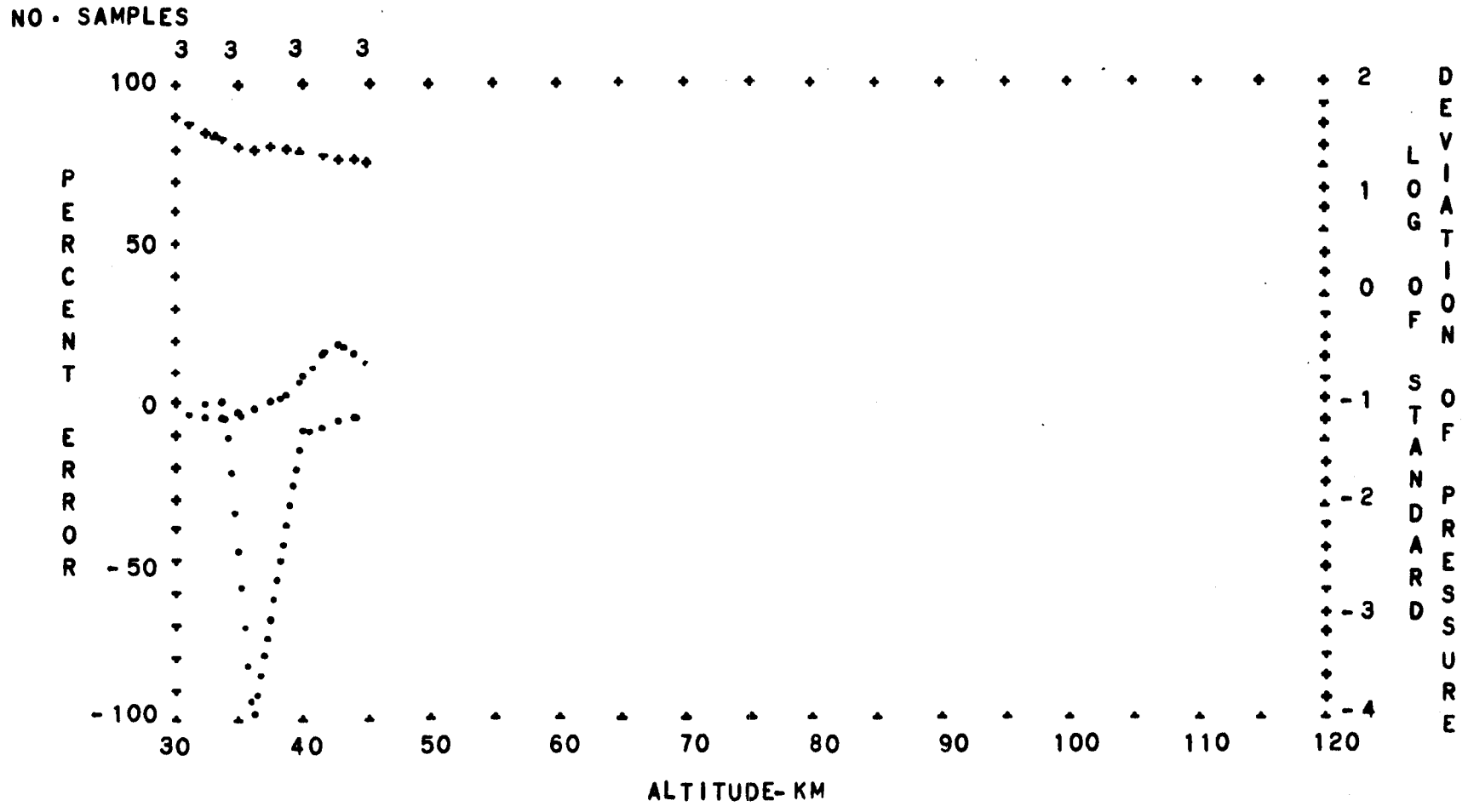

FIG. B-93. STANDARD DEVIATION OF PRESSURE AND PERCENT ERROR OF BUELL HYDROSTATIC EQUATION VERSUS ALTITUDE

ARCTIC SUMMER EXTREME DAYTIME

PERCENT ERROR--DOTS LOG DEVIATION--CROSSES

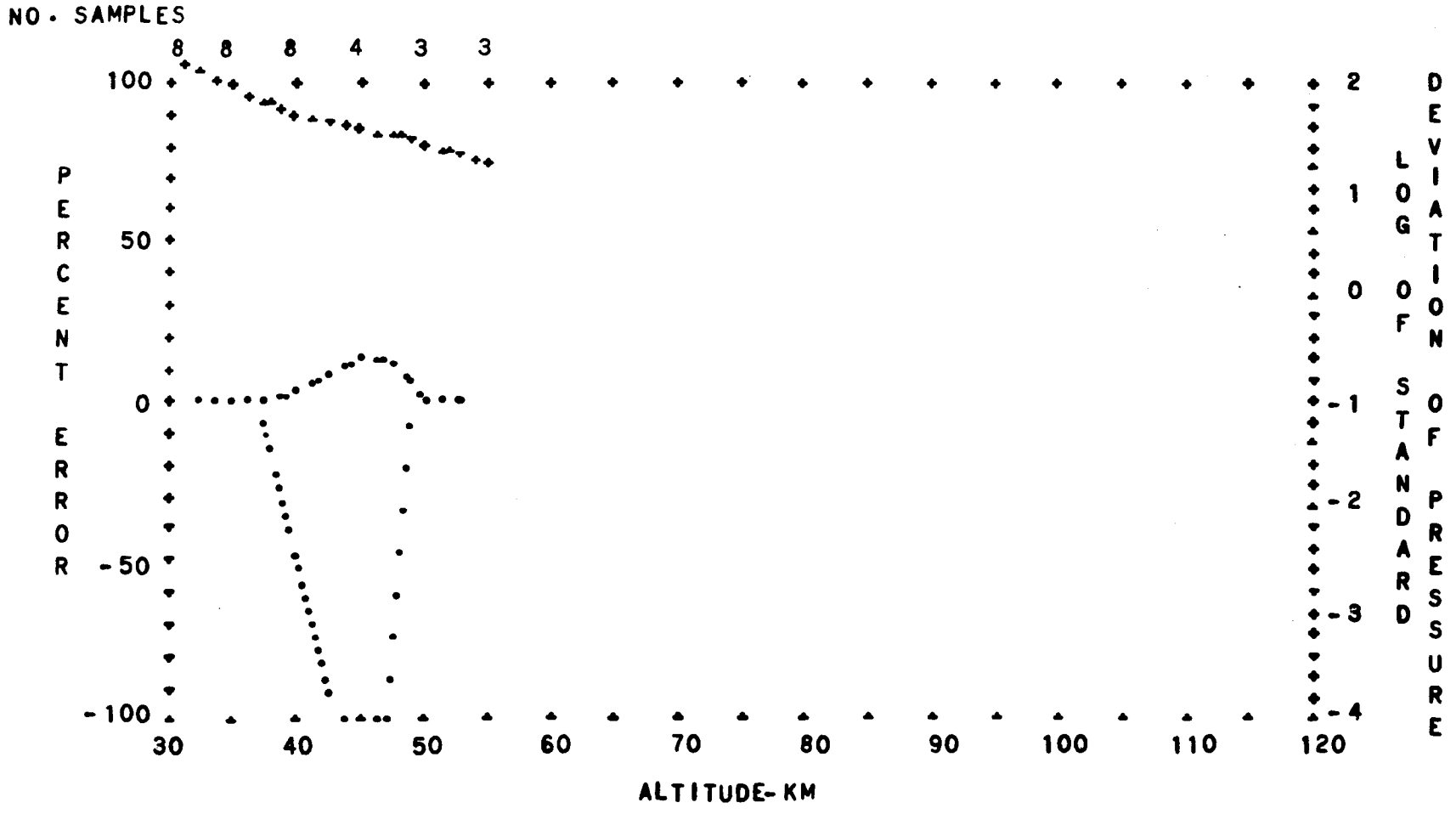

FIG. B-94. STANDARD DEVIATION OF PRESSURE AND PERCENT ERROR OF BUELL HYDROSTATIC EQUATION VERSUS ALTITUDE

ARCTIC SUMMER EXTREME DIURNAL MEAN

PERCENT ERROR--DOTS LOG. DEVIATION--CROSSES

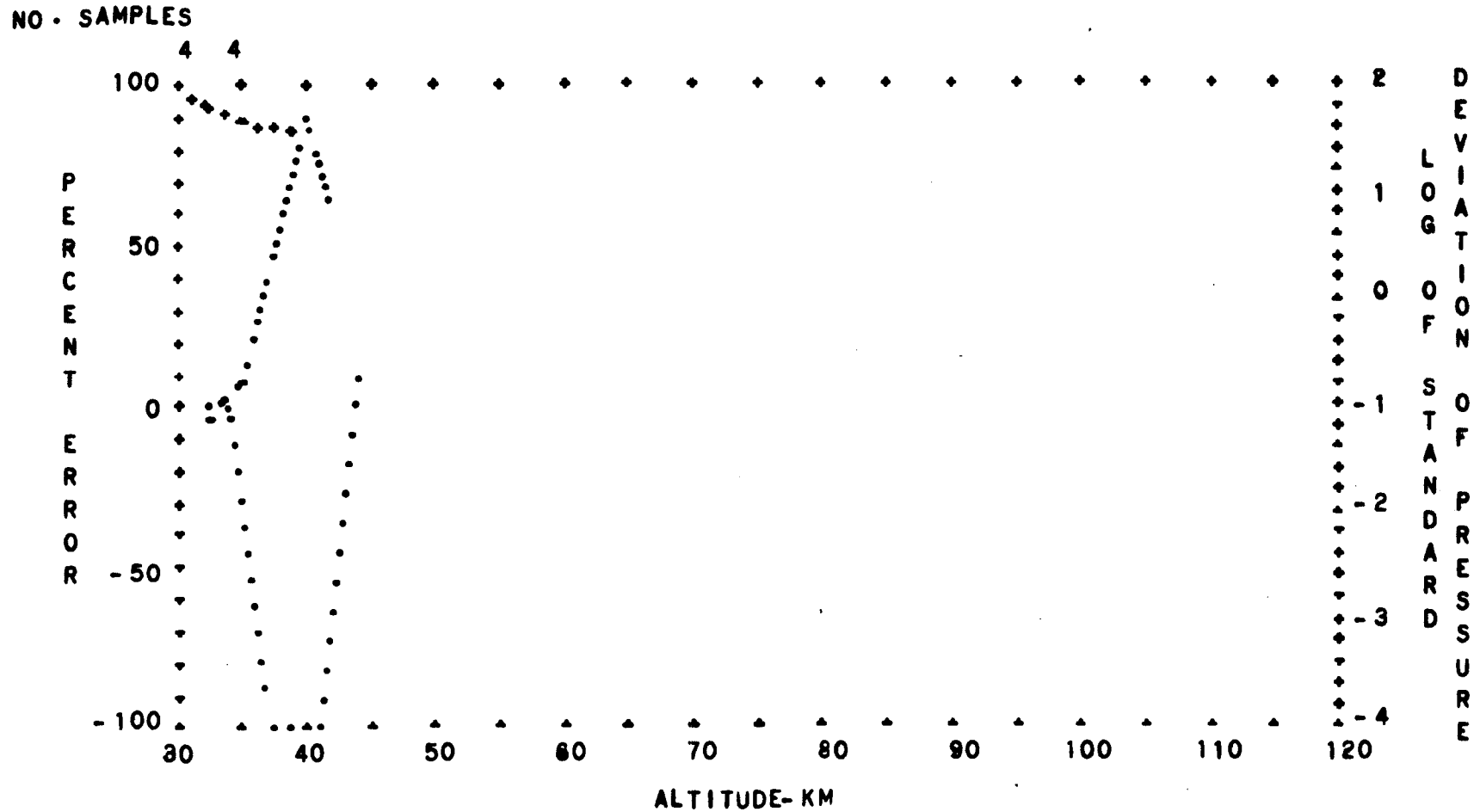

FIG. B-95. STANDARD DEVIATION OF PRESSURE AND PERCENT ERROR OF BUELL HYDROSTATIC EQUATION VERSUS ALTITUDE

ARCTIC WINTER EXTREME DIURNAL TRANSITION

PERCENT ERROR--DOTS LOG DEVIATION--CROSSES

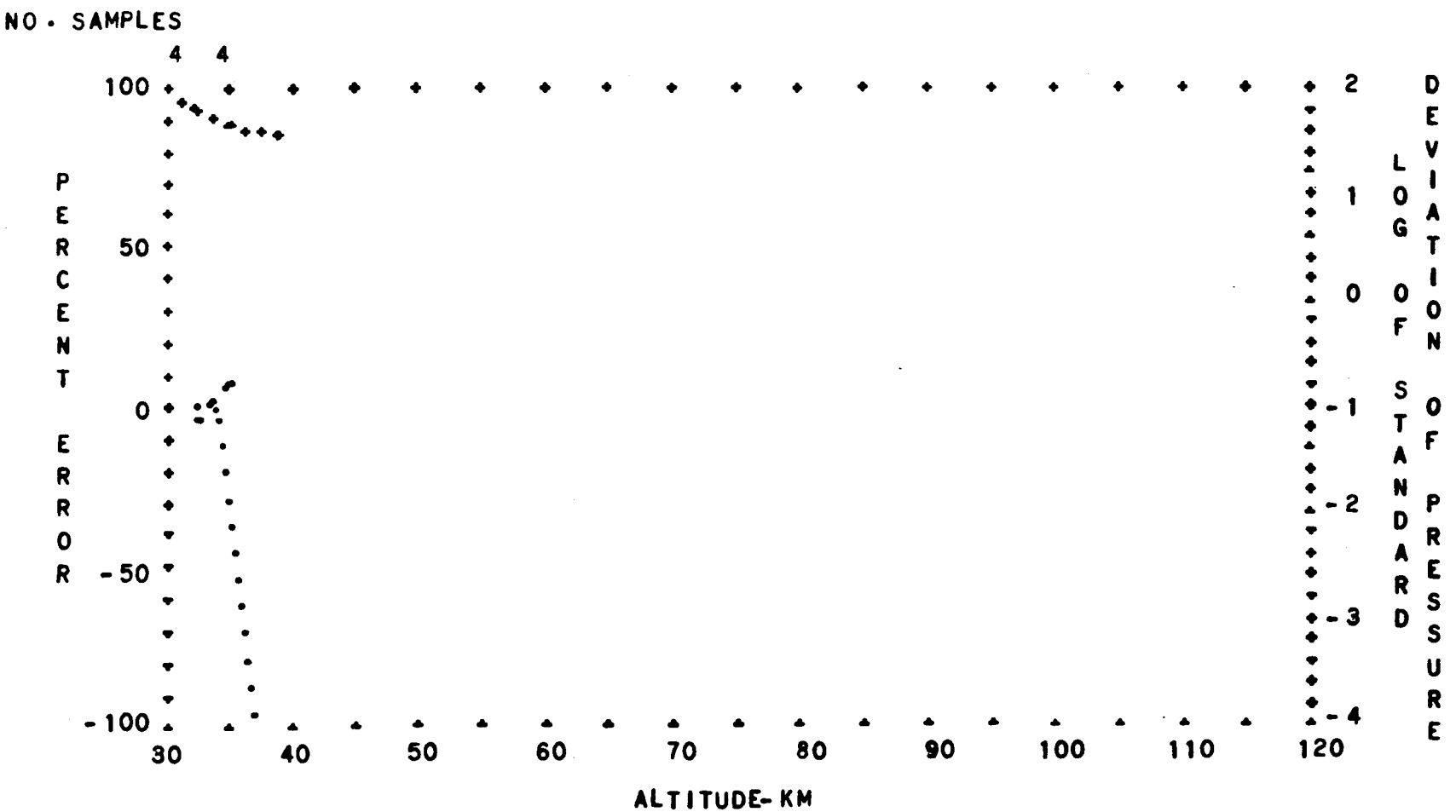

FIG. B-96. STANDARD DEVIATION OF PRESSURE AND PERCENT ERROR OF BUELL HYDROSTATIC EQUATION VERSUS ALTITUDE

ARCTIC WINTER EXTREME DIURNAL MEAN

PERCENT ERROR--DOTS LOG DEVIATION--CROSSES

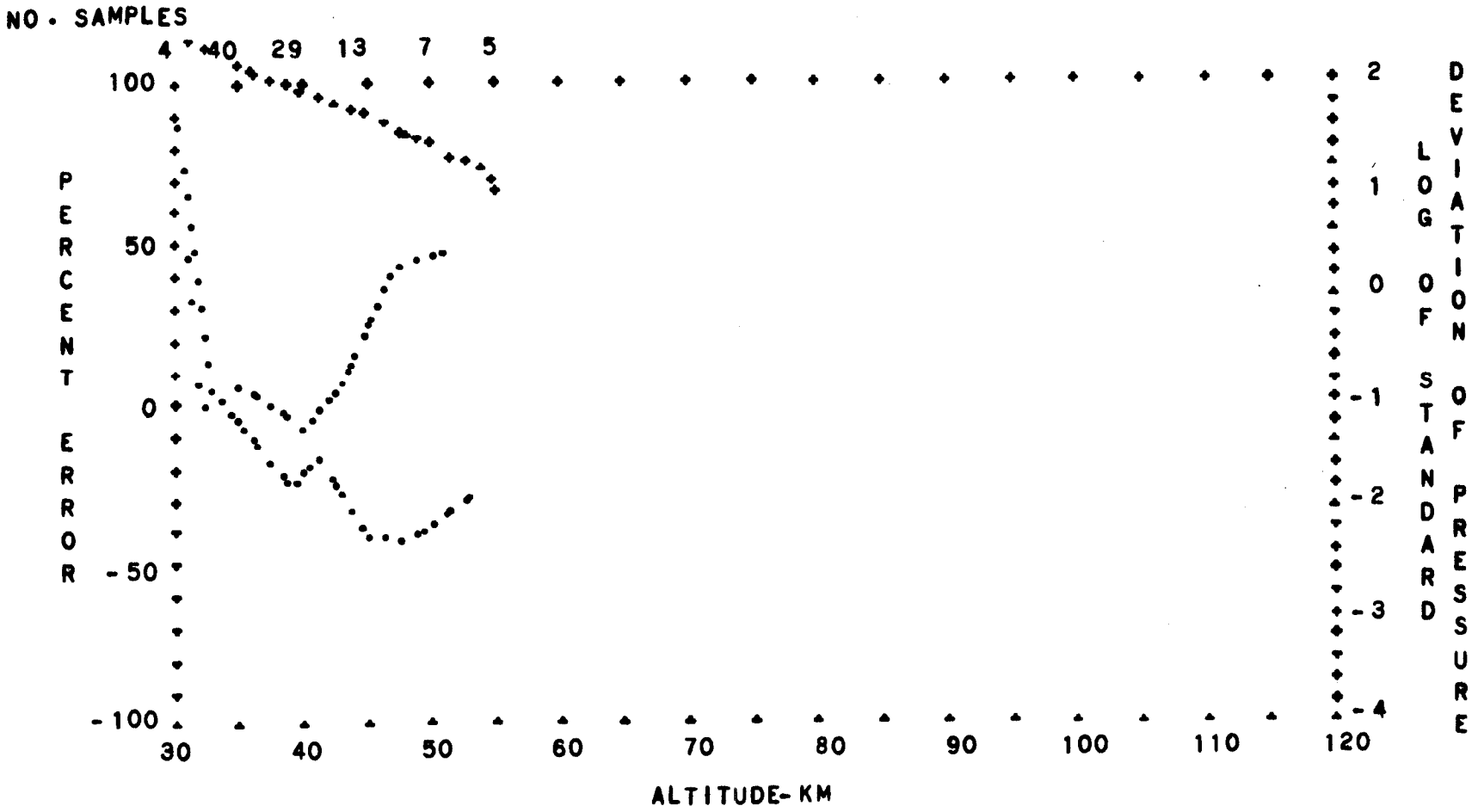

FIG. B-97. STANDARD DEVIATION OF PRESSURE AND PERCENT ERROR OF BUELL HYDROSTATIC EQUATION VERSUS ALTITUDE

ARCTIC ANNUAL MEAN DIURNAL TRANSITION

PERCENT ERROR--DOTS LOG. DEVIATION--CROSSES

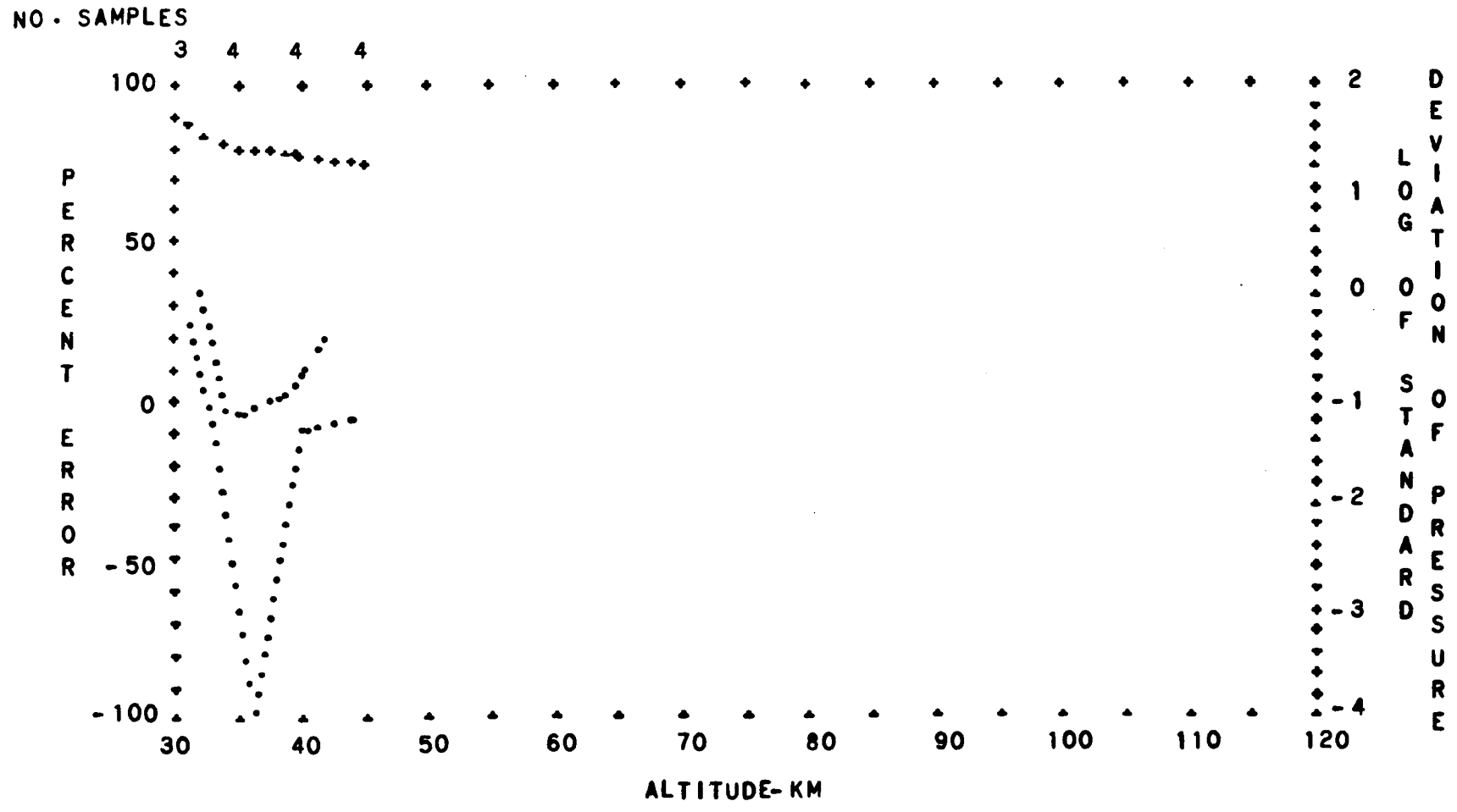

FIG. B-98. STANDARD DEVIATION OF PRESSURE AND PERCENT ERROR OF BUELL HYDROSTATIC EQUATION VERSUS ALTITUDE

ARCTIC ANNUAL MEAN DAYTIME

PERCENT ERROR--DOTS LOG. DEVIATION--CROSSES

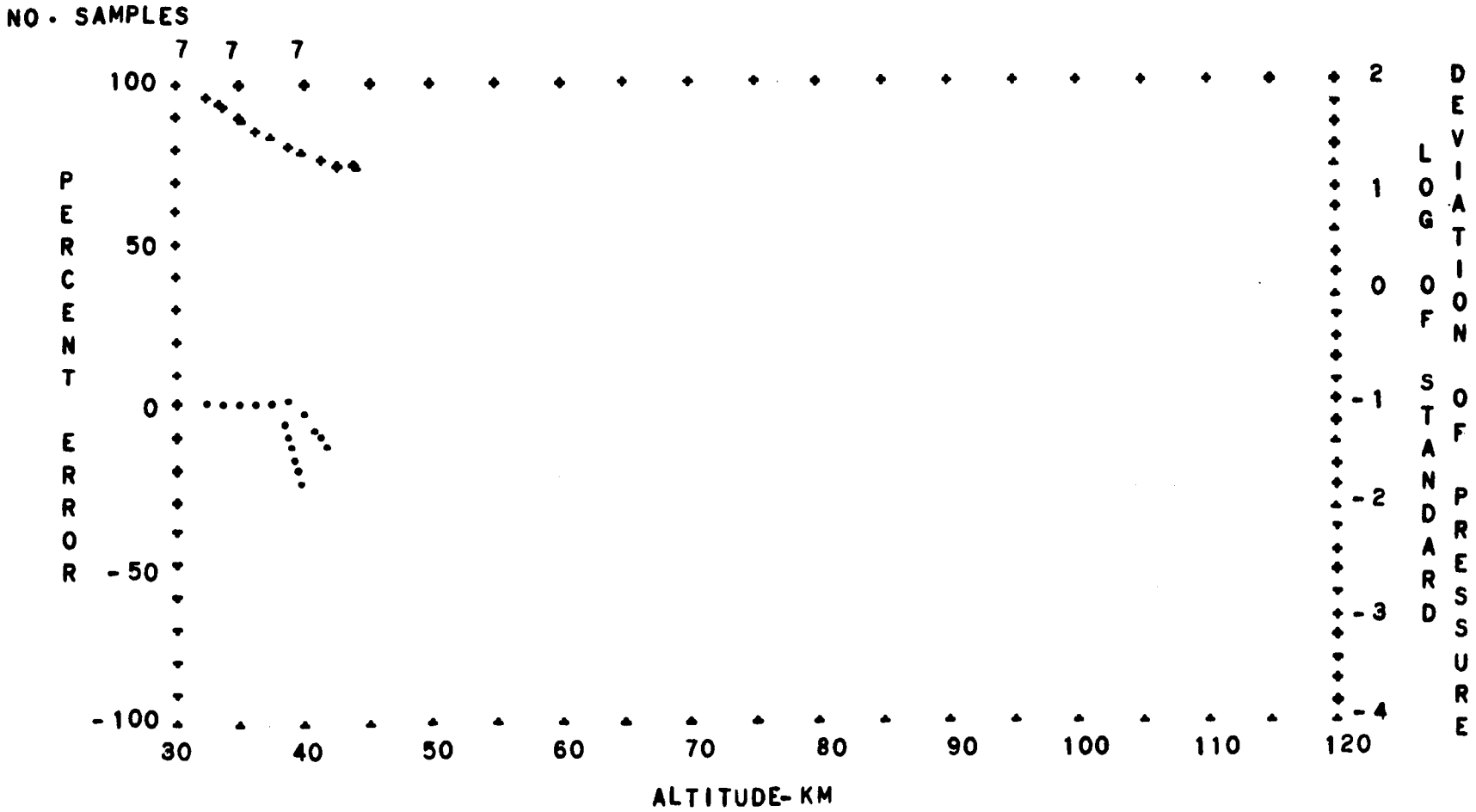

FIG. B-99. STANDARD DEVIATION OF PRESSURE AND PERCENT ERROR OF BUELL HYDROSTATIC EQUATION VERSUS ALTITUDE

ARCTIC ANNUAL MEAN NIGHTTIME

PERCENT ERROR--DOTS LOG. DEVIATION--CROSSES

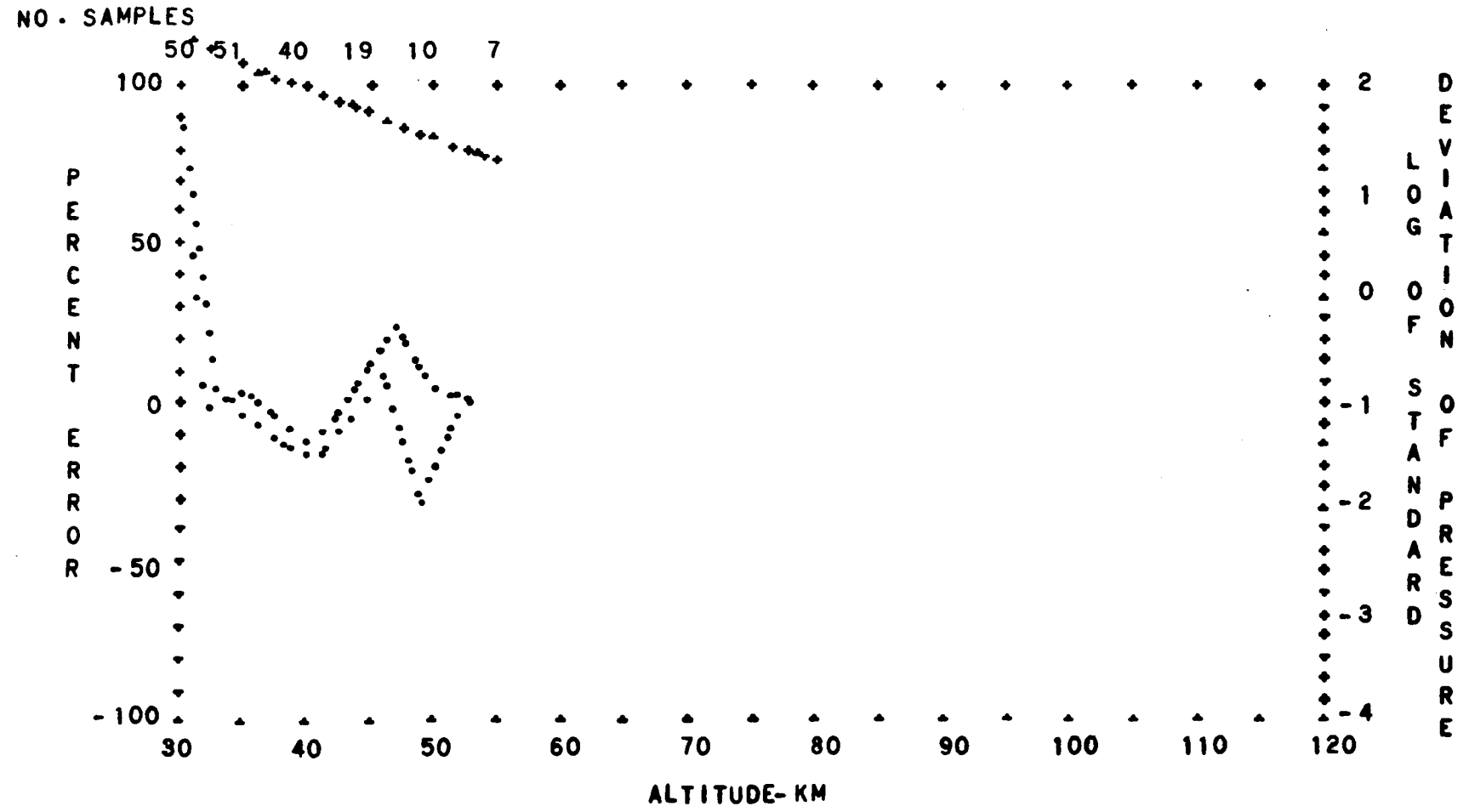

FIG. B-100. STANDARD DEVIATION OF PRESSURE AND PERCENT ERROR OF BUELL HYDROSTATIC EQUATION VERSUS ALTITUDE

ARCTIC ANNUAL MEAN DIURNAL MEAN

PERCENT ERROR--DOTS LOG. DEVIATION--CROSSES

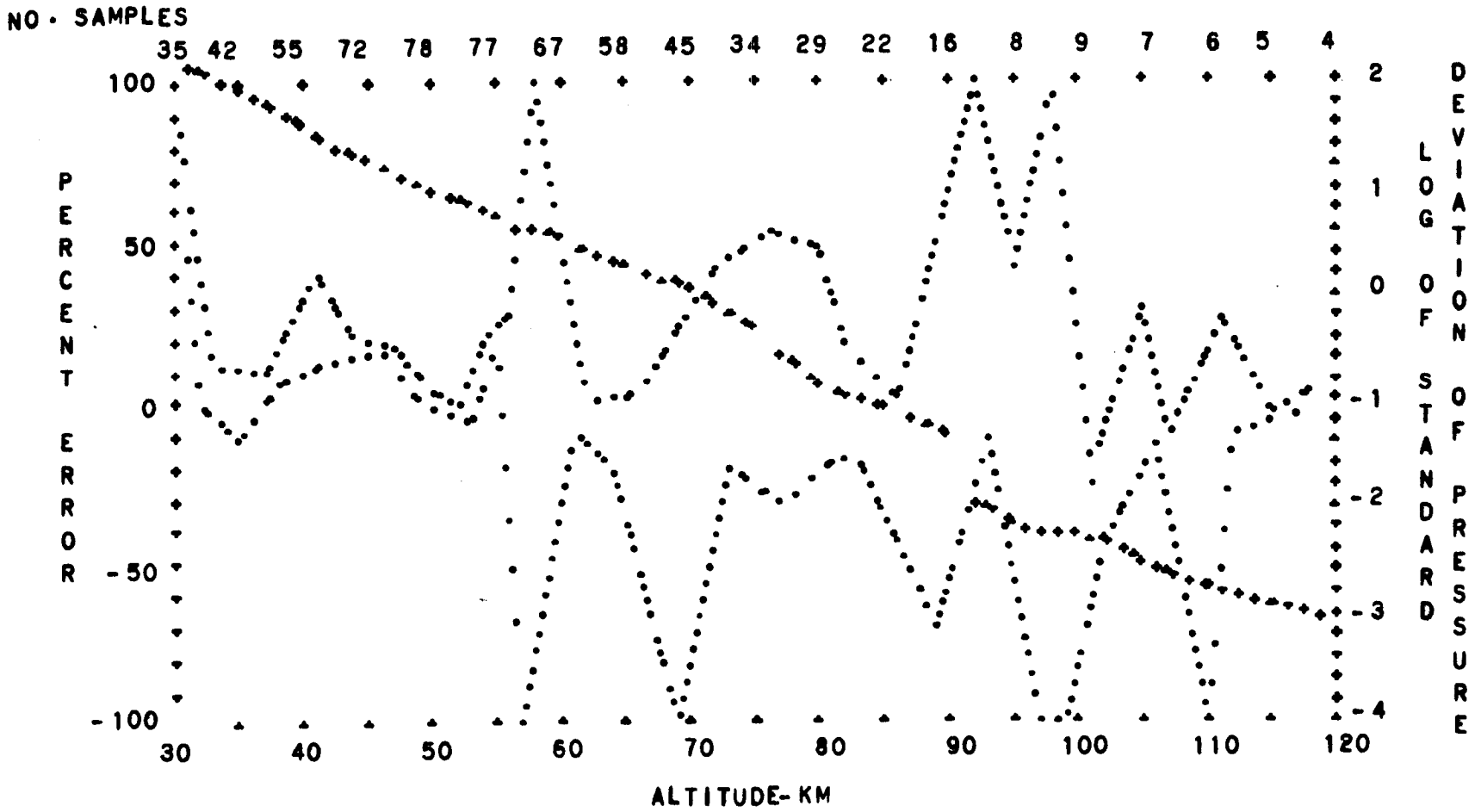

FIG. B-101. STANDARD DEVIATION OF PRESSURE AND PERCENT ERROR OF BUELL HYDROSTATIC EQUATION VERSUS ALTITUDE

HEMISPHERICAL MEAN PERCENT ERROR--DOTS SPRING DIURNAL MEAN LOG DEVIATION--CROSSES

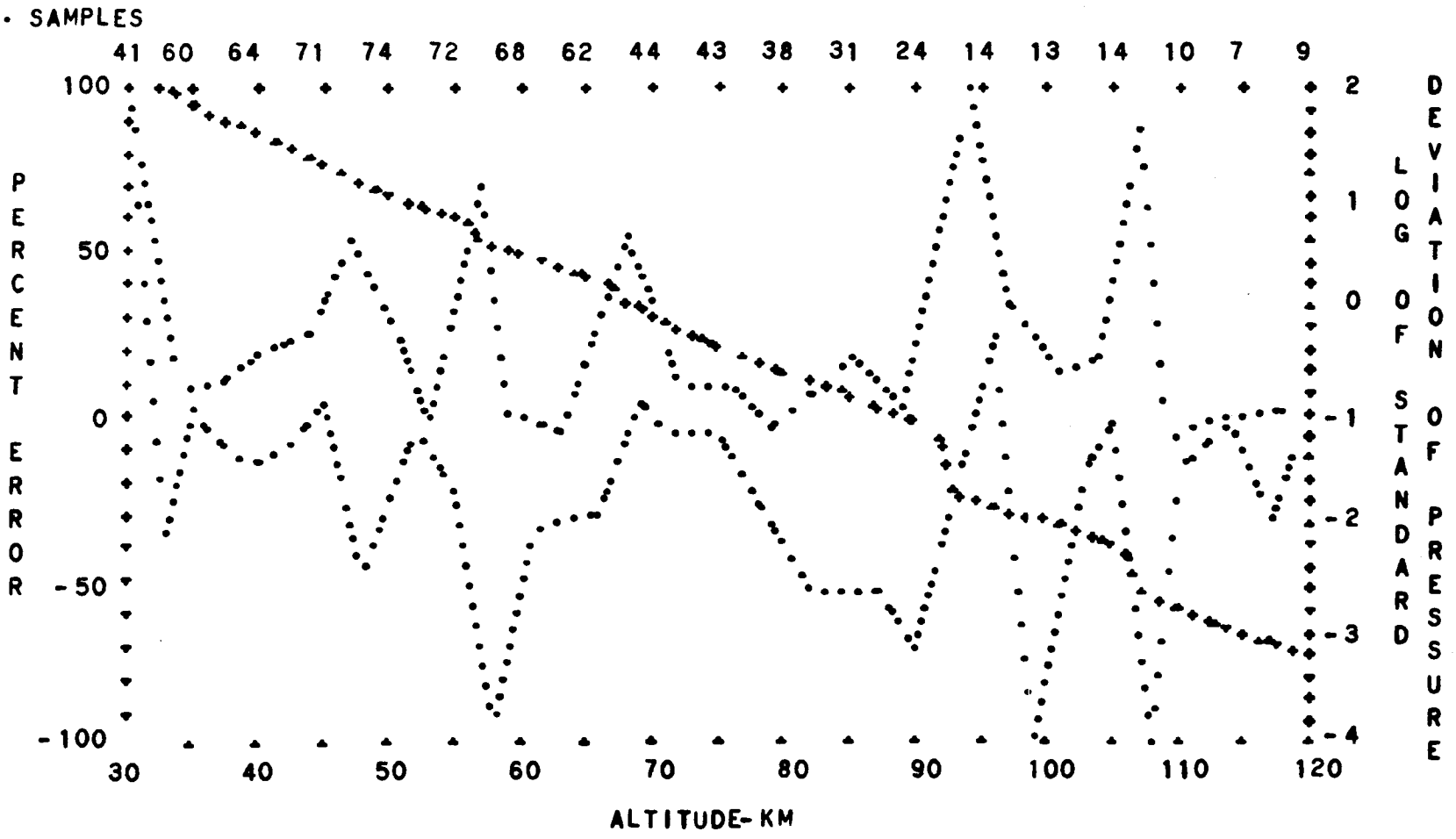

FIG. B-102. STANDARD DEVIATION OF PRESSURE AND PERCENT ERROR OF BUELL HYDROSTATIC EQUATION VERSUS ALTITUDE

HEMISPHERICAL MEAN SUMMER DIURNAL MEAN

PERCENT ERROR--DOTS LOG DEVIATION--CROSSES

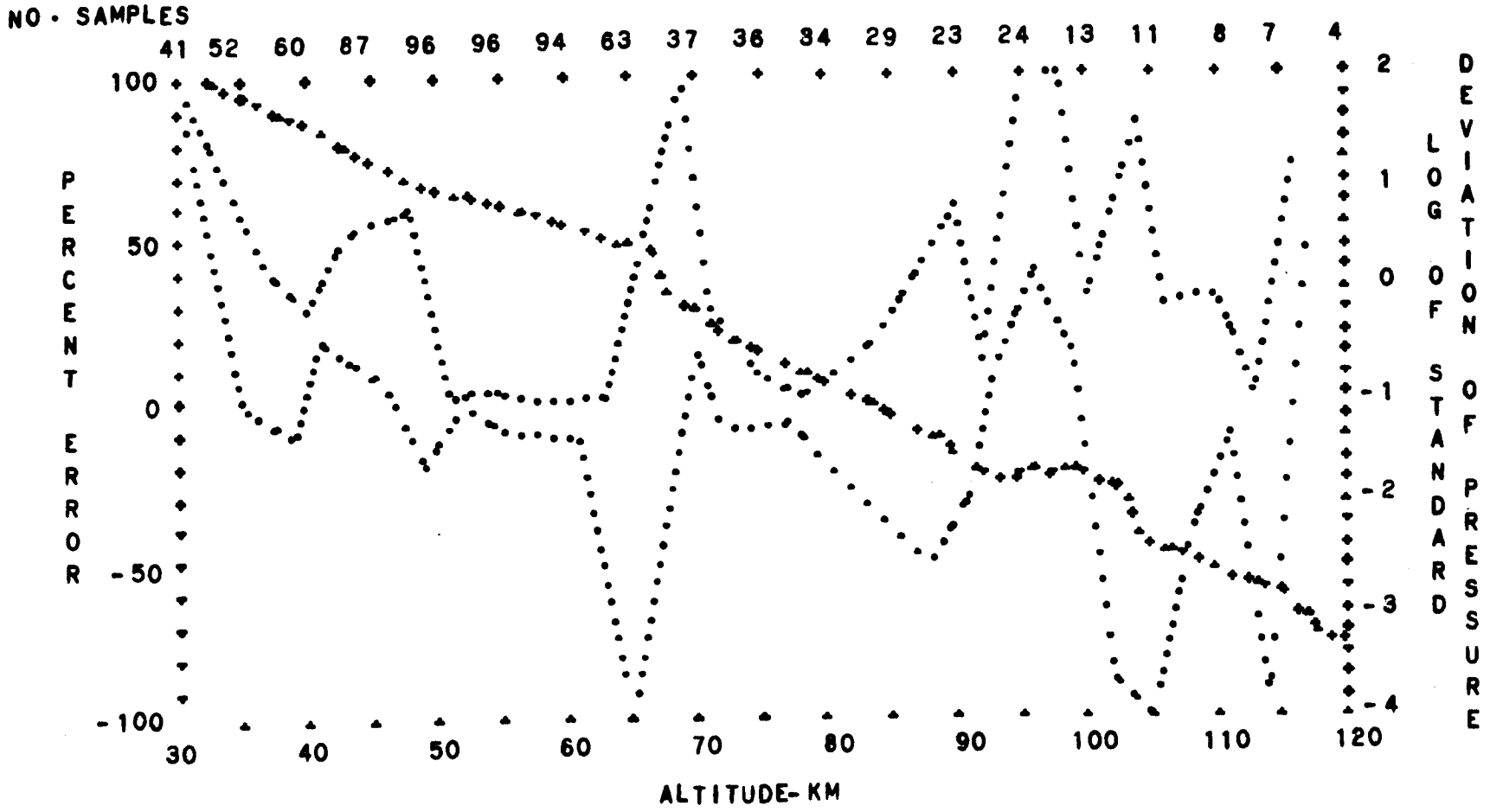

FIG. B-103. STANDARD DEVIATION OF PRESSURE AND PERCENT ERROR OF BUELL HYDROSTATIC EQUATION VERSUS ALTITUDE

HEMISPHERICAL MEAN AUTUMN DIURNAL MEAN

PERCENT ERROR--DOTS LOG DEVIATION--CROSSES

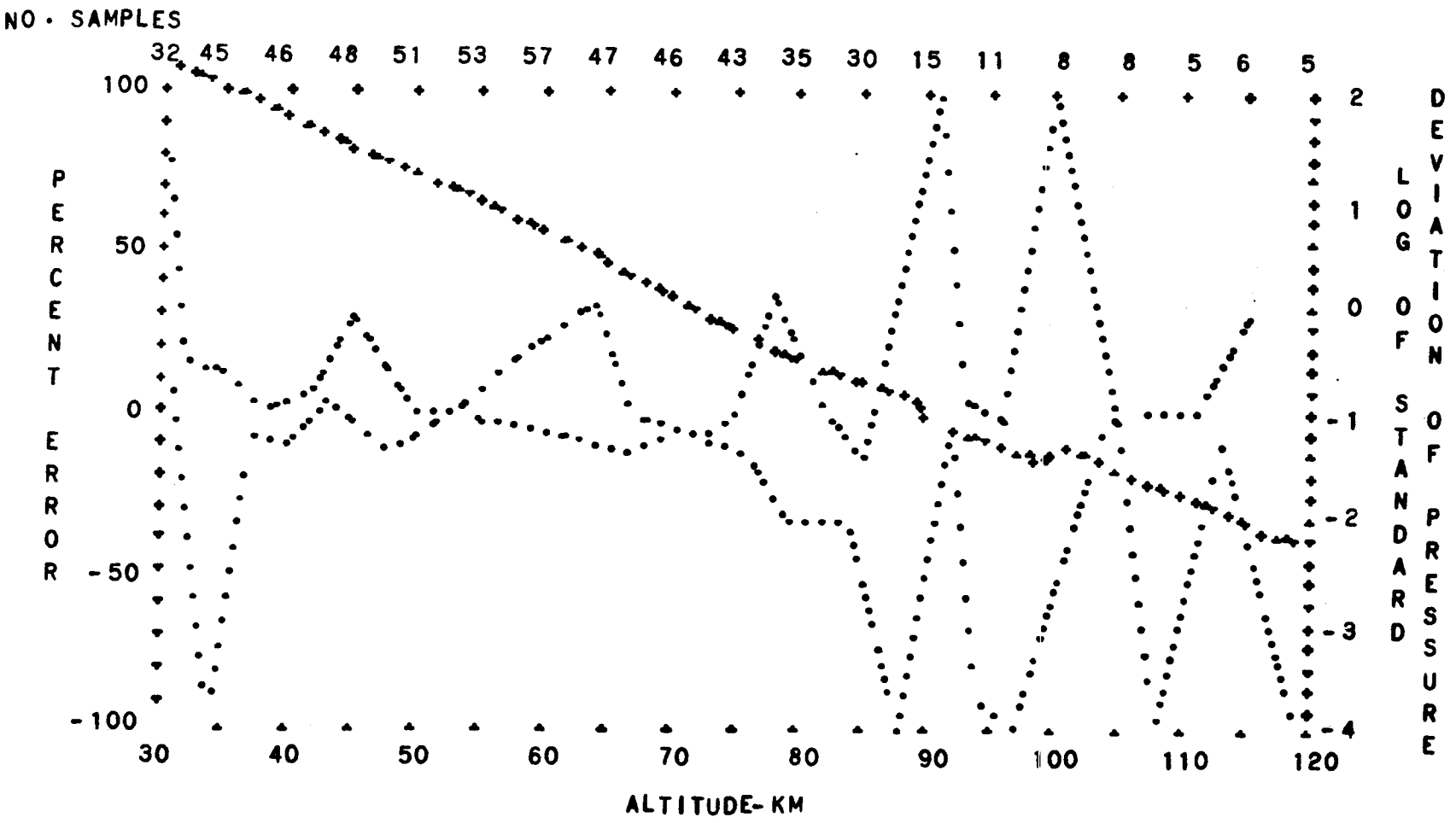

FIG. B-104. STANDARD DEVIATION OF PRESSURE AND PERCENT ERROR OF BUELL HYDROSTATIC EQUATION VERSUS ALTITUDE

HEMISPHERICAL MEAN PERCENT ERROR--DOTS WINTER DIURNAL MEAN LOG DEVIATION--CROSSES

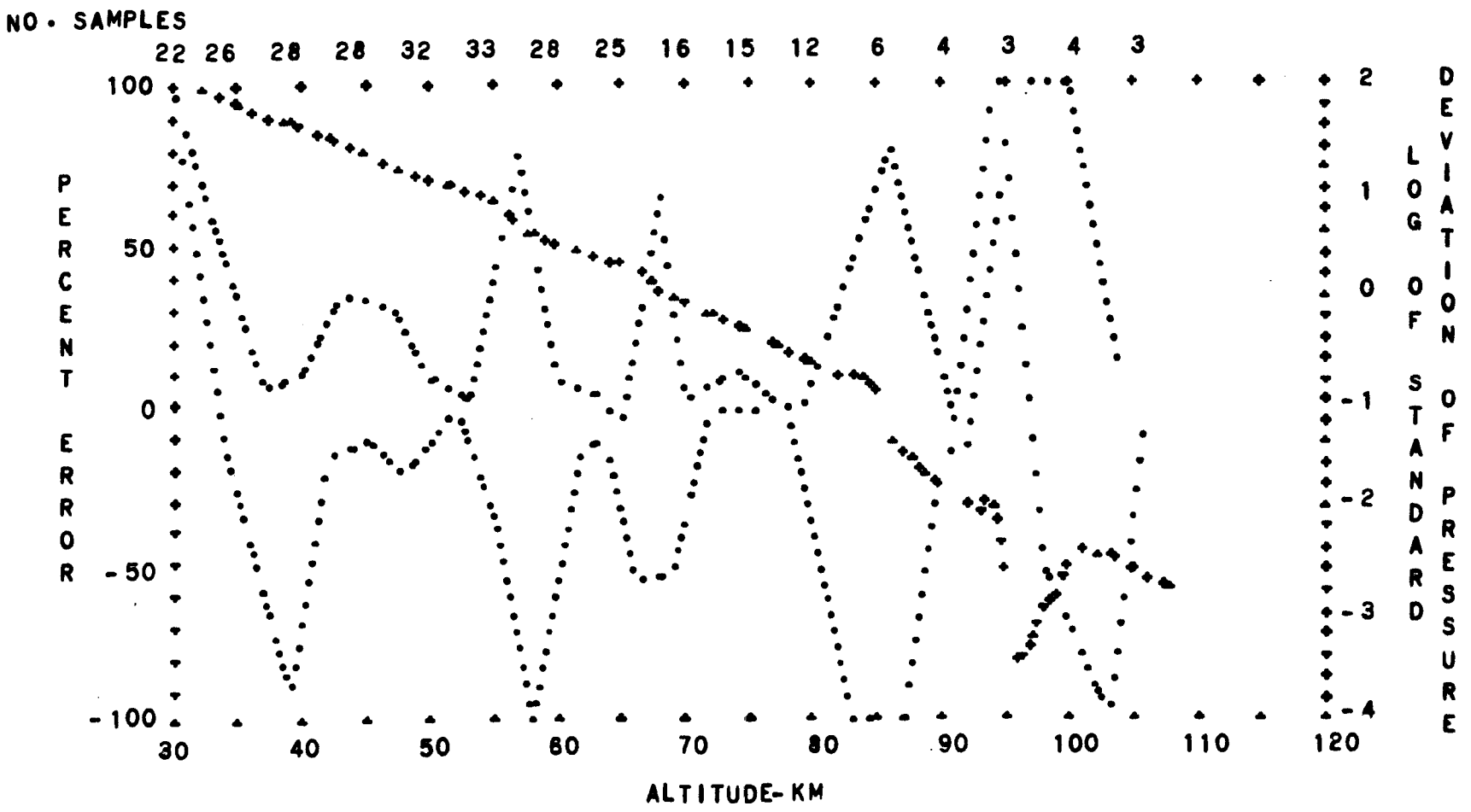

FIG. B-105. STANDARD DEVIATION OF PRESSURE AND PERCENT ERROR OF BUELL HYDROSTATIC EQUATION VERSUS ALTITUDE

HEMISPHERICAL MEAN PERCENT ERROR--DOTS SUMMER EXTREME DIURNAL MEAN LOG DEVIATION--CROSSES

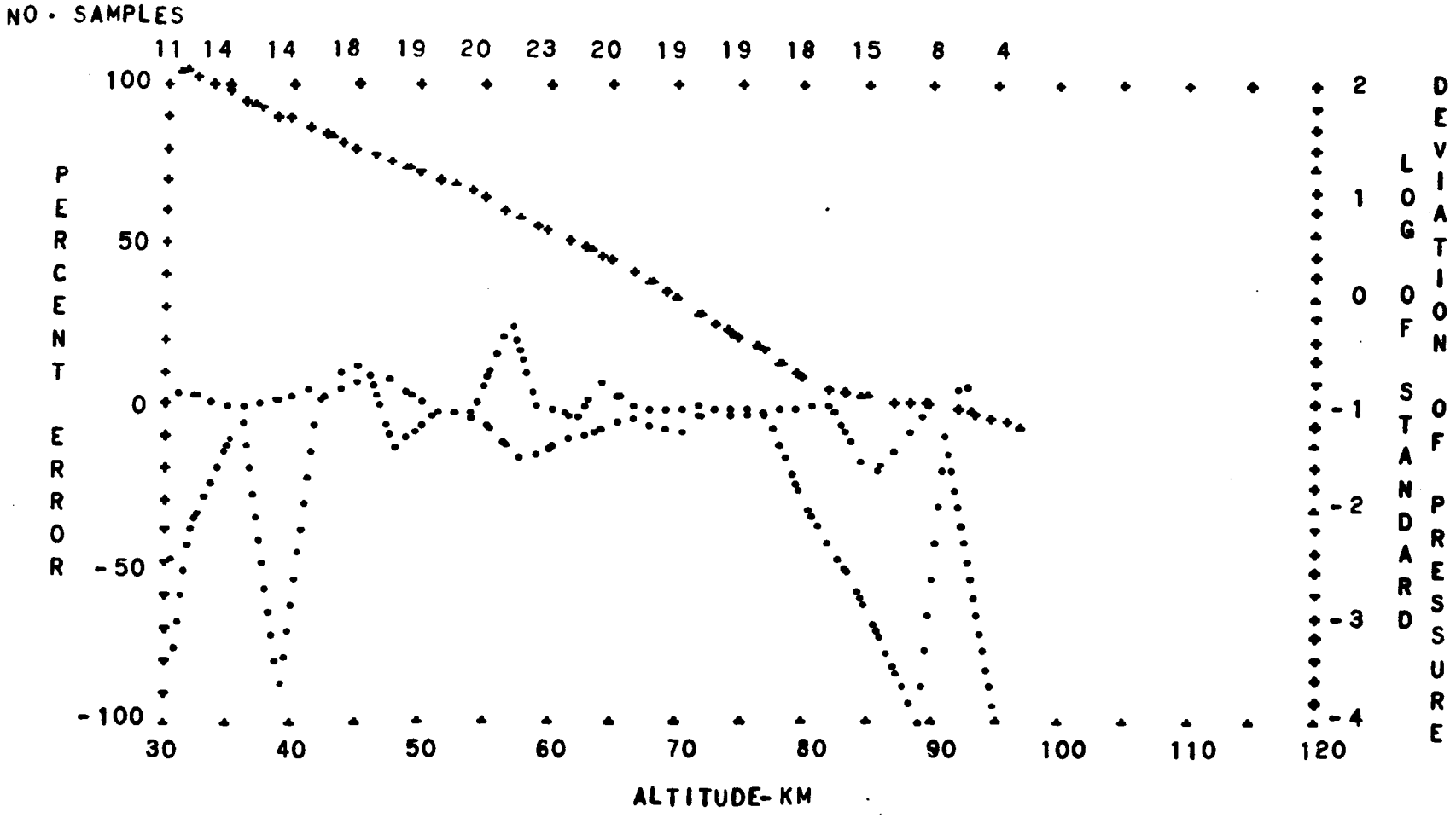

FIG. B-106. STANDARD DEVIATION OF PRESSURE AND PERCENT ERROR OF BUELL HYDROSTATIC EQUATION VERSUS ALTITUDE

HEMISPHERICAL MEAN WINTER EXTREME DIURNAL MEAN

PERCENT ERROR--DOTS LOG DEVIATION--CROSSES

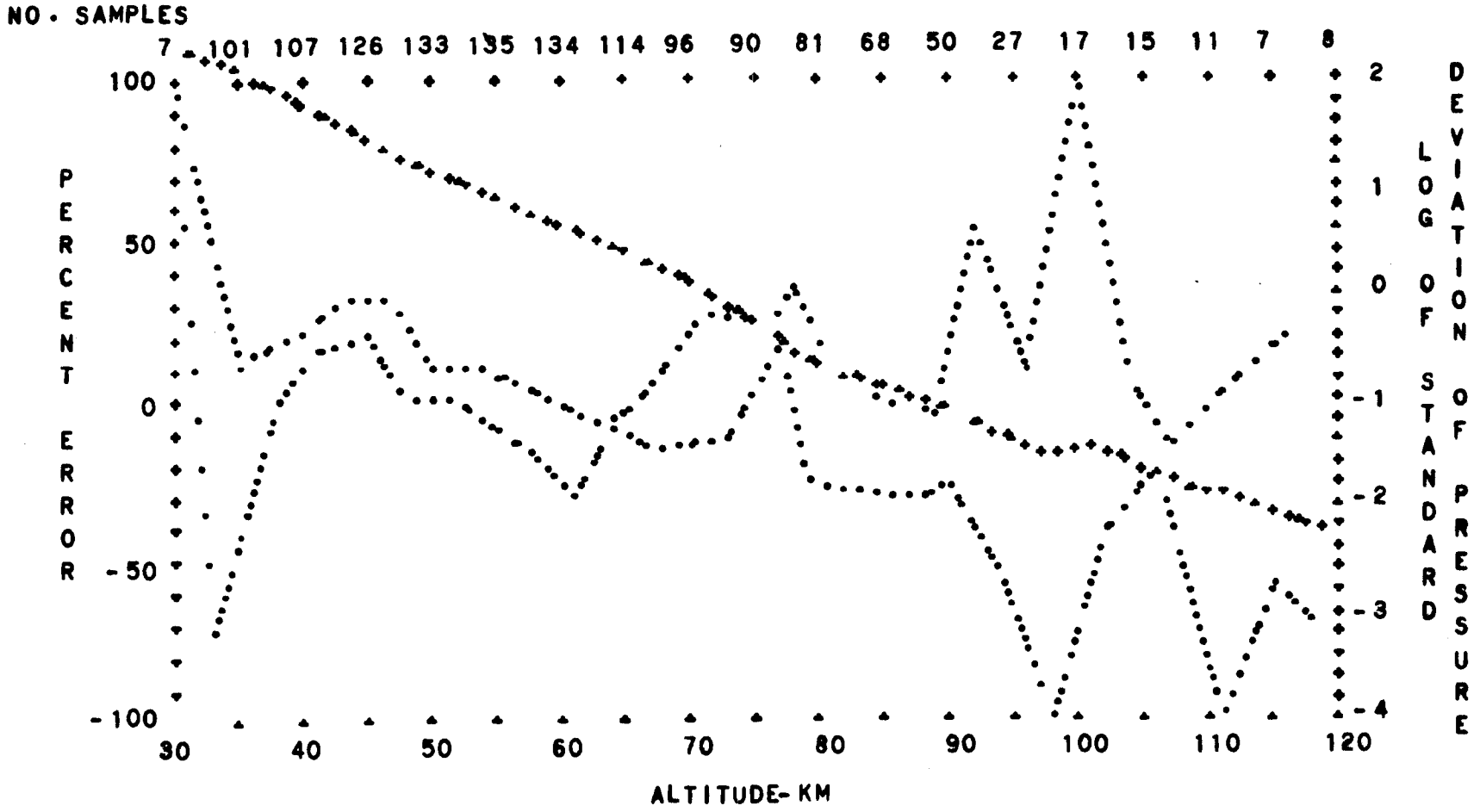

FIG. B-107. STANDARD DEVIATION OF PRESSURE AND PERCENT ERROR OF BUELL HYDROSTATIC EQUATION VERSUS ALTITUDE

HEMISPHERICAL MEAN ANNUAL MEAN DIURNAL TRANSITION

PERCENT ERROR--DOTS LOG DEVIATION--CROSSES

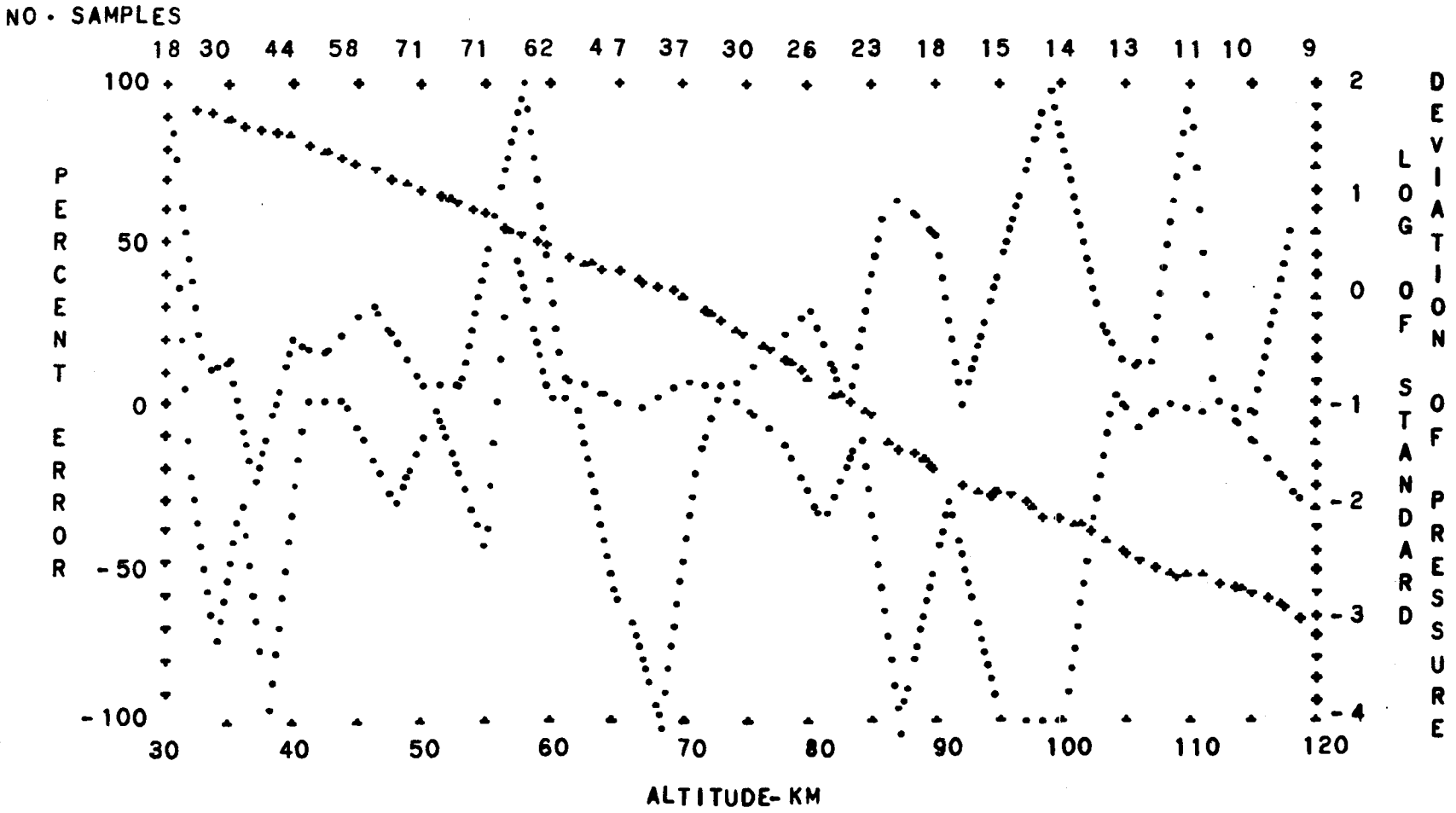

FIG. B-108. STANDARD DEVIATION OF PRESSURE AND PERCENT ERROR OF BUELL HYDROSTATIC EQUATION VERSUS ALTITUDE
HEMISPHERICAL MEAN ANNUAL MEAN DAYTIME
PERCENT ERROR--DOTS LOG DEVIATION--CROSSES

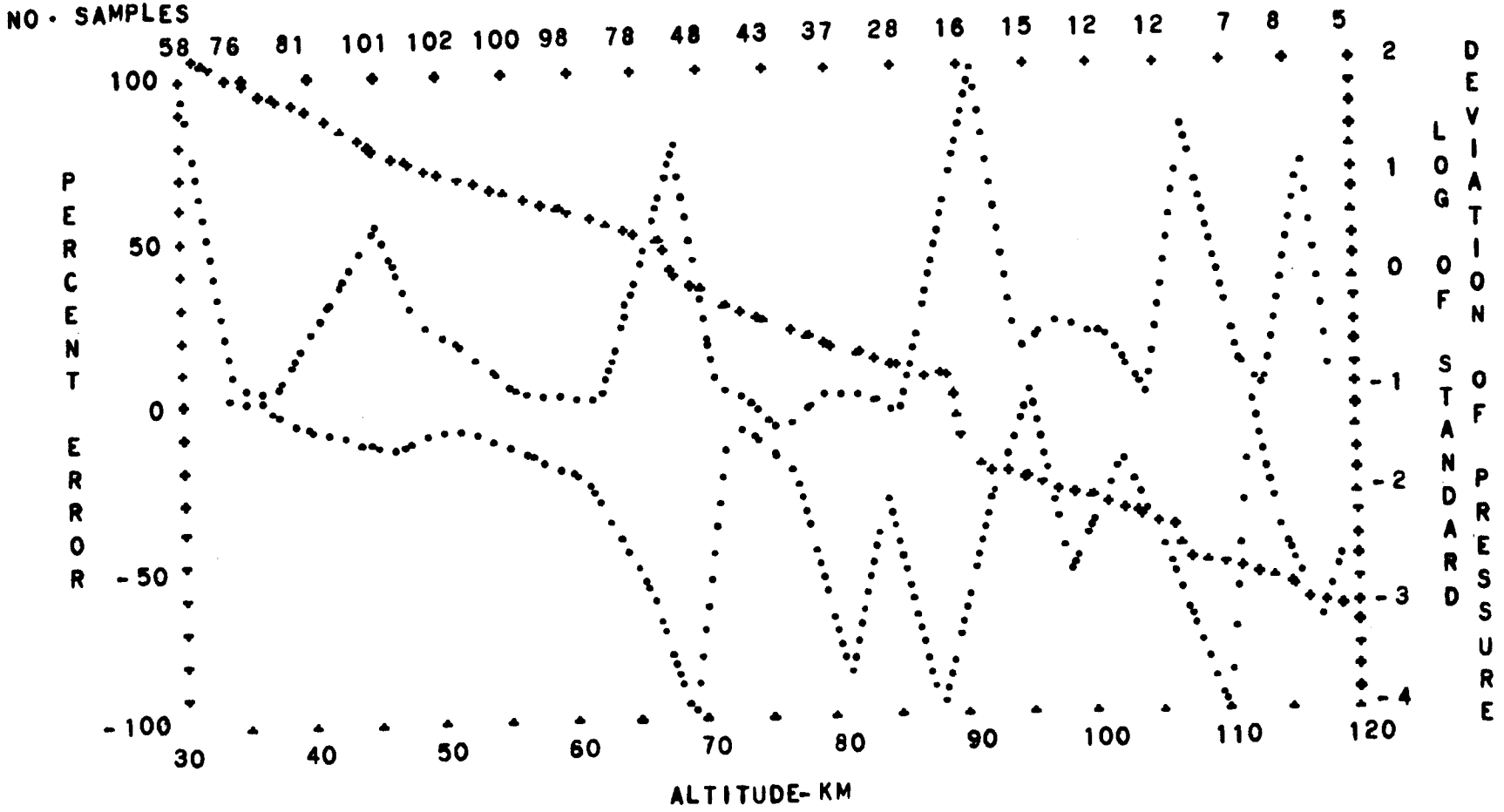

FIG. B-109. STANDARD DEVIATION OF PRESSURE AND PERCENT ERROR OF BUELL HYDROSTATIC EQUATION VERSUS ALTITUDE

HEMISPHERICAL MEAN ANNUAL MEAN NIGHTTIME

PERCENT ERROR--DOTS LOG DEVIATION--CROSSES

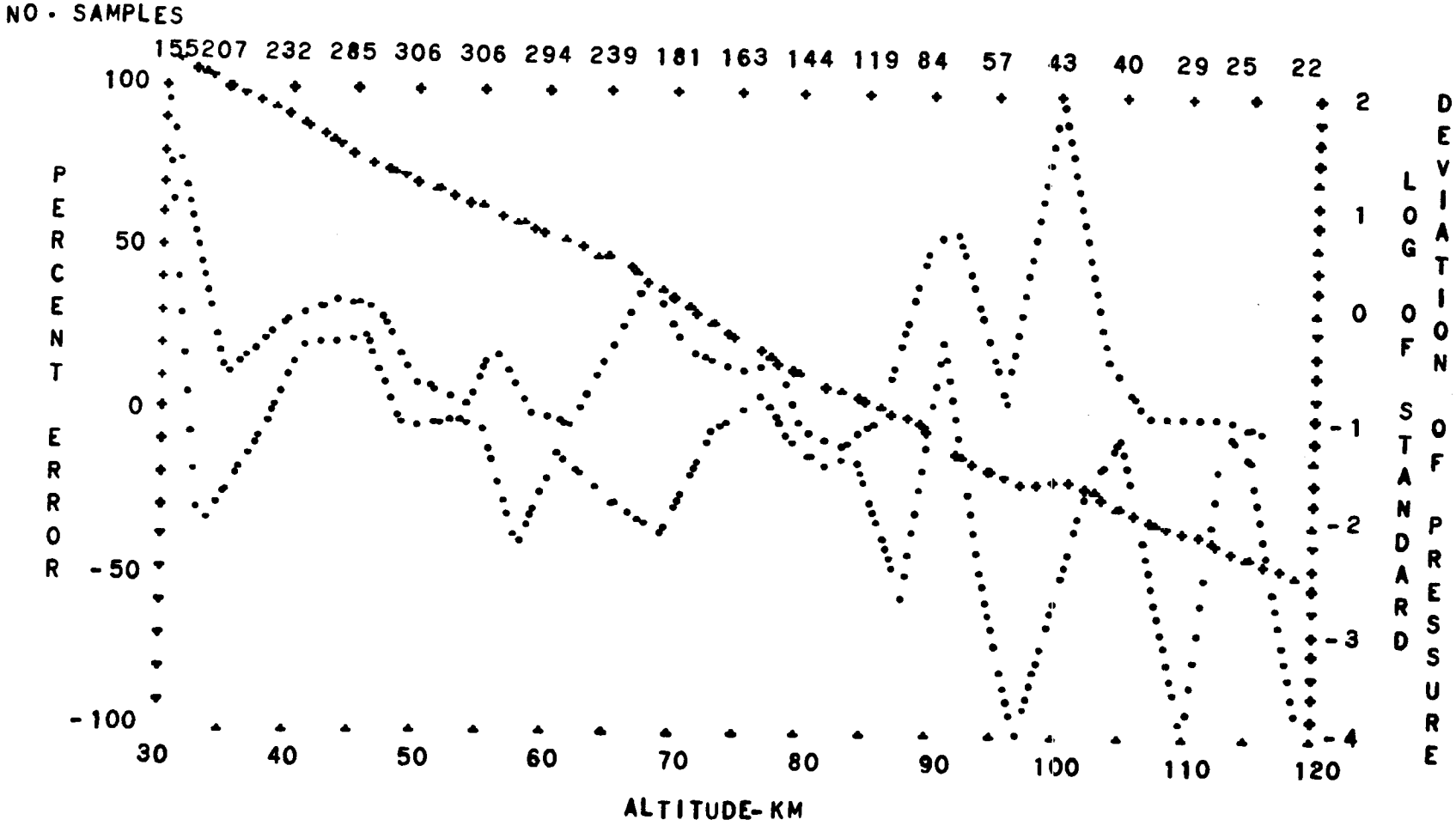

FIG. B-110. STANDARD DEVIATION OF PRESSURE AND PERCENT ERROR OF BUELL HYDROSTATIC EQUATION VERSUS ALTITUDE

HEMISPHERICAL MEAN ANNUAL MEAN DIURNAL MEAN

PERCENT ERROR--DOTS LOG DEVIATION--CROSSES

APPENDIX C

COMPUTATION PROCEDURE

The computations leading to the graphs of Appendix A and B were performed on an IBM 1620 digital computer and required several sequential stages of operation due to the limited storage capacity of this data processing system. The first stage dealt with the statistics of the 90 basic cells (not considering the equatorial belt) whose sounding distributions are depicted in Figures 2 and 4 of the basic text. This stage involved two programs:

The first program, called SUMMATION-1, calculated the sums of each thermodynamic variable, the sum of squares of these variables, and the sum of appropriate cross-products of these variables at each integral altitude for the number of samples in each of the basic cells. The input consisted of the processed sounding data within each latitude belt sorted according to altitude. The output of this program was presented on consecutive pairs of punched cards, each pair for a specific altitude of one cell, in accordance with the description in Tables C-1 and C-2. This output was used as the input to a second program, called STAT-1, which programmed the evaluation of the terms in the two Buell statistical equations being studied, and which determined the apparent discrepancies between the related terms of these equations for each altitude of each basic data cell. The output of STAT-1 was presented on consecutive sets of three punched cards, each set of 3 for a specific altitude within a particular cell, with a punch format as indicated in Tables C-3, C-4, and C-5.

In the second stage of calculation, the output of the SUMMATION-1 program, sorted according to altitude, was used as input ot a third computer program called STAT-2. This program performed three functions:

(1) It combined the summation values of the basic cells into compressed summations appropriate to the first-compression cells whose sounding distributions are presented in Figures 3 and 4 of the basic text.

(2) It also combined the summation values into compressed summations appropriate to those 5-second compression cells of Figure 3 of the basic text which represent compression across seasonal periods.

(3) It also performed the functions of the STAT-1 Program for each of these first-compression and second-compression cells. Summation cards 1 and 2, as well as Stat cards 1, 2, and 3, for these cells resulted from this program.

In the third stage, the summation data associated with those cells involved in the output of STAT-2 were used as input to STAT-3 Program. In a manner similar to the second-stage calculations, the data for the cells used as input were compressed, but this time, across latitude belts to yield

summation and stat cards appropriate to the remaining second-compression cells referred to in Figures 3 and 4 of the basic text and to the single third-compression cell referred to in Figure 4 of the basic text.

The interrelation between the summation input quantities and the stat output quantities applicable to all of the data cells is shown in Table C-6.

TABLE C-1

CONTENTS OF SUMMATION DATA CARD 1

COL. NO.	FORMAT	SYMBOL	COMMENTS
1-4	I4	IHT	Geometric Altitude in integer kilometers.
5-6	I2	ILAT	1-digit code designating latitude band (0 to 7).
7-8	I2	I	1-digit code designating season (0 to 9).
9-10	I2	J	1-digit code designating diurnal period (0 to 7).
11-24	E14.8	SD	Summation of Densities (kg/m^3).
25-38	E14.8	SDD	Summation of $(Densities)^2$.
39-52	E14.8	ST	Summation of Temperature (degrees K).
53-66	E14.8	STT	Summation of $(Temperature)^2$.

TABLE C-2

CONTENTS OF SUMMATION DATA CARD 2

COL. NO.	FORMAT	SYMBOL	COMMENTS
1-4	I4	IHT	Geometric altitude in integer kilometers.
5-6	I2	ILAT	1-digit code designating latitude (0 to 7).
7-8	I2	I	1-digit code designating season (0 to 9).
9-10	I2	J	1-digit code designating diurnal period (0 to 7).
11-24	E14.8	SP	Summation of pressure (newtons/m^2).
25-38	E14.8	SPP	Summation of(pressure)^2.
39-52	E14.8	SDT	Summation of density times temperature.
53-66	E14.8	SPD	Summation of pressure times density.
67-71	F5.0	EN	Number of samples in summations.

TABLE C-3

CONTENTS OF STAT CARD 1, STAT PROGRAM FORMAT 103

COL.NO.	FORMAT	SYMBOL	COMMENTS
1-4	I4	IHT	Geometric altitude in integer km. values.
5-8	I4	ISIJ	3-digit code specifying latitude, season, and diurnal period.
9-19	E11.5	AVGP	Average pressure in newtons/m^2.
20-30	E11.5	RMDT1	Average term of Buell Gas-Law Equation, i.e., the product of (R/M) times AVGD times AVGT. This product is a pressure in newton/m^2.
31-40	E10.4	RMDT2	Covariance term of Buell Gas-Law Equation.
41-45	F5.1	P1GL	Percent residual by which the sums of RMDT1 and RMDT2 fail to equal AVGP.
46-51	F6.1	P2GL	Percent contribution of RMDT1 to AVGP, i.e., (RMDT1 x 100)/AVGP.
52-57	F6.1	P3GL	Percent contribution of RMDT2 to AVGP, i.e., (RMDT2 x 100)/AVGP.
58-67	E10.4	AVGD	Average density in kg/m^3.
68-74	F7.1	AVGT	Average temperature in degrees Kelvin.
75-78	I4	N	Number of samples making up the average.
79-80	I2	N Card	Type number of data output card which is 1 in this instance.

TABLE C-4

CONTENTS OF STAT CARD 2, STAT PROGRAM FORMAT 104

COL. NO.	FORMAT	SYMBOL	COMMENTS
1-4	I4	IXHT	Geometric altitude in integer kilometers equal to IHT-2 to which altitude the contents of the particular card corresponds.
5-8	I4	ISIJ	3-digit code specifying latitude, season, and diurnal period.
9-18	E10.4	SLOPE	Partial derivative of SIGP with respect to geometric altitude (left side of Buell Hydrostatic Equation).
19-28	E10.4	GDR3(I,J)	Right side of Buell Hydrostatic Equation, i.e., 9.80665 (SIGD x RHOPD).
29-34	F6.1	P1HY	Departure of right side of equation from left side in percent, i.e., 100 - [GDR3(I,J) x 100]/SLOPE.
35-78	44X		
79-80	I2	N Card	Type number of data output card which is 2 in this instance.

See contents of Stat Card 3 for significance of SIGP, SIGD, and RHOPD.

TABLE C-5

CONTENTS OF STAT CARD 3, STAT PROGRAM FORMAT 105

COL. NO.	FORMAT	SYMBOL	COMMENTS
1-4	I4	IHT	Geometric altitude in integer kilometers.
5-8	I4	ISIJ	3-digit code specifying latitude, season, and diurnal period.
9-18	E10.4	SIGD	Standard deviation of density data.
19-24	F6.2	SIGT	Standard deviation of temperature data.
25-34	E10.4	SIGP	Standard deviation of pressure data.
35-40	F6.2	COEFD	Ratio (SIGD/AVGD) x 100.
41-46	F6.2	COEFT	Ratio (SIGT/AVGT) x 100.
47-52	F6.2	COEFP	Ratio (SIGP/AVGP) x 100.
53-57	F5.3	RHOPD	Coefficient of correlation between pressure and density.
58-62	F5.3	RHOPT	Coefficient of correlation between density and temperature.
63-74	12X		
75-78	I4	N	Number of samples involved in the calculations.
79-80	I2	N Card	Type number of data output card which is 3 in this instance.

TABLE C-6

INPUT DATA AND ITS RELATIONSHIP TO
PUNCHED INTERMEDIATE AND FINAL RESULTS OF BUELL-EQUATION ANALYSIS

		SIGD	SSTD	SSP	COEF	COTP	COPP	CVTD	RHTD	RHOD	AVGD	AVGT	AVGP	IHT	CARD	ITEM
	IHT													X		
	SD	X			X			X	X	X	X					
	SDD	X			X				X	X						
	ST		X			X		X	X			X				
INPUT	STT		X			X			X							
DATA	SP			X			X			X			X			
	SPP			X			X			X						
	SDT							X	X							
	SPD									X						
	AVGP												Y		1	3
	RMDT1										Y	Y			1	4
OUTPUT	RMDT2	I	I					Y	I						1	5
	P1GL							Y			Y	Y	Y		1	6
BUELL-	P2GL										Y	Y	Y		1	7
EQUATION	P3GL				I	I		Y	I				Y		1	8
RESULTS	SLOPE			Y										Y	2	3
	GDR3(I,J)	Y								Y					2	4
	P1HJ	Y		Y						Y				Y	2	5
	CARD	3	3	3	3	3	3	1	3	3	1	1	1	ALL OUTPUT CARD AND		
	ITEM	3	4	5	6	7	8	5	10	9	9	10	3	1	ITEM NUMBER	

X DESIGNATES RELATIONSHIP BETWEEN INPUT AND INTERMEDIATE QUANTITIES
Y DESIGNATES RELATIONSHIP BETWEEN INTERMEDIATE AND OUTPUT QUANTITIES
I DESIGNATES PUNCHED INTERMEDIATE VALUES IMPLICATE IN SPECIFIC OUTPUT

APPENDIX D

STATISTICAL DEFINITIONS AND SYMBOLS

The following equations serve to define certain statistical quantities used in the data processing related to this report.

1. The arithmetic average $\bar{x}$ of n separate observations of the variable x is defined by

$$\bar{x} = \frac{1}{n} \sum_{i=1}^{n} x_i \qquad \text{(D-1)}$$

2. The departure of any single observation x from the mean value $\bar{x}$ of a set of observations is designated by x′ so that

$$x' = x - \bar{x} \qquad \text{(D-2)}$$

Similarly

$$y' = y - \bar{y} \qquad \text{(D-3)}$$

3. The covariance c[x,y] between two variables x and y is defined as

$$c[x,y] \equiv \frac{1}{n} \sum_{i=1}^{n} (x_i' \; y_i') \qquad \text{(D-4)}$$

This can be expressed in a form more convenient for computation as

$$c[x,y] = \frac{n \, \Sigma(x,y) - \Sigma(x) \, \Sigma(y)}{n^2} \qquad \text{(D-5)}$$

4. The standard deviation of the variable x is defined by the relationship

$$\sigma[x] \equiv \left(\frac{\Sigma(x')^2}{n} \right)^{1/2} \qquad \text{(D-6)}$$

A more convenient computational form is

$$(\sigma[x])^2 = \frac{n\,\Sigma(x)^2 - (\Sigma x)^2}{n^2} \qquad \text{(D-7)}$$

5. The coefficient of correlation $r[x,y]$ between the two variables x and y is defined as

$$r[x,y] = \frac{c[x,y]}{\sigma[x]\ \sigma[y]} \qquad \text{(D-8)}$$

From Equations (D-5), (D-7), and (D-8) it follows that

$$r[x,y] = \frac{n\,\Sigma(xy) - (\Sigma x)(\Sigma y)}{\{n\,\Sigma(x^2) - (\Sigma x)^2\}^{1/2}\ \{n\,\Sigma(y^2) - (\Sigma y)^2\}^{1/2}} \qquad \text{(D-9)}$$

6. The above equations are the ones used in the calculations graphed in Appendices A and B. Each is written from the point of view that the sample size is relatively large. Small sample sizes are known to bias the results of the standard deviation so that this quantity tends to become increasingly too small as sample size is decreased. This situation is normally corrected by replacing n^2 by $n(n-1)$ in the denominator of Equation (D-7). Applying this factor to the standard deviation of each variable yields a corrected form for the covariance

$$c_r[x,y] = \left(\frac{n}{n-1}\right) \sigma[x] \cdot \sigma[y] \cdot r[x,y] \qquad \text{(D-10)}$$

The following tables provide a list of values of n/n-1 for sample sizes of 3 to 10 and represent the factors by which the various parts of the graphs in Appendix A should be increased to overcome the small sample bias.

TABLE D-1

CORRECTIONS TO BE APPLIED TO EQUATION D-10, AND HENCE TO THE GRAPHS OF APPENDIX A TO COMPENSATE FOR SMALL SAMPLE SIZE

n	n/(n-1)
3	1.50
4	1.33
5	1.25
6	1.20
7	1.17
8	1.14

TABLE D-1 (continued)

n	n/(n-1)
9	1.13
10	1.11
15	1.07
20	1.05
50	1.02
100	1.01

SECTION II

DENSITY DEVIATIONS FROM THE U. S. STANDARD ATMOSPHERE 1962 AND THE PATRICK REFERENCE ATMOSPHERE 1963

by

R. A. Minzner and S. Mello
GCA Corporation
GCA Technology Division
Bedford, Massachusetts

TABLE OF CONTENTS

INTRODUCTION

Standard and reference atmospheres have been prepared for various locations on earth and for other celestial bodies, frequently on the basis of minimal data and even on the basis of pure speculation. The utility of these standard or reference atmospheres is greatly increased when one has supplementary knowledge regarding the variability of the real atmosphere relative to these models. This present study is an attempt to improve the utility of both the U.S. Standard Atmosphere [1]* and the Patrick Reference Atmosphere [2] by comparing these models in the altitude range of 30 to 120 km with observations over various sites at various times of the year.

Comparisons such as those made in this study could be based on density, temperature, or pressure, or perhaps on some other atmospheric property. This study, however, is made on the basis of density data. This parameter was selected because many atmospheric-sounding techniques measure density more or less directly, and because most published sounding data include atmospheric density, even where temperature or pressure data are absent.

Summary of Results

This report consists primarily of a catalogue of two groups of machine plotted graphs. The first group consists of 48 graphs comparing various sets of data with the U.S. Standard Atmosphere. The second group consists of 48 graphs comparing the same sets of observed data with the Patrick Reference Atmosphere. Each graph contains a primary curve and two auxiliary curves for a particular combination of site r and season s, hereafter called the rs cell. The primary curve consists of a set of dots connected by a solid line, and represents the percentage departure of $\bar{\rho}(z)_{rs}$ the mean density-altitude profile for the rs cell from the density-altitude profile of a specified reference or standard atmosphere. The two auxiliary curves both designated by unconnected + signs fall one on each side of the primary curve, and deal with $\sigma(\rho)_{rs}$ the standard deviation of the data from which $\bar{\rho}(z)_{rs}$ was determined. One of these curves represents the percent departure of the quantity $[\bar{\rho}(z) + \sigma(\rho)]$ from the specified reference or standard atmosphere while the other represents a similar percent departure of the quantity $[\bar{\rho}(z) - \sigma(\rho)]_{rs}$.

*Numbers in [ ] are reference numbers.

ATMOSPHERIC SOUNDING DATA

Basic Data

The 48 density-altitude profiles which are compared with the two reference atmospheres were prepared from the data of 211 soundings. These come from summer and winter observations over 11 fixed land sites and 7 different ship sites. A chronological list of these soundings is given as Appendix A to this report. The density-altitude data for 176 of these soundings has been previously published as a data report [3].

Initial Grouping

Data for 10 or more soundings were available for most of the sites involved in the study. In the case of ship sites, however, the data consisted at most of the up and down legs of single soundings. Such a small sample size for seven or more sites was considered to be undesirable. Consequently, since five ship-based soundings existed for the subarctic latitude band, these five soundings were grouped together as a single site designated Ship (subarctic). The two remaining ship sites have latitudes 49°N and 74.5°N respectively, and could not readily be grouped with other soundings. These are designated Ship (midlat) and Ship (arctic) respectively. Thus, mean density-altitude profiles were computed for only three nominal ship sites. The three nominal ship sites plus the eleven fixed land sites are designated by name and latitude in Table 1.

Both summer and winter density-altitude profiles were available for most of the sites, and where possible separate mean-summer and mean-winter profiles were prepared for each site. Since soundings were available for only one of the two seasons at five of these sites, only 23 of the possible 28 different mean density-altitude profiles were prepared for the 14 sites. These are for the combinations of season and site designated by X's in Table 1.

The boundaries separating the winter half and the summer half of the year were taken to be identically 00:00 hours on March 16 GMT in the spring, and identically 00:00 hours on September 16 GMT in the fall. The period between September 16 and March 16 was taken to be the winter half of the year for northern-hemisphere sites. A reversal of this situation prevailed for the other half of the year.

Data Compression

Within the 23 X-type mean sets of data, no sounding is used more than once. The original soundings are reused however in 25 additional sets of data which were formed by compressing the 23 X-type sets in several different ways. One compression consists of a combining of the data from the various sites into latitudinal-mean sets according to the manner on which the site latitudes fall into the 15-degree-wide latitude bands designated in Table 1. Thus, the appropriate data for the tropical sites, Ascension, Kwajalein, and Guam, were

TABLE 1

LOCATION AND TIME OF SOUNDINGS

Site	Latitude	Seasons		
		Sum	Win	Ann
Ascension Island	07.98S	X		
Albuquerque	35.05N	X	X	O
Eglin AFB	30.38N		X	
Fort Churchill	58.73N	X	X	O
Guam	13.62N		X	
Holloman AFB	32.85N	X	X	O
Kwajalein	08.73N	X	X	O
Point Mugu	34.12N	X	X	O
Ship (Arctic)	74.57N	X		
Ship (Midlat)	49.0 N		X	
Ship (Subarctic)	59.6 N	X	X	
Wallops Island	37.83N	X	X	O
White Sands	31.11S	X	X	O
Woomera, Australia	32.38N	X	X	O
Tropics	7.5 - 22.5	Y	Y	O
Subtropics	22.5 - 37.5	Y	Y	O
Mid Latitudes	37.5 - 52.5	Y	Y	O
Subarctic	52.5 - 67.5	Y	Y	O
Arctic	67.5 - 82.5	Y		
All sites		Z	Z	W

combined into two latitudinal sets: a tropical summer set and a tropical winter set. Southern-hemisphere data were readily combined with northern-hemisphere data by virtue of the previously assigned convention regarding season. Similar compressions of summer and winter data were also made for soundings within four other latitudinal bends, with all of these compressions designated by Y's in Table 1. Thus, the data sets designated by Y's represent a regrouping of the entirety of the basic data, originally in 23 sets, now into 9 sets.

A further compression was made across all latitude bands. All the summer data for all sites were put into one set, and all the winter data for all sites were put into the other set. These two sets called All Sites are designated by Z's in Table 1. In this regrouping, the entirety of the basic data has been combined into two sets.

Yet another compression, that of the two Z sets into a single set, yielded a group of annual data for All Sites designated by W in Table 1.

Annual sets have also been formed by combining summer and winter sets for any particular site or latitude band. These are designated by O's in Table 1. No annual sets were formed for those sites or latitude bands not having both summer and winter data.

PROCESSING OF THE DATA

Initial Adjustment and Interpolation of the Basic Data

The basic data for this study consists of the density-altitude values from each of the 211 soundings listed in Appendix A. This data was obtained from the sources indicated in the associated references. Some of these density-altitude values were published for altitudes expressed in integer kilometer values, with densities expressed as kg per cubic meter. Others were published for altitude values expressed in kilometers plus decimal fractions of kilometers, with densities in grams per cubic centimeter. Still others were published for altitudes expressed in feet, and densities expressed in slugs per cubic ft. The initial step in the utilization of these data was the conversion to a single system of units, kilometers for altitude and kilograms per cubic meter for density, using standard conversion factors. In this form, the data were punched onto IBM cards.

Most of the data were still not in suitable form to permit combining the various soundings mathematically. This was because most density data were not presented for a common set of altitudes. This difficulty was eliminated by applying a semilogrithmic interpolation using a digital calculator. The process used is described in the following paragraph:

Assume that Z_e, ρ_e and Z_f, ρ_f are two consecutive density-altitude points in the tabulation of a sounding, such that

$$Z_e < Z_i \leq Z_f \tag{1}$$

where Z_i is the largest integer multiple of 1 km satisfying Relationship (1). If Z_i is equal to Z_f, no interpolation is required. If Z_i is less than Z_f but greater than Z_e, the density corresponding to Z_i is taken to be

$$\rho_i = \exp\left[\ln\rho_e + \frac{(\ln\rho_f - \ln\rho_e)}{(Z_f - Z_e)} (Z_i - Z_e)\right] \tag{2}$$

If consecutive data points are separated by 2 or more kilometers, several integer values of Z_i satisfy Relationship (1), and each of these values of Z_i is used in Equation (2). If consecutive data points are separated by less than 1 km, only those successive values which encompass integer-kilometer values are used in this interpolation process, and the remainder of the values are discarded.

Along with the density data for the appropriate integer-kilometer altitude, each data card is also punched with site and season information for sorting purposes.

Sorting Procedure

The data cards for all 211 soundings were first combined and chronologically sorted according to altitude. They were recombined in order of altitude from the highest to the lowest altitude, so that, for example, the entire set of data cards for 87 km altitude for all site-season cells followed directly after the similar set of data cards for 88 km. When the entire lot was then sorted according to site, fourteen sets of cards were established. Each of these sets was then sorted according to two seasons. Because of the absence of summer or winter data at particular sites, this sort yielded the 23 X-type sets shown in Table 1.

A card containing the greatest kilometer altitude of the set and the site-season code for the set was prepared for each of these 23 sets and placed at the beginning of each set. A card containing 1 in column 1 was placed at the end of each set, and the 23 sets were reassembled in alphabetical order of the initial letter of the site.

Computation of Averages

The program for computing averages was designed to compute and punch the following information on one card for each kilometer altitude in each of the 23 site-season sets:

n the number of values of density ρ at each altitude

$\bar{\rho}$ the average of n values of ρ at each altitude

$\overline{\rho^2}$ the average of n values of ρ^2 at each altitude

ID the site-season identification code

The equations for computing ρ and $\overline{\rho^2}$ are

$$\frac{\sum_{i=1}^{n} \rho_i}{n} = \bar{\rho} \tag{3}$$

$$\frac{\sum_{i=1}^{n} \rho_i^2}{n} = \overline{\rho^2} \tag{4}$$

When the values of n, $\bar{\rho}$, and $\overline{\rho^2}$ for lowest altitude in the set were computed, a separator card with a 1 in column 1 was punched.

The computation of the averages resulted in a considerable reduction in the total number of cards involved in the processing since this output yielded but one card per kilometer altitude per site. This computation was followed by the statistics program.

Statistics Program

The statistics program consisted of the application of five steps to each of the site-season sets of averages: The first of these involved the calculation of $\sigma(\rho)$ the standard deviation of the density values for each kilometer altitude. This was accomplished by the following equation:

$$\sigma(\rho) = \left[\frac{\overline{\rho^2} \cdot n - (\bar{\rho})^2 \cdot n}{n - 1} \right]^{1/2} \tag{5}$$

In the second step, PCDS the percent departure of $\bar{\rho}$ from ρST, the corresponding density of the U.S. Standard Atmosphere, was calculated as a means of detecting systematic differences of $\bar{\rho}(z)$ from the density-altitude profile of the U.S. Standard Atmosphere. This calculation was preceded by reading into the computer the set of standard atmosphere densities for altitudes from 1 km to 220 km, in increments of 1 km. The equation governing this calculation is

$$\text{PCDS} = \left(\frac{\bar{\rho} - \text{ST}}{\text{ST}} \right) 100 \tag{6}$$

The function, average density versus altitude, designated $\bar{\rho}(z)$ is essentially exponential, and when plotted on a semilogarithmic scale, small irregularities from one altitude to the next, resulting from irregularities in the original data, are frequently hardly discernible. When compared with the smooth computed density-altitude function $\rho ST(z)$, in the manner of Equation 6, the linear graph of the resulting values of PCDS appear to emphasize the irregularities in $\bar{\rho}(z)$ in a manner which often tends to obscure the systematic differences. Consequently, a 5-point smoothing process applied to the values of PCDS was incorporated into the calculation.

The third step in the statistic program was the smoothing of PCDS values over 5 km intervals using a set of smoothing formulae from Hildebrand [4]. This process is designed to yield a smoothed value SPCDS corresponding to each unsmoothed member PCDS in a site-season set. No data points are lost, but the smoothing formulae are different for the first two and the last two members of the set (i.e., for the two highest and two lowest altitudes), than for the remainder of the set. The successive members of the set of SPCDS values are designated by subscript indicies k as are the corresponding members of the set

of PDCS values. Thus, with index k = 1 designating the value associated with the highest altitude, and index k = N designating the value associated with the lowest altitude, we have:

$$SPCDS_1 = (3PCDS_1 + 2PCDS_2 + PCDS_3 - PCDS_5)/5 \quad (7)$$

$$SPCDS_2 = (4PCDS_1 + 3PCDS_2 + 2PCDS_3 + PCDS_4)/10 \quad (8)$$

$$SPCDS_k = (PCDS_{k-2} + PCDS_{k-1} + PCDS_k + PCDS_{k+1} + PCDS_{k+2})/5 \quad (9)$$

for those values of k meeting the condition $3 \leq n - 2$

$$SPCDS_{N-1} = (4PCDS_N + 3PCDS_{N-1} + 2PCDS_{N-2} + PCDS_{N-3})/10 \quad (10)$$

$$SPCDS_N = (3PCDS_N + 2PCDS_{N-1} + PCDS_{N-2} + PCDS_{N-4})/5 \quad (11)$$

Systematic differences between $\bar{\rho}$ and ρST are believed to be associated with layers whose thickness may be expressed in 10's of kilometers; consequently the 5-point smoothing should not significantly affect such differences, if they do exist.

The fourth step in the statistics program consisted of the generation of $S\bar{\rho}$, a smoothed value of average density, corresponding to each of the values of SPCD in a site-season set. This quantity is generated by the following equation:

$$S\bar{\rho}_k = \rho ST_k + \left[(SPCDS_k \cdot \rho ST_k)/100 \right] \quad (12)$$

The fifth step of the statistics program consisted of the generation of values for two additional quantities, UB and LB. These are the percentage of deviations from ρST_k, of $S\bar{\rho}_k$ plus and minus, respectively, the corresponding value of $\sigma(\rho)_k$ which was computed in step one. The values of UB and LB, when plotted as a function of altitude, provide a kind of smoothed set of upper and lower bounds, in terms of percentage deviation from the standard, within which about 67% of the data making up the altitude profile of SPCDS is located. Accordingly, these quantities are designated UB (upper bound) and LB (lower bound). They are computed by the following equations:

$$UB = \left[\frac{S\bar{\rho} + \sigma(\rho) - \rho ST}{\rho ST} \right] 100 \quad (13)$$

$$LB = \left[\frac{S\bar{\rho} - \sigma(\rho) - \rho ST}{\rho ST} \right] 100 \quad (14)$$

TABLE 2 PERCENT DEVIATION OF THE MEAN ATMOSPHERIC SUMMER DENSITY OVER ALBUQUERQUE FROM DENSITIES OF THE U.S. STANDARD ATMOSPHERE

Z	MEAN RHO	SMOOTH RHO	N	D	SMOOTH D	D1	D2
67.	.1735E-03	.1716E-03	11.	.3383E 02	.3238E 02	.5821E 01	.5894E 02 AU LS
66.	.1870E-03	.1876E-03	11.	.2709E 02	.2752E 02	.4306E 01	.5074E 02 AU LS
65.	.2020E-03	.2044E-03	11.	.2121E 02	.2267E 02	.4550E 00	.4488E 02 AU LS
64.	.2189E-03	.2237E-03	11.	.1620E 02	.1876E 02	-.4281E 01	.4180E 02 AU LS
63.	.2444E-03	.2479E-03	11.	.1500E 02	.1665E 02	-.3143E 01	.3644E 02 AU LS
62.	.2735E-03	.2764E-03	11.	.1428E 02	.1551E 02	-.1617E 01	.3264E 02 AU LS
61.	.3150E-03	.3113E-03	15.	.1654E 02	.1519E 02	-.1825E 01	.3221E 02 AU LS
60.	.3534E-03	.3523E-03	15.	.1552E 02	.1517E 02	-.7218E 00	.3107E 02 AU LS
59.	.3965E-03	.3981E-03	15.	.1461E 02	.1510E 02	-.1166E 00	.3032E 02 AU LS
58.	.4492E-03	.4472E-03	16.	.1492E 02	.1441E 02	-.1256E 01	.3009E 02 AU LS
57.	.5026E-03	.5014E-03	16.	.1391E 02	.1365E 02	-.1323E 01	.2862E 02 AU LS
56.	.5629E-03	.5610E-03	16.	.1311E 02	.1274E 02	-.2570E 01	.2805E 02 AU LS
55.	.6263E-03	.6250E-03	16.	.1168E 02	.1147E 02	-.3202E 01	.2614E 02 AU LS
54.	.6949E-03	.6949E-03	16.	.1006E 02	.1006E 02	-.3337E 01	.2346E 02 AU LS
53.	.7712E-03	.7700E-03	16.	.8575E 01	.8410E 01	-.3885E 01	.2070E 02 AU LS
52.	.8561E-03	.8567E-03	16.	.6882E 01	.6970E 01	-.4557E 01	.1849E 02 AU LS
51.	.9508E-03	.9600E-03	16.	.4840E 01	.5855E 01	-.5055E 01	.1676E 02 AU LS
50.	.1073E-02	.1078E-02	16.	.4489E 01	.5041E 01	-.6280E 01	.1636E 02 AU LS
49.	.1215E-02	.1215E-02	16.	.4489E 01	.4499E 01	-.6655E 01	.1565E 02 AU LS
48.	.1376E-02	.1371E-02	16.	.4503E 01	.4125E 01	-.6578E 01	.1483E 02 AU LS
47.	.1559E-02	.1551E-02	16.	.4176E 01	.3692E 01	-.6891E 01	.1427E 02 AU LS
46.	.1765E-02	.1768E-02	16.	.2969E 01	.3185E 01	-.7888E 01	.1425E 02 AU LS
45.	.2012E-02	.2017E-02	16.	.2324E 01	.2600E 01	-.7618E 01	.1282E 02 AU LS
44.	.2303E-02	.2303E-02	16.	.1952E 01	.1987E 01	-.8357E 01	.1233E 02 AU LS
43.	.2640E-02	.2637E-02	16.	.1581E 01	.1483E 01	-.9428E 01	.1239E 02 AU LS
42.	.3028E-02	.3022E-02	16.	.1108E 01	.9201E 00	-.1152E 02	.1336E 02 AU LS
41.	.3472E-02	.3465E-02	16.	.4513E 00	.2499E 00	-.1189E 02	.1239E 02 AU LS
40.	.3976E-02	.3974E-02	16.	-.4930E 00	-.5194E 00	-.9526E 01	.6487E 01 AU LS
39.	.4562E-02	.4573E-02	16.	-.1398E 01	-.1156E 01	-.7397E 01	.5084E 01 AU LS
38.	.5245E-02	.5279E-02	16.	-.2265E 01	-.1626E 01	-.8292E 01	.5039E 01 AU LS
37.	.6106E-02	.6116E-02	16.	-.2076E 01	-.1904E 01	-.8030E 01	.4220E 01 AU LS
36.	.7120E-02	.7112E-02	16.	-.1899E 01	-.2008E 01	-.7799E 01	.3782E 01 AU LS
35.	.8304E-02	.8307E-02	16.	-.1883E 01	-.1836E 01	-.7982E 01	.4308E 01 AU LS
34.	.9698E-02	.9730E-02	16.	-.1915E 01	-.1591E 01	-.8431E 01	.5248E 01 AU LS
33.	.1141E-01	.1141E-01	16.	-.1408E 01	-.1365E 01	-.8895E 01	.6164E 01 AU LS
32.	.1344E-01	.1339E-01	16.	-.8483E 00	-.1162E 01	-.9030E 01	.6705E 01 AU LS
31.	.1567E-01	.1566E-01	16.	-.7725E 00	-.8057E 00	-.8950E 01	.7339E 01 AU LS
30.	.1825E-01	.1834E-01	16.	-.8690E 00	-.3613E 00	-.9472E 01	.8749E 01 AU LS
29.	.2145E-01	.2163E-01	16.	-.1303E 00	.7107E 00	-.8152E 01	.9574E 01 AU LS
28.	.2528E-01	.2616E-01	16.	.8135E 00	.4334E 01	-.4127E 01	.1279E 02 AU LS
27.	.3062E-01	.3318E-01	16.	.4512E 01	.1326E 02	-.3276E 01	.2980E 02 AU LS
26.	.4020E-01	.4380E-01	16.	.1734E 02	.2786E 02	-.3362E 02	.8935E 02 AU LS
25.	.5763E-01	.5717E-01	16.	.4377E 02	.4262E 02	-.1198E 03	.2051E 03 AU LS
24.	.8114E-01	.7373E-01	16.	.7286E 02	.5709E 02	-.2190E 03	.3332E 03 AU LS
23.	.9606E-01	.9322E-01	16.	.7463E 02	.6947E 02	-.2128E 03	.3518E 03 AU LS
22.	.1141E 00	.1339E 00	16.	.7687E 02	.1076E 03	-.1774E 03	.3926E 03 AU LS
21.	.1357E 00	.1814E 00	16.	.7922E 02	.1396E 03	-.1400E 03	.4193E 03 AU LS
20.	.2974E 00	.2412E 00	5.	.2344E 03	.1713E 03	-.3188E 03	.6614E 03 AU LS

The quantities resulting from steps 3 and 5, i.e., SPCDS, UB and LB for each altitude within a site-season set, comprise the most significant results of the calculation, and these are then machine plotted as a function of altitude for each of the 23 basic site season sets of data.

In addition, seven of the computed quantities were tabulated as a function of altitude for each of the 23 basic site-season sets of data (as well as for the remaining 25 site-season sets of data designated in Table I for both the U. S. Standard and Patrick reference atmospheres). A sample tabulation is presented as Table 2, where the headings are related to the symbols in the equations as indicated in Table 3. The totality of the tabulation of the type of Table 2 for all cases examined consisted of several hundred pages. Because of its great bulk, this tabulation is not included in this report.

TABLE 3

RELATION BETWEEN SYMBOLS IN TEXT AND HEADINGS USED IN TABLE 2

Symbol	Heading
$\underline{Z}$	Z
$\underline{\rho}$	MEAN RHO
$S\underline{\rho}$	SMOOTH RHO
n	N
PCDS	D
SPCDS	SMOOTH D
UB	D1
LB	D2

Preparation of Compressed Sets

The preparation of the results of the several sets of compressed data, as designated by symbols Y, Z, W, and O in Table 1, did not require a return to the basic interpolated data. Rather, the various averages computed for the basic 23 sets of data served as the starting data for establishing new sets of averages in the averages-of-averages program. The simplest compression consisted of combining summer and winter data for a particular site as designated by O in Table 1. In this instance, the summer averages and winter averages for a single site were hand selected, combined, and sorted according to decreasing altitude. The set was preceded by a new header card designating the greatest altitude and ID of the new compressed sit-season designation. It was followed by a separator card which is blank except for a 1 in column 1.

The computer reads the quantities n, $\bar{\rho}$, and $\overline{\rho^2}$ on the first card for a given height and computes the corresponding quantities $n\rho$ and $n\overline{\rho^2}$. It performs the same operation on the data for each of m cards for a given altitude. The m values of n, $n\rho$, and of $n\rho^2$ are then combined to get the following three quantities [1]: M, the sum of the m values of n [2], $\bar{\bar{\rho}}$, the average of the m values of $\bar{\rho}$ [3], and $\overline{\overline{\rho^2}}$, the average of the m values of ρ^2. These quantities are obtained using the following equations:

$$\sum_{j=1}^{m} n_j = M \tag{15}$$

$$\frac{\sum_{j=1}^{m} (n\bar{\rho})_j}{M} = \bar{\bar{\rho}} \tag{16}$$

$$\frac{\sum_{j=1}^{m} (n\overline{\rho^2})_j}{M} = \overline{\overline{\rho^2}} \tag{17}$$

These quantities, along with the site-season ID for the compressed set, are then punched out for each altitude in the compressed site-season set, and these data serve as new input to the statistics program.

By combining the averages of the appropriate basic 23 sets of site-season data, the output is readily prepared for the graphs of all 48 site-seasons sets designated in Table 1. These graphs, using the U. S. Standard Atmosphere as a reference model, are designated Figures 1S through 48S.

Comparisons Relative to the Patrick Reference Atmosphere

The particular model, relative to which the data of the several site-season sets are compared, is introduced into the calculations in the statistics program. After the first 48 sets of output were computed and plotted relative to the U. S. Standard Atmosphere, the averages for each of the 48 site season sets were reintroduced into the statistics

program. This time, however, the Patrick Reference Atmosphere was used in place of the U. S Standard Atmosphere. This procedure resulted ultimately in the second set of 48 graphs designated 1P to 48P.

The study and analysis of these graphs is beyond the scope of this report but is being conducted independently.

REFERENCES

1. United States Standard Atmosphere, 1962. National Aeronautics and Space Administration, U.S. Air Force, and U.S. Weather Bureau, Government Printing Office, Washington, D.C.

2. O. E. Smith and D. K. Weidner, "A Reference Atmosphere for Patrick A.F.B., Florida, Annual (1963 revision)," NASA TMX-53139, Marshall Space Flight Center, Huntsville Alabama, September 23, 1964.

3. R. A. Minzner and S. M. Jacobson, "Density-Altitude Data from 150 Rocket Flights and 26 Searchlight Probings - 1947 through 1964," GCA Tech. Rpt. 66-4-N on contract NAS10-1225, 1964.

4. F. B. Hildebrand, Introduction to Numerical Analysis, p. 295, McGraw-Hill Book Co., Inc., 1956.

GRAPHICAL RESULTS

FIGURE 1S. PERCENT DEVIATION OF MEAN ATMOSPHERIC SUMMER DENSITIES OVER ASCENSION ISLAND FROM DENSITIES OF THE U.S. STANDARD ATMOSPHERE

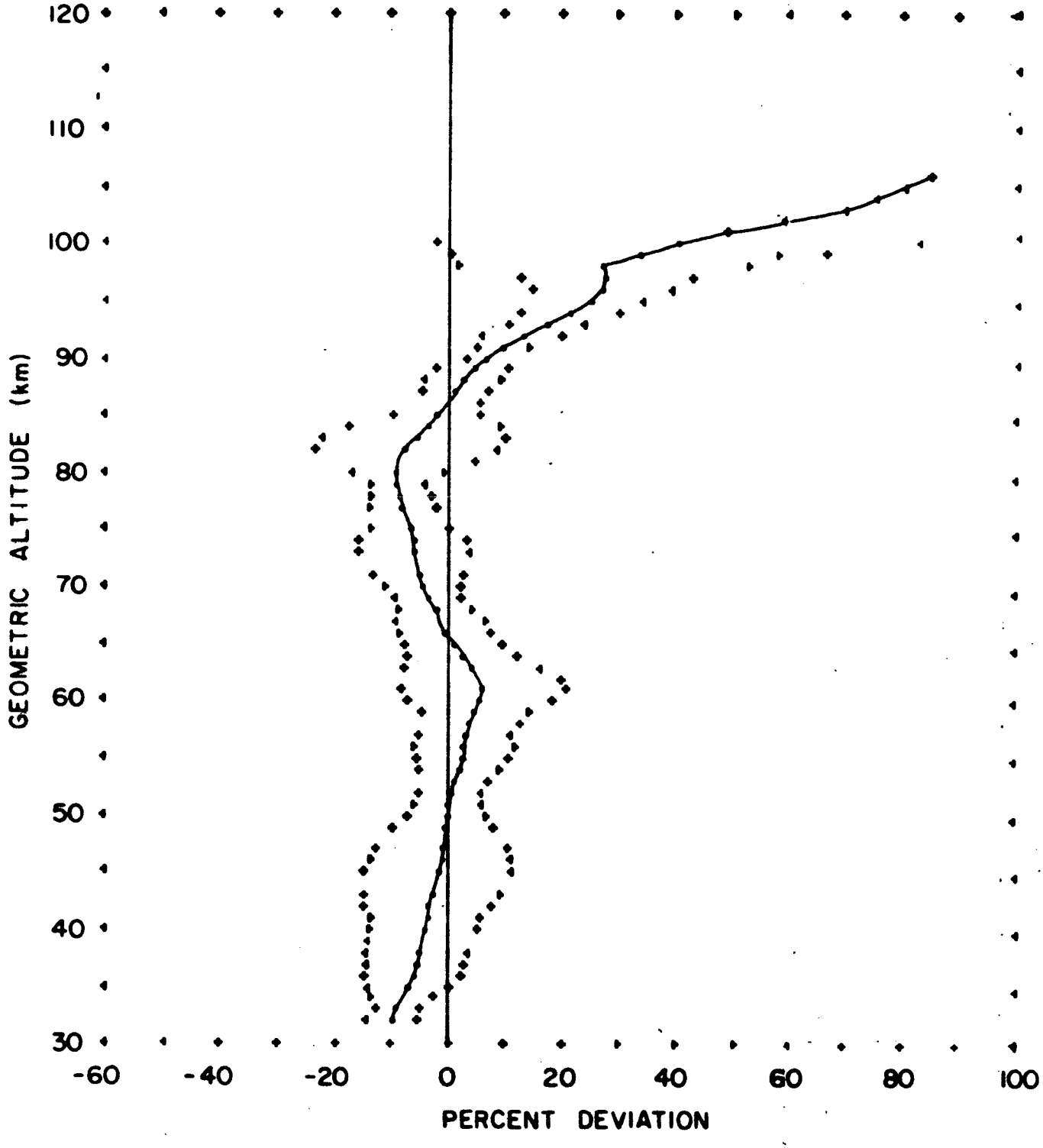

FIGURE 2S. PERCENT DEVIATION OF MEAN ATMOSPHERIC SUMMER DENSITIES OVER ALBUQUERQUE FROM DENSITIES OF THE U.S. STANDARD ATMOSPHERE

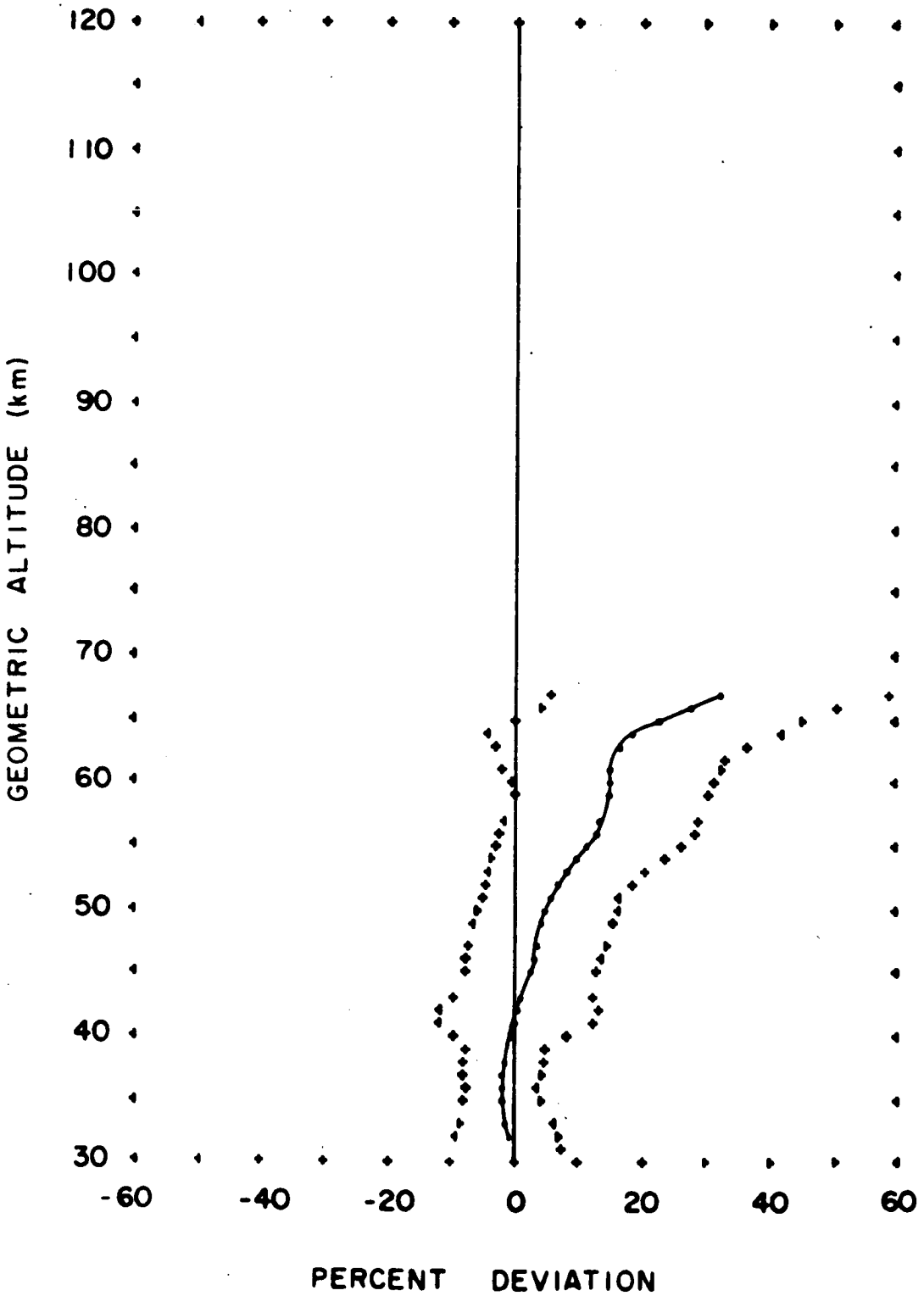

FIGURE 35. PERCENT DEVIATION OF MEAN ATMOSPHERIC WINTER DENSITIES OVER ALBUQUERQUE FROM DENSITIES OF THE U.S. STANDARD ATMOSPHERE

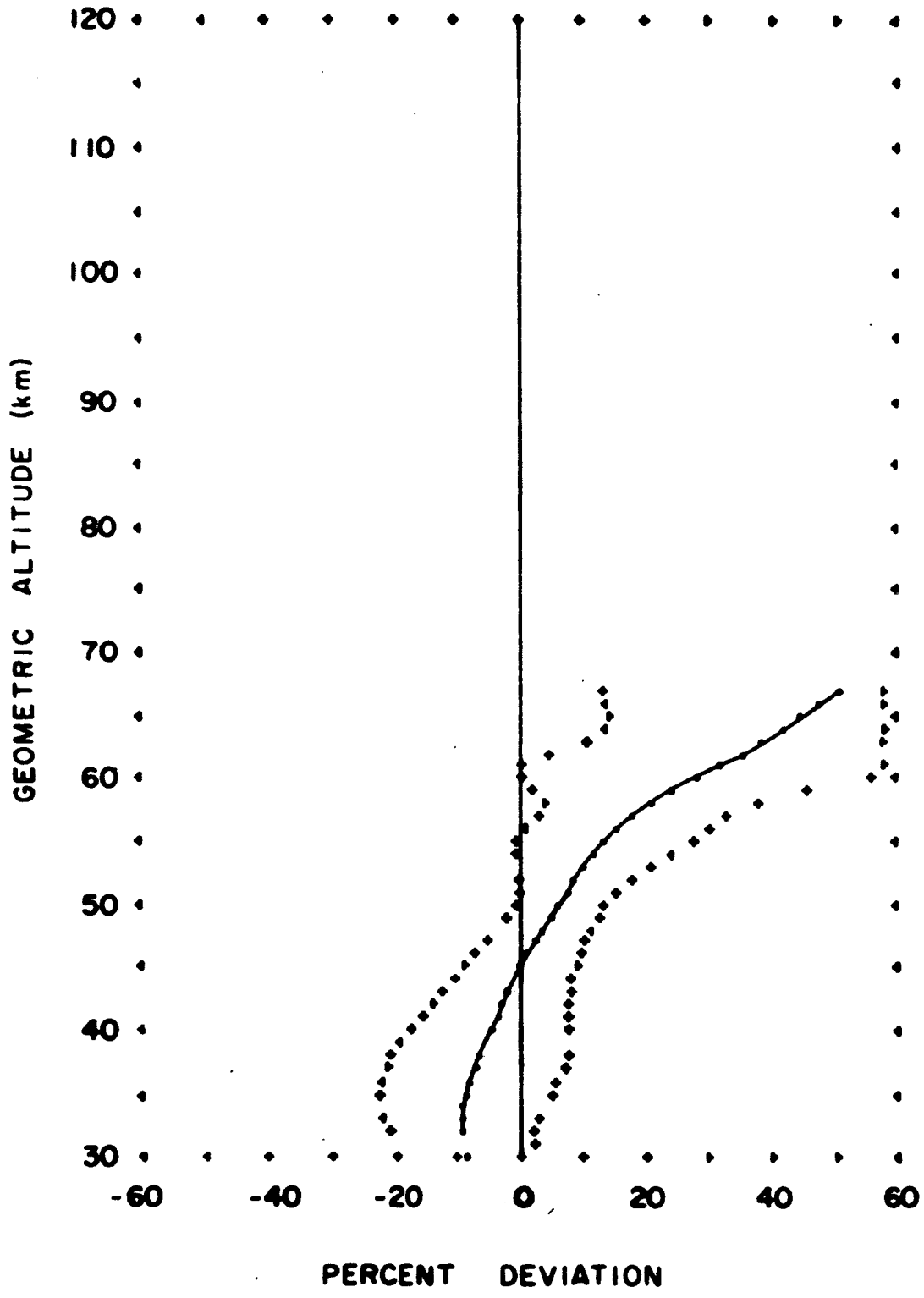

FIGURE 45. PERCENT DEVIATION OF MEAN ATMOSPHERIC ANNUAL DENSITIES OVER ALBUQUERQUE FROM DENSITIES OF THE U.S. STANDARD ATMOSPHERE

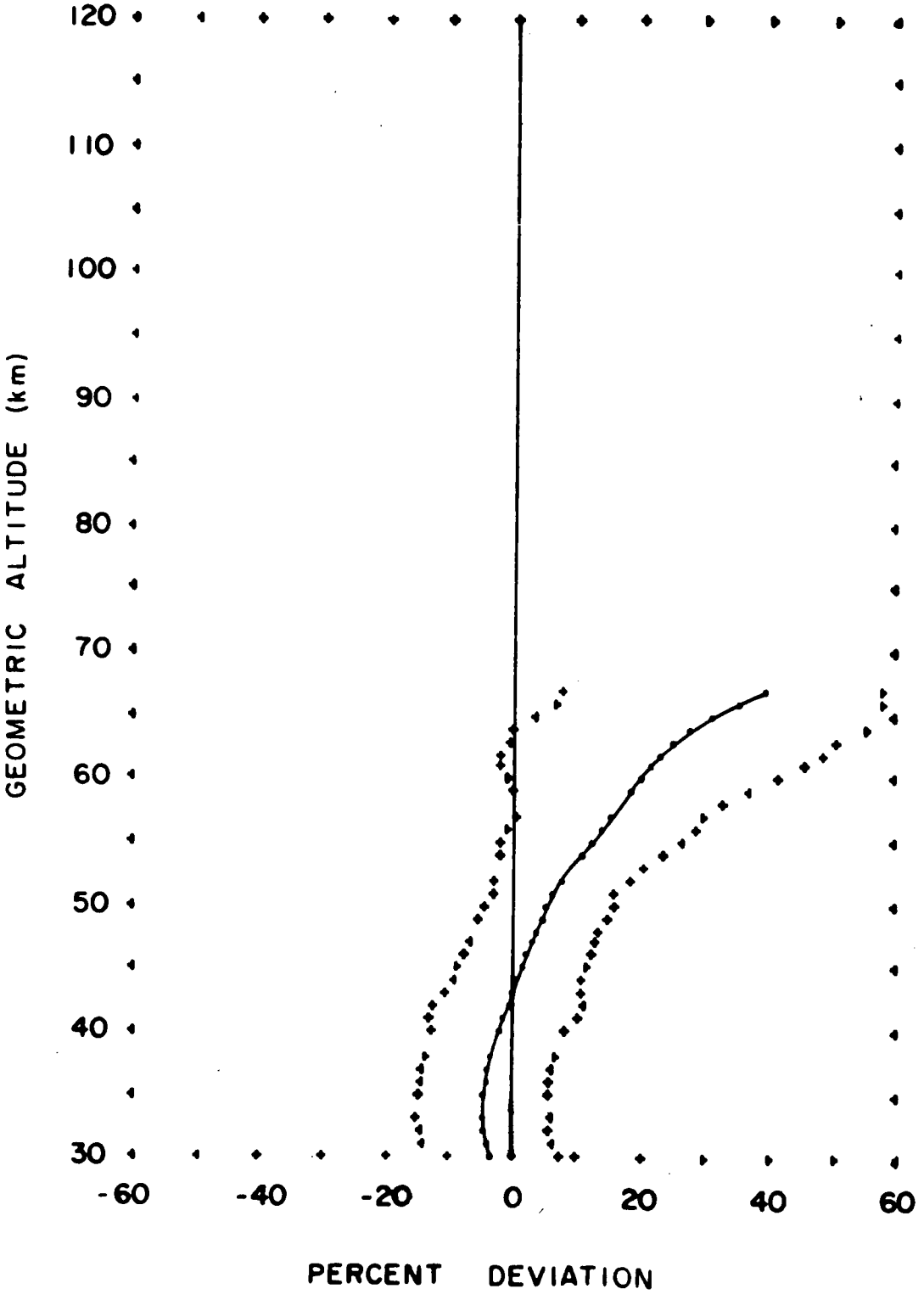

FIGURE 55. PERCENT DEVIATION OF MEAN ATMOSPHERIC WINTER DENSITIES OVER EGLIN RANGE FROM DENSITIES OF THE U.S. STANDARD ATMOSPHERE

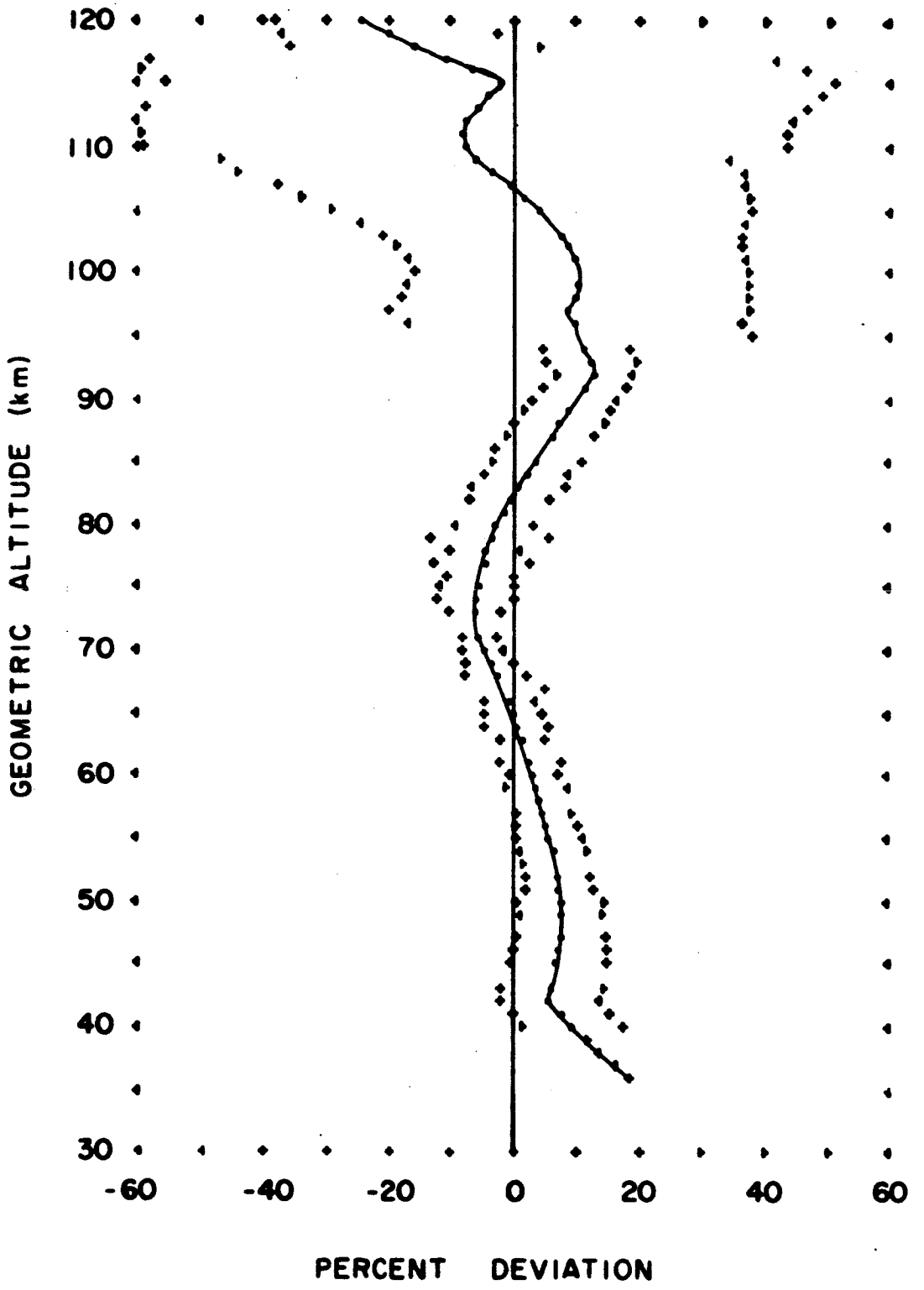

FIGURE 6S. PERCENT DEVIATION OF MEAN ATMOSPHERIC SUMMER DENSITIES OVER FORT CHURCHILL FROM DENSITIES OF THE U.S. STANDARD ATMOSPHERE

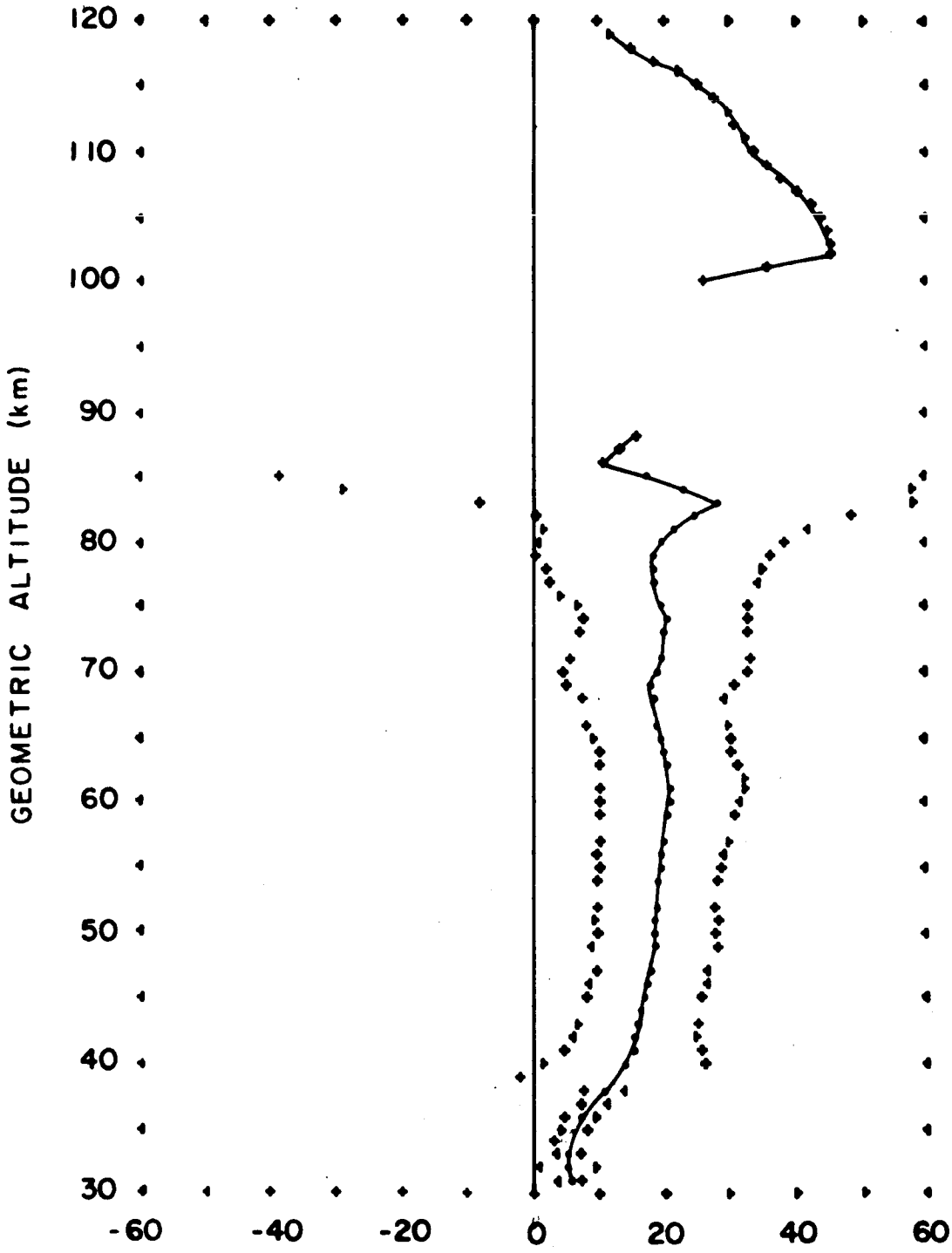

FIGURE 7S. PERCENT DEVIATION OF MEAN ATMOSPHERIC WINTER DENSITIES OVER FORT CHURCHILL FROM DENSITIES OF THE U.S. STANDARD ATMOSPHERE

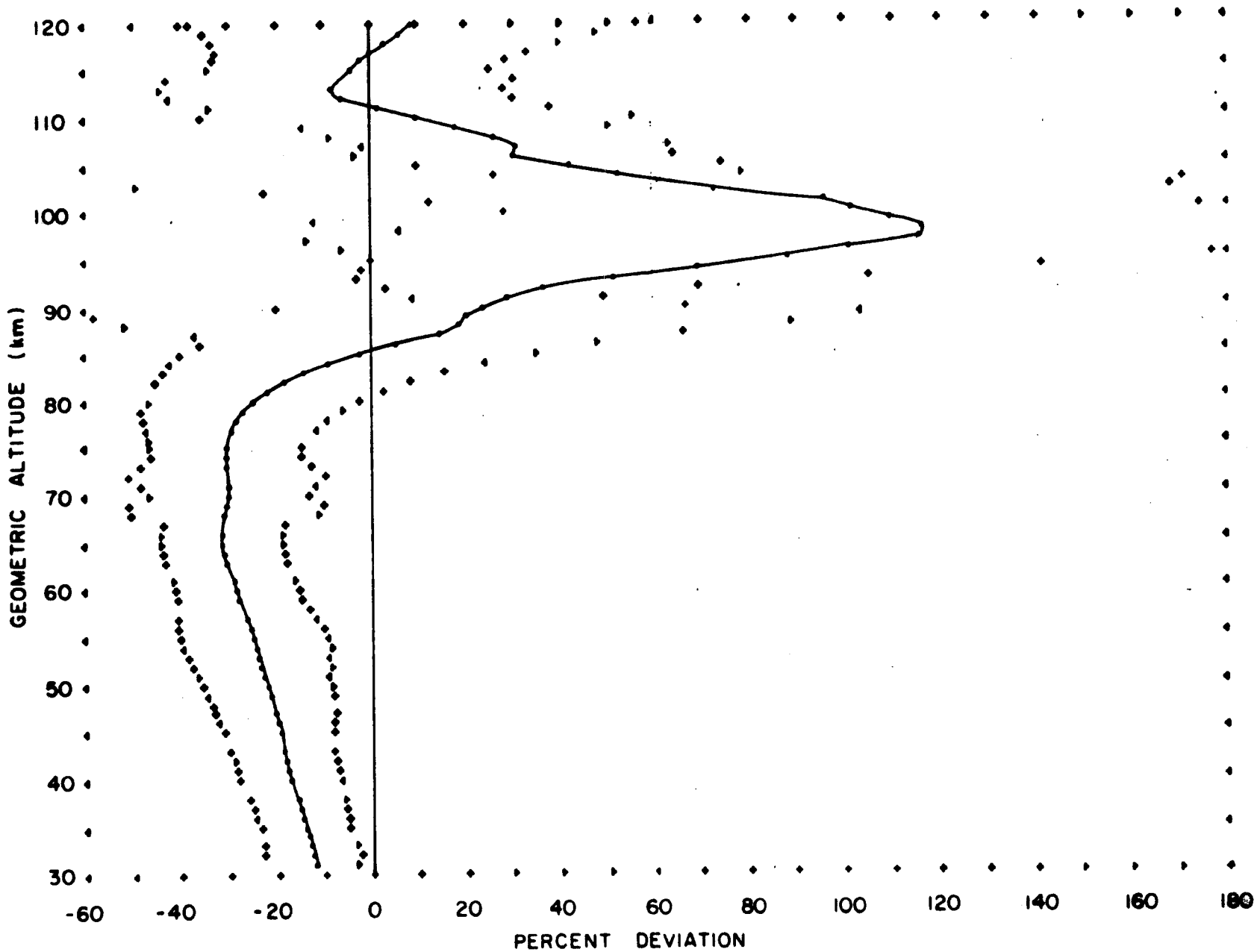

FIGURE 85. PERCENT DEVIATION OF MEAN ATMOSPHERIC
ANNUAL DENSITIES OVER FORT CHURCHILL
FROM DENSITIES OF THE U.S. STANDARD ATMOSPHERE

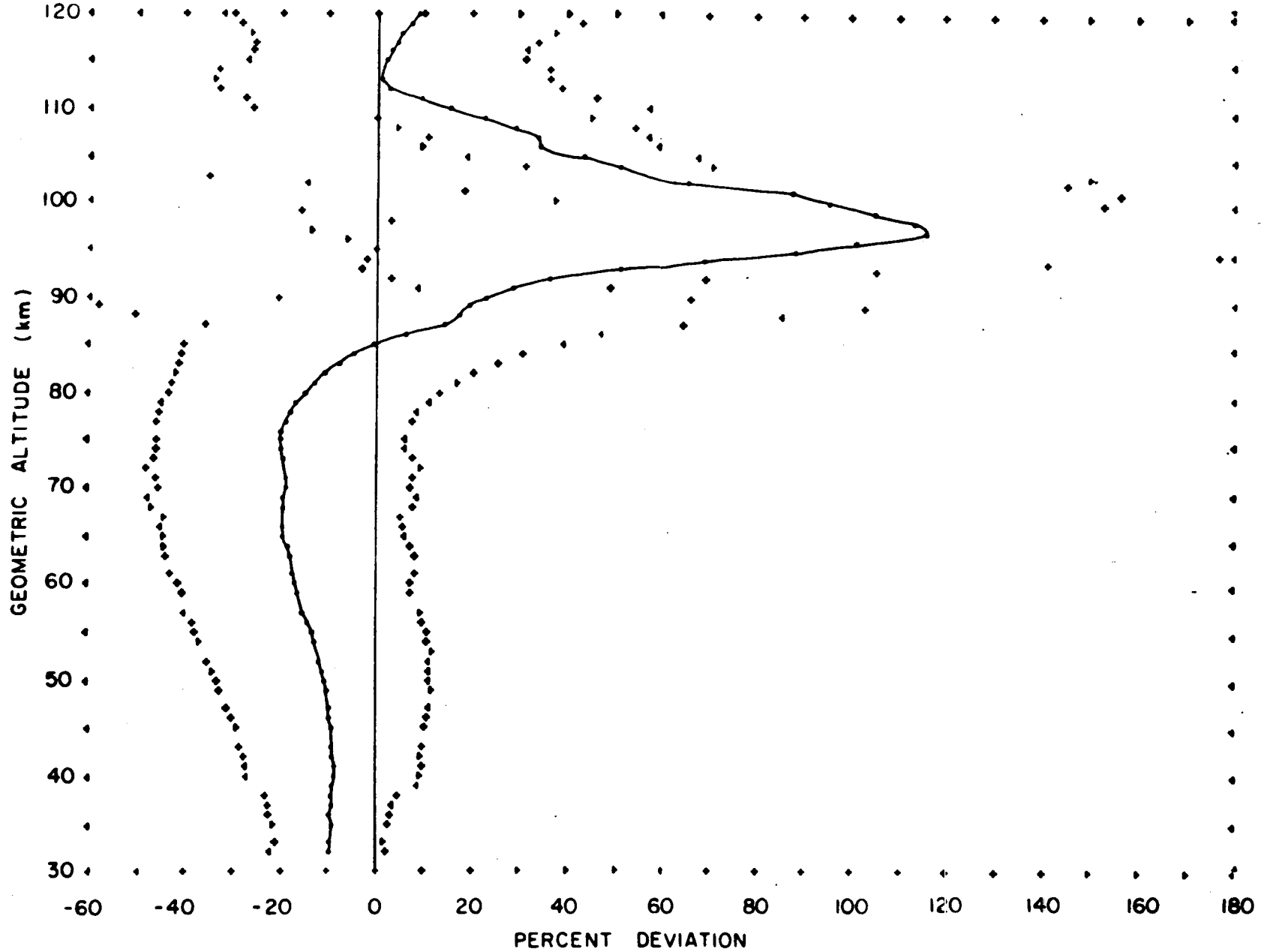

FIGURE 9S. PERCENT DEVIATION OF MEAN ATMOSPHERIC WINTER DENSITIES OVER GUAM FROM DENSITIES OF THE U.S. STANDARD ATMOSPHERE

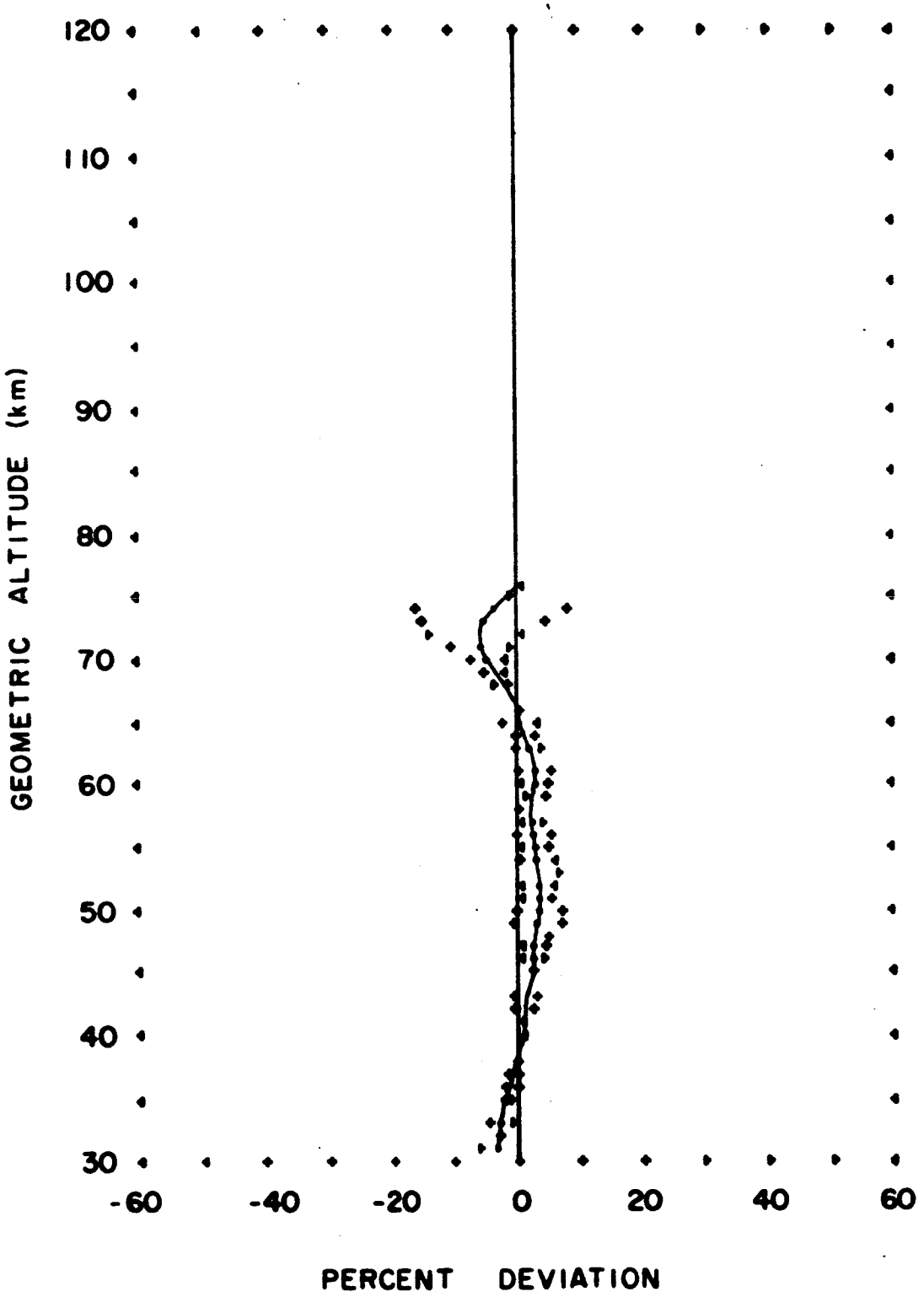

FIGURE 10S. PERCENT DEVIATION OF MEAN ATMOSPHERIC SUMMER DENSITIES OVER HOLLOMAN AFB FROM DENSITIES OF THE U.S. STANDARD ATMOSPHERE

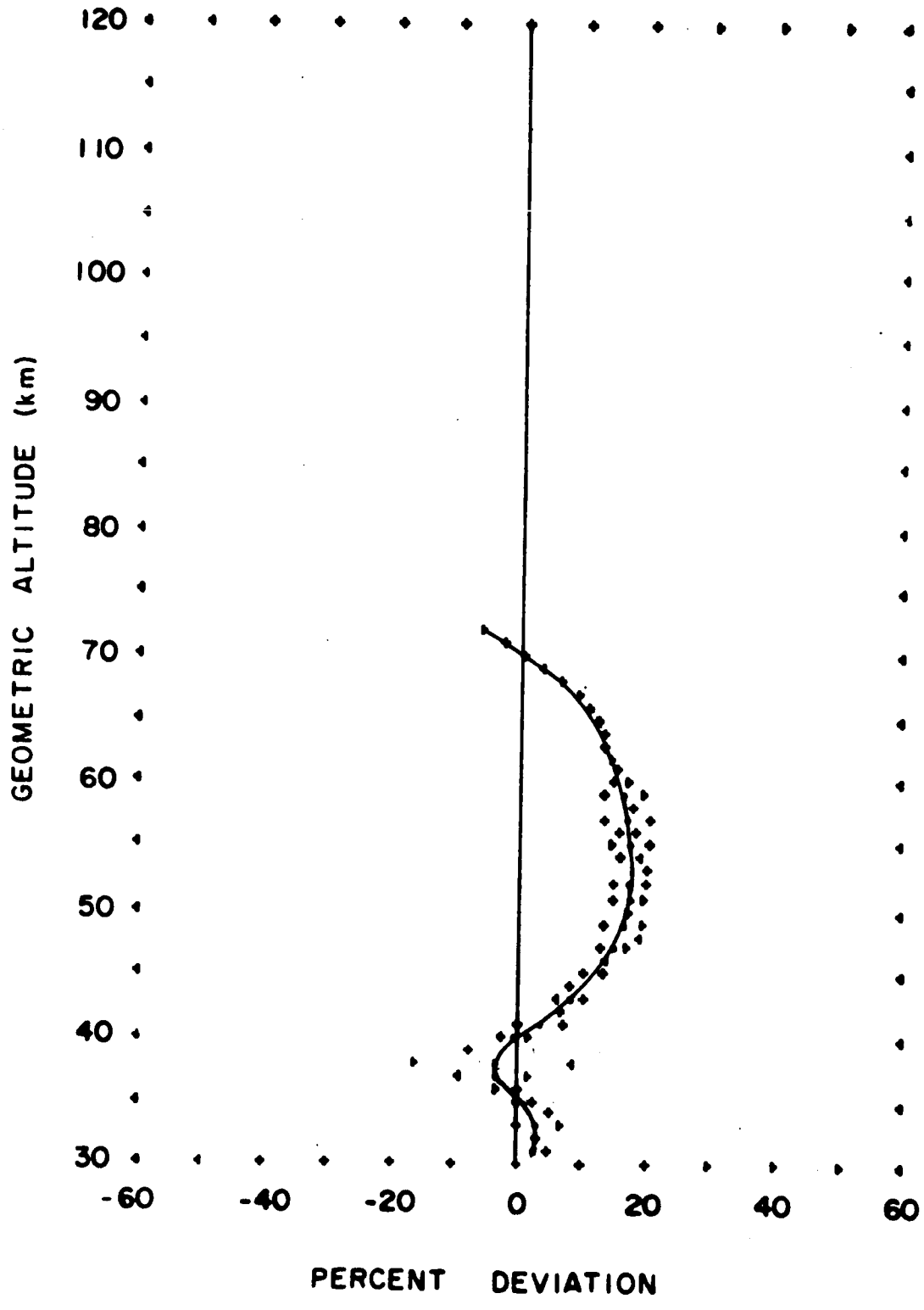

FIGURE 11S. PERCENT DEVIATION OF MEAN ATMOSPHERIC WINTER DENSITIES OVER HOLLOMAN AFB FROM DENSITIES OF THE U.S. STANDARD ATMOSPHERE

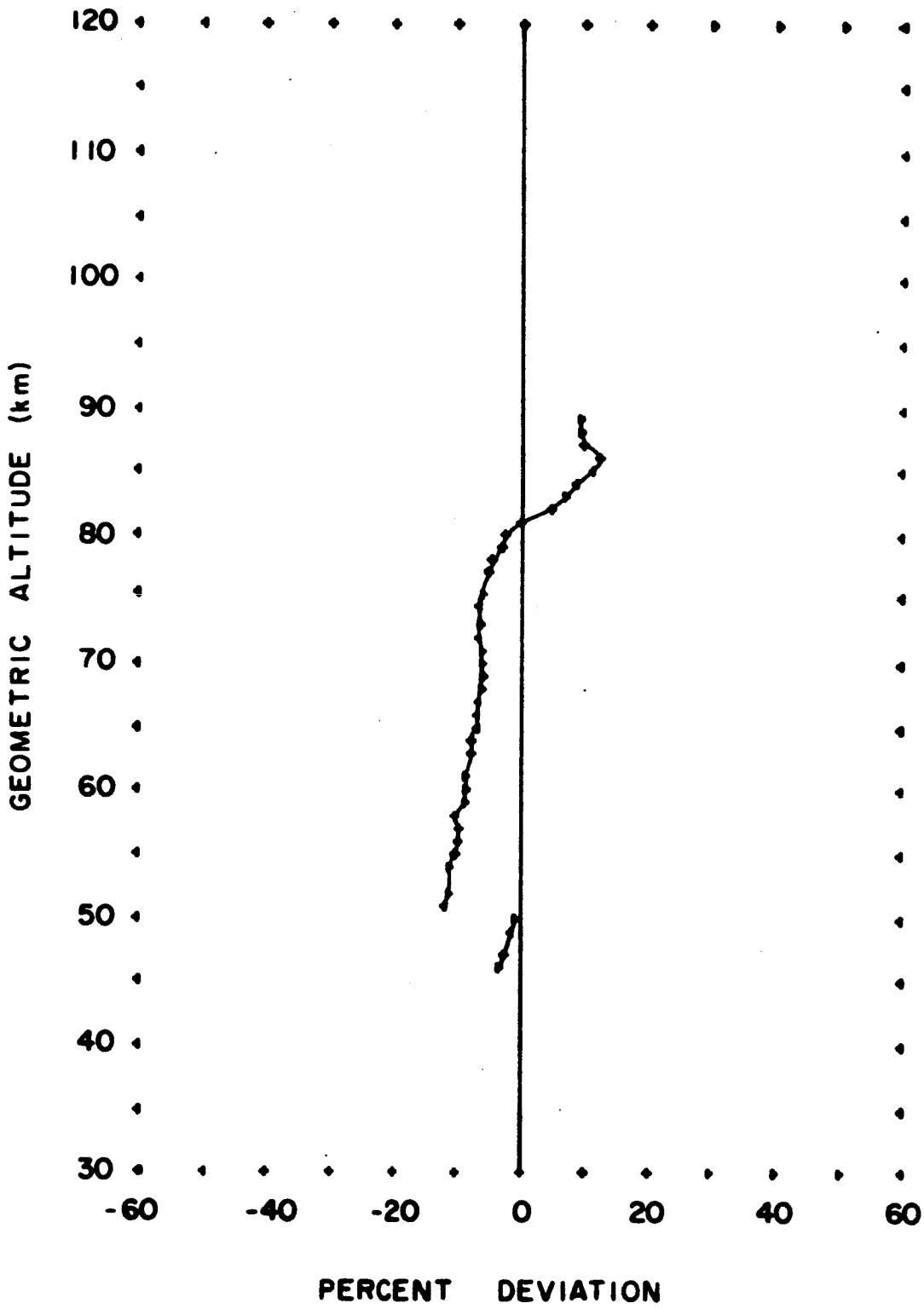

FIGURE 12S. PERCENT DEVIATION OF MEAN ATMOSPHERIC ANNUAL DENSITIES OVER HOLLOMAN AFB FROM DENSITIES OF THE U.S. STANDARD ATMOSPHERE

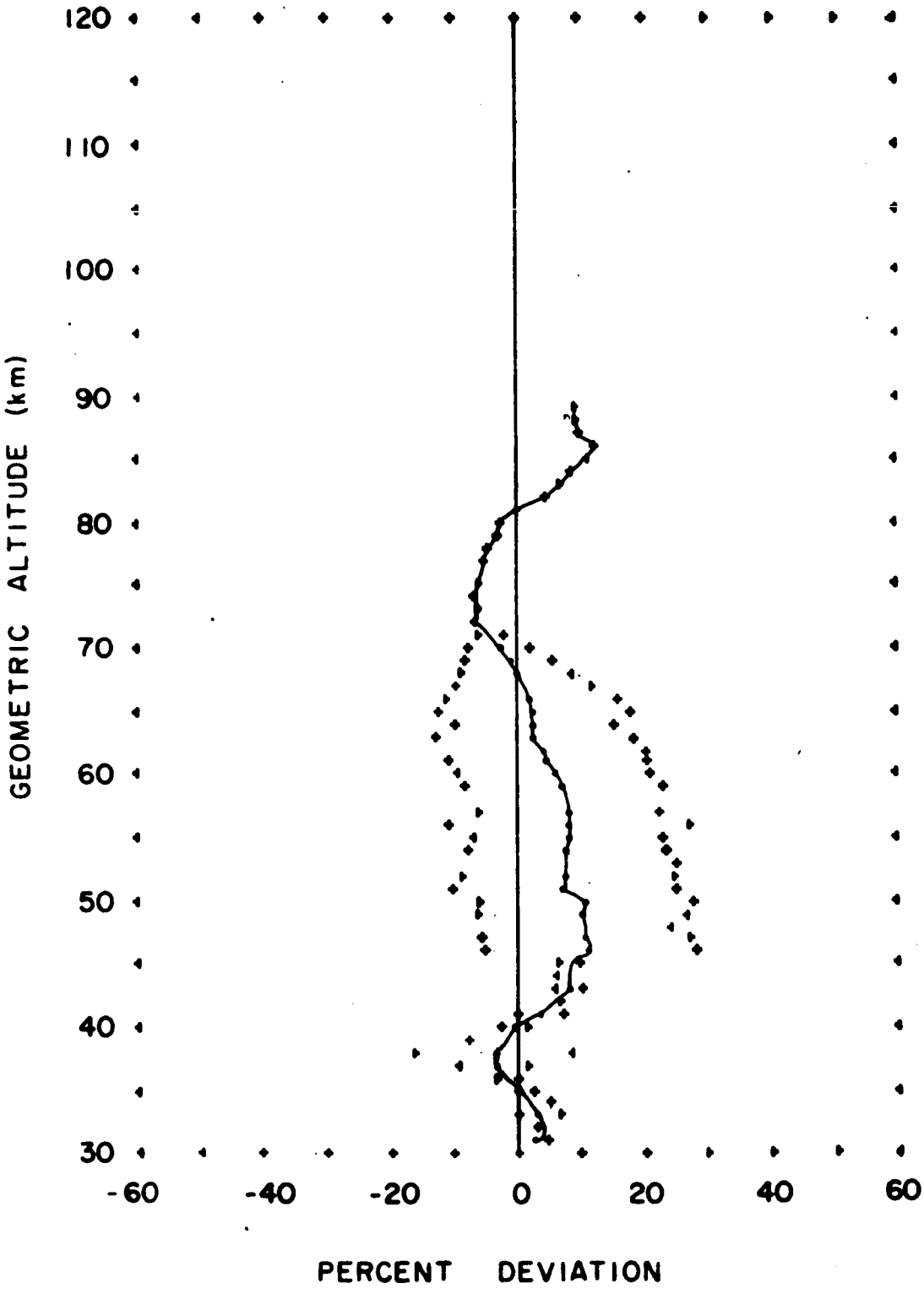

FIGURE 13S. PERCENT DEVIATION OF MEAN ATMOSPHERIC SUMMER DENSITIES OVER KWAJALEIN FROM DENSITIES OF THE U.S. STANDARD ATMOSPHERE

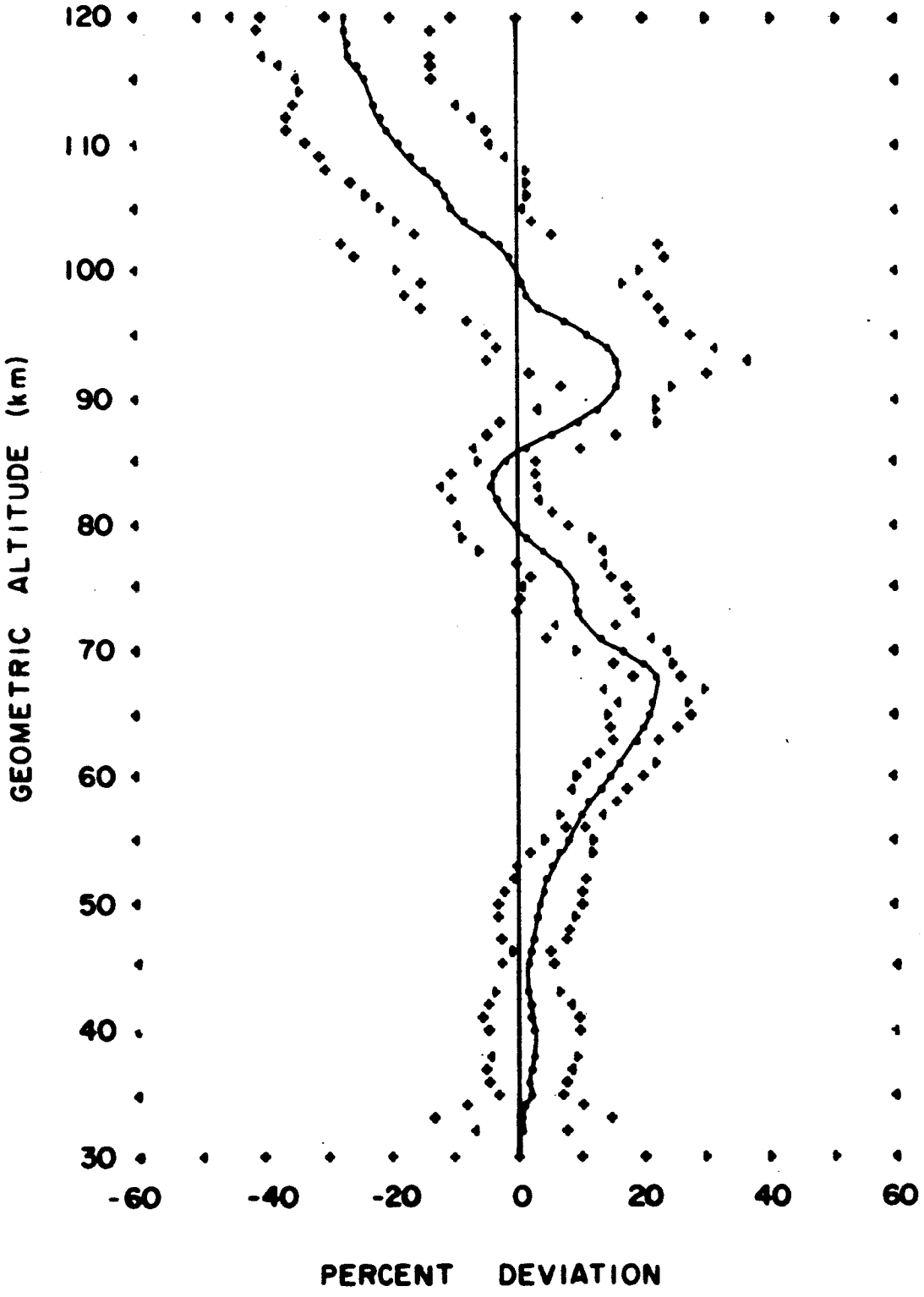

FIGURE 14S. PERCENT DEVIATION OF MEAN ATMOSPHERIC WINTER DENSITIES OVER KWAJALEIN FROM DENSITIES OF THE U.S. STANDARD ATMOSPHERE

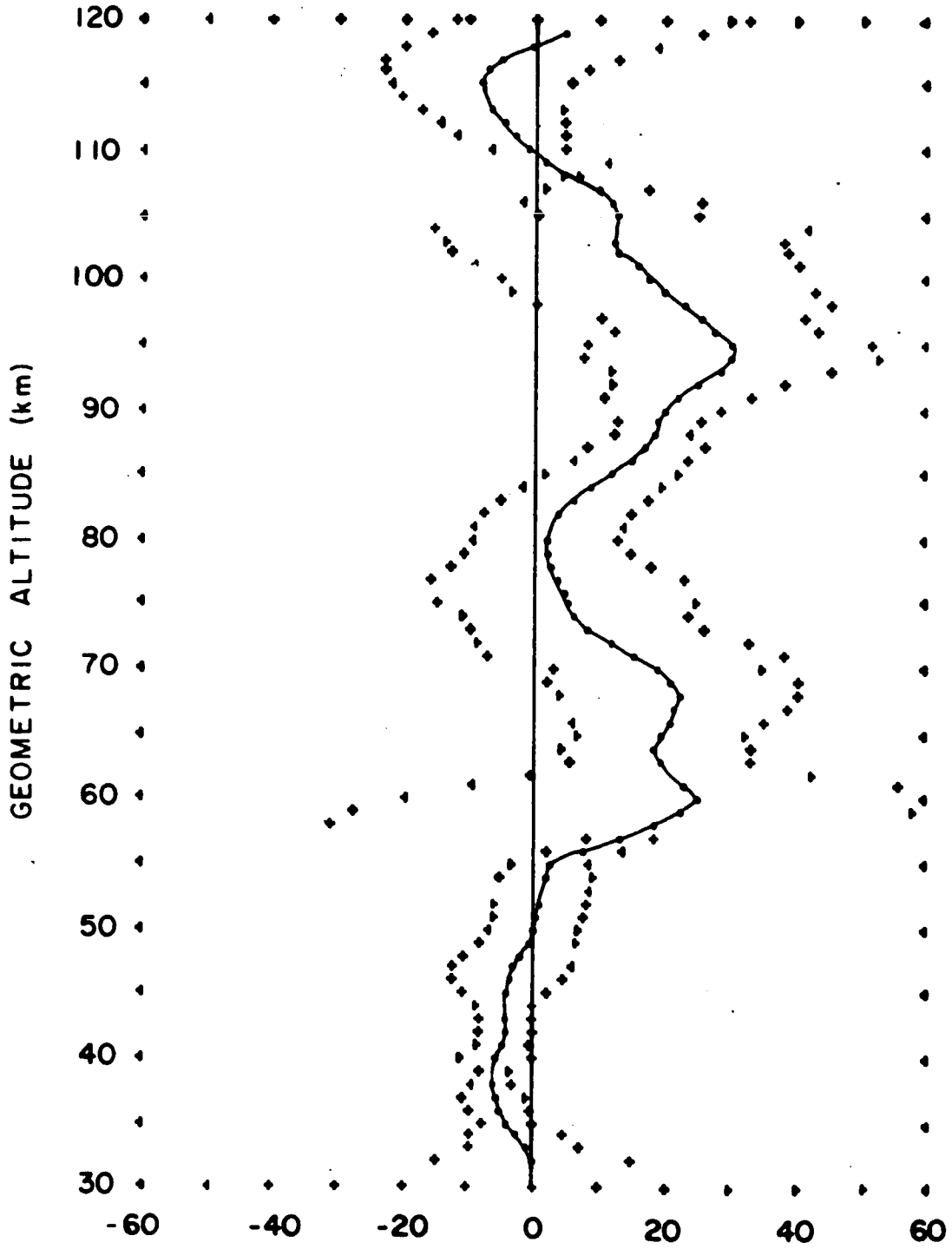

FIGURE 15S. PERCENT DEVIATION OF MEAN ATMOSPHERIC ANNUAL DENSITIES OVER KWAJALEIN FROM DENSITIES OF THE U.S. STANDARD ATMOSPHERE

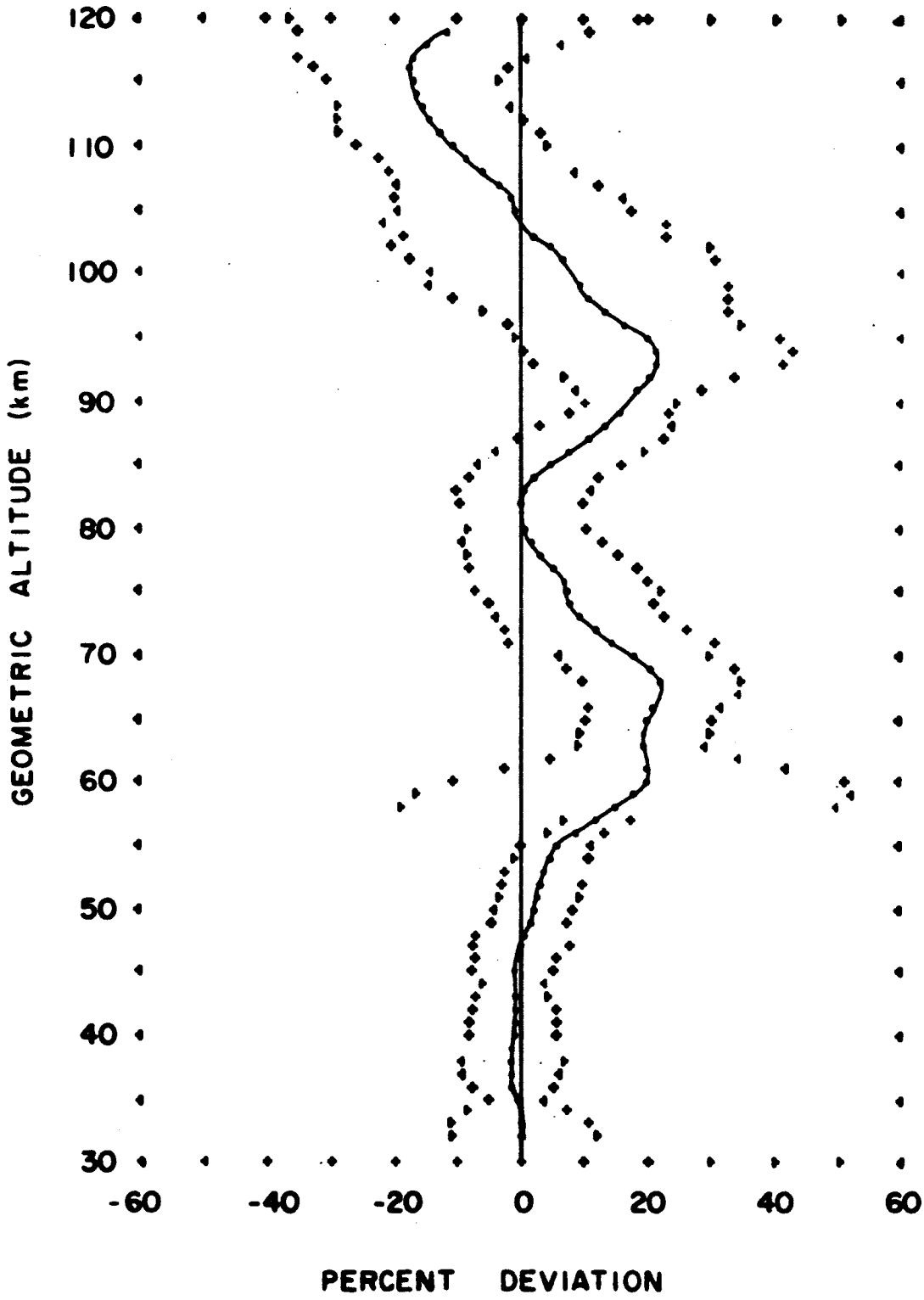

FIGURE 16S. PERCENT DEVIATION OF MEAN ATMOSPHERIC SUMMER DENSITIES OVER POINT MUGU FROM DENSITIES OF THE U.S. STANDARD ATMOSPHERE

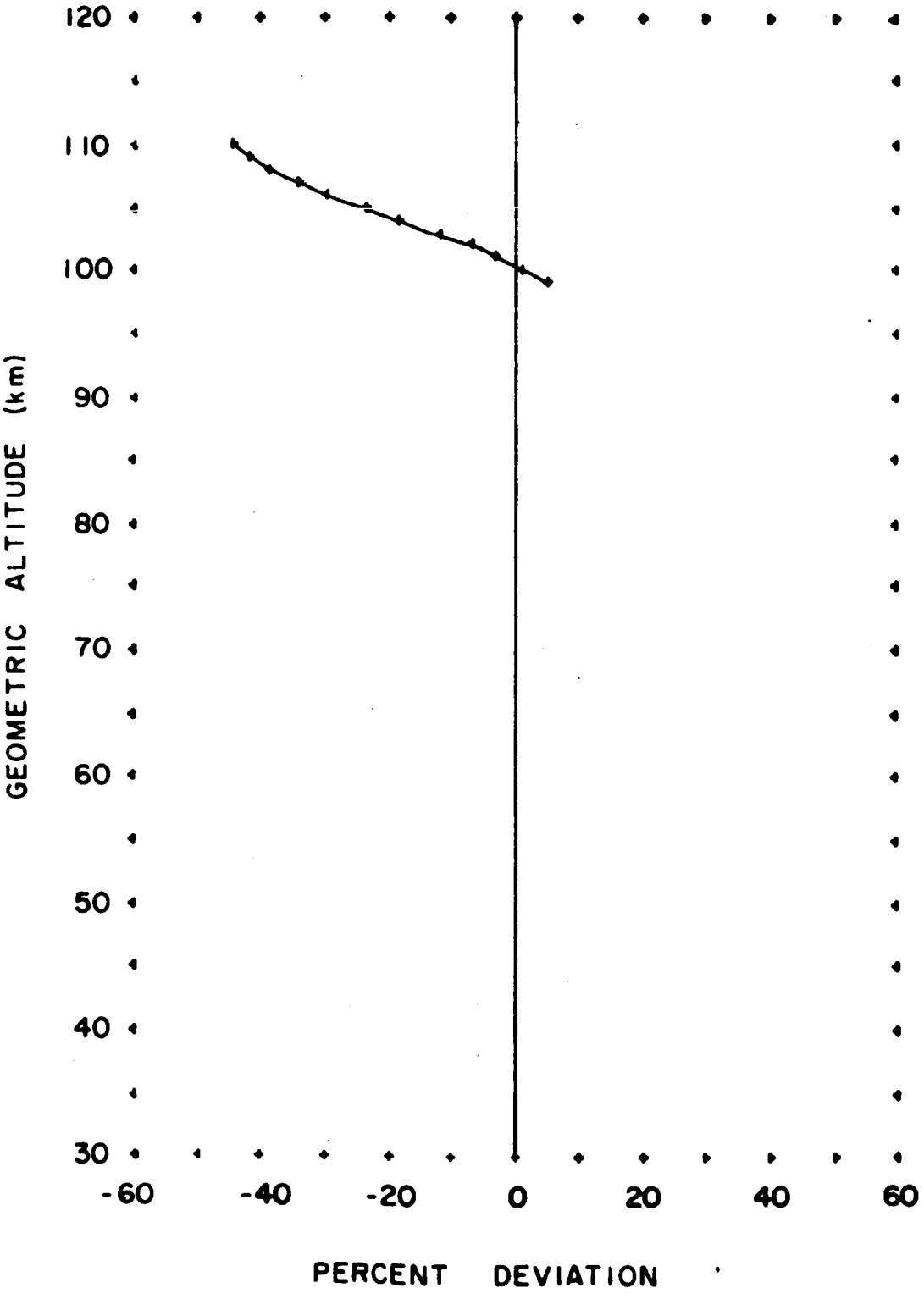

FIGURE 17S. PERCENT DEVIATION OF MEAN ATMOSPHERIC WINTER DENSITIES OVER POINT MUGU FROM DENSITIES OF THE U.S. STANDARD ATMOSPHERE

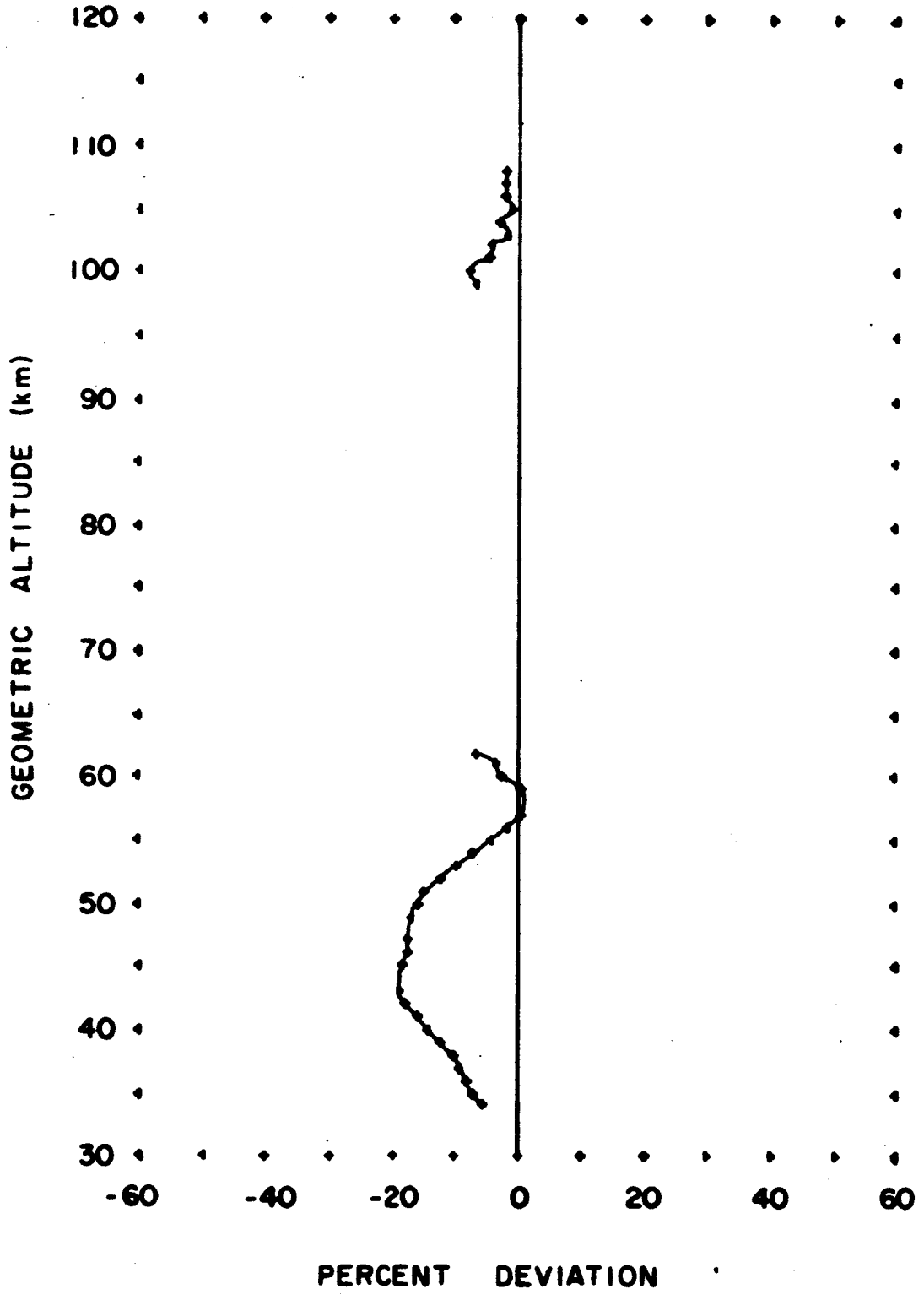

FIGURE 18S. PERCENT DEVIATION OF MEAN ATMOSPHERIC ANNUAL DENSITIES OVER POINT MUGU FROM DENSITIES OF THE U.S. STANDARD ATMOSPHERE

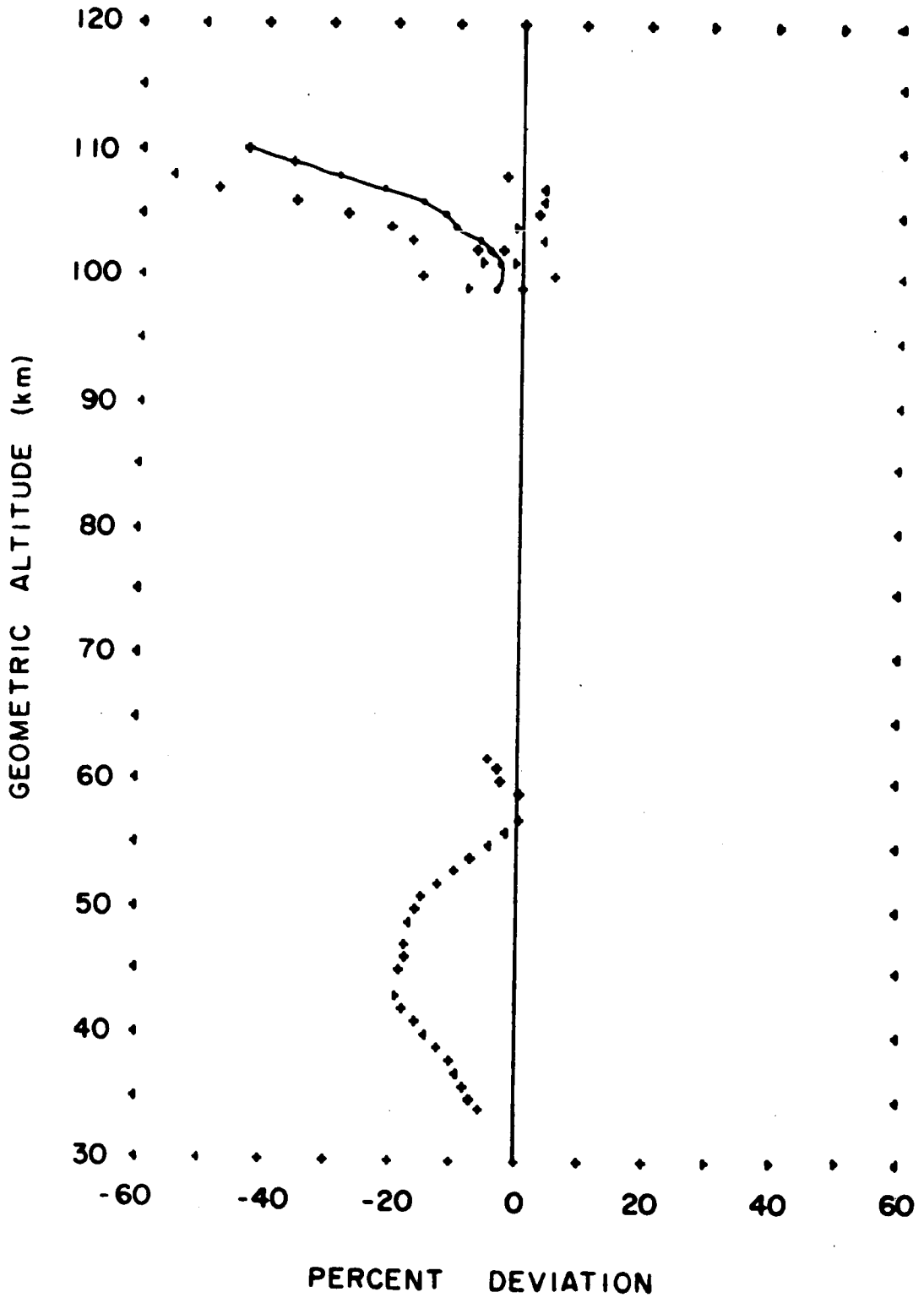

FIGURE 19S. PERCENT DEVIATION OF MEAN ATMOSPHERIC SUMMER DENSITIES OVER A SHIP (ARCTIC) FROM DENSITIES OF THE U.S. STANDARD ATMOSPHERE

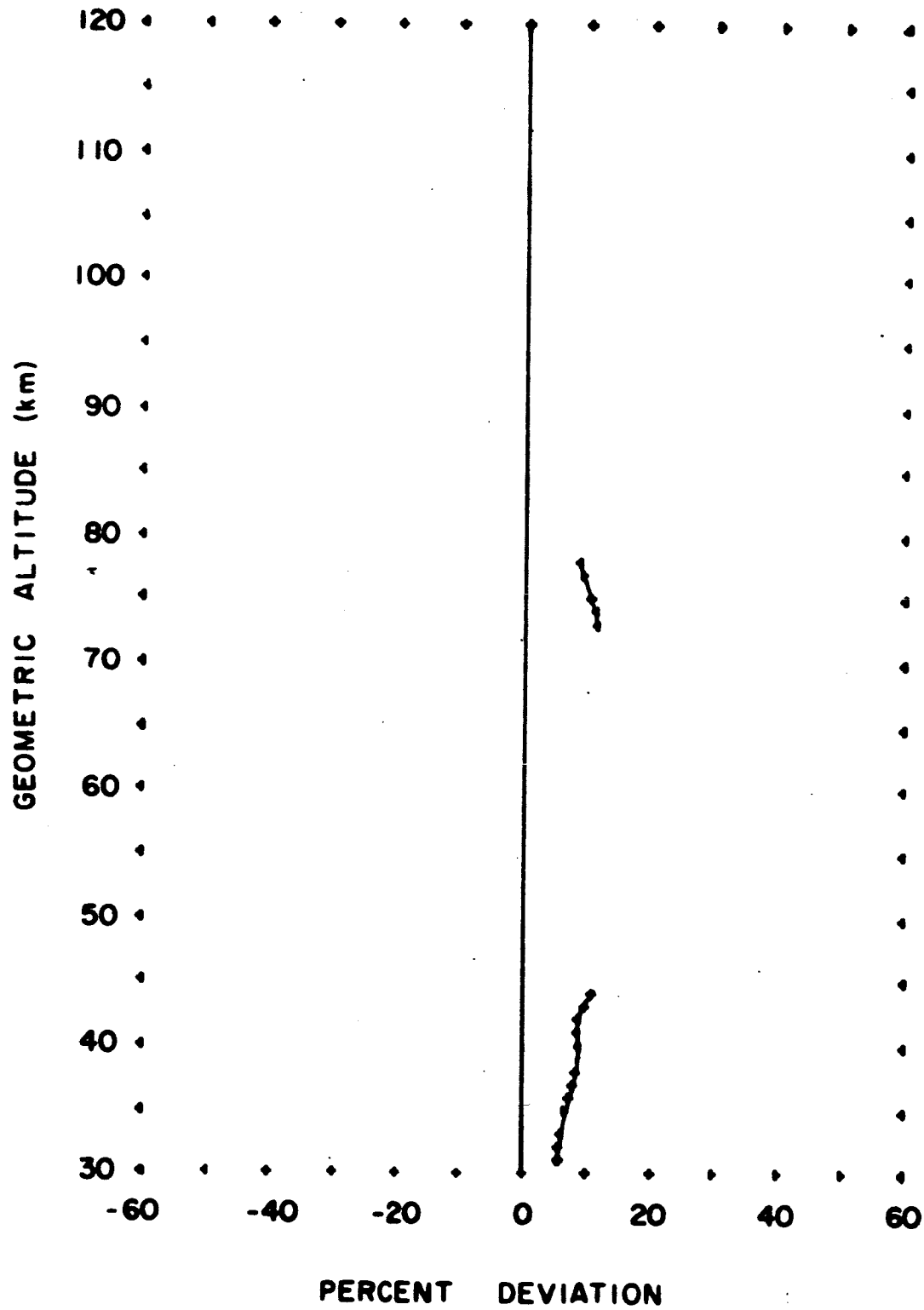

FIGURE 20S. PERCENT DEVIATION OF MEAN ATMOSPHERIC WINTER DENSITIES OVER A SHIP (MIDLAT.) FROM DENSITIES OF THE U.S. STANDARD ATMOSPHERE

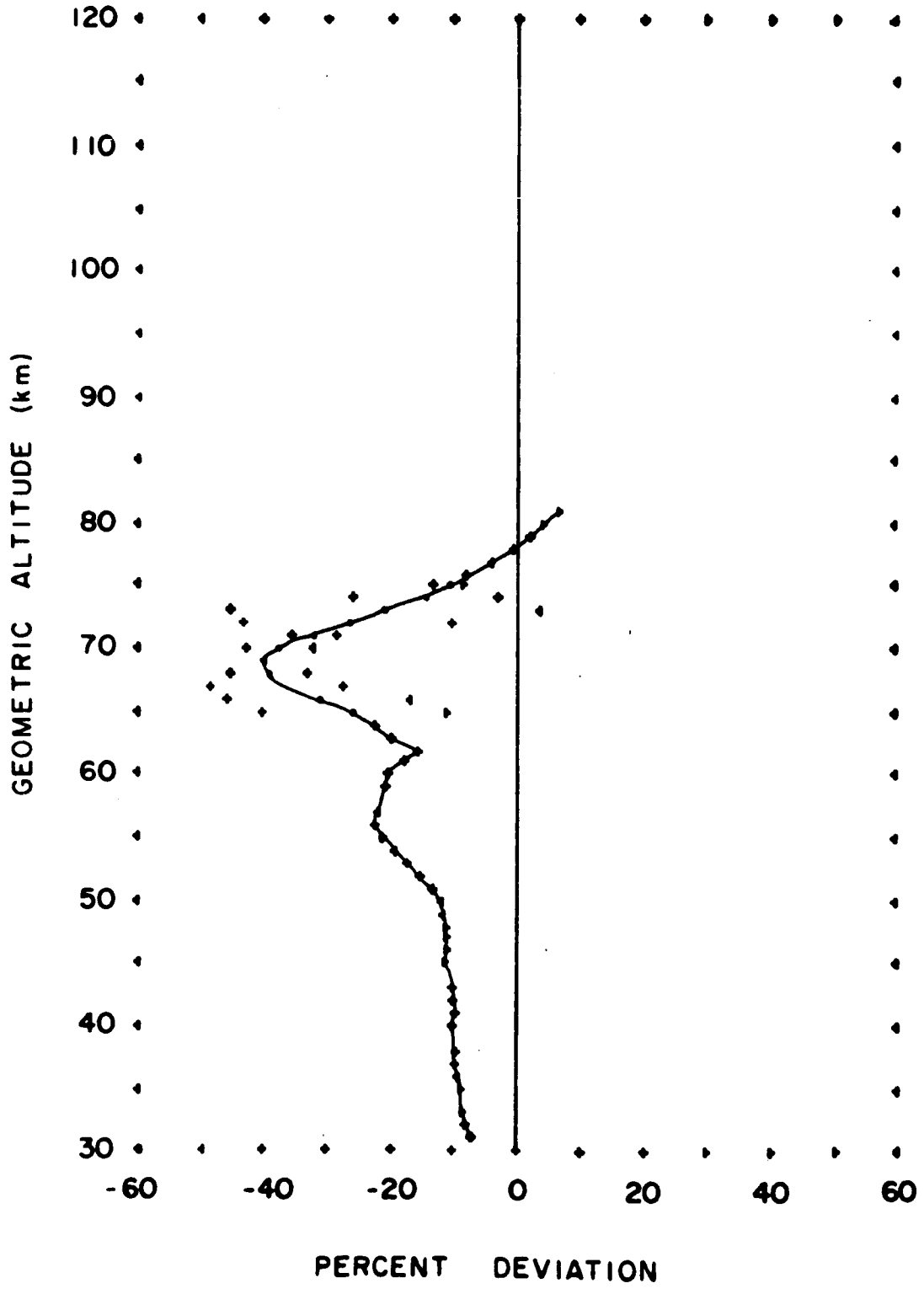

FIGURE 21S. PERCENT DEVIATION OF MEAN ATMOSPHERIC SUMMER DENSITIES OVER A SHIP (SUBARCTIC) FROM DENSITIES OF THE U.S. STANDARD ATMOSPHERE

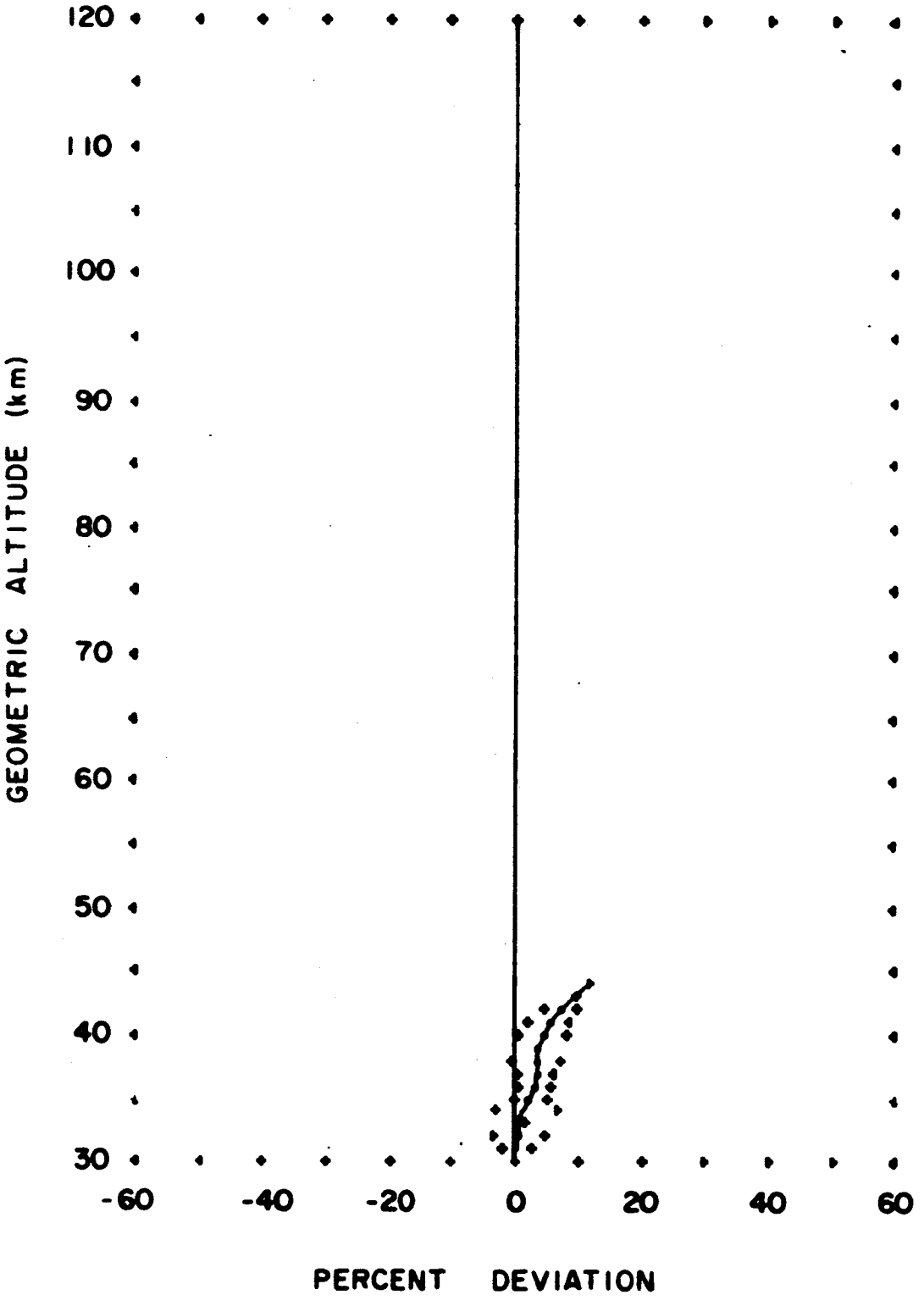

FIGURE 22S. PERCENT DEVIATION OF MEAN ATMOSPHERIC WINTER DENSITIES OVER A SHIP (SUBARCTIC) FROM DENSITIES OF THE U.S. STANDARD ATMOSPHERE

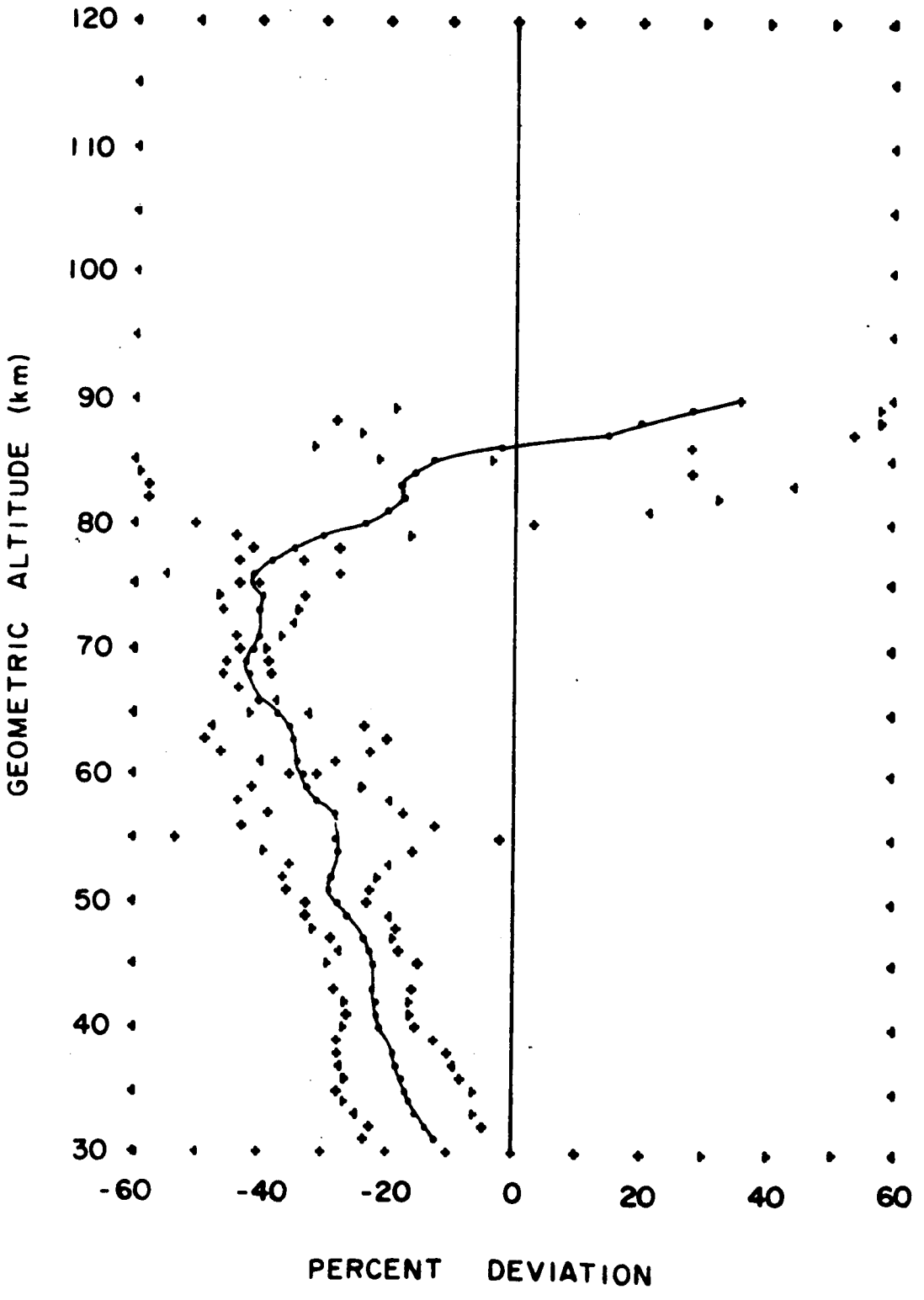

FIGURE 23S. PERCENT DEVIATION OF MEAN ATMOSPHERIC ANNUAL DENSITIES OVER A SHIP (SUBARCTIC) FROM DENSITIES OF THE U.S. STANDARD ATMOSPHERE

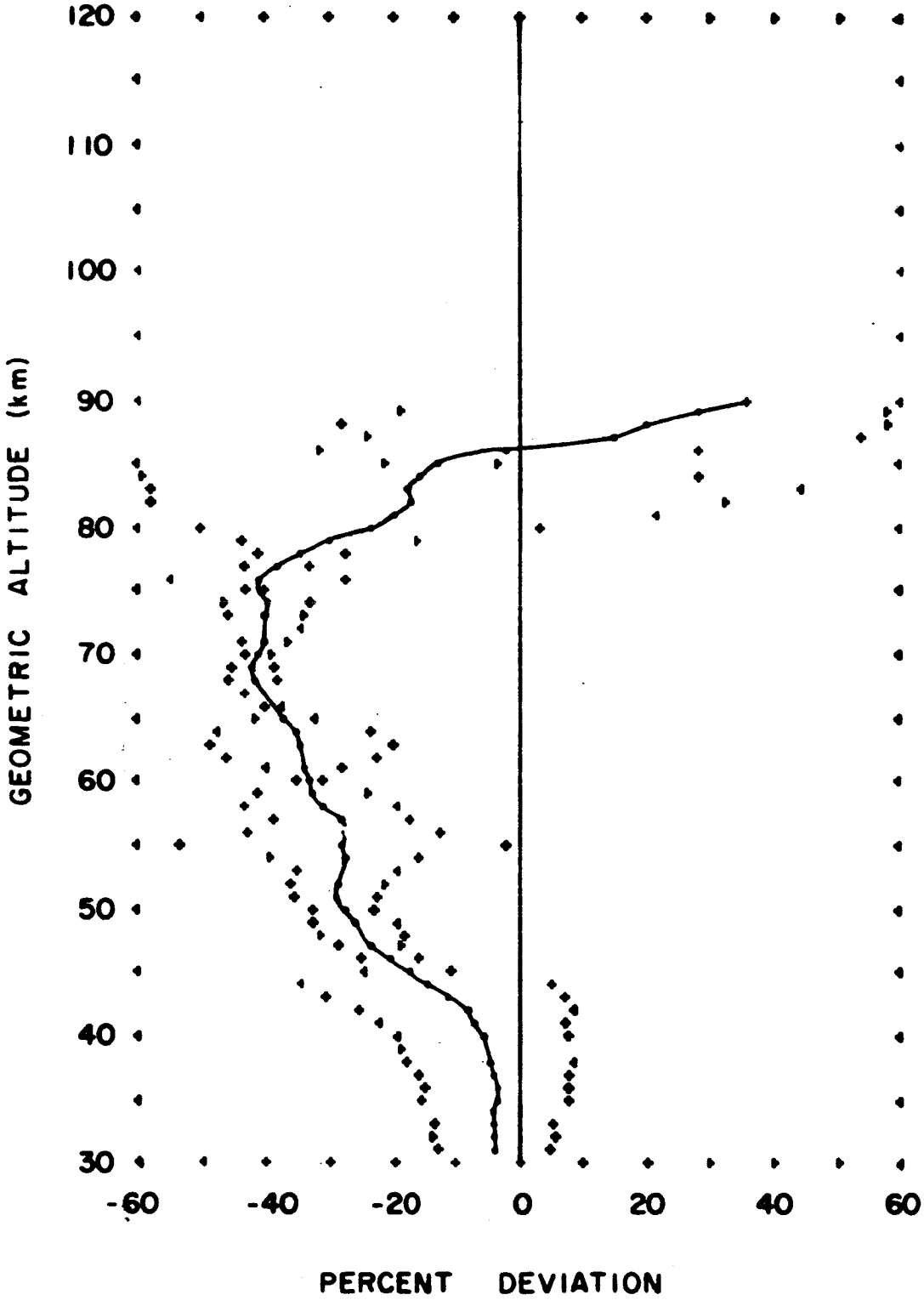

FIGURE 24S. PERCENT DEVIATION OF MEAN ATMOSPHERIC SUMMER DENSITIES OVER WALLOPS ISLAND FROM DENSITIES OF THE U.S. STANDARD ATMOSPHERE

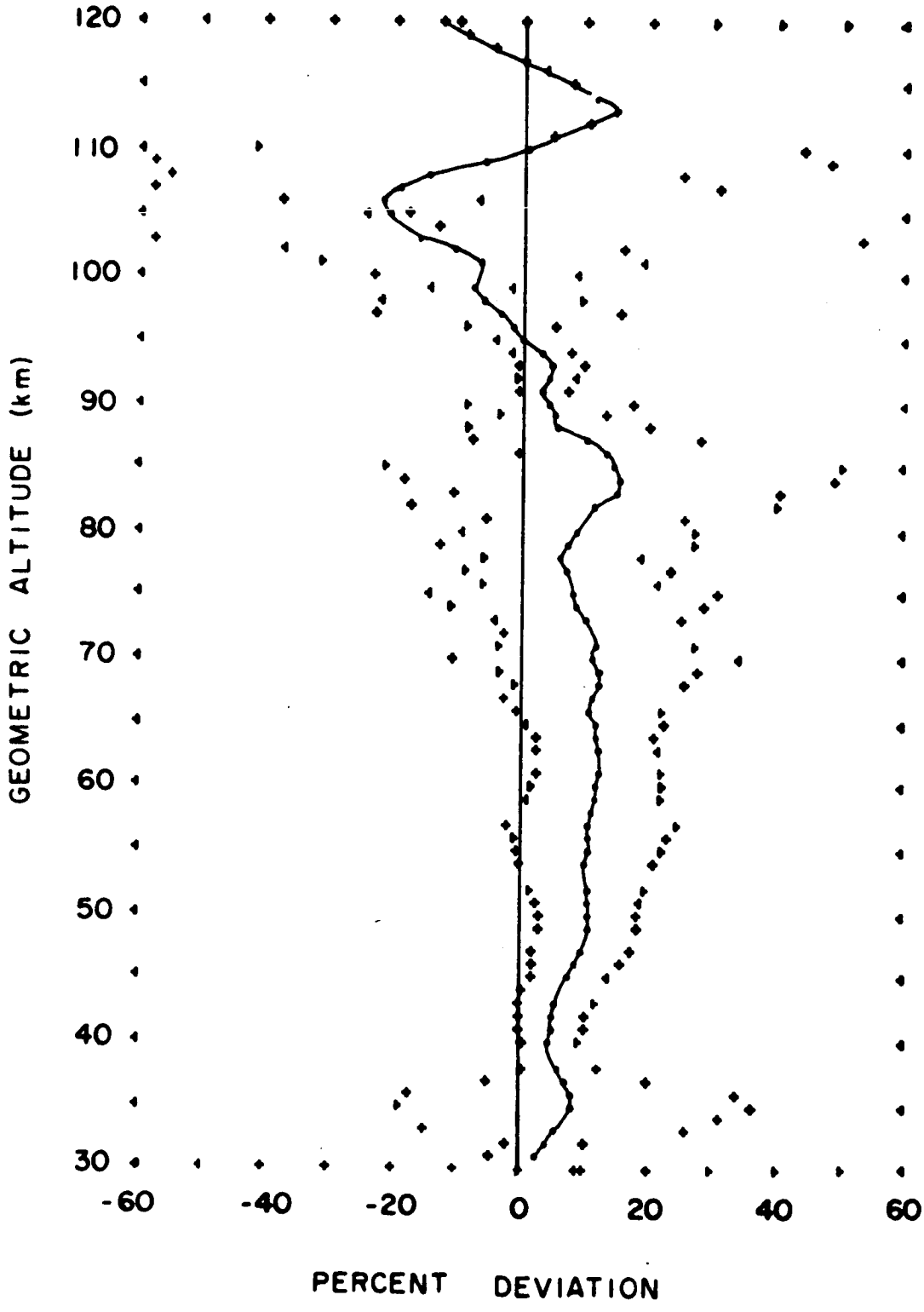

FIGURE 25S. PERCENT DEVIATION OF MEAN ATMOSPHERIC WINTER DENSITIES OVER WALLOPS ISLAND FROM DENSITIES OF THE U.S. STANDARD ATMOSPHERE

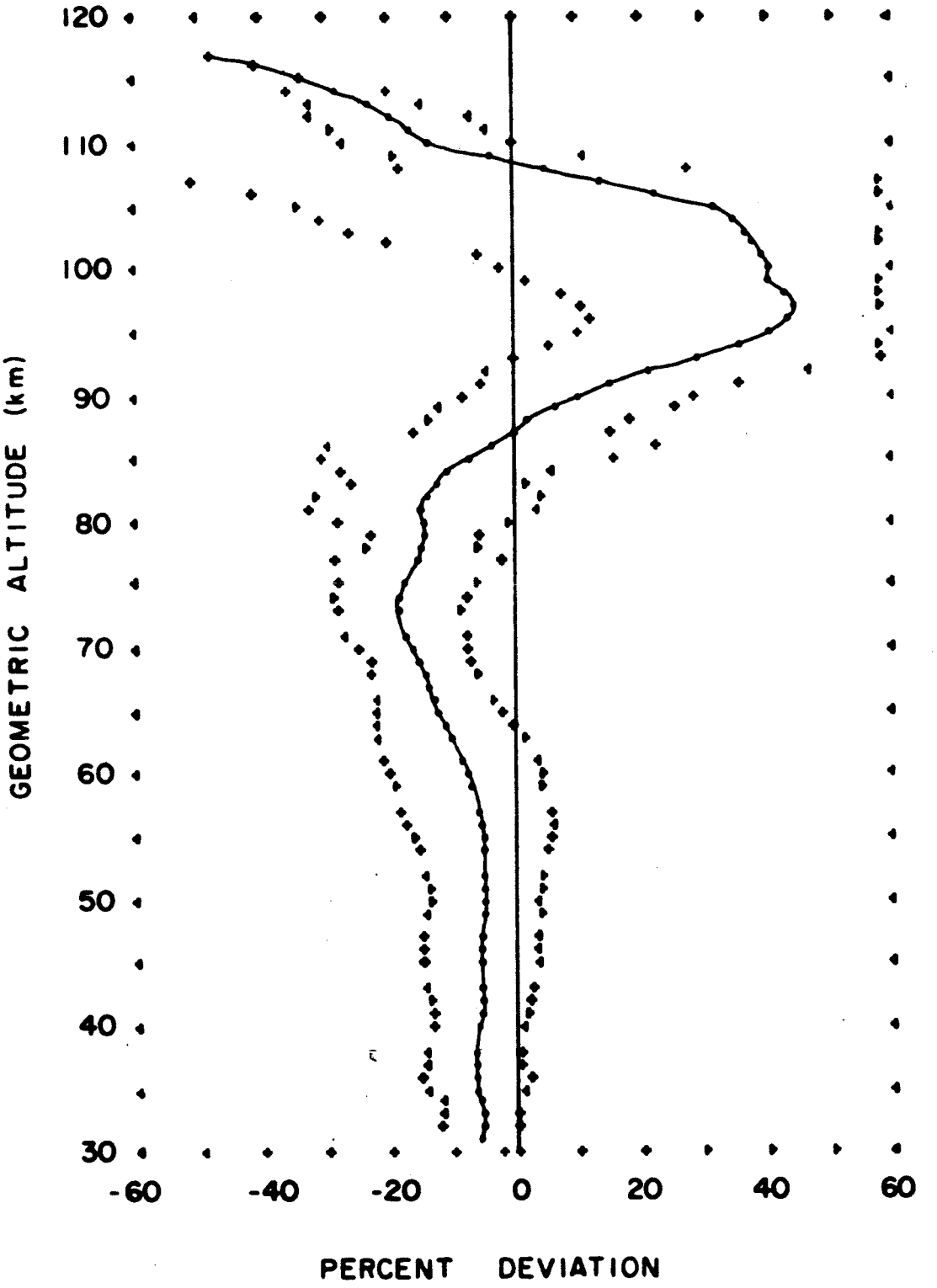

FIGURE 26S. PERCENT DEVIATION OF MEAN ATMOSPHERIC ANNUAL DENSITIES OVER WALLOPS ISLAND FROM DENSITIES OF THE U.S. STANDARD ATMOSPHERE

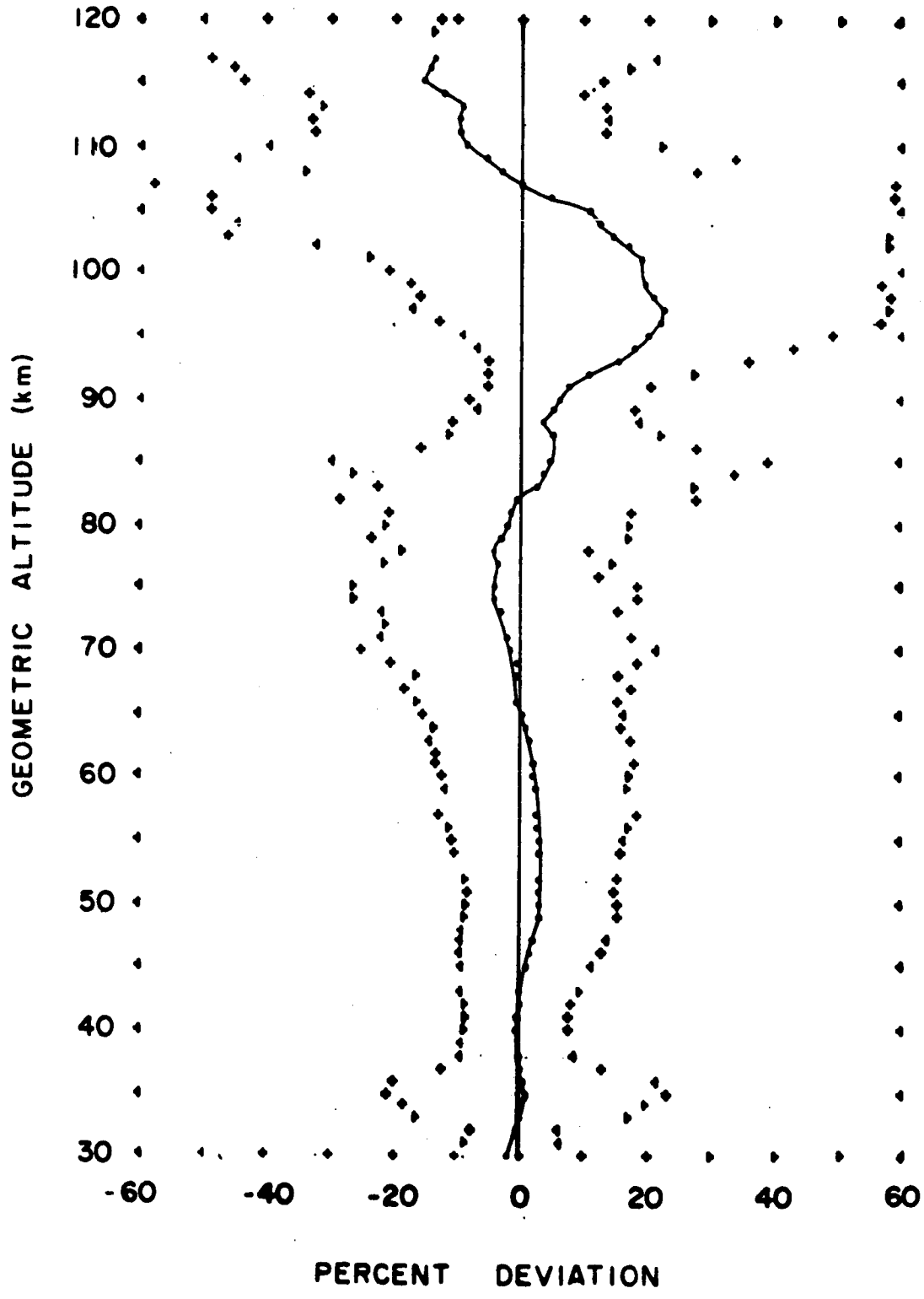

FIGURE 27S. PERCENT DEVIATION OF MEAN ATMOSPHERIC SUMMER DENSITIES OVER WHITE SANDS FROM DENSITIES OF THE U.S. STANDARD ATMOSPHERE

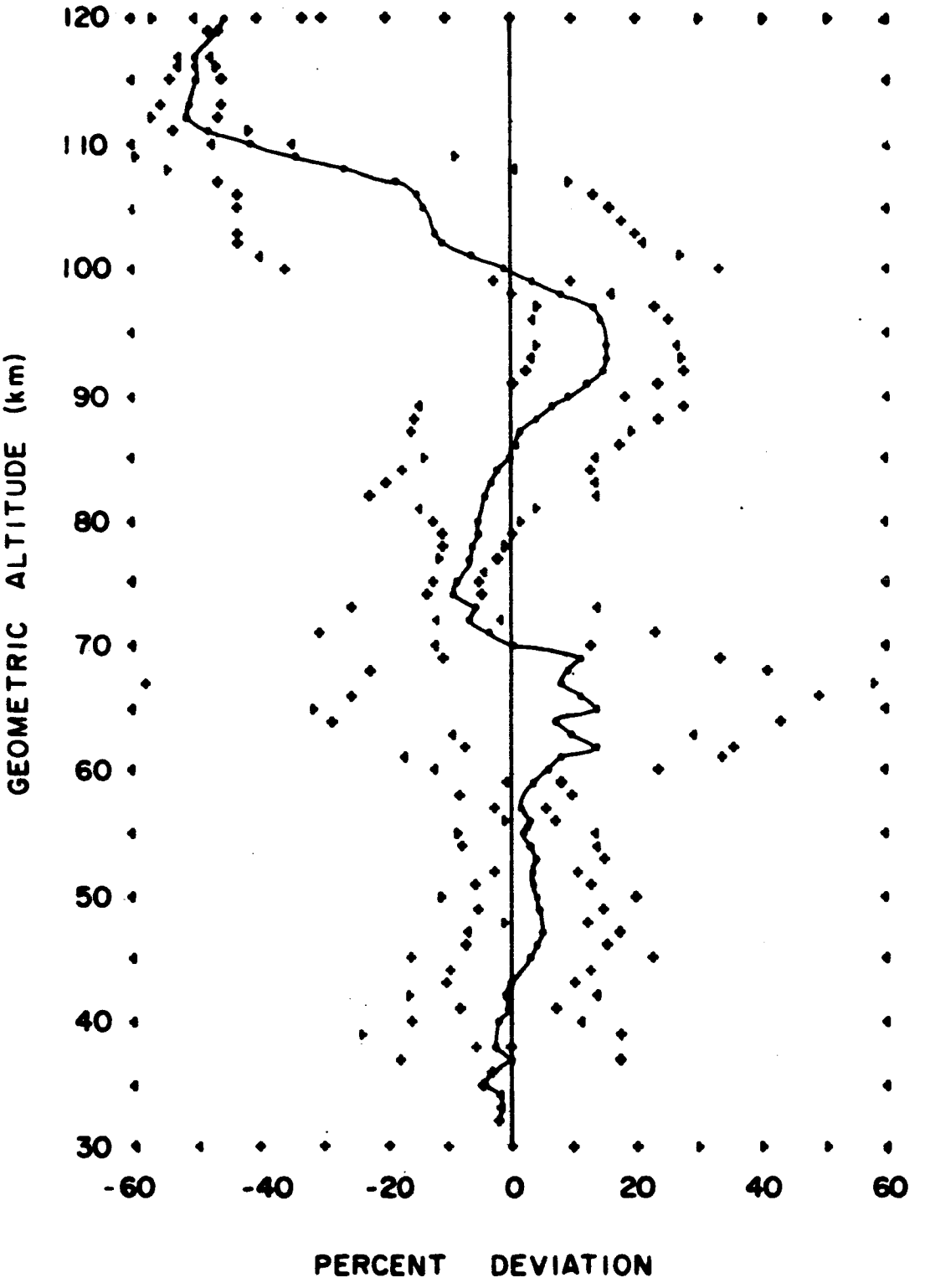

FIGURE 28S. PERCENT DEVIATION OF MEAN ATMOSPHERIC WINTER DENSITIES OVER WHITE SANDS FROM DENSITIES OF THE U.S. STANDARD ATMOSPHERE

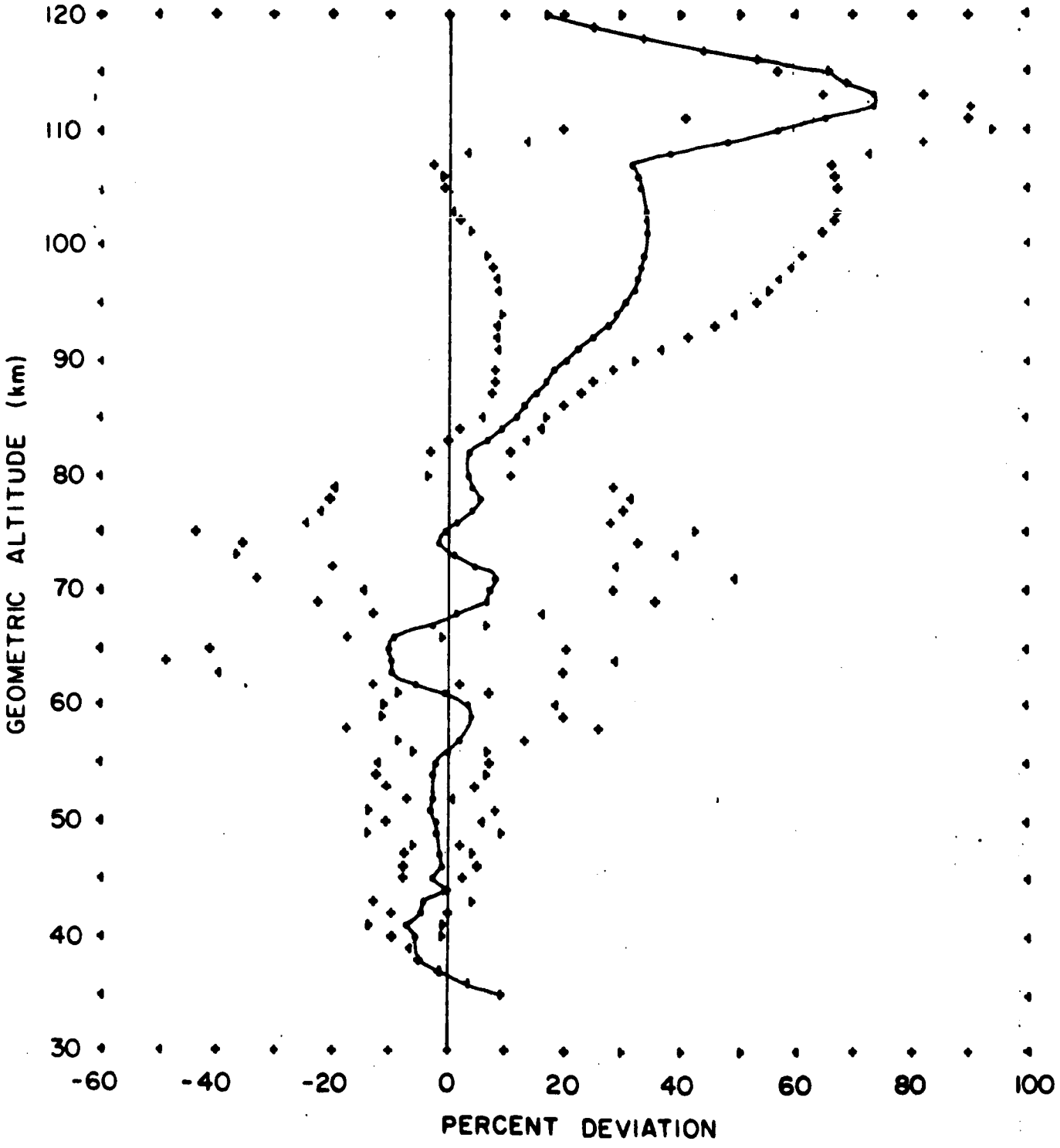

FIGURE 29S. PERCENT DEVIATION OF MEAN ATMOSPHERIC ANNUAL DENSITIES OVER WHITE SANDS FROM DENSITIES OF THE U.S. STANDARD ATMOSPHERE

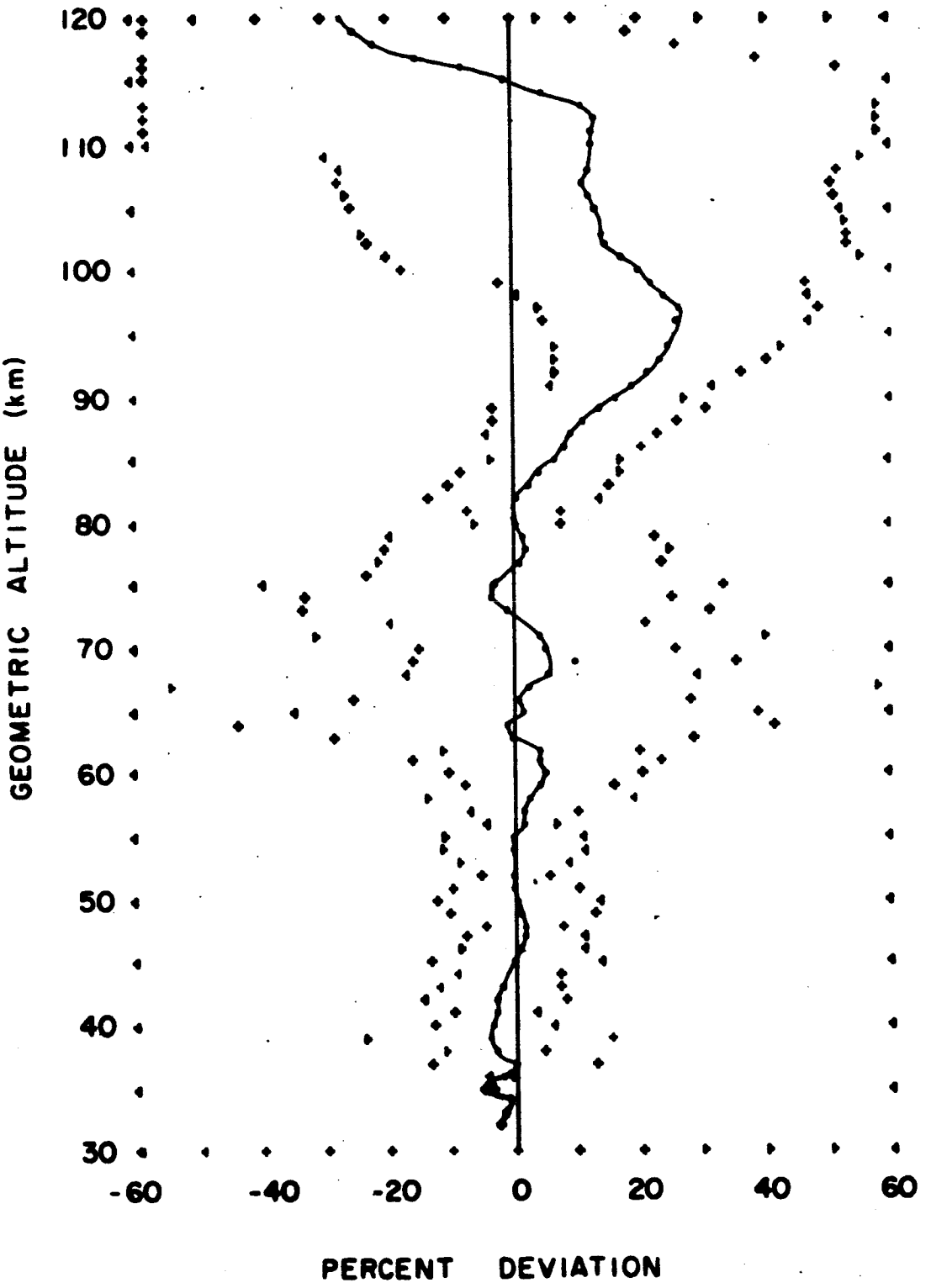

FIGURE 30S. PERCENT DEVIATION OF MEAN ATMOSPHERIC SUMMER DENSITIES OVER WOOMERA AUST. FROM DENSITIES OF THE U.S. STANDARD ATMOSPHERE

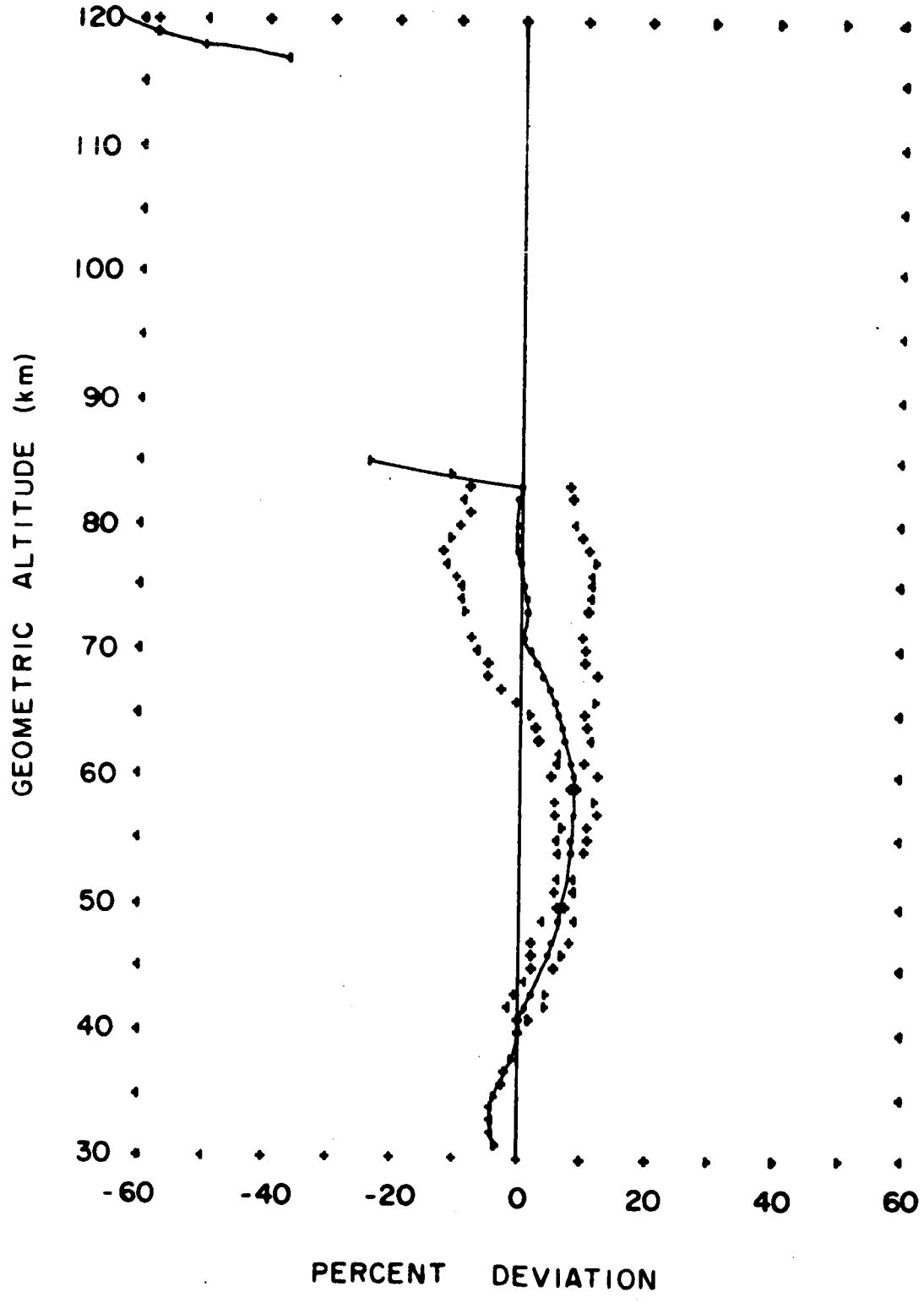

FIGURE 315. PERCENT DEVIATION OF MEAN ATMOSPHERIC WINTER DENSITIES OVER WOOMERA AUST. FROM DENSITIES OF THE U.S. STANDARD ATMOSPHERE

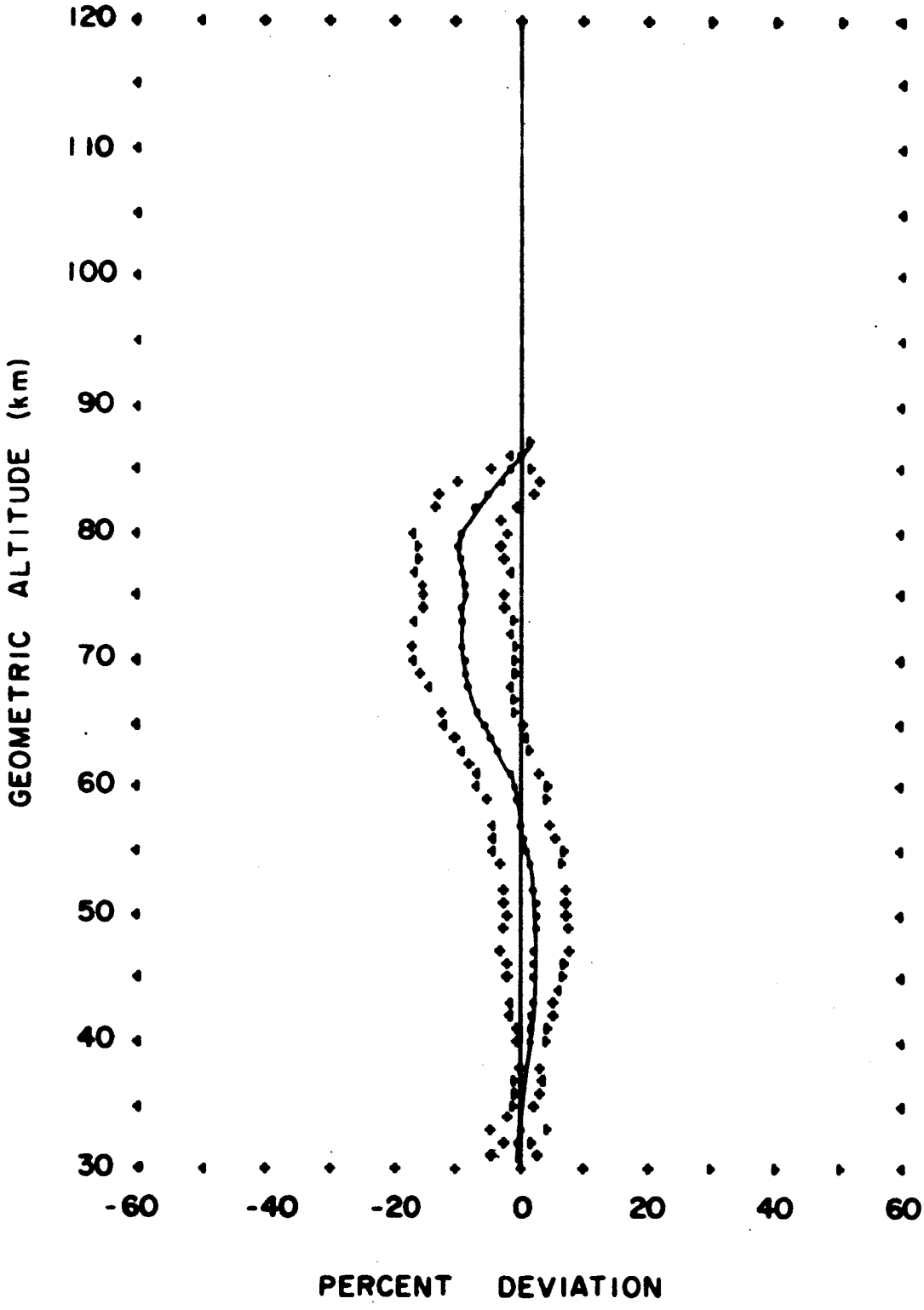

FIGURE 32S. PERCENT DEVIATION OF MEAN ATMOSPHERIC ANNUAL DENSITIES OVER WOOMERA AUST. FROM DENSITIES OF THE U.S. STANDARD ATMOSPHERE

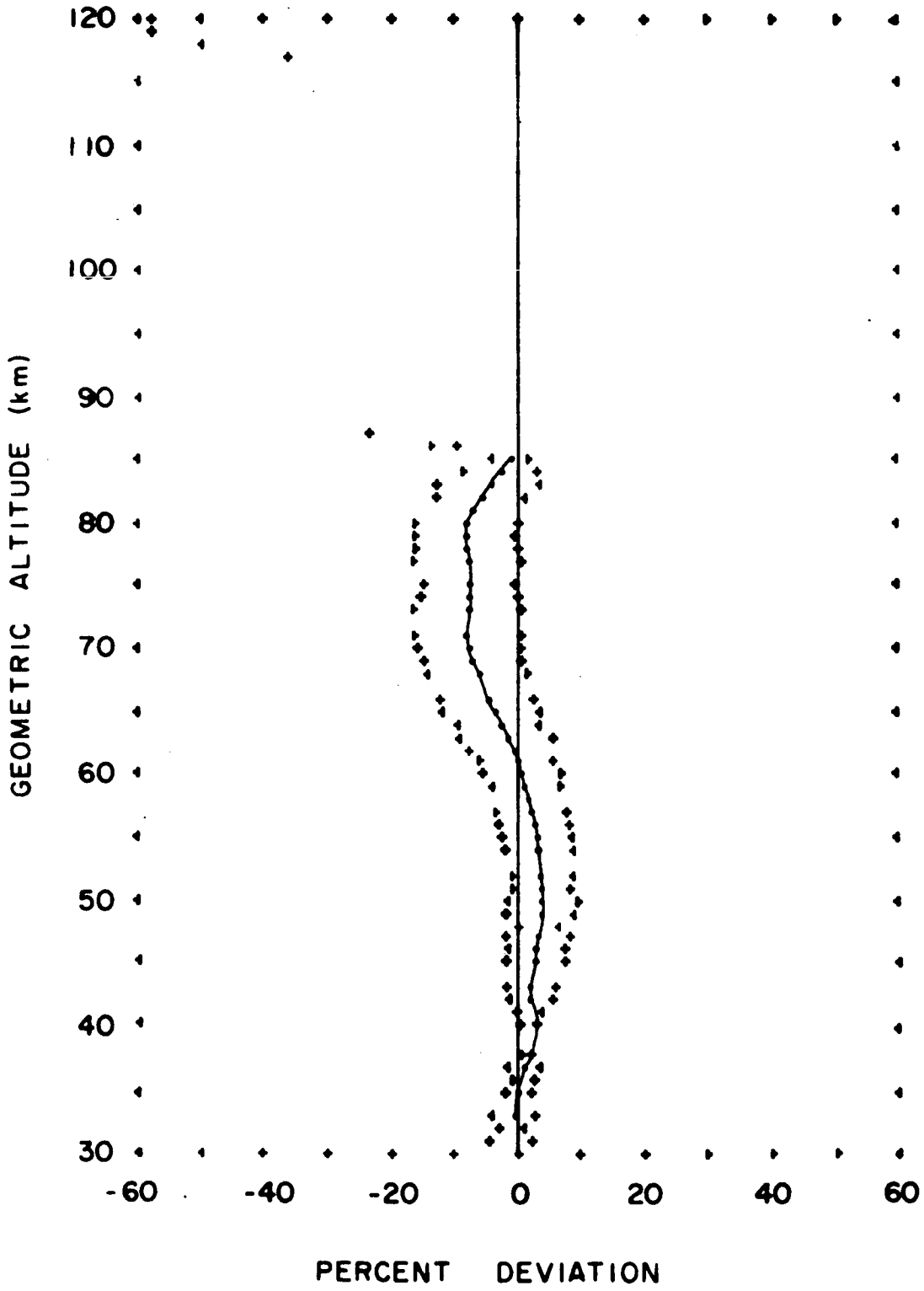

FIGURE 33S. PERCENT DEVIATION OF MEAN ATMOSPHERIC SUMMER DENSITIES OVER THE TROPICS FROM DENSITIES OF THE U.S. STANDARD ATMOSPHERE

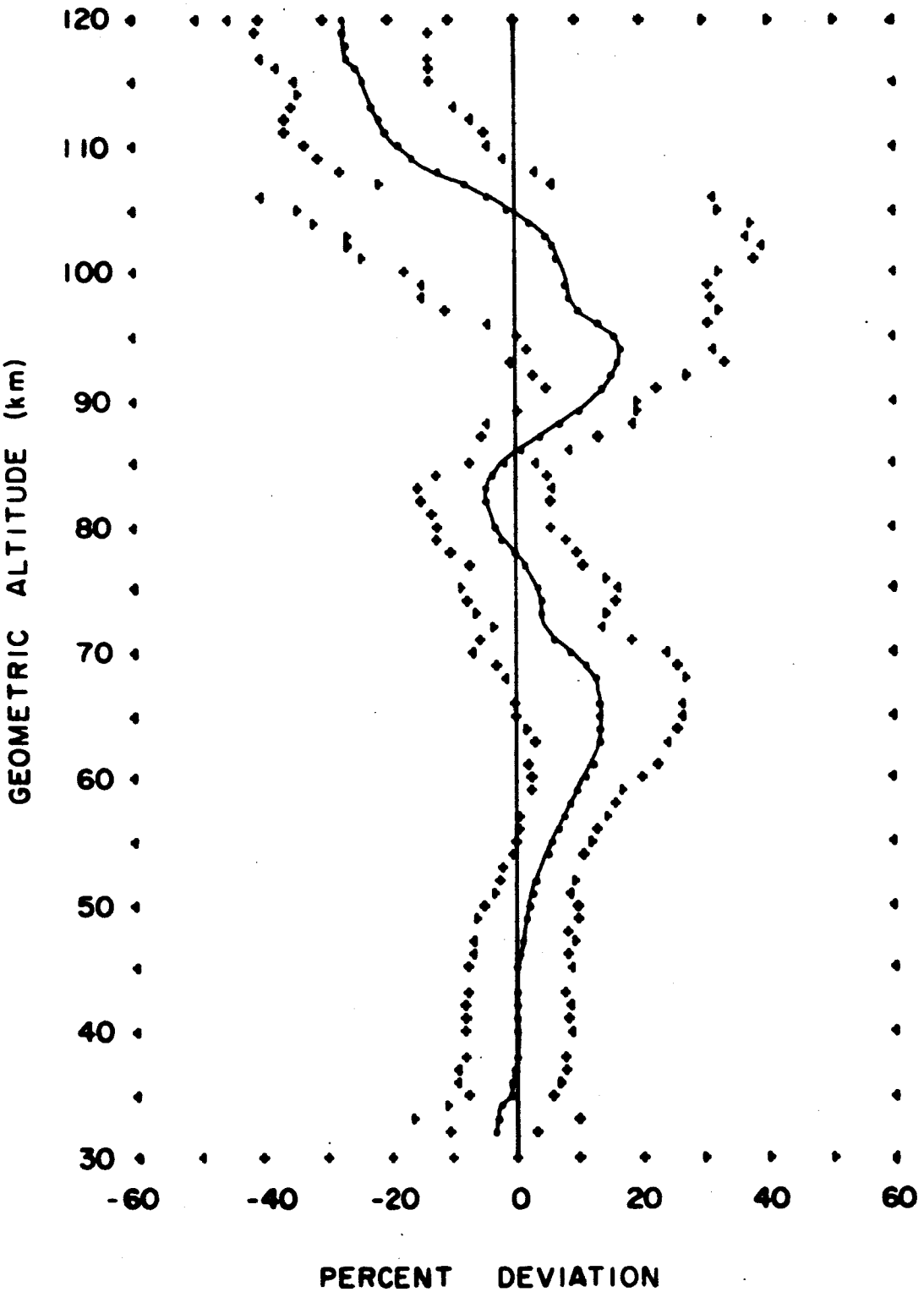

FIGURE 34S. PERCENT DEVIATION OF MEAN ATMOSPHERIC WINTER DENSITIES OVER THE TROPICS FROM DENSITIES OF THE U.S. STANDARD ATMOSPHERE

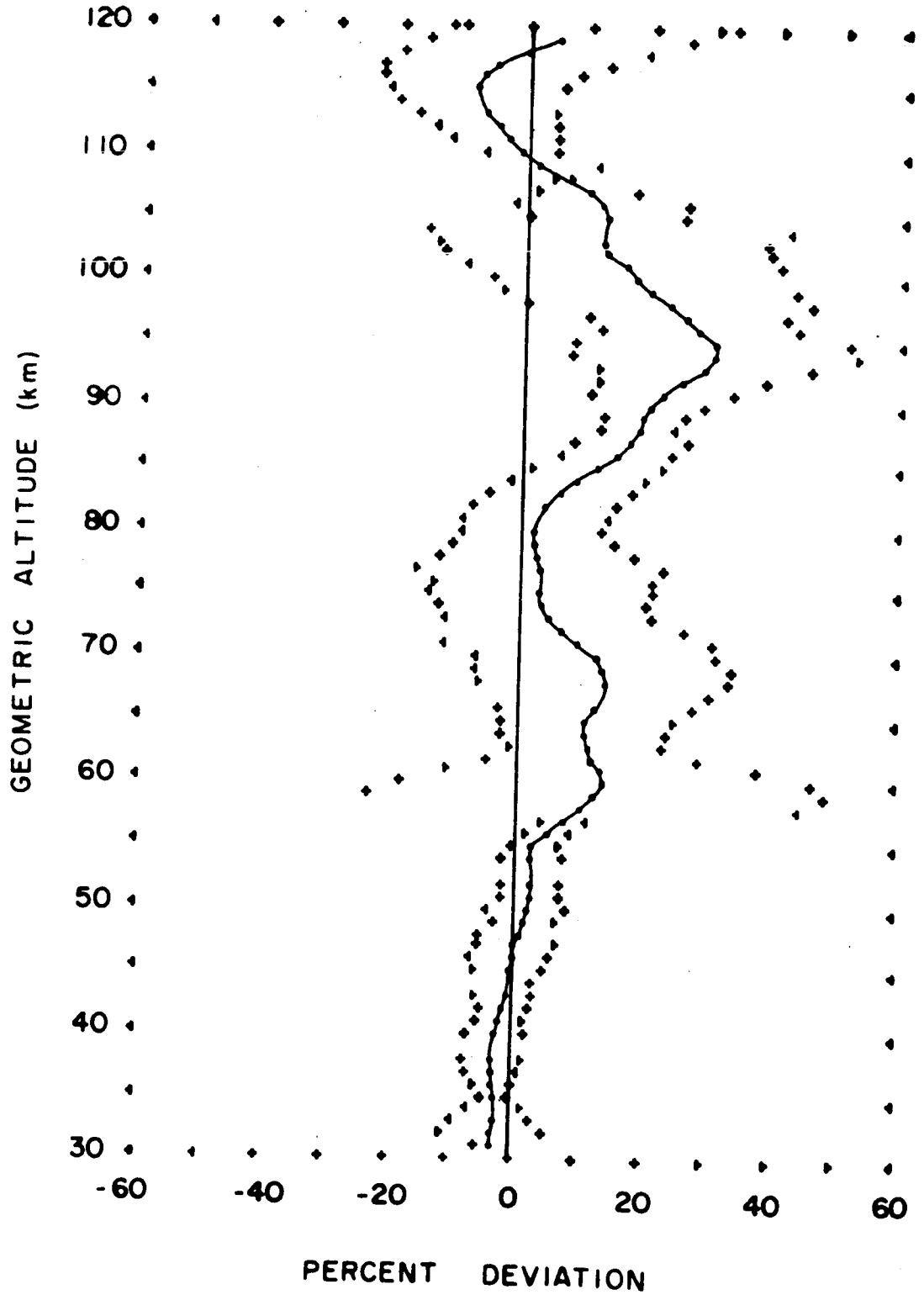

FIGURE 35S. PERCENT DEVIATION OF MEAN ATMOSPHERIC ANNUAL DENSITIES OVER THE TROPICS FROM DENSITIES OF THE U.S. STANDARD ATMOSPHERE

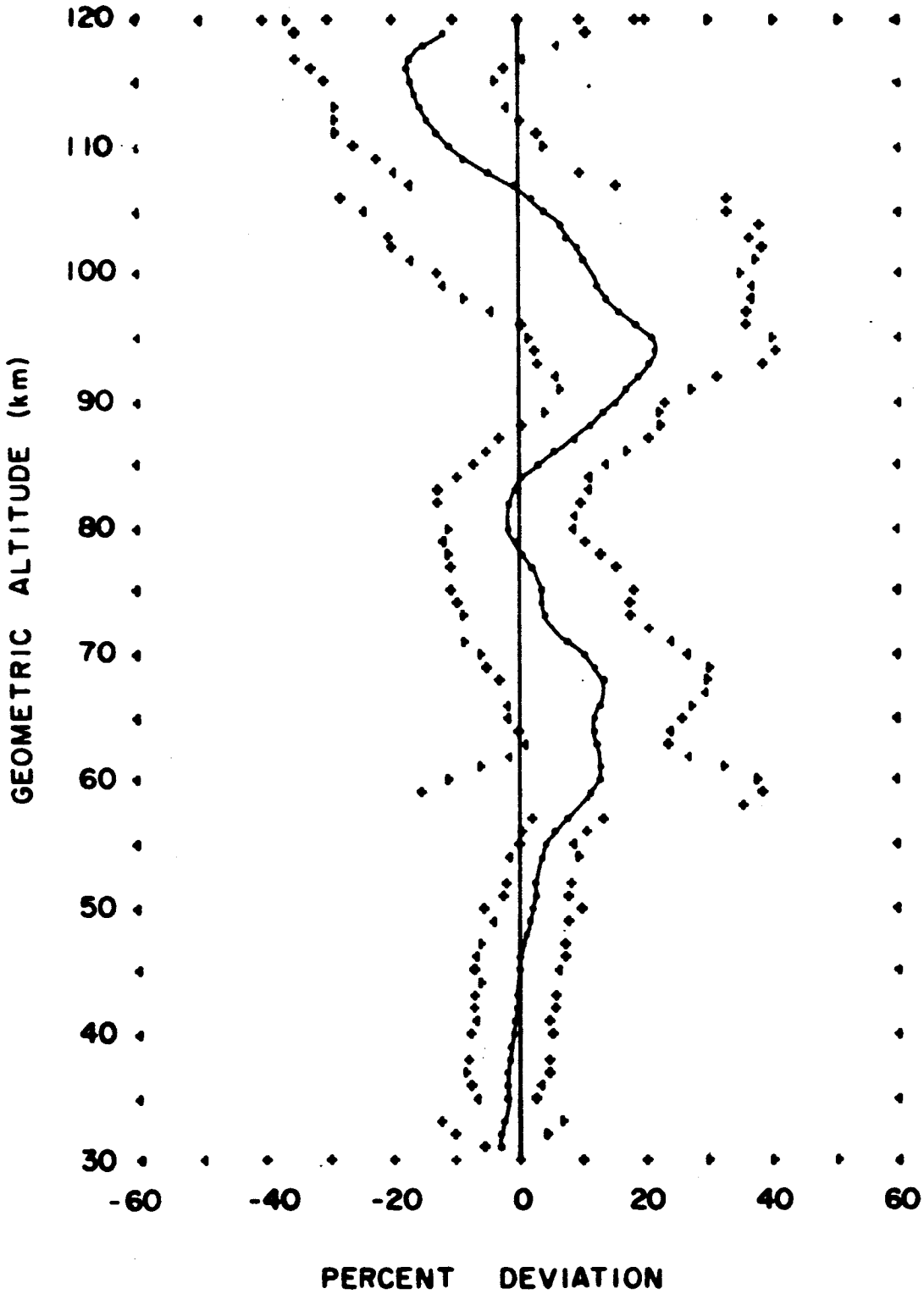

FIGURE 36S. PERCENT DEVIATION OF MEAN ATMOSPHERIC SUMMER DENSITIES OVER THE SUBTROPICS FROM DENSITIES OF THE U.S. STANDARD ATMOSPHERE

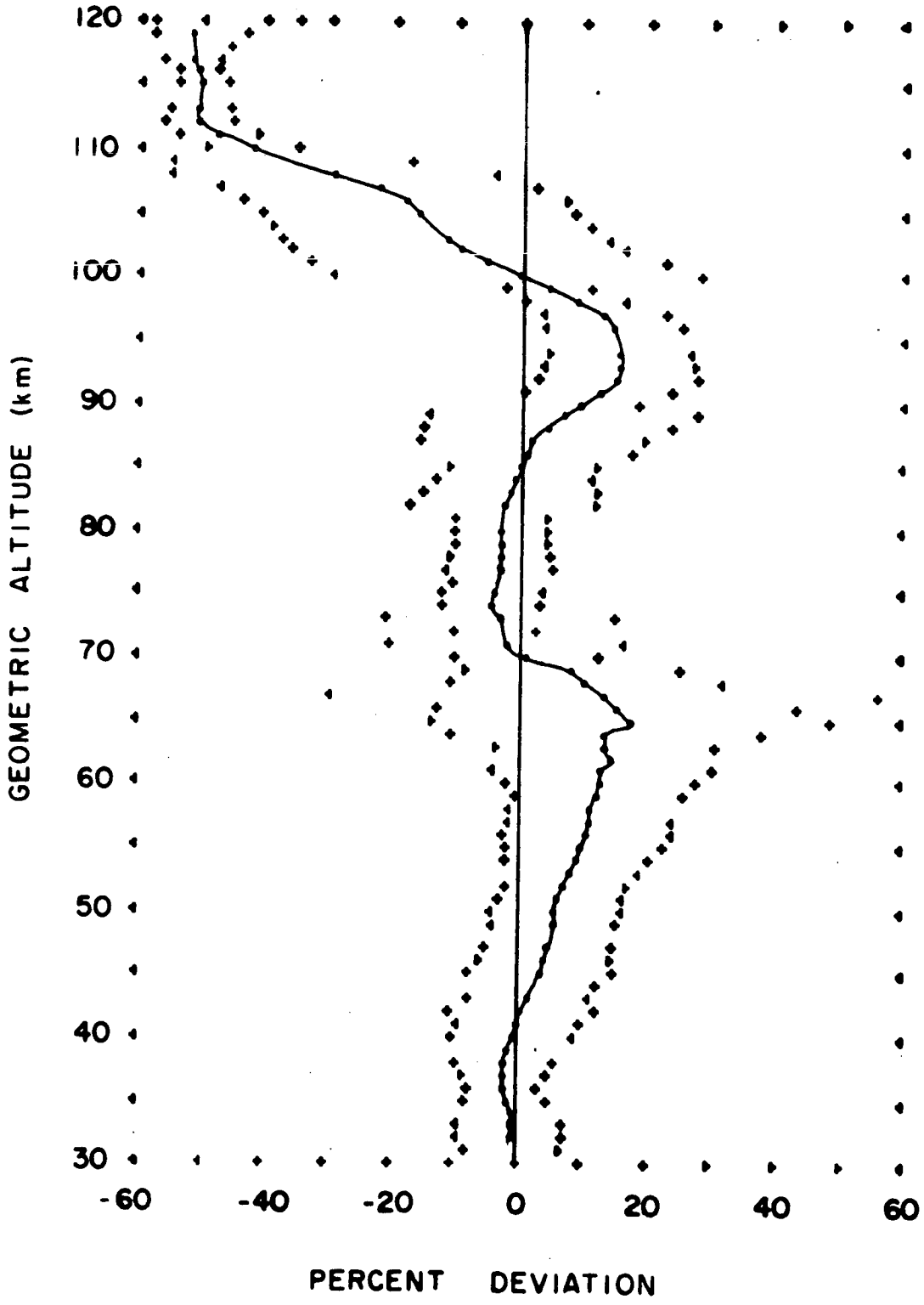

FIGURE 37S. PERCENT DEVIATION OF MEAN ATMOSPHERIC WINTER DENSITIES OVER THE SUBTROPICS FROM DENSITIES OF THE U.S. STANDARD ATMOSPHERE

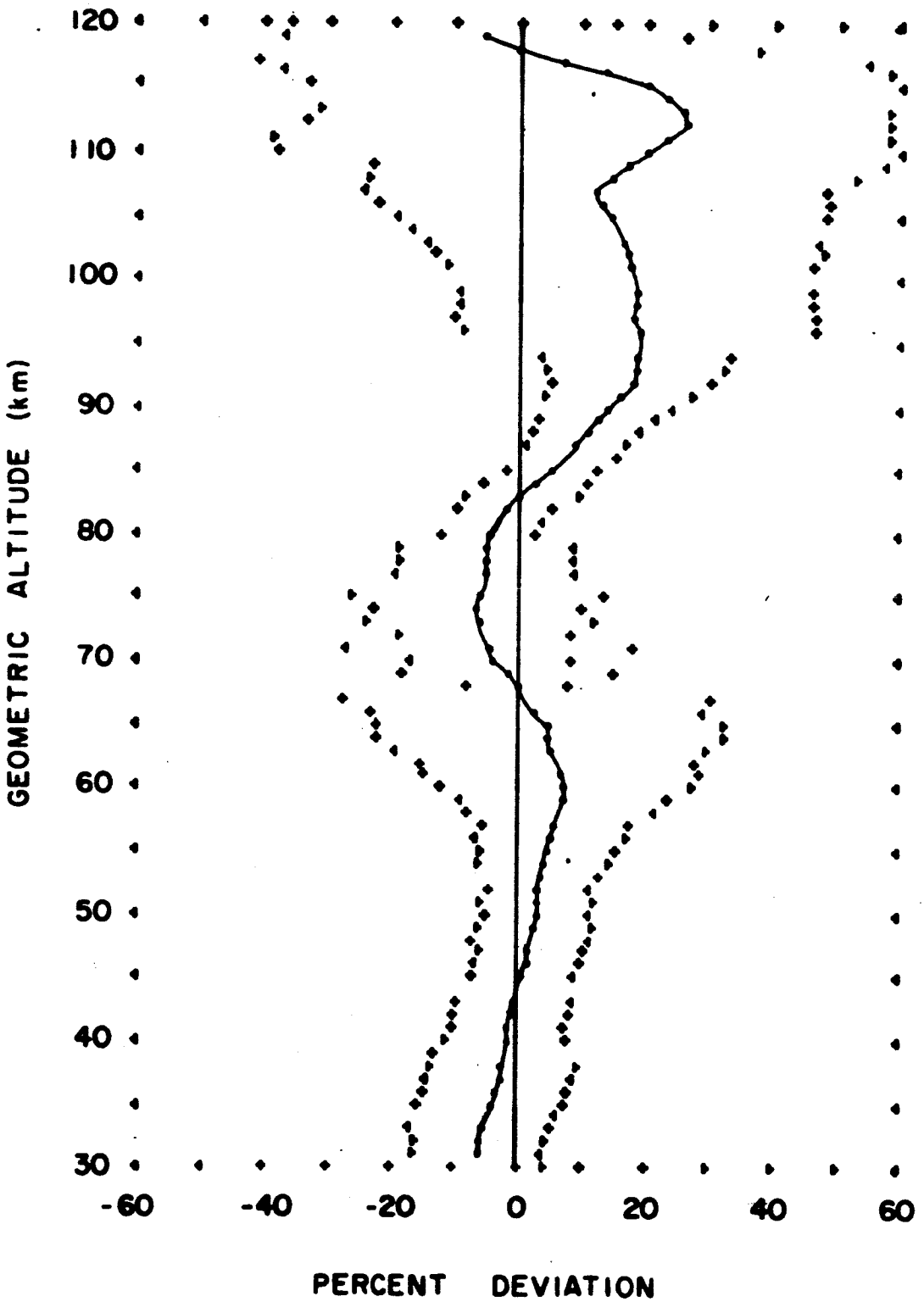

FIGURE 38S. PERCENT DEVIATION OF MEAN ATMOSPHERIC ANNUAL DENSITIES OVER THE SUBTROPICS FROM DENSITIES OF THE U.S. STANDARD ATMOSPHERE

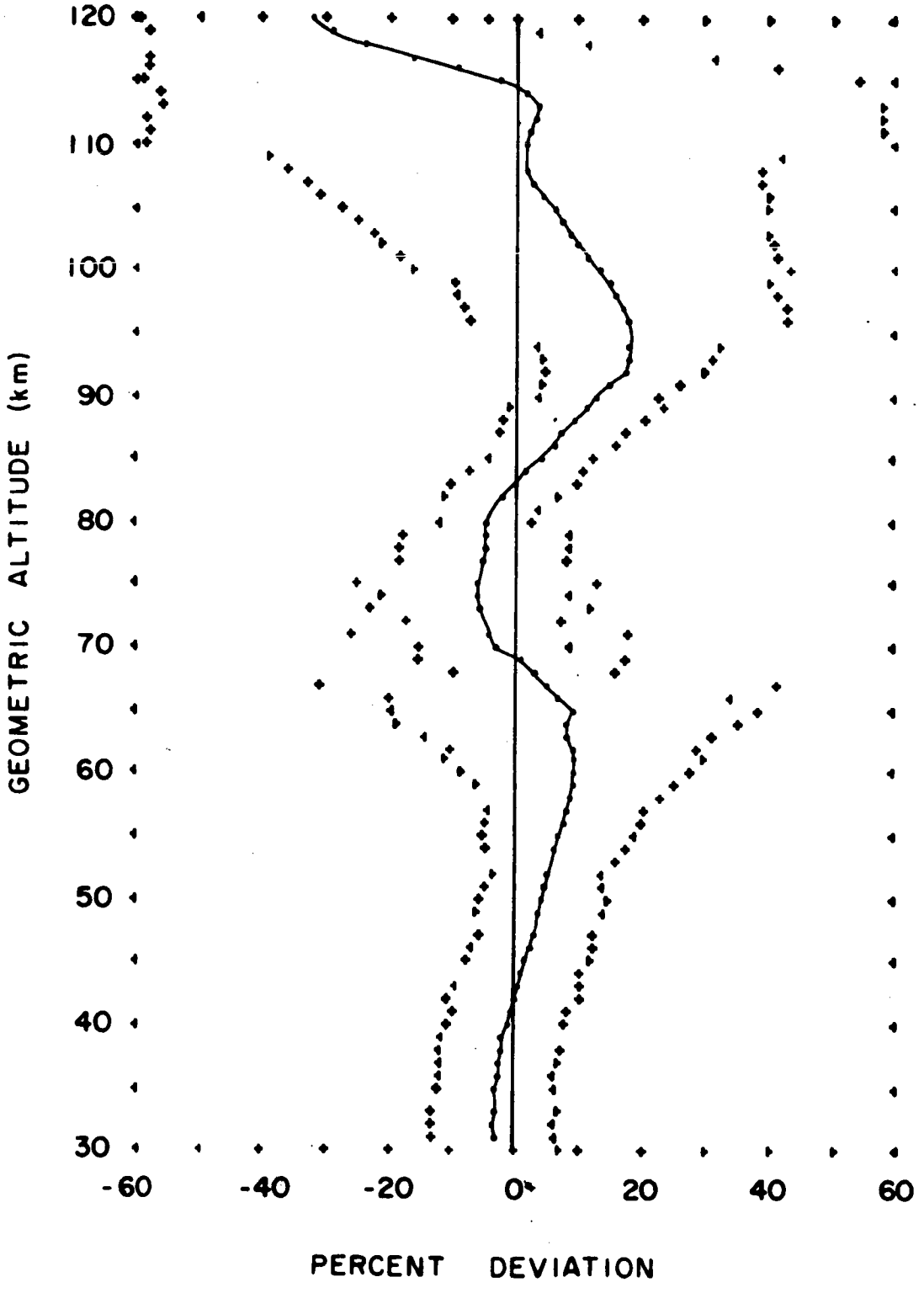

FIGURE 39S. PERCENT DEVIATION OF MEAN ATMOSPHERIC SUMMER DENSITIES OVER MIDLATITUDES FROM DENSITIES OF THE U.S. STANDARD ATMOSPHERE

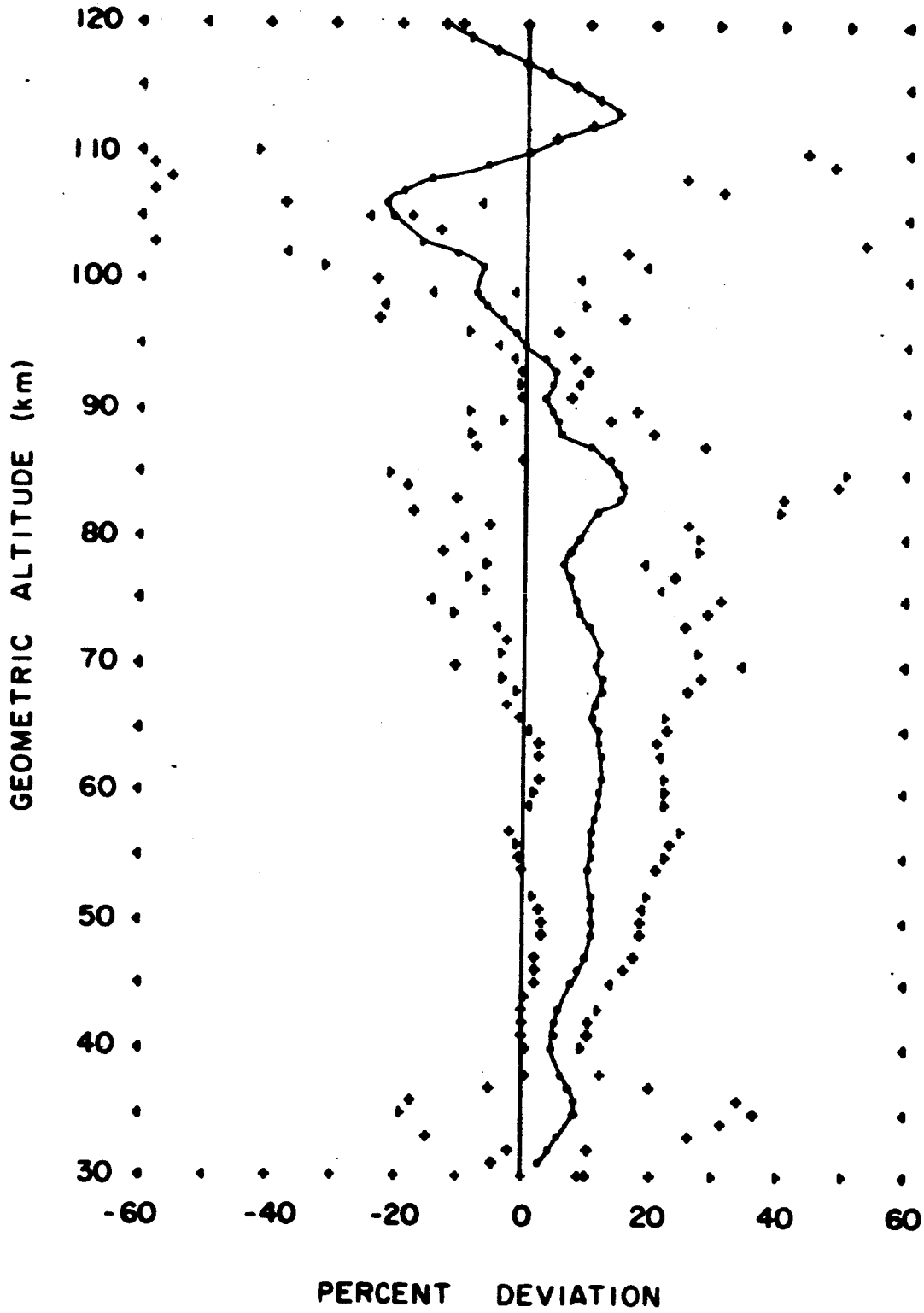

FIGURE 40S. PERCENT DEVIATION OF MEAN ATMOSPHERIC WINTER DENSITIES OVER MIDLATITUDES FROM DENSITIES OF THE U.S. STANDARD ATMOSPHERE

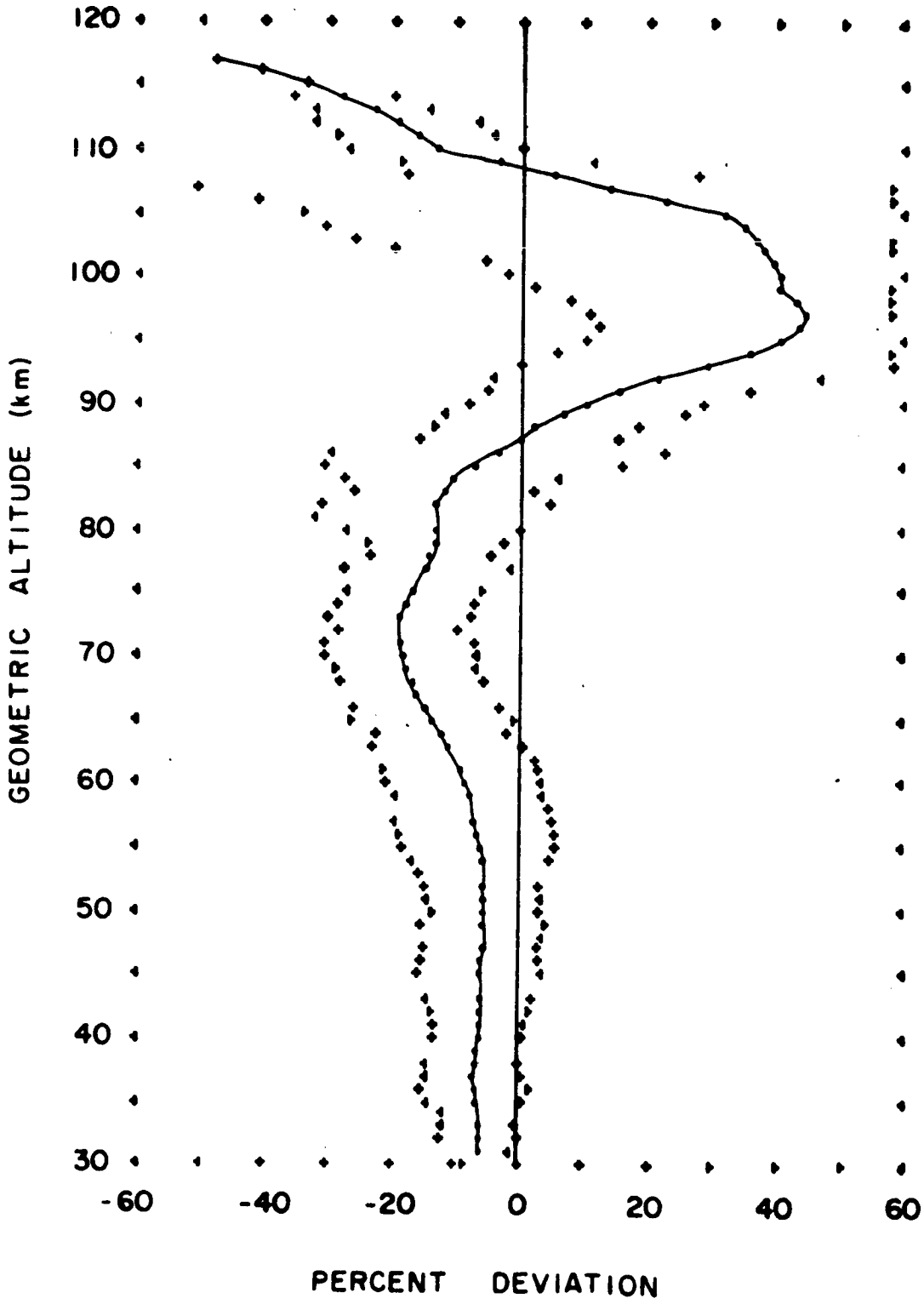

FIGURE 41S. PERCENT DEVIATION OF MEAN ATMOSPHERIC ANNUAL DENSITIES OVER MIDLATITUDES FROM DENSITIES OF THE U.S. STANDARD ATMOSPHERE

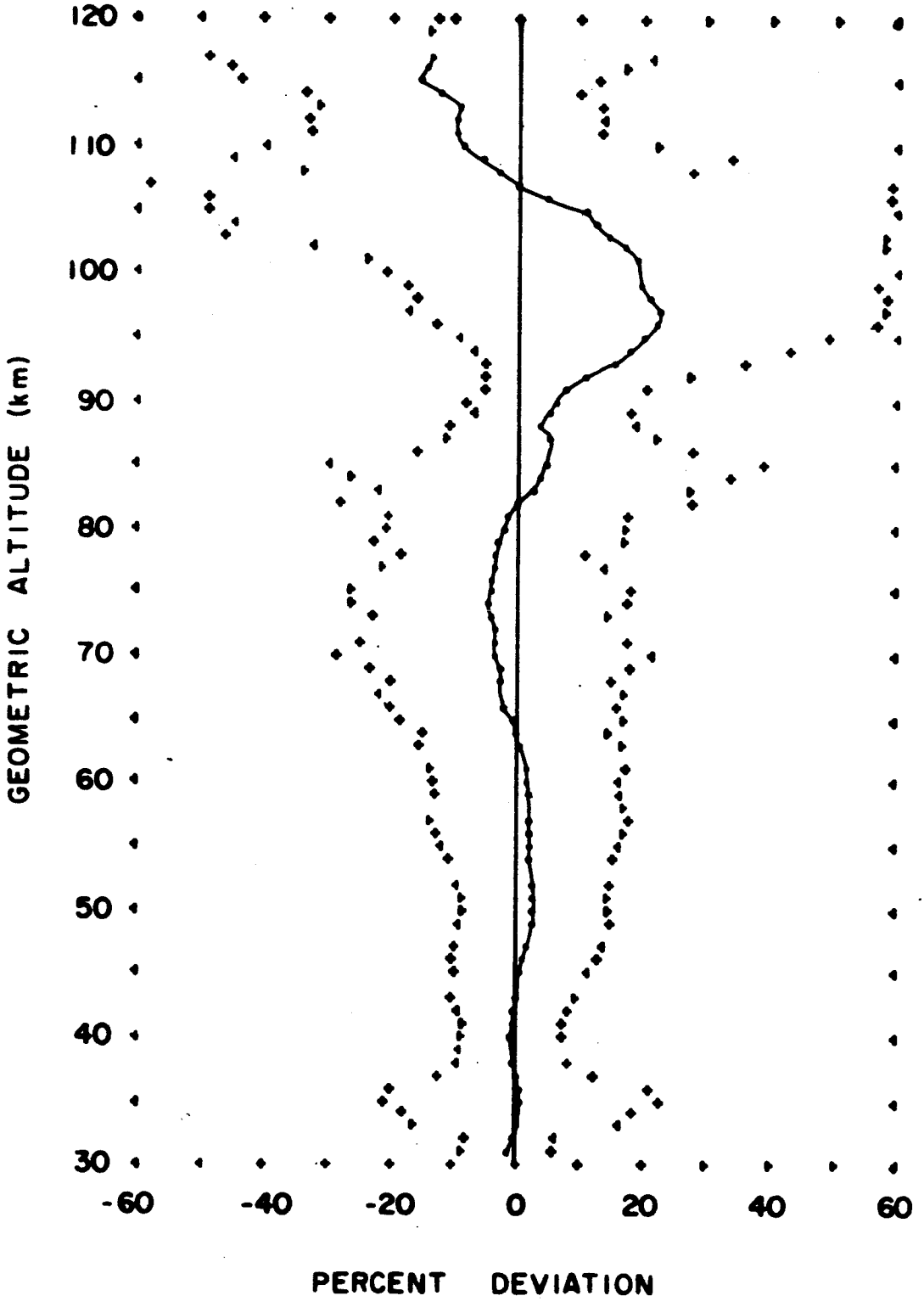

FIGURE 42S. PERCENT DEVIATION OF MEAN ATMOSPHERIC SUMMER DENSITIES OVER THE SUBARCTIC FROM DENSITIES OF THE U.S. STANDARD ATMOSPHERE

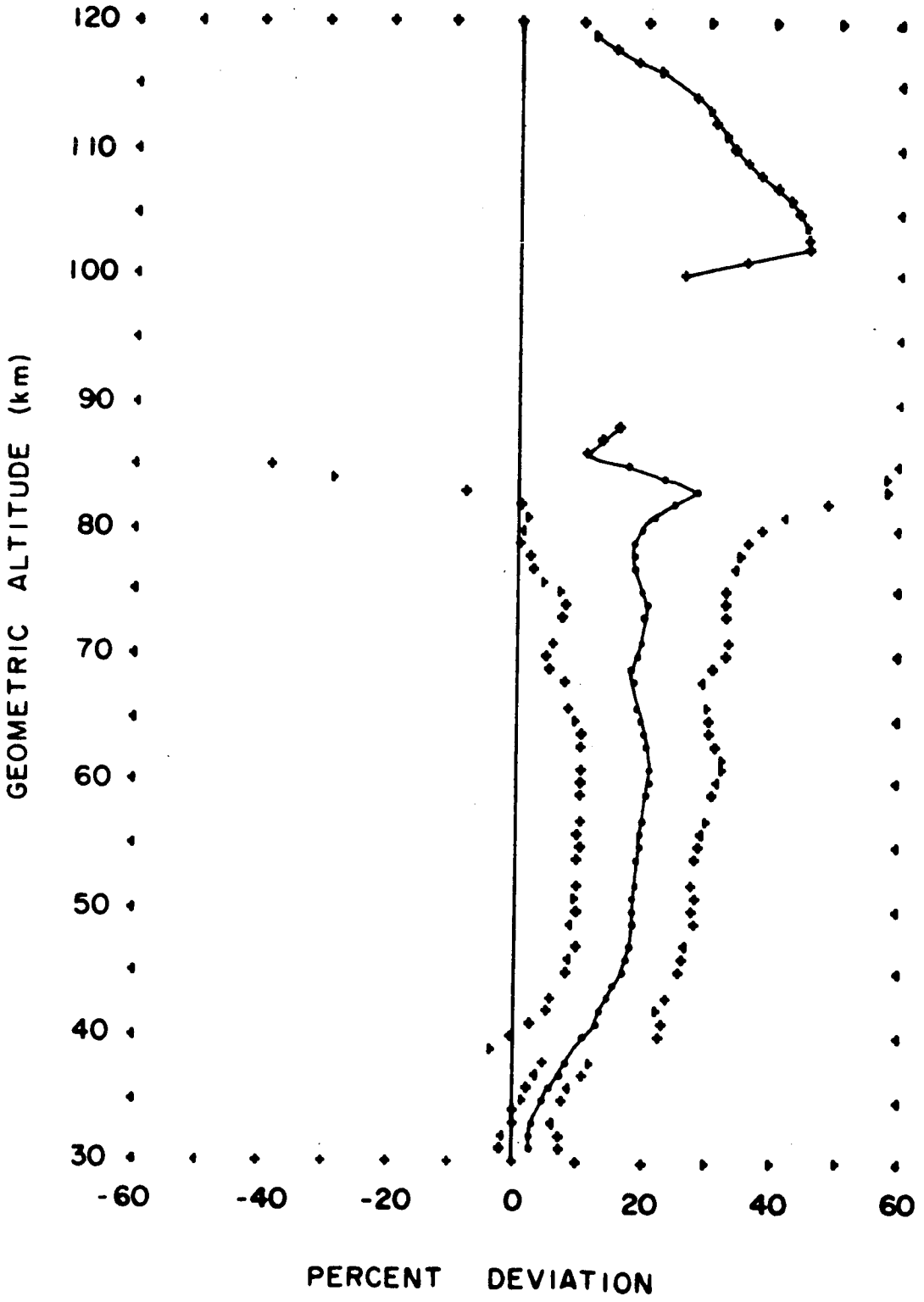

FIGURE 435. PERCENT DEVIATION OF MEAN ATMOSPHERIC
WINTER DENSITIES OVER THE SUBARCTIC
FROM DENSITIES OF THE U.S. STANDARD ATMOSPHERE

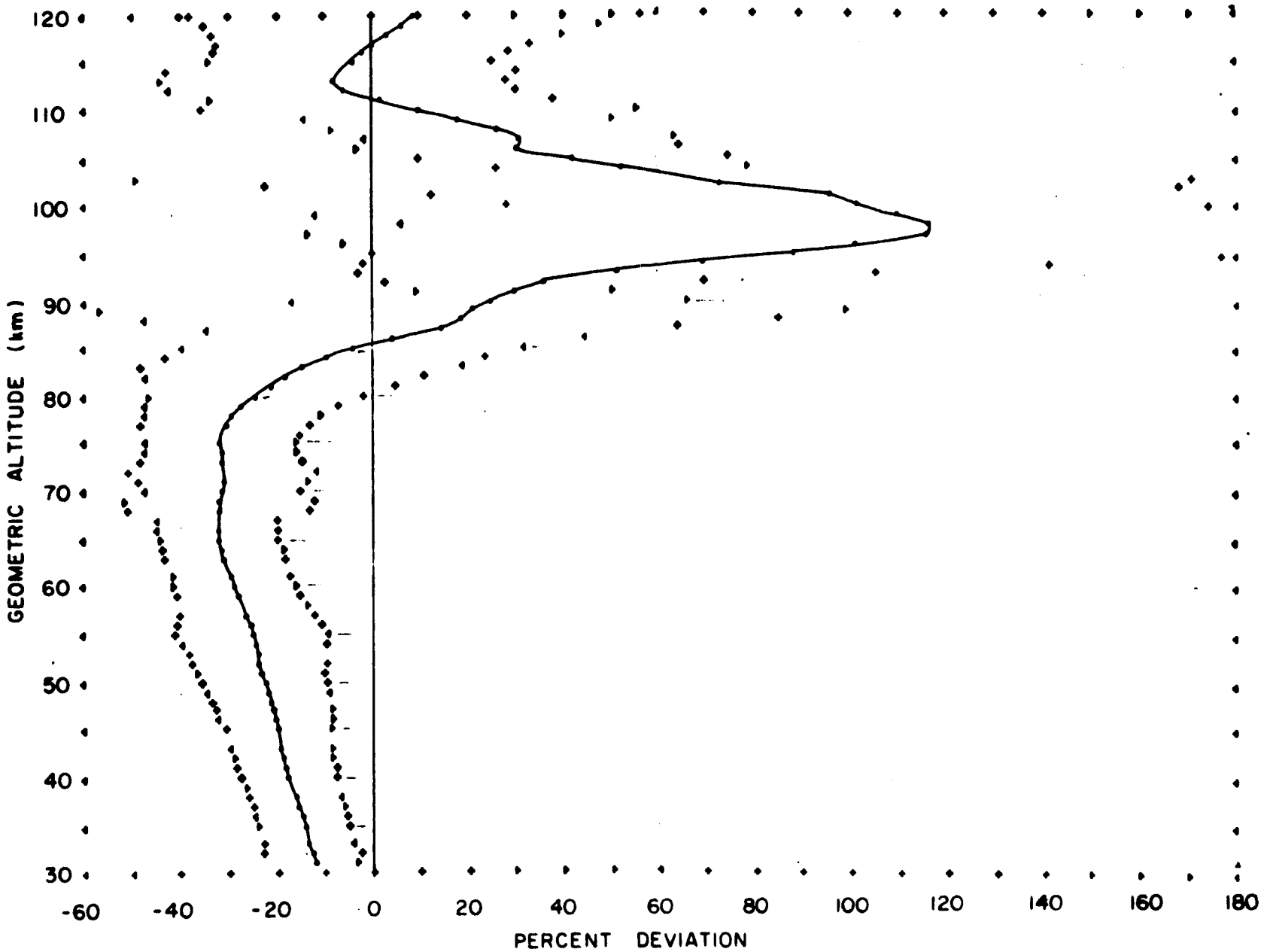

FIGURE 44S. PERCENT DEVIATION OF MEAN ATMOSPHERIC ANNUAL DENSITIES OVER THE SUBARCTIC FROM DENSITIES OF THE U.S. STANDARD ATMOSPHERE

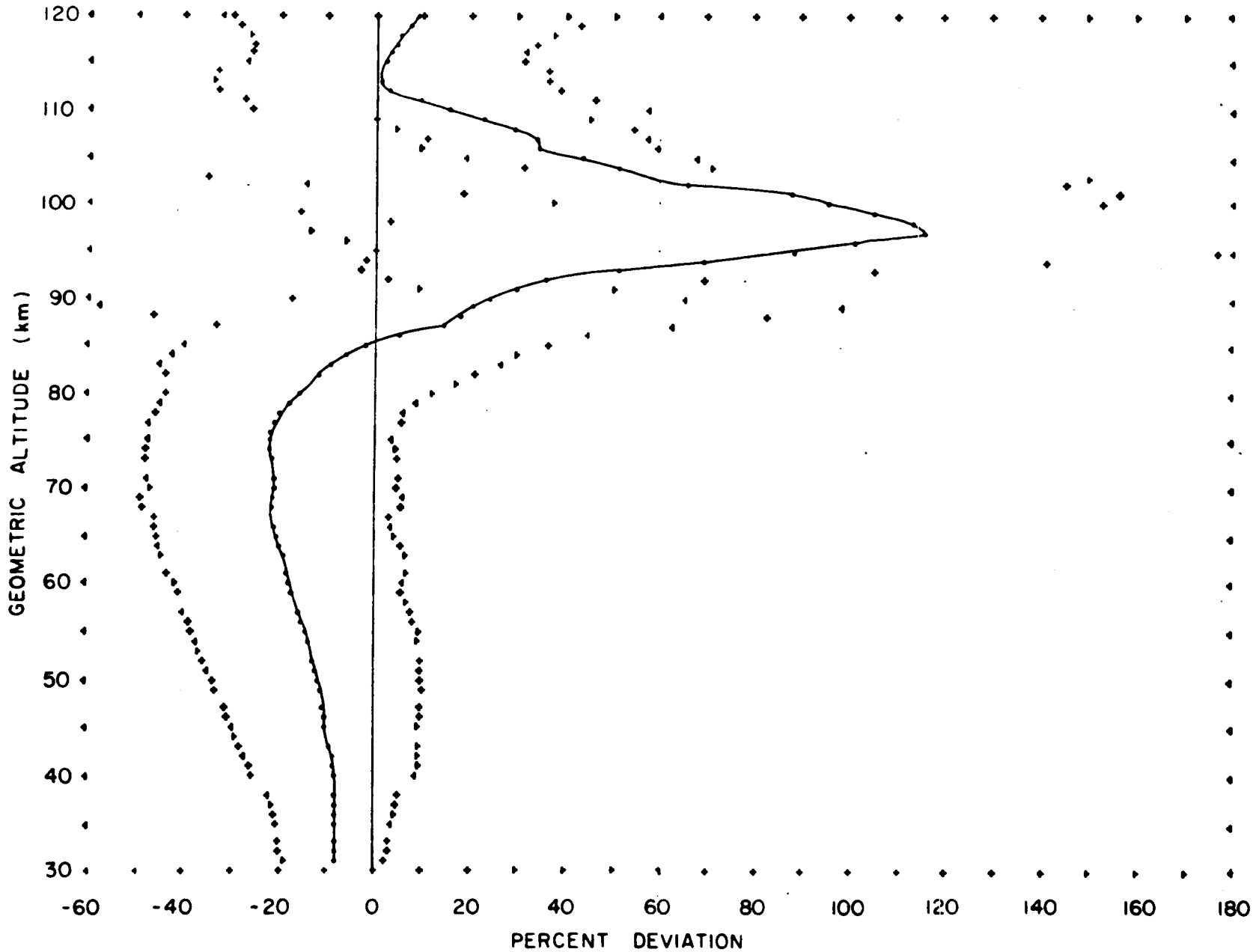

FIGURE 45S. PERCENT DEVIATION OF MEAN ATMOSPHERIC SUMMER DENSITIES OVER THE ARCTIC FROM DENSITIES OF THE U.S. STANDARD ATMOSPHERE

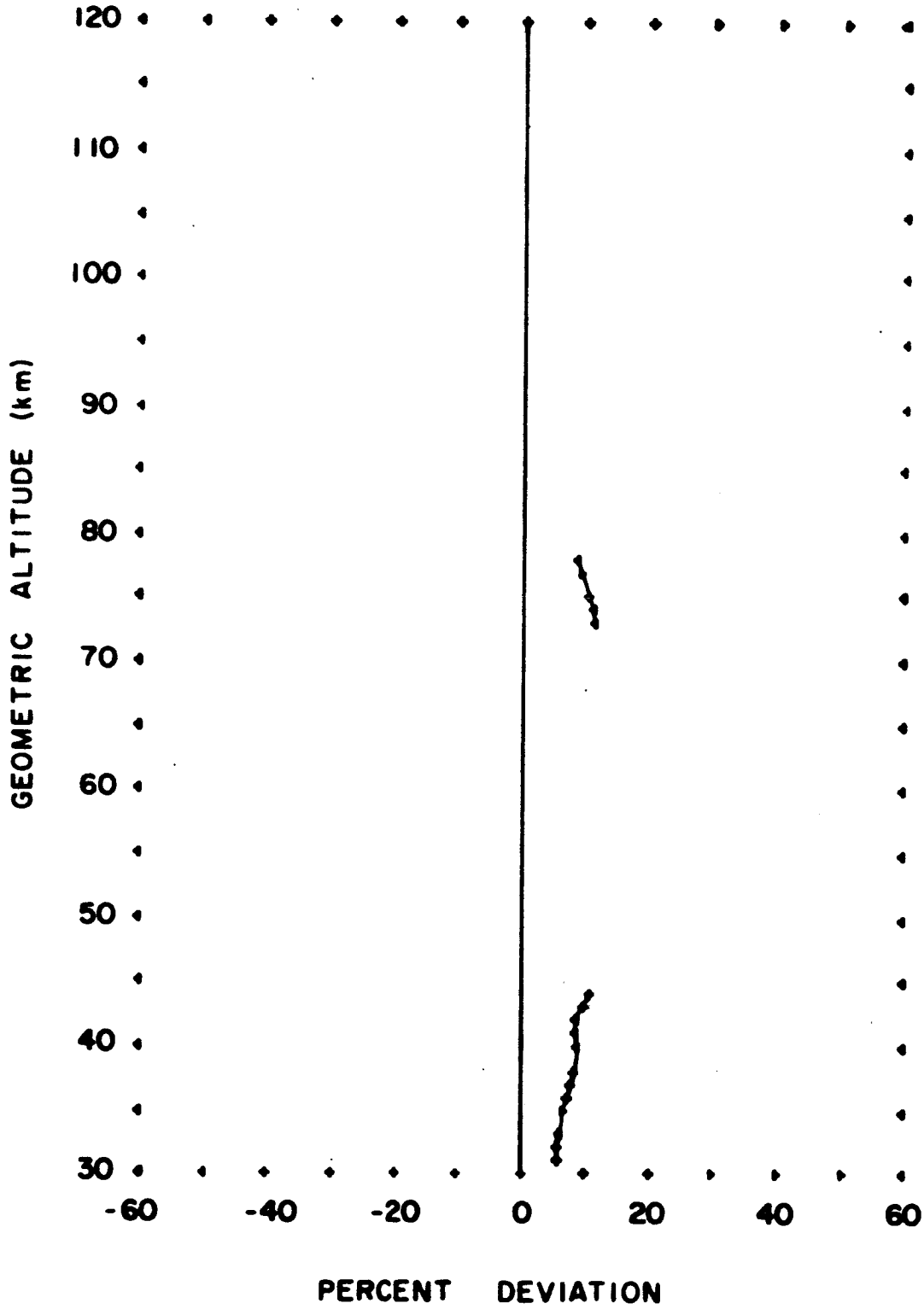

FIGURE 46S. PERCENT DEVIATION OF MEAN ATMOSPHERIC SUMMER DENSITIES OVER ALL SITES FROM DENSITIES OF THE U.S. STANDARD ATMOSPHERE

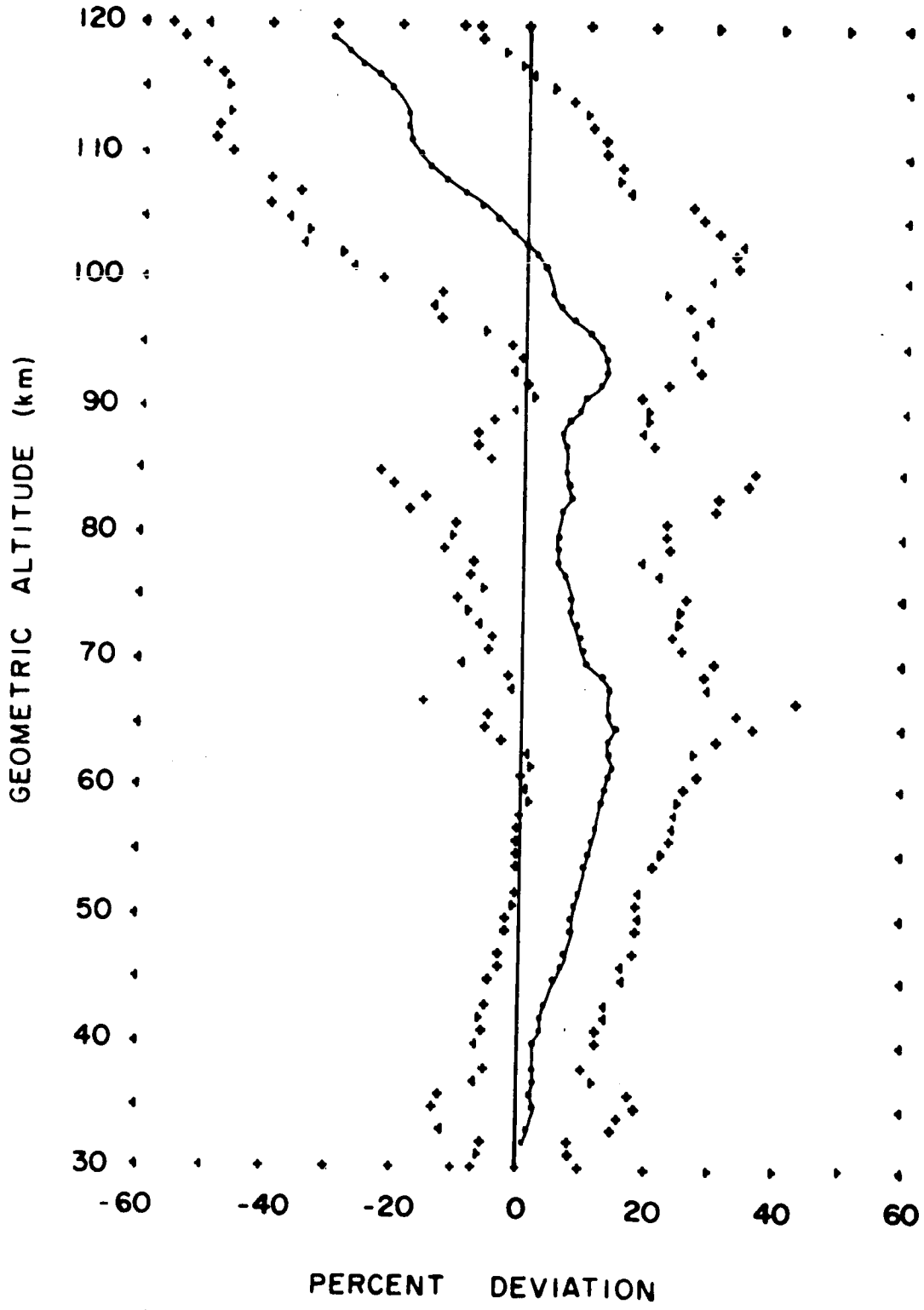

FIGURE 47S. PERCENT DEVIATION OF MEAN ATMOSPHERIC WINTER DENSITIES OVER ALL SITES FROM DENSITIES OF THE U.S. STANDARD ATMOSPHERE

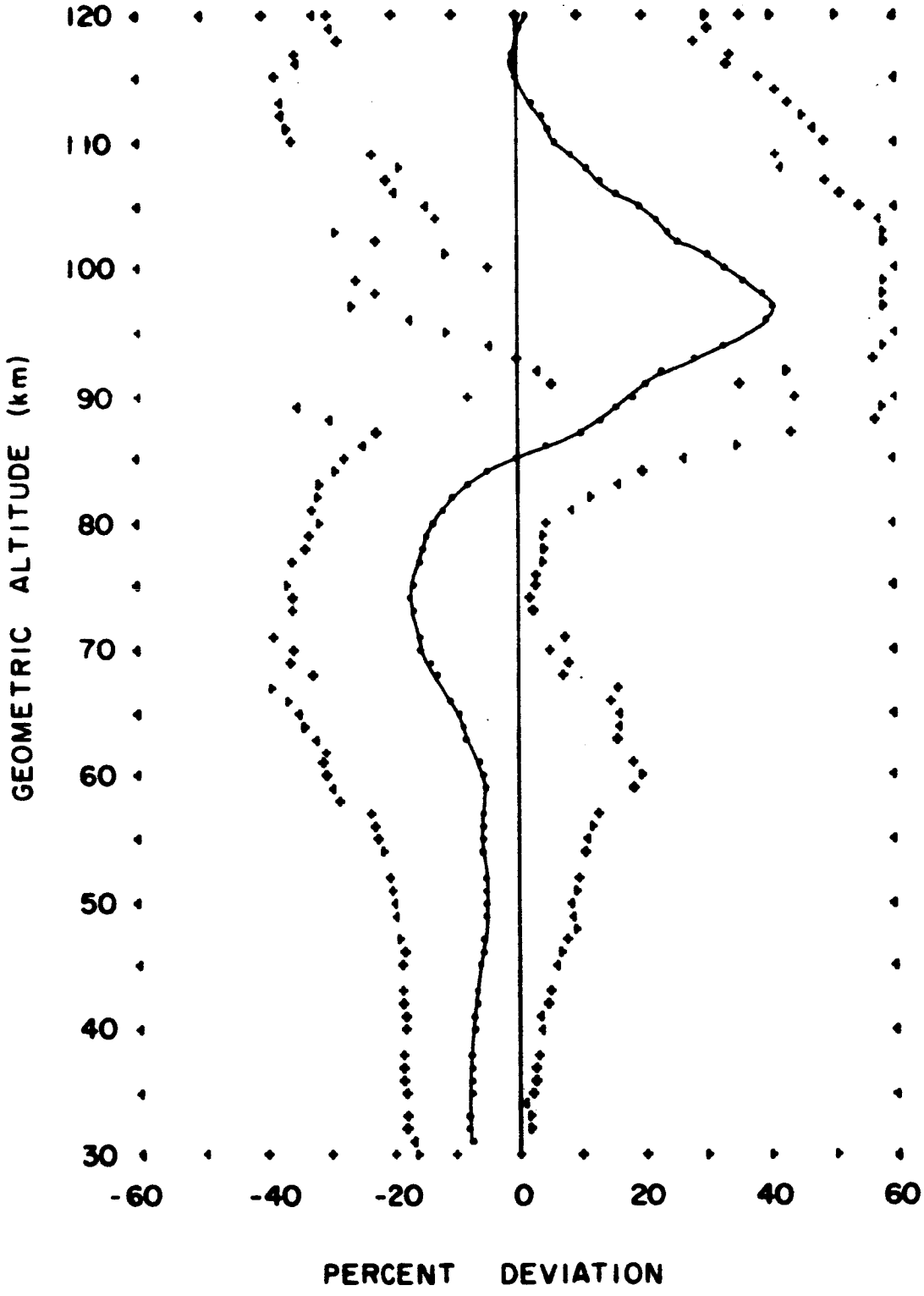

FIGURE 48S. PERCENT DEVIATION OF MEAN ATMOSPHERIC ANNUAL DENSITIES OVER ALL SITES FROM DENSITIES OF THE U.S. STANDARD ATMOSPHERE

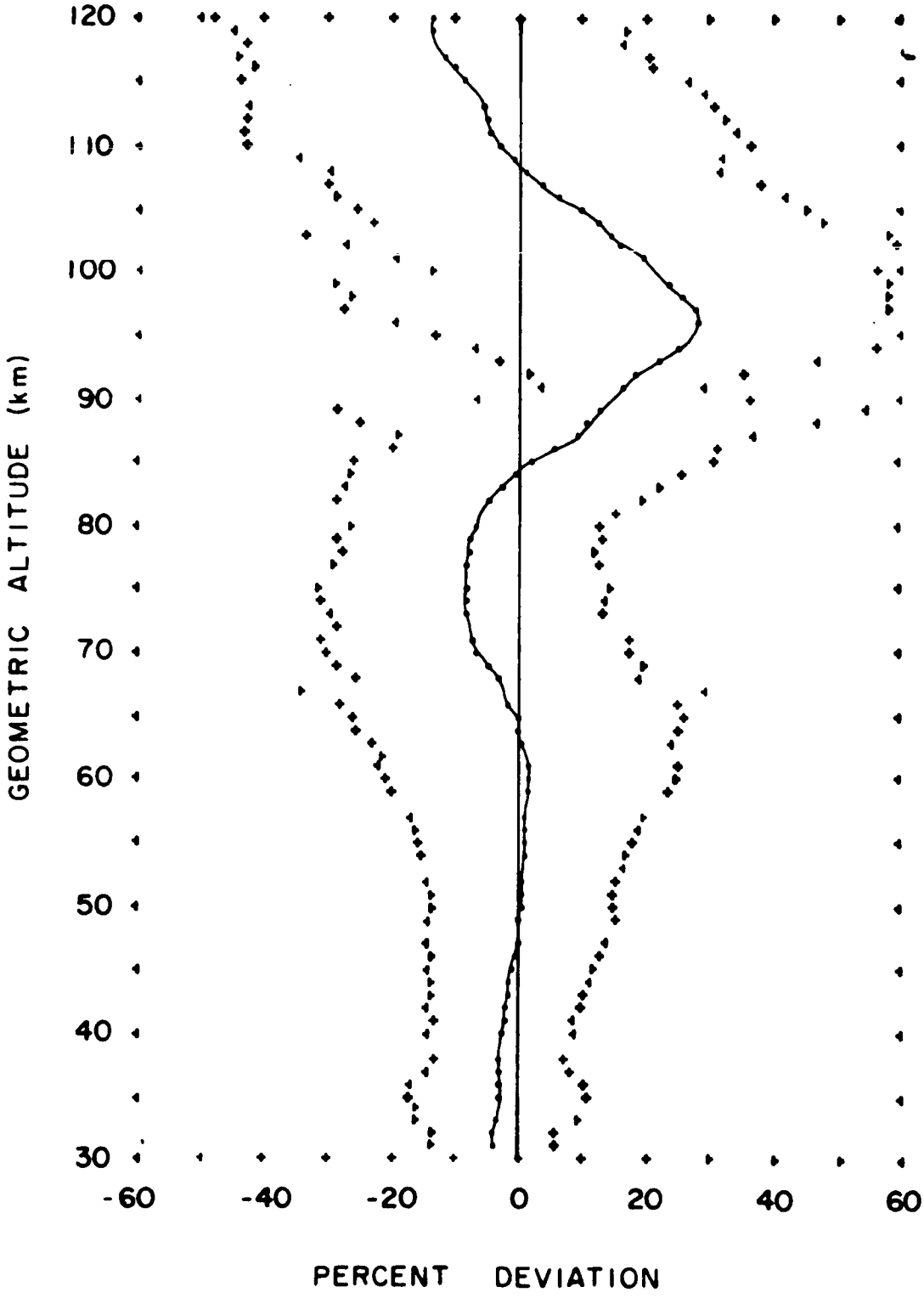

FIGURE 1P. PERCENT DEVIATION OF MEAN ATMOSPHERIC SUMMER DENSITIES OVER ASCENSION ISLAND FROM DENSITIES OF THE PATRICK REF. ATMOSPHERE

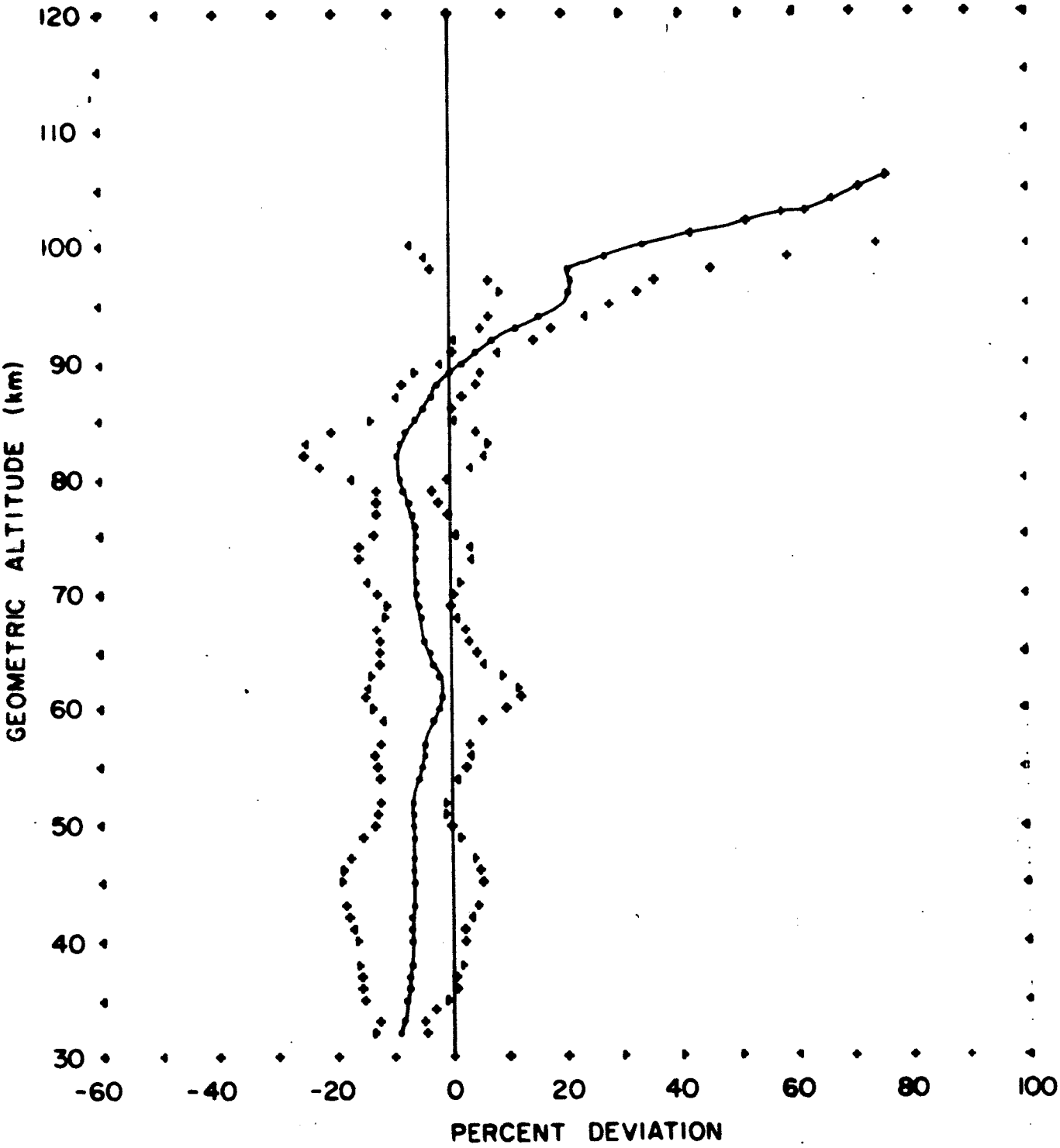

FIGURE 2P. PERCENT DEVIATION OF MEAN ATMOSPHERIC SUMMER DENSITIES OVER ALBUQUERQUE FROM DENSITIES OF THE PATRICK REF. ATMOSPHERE

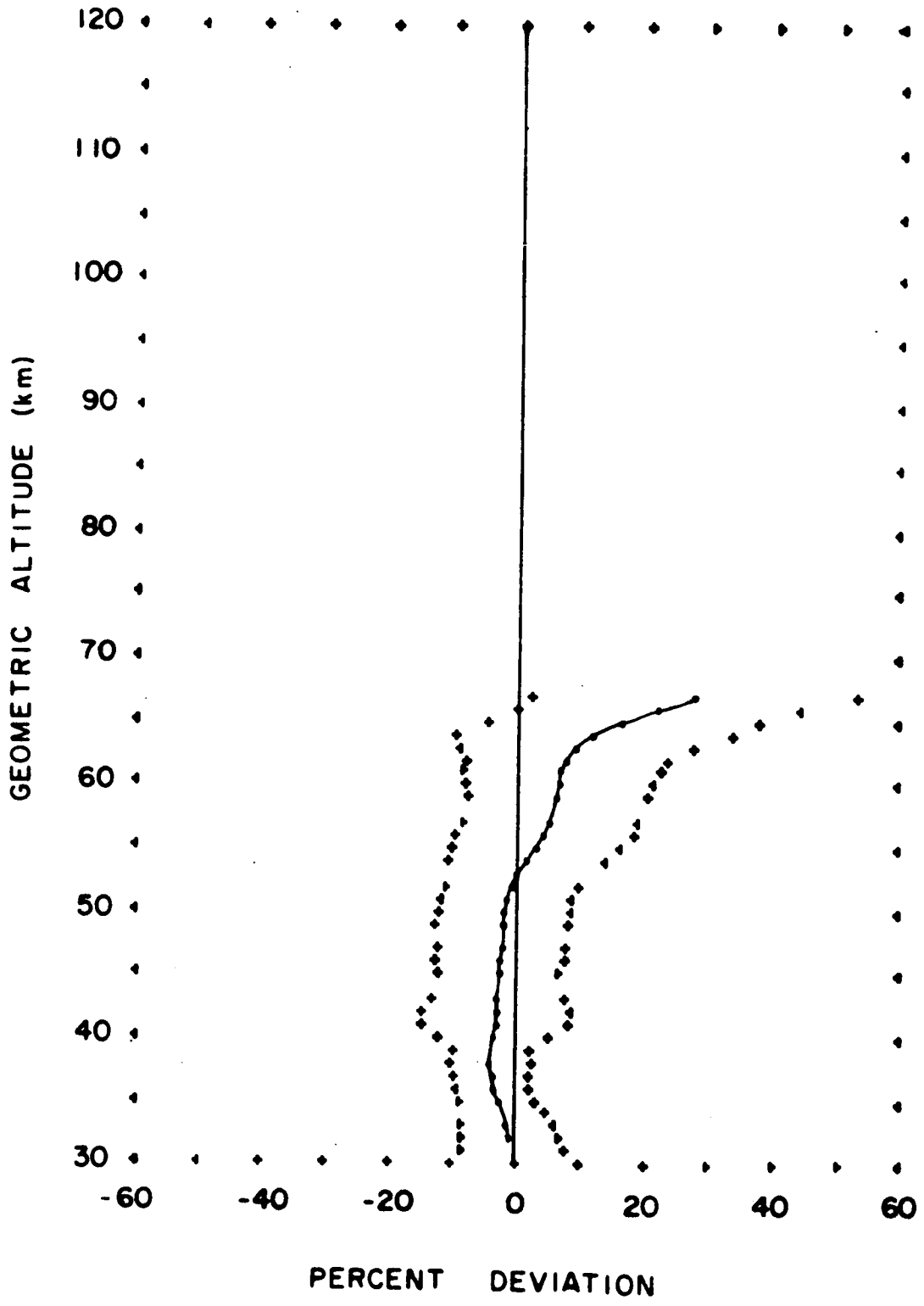

FIGURE 3P. PERCENT DEVIATION OF MEAN ATMOSPHERIC WINTER DENSITIES OVER ALBUQUERQUE FROM DENSITIES OF THE PATRICK REF. ATMOSPHERE

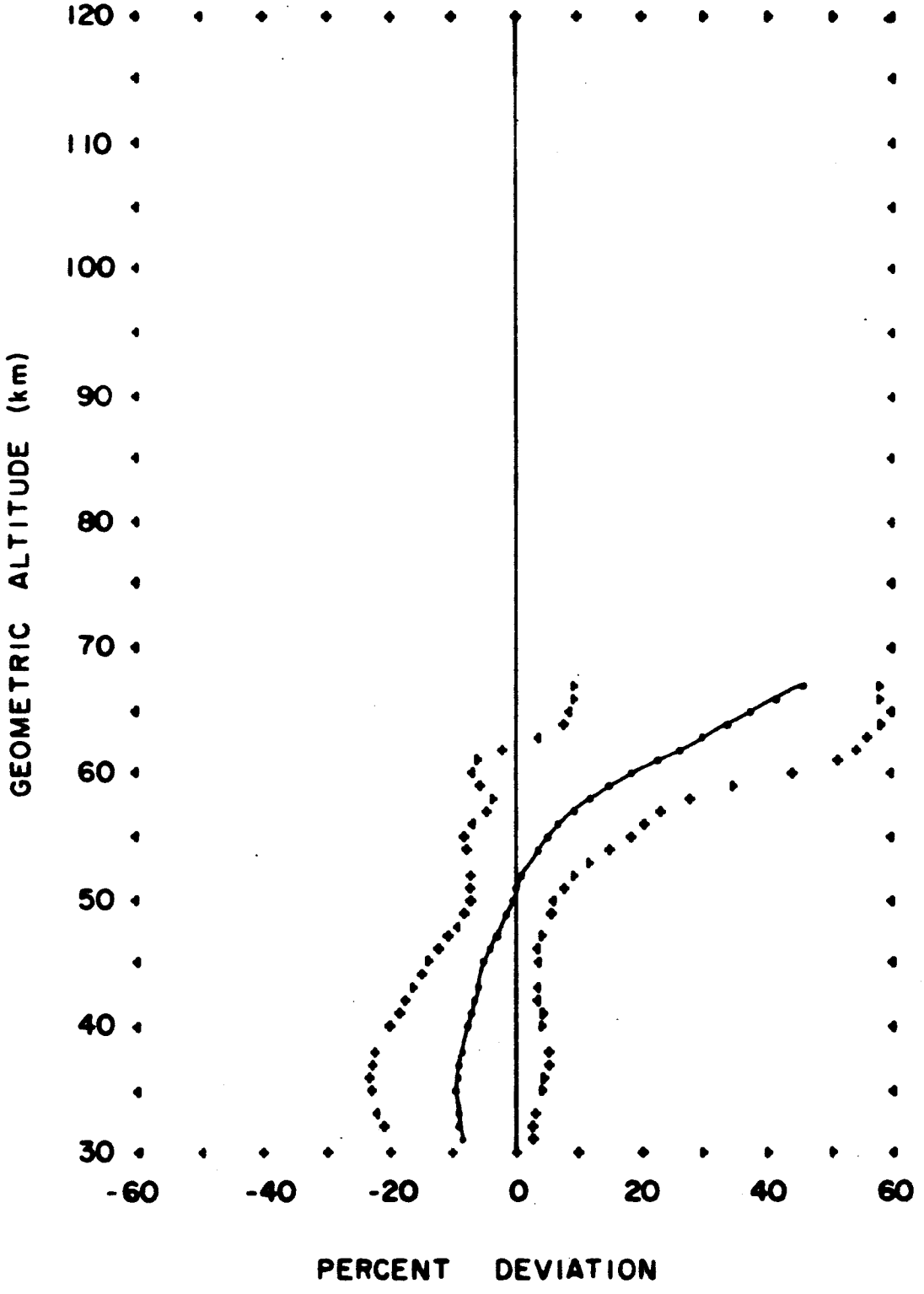

FIGURE 4P. PERCENT DEVIATION OF MEAN ATMOSPHERIC ANNUAL DENSITIES OVER ALBUQUERQUE FROM DENSITIES OF THE PATRICK REF. ATMOSPHERE

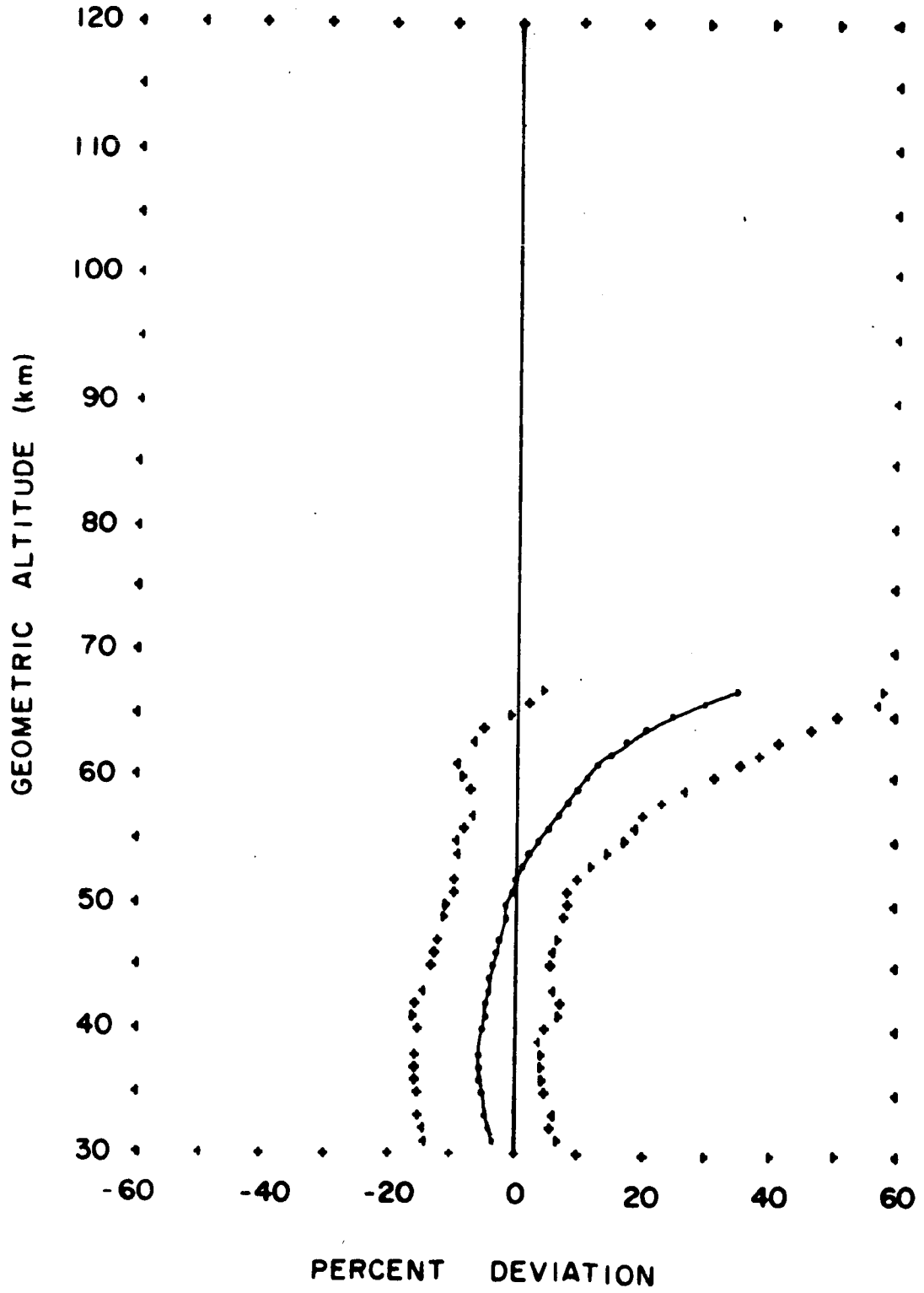

FIGURE 5P. PERCENT DEVIATION OF MEAN ATMOSPHERIC WINTER DENSITIES OVER EGLIN RANGE FROM DENSITIES OF THE PATRICK REF. ATMOSPHERE

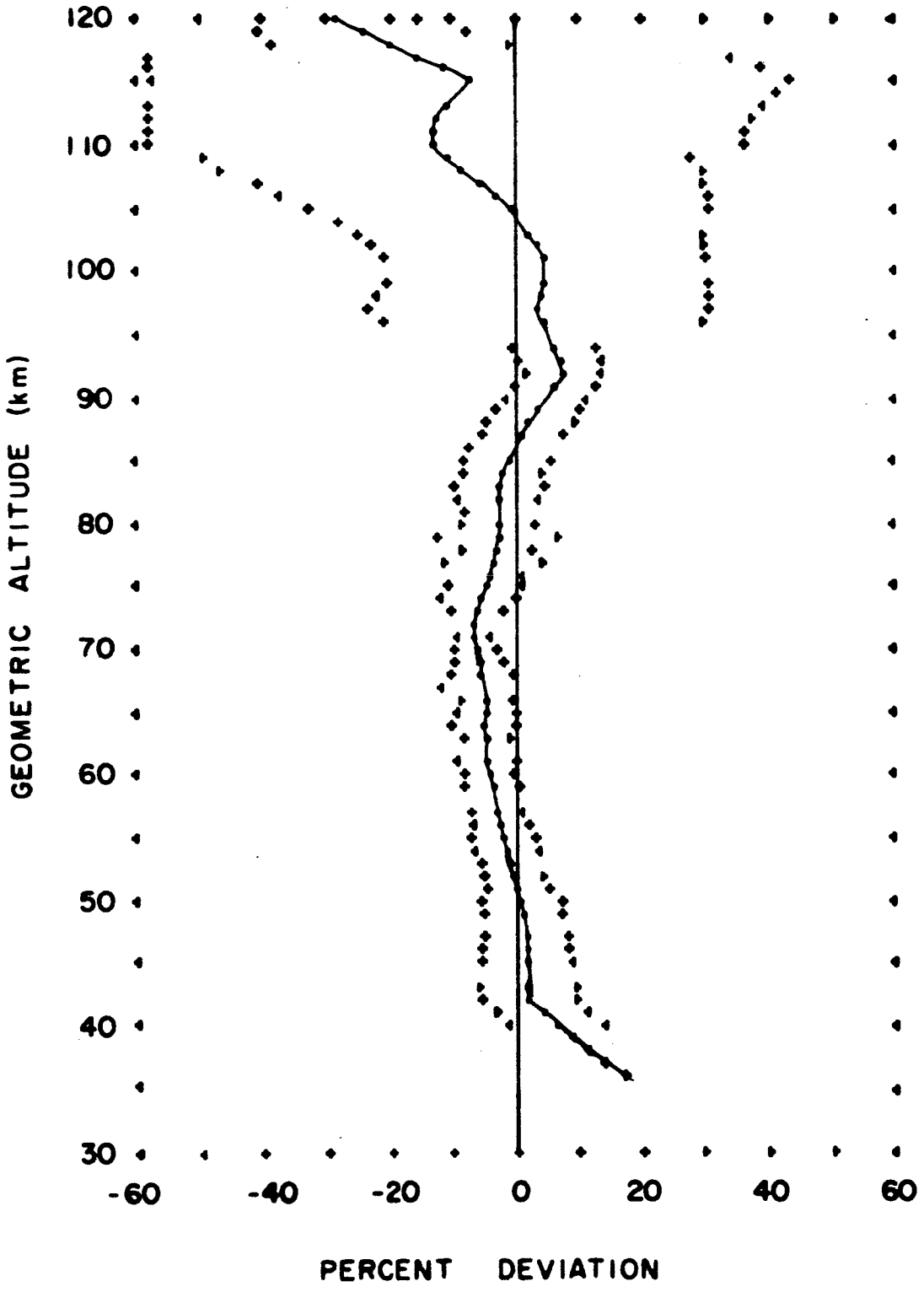

FIGURE 6P. PERCENT DEVIATION OF MEAN ATMOSPHERIC SUMMER DENSITIES OVER FORT CHURCHILL FROM DENSITIES OF THE PATRICK REF. ATMOSPHERE

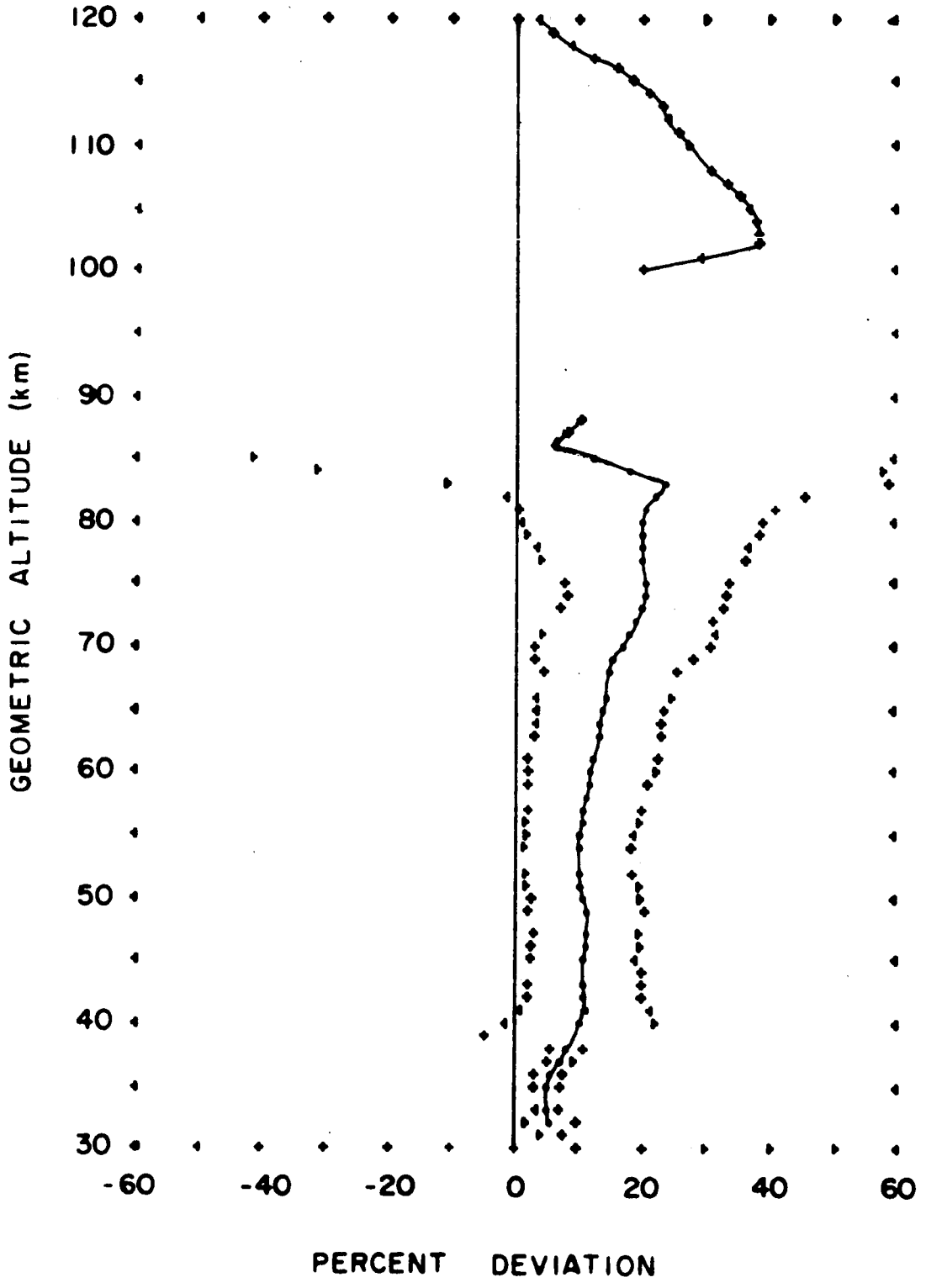

FIGURE 7P. PERCENT DEVIATION OF MEAN ATMOSPHERIC WINTER DENSITIES OVER FORT CHURCHILL FROM DENSITIES OF THE PATRICK REF. ATMOSPHERE

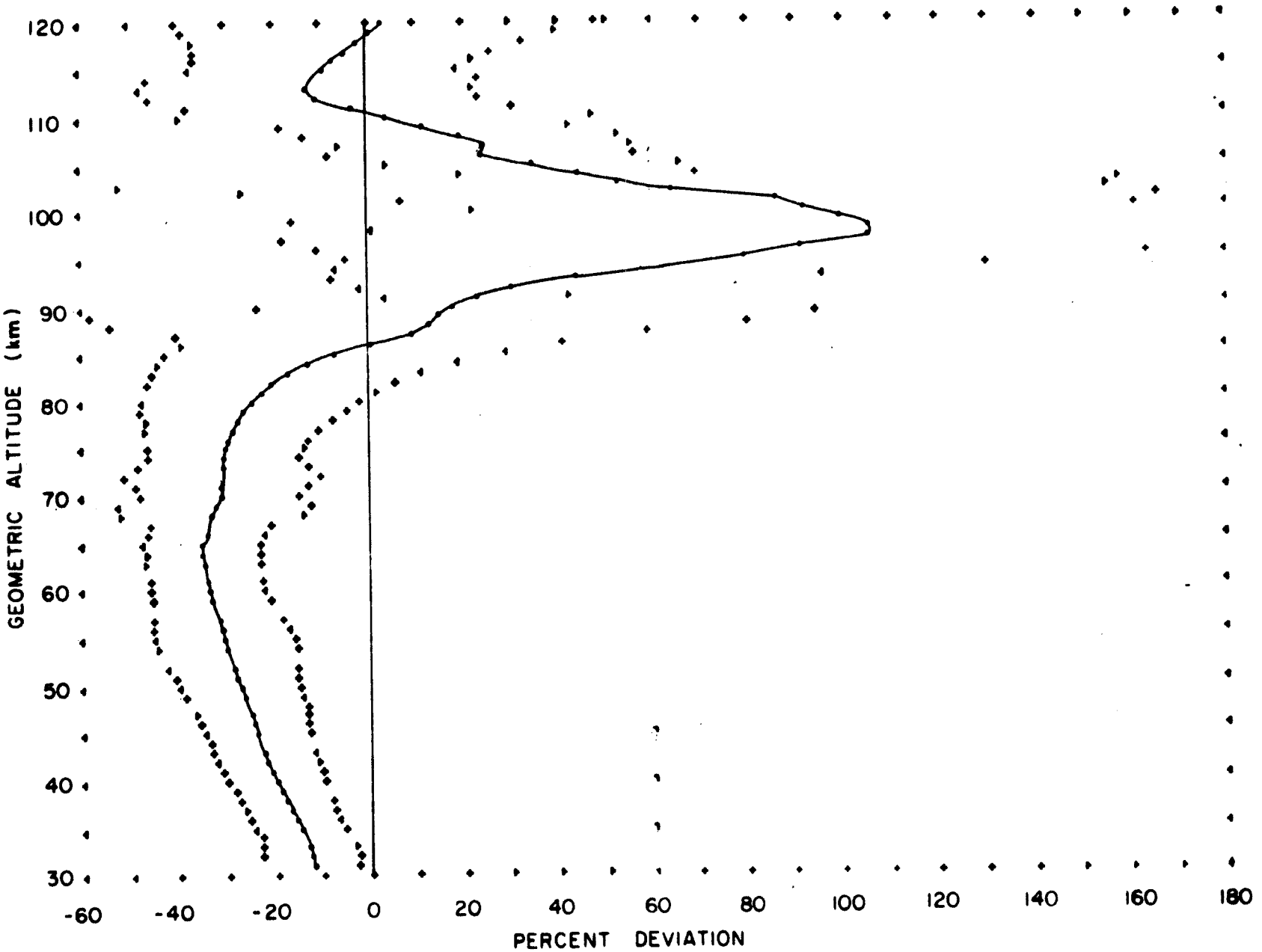

FIGURE 8P. PERCENT DEVIATION OF MEAN ATMOSPHERIC ANNUAL DENSITIES OVER FORT CHURCHILL FROM DENSITIES OF THE PATRICK REF. ATMOSPHERE

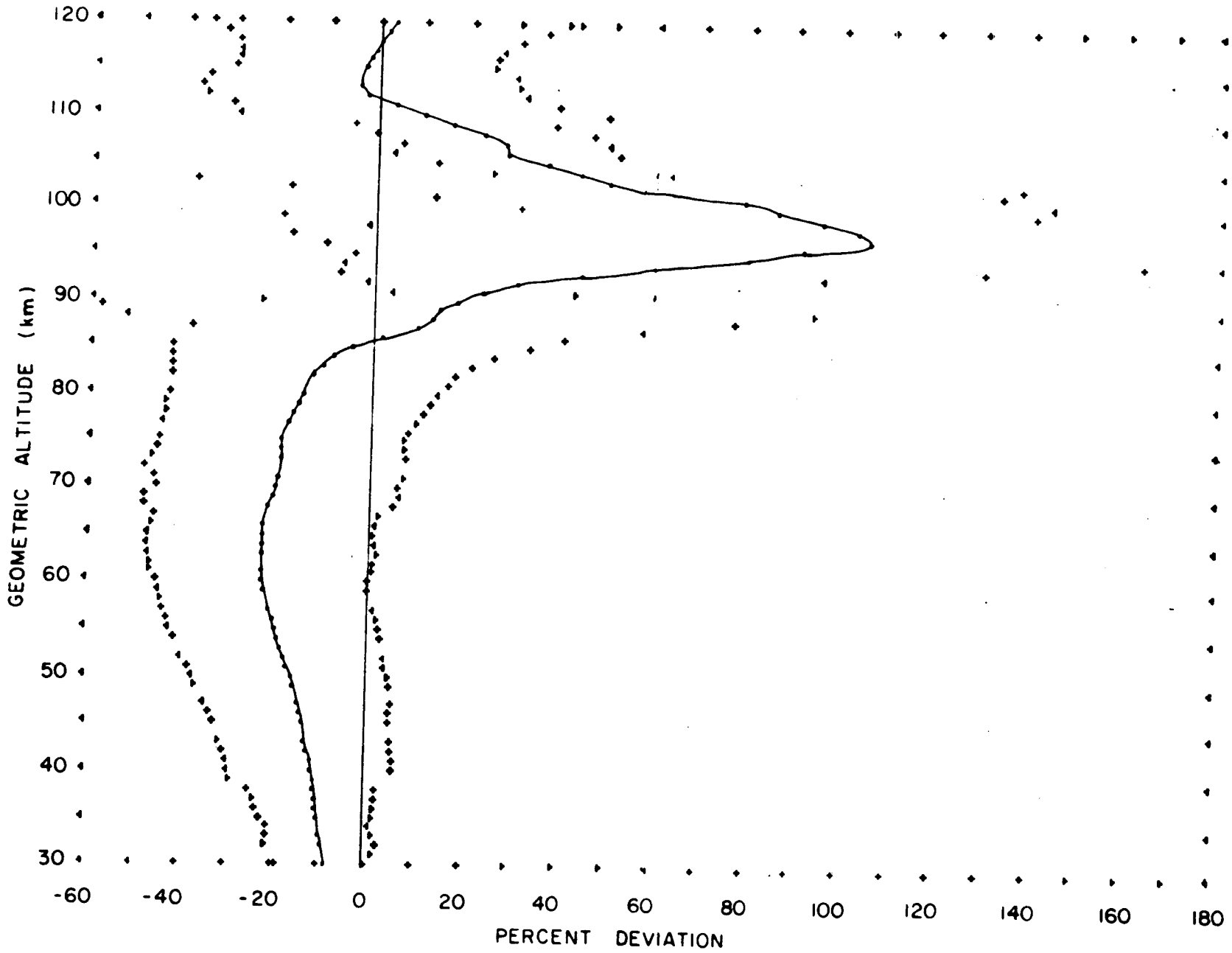

FIGURE 9P. PERCENT DEVIATION OF MEAN ATMOSPHERIC WINTER DENSITIES OVER GUAM FROM DENSITIES OF THE PATRICK REF. ATMOSPHERE

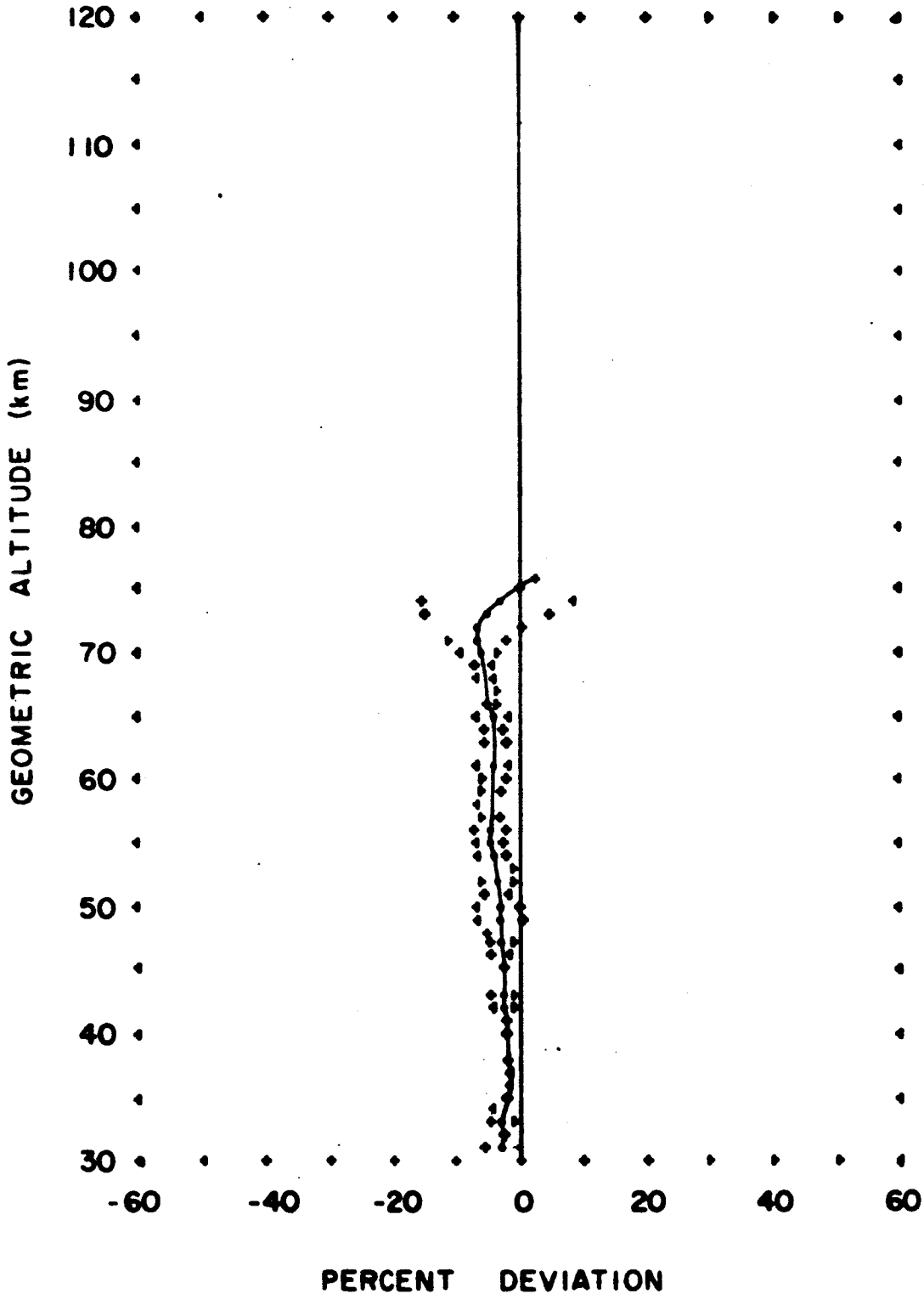

FIGURE 10P. PERCENT DEVIATION OF MEAN ATMOSPHERIC SUMMER DENSITIES OVER HOLLOMAN AFB FROM DENSITIES OF THE PATRICK REF. ATMOSPHERE

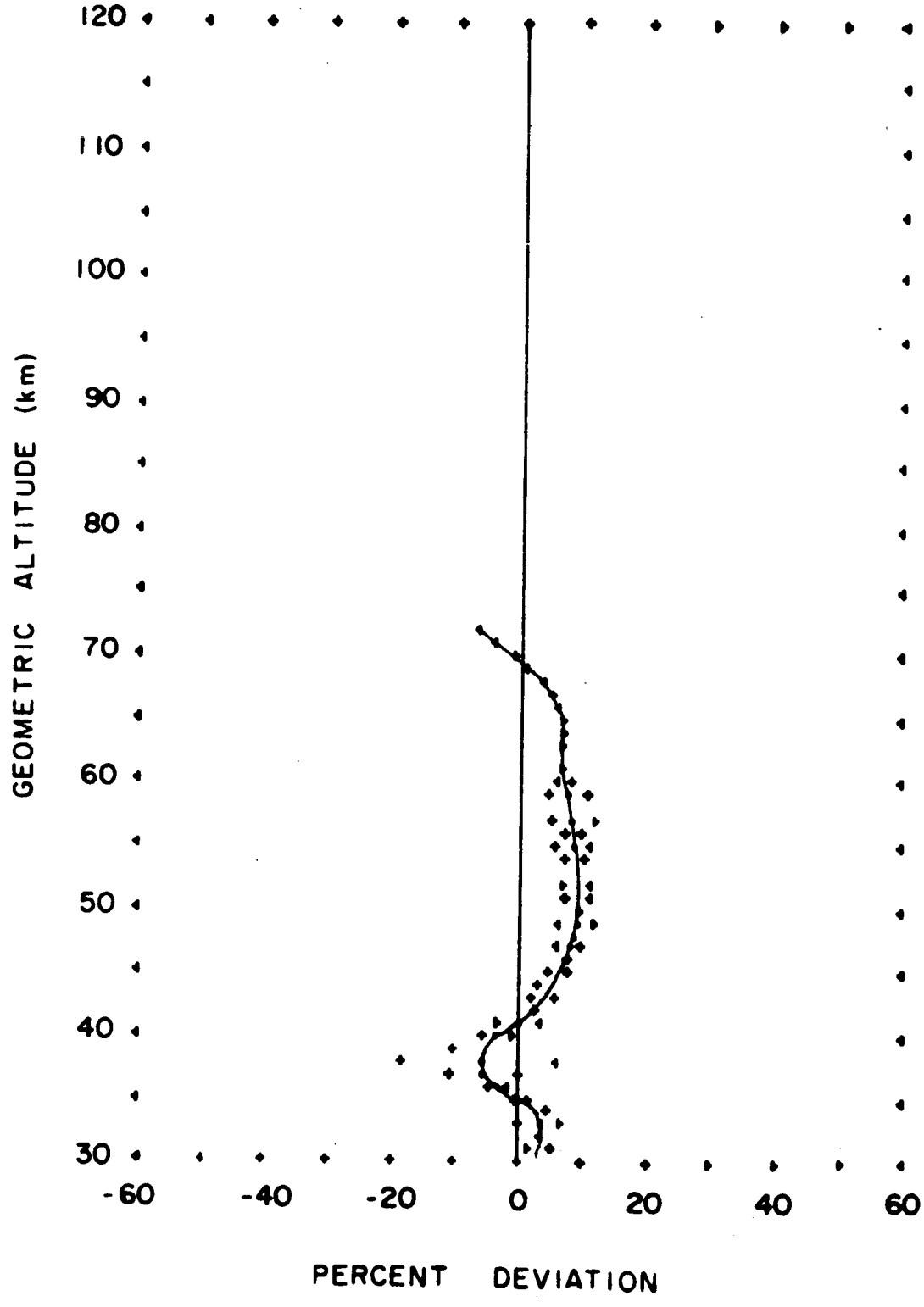

FIGURE 11P. PERCENT DEVIATION OF MEAN ATMOSPHERIC WINTER DENSITIES OVER HOLLOMAN AFB FROM DENSITIES OF THE PATRICK REF. ATMOSPHERE

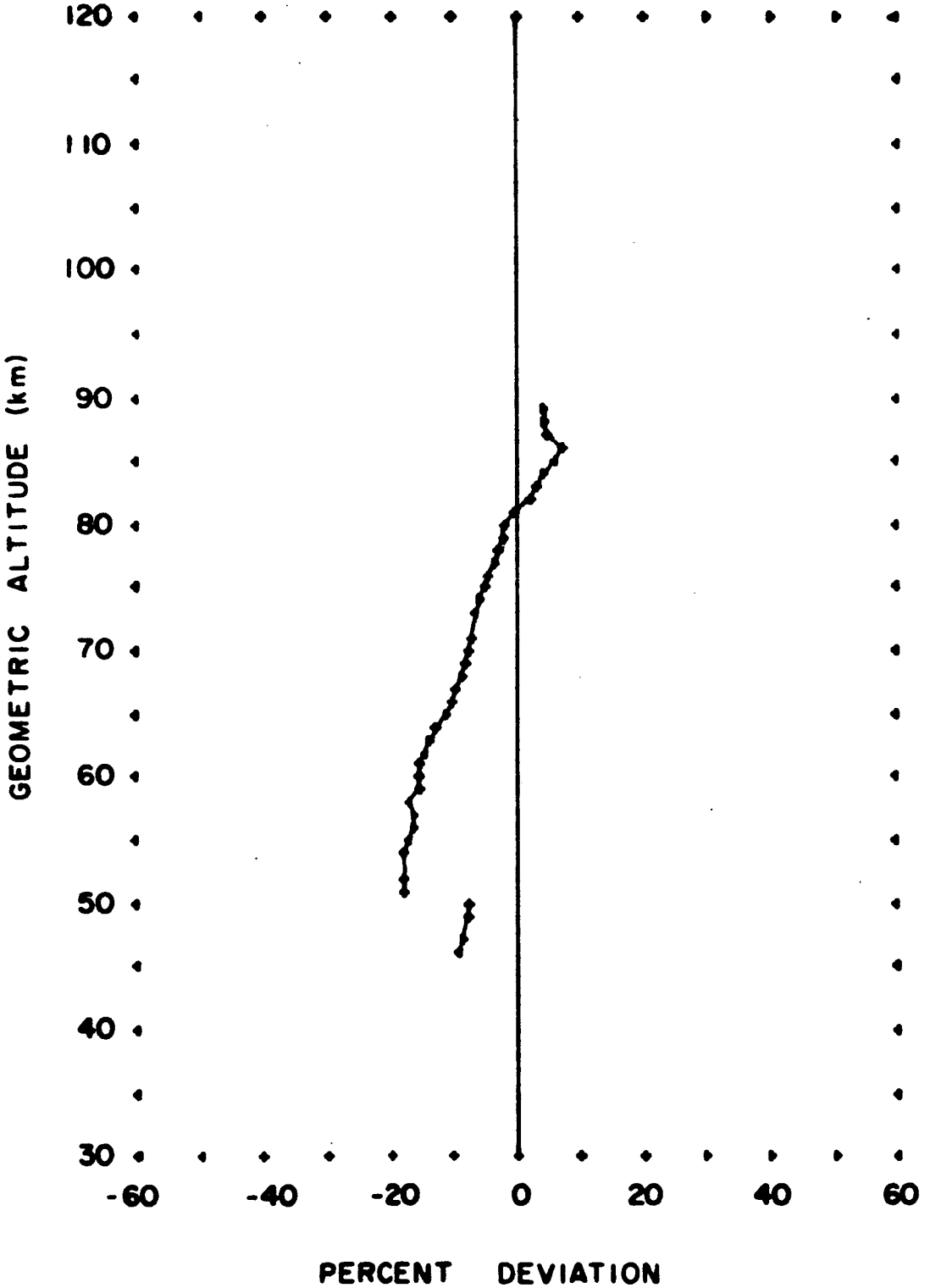

FIGURE 12P. PERCENT DEVIATION OF MEAN ATMOSPHERIC ANNUAL DENSITIES OVER HOLLOMAN AFB FROM DENSITIES OF THE PATRICK REF. ATMOSPHERE

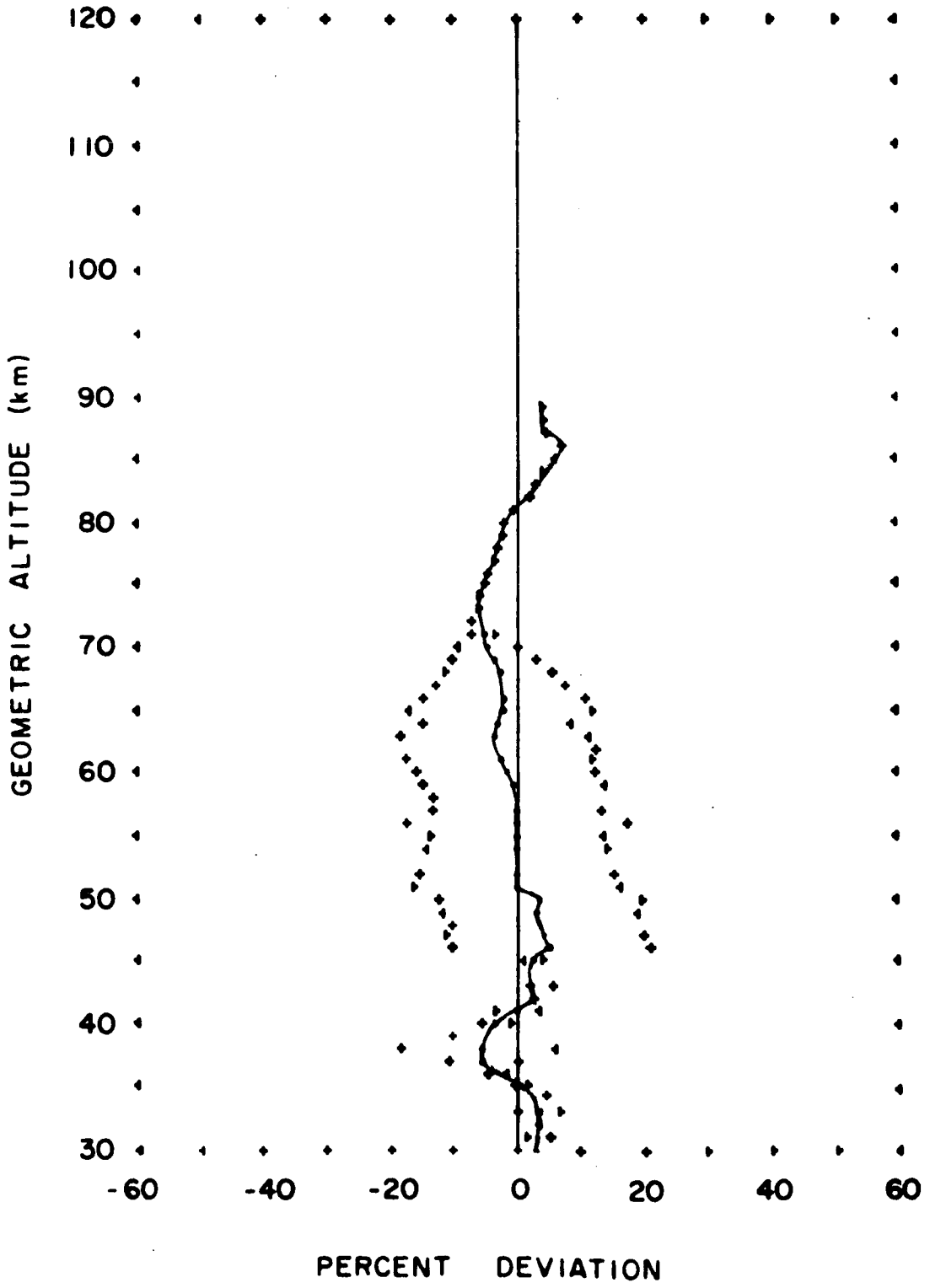

FIGURE 13P. PERCENT DEVIATION OF MEAN ATMOSPHERIC SUMMER DENSITIES OVER KWAJALEIN FROM DENSITIES OF THE PATRICK REF. ATMOSPHERE

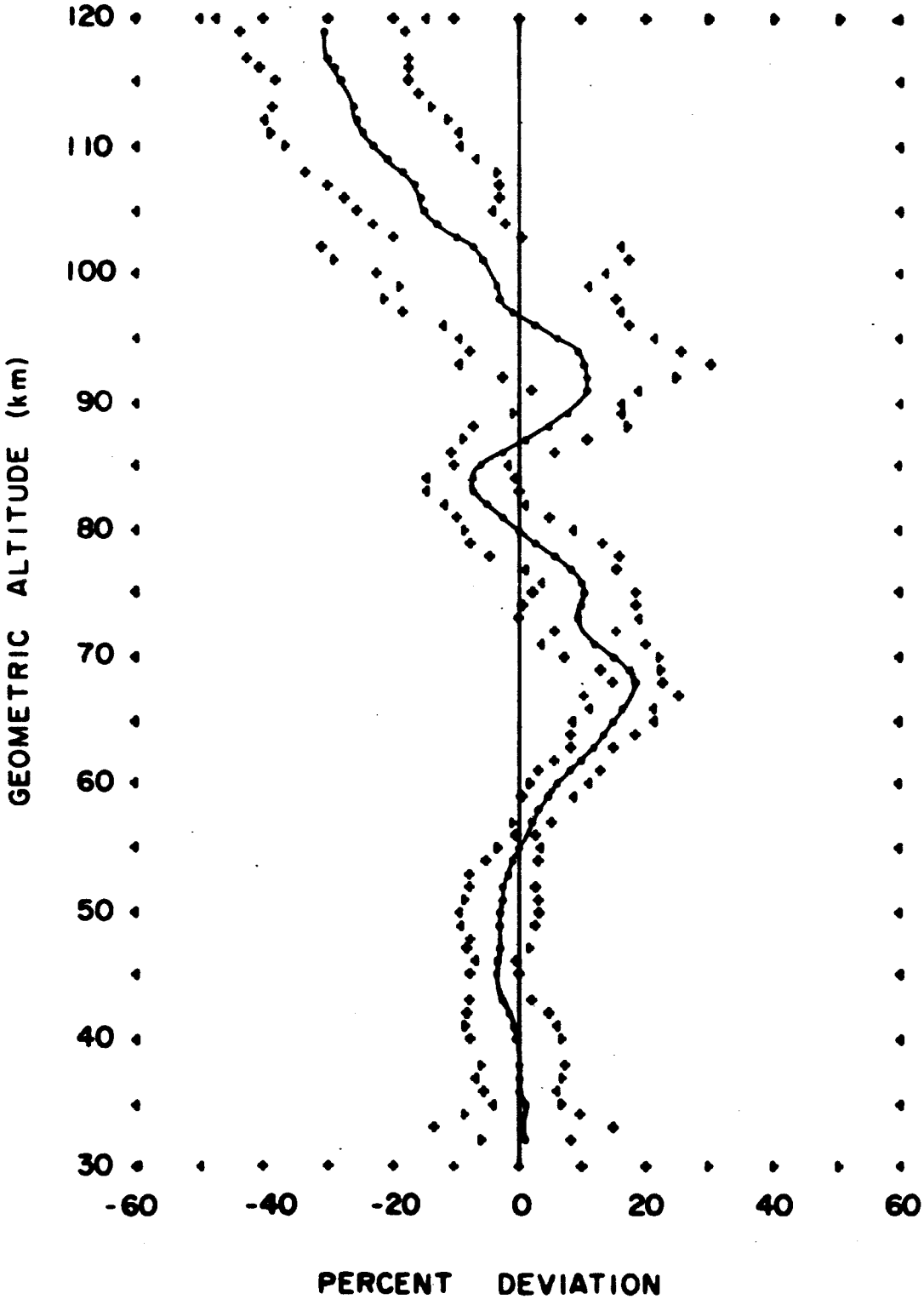

FIGURE 14P. PERCENT DEVIATION OF MEAN ATMOSPHERIC WINTER DENSITIES OVER KWAJALEIN FROM DENSITIES OF THE PATRICK REF. ATMOSPHERE

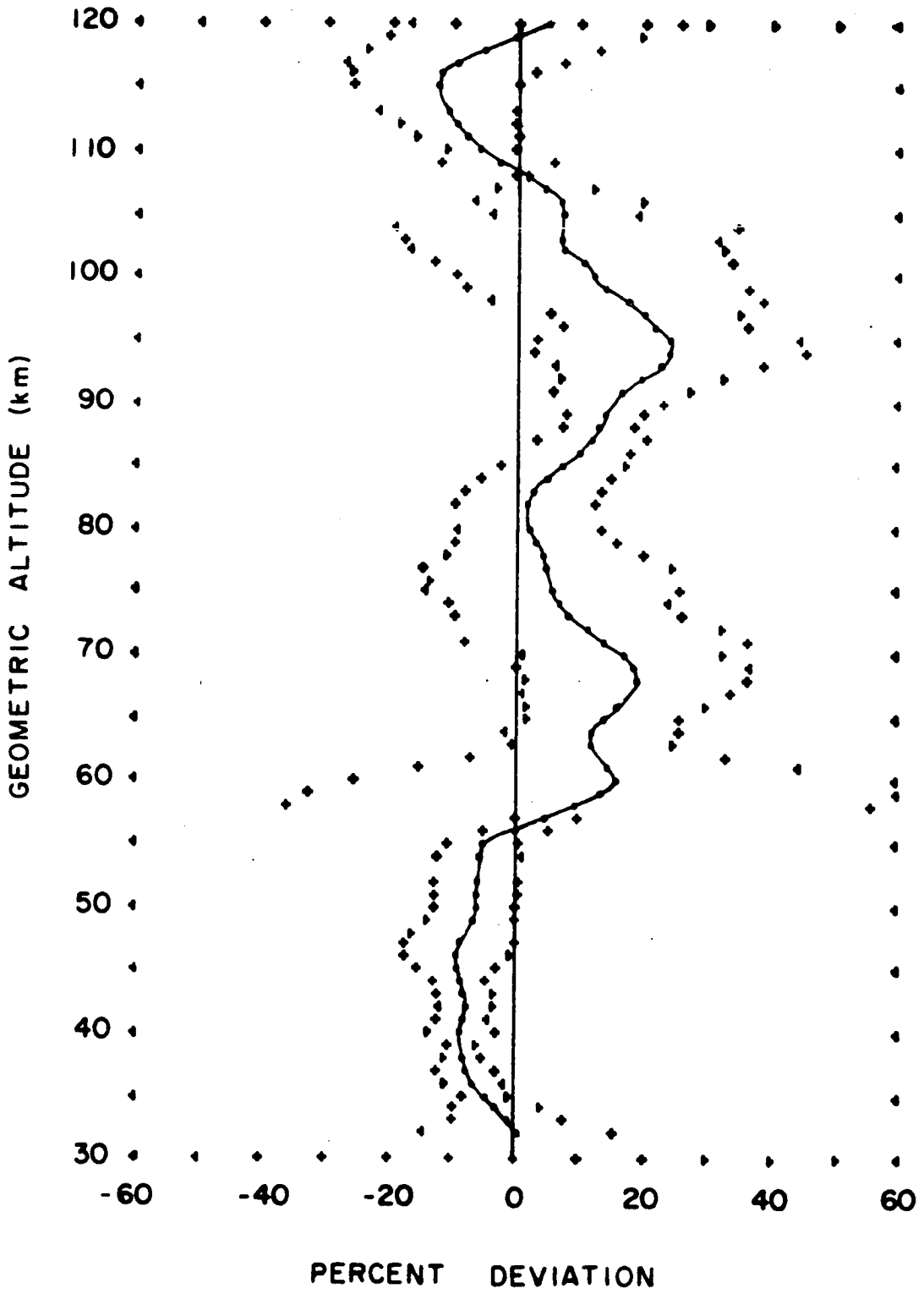

FIGURE 15P. PERCENT DEVIATION OF MEAN ATMOSPHERIC ANNUAL DENSITIES OVER KWAJALEIN FROM DENSITIES OF THE PATRICK REF. ATMOSPHERE

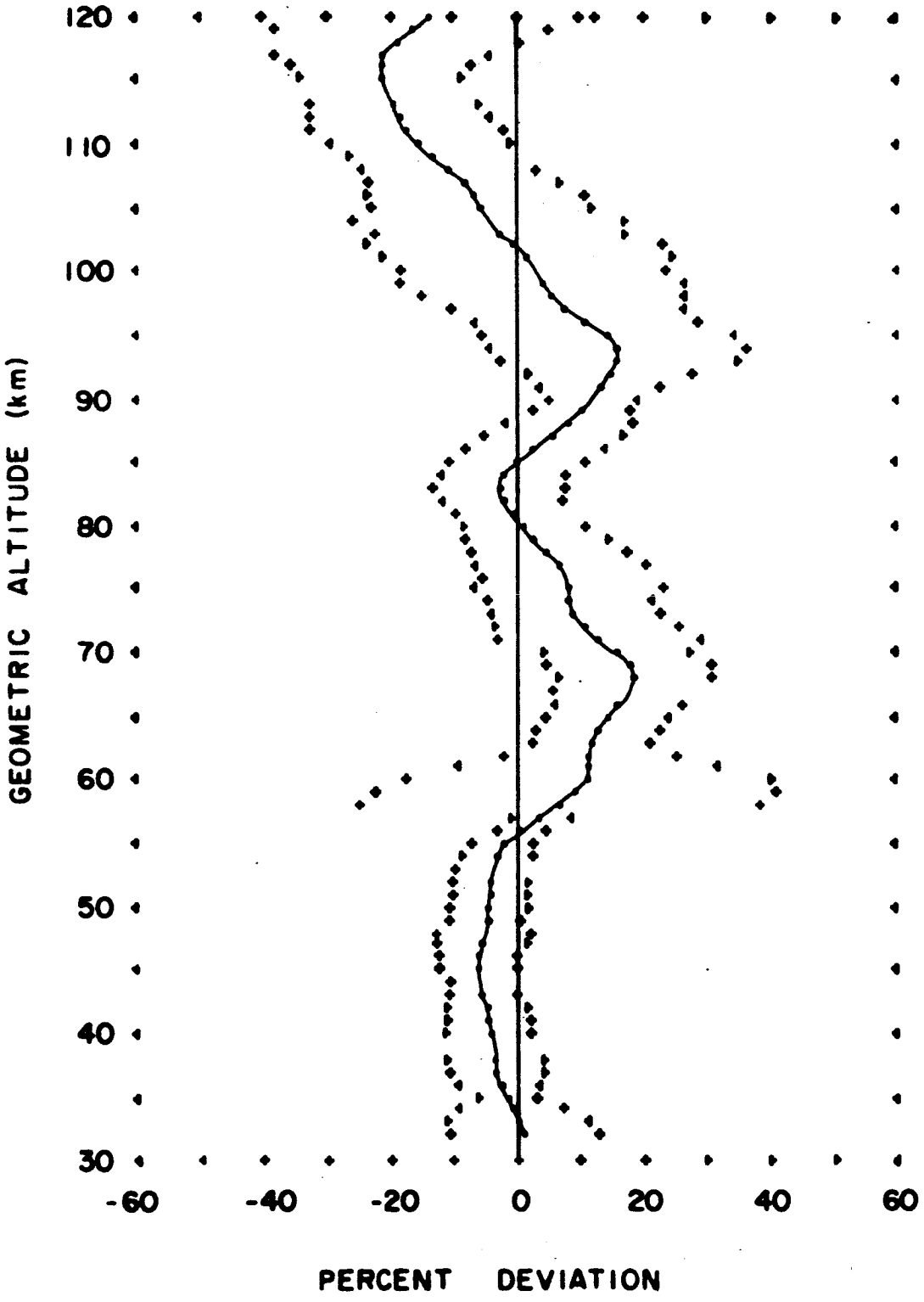

FIGURE 16P. PERCENT DEVIATION OF MEAN ATMOSPHERIC SUMMER DENSITIES OVER POINT MUGU FROM DENSITIES OF THE PATRICK REF. ATMOSPHERE

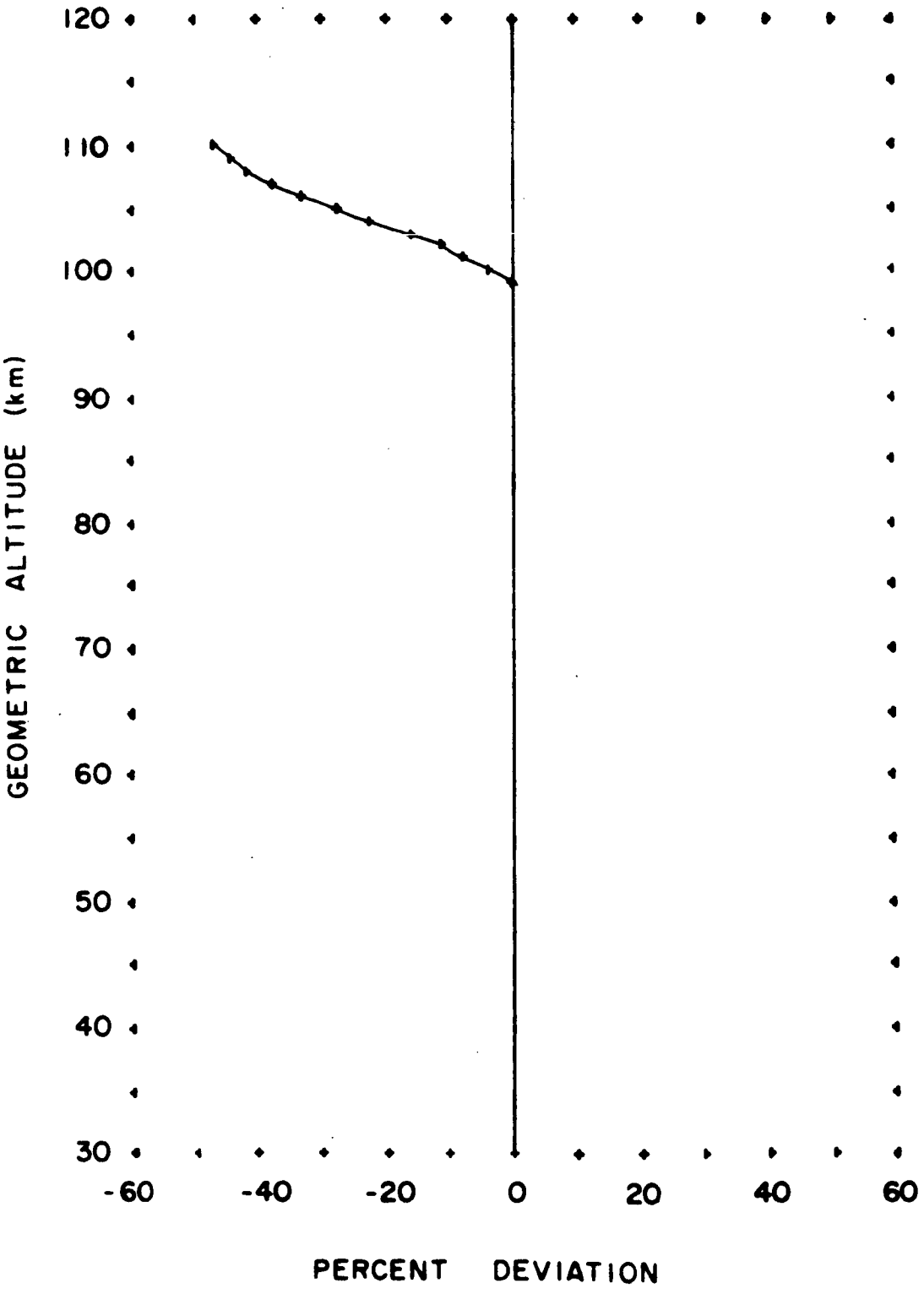

FIGURE 17P. PERCENT DEVIATION OF MEAN ATMOSPHERIC WINTER DENSITIES OVER POINT MUGU FROM DENSITIES OF THE PATRICK REF. ATMOSPHERE

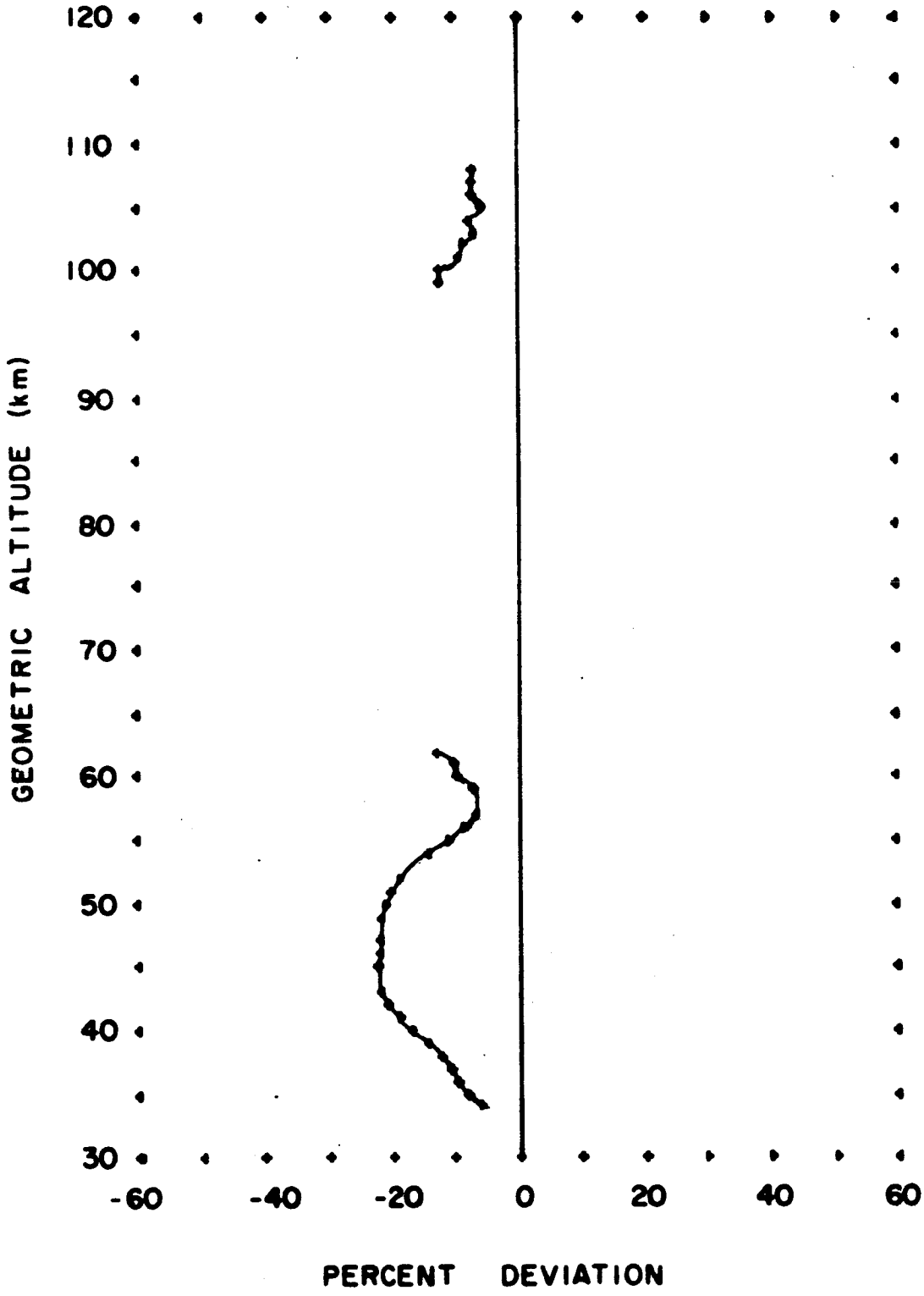

FIGURE 18P. PERCENT DEVIATION OF MEAN AIMOSPHERIC ANNUAL DENSITIES OVER POINT MUGU FROM DENSITIES OF THE PATRICK REF. ATMOSPHERE

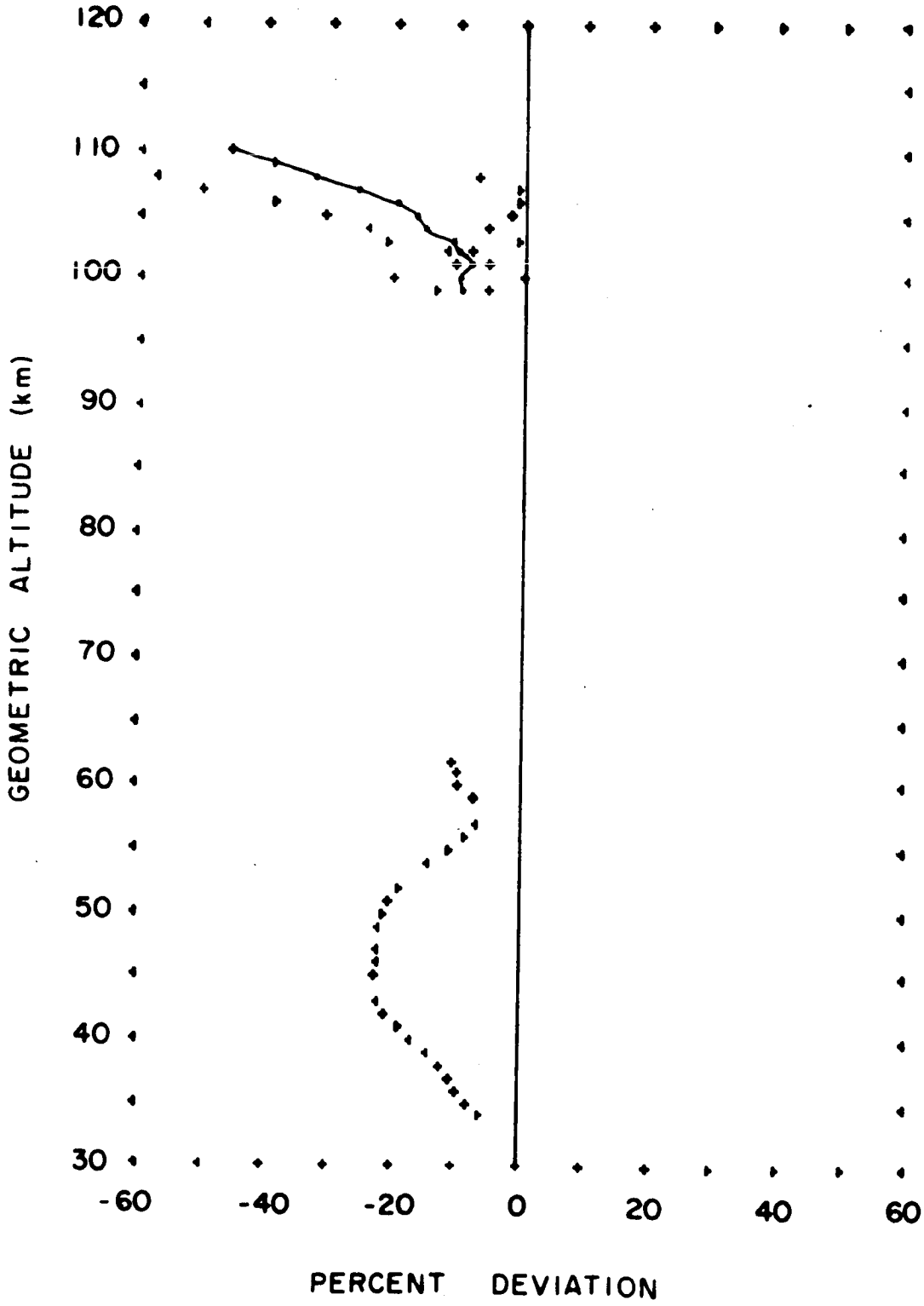

FIGURE 19P. PERCENT DEVIATION OF MEAN ATMOSPHERIC SUMMER DENSITIES OVER A SHIP (ARCTIC) FROM DENSITIES OF THE PATRICK REF. ATMOSPHERE

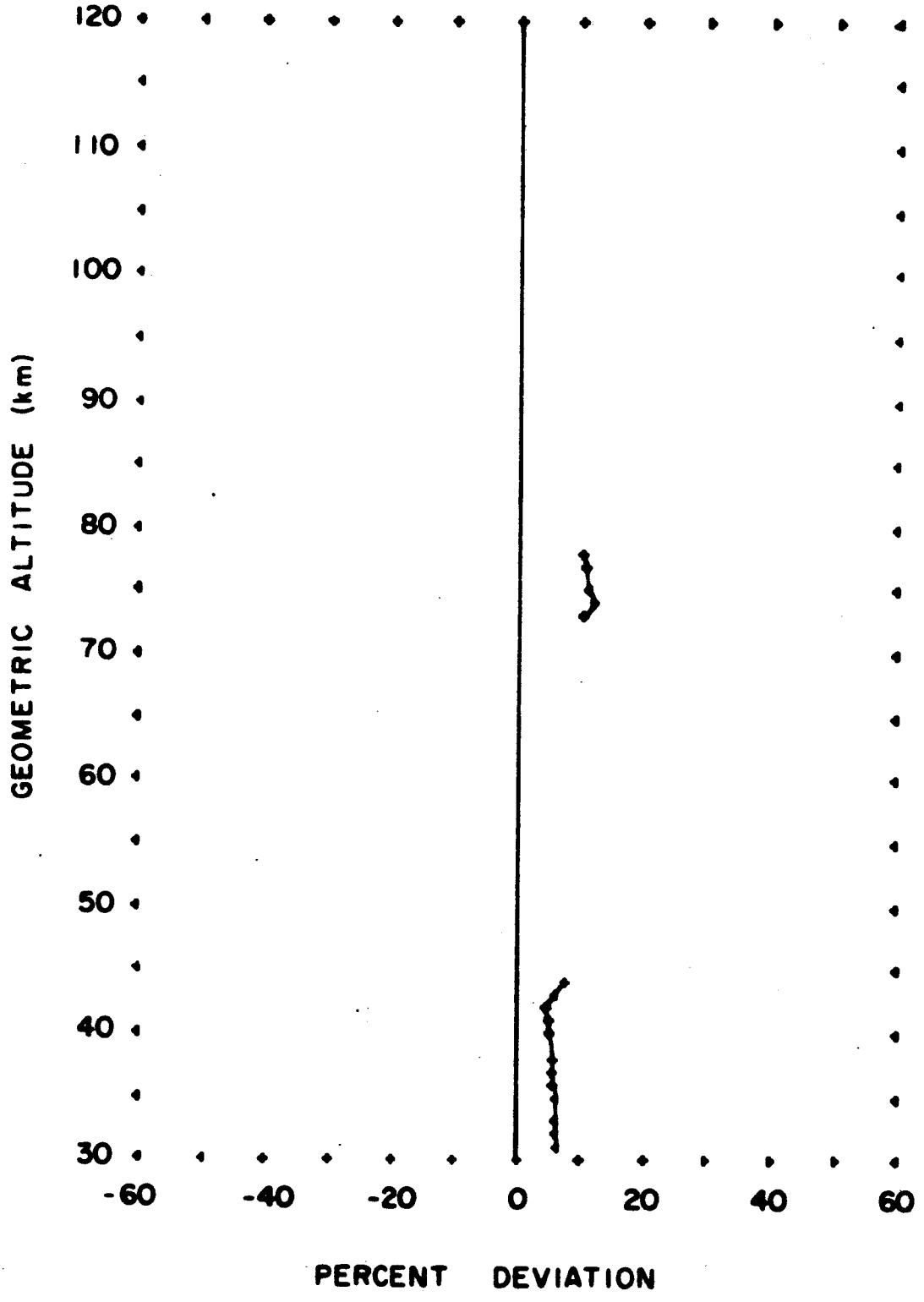

FIGURE 20P. PERCENT DEVIATION OF MEAN ATMOSPHERIC WINTER DENSITIES OVER A SHIP (MIDLAT.) FROM DENSITIES OF THE PATRICK REF. ATMOSPHERE

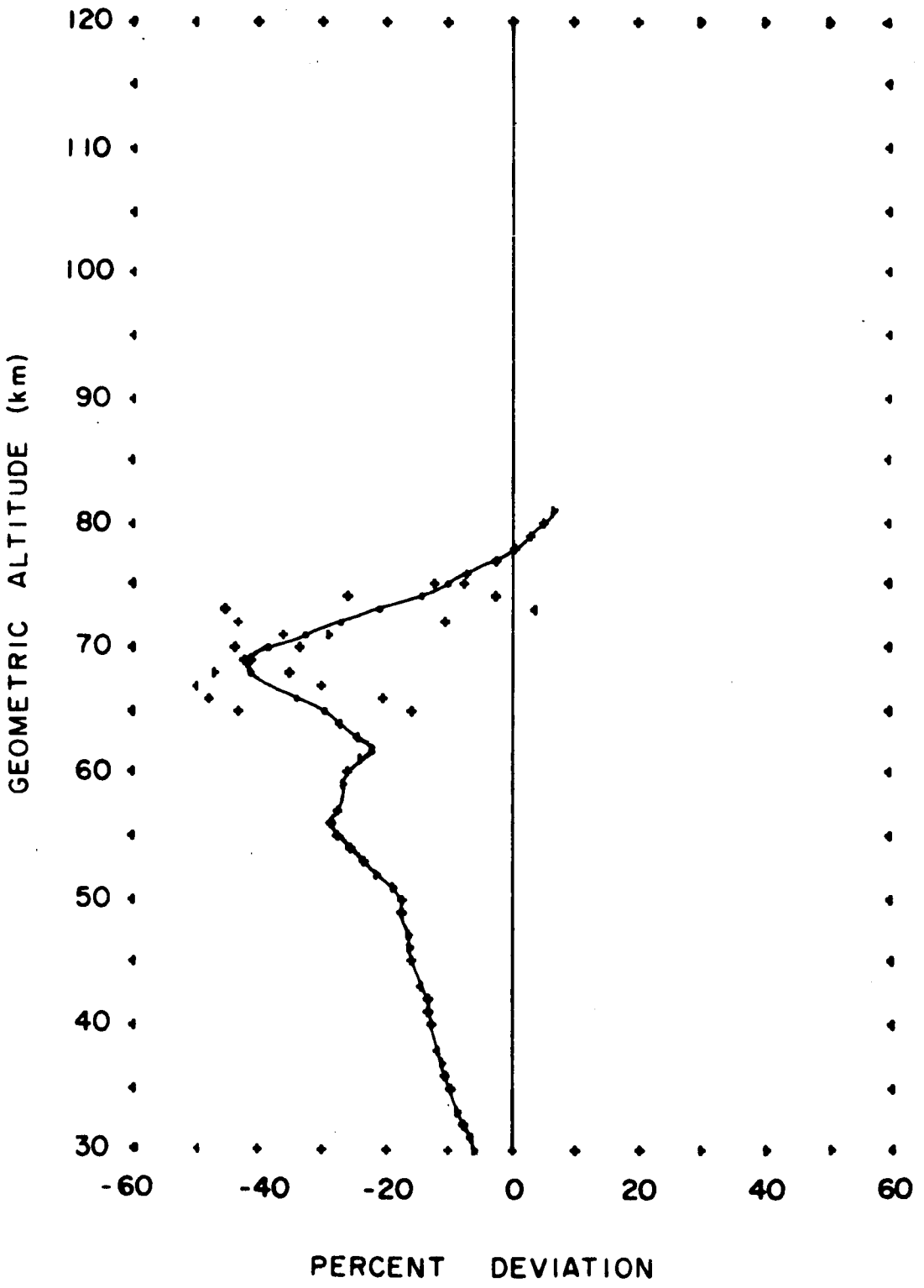

FIGURE 21P. PERCENT DEVIATION OF MEAN ATMOSPHERIC SUMMER DENSITIES OVER A SHIP (SUBARCTIC) FROM DENSITIES OF THE PATRICK REF. ATMOSPHERE

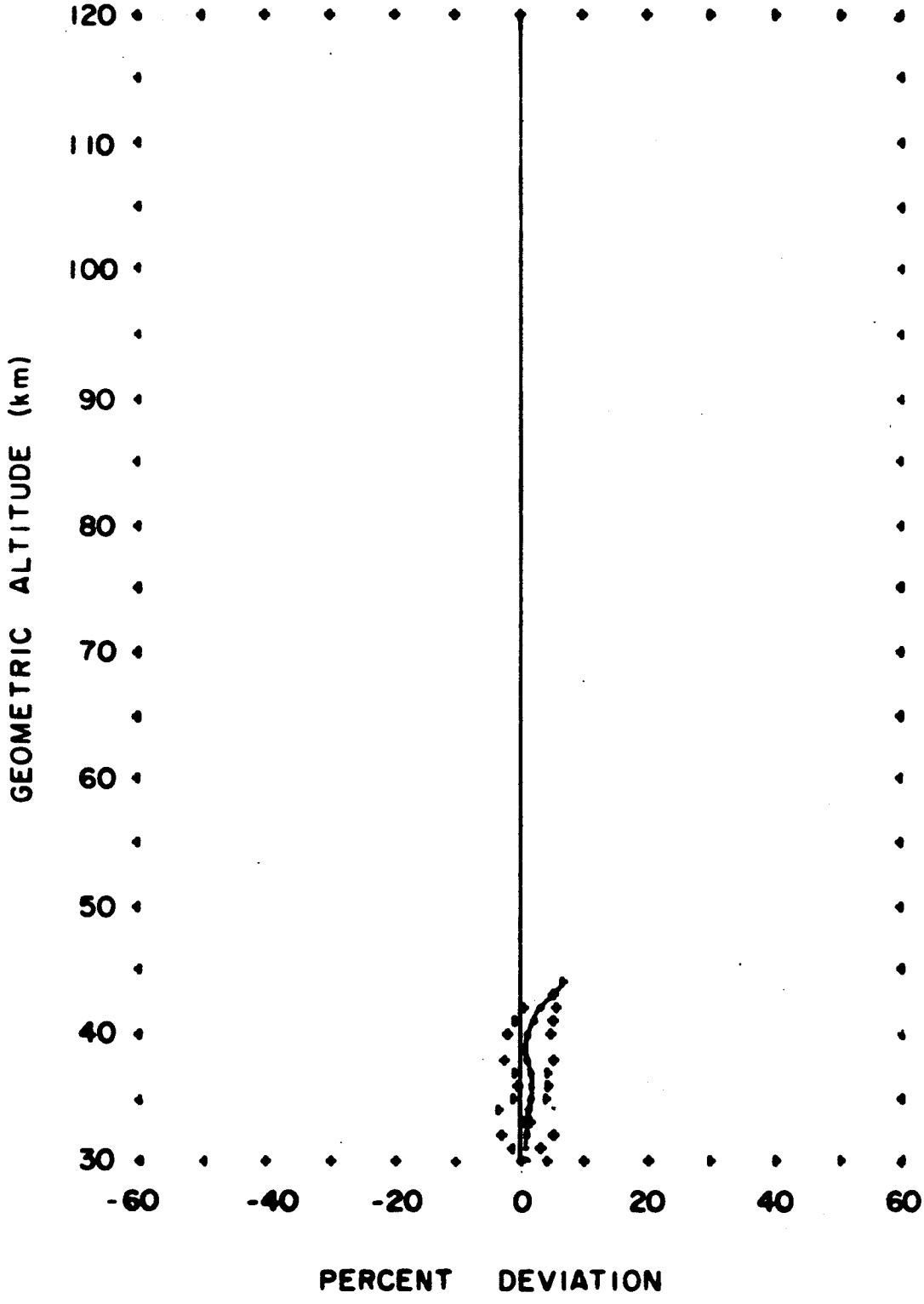

FIGURE 22P. PERCENT DEVIATION OF MEAN ATMOSPHERIC WINTER DENSITIES OVER A SHIP (SUBARCTIC) FROM DENSITIES OF THE PATRICK REF. ATMOSPHERE

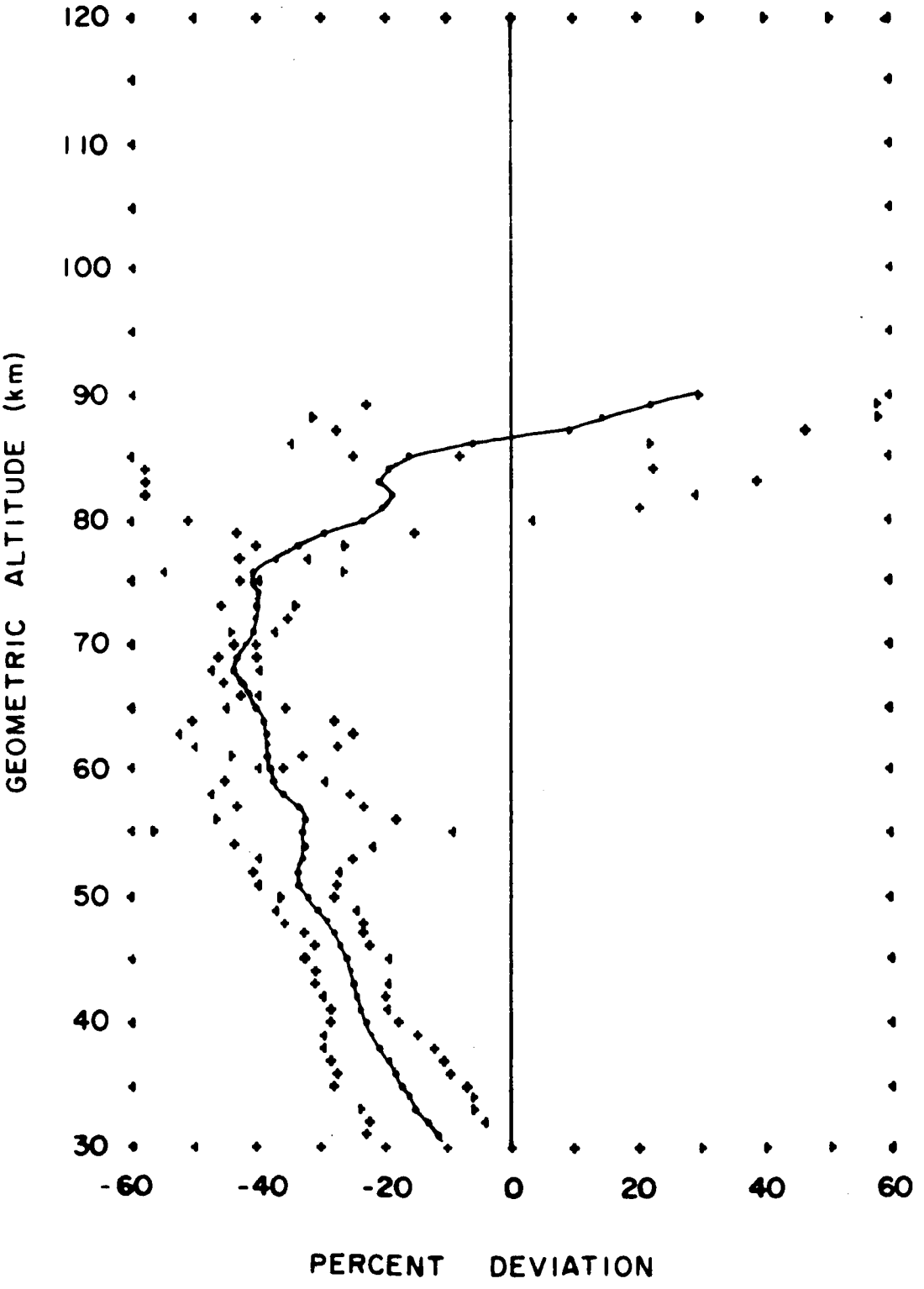

FIGURE 23P. PERCENT DEVIATION OF MEAN ATMOSPHERIC ANNUAL DENSITIES OVER A SHIP (SUBARCTIC) FROM DENSITIES OF THE PATRICK REF. ATMOSPHERE

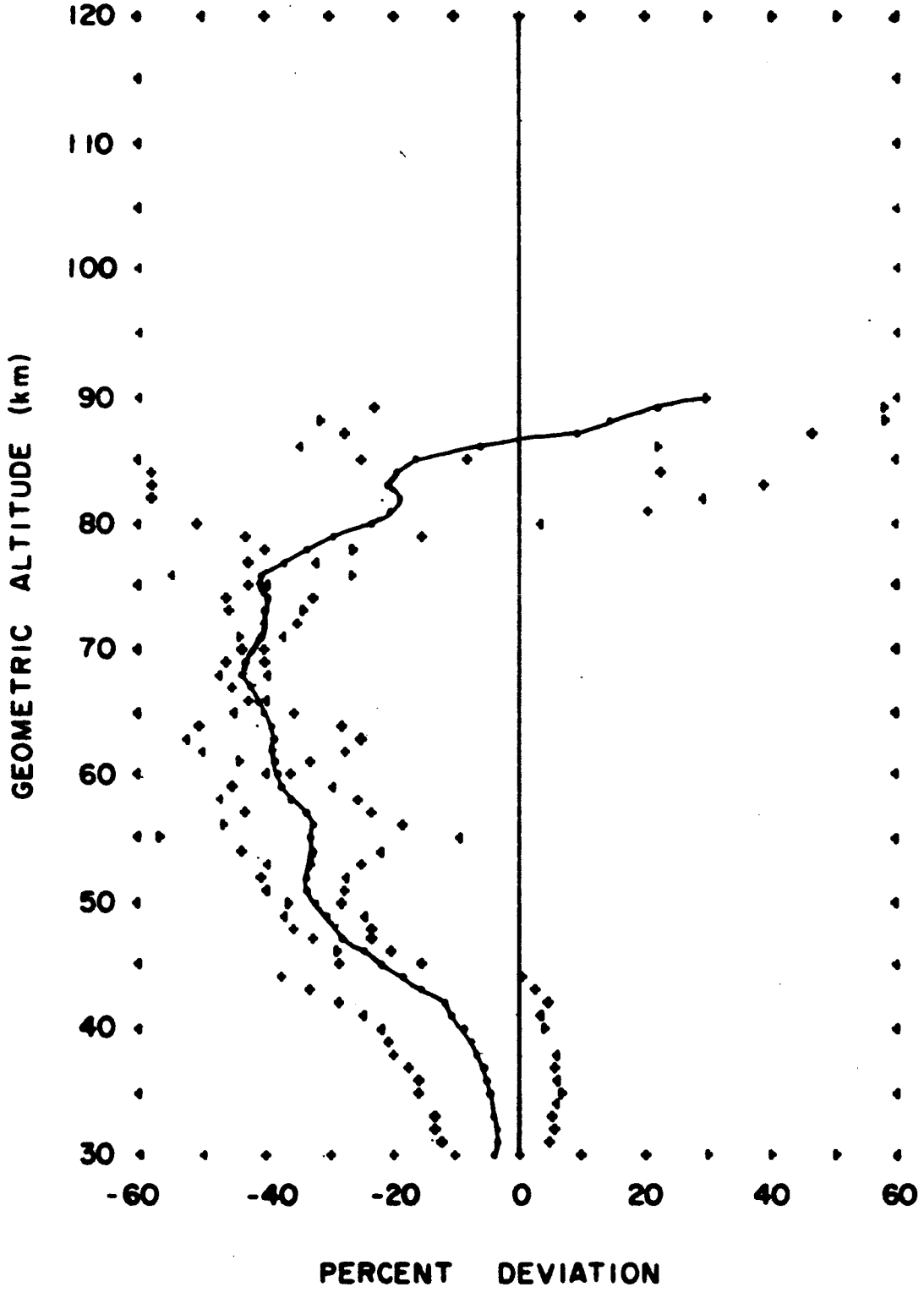

FIGURE 24P. PERCENT DEVIATION OF MEAN ATMOSPHERIC SUMMER DENSITIES OVER WALLOPS ISLAND FROM DENSITIES OF THE PATRICK REF. ATMOSPHERE

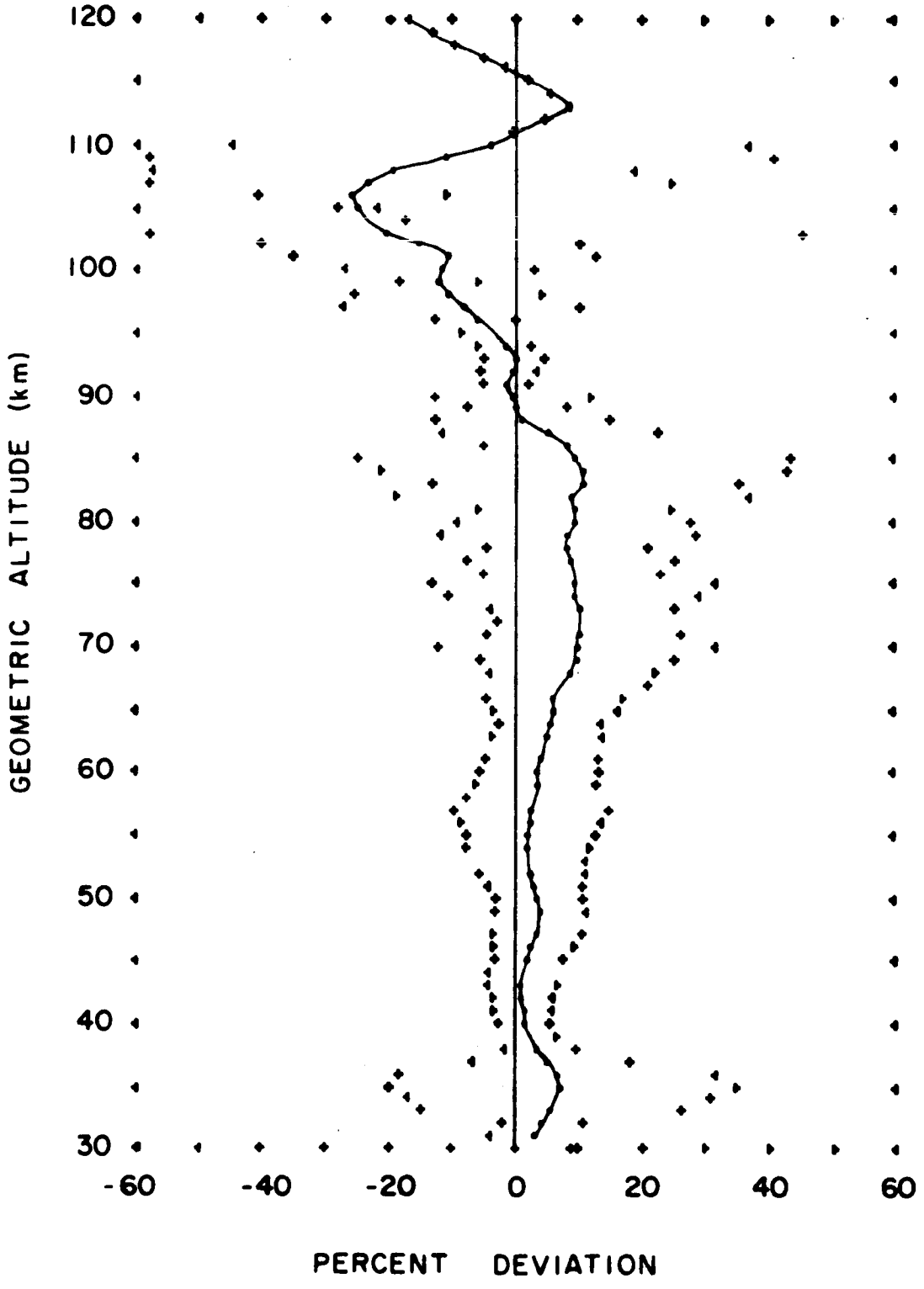

FIGURE 25P. PERCENT DEVIATION OF MEAN ATMOSPHERIC WINTER DENSITIES OVER WALLOPS ISLAND FROM DENSITIES OF THE PATRICK REF. ATMOSPHERE

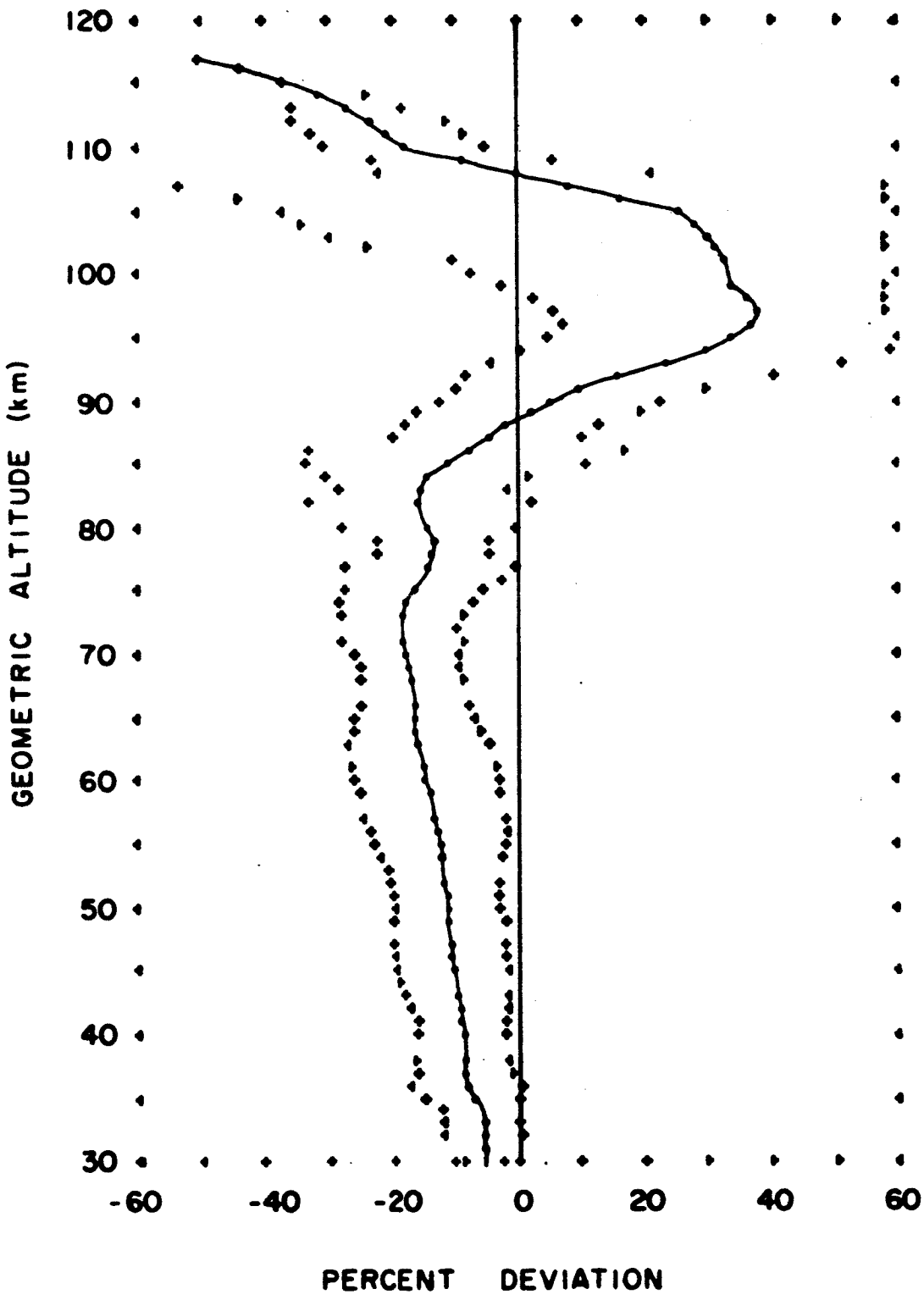

FIGURE 26P. PERCENT DEVIATION OF MEAN ATMOSPHERIC ANNUAL DENSITIES OVER WALLOPS ISLAND FROM DENSITIES OF THE PATRICK REF. ATMOSPHERE

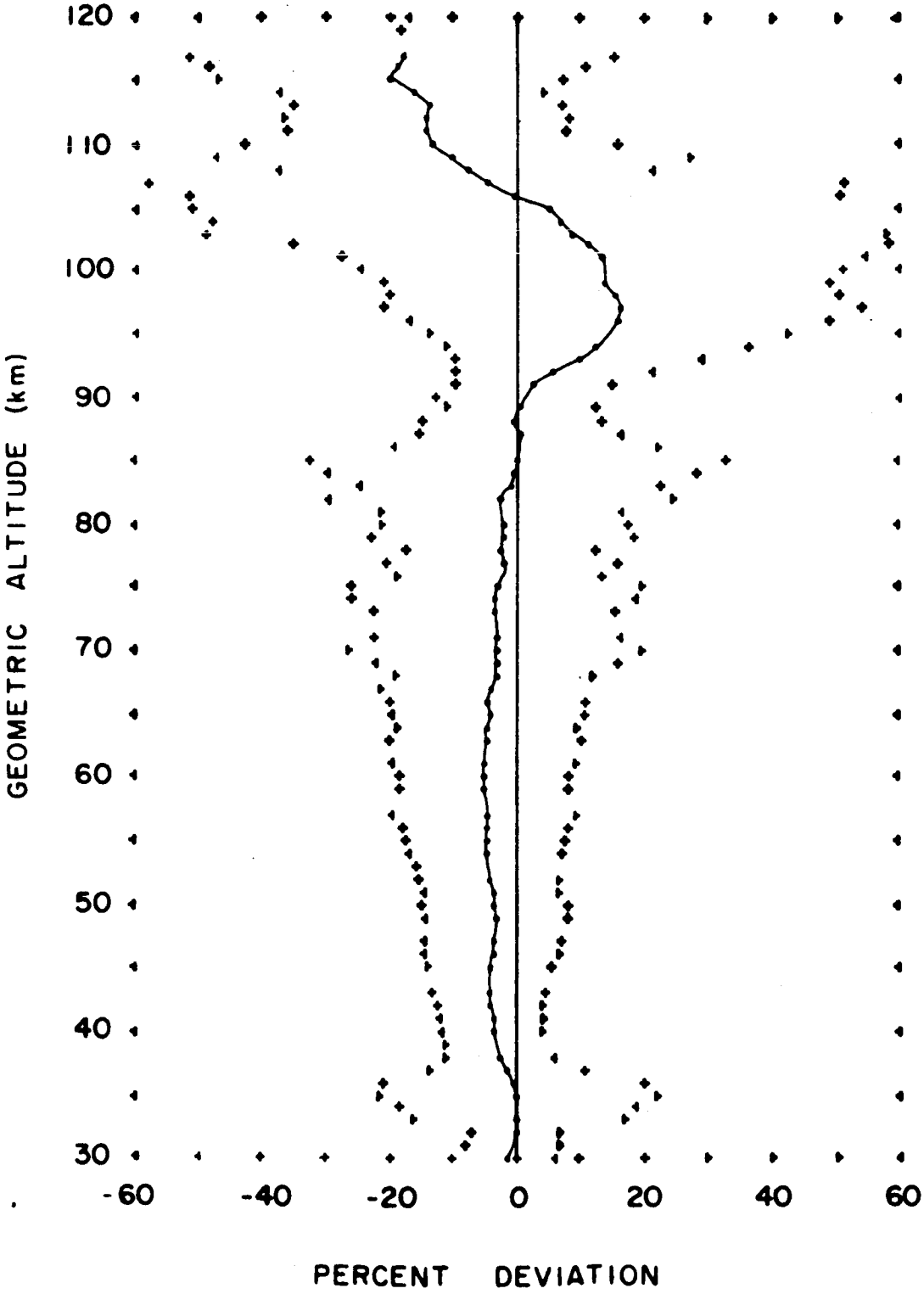

FIGURE 27P. PERCENT DEVIATION OF MEAN ATMOSPHERIC SUMMER DENSITIES OVER WHITE SANDS FROM DENSITIES OF THE PATRICK REF. ATMOSPHERE

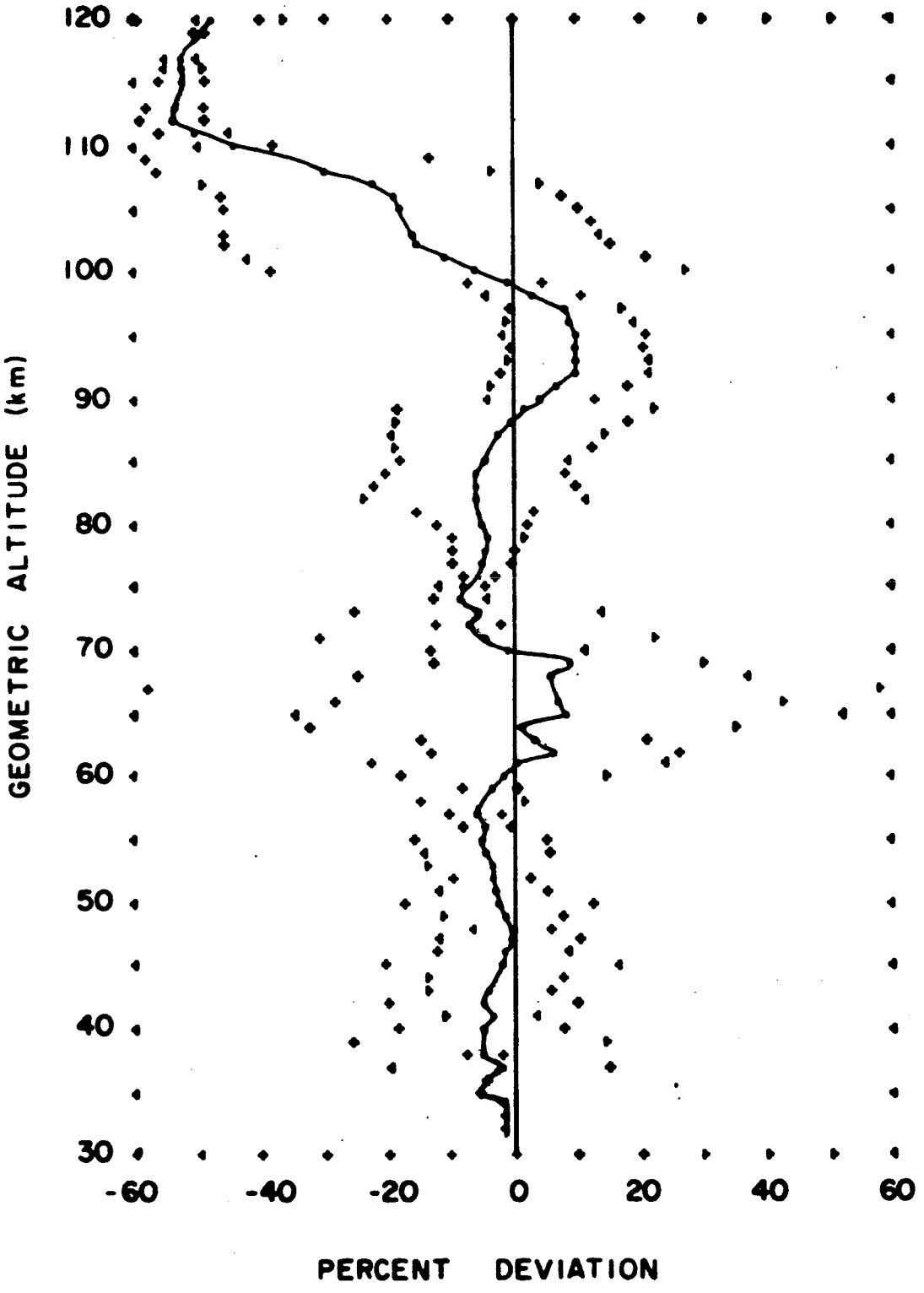

FIGURE 28P. PERCENT DEVIATION OF MEAN ATMOSPHERIC WINTER DENSITIES OVER WHITE SANDS FROM DENSITIES OF THE PATRICK REF. ATMOSPHERE

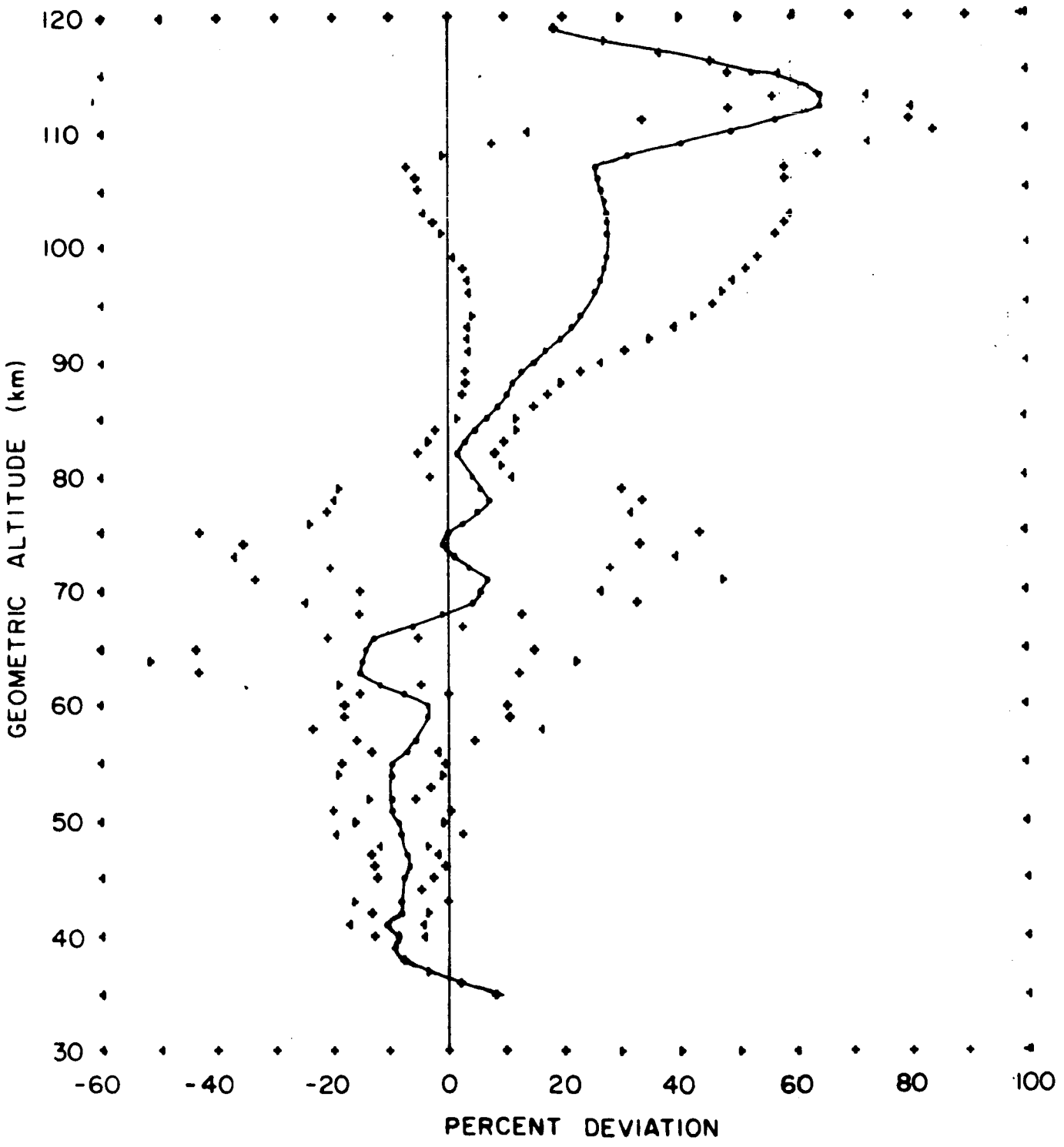

FIGURE 29P. PERCENT DEVIATION OF MEAN ATMOSPHERIC ANNUAL DENSITIES OVER WHITE SANDS FROM DENSITIES OF THE PATRICK REF. ATMOSPHERE

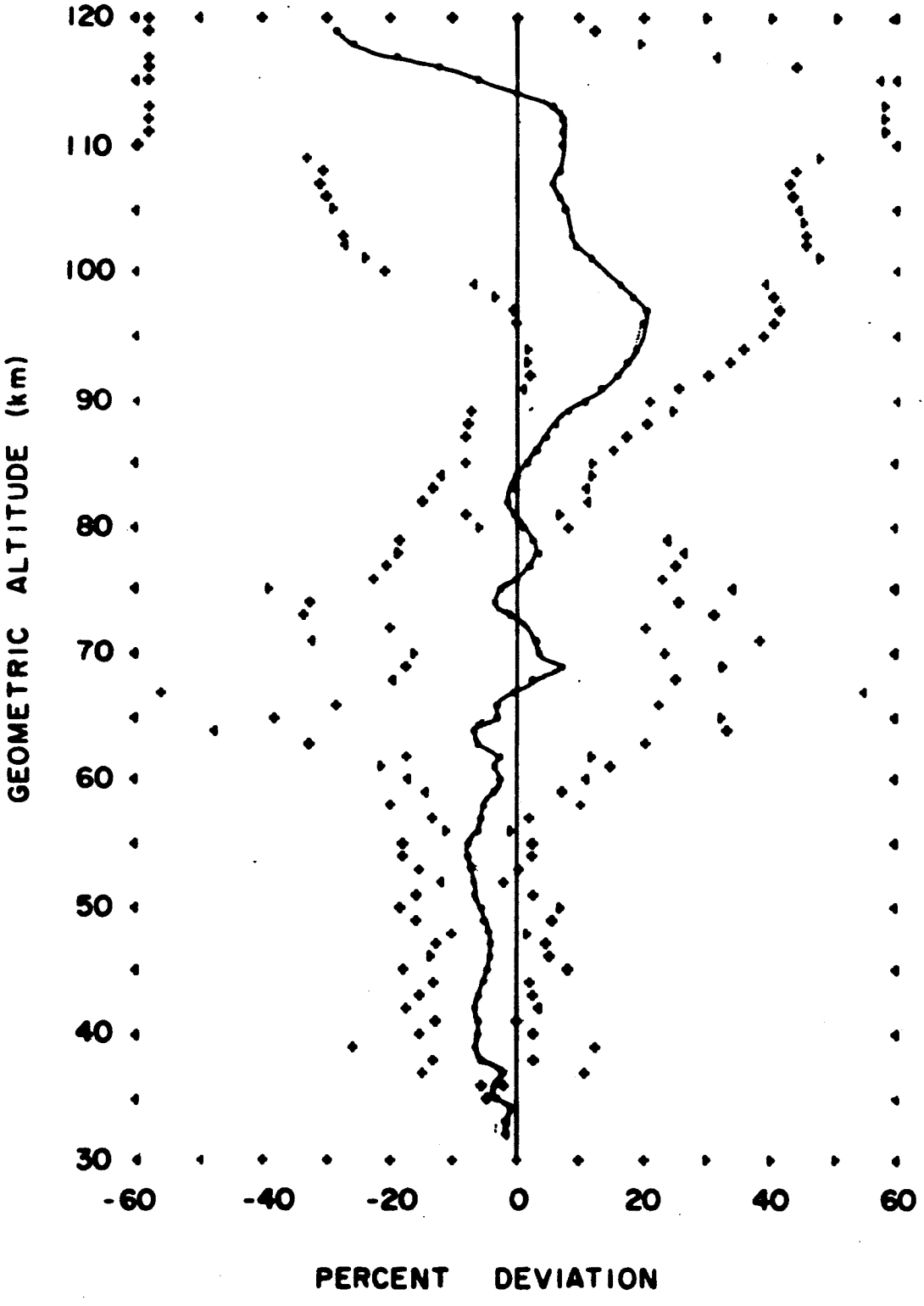

FIGURE 30P. PERCENT DEVIATION OF MEAN ATMOSPHERIC SUMMER DENSITIES OVER WOOMERA AUST. FROM DENSITIES OF THE PATRICK REF. ATMOSPHERE

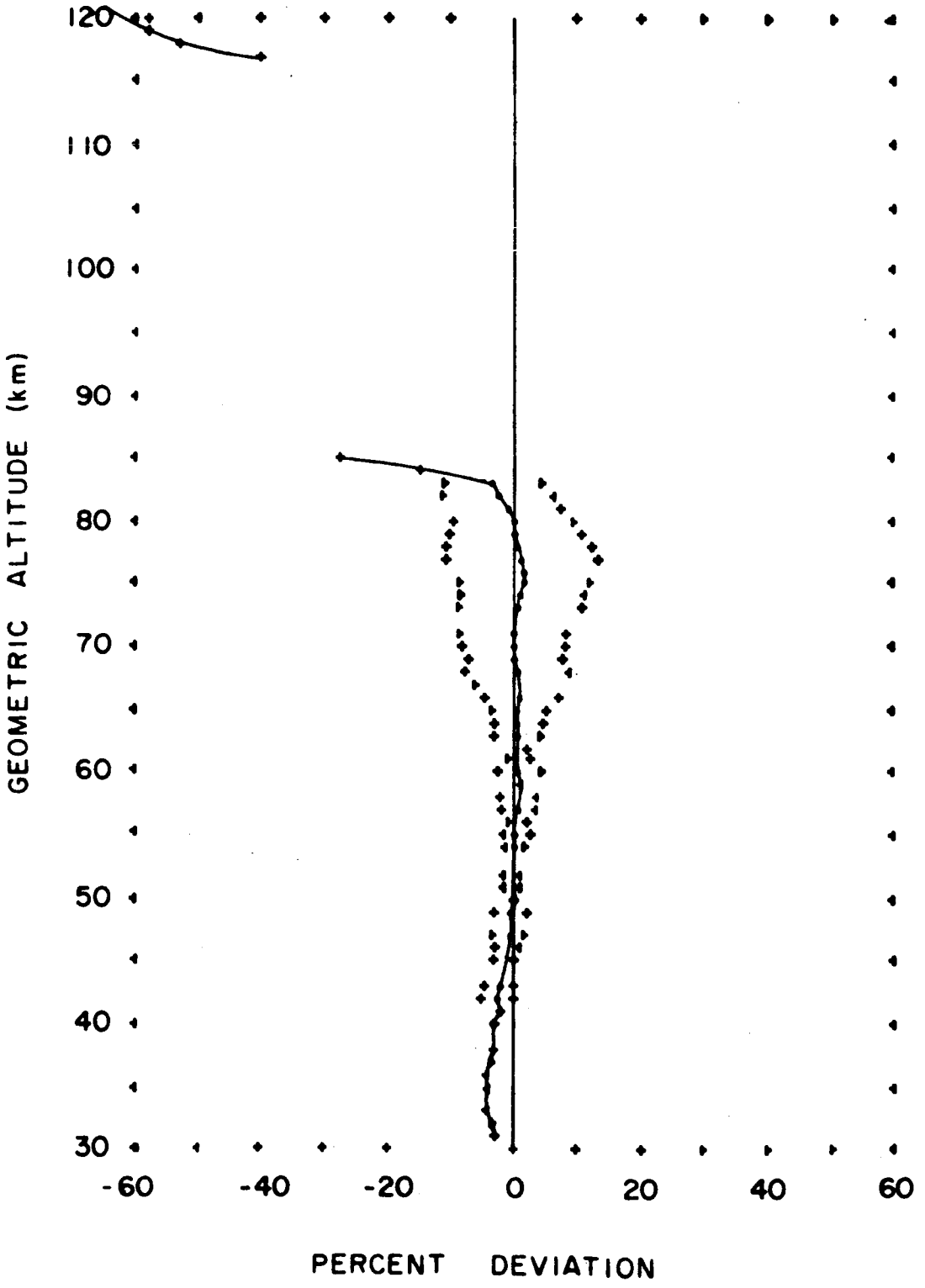

FIGURE 31P. PERCENT DEVIATION OF MEAN ATMOSPHERIC WINTER DENSITIES OVER WOOMERA AUST. FROM DENSITIES OF THE PATRICK REF. ATMOSPHERE

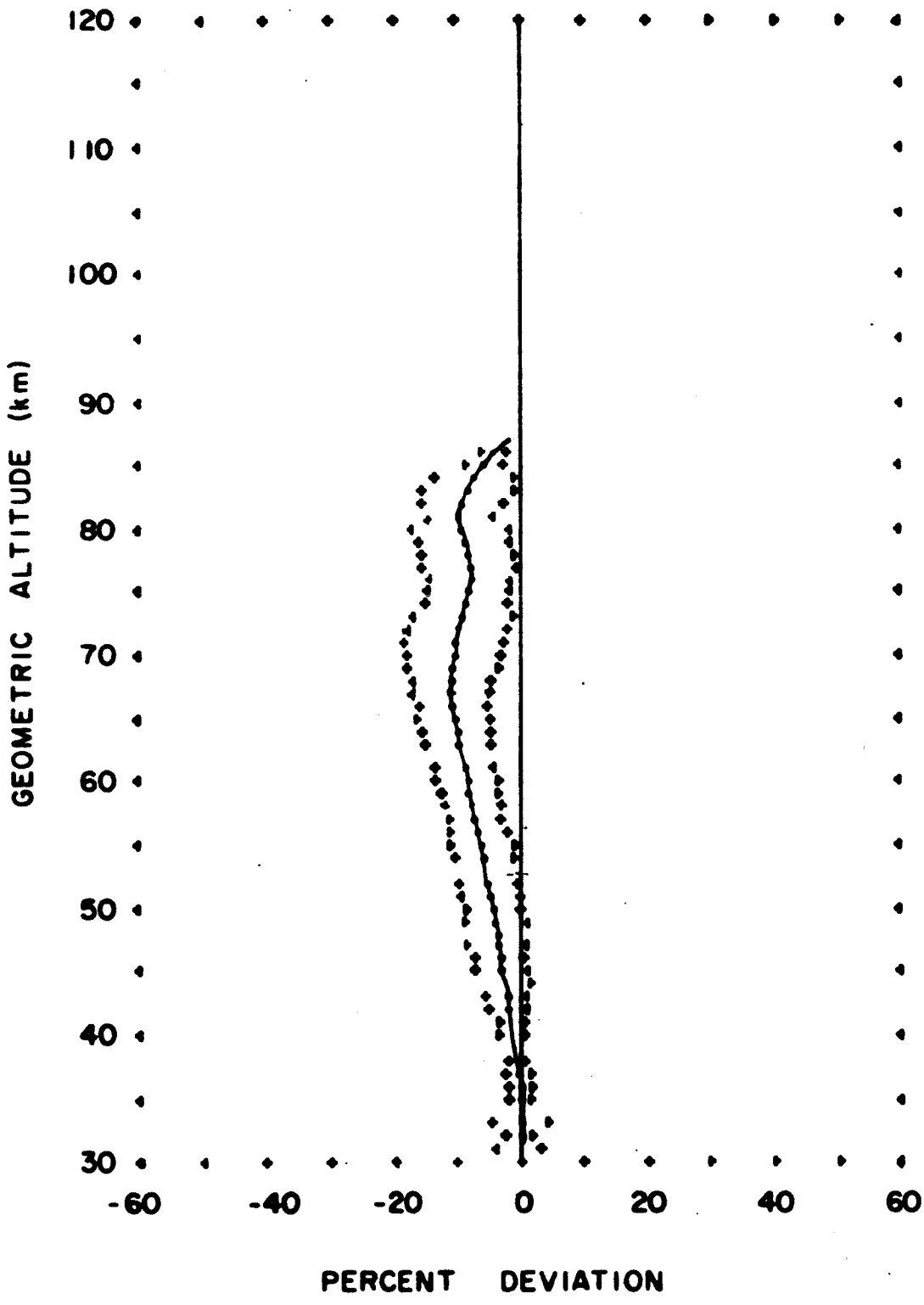

FIGURE 32P. PERCENT DEVIATION OF MEAN ATMOSPHERIC ANNUAL DENSITIES OVER WOOMERA AUST. FROM DENSITIES OF THE PATRICK REF. ATMOSPHERE

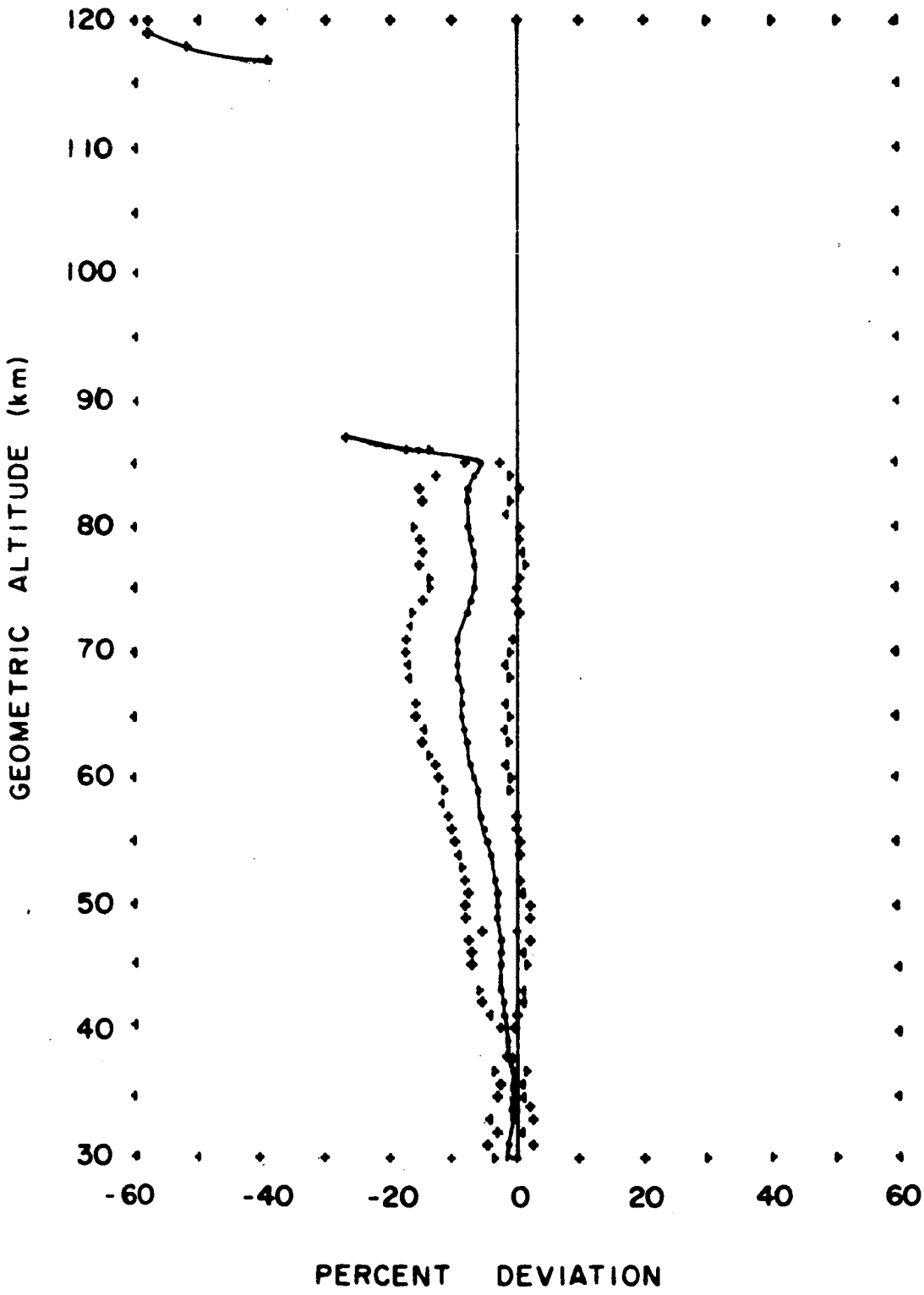

FIGURE 33P. PERCENT DEVIATION OF MEAN ATMOSPHERIC SUMMER DENSITIES OVER THE TROPICS FROM DENSITIES OF THE PATRICK REF. ATMOSPHERE

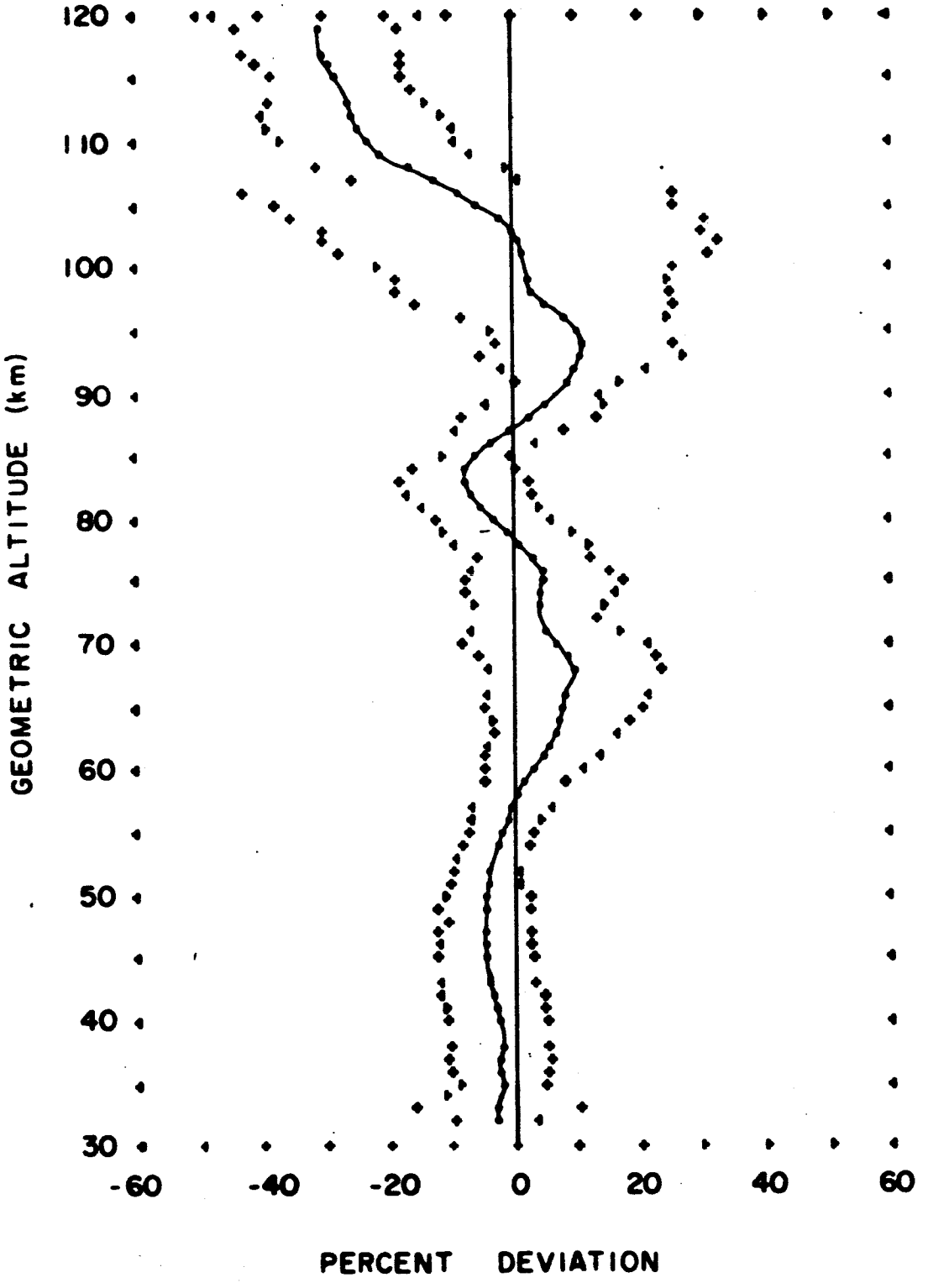

FIGURE 34P. PERCENT DEVIATION OF MEAN ATMOSPHERIC WINTER DENSITIES OVER THE TROPICS FROM DENSITIES OF THE PATRICK REF. ATMOSPHERE

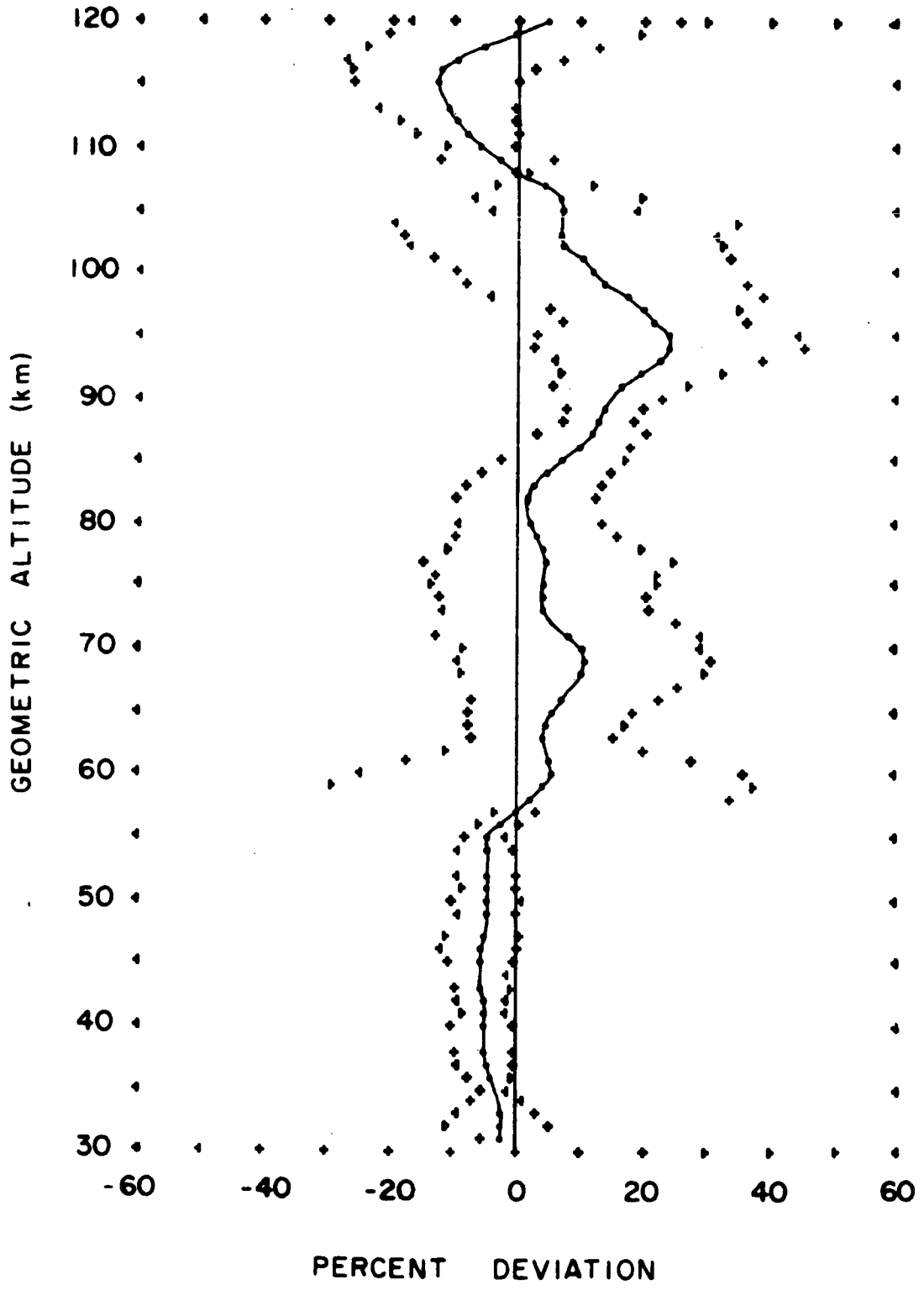

FIGURE 35P. PERCENT DEVIATION OF MEAN ATMOSPHERIC ANNUAL DENSITIES OVER THE TROPICS FROM DENSITIES OF THE PATRICK REF. ATMOSPHERE

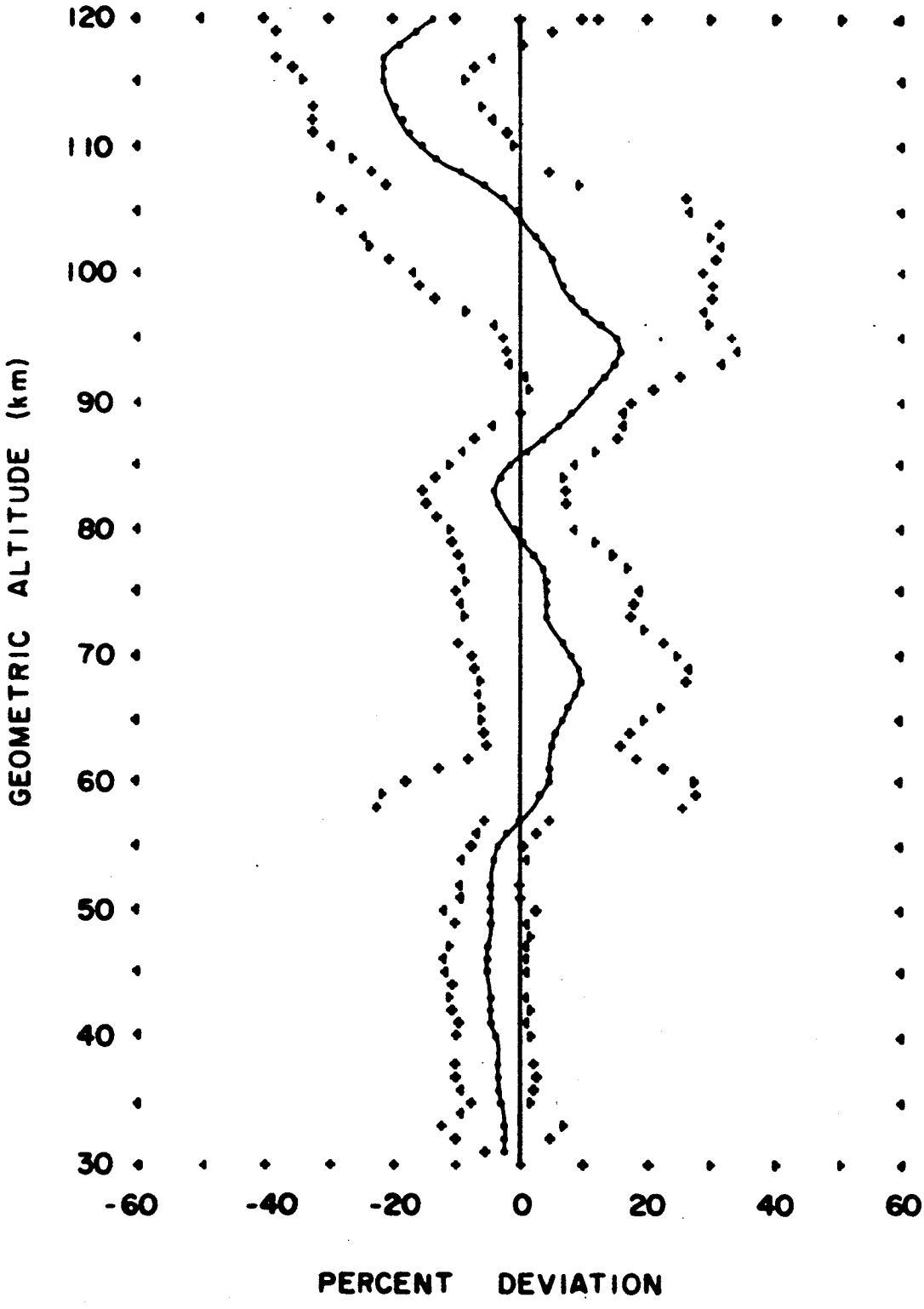

FIGURE 36P. PERCENT DEVIATION OF MEAN ATMOSPHERIC SUMMER DENSITIES OVER THE SUBTROPICS FROM DENSITIES OF THE PATRICK REF. ATMOSPHERE

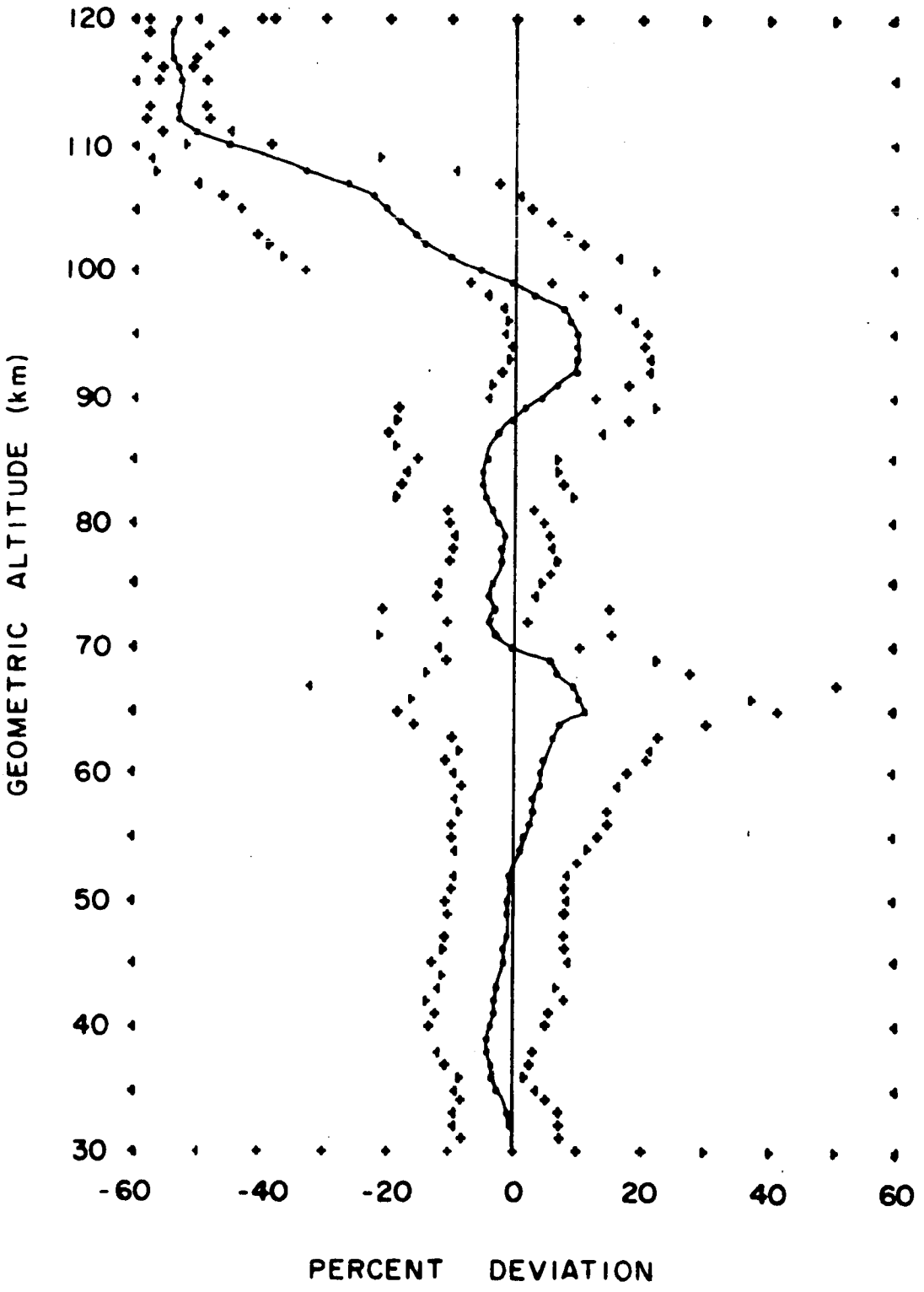

FIGURE 37P. PERCENT DEVIATION OF MEAN ATMOSPHERIC WINTER DENSITIES OVER THE SUBTROPICS FROM DENSITIES OF THE PATRICK REF. ATMOSPHERE

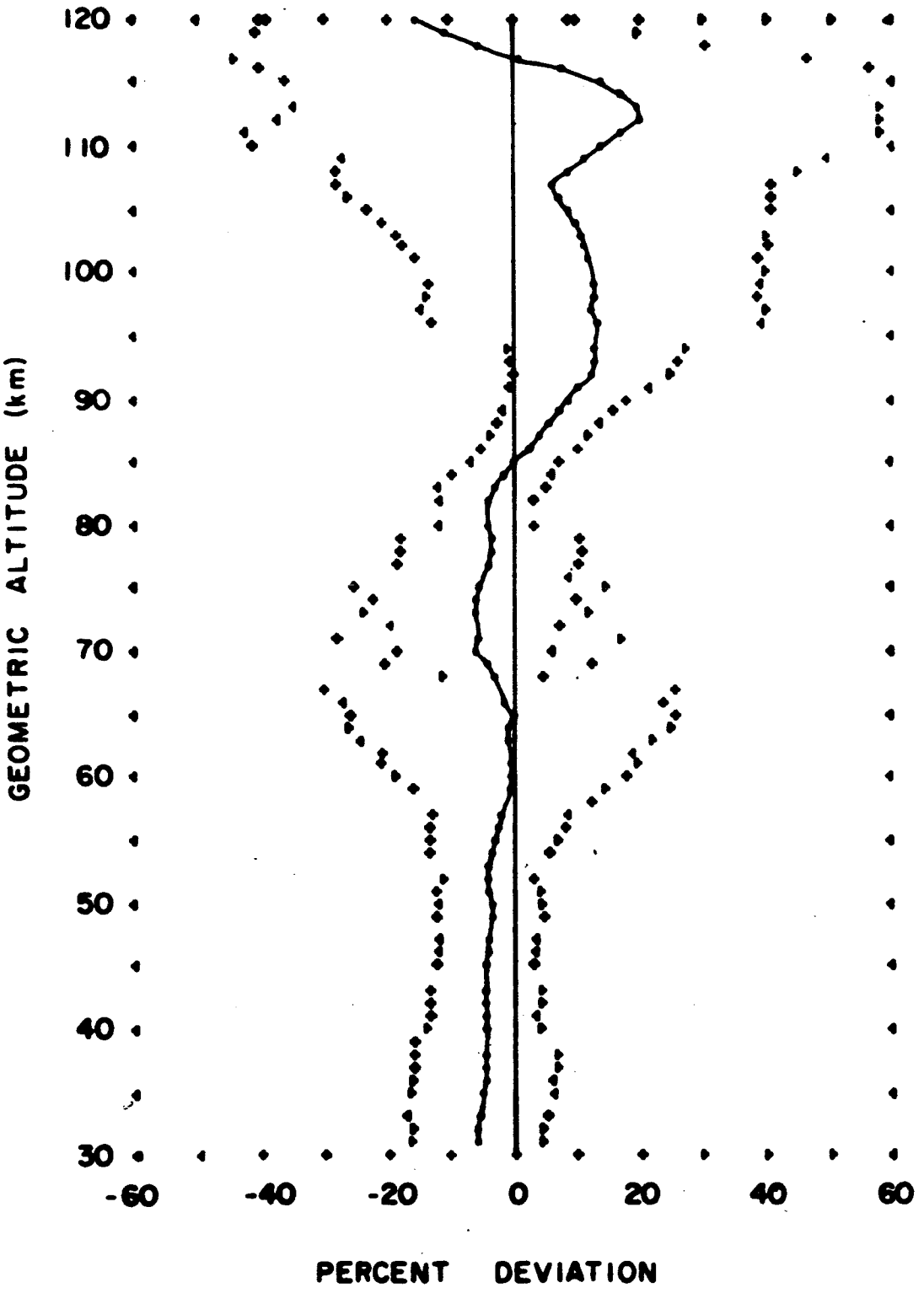

FIGURE 38P. PERCENT DEVIATION OF MEAN ATMOSPHERIC ANNUAL DENSITIES OVER THE SUBTROPICS FROM DENSITIES OF THE PATRICK REF. ATMOSPHERE

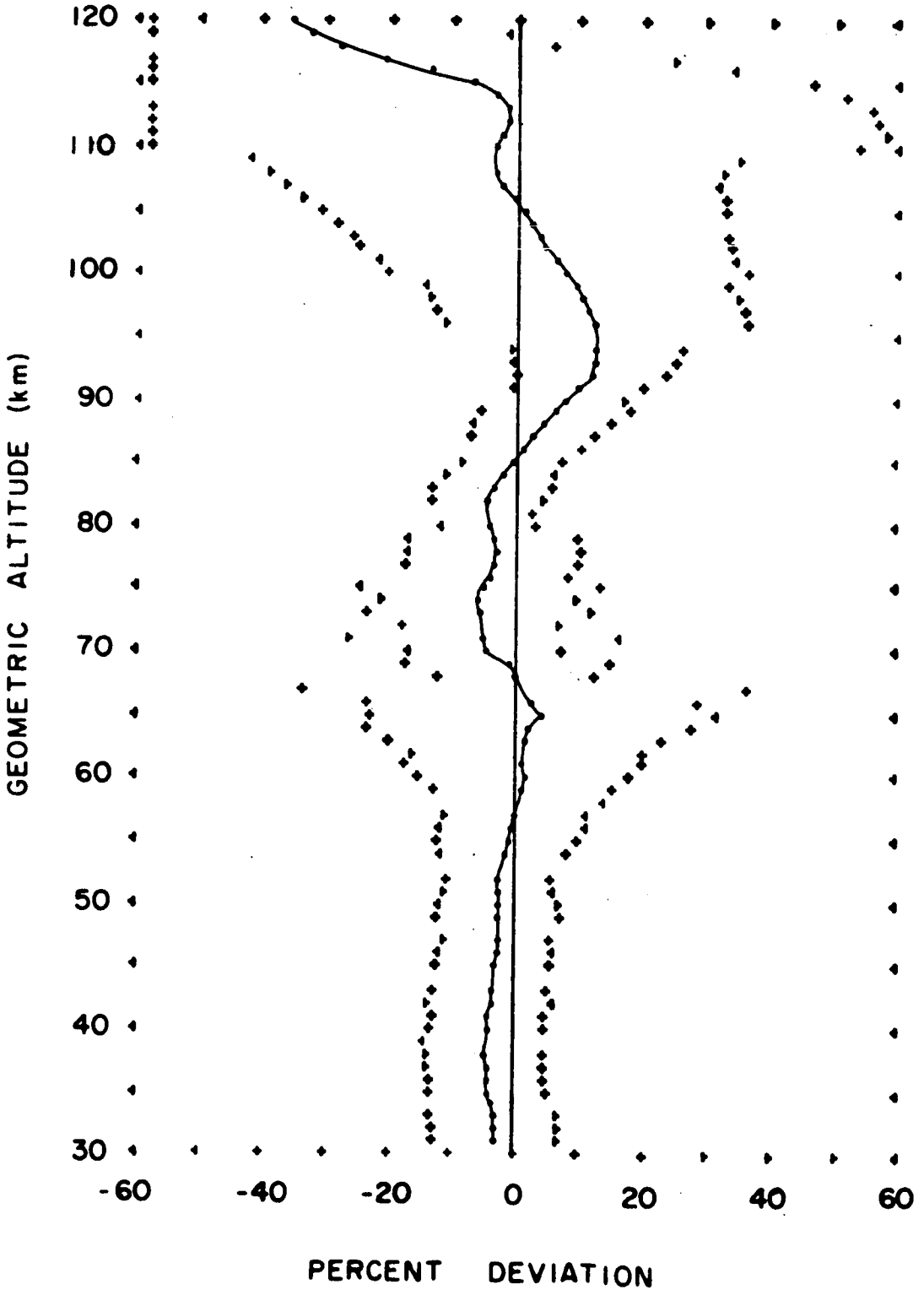

FIGURE 39P. PERCENT DEVIATION OF MEAN ATMOSPHERIC SUMMER DENSITIES OVER MIDLATITUDES FROM DENSITIES OF THE PATRICK REF. ATMOSPHERE

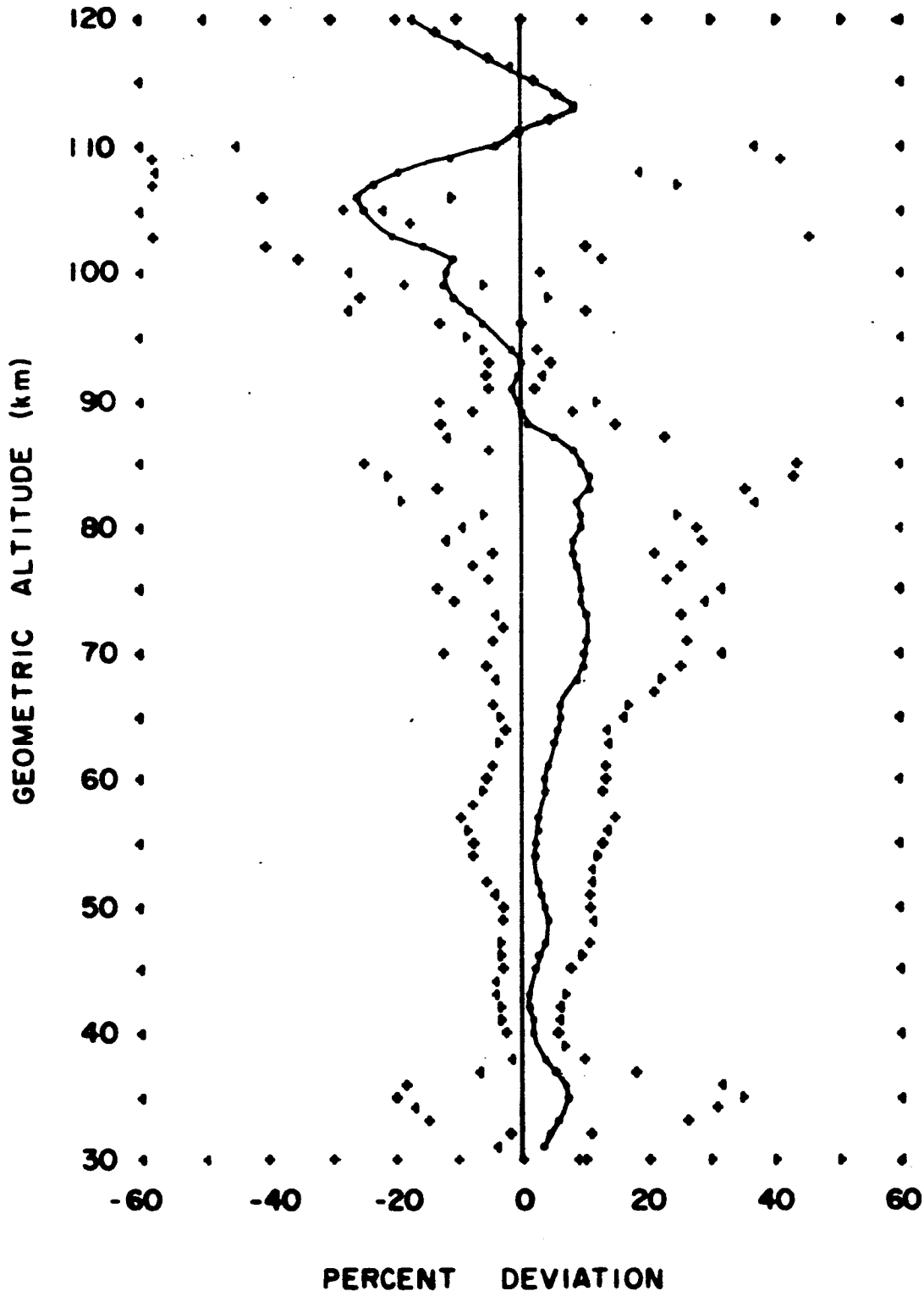

FIGURE 40P. PERCENT DEVIATION OF MEAN ATMOSPHERIC WINTER DENSITIES OVER MIDLATITUDES FROM DENSITIES OF THE PATRICK REF. ATMOSPHERE

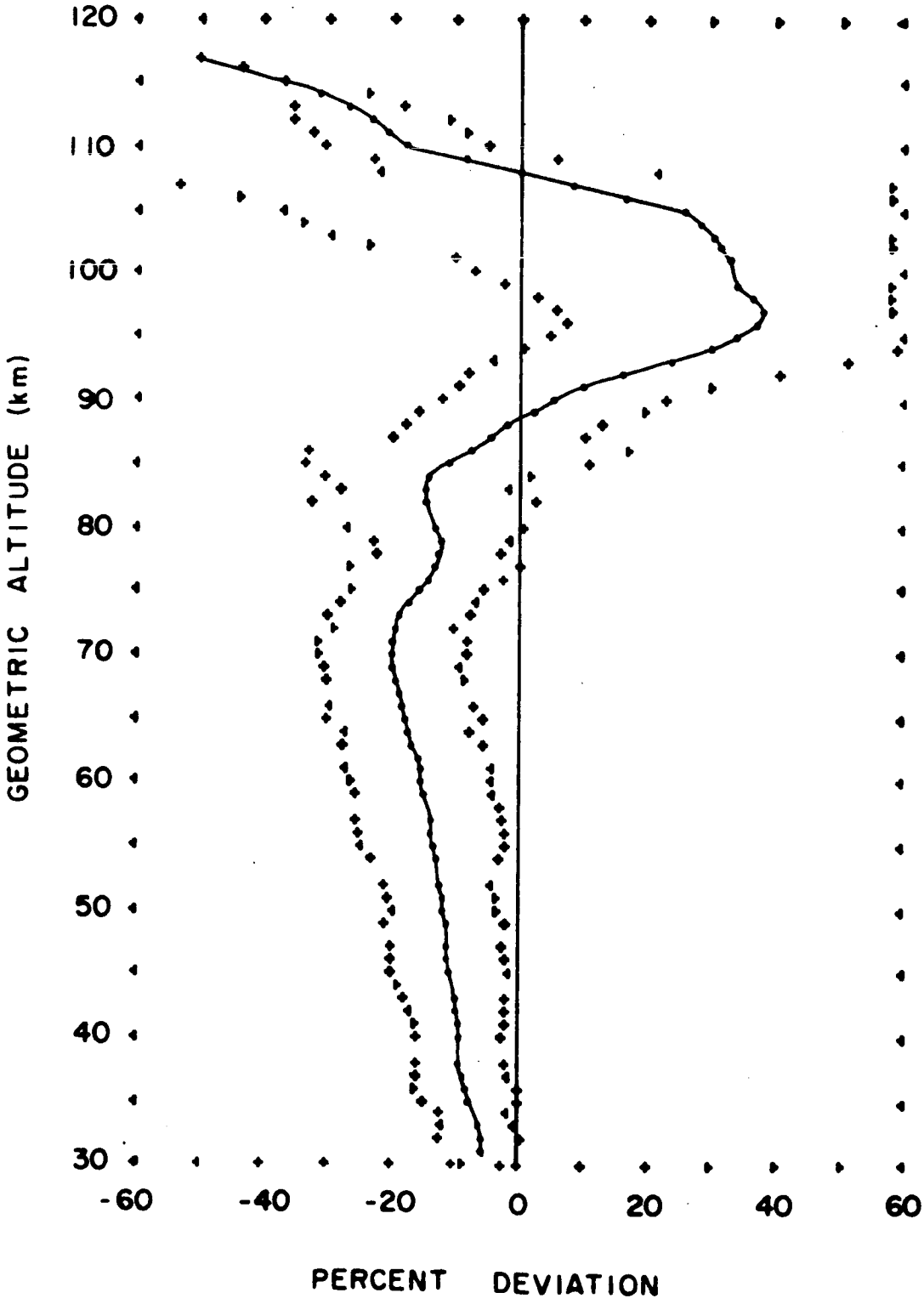

FIGURE 41P. PERCENT DEVIATION OF MEAN ATMOSPHERIC ANNUAL DENSITIES OVER MIDLATITUDES FROM DENSITIES OF THE PATRICK REF. ATMOSPHERE

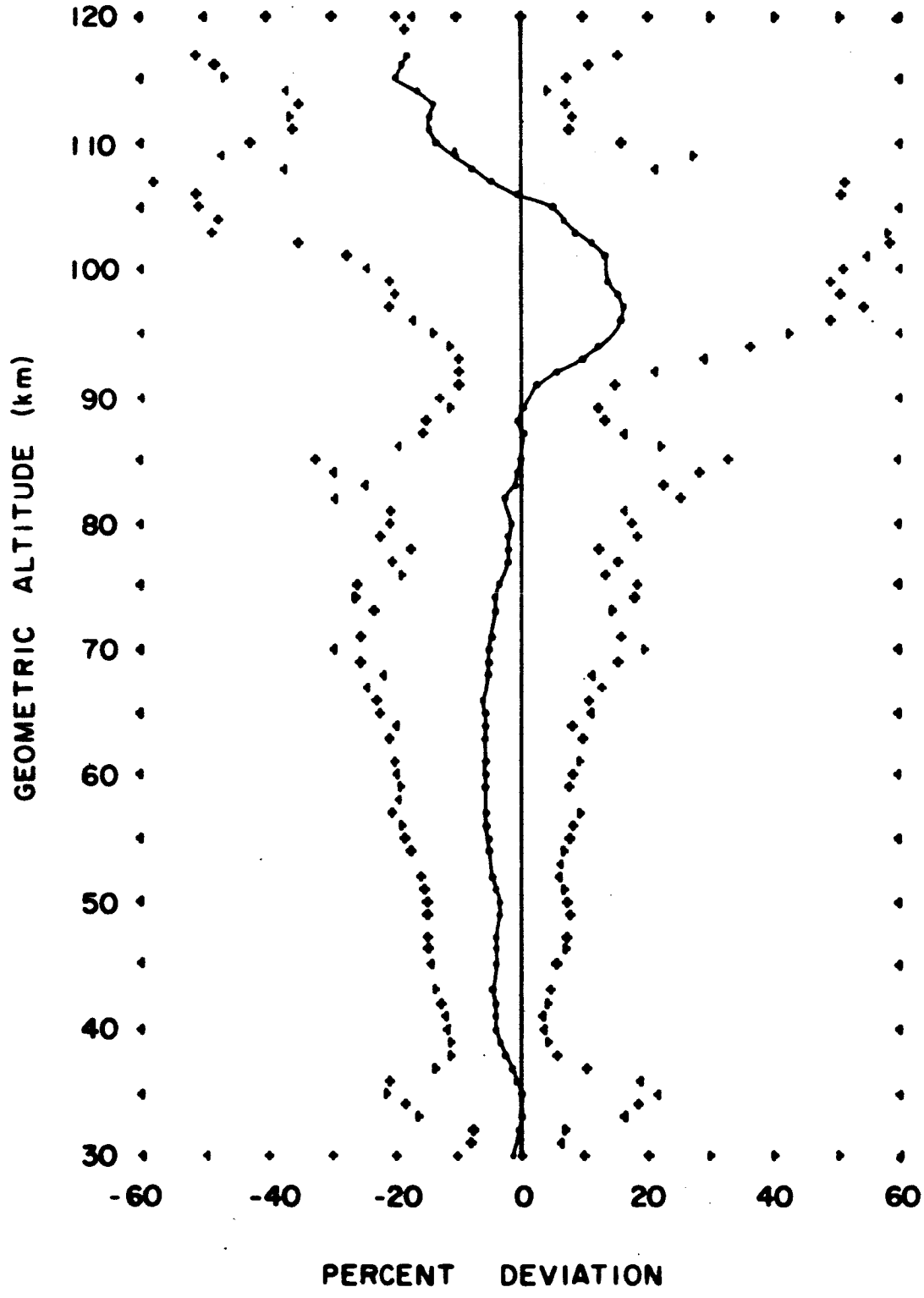

FIGURE 42P. PERCENT DEVIATION OF MEAN ATMOSPHERIC SUMMER DENSITIES OVER THE SUBARCTIC FROM DENSITIES OF THE PATRICK REF. ATMOSPHERE

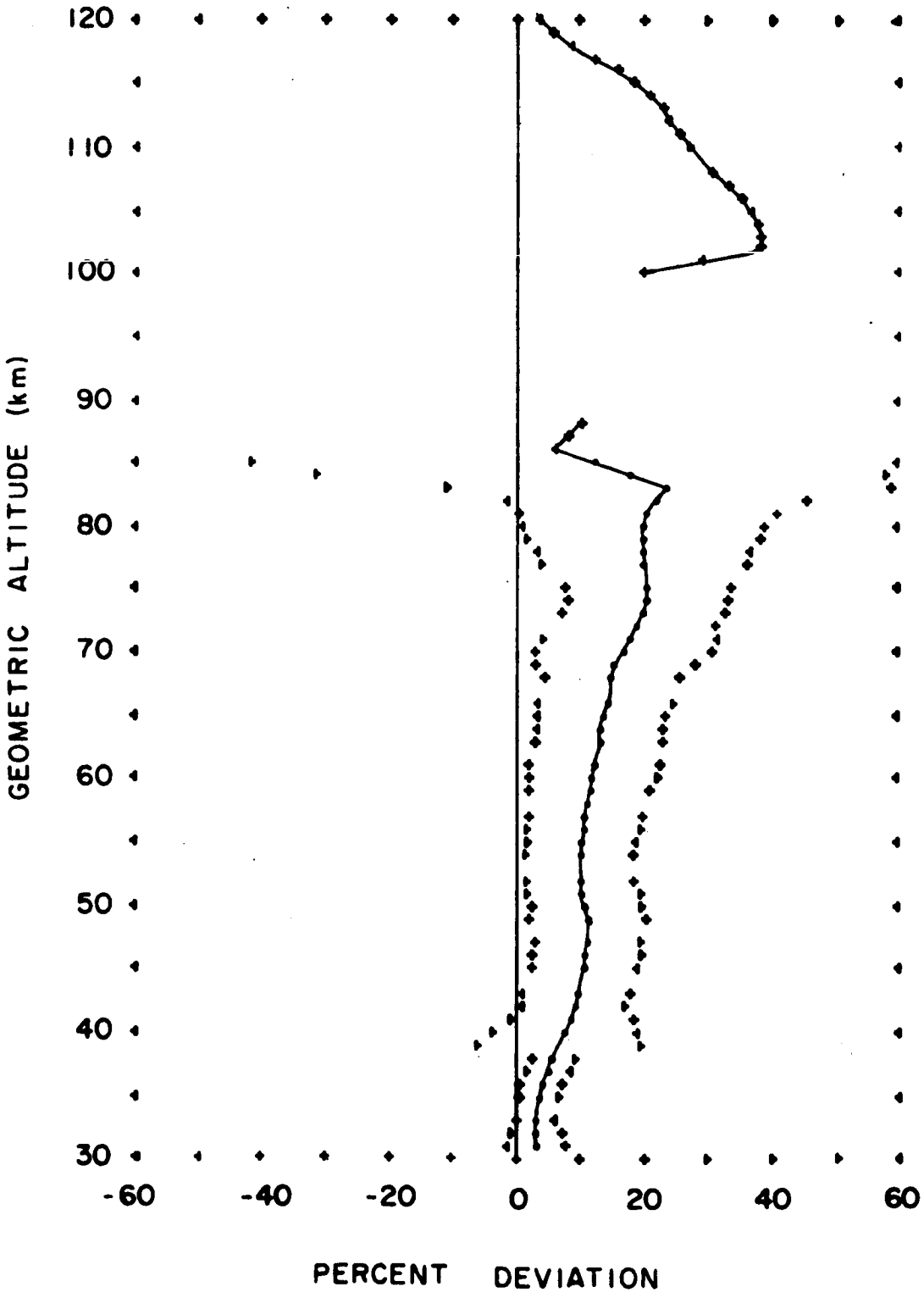

FIGURE 43P. PERCENT DEVIATION OF MEAN ATMOSPHERIC WINTER DENSITIES OVER THE SUBARCTIC FROM DENSITIES OF THE PATRICK REF. ATMOSPHERE

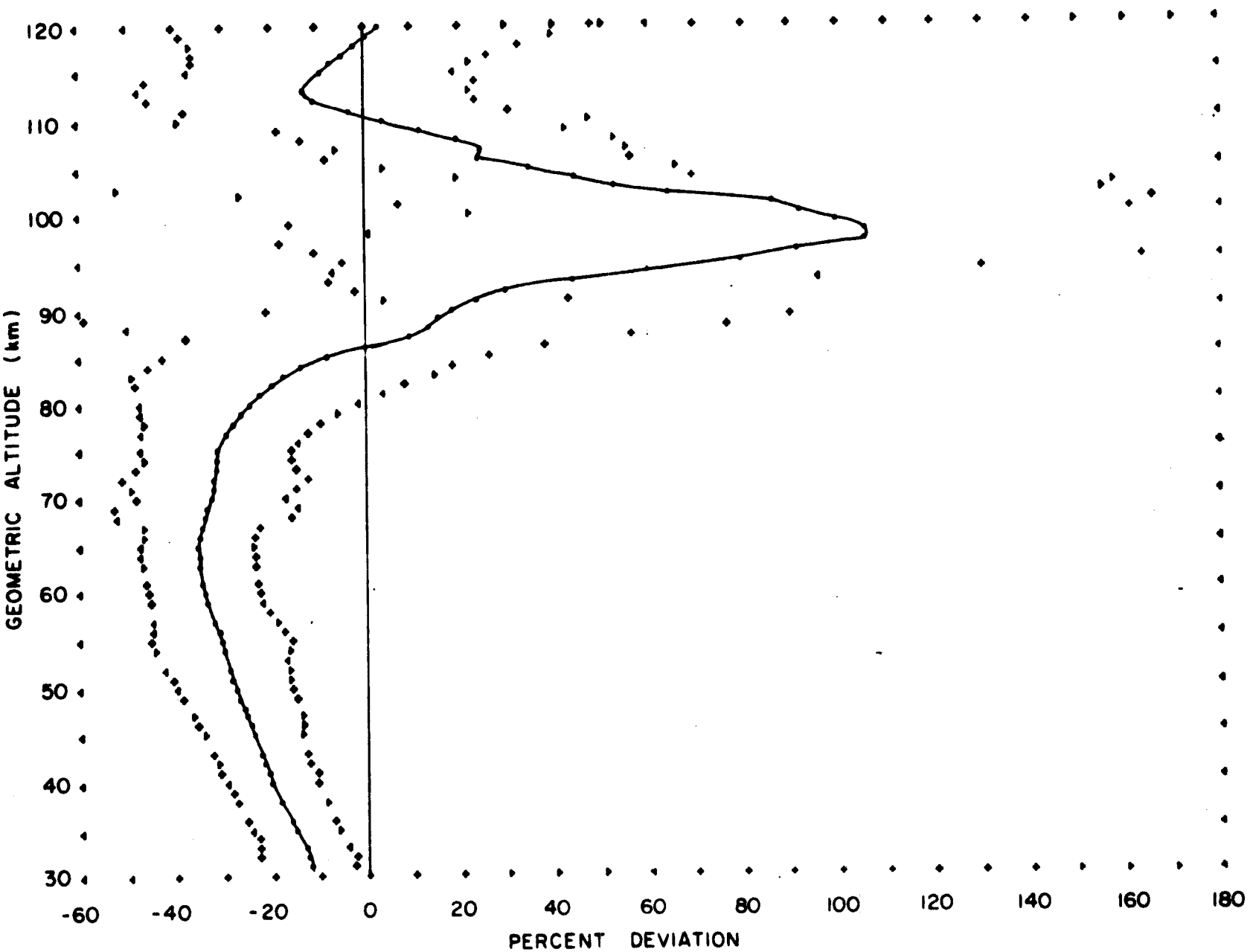

FIGURE 44P. PERCENT DEVIATION OF MEAN ATMOSPHERIC ANNUAL DENSITIES OVER THE SUBARCTIC FROM DENSITIES OF THE PATRICK REF. ATMOSPHERE

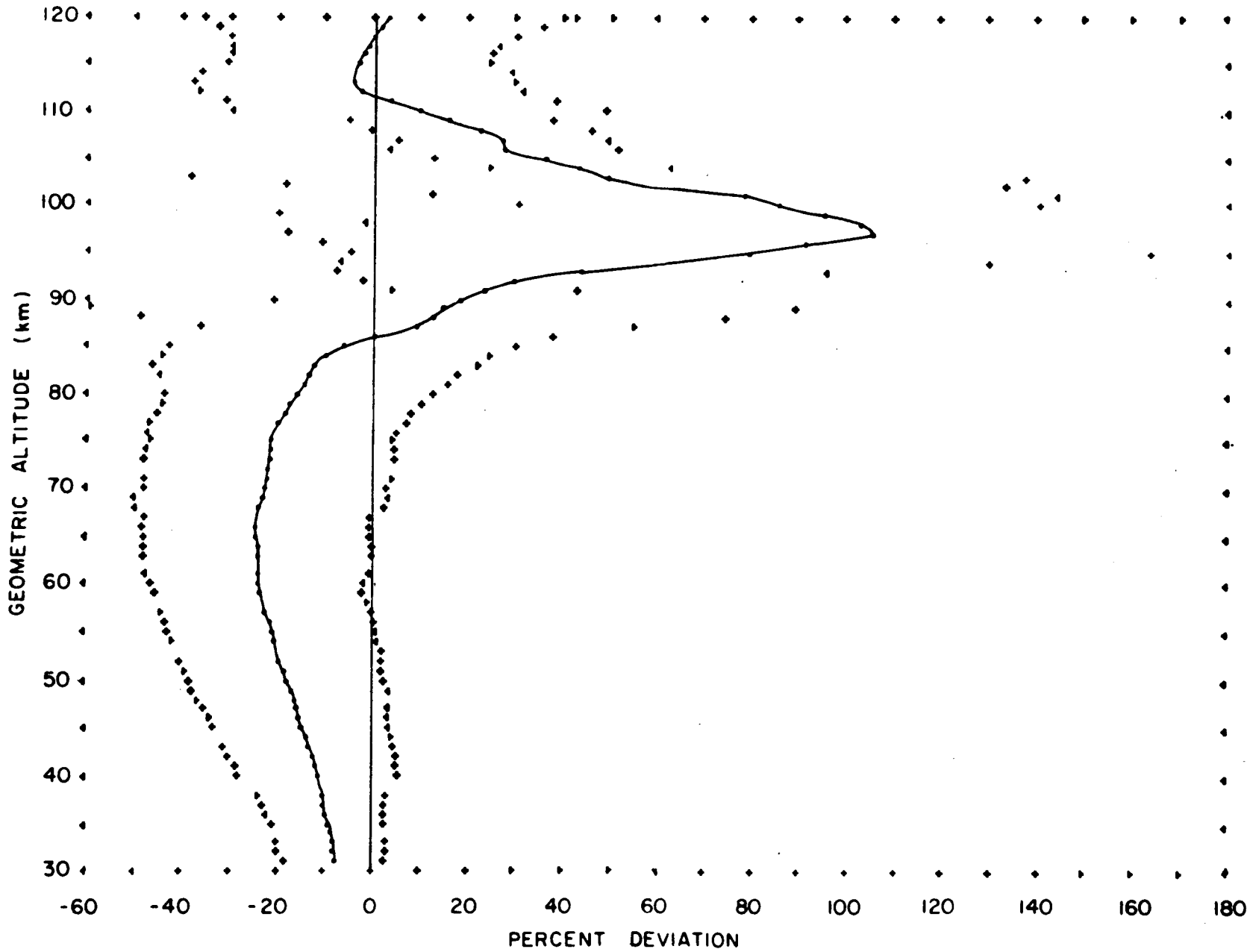

FIGURE 45P. PERCENT DEVIATION OF MEAN ATMOSPHERIC SUMMER DENSITIES OVER THE ARCTIC FROM DENSITIES OF THE PATRICK REF. ATMOSPHERE

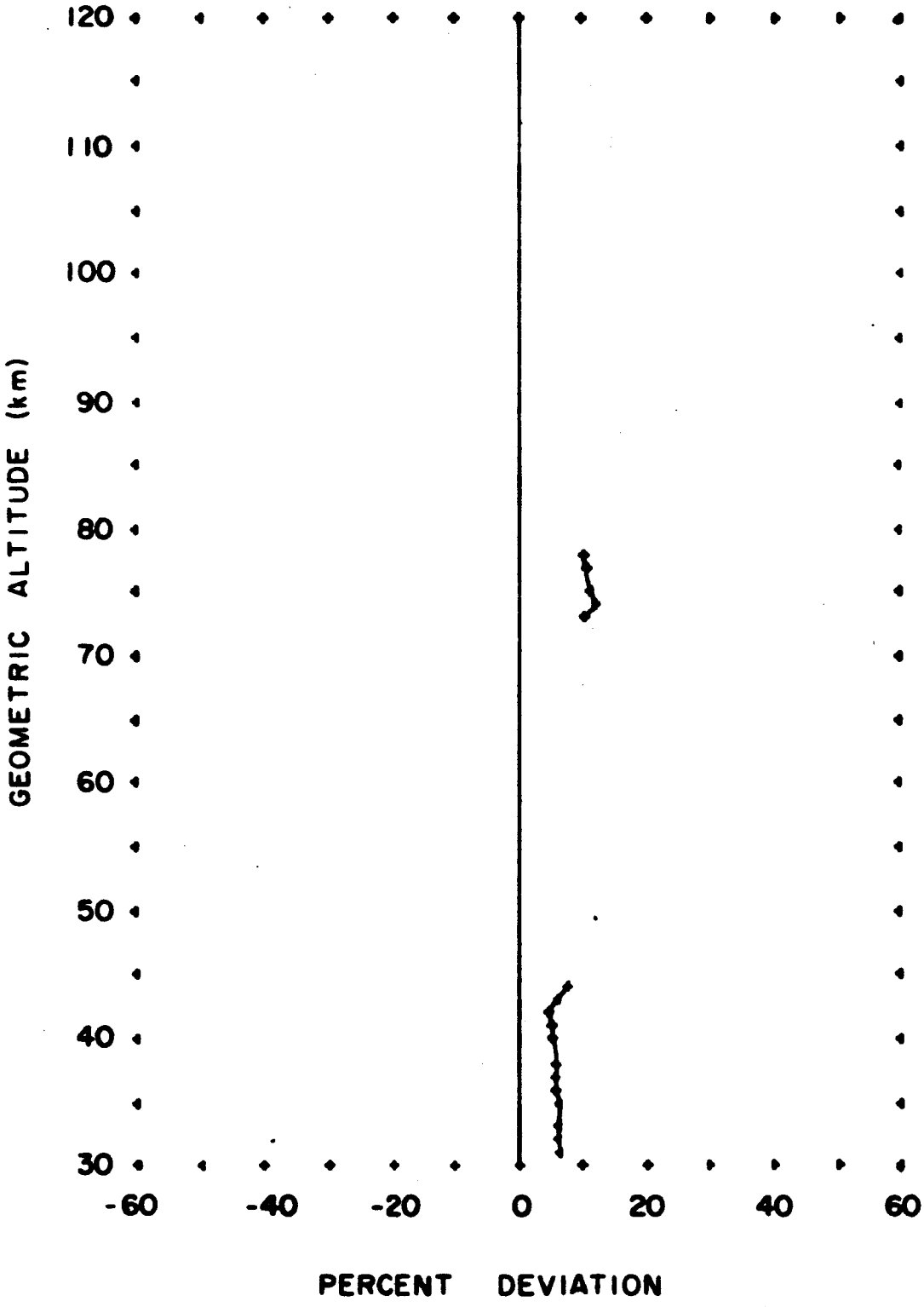

FIGURE 46P. PERCENT DEVIATION OF MEAN ATMOSPHERIC SUMMER DENSITIES OVER ALL SITES FROM DENSITIES OF THE PATRICK REF. ATMOSPHERE

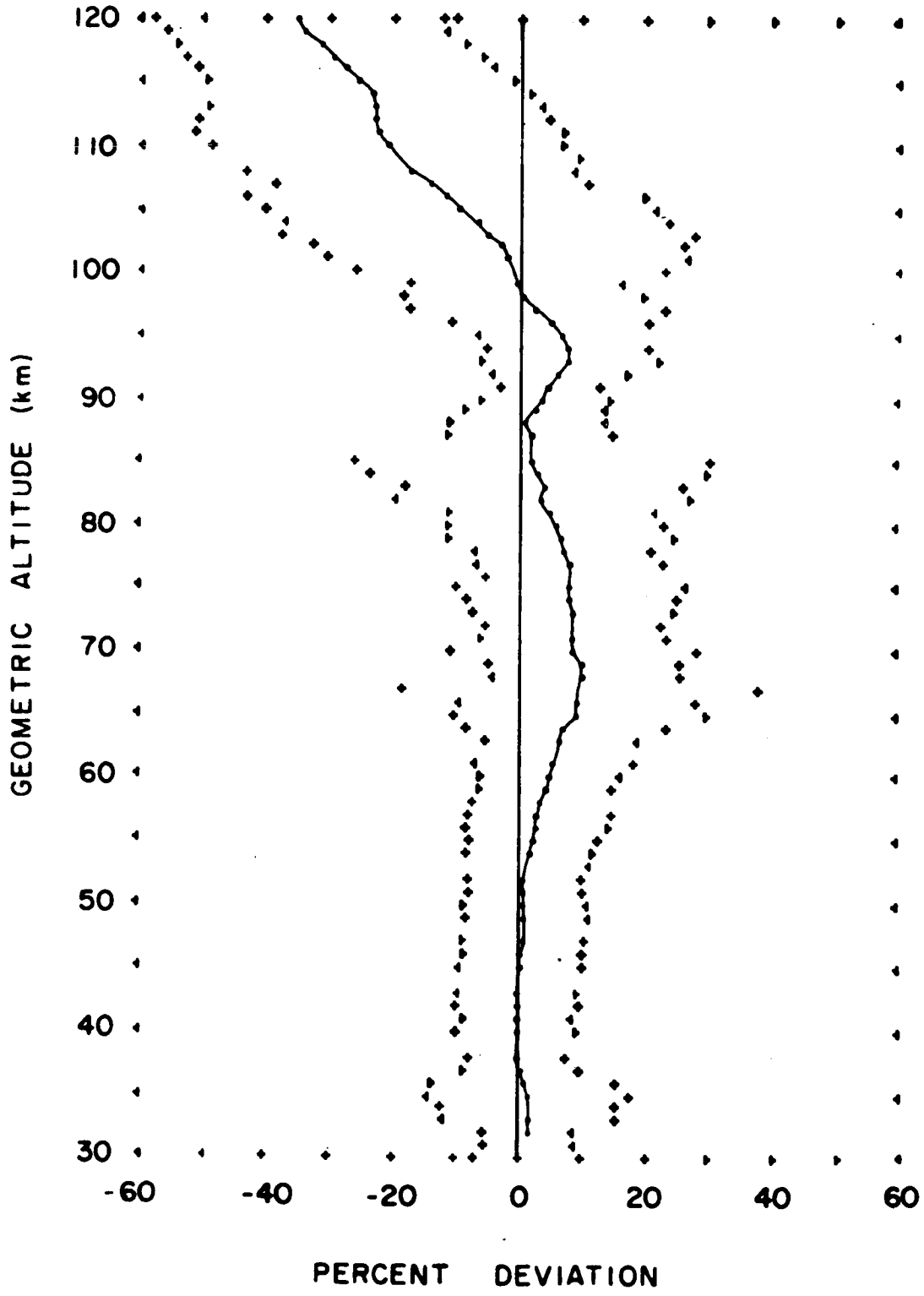

FIGURE 47P. PERCENT DEVIATION OF MEAN ATMOSPHERIC WINTER DENSITIES OVER ALL SITES FROM DENSITIES OF THE PATRICK REF. ATMOSPHERE

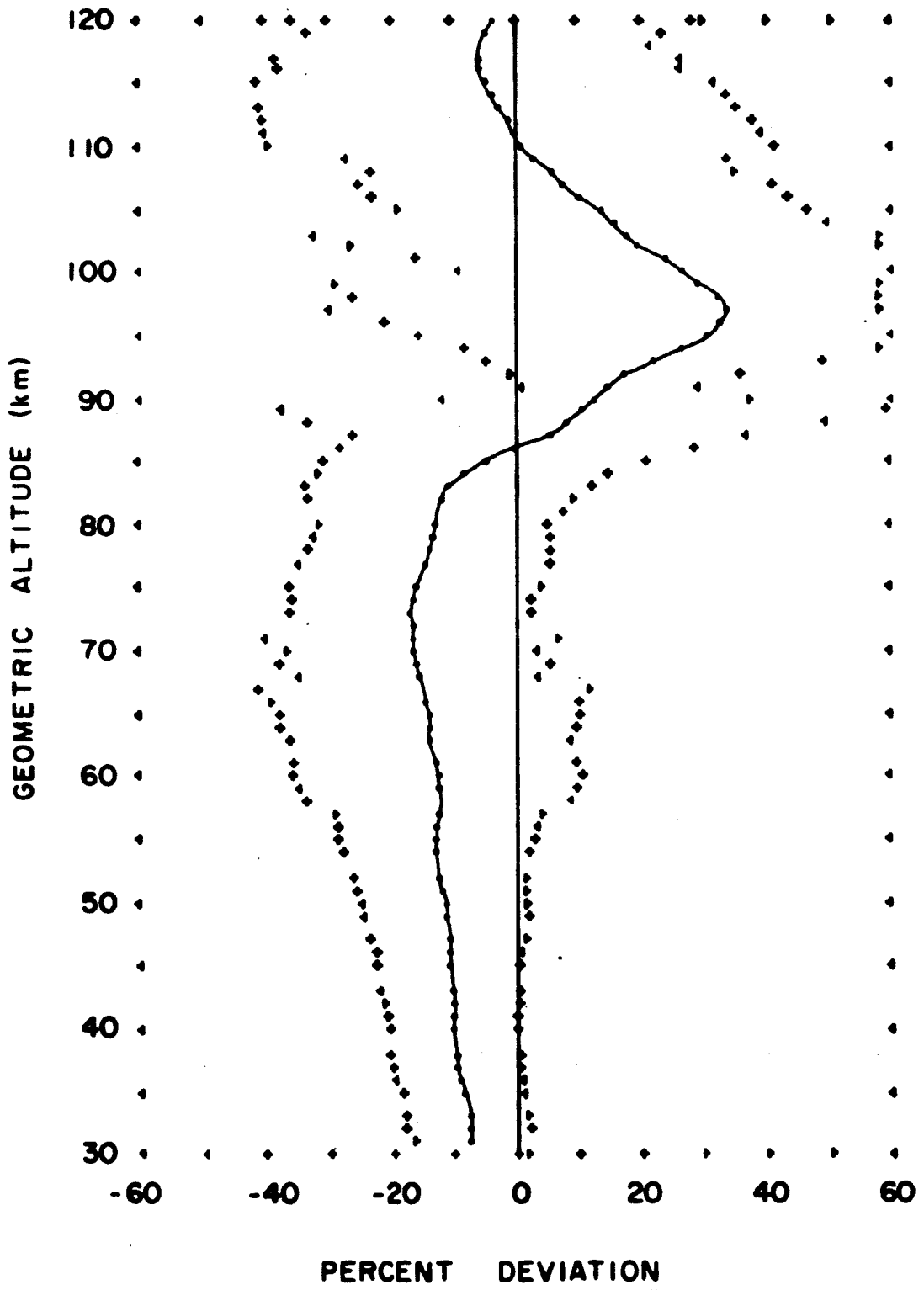

FIGURE 48P. PERCENT DEVIATION OF MEAN ATMOSPHERIC ANNUAL DENSITIES OVER ALL SITES FROM DENSITIES OF THE PATRICK REF. ATMOSPHERE

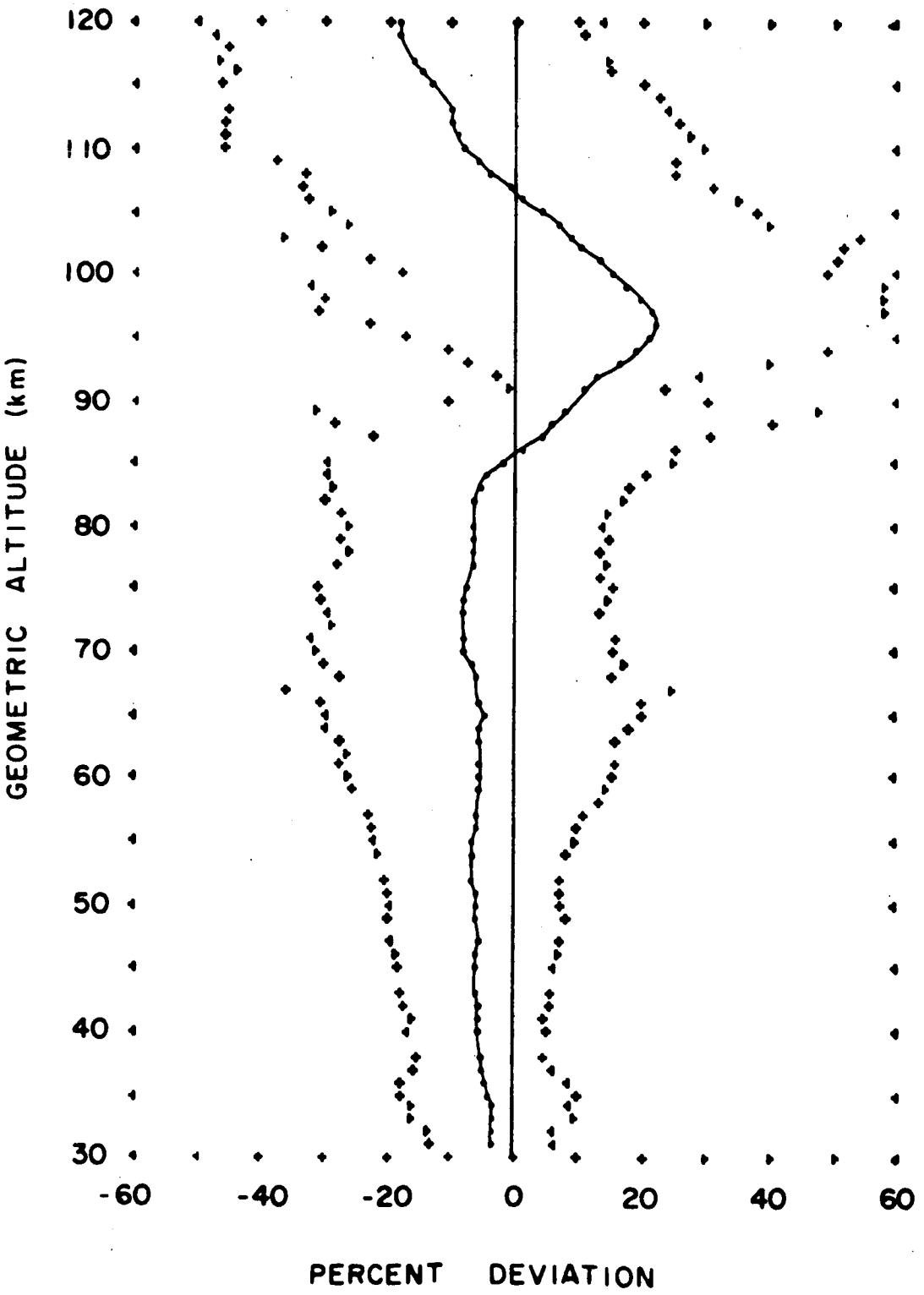

APPENDIX A

CHRONOLOGICAL LIST OF SOUNDINGS COMPRISING THE DATA AND THE SOURCES OF THESE DATA

TABLE A1

ATMOSPHERIC DENSITY OBSERVATIONS FOR ALTITUDES IN EXCESS OF 30 KILOMETERS FROM ROCKET SOUNDINGS AND GROUND-BASED SOUNDING PROBES LISTED CHRONOLOGICALLY

GMT DATE + TIME				PLACE AND TECH	SOLAR FLUX E+22 JOULE / SQ M		LOCAL SUN TIME	SUB-SOLAR ANGLE	MAXIMUM AND MINIMUM ALT KM		NUMBER OF DEN PTS AND		REF
MO DA YR	HR	MI		CODE	/ SEC	CPS	HOURS	DEG			CODE		
03/07/47	18	23		WS G	308.8	324.3	11.11	39.8	156	69	9	P	12
01/22/48	20	12		WS G	146.6	159.5			158	110	8	P/	12
08/06/48	01	37		WS G	206.0	185.8	18.43	86.4	69	61	8	P	12
09/29/49	16	58		WS G	130.5	128.8	10.04	44.6	89	82	3	P*	12
05/11/50	23	00		WS G	166.5	159.1	15.97	55.1	66	39	4	P	12
06/20/50	15	40		HA G	124.6	123.3	07.92	54.0	72	30	22	TP»	04
08/20/50	07	00		AQ L	N.D.	N.D.			59	21	13	=	05
09/08/50	07	00		AQ L	92.7	88.4			62	21	14	=	05
09/10/50	07	00		AQ L	88.0	N.D.			62	21	14	=	05
09/13/50	07	00		AQ L	97.0	106.9			62	21	14	=	05
09/14/50	07	00		AQ L	106.9	112.0			62	21	14	=	05
10/12/50	07	00		AQ L	113.3	106.9			62	21	14	=	05
10/14/50	07	00		AQ L	109.0	N.D.			62	21	14	=	05
11/16/50	07	00		AQ L	110.8	108.2			62	21	14	=	05
11/21/50	17	18		WS G	86.3	86.7	10.44	56.9	110	110	1	/	12
08/07/51	18	00		WS G	N.D.	130.5	10.82	22.6	220	110	13		14
09/13/51	11	37		HA G	129.1	121.1	03.96	112.9	60	30	16	TP»	04
05/15/52	01	16		WS D	74.9	74.5	18.24	82.9	67	50	68	T	19
05/30/52	08	22		AQ L	91.8	88.3			68	21	17	»	06
06/14/52	05	42		AQ L	75.3	76.6			68	21	17	»	06
06/16/52	06	45		AQ L	76.6	80.3			68	21	17	»	06
06/22/52	06	00		AQ L	90.9	91.3			68	21	17	»	06
06/23/52	06	00		AQ L	91.3	99.7			68	21	17	»	06
08/03/52	10	17		AQ L	83.8	87.2			68	21	17	»	06
09/18/52	04	32		AQ L	77.3	76.4			68	21	17	»	06
09/19/52	06	41		AQ L	76.4	82.3			68	21	17	»	06
09/25/52	06	07		AQ L	83.5	84.8			68	21	17	»	06
09/26/52	06	35		AQ L	84.8	82.2			68	21	17	»	06
09/27/52	07	35		AQ L	82.2	N.D.			68	21	17	»	06
10/11/52	03	35		AQ L	79.6	N.D.			68	21	17	»	06
10/12/52	03	00		AQ L	N.D.	82.2			68	21	17	»	06
10/17/52	04	30		AQ L	77.1	74.1			68	21	17	»	06
10/19/52	03	40		AQ L	74.1	78.3			68	21	17	»	06
10/22/52	09	55		AQ L	85.1	90.2			68	21	17	»	06
10/22/52	14	21		HA G	85.1	90.2	07.49	78.0	90	45	45	TP	20
10/23/52	05	30		AQ L	90.2	91.0			68	21	17	»	06
10/24/52	05	35		AQ L	90.1	91.5			68	21	17	»	06
12/11/52	23	47		WS D	89.2	94.3	16.80	88.3	75	34	110	T	19
04/23/53	19	33		WS D	75.4	77.0	12.49	20.8	81	37	92	T	19

TABLE A1 CONTINUED

08/05/53	21	54	SB	G	70.0	71.1	17.54	71.9	44	20	7	TP	2C
08/11/53	17	09	SB	G	80.8	89.3	10.77	60.2	44	20	7	TP	2C
09/29/53	20	50A	WS	D	71.8	71.3	13.85	40.9	54	46	33		19
09/29/53	20	50B	WS	D	71.8	71.3	13.85	40.9	53	31	167	T	19
07/19/54	16	00A	SB	G	66.6	67.2	12.34	33.4	43	32	4	*	2C
07/19/54	16	00B	SB	G	66.6	67.2	12.34	33.4	41	32	6	*	2C
07/25/54	18	45A	SB	G	N.D.	67.0	14.97	50.4	37	26	4	*	2C
07/25/54	18	45B	SB	G	N.D.	67.0	14.97	50.4	35	25	5	*	2C
06/24/55	18	04A	WI	D	93.2	82.9	13.00	19.3	70	61	34		19
06/24/55	18	04B	WI	D	93.2	82.9	13.00	19.3	78	31	75		19
07/06/56	18	00A	WI	D	158.	156.	12.89	19.0	87	61	23		19
07/06/56	18	00B	WI	D	158.	156.	12.89	19.0	73	49	54	T	19
10/23/56	08	40	FC	G	191.	184.	02.67	124.0	63	31	26		29
11/02/56	18	40A	SB	D	241.	225.	15.72	80.7	81	64	6		19
11/02/56	18	40B	SB	D	241.	225.	15.72	80.7	75	19	54	T	19
11/04/56	18	54A	SB	D	225.	251.	16.06	88.7	90	80	10		19
11/04/56	18	54B	SB	D	225.	251.	16.06	88.7	88	19	53	T	19
11/10/56	15	17A	SB	D	305.	284.	11.67	83.0	79	65	10		19
11/10/56	15	17B	SB	D	305.	284.	11.67	83.0	90	18	50	T	19
11/12/56	11	57	FC	S	283.	293.	05.96	105.4	59	19	41	T	02
11/17/56	16	48A	FC	G	257.	255.	10.80	79.2	39	20	10		01
11/17/56	16	48B	FC	G	257.	255.	10.80	79.2	195	195	1		20A
11/21/56	05	21	FC	M	216.	205.	22.86	139.3	210	110	18	/	21
07/22/57	04	16	FC	S	244.	236.	21.91	96.8	83	24	60	TP	02
07/24/57	05	29	FC	S	250.	255.	23.12	100.6	82	32	51	TP	02
07/29/57	22	00A	FC	G	212.	201.	15.64	56.1	82	20	38	TP	01
07/29/57	22	00B	FC	G	212.	201.	15.64	56.1	210	100	12	TP	15
08/12/57	16	00	FC	S	173.	177.	09.66	50.9	64	34	31	TP	02
08/20/57	02	30	FC	S	214.	199.	20.19	95.1	81	32	50	TP	02
08/25/57	14	08	FC	S	199.	210.	07.83	66.8	88	33	57	TP	02
09/01/57	22	28	FC	G	294.	275.	16.22	69.4	71	61	9		29
11/13/57	11	52	WO	S	257.	250.			69	40	8	P	9A
12/12/57	04	00	FC	S	211.	209.	21.85	137.7	76	21	56	TP	02
12/14/57	21	00	FC	S	248.	228.	14.83	89.2	86	30	57	TP	02
01/25/58	19	12A	FC	D	211.	206.	12.74	78.2	87	57	20	T	19
01/25/58	19	12B	FC	D	211.	206.	12.74	78.2	90	18	56		19
01/27/58	06	04	FC	S	220.	200.	23.60	139.6	86	27	60	TP	02
01/27/58	18	48A	FC	S	220.	200.	12.35	77.3	87	30	58	TP	02
01/27/58	18	48B	FC	D	220.	200.	12.34	77.3	90	19	47	T	19
01/27/58	19	18	FC	G	220.	200.	13.04	78.2	70	58	10		29
01/29/58	19	06A	FC	D	189.	194.	12.63	77.0	87	70	6		19
01/29/58	19	06B	FC	D	189.	194.	12.63	77.0	100	18	51	T	19
02/22/58	02	02	FC	M	172.	175.	19.55	110.9	215	115	21	/	21
02/24/58	07	00	FC	G	212.	220.	00.52	130.5	202	202	1		20A
02/24/58	07	35	FC	G	212.	220.			90	53	32		29
03/04/58	19	30A	FC	D	223.	232.	13.05	66.4	85	57	13		19
03/04/58	19	30B	FC	D	223.	232.	13.05	66.4	91	18	46	T	19
03/23/58	18	07	FC	M	266.	268.	11.75	57.8	180	110	15	/	21
03/24/58	22	00	FC	G	268.	274.	15.64	71.2	91	59	30		29

TABLE A1 CONTINUED

04/17/58	10	57	WO	S	197.	207.			84	26	13	P	9A
07/15/58	20	08	FC	G	182.	181.	13.78	41.9	85	39	44		27
10/15/58	01	05	FC	G	225.	228.	19.06	105.3	99	32	46		27
10/20/58	22	01	FC	G	296.	278.	16.02	84.4	72	53	17		27
10/31/58	19	59A	FC	G	228.	222.	14.00	49.8	110	22	41	TP	01
10/31/58	19	59B	FC	G	228.	222.	14.00	49.8	188	100	24	TP	16
11/12/58	11	40	GM	S	166.	166.	22.27	154.7	58	28	31	TP	02
11/14/58	11	10	GM	S	163.	166.	21.77	147.6	67	29	39	TP	02
11/19/58	18	02	GM	S	174.	183.	04.62	113.7	67	29	39	TP	02
11/20/58	14	39	GM	S	183.	187.	01.23	161.3	63	28	36	TP	02
11/22/58	09	58	GM	S	194.	200.	20.54	130.1	76	27	50	TP	02
11/22/58	17	06	GM	S	194.	200.	03.67	127.1	59	22	20		30
11/23/58	22	02	FC	G	200.	213.	16.01	93.2	103	55	50		29
11/24/58	17	27	GM	S	213.	229.	04.07	121.5	74	28	47	TP	02
11/30/59	09	58	WO	F	225.	230.	19.53	96.9	140	117	6	T	25
11/30/59	12	35	WO	S	225.	230.			86	48	6	P	9A
12/01/59	11	36	WO	S	230.	222.			54	41	4	P	9A
07/09/60	03	59	WI	S	176.	176.	22.87	117.7	81	25	57	TP	27
08/10/60	10	35	WO	S	152.	170.			74	63	3	P	9A
10/17/60	21	04	FC	G	165.	167.	15.06	77.6	93	28	32	/	17
11/17/60	10	06	WO	F	174.	164.	19.22	94.9	152	132	2		09
02/13/61	13	58	WO	S	98.	97.			78	44	17	P	9A
02/14/61	23	50	WI	S	97.	97.	18.56	104.4	73	30	44	TP	27
02/17/61	02	26	WI	S	96.	96.	21.17	134.3	77	30	48	TP	27
03/06/61	09	56	WO	S	94.	93.			86	42	17	P	9A
04/05/61	10	56	WO	S	103.	107.			86	45	9	P	9A
04/05/61	12	57	WI	S	103.	107.	07.87	64.2	76	29	48	TP	27
05/05/61	23	00	WI	S	104.	103.	18.03	80.4	81	22	60	TP	27
05/06/61	04	54	WI	S	103.	97.	23.93	125.7	87	22	66	TP	27
06/06/61	21	48A	WI	D	86.	88.	16.81	62.6	93	56	52	TP	24
06/06/61	21	48B	WI	D	86.	88.	16.81	62.6	91	46	69	TP	24
06/06/61	21	48C	WI	D	86.	88.	16.81	62.6	110	33	78	TP	24
07/04/61	10	32	WO	S	104.	103.			69	27	16	P	9A
07/13/61	22	07	WI	S	137.	141.	16.99	65.2	88	26	63	TP	27
07/14/61	16	02	WI	S	141.	136.	10.91	21.5	76	25	46	TP	27
07/20/61	10	30	WI	S	126.	123.	05.36	84.6	84	28	57	TP	27
08/23/61	17	03	WS	R	103.	98.	9.54	39.9	220	120	6	/	13
09/16/61	23	55	WI	S	135.	133.	19.07	101.1	61	28	34	TP	27
12/07/61	23	15	EG	D	101.	94.			132	98	50		08
03/01/62	18	07A	EG	D	122.	121.	12.13	38.0	97	60	31		07
03/01/62	18	07B	FG	D	122.	121.	12.13	38.0	95	36	41		07
03/02/62	00	05	WI	S	121.	112.	18.86	104.7	81	26	56	TP	27
03/02/62	11	15	WI	S	121.	112.	06.02	94.2	85	25	61	TP	27
03/06/62	12	35	WO	S	86.	81.			80	34	10	P	9A
03/23/62	23	54	WI	S	128.	130.	18.76	98.3	87	27	61	TP	27
03/28/62	00	04	WI	S	117.	109.	18.95	99.5	91	27	65	TP	27
03/29/62	11	04	WO	S	109.	103.			87	32	13	P	9A
04/05/62	15	47	WO	S	78.	76.			85	43	10	P	9A
04/17/62	09	29	WI	S	119.	114.	04.45	101.3	90	29	62	TP	27

TABLE A1 CONTINUED

05/18/62	18	02	WI	M	93.	95.	13.06	22.9	132	108	5	/	26		
06/05/62	12	45	WS	R	85.	85.			210	170	3	=	10		
06/06/62	23	40	WI	G	85.	87.	18.67	83.7	94	31	64	TP		18	
06/07/62	00	10	WI	D	85.	87.	19.17	89.0	110	30	81	TP		24	
06/07/62	01	05	WI	S	87.	92.	20.08	98.1	94	29	67	TP		27	
06/08/62	01	53	WI	S	92.	90.	20.87	105.0	90	31	60	TP		27	
07/05/62	03	46	WO	S	90.	88.			84	58	9	P		9A	
10/25/62	23	30	WS	R	89.	87.			210	170	3	=		10	
11/28/62	10	17	WO	S	75.	74.			84	40	10	P		9A	
12/01/62	20	34	WI	G	77.	77.	15.72	79.4	107	33	75	TP		18	
12/01/62	21	25	WI	S	77.	77.	16.57	87.7	91	29	63	TP		27	
12/04/62	07	05	FC	S	83.	82.			87	31	57	TP		27	
12/04/62	07	26	WO	S	83.	82.			59	29	9	P		9A	
12/06/62	05	32	WI	S	82.	83.	00.65	162.5	86	26	01	TP		27	
12/06/62	05	43	FC	S	82.	83.			89	28	62	TP		27	
02/14/63	00	30	EG	D	74.	74.	18.48	102.8	155	95	60			08A	
02/20/63	23	34	FC	S	79.	77.			72	29	50	TP		27	
02/20/63	23	47	WI	S	79.	77.	18.52	102.8	84	27	58	TP		27	
02/28/63	21	48	FC	S	75.	74.			88	33	55	TP		27	
02/28/63	22	11	WI	S	75.	74.	16.94	82.6	80	24	57	TP		27	
03/09/63	00	01A	FC	S	83.	82.			91	33	60	TP		27	
03/09/63	00	01B	WI	S	83.	82.	18.80	102.5	89	29	62	TP		27	
03/29/63	02	57A	KW	D	73.	75.	14.04	31.1	120	100	21	TP		23	
03/29/63	02	57B	KW	D	73.	75.	14.04	31.1	102	57	46	TP		23	
04/17/63	09	23	WO	S	88.	87.			85	52	7	P		9A	
06/06/63	14	30	WS	M	78.	77.	07.44	61.1	210	100	11			22	
06/18/63	03	28A	KW	D	86.	82.	14.64	40.3	120	99	22	TP		23	
06/18/63	03	28B	KW	D	86.	82.	14.64	40.3	102	33	42	TP	B	23	
06/20/63	03	00A	KW	D	79.	75.	14.16	34.0	110	104	07	TP		23	
06/20/63	03	00B	KW	D	79.	75.	14.16	34.0	98	33	66	TP		23	
07/10/63	17	04	WS	R	69.	69.	9.89	29.8	220	150	08	=		11	
08/02/63	23	33	WI	D	87.	87.	18.43	84.1	102	89	14	TP		23	
10/15/63	09	51	WO	S	86.	88.			83	34	13	P		9A	
10/15/63	11	48	WO	S	86.	88.			84	22	16	P		9A	
10/15/63	15	09	WO	S	86.	88.			81	21	15	P		9A	
10/15/63	19	22	WO	S	86.	88.			80	25	14	P		9A	
11/04/63	10	00A	WS	D	83.	83.	03.19	133.4	109	78	25	/		03	
11/04/63	10	00B	WS	D	83.	83.	03.19	133.4	114	35	62	/		03	
11/04/63	10	31	KW	D	83.	83.			45	40	06	TP		23	
11/04/63	12	27	KW	D	83.	83.			45	32	14	TP		23	
11/04/63	24	00A	WS	D	83.	83.	17.19	88.3	109	74	26	/		03	
11/04/63	24	00B	WS	D	83.	83.	17.19	88.3	110	35	79	/		03	
11/09/63	16	26A	KW	D	76.	75.	03.89	122.9	120	107	14	TP		23	
11/09/63	16	26B	KW	D	76.	75.	03.89	122.9	103	37	67	TP		23	
11/14/63	14	58A	KW	D	78.	81.	02.41	143.1	120	103	17	TP		23	
11/14/63	14	58B	KW	D	78.	81.	02.41	143.1	109	32	33	TP	B	23	
11/26/63	18	44A	WI	D	82.	82.	13.92	64.7	114	90	25	TP		23	
11/26/63	18	44B	WI	D	82.	82.	13.92	64.7	83	32	52	TP		23	
12/07/63	13	11A	WI	S	76.	77.	08.30	79.8	77	34	45			27	
12/07/63	13	11B	WI	D	76.	77.	08.30	79.8	88	58	31	TP		23	
12/07/63	13	43	WI	G	76.	77.	08.68	76.4	79	36	43	TP		18	

TABLE A1 CONCLUDED

01/23/64	18	25	KW	D	75.	75.	05.40	101.6	98	33	66	TP	23
02/04/64	01	35	AI	G	71.	71.	00.39	154.8	106	35	71	TP	18
02/18/64	21	50A	WS	D	74.	76.	14.51	56.9	114	56	58	/	03
02/18/64	21	50B	WS	D	74.	76.	14.51	56.9	111	42	35	/	03
02/19/64	21	30A	WS	D	76.	76.	14.18	53.8	114	61	45	/	03
02/19/64	21	30B	WS	D	76.	76.	14.18	53.8	104	32	74	/	03
03/13/64	18	20A	KW	D	77.	78.	05.36	99.9	120	99	22	TP	23
03/13/64	18	20B	KW	D	77.	78.	05.36	99.9	104	32	73	TP	23
04/15/64	01	22	AI	G	72.	71.	00.41	173.6	97	32	65	TP	18
04/15/64	15	56	AI	G	72.	71.	14.97	47.8	100	32	69	TP	18
05/07/64	02	31	PM	D	72.	71.	18.64	88.3	110	98	13	TP	23
05/12/64	11	25A	KW	D	70.	69.4	22.66	145.0	120	96	25	TP	23
05/12/64	11	25B	KW	D	70.	69.4	22.66	145.0	107	37	71	TP	23
06/17/64	01	01A	KW	D	70.6	71.1	12.19	14.2	120	102	19	TP	23
06/17/64	01	01B	KW	D	70.6	71.1	12.19	14.2	102	32	71	TP	23
06/18/64	02	19A	KW	D	71.1	71.7	13.48	25.4	120	100	21	TP	23
06/18/64	02	19B	KW	D	71.1	71.7	13.48	25.4	98	34	65	TP	23
06/18/64	16	30A	KW	D	71.7	70.1	03.66	117.1	120	102	19	TP	23
06/18/64	16	30B	KW	D	71.7	70.1	03.66	117.1	100	32	69	TP	23
11/17/64	21	10A	WI	D	71.9	75.5	16.39	84.0	117	96	22	TP	23
11/17/64	21	10B	WI	D	71.9	75.5	16.39	84.0	101	53	49	TP	23
12/17/64	19	54A	PM	D	79.9	79.6	12.02	57.5	109	99	12	TP	23
12/17/64	19	54B	PM	D	79.9	79.6	12.02	57.5	62	33	30	TP	23

DATA REFERENCES

1 AINSWORTH,J.E. FOX,D.E. AND LAGOW,H.E. 1961.
UPPER ATMOSPHERE STRUCTURE MEASUREMENT USING THE PITOT-STATIC TUBE.
J. GEO. RES. VOL. 66 (10) PP. 3191-3212.

2 BANDEEN,W.R. JUNE 2, 1965.
PRIVATE COMMUNICATION.

3 CHAMPION,K.S.W. AND FAIRE,A.C. JULY, 1964.
FALLING SPHERE MEASUREMENTS OF ATMOSHPERE DENSITY TEMPERATURE AND PRESSURE UP TO 115 KM.
AFCRL-64-554. AIR FORCE CAMBRIDGE RESEARCH LABS, BEDFORD, MASS.

4 DOW,W.G. AND SPENCER,N.W. AUGUST, 1953.
THE MEASUREMENT OF AMBIENT PRESSURE AND TEMPERATURE OF THE UPPER ATMOSPHERE.
UNIVERSITY OF MICHIGAN, ENGINEERING RESEARCH INSTITUTE, CONTRACT AF19(122)-55, FINAL REPORT.

5 ELTERMAN,L. DECEMBER, 1951.
THE MEASUREMENT OF STRATOSPHERIC DENSITY DISTRIBUTION WITH THE SEARCHLIGHT TECHNIQUE.
J. GEO. RES. VOL. 56 (4) PP. 509-520, ALSO
AFCRC, GEOPHYS. RES. PAPERS NO. 10, BEDFORD, MASS. DEC. 1951

6 ELTERMAN,L. JULY, 1954.
SEASONAL TRENDS OF TEMPERATURE, DENSITY AND PRESSURE IN THE STRATOSPHERE OBTAINED WITH THE SEARCHLIGHT-PROBING TECHNIQUE.
AFCRC. GEOPHYS. RES. PAPERS NO. 29, BEDFORD, MASS.

7 FAIRE,A.C. 1963.
PRIVATE COMMUNICATION.

8 FAUCHER,G.A. PROCUNIER,R.W. AND SHERMAN,F.S. 1963.
UPPER ATMOSPHERE DENSITY OBTAINED FROM MEASUREMENTS OF DRAG ON A FALLING SPHERE.
J. GEO. RES. VOL. 68, PP. 3437-3450.

9 GROVES,G.V. 22 MARCH 1963.
PRIVATE COMMUNICATION.

9A GROVES,G.V. MARCH 1965.
SEASONAL VARIATIONS OF TEMPERATURE, PRESSURE, DENSITY, AND WINDS TO 80 KM ALTITUDE AT WOOMERA, 1957-1963.
DEPT. OF PHYSICS, UNIV. COLLEGE, LONDON.

10 HALL,L.A. SCHWEIZER,W. AND HINTEREGGER,H.E. 1963.
DIURNAL VARIATION OF THE ATMOSPHERE AROUND 190 KM DERIVED FROM SOLAR EXTREME ULTRAVIOLET ABSORPTION MEASUREMENT.
J. GEO. RES. VOL. 68 (24) PP. 6413-6417.

11 HALL,L.A. SCHWEIZER,W. AND HINTEREGGER,H.E. JAN. 1965.
IMPROVED EXTREME ULTRAVIOLET ABSORPTION MEASUREMENTS IN THE UPPER ATMOSPHERE.
J. GEO. RES. VOL. 70, PP. 105-112.

12 HAVENS,R.J. KOLL,R.T. AND LAGOW,H.E. MARCH 1952.
THE PRESSURE, DENSITY, AND TEMPERATURE OF THE EARTH'S ATMOSPHERE TO 160 KM.
J. GEO. RES. VOL. 57 (1) PP. 59-72

13 HINTEREGGER,H.E. SEPT. 1962.
ABSORPTION SPECTROMETRIC ANALYSIS OF THE UPPER ATMOSPHERE IN THE E.U.V. REGION.
J. OF ATMOS. SCI. VOL. 19, PP. 351-368.

14 HOROWITZ,R. AND LAGOW,H.E. MARCH 1957.
UPPER AIR PRESSURE AND DENSITY MEASUREMENTS FROM 90 TO 220 KM WITH THE VIKING 7 ROCKET.
J. GEO. RES. VOL. 62 (1) PP. 57-78.

15 HOROWITZ,R. AND LAGOW,H.E. DEC. 1958.
SUMMER-DAY AURORAL-ZONE ATMOSPHERIC-STRUCTURE MEASUREMENTS FROM 100 TO 210 KM.
J. GEO. RES. VOL. 63 (4) PP. 757-773.

16 HOROWITZ,R. LAGOW,H.E. AND GIULIANI,J.F. DEC. 1959.
FALL-DAY AURORAL-ZONE ATMOSPHERIC STRUCTURE MEASUREMENTS FROM 100 TO 188 KM.
J. GEO. RES. VOL. 64 (12) PP. 2287-2295.

17 HORVATH,J.J. SIMMONS,R.W. AND BRACE,L.H. MARCH 1962.
THEORY AND IMPLEMENTATION OF THE PITOT-STATIC TECHNIQUE FOR UPPER ATMOSPHERE MEASUREMENTS.
SCI. REPORT NS-1 OF MICH. CONTRACT NASR-54(01), ALSO AF19(604)-6124

18 HORVATH,J.J. JAN. 28, 1965.
PRIVATE COMMUNICATION.

19 JONES,L.M. AND PETERSON,J.W. FEB. 1961.
UPPER AIR DENSITIES AND TEMPERATURES MEASURED BY THE FALLING SPHERE METHOD--- RESULTS FROM 13 FLIGHTS BETWEEN 1952 AND 1958 REVIEWED AND SUMMARIZED IN 1961.
U. OF MICHIGAN 03558-5-T, CONTRACT AF19(604)-6185.

20 LAGOW,H.E. AND AINSWORTH,J. MARCH 1956.
ARCTIC UPPER ATMOSPHERE PRESSURE AND DENSITY MEASUREMENTS WITH ROCKETS.
J. GEO. RES. VOL. 61 (1) PP. 77-92.

DATA REFERENCES CONCLUDED

20A LAGOW,H.E. HOROWITZ,R. AND AINSWORTH,J. 30 JULY 1958.
ROCKET MEASUREMENTS OF THE ARCTIC UPPER ATMOSPHERE.
IGY ROCKET REPORT SERIES NO. 1, NATIONAL ACADEMY OF SCI.

21 MEADOWS,E.B. AND TOWNSEND,J.W. JR. 1960.
IGY ROCKET MEASUREMENTS OF ARCTIC ATMOSPHERIC COMPOSITION ABOVE
100 KM. - ONE OF A SERIES OF PAPERS IN
KALLMAN,H., ED., SPACE RESEARCH, PROCEEDINGS OF THE FIRST INTER-
NATIONAL SPACE SCIENCE SYMPOSIUM, NICE, FRANCE, PP. 175-198.
NORTH-HOLLAND PUBLISHING COMPANY, AMSTERDAM.

22 HEDIN,A.E. AVERY,C.P. AND TSCHETTER,C.D. NOV. 1964.
AN ANALYSIS OF SPIN MODULATION EFFECTS ON DATA OBTAINED WITH
A ROCKET-BORNE MASS SPECTROMETER.
J. OF GEO. RES. VOL. 69, PP. 4637-4648.

23 PETERSON,J.W. 19 JAN. 1965.
PRIVATE COMMUNICATION.

24 PETERSON,J.W. AND MCWATTERS,K.D. APRIL 1964
THE MEASUREMENT OF UPPER-AIR DENSITY AND TEMPERATURE BY TWO
RADAR-TRACKED FALLING SPHERES.
NASA CR-29 (U. OF MICHIGAN CONTRACT NASW-138) WASHINGTON, D.C.

25 REES,J.A. 1961.
DIFFUSION COEFFICIENTS DETERMINED FROM SODIUM VAPORS TRAILS.
PLANET. SPACE SCI. VOL. 8, PP. 35-42.

26 SCHAEFER,E.J. AND NICHOLS,M.H. NOV. 1964.
UPPER AIR NEUTRAL COMPOSITION MEASUREMENTS BY A MASS SPECTROMETER
J. GEO. RES. VOL. 69 (21) PP. 4649-4660.

27 SMITH,W. KATCHEN,L. SACHER,P. SWARTZ,P. AND THEON,J. OCT. 1964.
TEMPERATURE, PRESSURE, DENSITY AND WIND MEASUREMENTS WITH THE
ROCKET GRENADE EXPERIMENT 1960-1963.
NASA TR R-211 GODDARD, GREENBELT, MARYLAND.

28 SPENCER,N.W. JUNE 1958.
RESEARCH IN THE MEASUREMENT OF AMBIENT PRESSURE, TEMPERATURE
AND DENSITY OF THE UPPER ATMOSPHERE BY MEANS OF ROCKETS.
AFCRC TR-58-264 U. OF MICH. FINAL REPORT, CONTRACT AF19(604)-545

29 SPENCER,N.W. BOGGESS,R.L. AND TAEUSCH,D.R. APRIL 1964.
SEASONAL VARIATION OF DENSITY AND TEMPERATURE OVER CHURCHILL,
CANADA, DURING SOLAR MAXIMUM.
J. GEO. RES. VOL. 69 (7) PP. 1367-1380.

30 QUIROZ,R.S. JAN. 1961.
AIR DENSITY PROFILES FOR THE ATMOSPHERE BETWEEN 30 AND 80
KILOMETERS.
AIR WEATHER SERVICE TECHNICAL REPORT 150. WASHINGTON, D.C.